LONDON NRM2018

NEURORECEPTORS AT WORK

BOOK OF ABSTRACTS

9 - 12 July 2018

www.nrm2018.org

WELCOME

It is our great pleasure to welcome you to NRM18 - 'Mapping Neuroreceptors at Work'. The meeting, established by Prof Albert Gjedde in 1997, represents a vibrant community of in vivo brain researchers deciphering the mysteries of the living human brain: exploring how CNS molecule - protein recognition makes us human – for better or for worse – in sickness and in health. This year's meeting is no exception and brings together delegates from around the globe to discuss the latest advances and controversies in this constantly evolving field. A record-breaking number of attendees (ca. 300) will be joining the 2018 meeting at KCL Waterloo Campus in central London.

In addition to keynote talks on 'The Neurobiology of Beauty' (Prof. Semir Zeki) and 'Of Psychotic Mice and Men' (Prof. Oliver Howes), the programme includes an impressive collection of the latest scientific research in the field, scheduled as oral and poster presentations. In order to maximise exposure of the submitted abstracts, we have also implemented two 'rapid-fire' sessions during the meeting. Other programme additions include the NRM18 'Grand Challenge', a session on 'Opportunities and Challenges for Total Body Imaging' and a status update on the 'Data Sharing Initiative'.

In addition to enjoying an excellent scientific program, the conference dinner and entertainment on Wednesday will be held aboard the 'Dixie Bell' for a cruise along the river Thames, details of which will be provided during the meeting.

The organization of NRM18 would not have been possible without the dedicated efforts of many individuals, including the local organising committee and administration, scientific advisory board, reviewers, session chairs, presenters, sponsors, exhibitors and supporters for their invaluable contribution to the conference. Most importantly we would like to thank YOU, the delegates, who never fail to provide lively scientific (and non-scientific) debate during the meeting. We hope you have a stimulating and enjoyable NRM18.

2018 COMMITTEES

LOCAL ORGANISING COMMITTEE

Jas Bains – King's College London
Ashley Little – King's College London
Salvatore Bongarzone – King's College London
Mattia Veronese – King's College London
Andreas Felser – European Association of Nuclear Medicine
Antony Gee – King's College London
Alexander Hammers – King's College London

LOCAL SCIENTIFIC COMMITTEE

Anne Lingford-Hughs – Imperial College London
David Nutt – Imperial College London
Federico Turkheimer – King's College London
Gaia Rizzo – Invicro/Imperial College London
Gemma Modinos – King's College London
Ilan Rabiner – Invicro/King's College London
Matthias Koepp – University College London
Nisha Singh – King's College London
Oliver Howes – King's College London/Imperial College London
Roger Gunn – Invicro/Imperial College London
Sajinder Luthra – King's College London
Salvatore Bongarzone – King's College London
Mattia Veronese – King's College London
Antony Gee – King's College London
Alexander Hammers – King's College London
Marios Politis – King's College London

INTERNATIONAL ADVISORY BOARD

Oral presentations

OP1	*Richard E. Carson*	Age and Sex Difference in Synaptic Density in Healthy Humans: A ^{11}C-UCB-J PET Study
OP2	*Min-Jeong Kim*	In vivo Distribution of Cyclooxygenase-1 in Brain and Peripheral Organs Demonstrated with a Novel PET Radioligand in Human and Rhesus Monkey
OP3	*Hanne D. Hansen*	Simultaneous measurement of cerebral blood flow and 5-HT1B receptor binding changes during a visual stimulus
OP4	*Sylvain Auvity*	Quantification of the efflux clearance role of the P-glycoprotein at the blood-brain barrier: a ^{11}C-metoclopramide PET study in baboons
OP5	*Gregor Gryglewski*	Correlation of serotonin transporter occupancy, brain connectivity and emotional processing investigated with PET/MR hybrid imaging
OP6	*Lars Jonasson*	Simultaneous functional-PET/fMRI imaging of glucose metabolism and BOLD-signal change during a complex working-memory task
OP7	*Samantha Rossano*	Fetal and Neonatal Imaging of Synaptic Density in the Developing Nonhuman Primate using ^{11}C-UCB-J PET
OP8	*Jouni Tuisku*	Effects of age, gender and body weight on the glial marker TSPO - a multicentre [^{11}C]PBR28 HRRT PET study
OP9	*Silvio Meier*	Antibody-based PET imaging detects lowered brain amyloid-beta levels after BACE-1 inhibition
OP10	*Cristian A. Salinas*	[^{18}F]MK-6240 for Imaging Tau in the Brain of Patients with Alzheimer's Disease: Evaluation of its Kinetic Properties, Test-retest Variability and Preliminary 6 Months Longitudinal Data
OP11	*Min Su (Peter)*	Amyloid driven tau deposition colocalizes with Braak Stages
OP12	*Tessa Timmers*	[^{18}F]AV1451 PET in relation to atrophy across the Alzheimer's disease spectrum
OP13	*Andrea Varrone*	Quantification and test-retest examination of [^{18}F]PF-06684511 - a novel radioligand for PET imaging of beta-secretase 1 in the human brain
OP14	*Xiaotian Tsong Fang*	High detection sensitivity with antibody-based PET radioligand for amyloid beta in brain
OP15	*Isadora Lopes Alves*	Event-based modeling of the temporal ordering of regional β-amyloid deposition in the brain
OP16	*Julie Ottoy*	Static and full-dynamic [^{18}F]florbetapir PET in relation to cognition for Alzheimer's disease
OP17	*Cristian C Constantinescu*	In vivo assessment of several fluorine-18 labeled PET tracers for synaptic vesicle protein 2A (SV2A)
OP18	*Zhengxin (Jason) Cai*	Discovery and translational evaluation of novel ^{18}F-labeled SV2A PET tracers in nonhuman primates
OP19	*Michel Koole*	Quantifying SV2A density and drug occupancy in the human brain using ^{11}C-UCB-J PET imaging and white matter as reference tissue
OP20	*Rajesh Narendran*	Imaging nociceptin receptors in cocaine use disorders with [^{11}C]NOP-1A and PET
OP21	*Yasmin Zakiniaeiz*	Sex Differences in Dorsolateral Prefrontal Cortical Amphetamine-Induced Dopamine Release in Tobacco Smokers

OP22	*Cristian C Constantinescu*	Positron Emission Tomography Study with [^{18}F]PF-05270430 to Determine Phosphodiesterase 2A Brain Enzyme Occupancy of TAK-915 in Healthy Human Subjects and Rhesus Macaques
OP23	*Patrick D Worhunsky*	An initial investigation of dissociable dopamine-serotonin subsystems in cocaine use disorder using [^{11}C](+)PHNO and [^{11}C]P943
OP24	*Jenny Ceccarini*	Cannabinoid Receptor Availability Regionally Modulates the Magnitude of Dopamine Release in vivo
OP25	*Christin Y. Sander*	Characterization of the partial agonist aripiprazole through its functional properties with combined PET/fMRI
OP26	*Dr. Daniel Martins*	Intranasal Oxytocin modulation of brainwide resting-state functional connectivity: a peripherally-controlled pharmaco-MRI study
OP27	*Jarkko Johansson*	Intranasal Naloxone Rapidly Occupies Brain mu-opioid Receptors in Human Subjects
OP28	*Lauri Nummenmaa*	Molecular signatures of psychiatric disorders: A volumetric meta-analysis of human neurotransmission imaging studies
OP29	*Yiyun (Henry) Huang*	A novel ^{18}F-labeled radiotracer for imaging 11β-HSD1: Synthesis and evaluation of ^{18}F-AS2471907 in non-human primates
OP30	*Mika Naganawa*	Strategies for Simplified ^{11}C-UCB-J PET Quantification: Ratio and Reference Tissue Methods
OP31	*Alex Whittington*	Ab_L – a more sensitive biomarker for amyloid imaging
OP32	*Nisha Singh*	Is intranasal radiotracer delivery feasible for PET imaging?
OP33	*Gregor Gryglewski*	Prediction of the human whole-brain transcriptome for integrative analysis in brain imaging
OP34	*Ryosuke Arakawa*	A methodology study to assess binding kinetics and test-retest repeatability of the PDE4B PET radioligand [^{18}F]PF-06445974 in healthy subjects
OP35	*Jessie Fanglu Fu*	Clinical Correlates of Complementary Spatial Patterns in [^{11}]C-DTBZ, [^{11}]C-MP, [^{11}]C-RAC, and [^{11}]C-DASB PET Images Revealed by Multiset Canonical Correlation Analysis in Parkinson's Disease
RF20	*Udunna Anazodo*	An approach for minimally-invasive quantification of ^{18}F-FEPPA PET in clinical populations using venous-metabolite correction and PET/MR-image derived input function
OP36	*Lawrence Fung*	GABAergic Dysfunction and Socio-communicative Deficits in Adults with Autism Spectrum Disorder
OP37	*Tonya M. Gilbert*	Epigenetic dysregulation in schizophrenia revealed by human histone deacetylase PET imaging and stem cell-derived neuronal modelling
OP38	*Faith Borgan*	Cannabinoid 1 receptor dysregulation in first episode psychosis: a positron emission tomography study
OP39	*Jennifer M. Coughlin*	Evaluation of the alpha7 nicotinic acetylcholine receptor in recent onset of psychosis using [^{18}F]ASEM PET
OP40	*Samuel Turton*	Combining mu-opioid receptor availability and endogenous opioid release with functional MRI measures of reward anticipation in alcohol and gambling addiction
OP41	*Dean F. Wong*	α7-nAChR: Brain imaging of [^{18}F] ASEM with reproducibility, specific binding, and changes in schizophrenia
OP42	*Patrik Fazio*	Brain mapping of dopaminergic and serotoninergic pathways in non depressed Parkinson's disease patients: a high resolution PET study with [^{18}F]FE-PE2I and [^{11}C]MADAM

OP43	*Adjmal Nahimi*	α_2 Adrenoceptors: Down-regulation in Parkinson's disease
OP44	*Albert Gjedde*	AADC and NET: Noradrenergic mechanisms in Parkinson's disease
OP45	*Shuiyu Lu*	[Carbonyl-^{11}C]N-(5-(((2S,4S)-4-(6-fluoropyridin-2-yloxy)-2-methylpiperidin-1-yl)methyl)thiazol-2-yl)acetamide ([^{11}C]OGA1) is an effective PET radioligand to image brain O-linked-b-N-acetyl-glucosamine hydrolase in monkey
OP46		*Abstract withdrawn*
OP47		*Abstract withdrawn*
OP48	*David Matuskey*	Measuring synaptic density in Parkinson's disease: Preliminary results from a PET imaging study of SV2A with ^{11}C-UCB-J
OP49		*Abstract withdrawn*
OP50	*Pedro Brugarolas*	Imaging multiple sclerosis by PET: development of a PET radioligand for K+ channels to image demyelination
OP51	*Hanne Demant Hansen*	Patients with migraine have high brain 5-HT levels: A PET neuroimaging study of the 5-HT$_4$ receptor in chronic and episodic migraine patients
OP52	*Takuya Toyonaga*	Comparison of In vivo and Ex vivo SV2A Density in Human Brain: A ^{11}C-UCB-J PET Study in Temporal Lobe Epilepsy
OP53	*Dr. Marian Galovic*	Measuring NMDA-receptor activation in focal epilepsy using [^{18}F]GE-179 PET
OP54	*Daniel S. Albrecht*	Frontolimbic connectivity mediates the link between neuroinflammation and depressive symptoms in human chronic pain
OP55	*Julia J Schubert*	Dynamic PET shows cerebral spinal fluid flow alterations in Alzheimer's disease and multiple sclerosis
OP56	*David Gorman*	Suitability of [^{18}F]FAZA to Measure Hypoxia in Glioblastoma Using PET

Rapid Fire Posters

RF1	*Hsiao-Ying Wey*	Comparisons of Biased and Non-biased μ-Opioid Receptor Agonists using PET/MRI
RF2	*Simon Cervenka*	Lower levels of the glial marker TSPO in psychosis patients – an individual participant data meta-analysis
RF3	*Audrey Fan*	Multi-delay arterial spin labeling MRI accurately identifies hypoperfusion in Moyamoya disease: comparison with a normative PET/MRI database
RF4	*Stal Shrestha*	Novel COX-2 PET radioligand, [^{11}C]MC1, can detect and quantify COX-2 upregulation during neuroinflammation in rhesus monkeys
RF5	*Nathalie Ginovart*	Striatal dopamine D2/3 receptors and amphetamine-evoked dopamine release in impulsivity and novelty-seeking traits : a SPECT imaging study using [123I]IBZM in rats
RF6	*Sophie E Holmes*	Investigating mGluR5 as a biomarker of suicidality in Bipolar Disorder: in-vivo and post-mortem evidence
RF7	*Samantha Rossano*	Estimation of V_{ND} of ^{11}C-UCB-J PET in an SV2A Occupancy Study
RF8	*Dean F. Wong*	An open label PET imaging study to evaluate the mGlu5 receptor occupancy following ADX48621 (dipraglurant) administration
RF9	*Nadja Van Camp*	A voxel-wise multimodal approach to evaluate the accuracy of simplified methods to quantify changes in TSPO binding using [^{18}F]-DPA-714
RF10	*Kelly Smart*	High resolution [^{11}C]ABP688 imaging of mGluR5 in healthy volunteers: sex differences and test-retest variability
RF11	*Luc ZIMMER*	Simultaneous PET/MR imaging of 5-HT_{1A} receptor 'biased' agonists
RF12	*Inés Mérida*	Kinetic modelling for endogenous neurotransmitter discharge characterization using PET imaging: optimization of lp-ntPET
RF13	*Samantha Reyes*	Pharmacokinetic modeling of sigma-1 radioligand [^{18}F]FTC-146 binding in brain
RF14	*Tobey J Betthauser*	Imaging considerations for dynamic and static PET imaging of tau pathology with [^{18}F]MK-6240
RF15	*Lisheng Cai, Ph. D.*	Synthesis of [^{11}C]NR2B-Me and its derivatives for evaluation as PET radioligands for NR2B subunits in NMDA receptors
RF16		*Abstract withdrawn*
RF17	*Sangram Nag*	Synthesis and biological evaluation of novel F-18 labelled peripheral benzodiazepine receptor PET radioligand: [^{18}F]fluorovinpocetine.
RF18	*Jimmy E. Jakobsson*	Synthesis and in vivo characterization of [^{11}C]Ro 04-5595 for PET imaging of NR2B subtype NMDA receptors
RF19		*Abstract withdrawn*
RF20	*Udunna Anazodo*	An approach for minimally-invasive quantification of ^{18}F-FEPPA PET in clinical populations using venous-metabolite correction and PET/MR-image derived input function

Posters

P1	*Martin Schain*	Likelihood Estimation of Drug Occupancy for Brain PET Studies
P2	*Anna Schildt*	Evaluation of [^{18}F]-FEOBV in rats
P3	*Lucas Rischka*	Optimized protocol for quantification of task-specific glucose metabolism and comparison to functional MRI
P4	*Soujanya Gade*	$GABA_A$ Receptors and Executive Function in Fragile X Syndrome
P5	*Michael S. Placzek*	Development of brain penetrant P2ry12 ligands towards microglia specific PET radiotracers
P6	*Granville J. Matheson*	Steps toward Promoting Reproducible Research Practices in PET through Open Data and Open Code
P7	*Andreas Hahn*	Reducing the duration and amount of task blocks in [^{18}F]FDG functional PET
P8	*Robert Doot*	Assessment of a statistical arterial input function extraction technique from [18F]fluortriopride PET images
P9	*Johanna Rokka*	Targeting brain HDAC6 using [^{18}F]Bavarostat
P10		Abstract withdrawn
P11	*Andrea Varrone*	In vivo measurement of brain exposure and distribution of [^{11}C]osimertinib in human subjects using positron emission tomography (PET)
P12	*Nandita Joshi*	Improved measurement of serotonin 1A receptor density with a novel image reconstruction technique: phantom and human studies
P13	*Jenny-Ann Phan*	Validation of VND estimates derived from Inhibition, Saturation and Occupancy plots of [^{11}C]raclopride binding in healthy human brain
P14	*Ryosuke Arakawa*	Target occupancy study and whole body dosimetry with a MAGL PET ligand [^{11}C]PF-06809247 in nonhuman primates
P15	*Emma Veldman*	Serotonin 1B receptor mapping in the human brainstem using Positron Emission Tomography and Autoradiography
P16	*Barbara Santangelo*	Modelling arterial input functions using data acquired with an MR- compatible sampler: a validation study using [18F]GE-179
P17	*Masahiro Fujita*	Selective imaging of phosphodiesterase-4 subtype D in monkey brain
P18	*Sandeep SV Golla*	Improved quantification of [^{18}F]flortaucipir uptake in the hippocampus after partial volume correction
P19	*Melanie Ganz-Benjaminsen*	False positive rates in positron emission tomography
P20	*Débora Elisa Peretti*	Optimization of the k2' parameter for the pharmacokinetic modelling of dynamic PIB scans using SRTM2
P21	*Bala Attili*	Evaluation of the new PET radiotracer ^{18}F-FC024 in the hCB_2-AAV rat model of human cannabinoid type 2 receptor local overexpression.
P22	*Francesca Zanderigo*	Application of a reference region-free HYbrid DEConvolution Approach for quantifying PET binding potentials in the absence of blood samples

P23	*Nicole Zurcher*	[^{11}C]PBR28 PET imaging reveals decreased regional brain expression of translocator protein (TSPO) in young adult males with autism
P24	*Granville J. Matheson*	Dopamine D1 receptor availability is not associated with delusional ideation measures of psychosis proneness
P25	*Karl Spuhler*	Elevated raphe 5-HT_{1A} binding is associated with gray matter diffusion entropy changes in temporal and frontal lobes
P26	*Carine SAN*	Evaluation of [^{18}F]-FEPPA as neuroinflammation PET radiotracer in a LPS injected mice model
P27	*Ulrich Sauerzopf*	Blood glucose levels interact with dopamine $D_{2/3}$ receptor availability at baseline and in presence of d-amphetamine inversely in patients with schizophrenia and in healthy volunteers. A [^{11}C]-(+)-PHNO PET study
P28	*Min Su (Peter)*	Brain glucose uptake is modulated by the interaction between microglial activation and amyloid load: a longitudinal microPET study
P29	*Catriona Wimberley*	Parametric maps of TSPO expression in a mouse model of epilepsy
P30	*Daniel Lewis*	[^{11}C]-(R) PK11195 uptake in sporadic vestibular schwannoma and a comparison of two referencing approaches
P31	*Elizabeth Bartlett*	Effects of Lithium Monotherapy on 5-HT1A [^{11}C]-CUMI-101 Binding in Bipolar Depression
P32	*Mala Ananth*	Effects of Lithium Monotherapy on [^{11}C]DASB Binding to the Serotonin Transporter in Bipolar Depression
P33	*Georgios Krokos*	Radioisotope Specific Resolution Kernel Improves Estimation Of Cerebral Perfusion From Dynamic [^{15}O]H_2O-PET Images In Patients With Glioblastoma
P34	*Erjon Agushi*	TSPO imaging in High Grade Glioma - a multitracer PET, MRI and neuropathology study
P35	*Catherine Gregory*	[^{11}C](R)-PK11195 PET imaging of microglial activation in recent onset and chronic schizophrenia
P36	*Matthäus Willeit*	Volumetric measures in selected areas of the prefrontal cortex are associated with amphetamine-induced dopamine release: Implications for psychosis research
P37		*Abstract withdrawn*
P38	*Yannis Paloyelis*	Oxytocin modulation of resting state regional cerebral blood flow: comparing the effects of intranasal and intravenous methods of administration
P39	*Martin Bauer*	First assessment of the P-glycoprotein substrate PET tracer [^{11}C]metoclopramide in healthy volunteers
P40	*Jacob Dubroff*	Greater dopamine D3 receptor availability in males than females as determined by [^{18}F] Fluortriopride, a D3 receptor selective radiotracer
P41		*Abstract withdrawn*
P42		*Abstract withdrawn*
P43	*Francesca Capotosti*	Novel alpha-Synuclein positron emission tomography (PET) Tracers for the Diagnosis of Parkinson's Disease
P44	*Catherine J Scott*	Reduced acquisition time amyloid PET quantification: sensitivity analysis
P45	*Tessa Timmers*	[^{18}F]Florbetapir specific binding in relation to cognition in subjective cognitive decline

P46	*Lyduine Collij*	Amyloid Staging Models: Semi-Quantitative versus Quantitative Measures
P47	*Sander Verfaillie*	Parametric imaging of [^{18}F]florbetapir: a test-retest study in healthy subjects and patients with Alzheimer's disease
P48	*Tatsuya Kikuchi*	Sulfate conjugation of [^{11}C]PBB3, a Tau imaging agent, in the brain
P49	*Nisha Kuzhuppilly Ramakrishnan*	Transgenic rat models of Tauopathy with potential application to PET radiotracer development
P50	*David Elmenhorst*	Impact of intermittent hypoxia on [^{18}F]CPFPX binding to cerebral A_1 adenosine receptors in humans
P51	*Steven Kealey*	In vivo PET evaluation of a potential PDE1 radiotracer – [^{11}C](±)-PF04822163
P52	*Waqas Rafique*	Radiosynthesis and characterization of 3-chloro-4-[^{18}F]fluoro-N-(1-(dimethylamino)cyclohexyl)methylbenzamide ([^{18}F]2a) in rats: Hunting for ^{18}F-labelled, selective mu opioid receptor agonists
P53	*My Jonasson*	Age-related dopamine transporter availability measured using [^{11}C]PE2I PET
P54	*Nicole Praschak-Rieder*	The influence of sex hormones on d-amphetamine induced changes in extracellular dopamine: a [^{11}C]-(+)-PHNO positron emission tomography
P55	*Enrico Glerean*	JABA: Flexible tool for volumetric meta-analysis of region-of-interest and voxel-based PET neuroimaging data
P56	*Swen Hesse*	An In vivo Approach to Assess Gut-Microbiome-Brain Axis Determinants of Human Obesity
P57	*Mi-Hyun Choi*	The observation of finger representations in somatosensory area by pressure tactile stimulation
P58	*Christin Y. Sander*	Stimulation in the VTA is partially driven by dopamine at both D1 and D2 receptors: A multi-modal evaluation with PET/fMRI
P59	*Stefanie D. Krämer*	Overcoming major challenges in input-function based PET kinetic modelling
P60	*Stergios Tsartsalis*	In vivo absolute quantification of striatal and extrastriatal $D_{2/3}$ receptors with [^{123}I]epidepride SPECT
P61	*Lucero G Aceves-Serrano*	Increase of ^{11}C-PBR28 binding after a clinical course of Theta Burst Stimulation in Non-Human Primates: a preliminary assessment
P62	*J. John Mann*	Radiosynthesis and in vivo evaluation of [^{11}C]MPC-6827, the first brain penetrant microtubule PET ligand
P63	*Paolo Zanotti Fregonara*	Head-to-head comparison of ^{11}C-PBR28 and ^{18}F-GE180 for the quantification of TSPO in the human brain
P64	*Yuichi Wakabayashi*	Assessment of a new semi-quantitative method "dopamine transporters standardized uptake value (DaTSUV)" in comparison with conventional specific binding ratio (SBR) in [123I] FP-CIT single-photon emission computed tomography (SPECT) (DaTscan).
P65	*Vesna Sossi*	Identification of a TSPO polymorphism dependant spatial covariance pattern in ^{11}C-PBR PET brain images.
P66	*Tomi Karjalainen*	Introducing AIVO: A centralized neuroinformatics database for brain-PET data
P67	*Paul Edison*	Single-subject Correlation Map (SCM): A novel approach to evaluate the pathological interaction in a single subject
P68	*Salvatore Bongarzone*	Radiosynthesis and In vitro Evaluation of [^{11}C]FPS-ZM1 as a PET Radiotracer to Quantify the Receptor for Advanced Glycation Endproducts in the Brain

P69	*Nicolas Tournier*	Impact of blood-brain barrier disruption induced by focused ultrasounds on the carrier-mediated efflux function: a ^{11}C-erlotinib PET study in rats
P70	*Matteo Tonietto*	A comparative study of stilbene derivatives repurposed for myelin imaging
P71	*Fiona Heeman*	Optimized coffee-break protocols for quantitative [^{18}F]flutemetamol and [^{18}F]florbetaben studies
P72	*Albert Gjedde*	AADC and NET: Noradrenergic mechanisms in Parkinson's disease
P73	*Karl Spuhler*	A convolutional neural network approach for synthesizing patient-specific transmission data using anatomical MRI
P74	*Jenny-Ann Phan*	Validation of dopamine D2 receptor density estimations in human brain with TRue EquilibriuM BoLus Estimation (TREMBLE)
P75	*Heather Liu*	Detecting and Characterizing Dopamine Dynamics in the Cortex with ^{18}F-fallypride PET: A Simulation Study of Time-Varying Models
P76	*Martin Nørgaard*	The Impact of Preprocessing Pipeline Choice on Serotonin Transporter Measurements
P77	*Ryosuke Arakawa*	Quantification of [^{11}C]PBR28 using venous blood sampling and population-based input function approach as less invasive method
P78	*Débora Elisa Peretti*	Relative cerebral flow from dynamic PIB scans as an alternative for FDG scans in Alzheimer's disease PET studies
P79	*Jenna M. Sullivan*	Development of a medium-throughput method to screen the effect of test articles on mouse brain activity using ^{14}C-2-deoxyglucose (14C-2DG) 3D autoradiography
P80	*Xuan He*	Image-derived input functions from heart and vena cava/aorta region for quantification of A1 adenosine receptors in mice brain using [^{18}F]CPFPX and PET
P81	*Pablo Rusjan*	Accounting for endothelial binding in the kinetic modeling of [^{18}F]FEPPA, a TSPO radioligand
P82	*Martin Schain*	Non-invasive estimation of [^{11}C]PBR28 binding potential – application to Alzheimer's Disease
P83	*Francesca Zanderigo*	Test-retest properties and noninvasive quantification of [^{11}C]Harmine binding to brain monoamine oxidase A
P84	*Jasper van der Aart*	Evaluation of the novel PET tracer [^{11}C]HACH242 for imaging the GluN2B NMDA receptor in non-human primates
P85	*Godber Mathis Godbersen*	Co-expression of 2 genes with the enzyme monoamine oxidase A quantified by PET in the human brain
P86	*Jakob Unterholzner*	Co-expression of fourteen genes with the serotonin-1A receptor quantified by PET in the human brain
P87	*Stephen Thompson*	Cu-catalysed methods for radiolabelling radioligands and radiotracers for neuroreceptors with ^{18}F and ^{11}C
P88	*Severi Santavirta*	MAGIA: Robust automated modelling and image processing pipeline for PET neuroinformatics
P89	*Kyle C. Wilcox*	Comparison of regional SV2A density in the rodent, monkey and human brain using ^{3}H-UCB-J
P90	*Akihiro Takano*	Characterization of [^{11}C]PXT012253 as a PET radioligand for mGlu4 allosteric modulators in non-human primates

P91		*Abstract withdrawn*
P92	*Hongmei Jia*	Evaluation of a novel radiotracer for PET imaging of sigma-1 receptors in the brain of nonhuman primates
P93	*Elina Tampio L'Estrade*	Synthesis, Radiolabeling and in vivo Evaluation of [^{18}F]ENL30, a Potential Positron Emission Tomography (PET) Radioligand for the 5-HT7 Receptor
P94	*Angel Torrado-Carvajal*	A Predictive Model of Chronic Low Back Pain Using Brain [^{11}C]-PBR28 Radiomic Features
P95	*Sangram Nag*	Synthesis and biological evaluation of a novel F-18 labelled radioligand [^{18}F]GEH200449 for detection of MAO-B activity
P96	*Ulrich Sauerzopf*	Blood glucose levels interact with dopamine D2/3 receptor availability at baseline and in presence of d-amphetamine inversely in patients with schizophrenia and in healthy volunteers. A (^{11}C)-(+)-PHNO PET study
P97	*Belen Pascual*	Evidence for neuroinflammation in semantic dementia
P98	*Wadad SABA*	PET imaging of the neuroimmune response to alcohol with [^{18}F]DPA-714 in an adolescent binge-drinking model
P99	*Selena M. Sephton*	Evaluation of binding and chemical development of [^{18}F]GE387 - a candidate radiotracer for Imaging TSPO with low binding sensitivity to human polymorphism rs6971.
P100	*Lidia Belles*	Effects of early environmental variables on striatal D2/3 receptors, impulsivity, novelty-seeking and cocaine-seeking behavior in rats
P101	*Matthew Zammit*	[^{11}C]clozapine PET in hemiparkinsonian rhesus with iPSC-derived dopaminergic neuronal grafts expressing DREADDs
P102	*Jeffrey M. Miller*	Serotonin 1A Autoreceptor Binding Correlates With Neural Responses to Emotion Reactivity and Regulation
P103	*Tatu Kantonen*	Endogenous opioid system is associated with inhibitory control: a combined fMRI-PET study
P104	*Euitae Kim*	Frontostriatal functional connectivity and its relationship with striatal dopamine capacity in schizophrenia
P105	*James B Lilleker*	Quantifying muscle amyloid content in inclusion body myositis using [^{18}F]florbetapir positron emission tomography
P106	*Teresa Mann*	Dopamine-D2-receptors in hemiparkinsonian rats - impact of intrastriatal Botulinum Neurotoxin-A Injection
P107	*Eszter Visi*	Microglial activation in recent ischemic stroke: comparison of two TSPO tracers
P108	*Tina Kroll*	Impact of electroconvulsive therapy on the adenosine A1 receptor in the human brain: A PET study in depressive patients
P109	*Nathan Kolla*	Borderline Personality Disorder and the Endocannabinoid System: A [^{11}C]-CURB Positron Emission Tomography Study
P110	*Christine Sandiego*	Evaluation of microglial activation and test-retest studies with [^{18}F]PBR06 in patients with amyotrophic lateral sclerosis and healthy volunteers
P111	*Julie C. Price*	Preliminary Imaging of Neuroepigenetics in Huntington's Disease

P112	*Pauline Roost*	Mapping alteration of dopaminergic neurons in a rat model of Parkinson Disease through the comparison of the presynaptic PET tracers, [^{18}F]-LBT999 and 6-[^{18}F]fluoro-L-m-tyrosine
P113	*Nisha Kuzhuppilly Ramakrishnan*	Preclinical evaluation of [^{18}F]GE387, a novel 18 kDa translocator protein (TSPO) PET radioligand with low binding sensitivity to human polymorphism rs6971
P114	*Colm J. McGinnity*	Two for the price of one: voxelwise “bandpass" spectral analysis of [^{11}C]Ro15-4513 PET reveals bidirectional GABAA receptor subunit expression changes in temporal lobe epilepsy
P115	*Jonas Svensson*	[^{11}C]raclopride – long term reliability and extrastriatal validity
P116	*Sylvain Auvity*	Evaluation of the new CB2R radioligand: a PET study with ^{18}F-FC024 in rhesus monkeys
P117	*Ana Weidenauer*	The Influence of Amphetamine Sensitization on the Binding Potential of [^{11}C]-(+)-PHNO to Dopamine D2/3 receptors: A Study in Healthy Humans
P118	*Leo Silberbauer*	Quantification of striatal serotonin transporter occupancy using reduced PET/MR scan time and [^{11}C]DASB bolus plus constant infusion
P119	*Sander Verfaillie*	Amyloid-β load is related to worries in individuals with subjective cognitive decline
P120	*Michel Bottlaender*	[^{18}F]-AV-1451 binding quantification in AD using SUVr: choosing the optimal time window
P121	*Kelly Mills*	α4β2-nicotinic receptor availability in Parkinson’s disease MCI and healthy controls: a pilot imaging study using [^{18}F]-XTRA PET
P122	*Tobias Gustavsson*	SPECT Imaging and brain retention of recombinant bispecific and unmodified antibodies in an amyloid beta mouse model
P123	*David John Williamson*	In vitro characterisation of TDP-43 and Tau protein distribution in frontotemporal lobe dementia (FTLD) using [^{18}F]AV-1451 autoradiography, T-557 fluorescence microscopy and immunohistochemistry
P124	*Rainer Hinz*	[^{18}F]Flutemetamol PET imaging reveals interaction between relative cerebral blood flow, fibrillar amyloid pathology and memory in non-demented elderly
P125	*Stina Syvänen*	Comparison of in vivo [^{11}C]DED imaging and immunohistochemical ex vivo markers of astrogliosis in a mouse model of Alzheimer’s Disease
P126	*Waqas Rafique*	Synthesis and characterization of heterocyclic sulfoxides: New reversibly binding radiotracers for positron emission tomography imaging of tau neurofibrillary tangles.
P127	*Joonas Majuri*	Dopamine synthesis capacity correlates with mu-opioid receptor availability in the human basal ganglia: a triple-tracer PET study
P128	*Vesa Putkinen*	Childhood family size is associated with striatal type 2 dopamine receptor density and protects against its age-related decline
P129	*Nina Karalija*	The relation between cerebrovascular stress, dopamine system integrity and cognitive performance
P130	*Anna Rieckmann*	Human fMRI response in striatum is accompanied by changes in dopamine D2-receptor occupancy: Results from an in-vivo hybrid PET-fMRI study in healthy humans during task performance
P131	*Roger L. Albin*	Regional Vesicular Acetylcholine Transporter Distribution in Human Brain: A [^{18}F]FEOBV Study
P132		*Abstract withdrawn*

P133	*Talakad G. Lohith*	Adaptive optimal design based PK/PD modeling determines enzyme occupancy of O-GlcNAcase (OGA) inhibitor by PET imaging
P134	*Stal Shrestha*	In vivo demonstration of COX-2 upregulation after neuroinflammation in monkey brain using the novel PET radioligand [^{11}C]MC1
P135	*J. John Mann*	Evaluation of [^{11}C]TMI as a COX-2 selective PET tracer in baboon
P136	*Aya Ogata*	Development of PET Imaging of Colony Stimulating Factor 1 Receptor expressed on microglia
P137	*Lucero G Aceves-Serrano*	Decrease in dopamine release in the striatum after a single session of continuous Theta Burst Stimulation (cTBS).
P138	*Sonia Lavisse*	TSPO radioligand ^{18}F-DPA-714 binding quantification in genotyped Parkinson patients and healthy volunteers
P139	*Ottavia Dipasquale*	Neuropharmacological fMRI of MDMA – A Novel, Multimodal Analytical Approach Informed by PET
P140	*Keisuke Takahata*	Association between tau neuropathology in TBI patients and late-onset psychiatric symptoms: A PET study
P141	*Pierluigi Selvaggi*	Multimodal ASL/PET/mRNA-expression analysis reveals CBF changes after single dose of antipsychotics depends on dopamine D2 receptor density profiles
P142	*Margaret Taylor Davis*	Dysregulation of mGluR5 in borderline personality disorder: A Pilot PET Study with [^{18}F]FPEB.
P143	*Mark M. Goodman*	Synthesis and microPET evaluation of [^{11}C]7-iodo-2-[4-methoxy-3-(2-(4-methylpiperidin-1-yl)ethoxy)phenyl]isoindolin-1-one as a candidate 5-HT2C receptor imaging agent
P144	*Albert Gjedde*	α7-nAChR: [^{18}F]ASEM binding potentials and receptor density in human brain in vivo

OP1
Age and Sex Difference in Synaptic Density in Healthy Humans: A ^{11}C-UCB-J PET Study

Richard E. Carson[1], Mika Naganawa[1], David Matuskey[1,2], Adam Mecca[2], Brian Pittman[2], Takuya Toyonaga[1], Yihuan Lu[1], Mark Dias[1], Nabeel B. Nabulsi[1], Sjoerd J. Finnema[1], Ming-Kai Chen[1], Robert Malison[2], Irina Esterlis[2], Christopher van Dyck[2], Yiyun Huang[1]

[1]PET Center, Department of Radiology and Biomedical Imaging, Yale University, New Haven, CT; [2]Department of Psychiatry, Yale University, New Haven, CT

Introduction:
^{11}C-UCB-J is a PET ligand for synaptic vesicle glycoprotein 2A (SV2A) (1-3), which is expressed ubiquitously in presynaptic terminals. SV2A has comparable distribution to synaptophysin, a common post-mortem synaptic density marker. Thus, ^{11}C-UCB-J may be a quantitative *in vivo* synaptic density marker, and we have found specific changes in epilepsy and Alzheimer's disease vs. age-matched controls. To date, there has been no *in vivo* assessment of aging effects on synaptic density. Studies in postmortem human brains with no dementia have found some loss of presynaptic terminals in healthy aged subjects (>60) compared to younger controls (4). Here, we used ^{11}C-UCB-J PET imaging in healthy controls to assess the effect of age and sex on synaptic density.

Materials and Methods:
A cohort of 47 healthy controls (17 females, 30 males) were scanned with the high resolution research tomograph (HRRT; mean dose: 14 mCi). The age range was 24-83 years (y) with 11 subjects >60 and no difference in mean age between females (46 y) and males (47 y). Arterial samples were used to measure the metabolite-corrected input function and plasma free fraction (f_P). V_T images were produced with the one-tissue model. Using the AAL template and individual MR images, 12 gray matter (GM) regions of interest (ROIs) were applied: frontal, occipital, parietal, and temporal cortices, anterior and posterior cingulate, hippocampus, precuneus, cerebellum, caudate, putamen, and thalamus. BP_{ND} was calculated with the centrum semiovale (CS) as reference region. Age and sex effects in V_T, K_1, and BP_{ND} were evaluated with regional correlations and t tests without multiple comparison correction. A mixed linear model was also applied to account for inter-regional covariance, followed by post-hoc tests.

Results:
Average cortical V_T was 18.2 mL/cm^3 with 14% intersubject SD. Average cortical K_1 was 0.34 mL/min/cm^3 (14% SD). Plasma free fraction was 0.29±0.03. In CS, mean V_T was 4.3 mL/cm^3 (15% SD) and mean K_1 was 0.11 (14% SD). There was a statistically significant reduction in CS V_T (Fig. 1A, 3.3% reduction per decade (RPD), p<0.02), with no significant

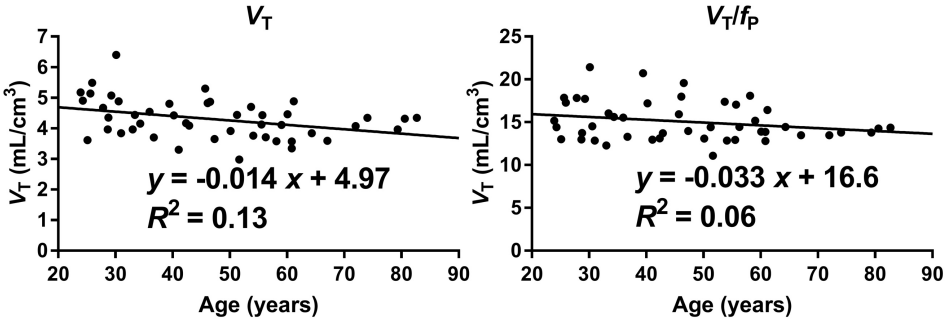

Fig. 1. Left: V_T in Centrum Semiovale vs. age with a statistically significant reduction; p < 0.02. Right: V_T/f_P in centrum semiovale showing no age effect (p > 0.010)

reduction in K_1 or f_P. Significant sex effects in CS V_T (4.59 (F), 4.14 (M), $p < 0.02$) and K_1 (0.126 (F), 0.108 (M), $p<0.0001$) were found with no significant difference in f_P. However, there was also a significant correlation between V_T and f_P ($r=0.39$, $p<0.01$), so we evaluated V_T/f_P in CS (mean: 15.1 mL/cm^3, 15% SD) and found that age (Fig. 1B, 2.2% RPD, $p>0.10$) and sex (15.6 (F), 14.7 (M), $p > 0.15$) effects were not significant. Thus, we attributed the age effect on V_T to age effects on plasma free fraction and subsequently used BP_{ND} as the primary outcome measure.

Average cortical BP_{ND} was 3.3 (16% SD). In the cortex, cerebellum and putamen, there were no age-related changes in BP_{ND} (mean RPD ~ 1%). Hippocampus showed a non-significant 2% RPD. However, in the caudate and thalamus, there were significant reductions in BP_{ND} with age (caudate: Fig. 2A, 8% RPD, $p<0.001$; thalamus: Fig. 2B, 4% RPD, $p< 0.01$). Across all regions, there was a 10±2% lower BP_{ND} in females than males, which reached significance in 5/12 ROIs; however, there were no significant sex effects in GM V_T.

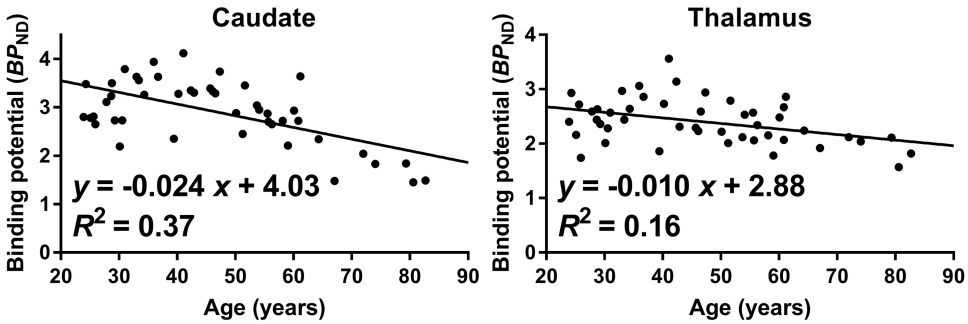

In the mixed model GM BP_{ND} analysis, an unstructured variance-covariance fit the data best. This structure uses separate variances for each region and separate covariances between pairs of regions. In general, correlations between regions were all high (median = 0.7), but were heterogeneous; e.g., frontal cortex correlations with other cortical regions were > 0.9). This analysis showed similar results to the individual-region analysis, with significance in age-by-region (caudate and thalamus, $p<0.01$), sex ($p<0.03$), and sex-by-region ($p<0.02$) effects.

Discussion/Conclusions:

Using ^{11}C-UCB-J, age-related synaptic density changes were found in caudate and thalamus; the functional significance of these reductions will require further study. BP_{ND} was 10% lower in females compared to males, and lower synaptic density in females than in males has been previously demonstrated in temporal cortex by stereology (5). However, both of these results should be carefully interpreted, since BP_{ND} depends on the accuracy of the reference region. Here, we saw age reductions and sex difference in CS V_T, but these may be due to differences in free fraction.

Further exploration of these effects on synaptic density will be focused on the following issues: 1) a more detailed and comprehensive set of ROIs, 2) an increase in the size of the older and female cohorts, 3) region-based partial volume correction to account for volume loss, and 4) assessment of the impact of atlas ROIs on these analyses. This last effect may be the most important, as anatomical standardization across age and sex could easily bias results.

References:

1. Nabulsi *et al.*, *JNMMI*, 57:777-84, 2016.
2. Finnema *et al.*, *Sci Transl Med*, 8:348:348ra96, 2016.
3. Finnema *et al.*, *JCBFM*, epub, 2017.
4. Masilah *et al., Neurology. 43:192-7, 1993.*
5. Alonso-Nanclares *et al.*, *PNAS*, 105: 14615-9, 2008.

OP2

In vivo Distribution of Cyclooxygenase-1 in Brain and Peripheral Organs Demonstrated with a Novel PET Radioligand in Human and Rhesus Monkey

Min-Jeong Kim, Prachi Singh, Jinsoo Hong, Cheryl Morse, Michelle Y. Cortes-Salva, Jeih-San Liow, Stal S. Shrestha, Denise Rallis-Frutos, Katharine Henry, Sami S. Zoghbi, Masahiro Fujita, Victor W. Pike, and Robert B. Innis

Molecular Imaging Branch, National Institute of Mental Health, National Institutes of Health, Bethesda, MD, USA

Introduction:
Cyclooxygenase-1 (COX-1) is constitutively expressed in most organs and produces prostanoids that mediate physiological functions. However, recent brain studies have also suggested proinflammatory roles of COX-1, which can be a potential therapeutic target in brain disorders, such as Alzheimer's disease. Our laboratory recently developed [^{11}C]PS13 as a novel PET radioligand for COX-1. In human and monkey whole blood assays, PS13 was highly potent and selective for COX-1 (IC_{50} = 1 nM) compared to COX-2 (IC_{50} > 1,000 nM). Using [^{11}C]PS13 in human and rhesus monkey, this study sought: 1) to image the in vivo distribution of COX-1 in brain and peripheral organs, and 2) to evaluate the in vivo selectivity of [^{11}C]PS13 for COX-1.

Materials and Methods:
Approximately 740 and 185 MBq of [^{11}C]PS13 were injected intravenously into healthy human subjects and rhesus monkeys, respectively, followed by dynamic positron emission tomography (PET) scans. One brain and seven whole-body scans were obtained in human subjects, and 16 whole-body scans were obtained in monkeys. To measure the in vivo selectivity, scans were also performed in monkeys pretreated with non-radioactive drugs that are preferential for COX-1 or COX-2. Blocking drugs were administered intravenously five to ten minutes before radioligand injection. Concurrent arterial samples for brain scan and venous samples for whole-body scans were obtained to measure the concentrations of parent radioligand and radiometabolites.

Results:
[^{11}C]PS13 showed specific (i.e., displaceable) uptake in most major organs including the spleen, gastrointestinal tracts, kidneys, and brain under baseline conditions in both human and monkey (Fig 1). [^{11}C]PS13 uptake in these organs was blocked by COX-1 preferential inhibitors (i.e., PS13, aspirin, and ketoprofen), but not by COX-2 preferential inhibitors (i.e., MC1 or celecoxib) in monkey. In the human brain scan, [^{11}C]PS13 showed prominent uptake in the choroid plexus and occipital cortex (Fig 2B).

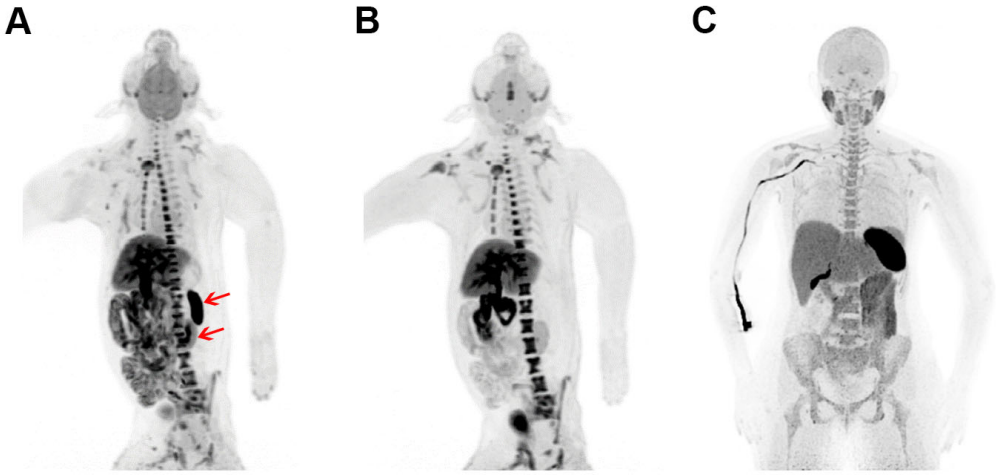

Fig 1. The maximum intensity projection images after injection of [^{11}C]PS13: Under baseline condition (A) and after injection of PS13 (0.3 mg/kg, intravenously) (B) in monkey, and in a healthy human subject (C). Upper arrow = spleen; lower arrow = left kidney.

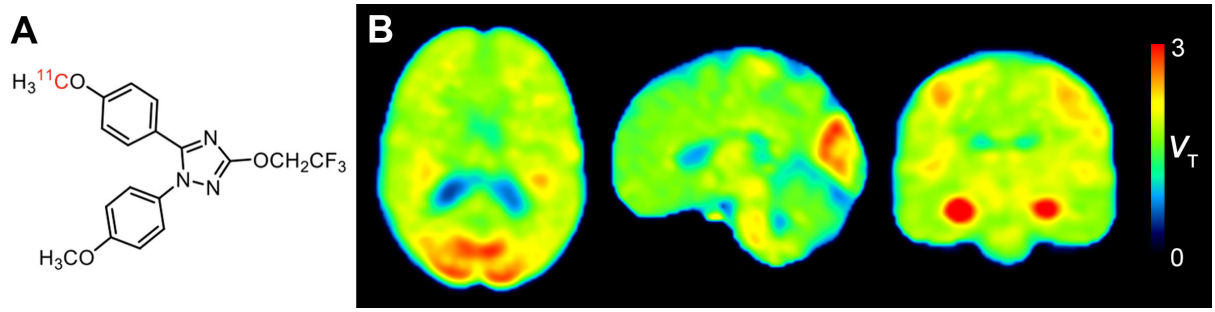

Fig 2. The chemical structure of [^{11}C]PS13 (A), and [^{11}C]PS13 parametric (V_T) brain PET images in a healthy human subject (B).

Conclusion:

Our results suggest that COX-1 is constitutively expressed in major organs such as the spleen, gastrointestinal tract, kidneys, and brain; especially in the choroid plexus and occipital cortex. The in vivo selectivity of [^{11}C]PS13 was also well demonstrated by pharmacological blockade in monkey. [^{11}C]PS13 is the first radioligand for COX-1 that acts directly at this target. It is a potential probe for measuring neuroinflammation in brain disorders, as well as for measuring target engagement by therapeutic drugs.

Reference

Choi SH, Aid S, and Bosetti F. [2009], Trends Pharmacol Sci, 30:174-81.

OP03

Simultaneous measurement of cerebral blood flow and 5-HT$_{1B}$ receptor binding changes during a visual stimulus

Hanne D. Hansen[1], Ulrich Lindberg[2], Patrick M. Fisher[1], Annette Johansen[1], Claus Svarer[1], Adam E. Hansen[2], Gitte M. Knudsen[1]

1. *Neurobiology Research Unit and NeuroPharm, Copenhagen University Hospital, Rigshospitalet, Copenhagen, Denmark*
2. *Department of Clinical Physiology, Nuclear Medicine and PET, Copenhagen University Hospital, Rigshospitalet, Copenhagen, Denmark*

Introduction:

PET-MR imaging enables the simultaneous assessment of brain neurochemistry and brain activity as well as characterization of drug functionality in the living brain [1]. Another unique feature is the opportunity to investigate the temporal correlation of these variables or to investigate brain networks and/or connectivity during a physiological stimulus or while performing a cognitive task.

The processing of affective input is known to be modulated by serotonin (5-HT), but no studies have directly linked affective visual stimuli and cerebral 5-HT release. The aim of this study was to investigate the changes in 5-HT, using serotonin 1B receptor (5-HT$_{1B}$R) binding as a proxy, during a visual stimulus with emotionally positive pictures and the associated neural responses.

Materials & Methods:

Eleven healthy subjects were scanned on the Siemens Biograph mMR scanner. 5-HT$_{1B}$R binding was measured with the radioligand [^{11}C]AZ10419369 while cerebral blood flow (CBF) was measured simultaneous with a 2D pseudo-Continuous Arterial Spin Labelling (pCASL) sequence from 35-80 min after [^{11}C]AZ10419369 injection (Figure 1). Subjects were scanned either with their eyes closed (n=7) or during a visual stimulus (n=10) 50-120 min after injection and comprising a selection of subject-selected personal and emotionally positive pictures.

pCASL data was analysed in blocks of 15 min using FSL. Reconstructed PET data were quantified using the extended simplified reference model [2]. All binding potentials (BP_{ND}) were normalized to the BP_{ND} in the precentral gyrus. This region was chosen as a reference region, given that the subjects did not move during the scan.

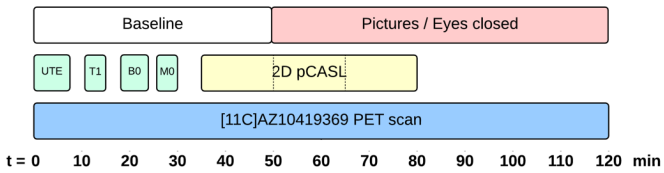

Figure 1: Experimental design of the PET/MR scans.

Results:

Voxel-based analysis of the pCASL data identified four regions of interest (ROIs) with significant increases in CBF when viewing emotionally positive pictures: occipital cortex, caudate nucleus, anterior cingulate and the thalamus (Figure 2A). When performing a ROI analysis and comparing $CBF_{50\text{-}65min}$ to $CBF_{35\text{-}50min}$ (see Figure 1), CBF increased 15 % in the primary visual cortex ($p<0.001$) and 4 % in the thalamus ($p=0.02$) but not in the caudate ($p=0.19$) or anterior cingulate ($p=0.75$). No differences were seen in the non-stimulated (eyes closed) group.

When visually stimulated, BP_{ND} decreased in the occipital cortex ($p=0.01$) compared to the control condition (eyes closed). No group differences were found in the caudate ($p=0.39$),

anterior cingulate cortex (p=0.12) or thalamus (p=0.53). A linear correlation was found between the percent change in CBF and BP_{ND} in the occipital cortex (p=0.03, Figure 2C).

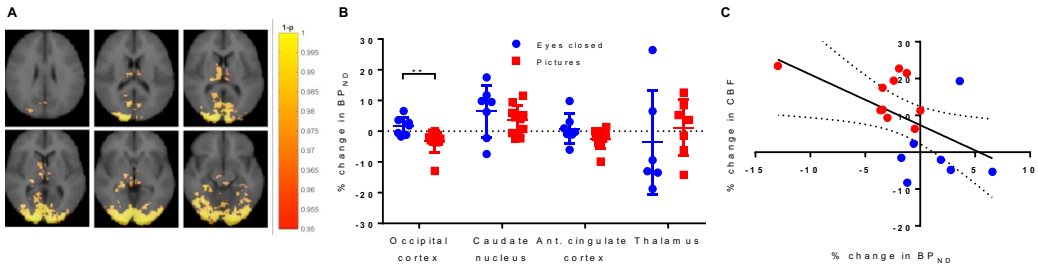

Figure 2: A) Brain regions with higher CBF during visual stimuli (50-65 min > 35-50 min, n=10). **B)** Changes in BP_{ND} in the two experimental settings and in four regions of interest. **C)** Linear correlation (with 95 % confidence interval) between the changes in BP_{ND} and the change in CBF in the occipital cortex (p=0.03, n=17). ** p < 0.01

Discussion:

As expected, we found a 15% increase in occipital cortex CBF as a result of emotionally positive visual stimuli. Interestingly, we also found a decrease in [^{11}C]AZ10419369 BP_{ND} in the occipital cortex in response to the stimuli. [^{11}C]AZ10419369 has previously been shown to be sensitive to changes in 5-HT [3, 4], and we therefore interpret the decreased binding in this study as increased 5-HT levels in response to emotionally positive visual stimuli. We believe it to be unlikely that a change in CBF is influencing the radioligand binding because of the low extraction of [^{11}C]AZ10419369.

Given that the visual stimuli consisted of personal, emotionally positive pictures, we hypothesized to see a 5-HT release in areas involved in emotional processing e.g. ventral striatum and anterior cingulate cortex. However, we were not able to detect any such changes in 5-HT release, but increased CBF was detected in these non-visual areas of the brain.

The linear correlation between changes in CBF and 5-HT_{1B}R binding indicates that the release of 5-HT and subsequent activation of receptors leads to a downstream activation of the neurons and a subsequent increased energy demand in occipital cortex, reflected by the increase in CBF. However, this is likely to be only one of several mechanisms involved in the processing of the stimuli.

To the best of our knowledge, this is the first-time simultaneous changes in CBF and 5-HT levels in response to physiological stimuli has been measured.

References:

1. Hansen HD, Mandeville JB et al (2017). J Neurosci 37:10671–10678
2. Zhou Y, Chen MK et al (2006). Neuroimage 33:550–563
3. Nord M, Finnema SJ et al (2013). Int J Neuropsychopharmacol 16:1577–1586.
4. Jørgensen LM, Weikop P et al (2018). J Cereb Blood Flow Metab

OP4

Quantification of the efflux clearance role of the P-glycoprotein at the blood-brain barrier: a ^{11}C-metoclopramide PET study in baboons

Sylvain Auvity[1,2,3,4], Solène Marie[1], Fabien Caillé[1], Catriona Wimberley[1], Martin Bauer[5,6], Oliver Langer[5,6], Irène Buvat[1], Sébastien Goutal[1] and Nicolas Tournier[1].

[1]UMR 1023 IMIV, Service Hospitalier Frédéric Joliot, CEA, Inserm, Université Paris Sud, CNRS, Université Paris-Saclay, Orsay, France
[2] Inserm, U1144, Paris, F-75006, France
[3]Université Paris Descartes, UMR-S 1144, Paris, F-75006, France
[4]Université Paris Diderot, UMR-S 1144, Paris, F-75013, France
[5]Health and Environment Department, AIT Austrian Institute of Technology GmbH, Seibersdorf, Austria.
[6]Department of Clinical Pharmacology, Medical University of Vienna, Vienna, Austria.

Introduction:
P-glycoprotein (ABCB1) is the most studied ATP-binding cassette (ABC) transporter expressed at the blood-brain barrier (BBB). Currently available PET radioligands such as ^{11}C-(R)-verapamil and ^{11}C-*N-desmethyl*-loperamide are high-affinity P-gp substrates. They convincingly highlighted the ability of P-gp to restrict the influx of its substrates from blood to the brain. Many CNS drugs such as metoclopramide are weaker P-gp substrates. They show sufficient permeability to cross the BBB and exert CNS effects, even when P-gp is fully functional. P-gp may be hypothesized to control the efflux clearance of CNS-active P-gp substrates from the brain, back to the blood. We developed ^{11}C-metoclopramide and showed its specificity for P-gp and suitable pharmacokinetic (PK) properties for such as the absence of brain radiometabolites and the lack of specific binding to other target structures in the brain [1]. In the present study, ^{11}C-metoclopramide was performed in non-human primates, a relevant animal model of the human BBB in terms of P-gp expression, to validate PK models and simplified methods to highlight and quantify the importance of the efflux clearance role of P-gp at the BBB.

Materials and Methods:
Four baboons were included in this study. Dynamic PET acquisitions were performed during 60 min after ^{11}C-metoclopramide injection (298.12 ± 44.13 MBq) under propofol anesthesia. Metabolite-corrected arterial input functions were measured during PET acquisitions. Each animal underwent a PET scan in the absence (baseline) and in the presence of the potent P-gp inhibitor tariquidar (TQD). TQD was i.v infused to ensure maintained plasma concentration during PET acquisition. PET images were co-registered onto corresponding MR images to generate time-activity curves (TACs) in selected brain regions. PK modeling was performed using a 1-tissue compartment model (1-TCM) analysis to estimate the influx (K_1) and efflux (k_2) rate constants and the total volume of distribution (V_T). The wash-out kinetics of ^{11}C-metoclopramide from the brain was also described by the elimination slope k_E, graphically measured from the log-transformed TACs in the elimination phase (30-60 min). Additional PET kinetic parameters were calculated, including the AUC of regional TACs from 0 to 30 min ($AUC_{0\text{-}30min}$). Correlation between full-kinetic modelling outcome parameters and image-derived parameters was tested using a linear regression.

Results:
TQD did not impact ^{11}C-metoclopramide plasma kinetics. Baseline PET images displayed the substantial brain distribution of ^{11}C-metoclopramide, which was homogeneously distributed among brain regions (Fig. 1). Baseline ^{11}C-metoclopramide distribution to the whole brain (V_T, 4.33±0.46 mL/cm3) was significantly increased by P-gp inhibition (V_T, 8.70±0.52 mL/cm^3, P<0.001). A significant 1.28±0.14-fold increase in K_1 (P<0.05) and a 1.64±0.20-fold decrease in k_2 (P<0.01) was observed. The effect on efflux rate constant k_2

was consistent with the significant 1.5±0.25-fold decrease in the elimination slope k_E ($P<0.01$). The effect of TQD on investigated parameters was similar across brain regions. The highest TQD/baseline ratios were obtained for V_T (2.02-fold increase).
A significant correlation was found between V_T and corresponding $AUC_{0\text{-}30min}$ ($P<0.001$, $R^2=0.87$). The elimination slope k_E of the regional TACs, measured from 30 to 60 min was better correlated with V_T ($P<0.001$, $R^2=0.62$) than k_2 ($P<0.001$, $R^2=0.53$)

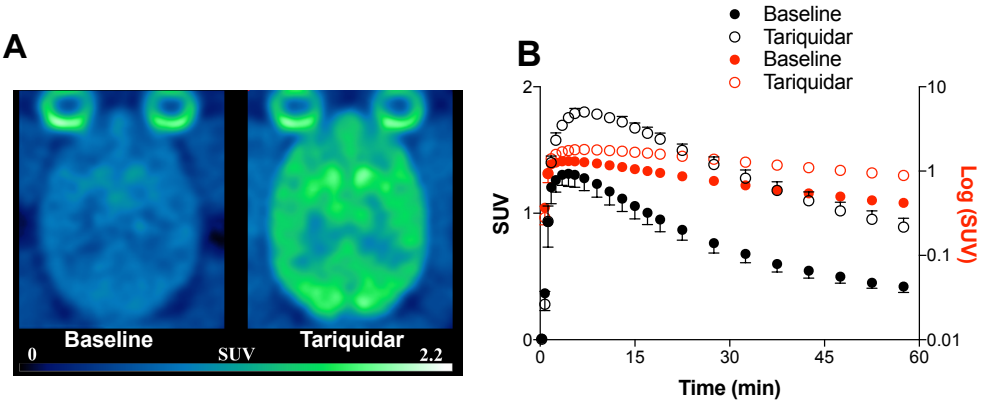

Figure 1: (A) Representative PET summation images (0-60 min) obtained for one baboon at baseline and during tariquidar-infusion. (B) Mean time-activity curves (SUV vs time) obtained in each condition (n =4) are represented using either a linear (black curves) or logarithmic scale (red curves).

Conclusion/Discussion:
Using ^{11}C-metoclopramide PET imaging and PK modelling in baboons, we showed that P-gp does not solely act as a "barrier" to limit the brain penetration of substrates from the blood. Once in the brain, P-gp also mediates the clearance of its substrates back to the blood, thus acting as a detoxifying system to limit overall brain exposure. The elimination slope k_E of the brain TACs offers a dynamic and PK relevant outcome parameter to describe P-gp function at the BBB, especially when arterial blood sampling is not possible.

References:
[1]. Pottier G, Marie S, Goutal S et al. [2016]. *J Nucl Med* 57(2):309–314.

OP5

Correlation of serotonin transporter occupancy, brain connectivity and emotional processing investigated with PET/MR hybrid imaging

Gregor Gryglewski[1], Manfred Klöbl[1], Neydher Berroterán-Infante[2], Lucas Rischka[1], Theresa Balber[2], Godber Mathis Godbersen[1], Verena Pichler[2], Leo Silberbauer[1], Eva-Maria Klebermass[2], Gregory Miles James[1], Markus Hartenbach[2], Wolfgang Wadsak[2,3], Markus Mitterhauser[2,4], Marcus Hacker[2], Andreas Hahn[1], Siegfried Kasper[1], Rupert Lanzenberger[1]

1 Department of Psychiatry and Psychotherapy, Medical University of Vienna, Austria
2 Department of Biomedical Imaging and Image-guided Therapy, Division of Nuclear Medicine, Medical University of Vienna
3 Center for Biomarker Research in Medicine (CBmed), Graz, Austria
4 Ludwig Boltzmann Institute Applied Diagnostics, Vienna, Austria

Introduction:
Despite the widespread use of selective serotonin reuptake inhibitors (SSRIs) in neuropsychiatry, the neurobiological mechanisms underlying their clinical efficacy are not entirely clear. Hybrid PET/MR imaging allows for the simultaneous investigation of pharmacological effects on outcomes acquired from multiple modalities in man. We studied the effects of SSRIs on brain connectivity at rest and activation during emotional processing and correlated these with the occupancy of the serotonin transporter (5-HTT).

Materials & Methods:
36 healthy subjects (27.8±9.6 years, 22 female) underwent two PET/MR measurements on a Siemens mMR scanner. PET data was acquired in listmode and [^{11}C]DASB was applied as bolus plus constant infusion. Citalopram 8 mg or saline was infused over 8 min starting 70 min after tracer bolus in a randomized double-blind design. Arterial blood samples were drawn at 50, 60 and 70 min after drug challenge for measurement of metabolite-corrected tracer activity [1]. Thalamus 5-HTT binding potentials (BP_P) were calculated by subtraction of activity in cerebellar gray matter and division by plasma activity [2]. Dynamic 5-HTT occupancy was obtained by scaling BP_P calculated by averaging three 5 min frames before drug challenge to be equal for both scans and calculating the relative difference in BP_P for each frame thereafter. The resulting time-course was fitted using three exponentials (Figure 1a). Equilibrium 5-HTT occupancy was calculated using an average of three 10 min frames corresponding to the blood samples.
Resting-state fMRI data was acquired for 40 min starting 10 min before drug infusion (TE/TR = 30/2440 msec, 2.1x2.1x3 mm). A sliding window approach (window length = 61 sec, step length = 2 TR) was used and dynamic connectivity matrices were calculated for 200 regions of interest [3]. Correlation strength between dynamic connectivity and dynamic 5-HTT occupancy was compared between placebo and citalopram condition using paired t-tests.
In 25 subjects, an event-related emotion-identification paradigm with happy, anxious, neutral and scrambled faces was performed before and after pharmacological challenge. Faces with emotional valence were contrasted with neutral faces. The difference in activation before and after challenge was compared between placebo and citalopram scans and correlated with 5-HTT occupancy in equilibrium.

Results:
Average equilibrium 5-HTT occupancy was 68.9±8.0%. A network with significantly lower correlation with the time-course of 5-HTT occupancy was identified in the citalopram condition (Figure 1b, $p_{FWE}<0.05$). The differences in brain activation of visual areas after SSRI application for the contrasts between happy and neutral faces ($p_{FWE}<0.001$), and between anxious and neutral faces ($p_{FWE}=0.033$) was significantly correlated with 5-HTT occupancy in equilibrium.

Discussion:

Significant drug effects in functional and molecular imaging outcomes within the first minutes after application of a low dose of SSRIs could be demonstrated. In detail, a reduction of connectivity in a network comprising the default mode system was observed to correlate with the reduction of available 5-HTT. On the other hand, 5-HTT occupancy correlated with the increase of brain activation to emotionally salient compared to neutral faces. The uncoupling of the default mode system associated with rumination and introspection [4], together with increased reactivity to outward emotional stimuli may underlie the postulated rapid shifts of bias in emotional processing elicited by antidepressants [5].

Acknowledgements:

G. Gryglewski, L. Rischka and M. Klöbl are recipients of DOC Fellowships of the Austrian Academy of Sciences at the Department of Psychiatry and Psychotherapy, Medical University of Vienna. This scientific project was performed with the support of the Medical Imaging Cluster of the Medical University of Vienna and a grant from the Else Kröner-Fresenius-Stiftung (2014_A192).

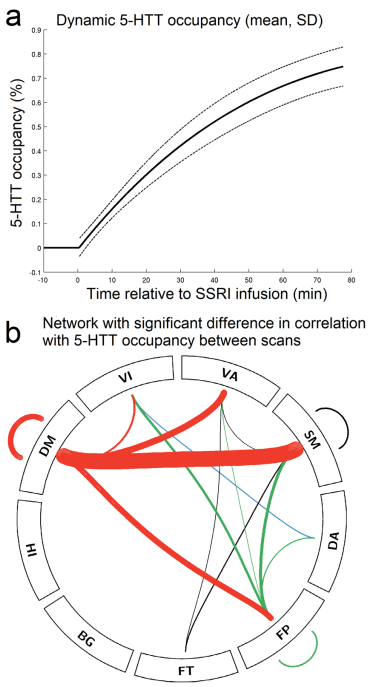

Fig 1: Dynamic 5-HTT occupancy and connectivity analysis.
VI: visual, SM: somatomotor, DA: dorsal attention, VA: ventral attention,
FT: fronto temporal, FP: fronto parietal, DM: default mode, HI: hippocampus + amygdala, BG: basal ganglia

References

[1] Ginovart N, Wilson AA, Meyer JH et al. [2001] J.Cereb.Blood Flow Metab. 21: 1342–1353
[2] Gryglewski G, Rischka L, Philippe C et al. [2017] NeuroImage 149: 23–32
[3] Craddock RC, James GM, Holtzheimer PE et al. [2012] Hum. Brain Mapp. 33: 1914-1928
[4] Hamilton JP, Furman DJ, Chang C et al. [2011] Biol. Psychiatry 70:327-333
[5] Harmer CJ, Bhagwagar Z, Perrett DI et al. [2003] Neuropsychopharmacology 28:148-152

OP6

Simultaneous functional-PET/fMRI imaging of glucose metabolism and BOLD-signal change during a complex working-memory task

Jonasson, L. S. [12], Grill, F. [23], Panes Lundmark, V. [23], Brynolfsson, P. [23], Axelsson, J. [23], Riklund, K. [23], Nyberg, L. [123], & Rieckmann, A. [123]

[1]*Department of Integrative Medical Biology, Umeå University*
[2]*Umeå Center for Functional Brain Imaging, Umeå University*
[3]*Department of Radiation Sciences, Umeå University*

Introduction:
In order to study the complexities of human brain function in vivo with *positron emission tomography* (PET), methodological advances such as improvements in time resolution are crucial. A major step in this direction was made when it was shown that constant infusion of [18F]fludeoxyglucose (FDG) could be used to *dynamically* measure metabolic changes in the brain during sensory and motor tasks (Villien et al. 2014; Hahn et al., 2016), i.e. *functional PET* (fPET). Extending this line of work, we investigate fPET signal in association cortex during working-memory task performance. We complement the dynamic fPET acquisition with simultaneous fMRI in order to test the assumption that task-dependent activation changes in large-scale association networks measured with fMRI reflect dynamic changes in glucose metabolism.

Methods:
The first three subjects from a recently launched data collection were included (3 females, age range 22-31). They were scanned on a SIGNA PET/MR 3.0T system (*GE Healthcare*). Structural images were acquired during the first 18 minutes of the scan, followed by a 42-minutes fMRI protocol. A verbal working memory task (Rieckmann et al., 2017) requiring manipulation and/or maintenance was performed in six-minute blocks (Figure 1). FDG was constantly infused over 60 minutes to enable simultaneous fPET analysis. fPET and fMRI data were modeled separately using general linear modeling (GLM).

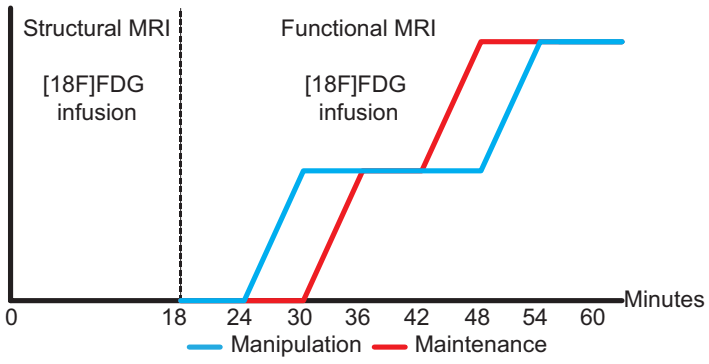

Figure 1. Simultaneous fPET/fMRI design. Constant infusion of [18F]FDG started at the beginning of the scan along with structural MRI collection. At the 18 minutes mark (dashed line) the fMRI protocol commenced. Shown are the ramp functions for manipulation (blue) and maintenance (red) used in the GLM analyses of the fPET data.

Results:
Preliminary analyses indicate areas in the frontoparietal control network and motor cortex, with increased metabolic demands during working-memory performance are successfully identified with fPET. A considerable overlap with regions simultaneously identified with fMRI was shown (Figure 2). Some differences between modalities were also evident in the data; for instance, cerebellar and occipital activations were only apparent in fMRI but not in fPET.

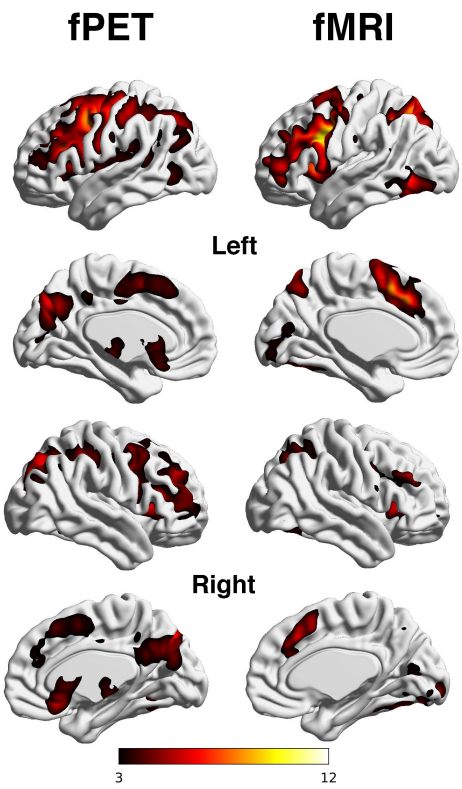

Figure 2. Manipulation vs. rest activations for fPET and fMRI. Areas with increased glucose uptake (left column) and fMRI response (right column) for the manipulation vs. rest blocks are shown. Results were similar for the maintenance condition.

Discussion:

This pilot study showed that constant infusion of FDG can be used to measure dynamic metabolic changes during higher order cognition tasks in vivo. The increase in fMRI BOLD response during working-memory overlap fairly well with increased glucose metabolism in frontoparietal and motor cortical regions, as measured by fPET. The assumption that changes in the BOLD response reflect underlying neuronal activity is supported by the present data. Nevertheless, we also observed some discrepancies between fMRI and fPET activations such that there are fMRI activations with no concomitant PET signal changes, and vice versa. Why this is the case is not yet fully understood but may depend on downstream changes in blood-flow not directly related to glucose and oxygen transport necessary for neural activity.

Data collection is still ongoing and the final sample will include n=20. Future analyses will focus on understanding the basis for non-overlapping networks as well as multi-modal associations to cognition. Here, we provide initial evidence that it is possible to measure metabolic and blood-flow changes simultaneously with fPET/fMRI during complex human cognition.

Acknowledgements:

This research was funded by the European Research Council (AR) and the Umeå University and Västerbotten County Council, Umeå, Sweden. We would like to thank Andreas Hahn for fruitful discussions. Contrast maps were visualized with the BrainNet Viewer (Xia et al., 2013, http://www.nitrc.org/projects/bnv/)

References:

Hahn, A., Gryglewski, G., Nics, L. et al. [2016], J. Nuclear Medicine, 12:1933
Villien, M., Wey, H., Mandeville, J. et al. [2014], NeuroImage, 100:192
Rieckmann, A., Pudas, S., and Nyberg, L. [2017], eNeuro, ePub

OP7

Fetal and Neonatal Imaging of Synaptic Density in the Developing Nonhuman Primate using ^{11}C-UCB-J PET

Samantha Rossano[1,2], Krista Fowles[2], Daniel Holden[2], Steven R. Wilson[3], Jennifer Asher[3], Helene Benveniste[4], Manuel L. Fontes[4], Richard Carson[1,2]

[1] Department of Biomedical Engineering, Yale University, New Haven, CT; [2] Yale PET Center, Department of Radiology and Biomedical Imaging, Yale School of Medicine, New Haven CT; [3] Yale School of Medicine, New Haven CT; [4] Department of Anesthesiology, Yale School of Medicine, New Haven CT

Introduction:

Synaptogenesis begins halfway through gestation in both nonhuman primates (NHP) and humans. The formation and presence of synapses allows for adequate signaling between neurons, which is critical for proper brain function. Previously, post-mortem histological analyses in NHPs using electron microscopy have shown changes in synaptic density throughout development. In most brain regions, synaptic density approaches the level of the adult by the end of gestation, continues to increase to almost twice the level of the adult by 4 postnatal months, before a decline and plateau at the adulthood level [1-4]. A limitation to these studies is the cross-sectional design. To limit confounding variables across subjects, a longitudinal *in vivo* measure of synaptic density in development is desirable. The objective of this study is to develop methodology and investigate the efficacy of using ^{11}C-UCB-J PET, which has been used in NHPs and humans to estimate synaptic density *in vivo*, to visualize synaptic vesicle glycoprotein 2A (SV2A) density in the fetal and neonatal NHP and monitor changes throughout development.

Figure 1: Fetal/Maternal Brain Volume (a) and SUVr (b) changes during fetal development.

A

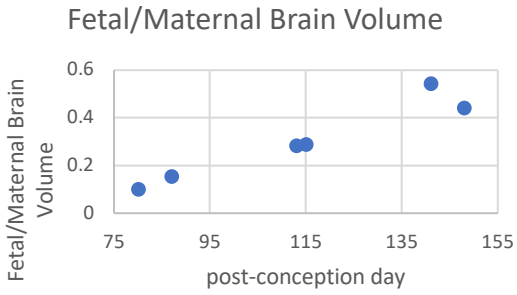

B

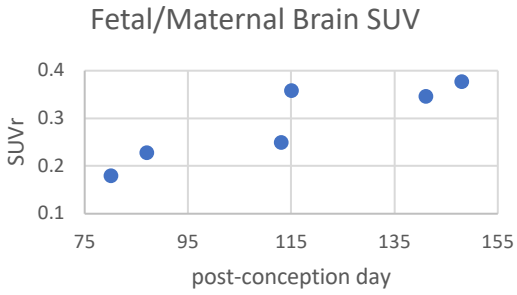

Materials & Methods:

Two pregnant rhesus macaques underwent monthly PET scans with ^{11}C-UCB-J during the final 3 months of gestation, at approximately 80, 110, and 140 post-conception days (pcd). Whole-body dynamic images were acquired on the Siemens Biograph mCT using continuous bed motion. A CT image was taken prior to PET scanning for attenuation correction and anatomical delineation. ^{11}C-UCB-J was administered with a bolus plus constant infusion (B/I) protocol (K_{bol} = 150), so that equilibrium is reached by ~60 min. Uptake within the fetal and maternal brain, delineated by the skull on the CT, were quantified as Standardized Uptake Values at equilibrium, and SUV ratios (SUVr) were calculated as fetal/maternal SUV. Relative brain volumes were defined from the CT images. Both NHPs successfully carried their offspring to term. Neonates (n=2, 1M/1F) were scanned on the Focus220 microPET system with <1mCi bolus of ^{11}C-UCB-J for one hour, at 16 and 58 days (neonate 1) or 34 days (neonate 2). Whole brain tracer uptake was quantified as SUV. No blood samples were acquired in the fetal or neonatal scans.

Results:

Fetal brain volume increased from 18 mL at 85pcd to about 69 mL (about half the maternal volume) at 140pcd (Figure 1a). SUVr increased from 0.20 at 85pcd to 0.36 at 140pcd (Figure 1b). Neonatal whole brain SUV slightly increased within the first 8 weeks after birth (Figure 2). Within the fetal and neonatal brain, tracer distribution was nonuniform, with higher midbrain and cerebellar activity than the cerebral cortex (Figure 3).

Discussion:

PET imaging with ^{11}C-UCB-J in the pregnant NHP demonstrates increasing tracer uptake with time and regionally-varying uptake in the fetal brain. By 140pcd, fetal brain tracer concentration reaches ~35% of the total maternal brain uptake, which is lower than values reported with postmortem NHP studies, in which the fetal synaptic density approaches 100% of the adult level in the month prior to birth [1]. Interestingly, the patterns of high activity in the fetal and neonatal brain resemble those of high glucose metabolism in newborn NHPs and human children investigated with ^{18}F-FDG [5, 6]. Future work is necessary for more accurate quantification of radiotracer distribution, including kinetic modeling with an image derived input function from the ventricular or aortic blood pools, partial volume corrections, and corrections for nondisplaceable uptake.

Figure 2: Brain SUV in early neonatal development.

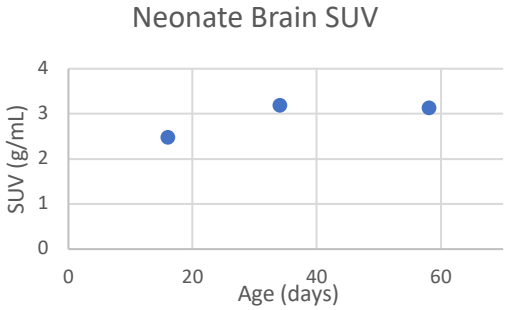

Figure 3: ^{11}C-UCB-J distribution in the fetal (A) and neonatal (B) brain. (scale: kBq/mL)

A.

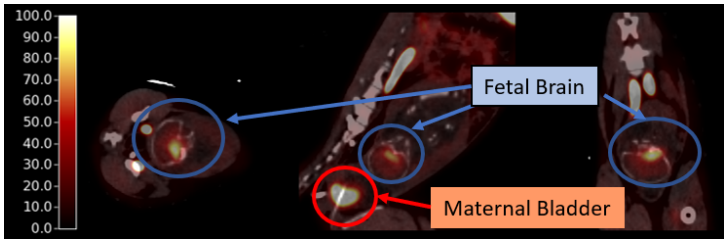

B.

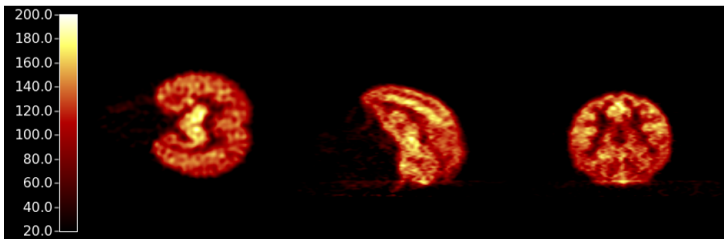

References:

1. Rakic, P., et al., [1986], Science, **232**(4747): p. 232-5.

2. Bourgeois, J.P. and Rakic P. [1993], J Neurosci, **13**(7): p. 2801-20.
3. Bourgeois, J.P., et al. [1994], Cereb Cortex, **4**(1): p. 78-96.
4. Zecevic, N., et al. [1989], Brain Res Dev Brain Res, **50**(1): p. 11-32.
5. Kennedy C., et al. [1982], Ann Neurol 12:333-340.
6. Chugani, H.T. and Phelps, M.E. [1986], Science, 231(4740): p. 840-843.

OP8

Effects of age, gender and body weight on the glial marker TSPO - a multicentre [^{11}C]PBR28 HRRT PET study

Jouni Tuisku[1,5], Pontus Plavén-Sigray[2,5], Edward C. Gaiser[3,5], Laura Airas[1,5], Haidar Al-Abdulrasul[1,5], Anna Brück[1,5], Richard E. Carson[3,5], Ming-Kai Chen[3,5], Kelly P. Cosgrove[3,4,5], Laura Ekblad[1,5], Irina Esterlis[3,4,5], Lars Farde[2,5], Anton Forsberg[2,5], Christer Halldin[2,5], Semi Helin[1,5], Ansel Hilmer[3,5], Eva Kosek[2,5], Mats Lekander[2,5], Noora Lindgren[1,5], Päivi Marjamäki[1,5], Eero Rissanen[1,5], Marcus Sucksdorff[1,5], Andrea Varrone[2,5], Juha Rinne[1,5], David Matuskey[3,5], Simon Cervenka[2,5]

[1]Turku PET Centre, Turku University Hospital and University of Turku, Turku, Finland. [2]Department of Clinical Neuroscience, Karolinska Institutet, Stockholm, Sweden. [3]PET Center, Department of Radiology and Biomedical Imaging, Yale University, New Haven, CT 06520. [4]Department of Psychiatry, Yale University, New Haven, CT 06511. [5]HRRT [^{11}C]PBR28 study group

Introduction:

Translocator protein (TSPO) is an 18 kDa protein structure located on the outer mitochondrial membrane of microglia and astrocytes. TSPO expression has shown to be increased as a response to immune activation (Selvaraj and Stocco, 2015) and is therefore considered a putative marker of neuroinflammation. While aging has shown to be associated with increases in peripheral markers of inflammation, previous PET studies on brain TSPO in relation to age have been inconclusive. However, the sample sizes have been small, limiting the conclusions that can be drawn. In this study we aimed to investigate the effects of aging, gender and body weight to TSPO binding within a large database of healthy control subjects imaged using the 2nd generation TSPO radioligand [^{11}C]PBR28.

Materials & Methods:

[^{11}C]PBR28 data from 143 healthy volunteers (66 males and 77 females; n=80 with HAB and n=63 MAB genotype; age range 19-80 years; body weight range 50 – 129 Kg) were acquired with High Resolution Research Tomograph (HRRT, Siemens/CTI, Knoxville, TN, USA) at three centers: Karolinska Institutet (n=54), Turku PET center (n=67) and Yale University PET center (n=22). All data were preprocessed in a standard manner, in which PET images were realigned and coregistered to anatomical MR images. The MR images were further segmented into tissue classes using SPM, after which the thresholded cortical grey matter segment (GM>0.5) was used as the region of interest for the analysis. The total volume of distribution (V_T) was estimated on 70 min long time-activity curves (t* = 30min) using Ichise's multilinear analysis 1 approach (Ichise et al., 2002) with metabolite corrected arterial plasma samples as an input function. The effects of age, weight and gender on [^{11}C]PBR28 binding were investigated using linear mixed effects model with random intercepts for the TSPO genotype and PET center. The results are presented as effect estimates with 95% confidence intervals.

Results:
Body weight was significantly associated with lower [^{11}C]PBR28 V_T (-0.021 [-0.034,-0.007], p = .003), where the relationship was stronger for HAB genotype group compared to MABs (Figures 1A and 1B). No significant association was observed for age (-0.002 [-0.014, 0.010], p = .785), (Figures 1C and 1D). Furthermore, no difference was observed between males and females for the whole sample (0.320 [-0.050, 0.690], p = .092), but when analyzing TSPO genotype groups separately females showed higher [^{11}C]PBR28 binding in the HAB group (Figs 1E and 1F).

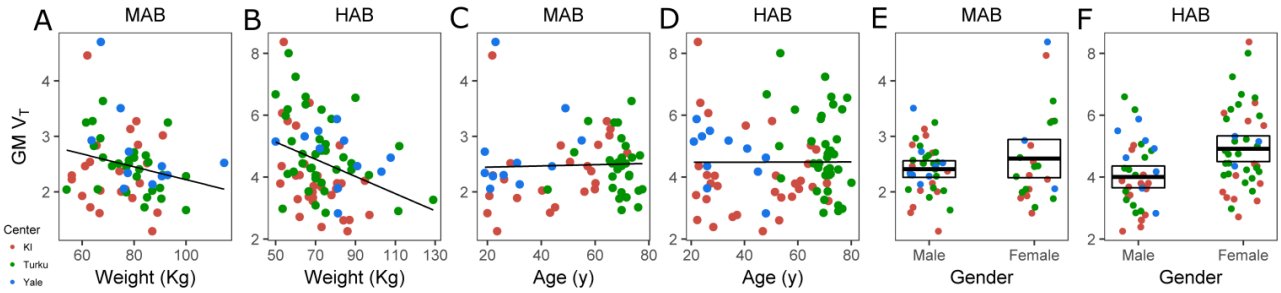

Fig1. Body weight vs. [^{11}C]PBR28 GM V_T in MAB genotype subjects (β = -0.014, CI = [-0.026, -0.002]) (**A**) and HAB genotype subjects (β = -0.031, CI = [-0.049, -0.013]) (**B**). Age vs. [^{11}C]PBR28 GM V_T in MAB genotype subjects (β = 0.003, CI = [-0.007, 0.013]) (**C**) and HAB genotype subjects (β = -0.017, CI = [-0.037, 0.003]) (**D**). Gender vs. [^{11}C]PBR28 GM V_T in MAB genotype subjects (β = 0.190, CI = [-0.126, 0.506]) (**E**) and HAB genotype subjects (β = 0.871, CI = [0.340, 1.402]) (**F**).

Discussion:
Using a several-fold larger dataset, our observation of no effect of age on [^{11}C]PBR28 binding in cortical GM is in line with a previous study employing the 2nd generation TSPO radioligand [^{18}F]FEPPA (Suridjan et al., 2014). These results are in contrast to a small study using the 1st generation TSPO radioligand [^{11}C]PK11195 (Schuitemaker et al., 2012). To our knowledge this is the first study to report effects of body weight and gender on TSPO levels, suggesting that hormonal effects may be a factor in determining TSPO expression. Stronger effects were observed for the HAB genotype subgroup, which is expected since the specific binding is twice as high compared to the MAB group (Owen et al., 2014). The present study is an example of how multicentre collaborations can mitigate the problem of small sample sizes in PET research, providing increased power to detect clinically relevant effects.

Acknowledgements:
Additional members of the HRRT PBR28 study group: Karin Collste, Jean-Dominique Gallezot, Yiyun Huang, Jarkko Johansson, Aurelija Jucaite, Jon Lampa, Nabeel Nabulsi, Caroline Olgart Höglund, Brian Pittman, Christine M. Sandiego, Per Stenkrona.

References:
Ichise, M., et al., 2002. J. Cereb Blood Flow Metab. 22, 1271–1281.
Owen, D.R., et al., 2014. J. Cereb. Blood Flow Metab. 34, 989–94.
Schuitemaker, A, et. al., 2012. Neurobiol Aging. 33, 1067-72.
Selvaraj, V., Stocco, D.M., 2015. Trends Endocrinol. Metab. 26, 341–348.
Suridjan, et al., 2014. Neuroimage 84, 868–875.

OP9
Antibody-based PET imaging detects lowered brain amyloid-beta levels after BACE-1 inhibition

Silvio R Meier[1], Greta Hultqvist[2], Xiaotian T Fang[1], Sahar Roshanbin[1], Lars Lannfelt[1], Ulf Neumann[4], Stina Syvänen[1], Dag Sehlin[1]

[1] Department of Public Health and Caring Sciences / Geriatrics, Uppsala University, Dag Hammarskjölds väg 20, 751 85 Uppsala, Sweden
[2] Department of Pharmaceutical Biosciences, Uppsala University, Hussargtan 3, 751 24 Uppsala,
[3] BioArctic AB, Stockholm, Sweden
[4]Neuroscience Research, Novartis Institutes for BioMedical Research, 4002 Basel, Switzerland

Introduction:
Amyloid-beta (Aβ) positron emission tomography (PET) has become an important tool for diagnosis of Alzheimer's disease (AD) and as an inclusion criterion for enrolment of patients in clinical trials. However, all available radioligands, such as [^{11}C]PIB[1], reflect levels of insoluble Aβ plaques and may thus not be sensitive to treatment aimed at reducing soluble Aβ, e.g. by inhibiting Aβ production. The aim of the present study was to investigate if a novel PET radioligand, based on an antibody directed towards soluble aggregates of Aβ, could be used to detect changes in Aβ levels after treatment with a β-secretase (BACE-1) inhibitor.

Materials and Methods:
Transgenic mice (tg-ArcSwe[2], model of Aβ pathology), were treated during 3 months with BACE-1 inhibitor NB-360[3] and compared to an untreated control group. After treatment, at the age of 13 months, animals were PET scanned with Aβ protofibril selective radioligand [^{124}I]RmAb158-scFv8D3[4]. A baseline group, aged 10 months, also underwent PET scanning. Brain tissue was isolated after PET and Aβ levels were measured in tissue homogenates.

Results:
Treated animals showed significantly lower *in vivo* [^{124}I]RmAb158-scFv8D3 concentrations quantified and visualized with PET than untreated animals. Further, treated animals showed similar [^{124}I]RmAb158-scFv8D3 binding in the brain as the baseline group (Figure 1A and B). The PET results corresponded well with decreased Aβ levels measured in post mortem brain tissue (Figure 1C)

Discussion:
Antibody based PET imaging benefits from very specific binding to the target structure. With protofibril selective radioligand [^{124}I]RmAb158-scFv8D3 we are able to image soluble Aβ protofibrils, which seem to be a promising target for early diagnosis, for following disease progression[5] and for quantification of treatment effects.

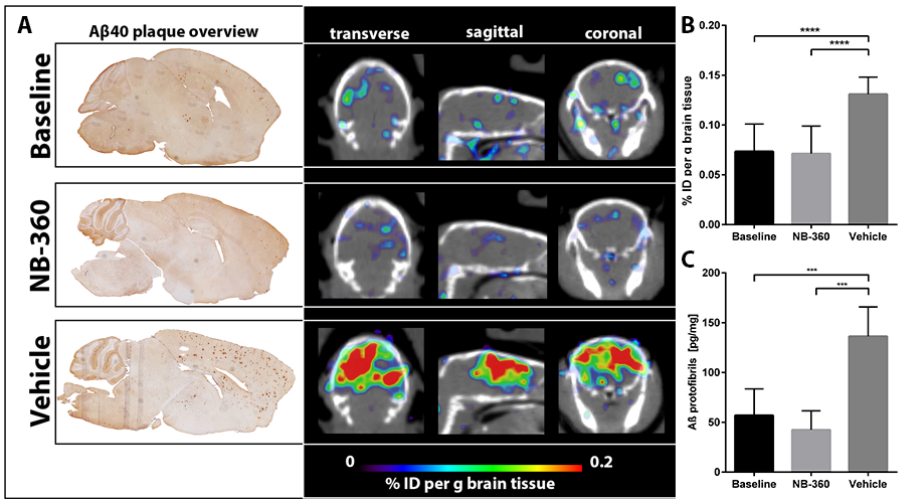

Figure 1: PET analysis of different brain regions. **A:** After a treatment period of 3 months with either food pellets supplemented with BACE-1 inhibitor NB-360 or control food, tg-ArcSwe animals were PET scanned and histopathologically analyzed at the age of 13 months. A third, baseline group was scanned and analyzed at the starting age of 10 months. The untreated control group showed higher degree of plaque pathology and higher PET signals compared with treated animals. In contrast, NB-360 treated animals showed similar plaque pathology and a PET outcome similar to the baseline group, indicating a halting of disease progression due to treatment. **B:** [^{124}I]RmAb158-scFv8D3 in cortex, displayed as percent of injected dose per gram brain tissue. While there was no significant difference between the baseline and NB-360 groups, the vehicle group showed significantly higher radioactivity concentrations ($P<0.0001$ in cortex). **C:** Mesoscale analysis of soluble Aβ40 in brain homogenates. The control group showed significantly higher Aβ40 levels than the baseline and the NB-360 treated group.

Conclusions:

Several AD treatments[6] are currently in phase II and III clinical trials but there are limited possibilities to study their effects on a molecular level *in vivo*. With our previously developed protofibril selective radioligand [^{124}I]RmAb158-scFv8D3 we here demonstrate the ability to monitor treatment effects with PET imaging in tg-ArcSwe mice.

References:

1. Klunk, W. E. *et al.* Imaging brain amyloid in Alzheimer's disease with Pittsburgh Compound-B. *Ann. Neurol.* 55, 306–319 (2004).
2. Lord, A. *et al.* The Arctic Alzheimer mutation facilitates early intraneuronal Abeta aggregation and senile plaque formation in transgenic mice. *Neurobiol. Aging* 27, 67–77 (2006).
3. Neumann, U. *et al.* A novel BACE inhibitor NB-360 shows a superior pharmacological profile and robust reduction of amyloid-β and neuroinflammation in APP transgenic mice. *Mol. Neurodegener.* 10, 44 (2015).
4. Hultqvist, G., Syvänen, S., Fang, X. T., Lannfelt, L. & Sehlin, D. Bivalent Brain Shuttle Increases Antibody Uptake by Monovalent Binding to the Transferrin Receptor. *Theranostics* 7, 308–318 (2017).
5. Sehlin, D. *et al.* Antibody-based PET imaging of amyloid beta in mouse models of Alzheimer's disease. *Nat. Commun.* 7, 10759 (2016).
6. Hung, S.-Y. & Fu, W.-M. Drug candidates in clinical trials for Alzheimer's disease. *J. Biomed. Sci.* 24, (2017).

OP10

[18F]MK-6240 for Imaging Tau in the Brain of Patients with Alzheimer's Disease: Evaluation of its Kinetic Properties, Test-retest Variability and Preliminary 6 Months Longitudinal Data

Cristian A. Salinas[1], R.Matthew Hutchison[1], Ajay Purohit[1], Talakd Lohith[2], Idriss Bennacef[2], Arie Struyk[2], Cyrille Sur[2], Olivier Barret[3], Cristian Constantinescu[3], Ken Marek[3], Jennifer Madonia[3], Rick Hiatt[4], John Beaver[1], Laurent Martarello[1]

1.-Biogen, 2.- Merck Sharp & Dhome, 3.-InviCRO, 4.- Cerveau technologies

Introduction:

[18F]MK-6240 is a high affinity selective tau PET tracer currently under investigation for clinical assessment in patients with Alzheimer's disease. In previous studies, [18F]MK-6240 demonstrated properties consistent with a best in class tau radiotracer, that is, low retention in healthy volunteers (HV), high dynamic range of uptake in subjects with AD in brain regions associated with neurofibrillary tangles (NFT) deposition and low test-retest variability[1]. Herein we report the pharmacokinetic properties of [18F]MK-6240, its quantification, test-retest properties and the preliminary results of a six months longitudinal study in HVs and subjects with AD.

Material & Methods:

Three HVs and five amyloid-beta positive (Florbetapir) AD subjects (MMSE 17-24, age=65±10y) underwent three high specific activity [18F]MK-6240 PET scans (235±75MBq). The first two [18F]MK-6240 scans occurred within an average time window of 14 days. The third scan was performed 6 months (± 20 days) after the first scan (Figure 1).

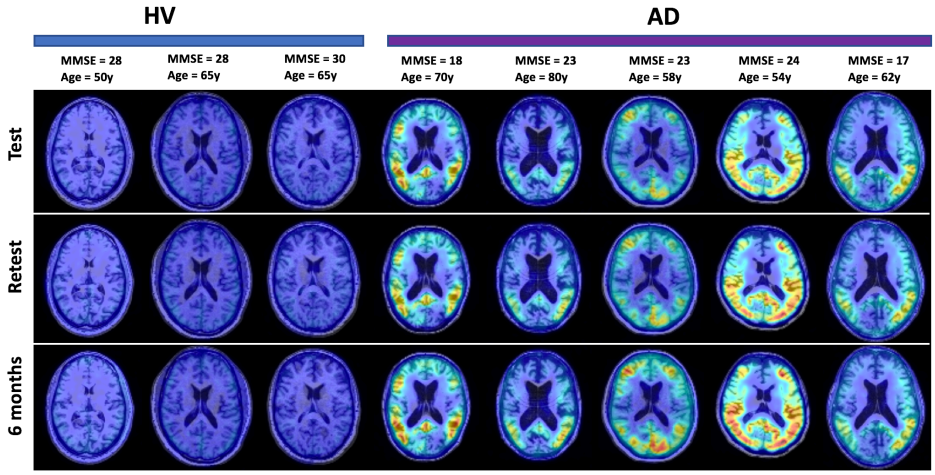

Figure 1: Brain distribution of [18F]MK-6240 at test, retest and six month

In each [18F]MK-6240 visit subjects were dynamically scanned for a 3 hour period post-injection. For each data set a standard image analysis was applied that included PET motion correction, MRI atlas registration and generation of time activity curves. Arterial blood samples were collected to generate a plasma input function corrected for radiometabolites. Regional specific binding was assessed by volumes of distribution (VTs, 2TC), SRTM derived BPNDs and standardized uptake value ratios (SUVRs) using the cerebellar grey matter as reference tissue. Test-retest variability was calculated using the first two scans. Additionally, multiple exploratory metrics were used to estimate tau spread between baseline and 6 month.

Results:
Intravenous administration of [18F]MK-6240 was well tolerated. [18F]MK-6240 rapidly partitioned into brain and its distribution pattern was consistent with NFT pathology in AD. SUVR curves in NFT associated regions were high in AD (>2-3). In contrast a uniform distribution (~1) was consistently observed in healthy subjects. A linear correlation was observed between SUVR and BPnd whilst a non-linear monotonic relationship was observed between SUVR and two tissue compartment derived VTs. SUVRs (90-120 minutes) showed an average TRT variability ≤7% and high correlation with clinical measurements of disease stage (Figure 2)

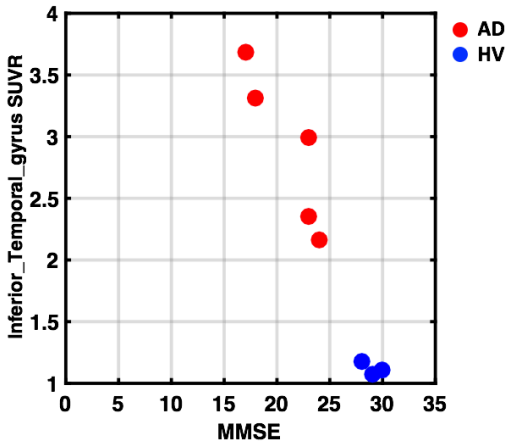

Figure 2: Relatisohip between [18F]MK-6240 SUVR in the inferior temporal lobe and MMSE scores

Exploratory metrics of tau signal spread suggest a change between baseline and six months in subject with AD whilst no change in HVs.

Discussion/Conclusions:
Good sensitivity and correlation with clinical scores, low test-retest variability, and first evidence of sensitivity to the pathology longitudinal changes provide further evidences of [18F]MK-6240 value as biomarker to support the development of novel tau targeting therapies. Further characterization of the tracer and spread metrics is ongoing focusing on the collection of additional subjects and time points (12 and 18 months)

References:
1- Salinas et al., 2018, Test-retest characterization and pharmacokinetic properties of [18F]MK-6240, Human Amyloid imaging 2018, Oral presentation, Session 3

OP11
Amyloid driven tau deposition colocalizes with Braak Stages

Min Su Kang[1,2], Sulantha Mathotaarachchi[1,2], Andrea L. Benedet[1,2], Tharick A. Pascoal[1,2], Mira Chamoun[1,2], Melissa Savard[1,2], Joseph Therriault[1,2], Monica Shin[1,2], Jean-Paul Soucy[3], Gassan Massarweh[3], Serge Gauthier[1,2], Pedro Rosa-Neto[1,2,3]

Translational Neuroimaging laboratory - McGill Centre for Studying in Aging[1], Brain Imaging Centre – Douglas Research Centre[2], McConnell Brain Imaging Centre – McGill University[3], Department of Pharmacology – McGill University[4].

Background:
The amyloid plaques and neurofibrillary tangles (NFTs) are the two major hallmarks of Alzheimer's disease (AD). The histopathological studies hint distinct spreading and progression of amyloidosis and NFTs across AD stage[1,2]. Given the divergent spatial patterns of the hallmarks, the association between the two abnormal protein aggregates in different brain regions is elusive. Here, we reveal the association between amyloidosis and NFTs in cognitively normal (CN), mild cognitive impairment (MCI), and AD individuals with positron emission tomography (PET). The emergence of novel PET tracers of [^{18}F]AZD4694 for amyloidosis and [^{18}F]MK6240 for NFTs allows precise investigation of each pathological progression in temporal and spatial in vivo. Here, we hypothesize that association between the two hallmarks spreads from posterior to anterior regions following the disease progression.

Methods:
A total of 16 CN, 11 MCI, and 11 AD patients was used. Each subject underwent PET [^{18}F]AZD4694 and [^{18}F]MK6240 acquisitions. [^{18}F]AZD4694 image was processed from 40 minutes post-injection for 30 minutes. [^{18}F]MK6240 image was processed from 90 minutes post-injection for 20 minutes. All images were registered to individual MRI with lsq6. Then, they are transformed into ADNI template using lsq12 with nonlinear transformations. The SUVR parametric map was generated using cerebellar grey matter as a reference region for both images. For statistical analysis, we performed voxel-wise analysis to show the association between amyloidosis and NFTs following the model in each group using VoxelStats[3]. [^{18}F]MK6240 SUVR ~ [^{18}F]AZD4694 SUVR + age + gender + APOE + education.

Results:
The unique association between amyloidosis and NFTs was present in entorhinal cortex and PCC in CN; precuneus, PCC, and parahippocampal gyrus in MCI; ACC, entorhinal cortex, parahippocampal gyrus, and orbitofrontal cortex in AD. All groups showed the association in lateral temporal and middle frontal gyrus.

Conclusion:
Our results revealed both similar and different association patterns between amyloidosis and NFTs across AD stage. Most common association pattern was present at left lateral temporal cortex while the different association pattern moved from PCC, precuneus, to orbitofrontal cortex in CN, MCI, and AD, respectively. This corroborates the two pathologies spread from the posterior to anterior regions of the brain.

Figure1.

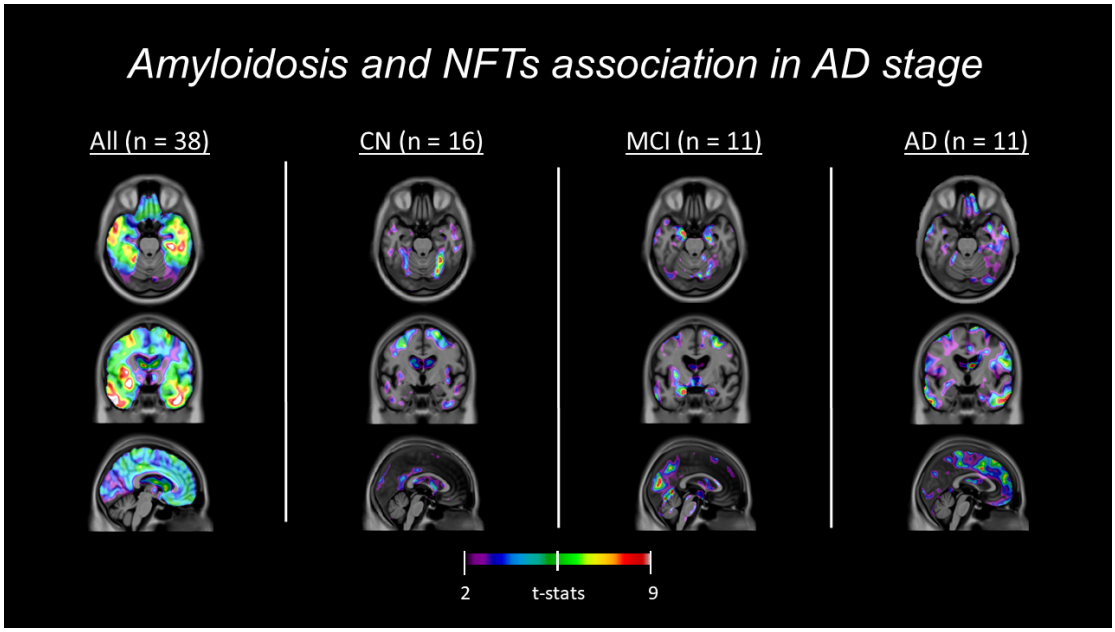

References:

1. Braak, Heiko, and E. V. A. Braak. [1995] "Staging of Alzheimer's disease-related neurofibrillary changes." *Neurobiology of aging* 16.3: 271-278.
2. Thal, Dietmar R., et al. [2002] "Phases of Aβ-deposition in the human brain and its relevance for the development of AD." *Neurology*58.12: 1791-1800.
3. Mathotaarachchi, Sulantha, et al. [2016] "VoxelStats: a MATLAB package for multi-modal voxel-wise brain image analysis." Frontiers in neuroinformatics 10: 20.

OP12
[^{18}F]AV1451 PET in relation to atrophy across the Alzheimer's disease spectrum

Tessa Timmers[1,2], Rik Ossenkoppele[2,3], Emma E. Wolters[1,2], Denise Visser[1], Frederik Barkhof[1,4], Sandeep SV Golla[1], Ronald Boellaard[1], Bert Windhorst[1], Philip Scheltens[2], Wiesje M. van der Flier[2,5], Bart N.M. van Berckel[1]

[1]Department of Radiology & Nuclear Medicine, VU University Medical Center, Amsterdam, The Netherlands
[2]Alzheimer Center, Department of Neurology, VU University Medical Center, Amsterdam, The Netherlands
[3]Clinical Memory Research Unit, Lund University, Lund, Sweden
[4]Institutes of Neurology and Healthcare Engineering, UCLK, London, UK
[5]Department of Epidemiology and Biostatistics, VU University Medical Center, Amsterdam, The Netherlands

Introduction:
Neuropathological Braak staging of neurofibrillary tangles has been introduced to capture the spatial spreading of tau. Using [^{18}F]AV1451 PET, it is now possible to visualize these Braak stages in vivo. The aim of this study was to investigate whether and how specific [^{18}F]AV1451 binding in ascending Braak stages relates to regional atrophy patterns across the Alzheimer's disease (AD) spectrum.

Materials & Methods:
We included 70 subjects (35 subjective cognitive decline [SCD], 6 mild cognitive impairment [MCI] and 29 AD dementia) who underwent a 130-minute dynamic [^{18}F]AV1451 PET scan and structural MRI. For [^{18}F]AV1451, receptor parametric mapping (RPM) with cerebellar grey matter as reference region was used to calculate binding potential (BP_{ND}). Using parametric [^{18}F]AV1451 BP_{ND} images, separate regional values for 1) Braak stage I/II (enthorinal), 2) Braak stage III/IV (limbic) and 3) Braak stage V/VI (neocortical) (Schöll et al, 2016) were extracted (*figure 1*). T1-weighted MR images were used to assess grey matter (GM) volumes. We performed whole-brain voxelwise analyses using the 3 regional Braak [^{18}F]AV1451 BP_{ND} as independent variables, and GM volumes as the dependent variable, adjusting for age, sex and total intracranial volume, with a threshold of $p<0.001$ (uncorrected for multiple comparisons). These analyses were repeated using region-of-interest analyses for both [^{18}F]AV1451 BP_{ND} and GM volumes.

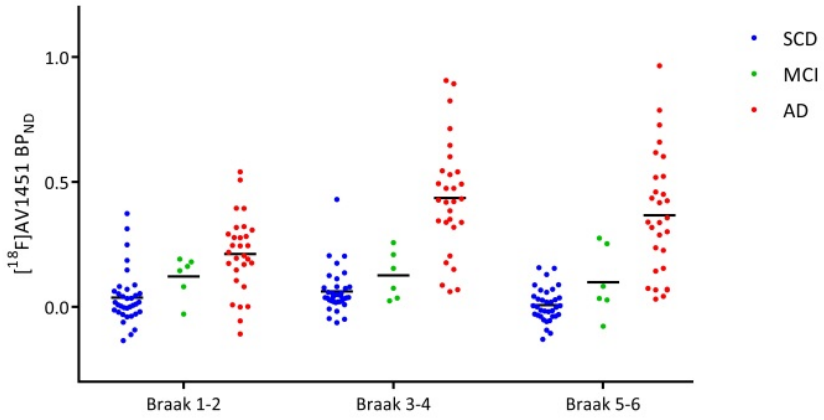

Figure 1: [^{18}F]AV1451 BP_{ND} values per Braak region, according to diagnosis
Abbreviations: BP_{ND} = binding potential, SCD = subjective cognitive decline, MCI = Mild Cognitive Impairment, AD = Alzheimer's Disease

Results:

In the MCI/AD group, [^{18}F]AV1451 BP_{ND} in Braak stage I/II showed limited associations with GM volumes. Greater [^{18}F]AV1451 BP_{ND} in Braak stage III/IV, however, was associated with lower GM volumes in temporal, parietal and frontal cortices (*figure2*). These associations were similar for [^{18}F]AV1451 BP_{ND} in Braak stage V/VI, although slightly less widespread (*figure2*). For SCD, only subtle associations between [^{18}F]AV1451 BP_{ND} in Braak III/IV and GM volumes were observed (*figure3*). Region-of-interest analyses were in line with these findings.

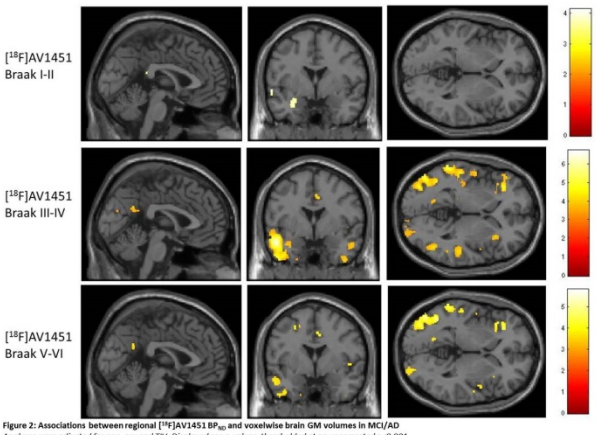

Figure 2: Associations between regional [^{18}F]AV1451 BP_{ND} and voxelwise brain GM volumes in MCI/AD

Analyses were adjusted for age, sex and TIV. Displayed are p-values, thresholded at an uncorrected p<0.001.

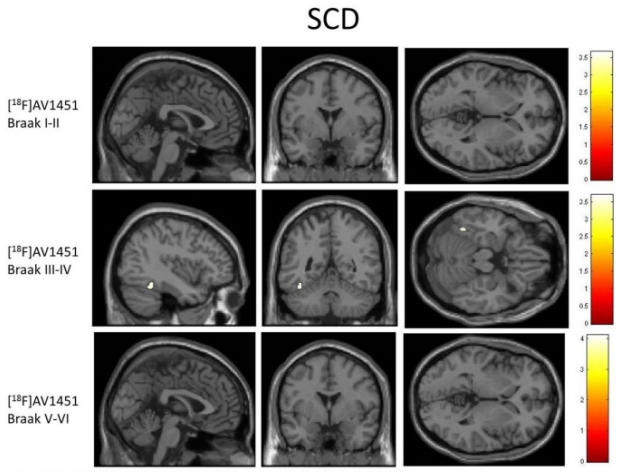

Figure 3: Associations between regional [^{18}F]AV1451 BP_{ND} and voxelwise brain GM volumes in SCD

Analyses were adjusted for age, sex and TIV. Displayed are p-values, thresholded at an uncorrected p<0.001.

Discussion/Conclusion:

These data suggest that tau pathology in Braak stages III/IV is most strongly associated with gray matter volume loss in patients with MCI and AD. Higher tau specific binding in Braak stage V/VI is not related to more extensive atrophy. In SCD and in Braak stage I/II in MCI/AD, only subtle associations between tau pathology and gray matter were observed. These findings could possibly be influenced by partial volume effects.

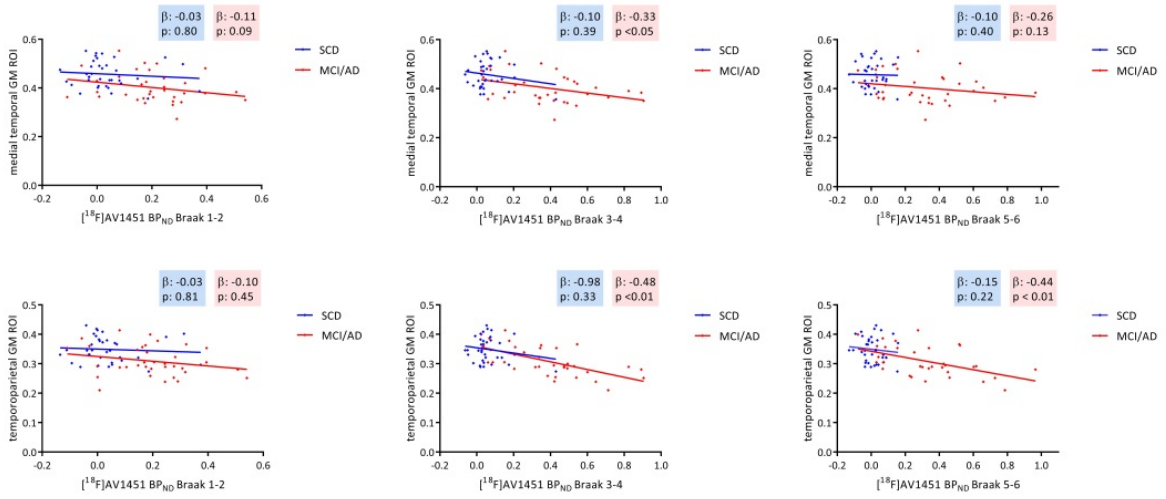

Figure 4: Relationships between [^{18}F]AV1451 BP_{ND} and gray matter ROIs

Displayed are relationships between [^{18}F]AV1451 BP_{ND} in Braak 1-2 (panel A,D), Braak 3-4 (panel B,E) and Braak 5-6 (panel C,F) and gray matter in medial temporal lobe (panel A-C) and temporoparietal lobe (panel D-F). Data are shown for SCD in blue and MCI/AD in red. Beta coefficients and p-values are displayed in blue boxes for SCD and in red boxs for MCI/AD. Abbreviations: BP_{ND} = binding potential, GM = gray matter, ROI = region of interest, SCD = subjective cognitive decline, MCI = mild cognitive decline, AD = Alzheimer's disease

OP13

Quantification and test-retest examination of [^{18}F]PF-06684511 - a novel radioligand for PET imaging of beta-secretase 1 in the human brain

Andrea Varrone[1], Ryosuke Arakawa[1], Akihiro Takano[1], Per Stenkrona[1], Sangram Nag[1], Vladimir Stepanov[1], Mahabuba Jahan[1], Laigao Chen[2], Lei Zhang[2], Ping He[2], Anabella Villalobos[3], Timothy McCarthy[2], Christer Halldin[1]

1. Department of Clinical Neuroscience, Centre for Psychiatry Research, Karolinska Institutet and Stockholm County Council, Stockholm SWEDEN
2. Worldwide Research & Development, Pfizer Inc., Cambridge, MA, USA
3. Worldwide Research & Development, Pfizer Inc., Groton, CT, USA

Introduction:
Beta secretase 1 (BACE1) is an enzyme implicated in the pathophysiology of brain amyloid-beta (Aβ) accumulation in Alzheimer´s disease (AD). BACE1 inhibitors are currently under development as potential therapy for AD. PET imaging of the brain BACE1 level would be a valuable tool in the drug development of Aβ related AD treatments such as BACE1 inhibitors. The PET radioligand [^{18}F]PF-06684511 (IC50=0.7 nM) has been developed for in vivo imaging and quantification of BACE1. The aim of this study was to examine the quantification and test-retest repeatability of [^{18}F]PF-06684511 binding in the brain of healthy human subjects.

Materials & Methods:
Seven healthy subjects (6 females, 1 male, 49±8 y) underwent two PET measurements with [^{18}F]PF-06684511 within 5 to 19 days. The radioactivity and mass injected were 123±24 MBq and 1.1±0.4 µg, respectively, in test studies and 121±24 MBq and 1.0±0.3 µg, respectively, in retest studies. For technical reasons, PET studies were performed with an ECAT EXACT HR system in the first 5 subjects and with a HRRT system in the last two subjects. PET data were acquired for 123 min. Arterial blood samples were collected for the measurement of the plasma free fraction (f_P), the blood and plasma radioactivity concentration as well as for the radiometabolite analysis. Volumes of interest (VOIs) were delineated using the AAL template applied on coregistered 1.5T MRI images. Quantification was performed with the kinetic (1- and 2-tissue compartment modeling) and the Logan graphical analysis (GA) using the metabolite corrected arterial input function. The outcome measure was the total distribution volume (V_T, mL*cm^{-3}). Absolute differences between test and retest measurements relative to mean test-retest values were obtained as measures of repeatability. Mean differences of V_T between models and their 95% C.I. were obtained as the measure of the agreement.

Results:
[^{18}F]PF-06684511 distributed rather uniformly in the brain (Figure 1A). The mean whole brain uptake was peaked around 1.8 SUV at approximately 20 min after injection (Figure 1B) with relatively slow wash-out (mean SUV 1.6 at 120 min). The lowest brain uptake was in the cerebellum and the highest in the anterior cingulate cortex and amygdala (Figure 1C). [^{18}F]PF-06684511 in the plasma was rather stable, with ~70% of the unchanged radioligand still present at 60 min after injection (Figure 1D). The mean f_P was approximately 10% with a test-retest repeatability (TRR) of 19±8%.

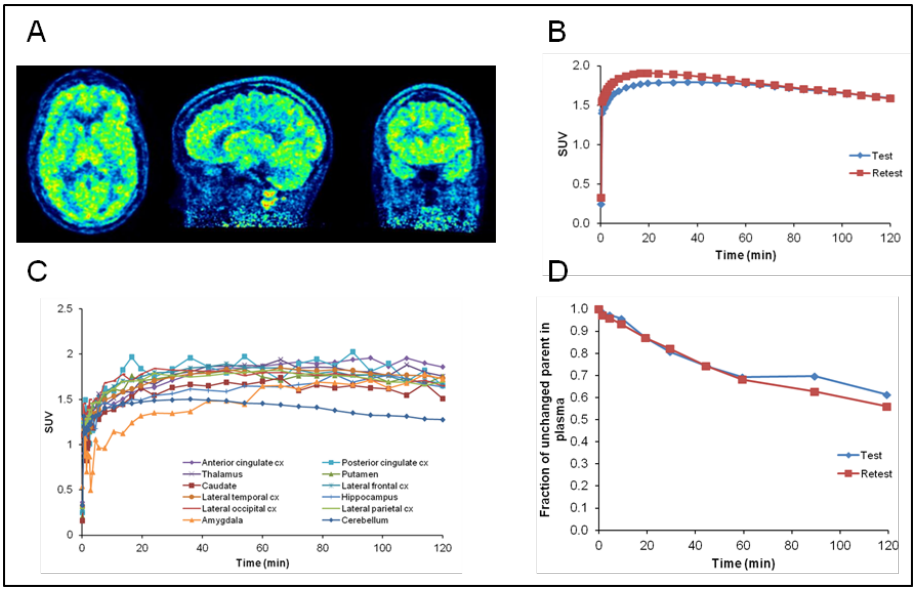

Figure 1.
A) Representative image of [^{18}F]PF-06684511 from one subject using the HRRT system.
B) Mean test and retest whole brain time-activity curves.
C) Regional brain uptake in the same subject as in A.
D) Mean test and retest fractions of unchanged [^{18}F]PF-06684511 in plasma.

The whole brain V_T estimated with 2-TCM ranged between 4.1 and 5.9 mL*cm^{-3}. The lowest V_T values were in the cerebellum (test: 4.1±0.9, retest: 4.6±0.9) and the highest in the amygdala (test: 5.9±1.1, retest: 6.9±1.5) and anterior cingulate cortex (test: 6.0±1.0, retest: 6.6±1.1). The TRT of V_T in the whole brain ranged from 9% to 26% (mean: 18%). It was the lowest in the cerebellum (14±13%), and the highest in the putamen (23±11%). 1-TCM and Logan GA underestimated V_T as compared to 2-TCM by up to 7%. The mean difference of whole brain V_T between 1-TCM and 2-TCM was -0.15 (95% C.I.: -0.20, -0.09) for the test and -0.16 (95% C.I.: -0.20, -0.12) for the retest studies. The mean V_T difference between Logan GA and 2-TCM was -0.13 (95% C.I.: -0.27, 0.1) for the test and -0.06 (95%C.I.: -0.13, 0.00) for the retest studies. The TRR of V_T estimated with 1-TCM and Logan GA was similar to that measured with 2-TCM.

Discussion/Conclusion:
These preliminary data suggest that [^{18}F]PF-06684511 is a suitable radioligand for imaging BACE1 in the human brain. [^{18}F]PF-06684511 displayed relatively slow kinetics, which requires an imaging duration of at least 90 to 120 min for full quantification. 1-TCM and Logan GA provided outcome measures in close agreement with 2-TCM. Further analysis is needed to assess whether simplified methods, such as SUV, can be used in clinical studies in AD patients. The TRR of V_T was similar to that observed for other radioligands without a reference region, such as [^{11}C]PBR28.

Acknowledgements:
The study has been supported by funds from Worldwide Research & Development, Pfizer Inc.

References
Lei Zhang, Laigao Chen, Jason K. Dutra, et al. J Medicinal Chemistry [2018] in press DOI: 10.1021/acs.jmedchem.7b01769.

OP14
High detection sensitivity with antibody-based PET radioligand for amyloid beta in brain

Xiaotian T. Fang[a], Greta Hultqvist[a,b], Silvio R. Meier[a], Gunnar Antoni[c,d], Dag Sehlin[a], Stina Syvänen[a]*

[a] *Department of Public Health and Caring Sciences / Geriatrics, Uppsala University, Uppsala, Sweden*

[b] *Department of Pharmaceutical Biosciences, Uppsala University, Uppsala, Sweden*

[c] *Department of Medicinal Chemistry, Preclinical PET Platform, Uppsala University, Uppsala, Sweden*

[d] *PET Centre, Uppsala University Hospital, Uppsala, Sweden.*

Introduction:

PET imaging of amyloid-beta (Aβ) deposits in the brain, introduced more than a decade ago, has become an important aid in the diagnosis of Alzheimer's disease, and an inclusion criterion for enrolment of patients into clinical trials of potential new anti-Aβ treatments. All available PET radioligands visualizing Aβ bind to the insoluble fibrils, i.e. the main constituent of Aβ plaques. It appears that levels of prefibrillar Aβ forms, e.g. soluble oligomers and protofibrils, correlate better than plaques with disease severity and further that these soluble species are the neurotoxic form of Aβ that eventually leads to neurodegeneration. Thus, the goal of this study was to create a radioligand, based on an antibody that would recognize not only fibrillary Aβ, but also smaller and still soluble aggregates. We therefore designed and expressed a small recombinant bispecific antibody construct, di-scFv 3D6-8D3 targeting both the N-terminus of Aβ and the transferrin receptor.

Materials & Methods:

The light and heavy chain variable fragments of 3D6 were linked together with a 19 amino acid length linker to the scFv 8D3 sequence, forming a di-scFv antibody-like construct: 3D6-8D3, which was transiently expressed by Expi293f mammalian cells and purified from the cell media with a nickel column. Two mouse models were used in this study: tg-Swe (*AβPP* KM670/671NL) harbouring the Swedish AβPP, and tg-ArcSwe which has both the Swedish and the Arctic (*AβPP* E693G) mutations. Wildtype littermates were used as controls. Di-scFv 3D6-8D3 was iodine-124 labelled using a direct radioiodination method with Chloramine-T. Animals were injected intravenously with di-scFv ^{124}I-3D6-8D3 (6.0 ± 2.2 MBq), then scanned either 14, 24 and/or at 72 h post-injection.

Results:

The transferrin receptor, expressed at the blood-brain barrier, could thus be used as a shuttle between the blood and the brain. Di-scFv 3D6-8D3 bound to Aβ1-40 (K_D: 1.22 nM) and to the transferrin receptor (K_D: 12.19 nM) both pre- and post- radiolabeling with radionuclide iodine-124. Di-scFv ^{124}I-3D6-8D3 was injected in two transgenic mouse models overexpressing human Aβ and wild-type control mice and PET scanned at 14h, 24h or 72h after injection. Di-scFv ^{124}I-3D6-8D3 was retained in the brain of transgenic animals while it was cleared from the wild-type brain that lacked Aβ. This difference was observed from 24h onwards, and at 72h, 18 months old transgenic animals displayed SUVR of 2.2-3.5 in brain while wild-type mice showed ratios close to unity. A subset of the mice were also scanned with ^{11}C-PiB. Again wt mice displayed ratios of unity while transgenes showed only slightly, and not significantly, elevated SUVR of 1.2, indicating improved sensitivity with novel di-scFv ^{124}I-3D6-8D3 compared with ^{11}C-PiB. Brain concentrations of di-scFv ^{124}I-3D6-8D3 correlated with soluble Aβ ($p < 0.0001$) but not with total Aβ corresponding to plaque load ($p = 0.34$).

Discussion/Conclusions:
In summary, we have successfully created a small bispecific antibody-based radioligand capable of crossing the BBB, subsequently binding to and visualizing intrabrain Aβ. The radioligand displayed better sensitivity compared with ^{11}C-PiB, and brain concentrations correlated with soluble neurotoxic forms of Aβ.

OP15

Event-based modeling of the temporal ordering of regional β-amyloid deposition in the brain

Isadora Lopes Alves[1], Lyduine Collij[1], Fiona Heeman[1], Viktor Wottschel[1], Elles Konijnenberg[2], Anouk den Braber[2], Maqsood Yaqub[1], Ronald Boellaard[1], Pieter Jelle Visser[2], Bart van Berckel[1], Philip Scheltens[2], Mark Schmidt[4], Frederik Barkhof[1,3]

[1]Dept. of Radiology and Nuclear Medicine, VU University Medical Center, Amsterdam, The Netherlands; [2]Alzheimer Center and Dept. of Neurology, VU University Medical Center, Amsterdam, The Netherlands; [3]Institute of Neurology and Healthcare Engineering, University College London, London, United Kingdom; [4]Janssen Pharmaceutica, Beerse, Belgium.

Introduction:

Unraveling the spatio-temporal trajectory of β-amyloid brain deposition may improve early diagnosis and support future secondary prevention trials in Alzheimer's disease. This study applied event-based modeling (EBM)[1] to determine the temporal ordering of amyloid accumulation in cognitively healthy elderly subjects.

Materials & Methods:

Cognitively healthy subjects (n=190) from the EMIF-AD PreclinAD Study were included and underwent dynamic PET scans (0-30min, 60min break, 90-110min), started at injection (185±10%MBq of [^{18}F]flutemetamol). Amyloid status (positive or negative) was determined by the majority vote of three independent readers who visually assessed the images blinded to clinical information. Quantitative (regional) non-displaceable binding potentials (BP_{ND}) and standard uptake values (SUVR) were calculated from parametric images using cerebellar gray matter as a reference region. EBM was fitted to BP_{ND} and SUVR results, where each regional value corresponds to an event. The control group was composed of negative scans; the affected group of positive scans.

Results:

Twenty six subjects (13%) were visually classified as positive using BP_{ND} images, and 28 (14%) using SUVR images. Figure 1 shows the positional variance diagrams for the ordering of amyloid abnormality in this population for each metric. BP_{ND} based EBM showed better agreement with recent studies of early amyloid deposition patterns, and greater certainty in event ordering and staging placement (Figure 2a). Earliest BP_{ND} regions included the parahippocampal and fusiform gyri; latest consisted of thalamus, hippocampus, cuneus and lingual gyrus. In contrast, SUVR displayed higher uncertainty, suboptimal staging (Figure 2b), and regional contradictory ordering, e.g. lingual gyrus as earliest positive region and fusiform gyrus and parahippocampal and fusiform gyri at later stages. A high proportion (60% with BP_{ND} and 54% with SUVR) of subjects were classified as stage 0, in line with the small number of positive scans and confirming the presence of pathological changes missed by global classifications of β-amyloid status.

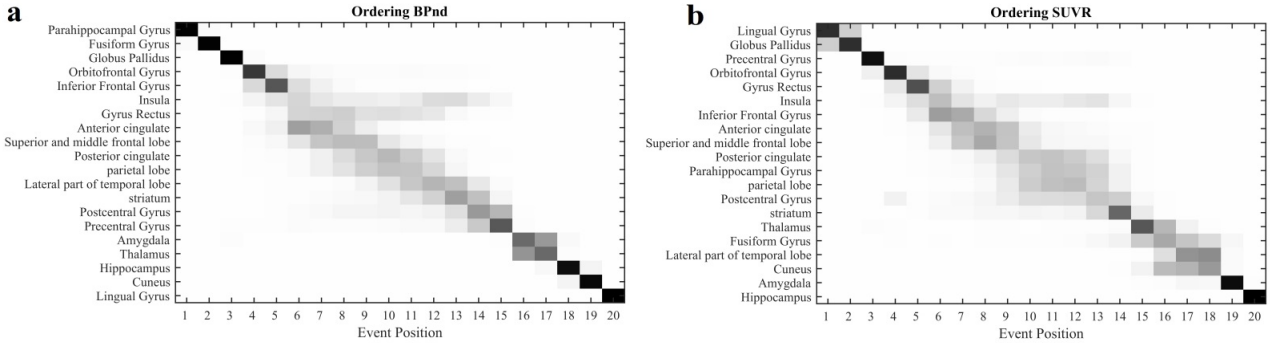

Figure 1. Positional variance diagrams of the uncertainty in the maximum likelihood event ordering estimated by taking MCMC (Markov chain Monte Carlo) samples using the EBM to fit (a) BPnd and (b) SUVR data.

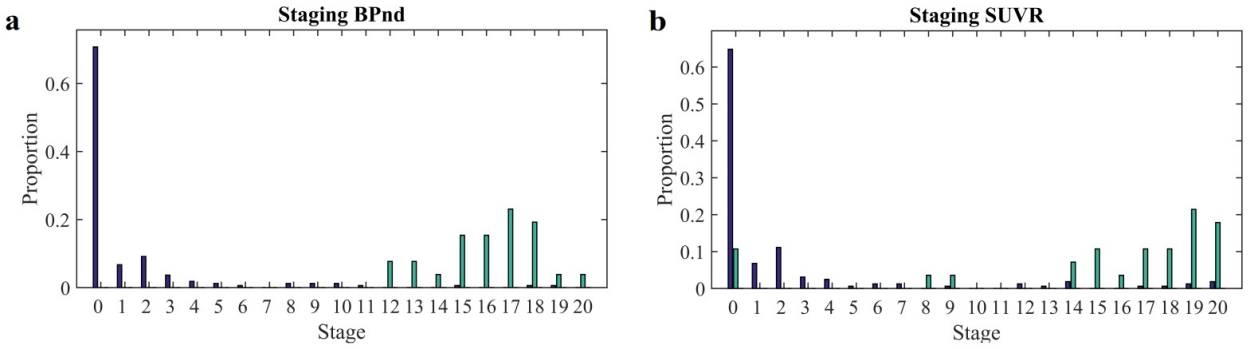

Figure 2. Proportion of subjects in each category (normal vs abnormal) at each EBM stage. Proportion of negative scans in dark blue and positive scans in green. Each EBM stage on the x-axis corresponds to the occurrence of a new regional transition event. Stage 0 corresponds to no events having occurred and stage 20 is when all events have occurred. Events are ordered by the maximum likelihood event sequence for the whole population as shown in Figure 1.

Discussion/Conclusion:

EBM reconstructed the ordering of amyloid accumulation in a data-driven manner from a cross-sectional cohort without the use of pre-defined cut-offs for positivity. As expected, the resulting event order using BP_{ND} outperformed SUVR, showing greater agreement with recent staging studies and suggesting higher sensitivity to early pathological changes.

Acknowledgements:

This work has received support from the EU/EFPIA Innovative Medicines Initiative Joint Undertaking EPAD grant agreement n°115736. The authors would like to acknowledge the AMYPAD Consortium, as well as collaborating projects such as EMIF and EuroPOND.

References:

[1] Young AL et al. 2014, Brain. A data-driven model of biomarker changes in sporadic Alzheimer's disease. 137(Pt 9):2564-77.

OP16
Static and full-dynamic [^{18}F]florbetapir PET in relation to cognition for Alzheimer's disease.

Julie Ottoy[1], Jeroen Verhaeghe[1], Ellis Niemantsverdriet[2], Ellen De Roeck[2], Hanne Struyfs[2], Charisse Somers[2], Leonie wyffels[3], Tobi Van den Bossche[4], Sara Van Mossevelde[4], Sarah Ceyssens[3], Christine Van Broeckhoven[4], Sigrid Stroobants[3], Maria Bjerke[2], Sebastiaan Engelborghs[2] and Steven Staelens[1].

[1] *Molecular Imaging Center Antwerp, University of Antwerp, Antwerp, Belgium*
[2] *Reference Center for Biological Markers of Dementia (BIODEM), Laboratory of Neurochemistry and Behavior, Institue Born-Bunge, University of Antwerp, Antwerp, Belgium*
[3] *Department of Nuclear Medicine, Antwerp University Hospital, Edegem, Belgium*
[4] *Department of Molecular Genetics, VIB, University of Antwerp, Antwerp, Belgium*

Introduction:
The aim of this study was to investigate the associations of [^{18}F]florbetapir binding measures from static and full-dynamic PET imaging with CSF, MRI, and cognition measures at baseline as well as with longitudinal cognitive performance in the Alzheimer's disease (AD) spectrum.

Materials and Methods:
At baseline 45 subjects (11 healthy controls, 24 MCI, 10 AD) underwent 60 min dynamic [^{18}F]florbetapir PET with continuous arterial sampling. Two-tissue compartment modeling with a metabolite-corrected plasma input function was used to calculate V_T and DVR in frontal, parietal, temporal, occipital, ACC, PCC, precuneus and global regions (i.e., volume-weighted average of frontal, parietal and temporal uptake). Static SUV(R) was calculated at 50-60 min p.i.. Both DVR and SUVR were normalized to the cerebellar gray matter. Neuropsychological tests, including MMSE and RBANS, were performed at baseline and for a subset at follow-up (n=40 at follow-up year 1; n=33 (MMSE) and n=21 (RBANS) at follow-up year 2). ANCOVA, adjusted for age, sex, education, APOE-e4, baseline diagnosis (and cognition interval as well as baseline score), were used to determine the associations between PET and the other biomarkers. Linear-mixed models, adjusted for age, sex, education, and APOE-e4, were used to assess the difference in cognitive performance over time between Aβ+ and Aβ- subjects stratified based on either V_T, DVR, SUV or SUVR (i.e., global measure > average controls + 1.5 SD).

Results:
At baseline, all [^{18}F]florbetapir measures were significantly associated with CSF (Ab_{1-42}/Ab_{1-40}, Ab_{1-42}, $Ptau_{181}$ and $Ptau_{181}/Ab_{1-42}$). All global [^{18}F]florbetapir measures except SUV were significantly and inversely associated with cortical grey matter volume on MRI, but only the relative (both global and regional) measures were significantly and inversely associated with hippocampal volume. All [^{18}F]florbetapir measures were significantly and inversely associated with cognition (e.g., global V_T with language (p=0.008), immediate recall (p=0.009) and story recall (p=0.024); SUV with figure recall (p=0.030); both DVR and SUVR with story recall (p=0.021 and p=0.043, resp.)). Higher V_T (parietal and precuneus) and DVR (parietal, temporal, PCC, precuneus and global cortical) at baseline were significantly associated with steeper cognitive decline (Δ word list recall) over 1 year (Fig.1). Baseline SUV(R) was not significantly associated with change in cognition.
Based on mixed model analysis over 2 years, Aβ+ showed significant lower cognition score than Aβ- when the groups were stratified based on V_T (all cognitions, p=0.008-0.067), DVR (all cognitions, p=0.018-0.068), SUV (all cognitions except story (p=0.100) and list (p=0.091) recall), and SUVR (all cognitions except immediate (p=0.084) and delayed (p=0.150) recall).

Aβ+ showed a faster cognitive decline over time compared to Aβ- when the groups were stratified based on V_T (MMSE, immediate and list recall), SUV (list recall), and DVR and SUVR (MMSE) (Fig. 2).

Conclusion:

Both static and dynamic [^{18}F]florbetapir PET measures were well associated with CSF, MRI, and cognition measures at baseline. Dynamic [^{18}F]florbetapir PET was a stronger predictor of longitudinal cognitive change.

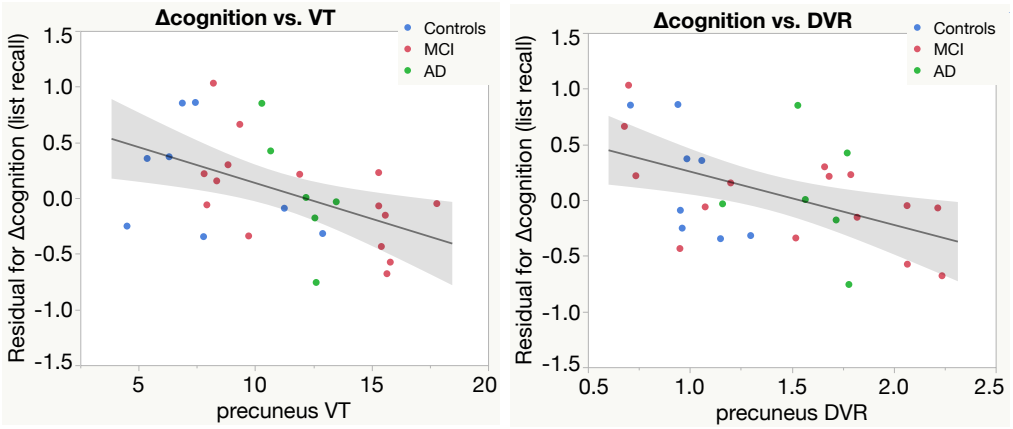

Fig 1. Relationship between change in cognition (Δ word list recall) and V_T (left) or DVR (right) in the precuneus. Residuals are extracted from an ANCOVA including Δ word list recall as dependent variable and age, education, gender, APOE-e4, baseline diagnosis, baseline cognition score and cognition interval as covariates/factors. Both V_T and DVR were significant predictors of Δ word list recall ($p=0.038$, $R^2=0.21$ (including all predictors: $R^2=0.65$), and $p=0.016$, $R^2=0.27$ (including all predictors: $R^2=0.68$), resp.).

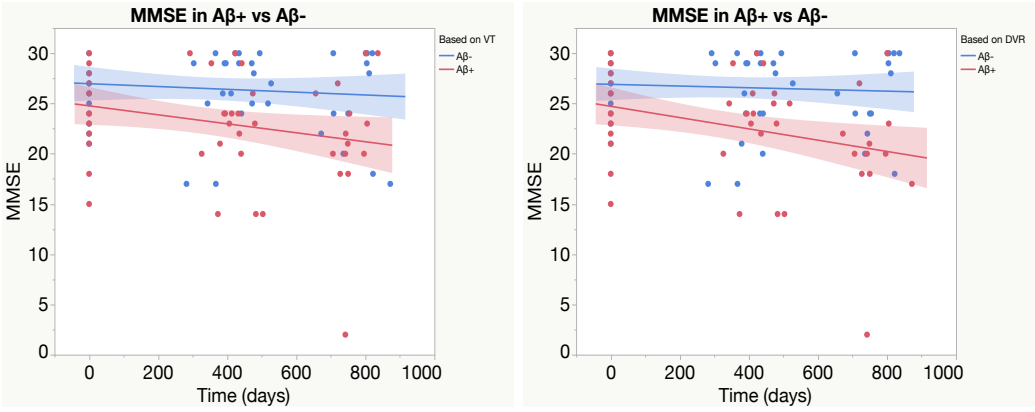

Fig 2. MMSE score versus time (2 years span) in Aβ+ versus Aβ- subjects, stratified based on V_T (left) and DVR (right). There was a significant group as well as group*time interaction effect for V_T ($p=0.063$ and $p=0.050$, resp.) and DVR ($p=0.018$ and $p=0.007$, resp.).

OP17
In vivo assessment of several fluorine-18 labeled PET tracers for synaptic vesicle protein 2A (SV2A)

Cristian C. Constantinescu, Vincent Carroll[1], David Alagille[1], Cedric Tresse[1], Laetitia Mistico[1], Christine Sandiego[1], Caroline Papin[1], Alexandra Gouasmat[1], MingQiang Zheng[1], Kenneth Marek[1], John P. Seibyl[1], Gilles D. Tamagnan[1,2], and Olivier Barret[1]

[1]*Invicro, New Haven, CT, 06510, USA;* [2]*Xingimaging, LLC, USA*

Introduction:

Synaptic vesicle protein 2A (SV2A) serves as a biomarker of synaptic density and PET imaging targeting of SV2A could provide a tool to assess progression of neurodegenerative diseases. Two tracers have primarily been reported and characterized in vivo: [^{11}C]UCB-J and [^{18}F]UCB-H. In early human studies, [^{11}C]UCB-J showed promising results by demonstrating reduced signal in Alzheimer's and Parkinson disease subjects compared to healthy volunteers, while its ^{18}F labeled analogue, [^{18}F]UCB-H showed suboptimal specific signal in comparison to [^{11}C]UCB-J. Considering the limited use of [^{11}C]UCB-J to facilities with a cyclotron, having a ^{18}F tracer would facilitate large, multicenter imaging trials. We have screened several ^{18}F derivatives of UCB-J in non-human primates to identify a promising ^{18}F PET candidate, [^{18}F]MNI-1038, with additional investigations of the active enantiomer [^{18}F]MNI-1126, affording a signal comparable to [^{11}C]UCB-J. Further in vivo studies with both tracers were aimed to characterize their kinetics and specificity for SV2A.

Methods:
[^{18}F]UCB-J, [^{18}F]UCB-H and five ^{18}F derivatives were administered in non-human primates (173 ± 44 MBq) and microPET imaging was carried out over 2-3 hours. Blood samples were taken at different time points (3, 10, 30 and 60 min) to evaluate the metabolism of the different tracers by HPLC.
Following screenings, [^{18}F]MNI-1038 was identified as the F-18 derivative with the highest signal and favorable kinetics. Two pre-block scans with Levetiracetam (LEV, 30 mg/kg, iv) were performed in 1 cynomolgus and 1 rhesus macaques. Two more baseline scans and one LEV pre-block (30 mg/kg, iv) were further carried out with the enantiomer [^{18}F]MNI-1126 (DCY~15-20%, SA ~185-370 GBq/μmol) in 2 rhesus macaques. Kinetic modeling with one- and two-tissue compartmental models was applied to PET data using metabolite-corrected arterial input function. Non-invasive graphical analysis methods with centrum semiovale as reference region have also been explored. Two whole-body PET studies were performed with MNI-1038 in one male and one female rhesus, and radiation absorbed dose estimates and effective dose (ED, ICRP-103) were estimated with OLINDA/EXM 2.0.

Results:

All compounds screened displayed very good brain penetrability with a maximum SUV of 5-8 within 10 min of injection. *rac*-[^{18}F]UCB-J showed uptake and kinetics consistent with literature reports for [^{11}C]UCB-J, but its radiosynthesis could not be reliably reproduced for further in vivo studies. [^{18}F]UCB-H *(R)*-isomer displayed higher signal compared to the racemate, as recently reported in the literature, but showed sub-optimal signal compared to [^{18}F]UCB-J. All other ^{18}F derivatives, except [^{18}F]MNI-1038 and [^{18}F]MNI-1126, showed suboptimal results, with similar or lower uptake than [^{18}F]UCB-H. All tracers showed a similar metabolism with a free fraction of ~40%. [^{18}F]MNI-1038 and [^{18}F]MNI-1126 showed uptake and distribution the most consistent with UCB-J, with V_T being highly correlated ($r>0.99$). Pre-block of [^{18}F]MNI-1038 or [^{18}F]MNI-1126 with LEV showed robust occupancy across all cortical regions, similar to that reported with [^{11}C]UCB-J (~85%). BP_{ND} values with respect to centrum semiovale of [^{18}F]MNI-1126 were higher than those reported for [^{11}C]UCB-J by

~30 to 40%. From whole-body imaging average ED of [^{18}F]MNI-1038 was estimated to be 0.033 mSv/MBq, with tracer being eliminated *via* both urinary and hepatobiliary pathways.

Conclusion:

Screening of 5 derivatives of UCB-J allowed identification of a ^{18}F labeled radiotracer ([^{18}F]MNI-1126) that exhibits improved *in vivo* characteristics to that of [^{11}C]UCB-J in non-human primates. Both tracers, [^{18}F]MNI-1126 and [^{11}C]UCB-J, have similar specificity as indicated by similar LEV occupancy at the same dose, which makes [^{18}F]MNI-1126 a promising PET radiotracer for imaging SV2A in human trials.

Figure Top: [^{18}F]MNI-1126 images (SUV 30-120 min) acquired at baseline and LEV pre-block. Left: Comparison of [^{18}F]MNI-1126 time-activity curves (baseline, LEV pre-block) and [^{11}C]UCB-J from literature (Nabulsi *et al*. 2016).

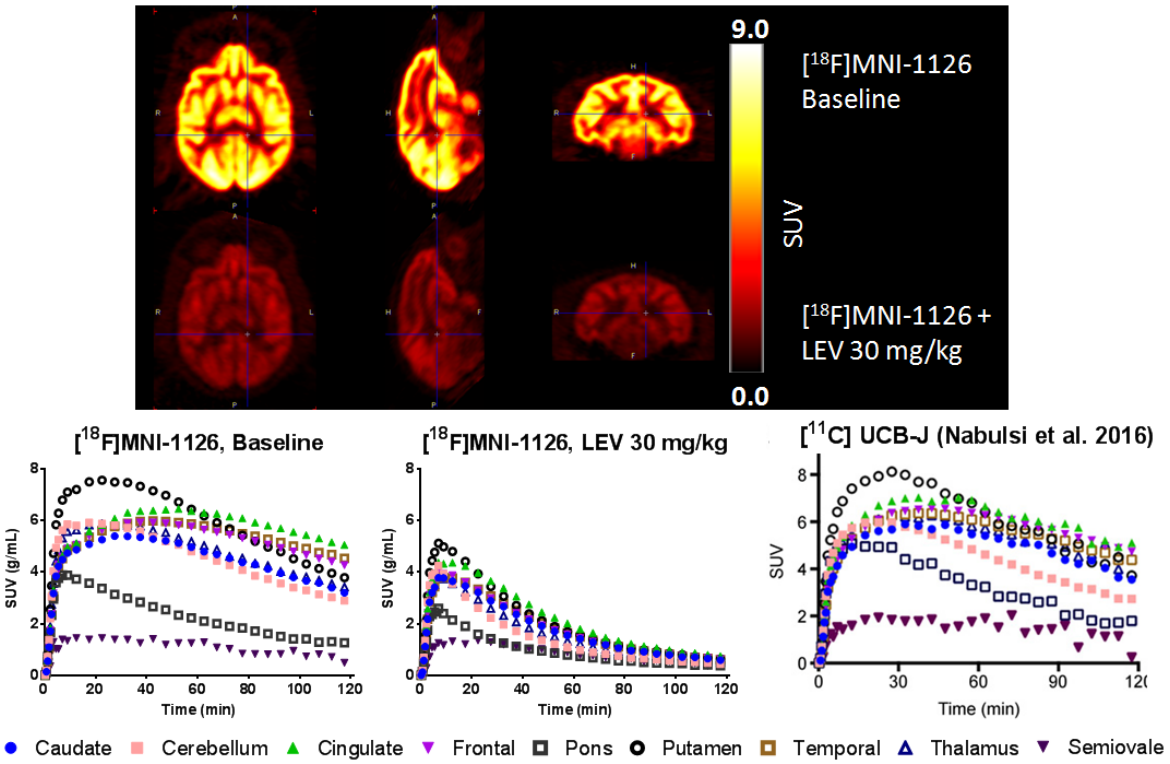

References:

1. Nabulsi NB, Mercier J, Holden D, et al. [2016], J Nucl Med, 57(5):777-84.

OP18
Discovery and translational evaluation of novel ^{18}F-labeled SV2A PET tracers in nonhuman primates

Zhengxin Cai, Songye Li, Daniel Holden, Shu-fei Lin, Anupama Shirali, Hong Gao, Paul Emery, Mike Kapinos, Jim Ropchan, Nabeel Nabulsi, Richard E. Carson, Yiyun Huang

PET Center, Department of Radiology and Biomedical Imaging, Yale University, New Haven, CT, USA

Introduction:
Synaptic abnormality is believed to be associated with a variety of neurologic and psychiatric disorders such as Alzheimer's disease, epilepsy, Parkinson's disease, autism, stroke, traumatic brain injury, schizophrenia, and depression. *In vivo* PET imaging of synaptic density may provide pathophysiological information unattainable through other approaches. We have validated imaging of synaptic vesicle glycoprotein 2A (SV2A) with ^{11}C-UCB-J as a method for *in vivo* measurement of synaptic density [1, 2]. To enable facile clinical translation and multicenter trials to validate SV2A PET imaging for the diagnosis of neuropsychiatric diseases and monitoring of treatment efficacy for disease-modifying therapies targeted at synaptic repair and recovery, we developed a series of ^{18}F-labeled SV2A radiotracers and assessed their pharmacokinetic and imaging characteristics in nonhuman primates. Herein, we report the synthesis and evaluation of two such novel radiotracers.

Materials & Methods:
The SV2A ligands and their ^{18}F-fluorination precursors were synthesized from commercially available starting materials in 4 or 5 steps. Enantiomerically pure compounds were obtained through chiral HPLC separation. Binding affinities were measured via radioligand competition assays using rat brain homogenates. The precursors were radiolabeled with ^{18}F-fluoride at 100-150 °C for 10-20 min. The enantiopure tracers were evaluated in rhesus monkeys. Brain PET imaging was performed on the FOCUS 220 scanner for 120-180 min. Levetiracetam (30 mg/kg, *i.v.*) was used in displacement experiments to determine binding specificity of the new tracers. Arterial blood was taken for metabolite analysis and measurement of arterial input functions (AIF). Regional brain time-activity curves (TACs) data was analyzed with one-tissue (1T), two-tissue (2T) compartment models, and by multilinear analysis-1 (MA1) method to obtain regional volumes of distribution (V_T). Regional binding potential (BP_{ND}) values were estimated using white matter as the reference region for comparison with those of ^{11}C-UCB-J.

Results:
The novel SV2A ligands SDM-7 and SDM-8 and their corresponding radiolabeling precursors were synthesized in good yields. Binding assays demonstrated higher affinities for the (*R*)-enantiomers with K_i of 2.1 and 0.6 nM, respectively, for (*R*)-SDM-7 and (*R*)-SDM-8, compared with K_i of 0.27 nM for UCB-J. The radiotracers (*R*)-^{18}F-SDM-7 and (*R*)-^{18}F-SDM-8 were prepared in >98% radiochemical purity, and >99% enantiomeric purity. In rhesus monkeys, both tracers showed similar rate and pattern of metabolism, with all radioactive metabolites more polar than the parent tracers. Plasma free fractions were 37% and 42% for (*R*)-^{18}F-SDM-7 and (*R*)-^{18}F-SDM-8, respectively. The tracers displayed high brain uptake with peak SUV of 6-9 (**Figure 1**). Displacement with levetiracetam reduced the regional uptake of (*R*)-^{18}F-SDM-7 and (*R*)-^{18}F-SDM-8 to background levels, confirming their *in vivo* binding specificity. Kinetics was faster or similar to that of ^{11}C-UCB-J, with brain-to-AIF ratios plateauing at ~20 min for (*R*)-^{18}F-SDM-7, and ~50 min for (*R*)-^{18}F-SDM-8 (and ^{11}C-UCB-J). Both 1T and MA1 models produced good fits of regional TACs and reliable V_T estimates. Compared with ^{11}C-UCB-J, regional BP_{ND} values were higher for (*R*)-^{18}F-SDM-8, and slightly lower for (*R*)-^{18}F-SDM-7 (**Table 1**).

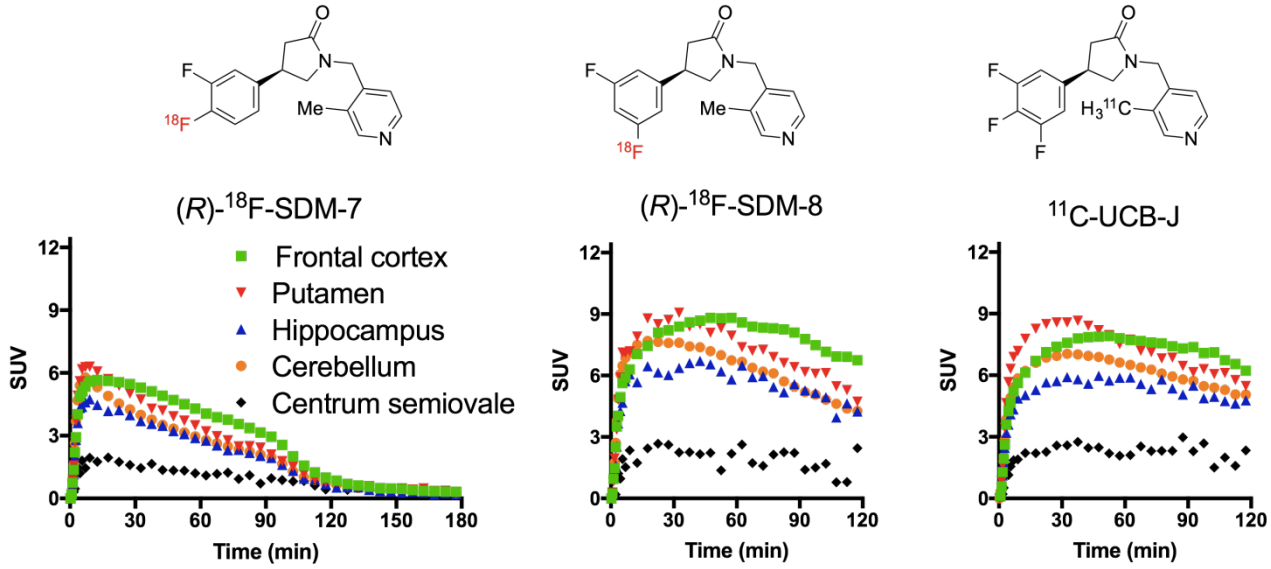

Figure 1. TACs for (*R*)-^{18}F-SDM-7, (*R*)-^{18}F-SDM-8, and ^{11}C-UCB-J in selected brain regions of the same rhesus monkey. Levetiracetam (30 mg/kg, *i.v.*) was infused at 90 min for the scan with (*R*)-^{18}F-SDM-7.

Table 1. Regional BP_{ND} values* for (*R*)-^{18}F-SDM-7, (*R*)-^{18}F-SDM-8, and ^{11}C-UCB-J.

	(*R*)-^{18}F-SDM-7 (n = 1)	(*R*)-^{18}F-SDM-8 (n = 2)	^{11}C-UCB-J (n = 6)
Cingulate cortex	2.60	4.49	3.17
Frontal cortex	2.51	4.26	3.18
Insular cortex	2.41	4.16	3.12
Occipital cortex	2.30	3.75	2.97
Temporal cortex	2.21	3.60	2.79
Putamen	1.86	3.03	2.42
Thalamus	1.65	3.08	2.03
Hippocampus	1.35	2.36	1.59
Pons	0.73	0.80	0.75

*Values are either single measurement or the average of n measurements.

Conclusions:

We have successfully synthesized and evaluated a number of novel ^{18}F-labeled SV2A radiotracers in nonhuman primates. Among these tracers, (*R*)-^{18}F-SDM-7 and (*R*)-^{18}F-SDM-8 possess attractive imaging properties, with high brain uptake, fast tissue kinetics, and high specific binding in brain. Comprehensive characterizations of these novel SV2A PET tracers are underway for advancement to first-in-human studies.

Acknowledgements:

The authors would like to thank the Yale PET Center staff for their expert technical assistance, the internal funding from Yale, and funding from NIH/NIBIB K01EB023312.

References: **[**1]. Finnema JF et. al. [2016] Sci Transl. Med. **8**:348. [2]. Nabulsi NB et. al. [2016] J. Nucl. Med. **57**:777.

OP19
Quantifying SV2A density and drug occupancy in the human brain using ^{11}C-UCB-J PET imaging and white matter as reference tissue

Michel Koole[1], June van Aalst[1], Martijn Devrome[1], Nathalie Mertens[1], Kim Serdons[1], Brigitte Lacroix[2], Joel Mercier[2], David Sciberras[2], Paul Maguire[2], Koen Van Laere[1]

[1]*Department of Nuclear Medicine and Molecular Imaging, KU Leuven, Leuven, Belgium*
[2] *UCB Pharma S.A., Braine-l'Alleud, Belgium*

Introduction:
Synaptic pathology is associated with many neurological and psychiatric disorders. ^{11}C-UCB-J was developed as a Positron Emission Tomography PET ligand specific for quantifying presynaptic SV2A expression in vivo. As such, ^{11}C-UCB-J binding is also considered as an excellent proxy of synaptic density. We performed a ^{11}C-UCB-J displacement study in human volunteers to determine the most suitable compartmental model for ^{11}C-UCB-J quantification in the human brain and to validate simplified, non-invasive measures using white matter as a reference tissue.

Materials and Methods:
^{11}C-UCB-J PET was performed in 10 healthy volunteers (8M/2F; mean age 27.6 yrs), before and after administration of a novel chemical entity with selective affinity for presynaptic SV2A. A ninety-minute dynamic PET with full arterial blood sampling was performed, to determine the optimal kinetic model for regional tissue distribution volume (V_T) and SV2A occupancy using a Lassen plot. The centrum semi-ovale (SO) was evaluated as a potential reference region by comparing baseline and post-drug V_T. Binding Potential (BP_{ND}) using a Simplified Reference Tissue Model (SRTM2, a two-step method using a fixed value of k'_2) for 90 min. and reduced acquisition times, and Standardized Uptake Value Ratios between 60 to 90-min. acquisition ($SUVR_{60\text{-}90min}$), were compared with V_T ratios (DVR). Time-stability of the kinetic parameters was established down to 60 min.

Results:
A 1-Tissue Compartmental Model (1TCM) was confirmed as the most appropriate model for ^{11}C-UCB-J kinetics in the human brain. After drug pre-treatment, regional 1TCM V_T was reduced significantly except for SO (Fig 1). Occupancy estimates (range 10-100%) with SO as the reference region, were not significantly different from estimates with a Lassen plot (1.9 ± 2.8% bias, Fig 2). Highly significant correlations were present between 1TCM DVR-1, SRTM2 BP_{ND} and $SUVR_{60\text{-}90min}$-1 with SO as the reference region. Baseline SRTM2 BP_{ND} and 1TCM DVR-1 showed a small bias (≤ 6.1%) with lower precision for shorter acquisition times, while $SUVR_{60\text{-}90min}$-1 showed 3.5% bias with similar precision (Fig 3). Differences between occupancy values based on $SUVR_{60\text{-}90min}$-1 and occupancy estimates using 1TCM V_T and a Lassen plot were small (Table1), while negligible bias was found for SRTM2 based occupancy estimates (at least 70-min. acquisition time).

Conclusion:
Dynamic ^{11}C-UCB-J human brain PET imaging was performed with varying doses of novel chemical entity with selective affinity for presynaptic SV2A. Findings showed that SO is a suitable reference region for the quantification of SV2A availability and drug occupancy in the human brain. Accurate quantification is achieved by SRTM2 with at least 70-min. data but also with $SUVR_{60\text{-}90min}$.
STUDY SUPPORTED BY: UCB Pharma

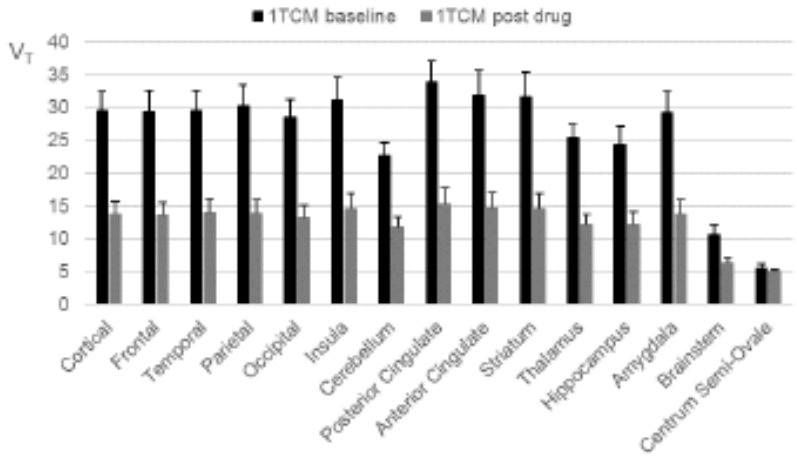

Fig1: Mean baseline and post drug 1TCM V_T values (SD as error bar, n=5). Post drug scans correspond to a mean occupancy level of 61.1 ± 2.9% (mean ± SD).

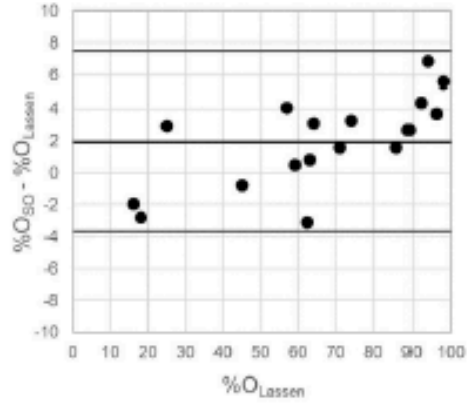

Fig2: A Bland Altman comparison between SO based occupancy estimates O_{SO} and 1TCM V_T based occupancy estimates O_{Lassen} using a Lassen plot.

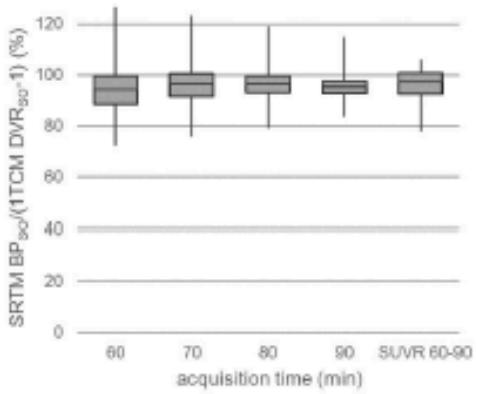

Fig3: A box plot of the ratio of baseline SRTM2 $BP_{SO,x}$ and $SUVR_{SO,60-90min} - 1$ values relative to baseline 1TCM $DVR_{SO} - 1$ values for the different acquisition time intervals.

	SUVR-1 (60-90min)	SRTM2 BP_{SO} 90 min	SRTM2 BP_{SO} 80 min	SRTM2 BP_{SO} 70 min	SRTM2 BP_{SO} 60 min
Bias (%)	3.5	-1.2	-0.6	-0.6	3.7
SD of bias (%)	6.5	5.3	5.9	6.3	13.0
95% limits of agreement (%)	[-9.7,15.6]	[-11.6,9.2]	[-12.2,11.0]	[-13.0,11.8]	[-21.8,29.3]

Table1: Bland Altman comparison of occupancy values based on SUVR-1 using a 60- to 90-min. acquisition time interval after tracer injection and SRTM2 BP_{SO} for a 90-, 80-, 70- and 60-min. acquisition time interval starting at tracer injection respectively with 1TCM V_T occupancy values using a Lassen plot (% difference vs mean). All but the latter approach use SO as brain reference tissue.

OP20
Imaging nociceptin receptors in cocaine use disorders with [^{11}C]NOP-1A and PET

Rajesh Narendran, Savannah Tollefson, Michael Himes, Brian Lopresti and N. Scott Mason
Department of Radiology, University of Pittsburgh, Pittsburgh, USA

Introduction:
No previous PET studies have characterized neuropeptides in the brain stress (e.g., corticotrophin releasing factor, CRF) and anti-stress systems (e.g., nociception and neuropeptide Y) that underlie negative reinforcement and relapse in human addicts (1). Nociceptin, which binds to the nociceptin/orphanin FQ peptide (NOP) receptor, is one such neuropeptide transmitter that exerts anti-stress effects by counteracting the functional effects of endogenous CRF in the brain. Basic investigations are mixed in supporting a role for both NOP agonists and antagonists in the treatment of addictive disorders. Thus, clarification of the in vivo status of NOP receptors in human addicts and linking it to relapse has the potential to inform NOP medication development. Here, we capitalize on the validation of [^{11}C]NOP-1A as a selective NOP receptor PET radiotracer (2) to report on the in vivo status of NOP receptors in cocaine use disorders (CUD).

Materials and Methods:
[^{11}C]NOP-1A and PET was used to measure the in vivo binding to NOP receptors in 17 individuals with CUD and 16 healthy controls (HC) matched for age and gender. CUD with no comorbid psychiatric, medical, or drug and alcohol use disorders were scanned following 10-14 days of outpatient monitored abstinence (3x/week urine drug screens). [^{11}C]NOP-1A distribution volume (V_T) in regions of interest including the amygdala, hippocampus, midbrain, cerebellum, striatal (ventral striatum, caudate and putamen), and prefrontal cortical (anterior cingulate, dorsolateral, orbitofrontal, and medial prefrontal cortex) subdivisions were measured with kinetic analysis using the arterial input function. To document relapse, CUD subjects were followed for 12-weeks after the PET scan using contingency management in which they were paid money to remain abstinent.

Results:
The CUD included 8 female and 12 smokers (n=17). The HC group included 9 females and 6 smokers (n=16). The mean age of CUD and HC were 41 $\pm$ 8 and 40 $\pm$ 8 years old. CUD self-reported spending \$106 $\pm$ 75/week on cocaine for the past 15 $\pm$ 8 years. There were no significant differences in [^{11}C]NOP-1A injected dose between CUD (12.4 $\pm$ 0.6 mCi) and HC (12.3 $\pm$ 0.8 mCi). There was a trend level difference in injected mass between the groups (CUD 2.9 $\pm$ 1.1 μg; HC 2.2 $\pm$ 0.8 μg, p =0.052). No differences were noted in plasma free fraction (fp).
[^{11}C]NOP-1A V_T was higher in CUD compared to HC (linear mixed model, diagnosis, p = 0.043; region, p < 0.001, diagnosis*region, p = 0.21). Unpaired t tests in the individual regions showed a higher V_T in CUD in six out of eleven regions of interest that were examined including the hippocampus, midbrain, ventral striatum, putamen, anterior cingulate cortex and cerebellum (p < 0.05, not corrected for testing multiple regions). The remaining regions except for the caudate were at trend level (p < 0.1). No relationship between [^{11}C]NOP-1A V_T and other clinical measures (including duration and severity of cocaine abuse, craving, stress and anxiety) were significant. Of the subjects enrolled in the 12-week follow-up phase, n=4 subjects did not relapse, n=7 relapsed, and n=6 were lost during follow-up. No differences in baseline [^{11}C]NOP-1A V_T were observed between these three groups (LMM, relapse status, p =0.96). A Cox proportional hazards analysis used to determine the association between time to relapse and [^{11}C]NOP-1A V_T in ROIs in the CUD group was also not significant. This might have been due to relatively small number of

subjects who had a documented relapse. Data acquisition is continuing which will allow for an updated analysis at the conference.

Discussion:
CUD subjects compared to HC demonstrated an increase in [^{11}C]NOP-1A V_T in the regions examined. An upregulation of NOP receptors is consistent with basic investigations that suggest lower nociceptin levels in animal models of addiction. It may also be suggestive of a compensatory adaptation in the brain anti-stress system to counteract increased CRF transmission. Finally, increases in NOP in CUD is inconsistent with the lack of alterations in NOP reported recently in alcohol dependence (3). The relatively small increase in NOP V_T (~10%), lack of regional selectivity (e.g., amygdala), and failure to predict relapse are concerns that somewhat diminish this finding.

Acknowledgements: National Institute on Drug Abuse

References:
1. Tollefson S, Himes M, Narendran R (2017): Imaging corticotropin-releasing-factor and nociceptin in addiction and PTSD models. *Int Rev Psychiatry*. 29:567-579.
2. Pike VW, Rash KS, Chen Z, Pedregal C, Statnick MA, Kimura Y, et al. (2011): Synthesis and evaluation of radioligands for imaging brain nociceptin/orphanin FQ peptide (NOP) receptors with positron emission tomography. *J Med Chem*. 54:2687-2700.
3. Narendran R, Ciccocioppo R, Lopresti B, Paris J, Himes ML, Mason NS (2017): Nociceptin Receptors in Alcohol Use Disorders: A Positron Emission Tomography Study Using [11C]NOP-1A. *Biol Psychiatry*.

OP21
Sex Differences in Dorsolateral Prefrontal Cortical Amphetamine-Induced Dopamine Release in Tobacco Smokers

Yasmin Zakiniaeiz[1], Ansel T. Hillmer[2], Patrick D. Worhunsky[3], Jean-Dominique Gallezot[2], David Matuskey[2,3], Nabeel Nabulsi[2], Yiyun Huang[2], Jim Ropchan[2], Sherry McKee[3], Evan D. Morris[1,2,3,4], Kelly P. Cosgrove[1,2,3]

[1]*Interdepartmental Neuroscience Program, Yale University, New Haven, CT*
[2]*Yale Positron Emission Tomography (PET) Center, Yale University, New Haven, CT*
[3]*Department of Psychiatry, Yale University, New Haven, CT*
[4]*Department of Biomedical Engineering, Yale University, New Haven, CT*

Introduction:
The behavioral and molecular mechanisms underlying tobacco smoking vary by sex. Men tend to smoke for the reinforcing effects of nicotine and women tend to smoke to regulate stress and mood.[1,2] The mesolimbic dopamine (DA) system drives the reinforcing effects of tobacco smoking, whereas the mesocortical DA system—including the dorsolateral prefrontal cortex (dlPFC)—is critical for inhibitory control and working memory function, both compromised by stress. The goals of this study were to investigate sex differences in dlPFC DA D_2 receptor (D_2R) availability and amphetamine-induced cortical DA release in tobacco smokers and nonsmokers.

Methods:
Twenty-four tobacco smokers (12 females) and 25 sex- and age-matched nonsmokers participated in two [^{11}C]FLB457 positron emission tomography (PET) scans on the same day before and 3 hours after amphetamine administration (0.4-0.5mg/kg, PO). Same-day scans did not differ in injected activity (349.48±45.14 MBq baseline, 325.51±72.81 MBq post-amphetamine, p=0.145), injected mass (0.40±0.15 µg baseline, 0.46±0.14 µg post-amphetamine, p=0.092), or injected mass per bodyweight (0.01±0.0003 µg/kg baseline, 0.01±0.0003 µg/kg post-amphetamine, p=0.722). Smokers abstained from smoking overnight. Male (MS) and female smokers (FS) were matched for age (MS: 35±3, FS: 33±3, p=0.52), cigarettes smoked per day (MS: 13.6±1.5, FS: 12.8±1.5, p=0.70), and years of smoking (MS: 16.1±1.9, FS: 13.5±2.0, p=0.36). PET data were analyzed with SRTM using cerebellum as the reference region[2] to measure non-displaceable binding potential (BP_{ND}) in dlPFC. The percent fractional change in BP_{ND} (%ΔBP_{ND}) before and after amphetamine, an index of DA release, was calculated as %ΔBP_{ND} = (1–$BP_{ND(Amphetamine)}$/$BP_{ND(Baseline)}$)*100. Baseline BP_{ND} and %ΔBP_{ND} in the dlPFC were compared between smokers and nonsmokers and between MS and FS. BP_{ND} was estimated regionally (using the AAL template), and at the voxel level (using SPM) (FWE corrected at p<0.05). Subject-level BP_{ND} values were extracted and averaged from significant clusters in SPM.

Results:
At baseline, dlPFC D_2R availability was significantly lower in smokers (BP_{ND}=0.77±0.05) than nonsmokers (BP_{ND}=0.92±0.04), p=0.016, as shown using regional (Figure 1a; left) and voxel-wise t-tests (1a; right) analyses. All females had significantly less amphetamine-induced DA release in dlPFC (%ΔBP_{ND}=5.64±2.31%) than all males (%ΔBP_{ND}=12.5±2.40%), p=0.042, as shown using regional (Figure 1b; left) and voxel-wise t-tests (1b; right) analyses. Exploratory voxel-wise analysis identified an interaction of sex and smoking status on dlPFC %ΔBP_{ND} (Figure 1c; left, F-values of interaction shown) and averaged %ΔBP_{ND} values within the clusters plotted per group (1c; right) (FNS: female nonsmokers, MNS: male nonsmokers). Female smokers had significantly less amphetamine-induced DA release in dlPFC (%ΔBP_{ND}=1.95±2.96%) than male smokers

(%ΔBP_{ND}=14.0±4.35%), p=0.033, as shown using regional (Figure 1d; left) and voxel-wise t-tests (1d; right) analyses (B: baseline, A: post-amphetamine).

Discussion/Conclusions:

Previous literature has identified patterns of lower striatal D_2R availability in tobacco smokers[4] and other substance-abuse populations compared to controls.[5-7] This study is the first to show that tobacco-smokers have lower cortical D_2R availability than nonsmokers using regional and voxel-based analyses. This study is the first to identify sex differences in amphetamine-induced cortical DA release. Female smokers had lower amphetamine-induced DA release compared to male smokers, while female nonsmokers and male nonsmokers were not different from each other. These findings demonstrate that the cortical DA system is differentially affected in male and female tobacco smokers, suggesting an underlying neurochemical mechanism for the reported sex differences in behavior.

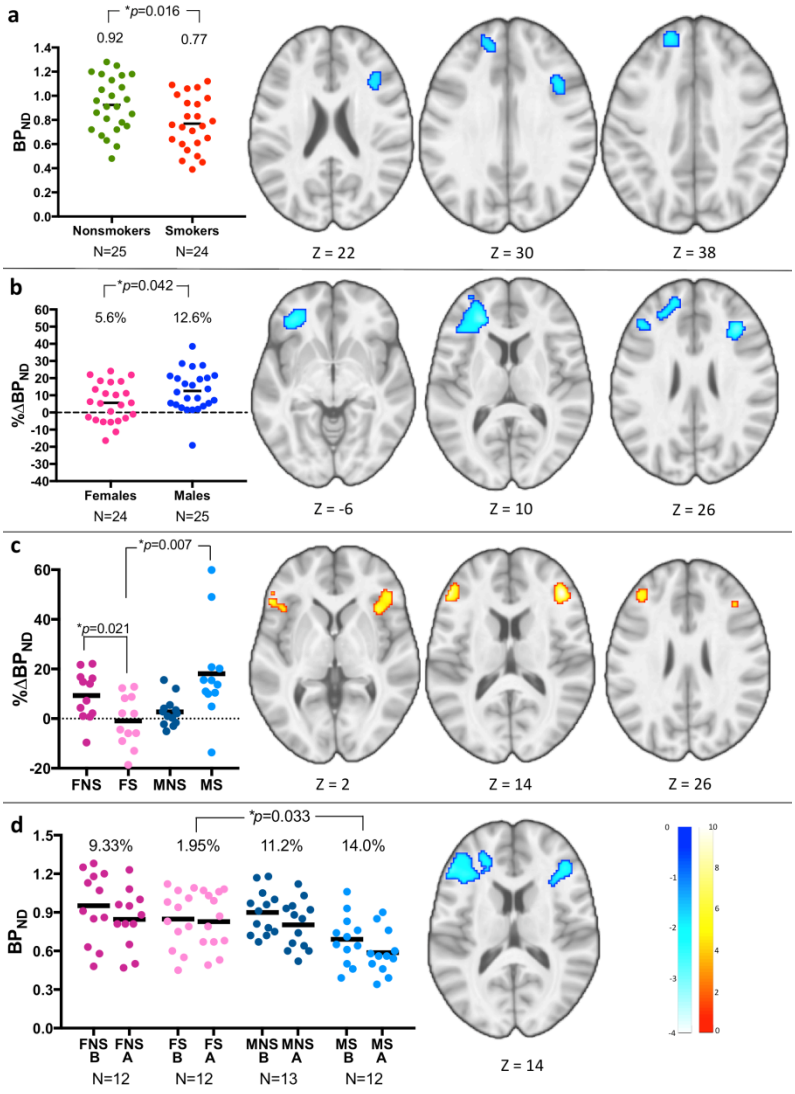

Acknowledgments: Research support provided by P50DA033945 (McKee), K02 DA03175 (Cosgrove), K01 AA024788 (Hillmer), T32NS4122813, Gruber Science Fellowship, and NSF-GRFP (Zakiniaeiz).

References:

1. Perkins, KA [2009] Nebr Symp Motiv 55: 143
2. Cosgrove KP, Wang S, et al. [2014], J Neurosci, 34(50):16851.
3. Sandiego et al. [2015], JCBF&M. 35:623.
4. Fehr C et al. [2008] Am J Psychiatry, 165:507-514.
5. Martinez D et al. [2005]. Biol Psychiatry. 58:779.
6. Volkow ND et al. [2001], Am J Psychiatry. 158:2015.
7. Martinez D et al. [2004], Neuropsychopharm. 29:1190.

OP22

Positron Emission Tomography Study with [^{18}F]PF-05270430 to Determine Phosphodiesterase 2A Brain Enzyme Occupancy of TAK-915 in Healthy Human Subjects and Rhesus Macaques

Cristian C Constantinescu, PhD[1]; Patricia E Cole, PhD, MD[2]; Tolga Uz, MD, PhD[3]; Hiroki Iwashita, PhD[4],Terry Brown, CNMT [4]; Thomas Morley, PhD [1]; Caroline Papin, PhD [1]; David Alagille, PhD [1]; Danna Jennings, MD [5]; David Russell, MD [1]; Gilles Tamagnan, PhD[1]; John Seibyl, MD [1,6]; John Wagner, MD, PhD[4]; Kenneth Marek, MD [1,6]; Olivier Barret, PhD[1]; Johannes Tauscher, MD [4]

[1]Invicro, New Haven, CT, USA, [2]Bayer Pharmaceuticals, Whippany, NJ, USA, [3]Astellas Pharma Global Development, Inc., Northbrook, IL; [4]Takeda Pharmaceuticals, Inc., Cambridge, MA, USA, [5]Eli Lily and Company, Indianapolis, IN, USA, [6]Institute for Neurodegenerative Disorders, New Haven, CT, USA

Introduction:
Phosphodiasterase 2A (PDE2A), a dual specificity enzyme for second messengers cAMP and cGMP, is a potential target of interest for therapeutics seeking to alter and improve synaptic plasticity and memory functions. We have conducted a series of PET imaging studies in rhesus macaques and human volunteers with the PDE2A radiotracer [^{18}F]PF-05270430 (also known as [^{18}F]MNI-794) to determine brain penetration as well as the degree and duration of PDE2A target engagement of TAK-915, a PDE2A inhibitor intended for adjunct therapy for cognitive deficits and negative symptoms which are present in virtually all subjects with schizophrenia.

Methods:
Preclinical studies were first conducted in two rhesus macaques, with each receiving four 120 min dynamic PET scans with [^{18}F]PF-05270430 (178 ± 7 MBq, microPET Focus 220), two at baseline (test/retest) and two pre-blocking with TAK-915. TAK-915 was administered as 5 min iv bolus starting 30 min before tracer injection, at two dose levels, low (0.53 and 0.51 mg/kg) and high (1.34 and 1.57 mg/kg), respectively. Plasma samples were collected following TAK-915 and throughout imaging for pharmacokinetic measurements.
An open-label, non-randomized clinical study was conducted in 12 healthy human subjects. TAK-915 was administered as a single oral dose of 30, 75, 100, or 200 mg. Each subject received either two, or three 90-min dynamic brain imaging scans with [^{18}F]PF-05270430 (163 ± 14 MBq, ECAT HR+) at baseline, and at either one (~5h) or two (~4-5h and ~28-29h) time points following administration of TAK-915.
PET data were modeled with non-invasive Logan graphical analysis (NI-LGA) with cerebellar cortex as reference region to estimate [^{18}F]PF-05270430 binding potential, BP_{ND}. Based on BP_{ND} values at baseline and post TAK-915 occupancy was calculated in striatum (putamen, caudate, and nucleus accumbens) and pallidum, regions with highest PDE2A density. Occupancy was modeled against the plasma TAK-915 with a one-site specific binding model.

Results:
In primates TAK-915 showed brain penetration and successful target engagement with dose dependent average striatal PDE2A occupancies of 57% - 84%. TAK-915 plasma and dose-occupancy modeling resulted in ED_{50} and EC_{50} values of 0.32 ± 0.04 mg/kg and 64.53 ± 6.36 ng/mL, respectively.
In human volunteers, blockade of [^{18}F]PF-05270430 by TAK-915 was observed at all doses tested, indicating that TAK-915 binds specifically to the PDE2A enzyme in the brain. At both imaging time points the PDE2A occupancy increased with the TAK-915 dose, but plateaued at ~ 70-80% in the caudate nucleus and nucleus accumbens, and to ~ 60% in putamen and pallidum for doses of 100 and 200 mg. An occupancy of at least 50% was consistently

reached at 75 mg TAK-915 dose. TAK-915 and imaging conditions were well tolerated by the participants in the study, with no significant adverse effects.

Conclusion:
TAK-915 showed brain penetration and PDE2A target engagement in both macaques and human volunteers. In humans, the TAK-915 effects were long lasting, with occupancy levels maintained up to 28-29h post dosing. The results of our studies demonstrated that TAK-915 is a brain-penetrant PDE2A inhibitor that can be used for further clinical studies.

Figure: Right: Baseline (top), 4h (middle) and 28h (bottom) post 30 mg TAK-915 oral dose demonstrating striatal occupancy. Left: %Occupancy (mean and SD) at the 2 time points following administration of TAK-915 as a function of TAK-915 dose for putamen, and caudate nucleus.

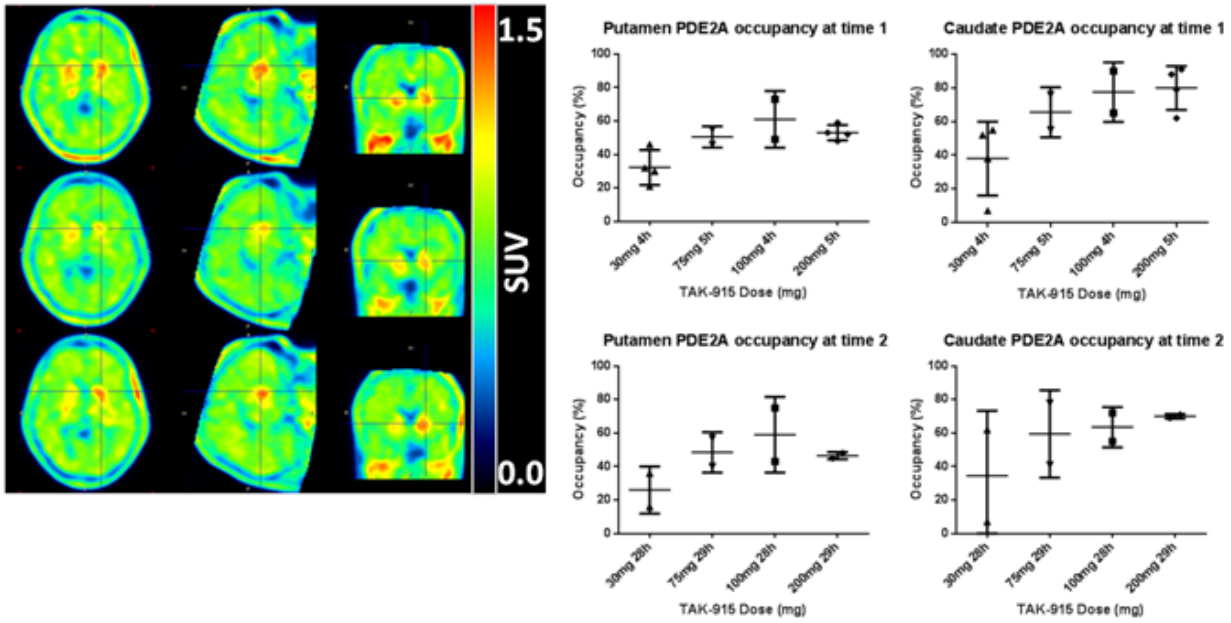

References

1. Boess FG, Hendrix M, van der Staay FJ, et al. [2004], Neuropharmacology, 47(7):1081-92.
2. Stephenson DT, Coskran TM, Wilhelms MB et al. [2009], J Histochem Cytochem., 57(10):933-949.
3. Naganawa M, Waterhouse RN, Nabulsi N et al. [2016], J Nucl Med., 57(9):1388-1395.
4. Chen L, Nabulsi N, Naganawa M et al. [2016], J Nucl Med., 57(9):1448-1453.

OP23
An initial investigation of dissociable dopamine-serotonin subsystems in cocaine use disorder using [^{11}C](+)PHNO and [^{11}C]P943

Patrick D. Worhunsky[1], David Matuskey[1], Gustavo A. Angarita[1], Vince D. Calhoun[2], Marc N. Potenza[1], Richard E. Carson[1], Robert T. Malison[1]
[1]Yale University, New Haven, CT, USA; [2]University of New Mexico, Albuquerque, NM, USA

Introduction:
Dopamine and serotonin systems, including D_2/D_3 and 5-HT_{1B} receptors, have been implicated in addiction. Cocaine-use disorder (CUD) has been associated with lower D_2R [1,2], greater D_3R [2,3], and lower 5-HT_{1B} availability[4]. These alterations have been associated with years of cocaine use, suggesting potentially concurrent and complementary neuroadaptations across the two neuroreceptor systems. The current study explored the relationships between regional D_2/D_3 and 5-HT_{1B} receptor availability in individuals with CUD using general linear models and joint independent component analysis (jICA). jICA is a data-driven, multivariate computational procedure that can be used to identify common sources of subject-related modulation across imaging modalities[5].

Materials & Methods:
Ten individuals with CUD (age: 40.7 ± 7.4; 3 female; 17.9 ± 8.1 years of cocaine use) completed [^{11}C](+)PHNO and [^{11}C]P943 positron emission tomography (PET) scans to assess D_2/D_3 and 5-HT_{1B} receptor availability respectively. Seven participants completed both scans on the same day, 3 participants completed scans 44, 56, and 198 days apart. Parametric images of [^{11}C](+)PHNO binding potential (BP_{ND}) were computed using a simple reference tissue model (SRTM2) with the cerebellum as reference. Parametric images of [^{11}C]P943 BP_{ND} were computed using a multilinear reference tissue model (MRTM2) with the cerebellum as reference. Images were registered into 2mm^3 standard space using the Computational Anatomy Toolbox (CAT12) for SPM12 (Wellcome Trust Centre for Neuroimaging) using high-resolution T1 MR images of each subject. Registered [^{11}C](+)PHNO BP_{ND} and [^{11}C]P943 BP_{ND} images were smoothed with 4mm and 10mm FWHM Gaussian kernels respectively, due to different spatial characteristics of the two radiotracers. For general linear analysis, average [^{11}C](+)PHNO BP_{ND} values in the D_2-rich dorsal putamen and D_3-rich substantia nigra were computed using previously defined regional masks[2], and included in a multiple regression model to investigate associations with whole-brain [^{11}C]P943 BP_{ND} at an uncorrected voxel-wise threshold of P<0.01 with an uncorrected cluster-level threshold of P<0.05 (>328 contiguous voxels). jICA was performed using the Fusion ICA Toolbox (FIT; http://mialab.mrn.org/software/fit) to identify 3 joint components (JC) from the parametric images of both radiotracers through averaging 20 iterated extractions using Infomax. Source maps for each JC for each radiotracer were scaled to jICA-estimated binding potential ($\widetilde{BP}$), and thresholded at $\widetilde{BP}$>0.5 to identify regions integrated into each JC source.

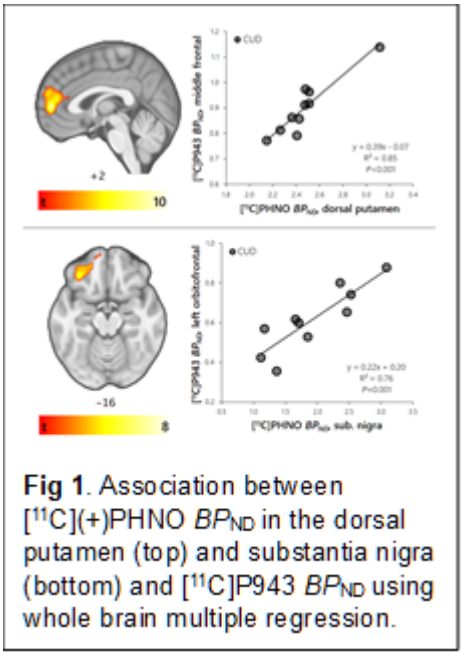

Fig 1. Association between [^{11}C](+)PHNO BP_{ND} in the dorsal putamen (top) and substantia nigra (bottom) and [^{11}C]P943 BP_{ND} using whole brain multiple regression.

Results:
Using multiple regression models, D_2-related [^{11}C](+)PHNO BP_{ND} in the dorsal putamen was associated with [^{11}C]P943 BP_{ND} in the medial prefrontal cortex (Fig. 1; top). By comparison, D_3-related [^{11}C](+)PHNO BP_{ND} in the substantia nigra was associated with [^{11}C]P943 BP_{ND} in the left orbitofrontal cortex (Fig. 1; bottom). Source maps and subject-loading

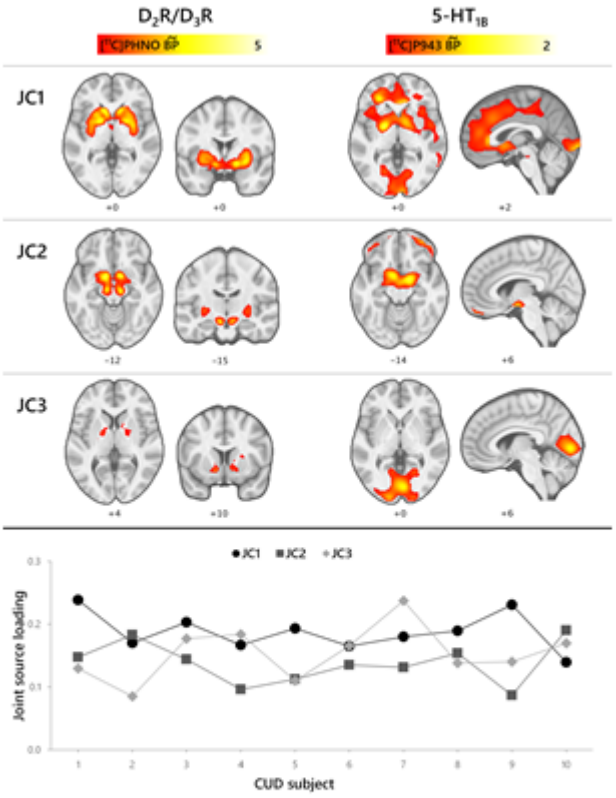

Fig 2. jICA identified source maps (top) and subject loadings (bottom) of joint components of [^{11}C](+)PHNO and [^{11}C]P943 BP_{ND}.

of the 3 JCs identified by jICA are shown in Fig. 2. JC1 involved covariation of [^{11}C](+)PHNO BP_{ND} in D_2-rich regions with [^{11}C]P943 BP_{ND} in striatal, prefrontal, and occipital regions. By comparison, JC2 involved covariation of [^{11}C](+)PHNO BP_{ND} in D_3-rich regions with [^{11}C]P943 BP_{ND} in ventral basal ganglia, amygdala, and lateral orbitofrontal regions. JC3 involved covariation of [^{11}C](+)PHNO BP_{ND} in pallidal regions with [^{11}C]P943 BP_{ND} in the occipital cortex. JC1 loading was correlated with [^{11}C](+)PHNO BP_{ND} in the dorsal putamen (r=0.81, P=0.005), and JC2 loading was correlated with [^{11}C](+)PHNO BP_{ND} in the substantia nigra (r=0.91, P<0.001). A correlation between JC2 loading and years of cocaine use trended toward, but did not reach significance (r=0.57, P=0.08).

Discussion/Conclusion:

This study represents an initial exploration of dissociable subsystems in the relationship between D_2/D_3 and 5-HT_{1B} receptor alterations in humans with CUD. Results suggest that established reductions in D_2-receptor availability in CUD may be associated with complementary reductions in 5-HT_{1B} availability, particularly in prefrontal and striatal regions. By comparison, increases in D_3-receptor availability in CUD may be associated complementary increases in 5-HT_{1B} availability in ventral basal structures and lateral orbitofrontal regions. Functionally, circuitry encompassing these two systems (1: dorsal striatal dopamine and prefrontal serotonin; and 2: midbrain/ventral striatal dopamine and orbitofrontal serotonin) have been proposed to represent distinct cognitive and reward-related mechanisms related to addiction respectively. The current results support these models of dissociable dopamine-serotonin subsystems and warrant further study to examine the specificity of these findings for CUD through direct comparison with healthy control and non-addicted individuals, and to explore associations with hypothesized pathophysiology.

Acknowledgements:

Research support provided by K01-DA042998, K12-DA000167, P20-DA027844, R03-DA027456, R01-DA039136, P20-GM103472, R01-EB005846, CT-DMHAS, and UL1-TR000142

References:

1. Volkow N, et al. [1997], Nature, 386:830-833. **2.** Worhunsky PD, et al. [2017], Neuroimage, 148:343-351. **3.** Payer DE, et al. [2014], Neuropsychopharmacology, 39:321-28. **4.** Matuskey D, et al. [2014], Bio. Psychiatry, 76:816–822. **5.** Calhoun VD, et al. [2006], Hum. Brain Mapp., 27:598–610.

OP24
Cannabinoid Receptor Availability Regionally Modulates the Magnitude of Dopamine Release *in vivo*

Jenny Ceccarini[1], Michel Koole[1], Koen Van Laere[1]
Department of Nuclear Medicine and Molecular Imaging, University Hospital Leuven, KU Leuven, Belgium

Introduction:
The type 1 cannabinoid receptor (CB_1R) is among the most abundant G-protein coupled receptors in the human brain, predominantly located presynaptically and highly concentrated in the hippocampus, amygdala, basal ganglia, and prefrontal cortex. CB_1R activation modulates synaptic release of major neurotransmitter systems such as glutamate, GABA, and also indirectly modulates dopamine (DA) transmission[1]. Thus, CB_1R pathways may have an important influence on various DA-related neurobiological processes and on the neurobiology of disorders affected by these processes, such as drug addiction and schizophrenia[2]. Despite preclinical evidence for a number of functional CB_1R-DA interactions, the relation between *in vivo* human CB_1R availability and DA release capacity has not been investigated so far.

Materials and Methods:
Ten physically and psychiatrically healthy male subjects (mean age = 24.8 years, range = 19.8-30.0 years) were scanned on three separate days, once with the CB_1R radioligand [^{18}F]MK-9470, an inverse agonist with a high-affinity and specificity for the human CB_1R[3], and twice with the $D_{2/3}R$ radioligand [^{18}F]Fallypride after placebo and following AMPH. The two [^{18}F]Fallypride scans occurred 3 hours after oral administration of identical-appearing opaque gelatine capsules containing or oral dexamfetamine sulfate (AMPH; 30 mg) or placebo according to a single-blinded design in which the subject did not know what drug was being administered. All PET scans were performed on the HiRez Biograph 16 slice PET/CT camera (Siemens Inc) in three-dimensional mode. Dynamic CB_1R PET scans were started 120 minutes after [^{18}F]MK-9470 injection (in average 146.7 MBq) with 60-minutes scanning session. Protocols for [^{18}F]Fallypride $D_{2/3}R$ PET acquisition were derived from previous AMPH challenge studies[4]. [^{18}F]Fallypride PET scans were started simultaneously with the intravenous [^{18}F]Fallypride injection (in average 155.7 MBq) and were obtained for 3.5 hours with two 20-minute breaks. For each placebo and AMPH condition, we generated individual voxelwise $D_{2/3}R$ BP_{ND} maps with a multilinear reference tissue model (MRTM2). SPM analysis was used to compare $D_{2/3}R$ BP_{ND} maps obtained for placebo and AMPH by using a paired t-test. We additionally performed a VOI-based analysis where we compared placebo *vs* AMPH $D_{2/3}R$ BP_{ND} in each VOI. To examine whether the magnitude of DA release was modulated by CB_1R availability, a voxel-based correlation analysis was performed between the parametric fractional uptake ratio CB_1R maps[5] and the percentage change in [^{18}F]Fallypride BP_{ND} between placebo and AMPH (ΔBP_{ND} = [($BP_{ND\text{-}AMPH}$ / $BP_{ND\text{-}PLAC}$) -1)] x 100%) for those VOIs showing significant voxel-based AMPH-induced DA release.

Results:
Decreases in [^{18}F]Fallypride binding after AMPH indicate endogenous DA release after AMPH administration (*Figure a*). Consistent with the voxel-based analysis, we found a significant AMPH effect in the dorsal striatum (mean ΔBP_{ND} = -7.8%, range : -21.9-11.6%; p=0.03), including the putamen (p=0.004) and globus pallidus (p=0.01), in the hypothalamus (p=0.01), and in the mesotemporal lobe (mean ΔBP_{ND} = -5.6%, range : -18.9-3.9%; p=0.03). Correlations between DA release and CB_1R availability demonstrated that the magnitude of AMPH-induced DA release was correlated with CB_1R availability in specific cerebral regions. SPM analysis revealed that striatal ΔBP_{ND} was inversely correlated with CB_1R availability in

a cluster located in the medial orbitofrontal cortex (t=7.48, at voxel-level $p=3.54 \cdot 10^{-5}$) (*Figure b-c*). For extrastriatal regions, such as mesotemporal regions, where AMPH had a significant effect on BP_{ND}, a positive correlation was observed between AMPH-induced ΔBP_{ND} in the parahippocampal gyrus and CB_1R availability in a cluster located at the dorsal anterior cingulate cortex (t=6.80, at cluster-level p=0.001).

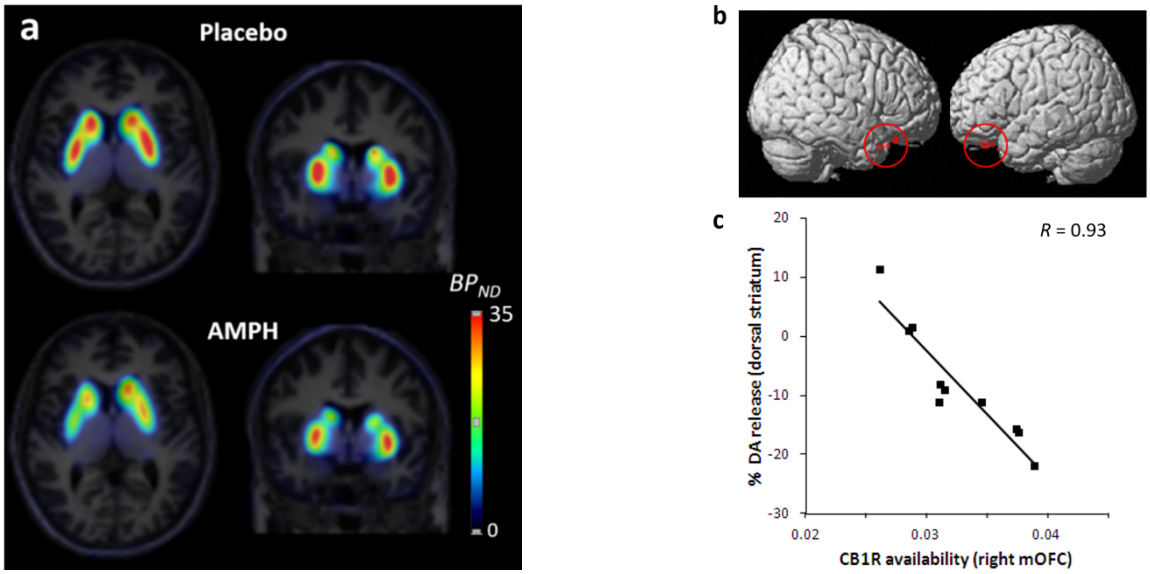

Figure: a) Effect of AMPH on [^{18}F]Fallypride BP_{ND} maps copared to the placebo condition for a representative subject; **b)** SPM maps and **c)**, individual correlation scatterplot showing the correlation of the AMPH-induced DA release in the dorsal striatum with CB_1R availability in the right mOFC (P_{uncor}=0.003; t=7.48; K_{ext}=131; [x, y, z] = [26, 30, -28]).

Discussion:

In the dorsal sensorimotor striatum that mediates habitual drug seeking, DA increases were directly associated with CB_1R availability in the medial orbitofrontal cortex, a region involved with salience attribution, motivation, decision making, sensory integration, reward, hedonic experience and therefore also implicated in compulsive and addictive behaviors. Therefore, DAergic transmission in dorsal striatum is modulated not only by striatal endogenous cannabinoid release, but also by CB_1R in mOFC, where CB_1R activation reduces the negative feedback of striatal DA neural activity presumably by influencing the GABAergic transmission directly. On the other hand, we found that in specific limbic structures such as the parahippocampal gyrus, where CB1Rs are mainly located in the excitatory glutamatergic inputs, the magnitude of DA release was greater in those subjects with lower CB_1R availability in the anterior cingulate cortex, a prefrontal region involved in regulating cognitive control over goal-directed behaviour and ongoing behavioural adaptation. In conclusion, our results represent the first direct demonstration that CB_1R availability is a determinant of DA transmission in mesocorticolimbic structures in vivo. The findings are shown in a group of healthy controls, and warrant further investigation in pathological conditions characterized by either hypo- or hyper-excitability of DA release (e.g., addiction or psychosis) in relation to CB_1R availability.

References:

[1] Katona I, Freund T.F [2008] Nat Med 14(9):923-30. [2] Fernandez-Ruiz J, Hernandez M, Ramos J.A [2010] CNS. Neurosci. Ther 16: 72-91. [3] Burns H.D, et al. [2007] Proc Natl. Acad. Sci. U.S.A 104, 9800-5. [4] Riccardi P, et al. [2006] Neuropsychopharmacology 31, 1016-26. [5] Sanabria-Bohorquez, S.M. et al. [2010] Eur. J. Nucl. Med. Mol. Imaging 37, 920-33.

OP25
Characterization of the partial agonist aripiprazole through its functional properties with combined PET/fMRI

Christin Y. Sander[1], Bruce R. Rosen[1,2] and Joseph B. Mandeville

[1]Athinoula A. Martinos Center, Department of Radiology, Massachusetts General Hospital, Charlestown, MA,
[2]Division of Health Sciences and Technology, Harvard-MIT, Cambridge, MA

Introduction:
The binding of a drug or neurotransmitter to a receptor is the basis of neuronal signal transmission and modulation in the brain. Neurovascular coupling to receptor occupancy has been previously shown to occur for antagonist and agonist drugs specific to the D2/D3 dopamine receptor system using simultaneous receptor-specific PET and fMRI measurements[1,2]. In this study, we extend this concept to current third generation antipsychotic drugs that are classified as partial agonists at the D2/D3 dopamine receptor. Our goal was to characterize the *in vivo* functional response at D2/D3 receptors of partial agonists in the context of full D2/D3 antagonists and agonists using simultaneous PET/fMRI.

Materials & Methods:
Dynamic [^{11}C]raclopride PET (specific to D2/D3 dopamine receptors) and fMRI were acquired in three anesthetized non-human primates (*rhesus macaque*) on an integrated PET/MR scanner. Three different doses (0.02, 0.05, 0.1mg/kg) of the antipsychotic aripiprazole were injected intravenously as a within-scan challenge at ~35 minutes and/or 70 minutes after the start of a bolus plus infusion of [^{11}C]raclopride. Comparisons were made to previously acquired data[1,2] of two full antagonists (prochlorperazine, raclopride) and two agonists (ropinirole, quinpirole), two of which are clinically relevant (prochlorperazine, ropinirole), with the others being preclinical drugs. Gradient-echo echo planar imaging was acquired throughout the dynamic PET acquisition of 100 minutes. Before each scan, iron oxide was injected to improve fMRI contrast and detection power[3]. fMRI data were analyzed with the GLM and cerebral blood volume (CBV) changes were derived. PET data were analyzed with a simplified reference tissue model (SRTM) that included a term for dynamic binding changes and used the cerebellum as the reference tissue in order to determine receptor occupancy[4]. A neurovascular coupling model previously introduced[2] was used to predict functional responses from drugs that exhibit partial agonist and antagonist properties.

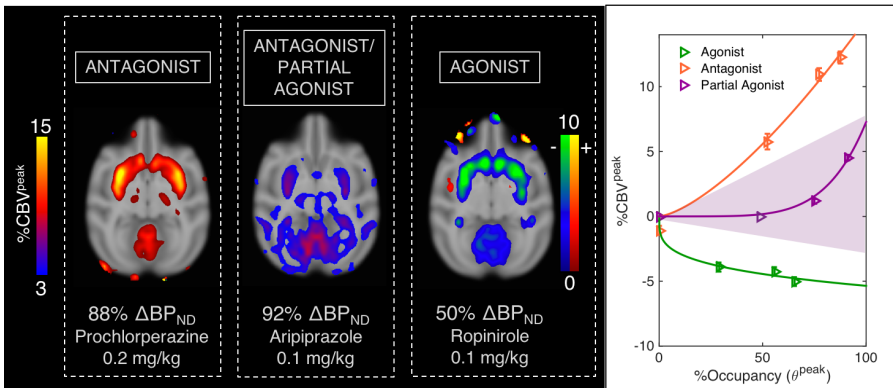

Figure 1.
Left: Voxelwise maps of CBV signals of the partial agonist aripiprazole compared to the full agonist prochlorperazine and ropinirole at their highest occupancies.
Right: Plot of CBV vs. D2/D3 receptor occupancy for a range of drug doses.

Results:
The highest doses of all administered drugs gave the largest D2/D3 receptor occupancy values as measured by [^{11}C]raclopride PET data and corresponded to the largest CBV change for each drug in the striatum. Figure 1 (*left*) shows the voxelwise CBV maps from the highest dose of aripiprazole in comparison to the two clinically relevant full agonist and antagonist responses, together with the simultaneously acquired occupancy measurement. Interestingly, the atypical antipsychotic aripiprazole showed an overall positive CBV response that was
markedly lower in magnitude, despite higher D2/D3 receptor occupancy, compared to the full ant-/agonist. The full agonists consistently showed a negative response and full antagonists a positive CBV response in the striatum. Figure 1 (*right*) shows a direct comparison of CBV values for each occupancy. D2/D3 occupancy values for the three doses of aripiprazole were 49%, 74% and 92% in the putamen. Simultaneously acquired %CBV values were not significant for the lowest dose of aripiprazole, but showed positive %CBV of 1.2% and 4.5% for the two higher doses in the putamen. Figure 3 shows time-activity curves for a single vs. double injection of aripiprazole. A double injection of 2×0.02mg/kg or 2×0.05mg/kg aripiprazole
separated by 35 minutes led to a similar overall occupancy compared to a single injection of 0.05mg/kg or 0.1mg/kg, respectively, but could be clearly distinguished in kinetic modeling as separate occupancy curves.

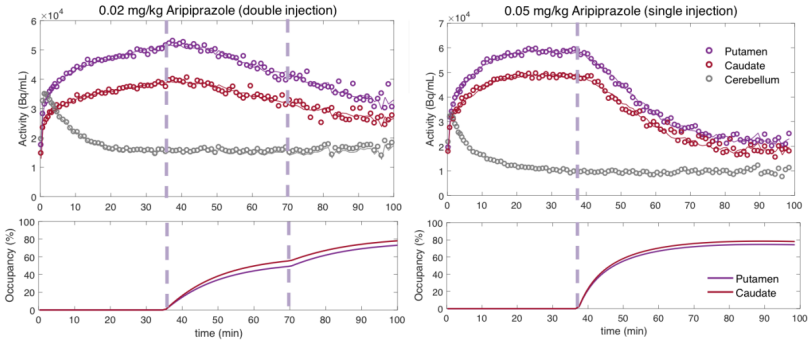

Figure 2.
Left: TAC and calculated occupancy of a double injection of aripiprazole is clearly distinguished through modeling of two separate challenges. *Right:* TAC from a single challenge injection with double the dose shows similar occupancy values.

Discussion/Conclusion:

The atypical antipsychotic aripiprazole that is classified as a partial agonist *in vitro* could be characterized as a partial agonist *in vivo*, using comparisons to full and partial agonists in agreement with a neurovascular coupling model[1]. Together with the results from full agonist and antagonists, this brings together a comprehensive dataset that shows that the combination of PET/fMRI can be used to classify D2/D3 drugs according to their *in vivo* pharmacodynamic profile. Our *in vivo* results agree with classifications from *in vitro* studies, but will be especially useful for drugs that are classified as partial agonists or atypical and may not have a defined functional response *in vivo*. It is of interest to note that the CBV-occupancy curve for the partial agonist seems to be more convex than that for the antagonist. This may be due to pre-synaptic autoreceptors having a comparatively larger effect at increasing occupancy, thus more effectively cancelling out small signals from a partial agonist at lower occupancy. In addition, we demonstrated that a double challenge injection spaced apart from each other by ~35min during a [^{11}C]raclopride bolus plus injection scan can yield distinguishable occupancy values that are equivalent to a single injection. While we investigated D2/D3 receptors, the fMRI response from non-specific drugs such as aripiprazole could also be modulated by other receptors. Further experiments with other partial agonists or clinical antipsychotics may reveal further insight on *in vivo* drug function that may be invaluable for predicting therapeutic effects of drugs.

Acknowledgements: This work was supported by NIH grants 1K99DA043629, P41EB015896, S10RR026666, S10RR022976, S10RR019933 and S10RR017208.

References:

[1]Sander CY, Hooker JM, Catana C, et al. [2013], *PNAS*, 110:11169-74. [2]Sander CY, Hooker JM, Catana C, et al. [2015], *Neuropsychopharmacology* 41:1427-1436. [3]Mandeville JB, Marota JJA, Kosofsky BE, et al. [1998] *MRM* 39:615-624. [4]Lammertsma AA, Hume SP [1996], *NeuroImage* 4:153-158.

OP26
Intranasal Oxytocin modulation of brainwide resting-state functional connectivity: a peripherally-controlled pharmaco-MRI study

D. Martins[1], O. Dipasquale[1], F. Zelaya[1], N. Mazibuko[1], O. O'Daly[1], J. O'Muircheartaigh[2], S. Maltezos[2], U. Schuschnig[3], S. Williams[1], Y. Paloyelis[1]

[1] King's College London, Department of Neuroimaging, Institute of Psychiatry, Psychology and Neuroscience, London, UK
[2] King's College London, Department of Forensic and Neurodevelopmental Science (SM), Institute of Psychiatry, Psychology and Neuroscience, London, UK
[3] PARI Pharma GmbH, Gräfelfing, Germany

Introduction:
Intranasal oxytocin (OT) has been proposed as an experimental therapeutic for several human neuropsychiatric conditions characterized by deficits in social functioning. However, it is currently under debate whether the effects of intranasal OT on social cognition in humans do reflect privileged delivery of OT to the brain. OT is a large hydrophilic peptide and thus is unlikely to cross the blood-brain barrier (BBB) in abundance. Although intranasal OT use typically derives from the assumption it may represent a privileged way for circumventing the BBB, intranasal administration of OT does produce significantly higher elevation of OT levels in the plasma than those observed in the cerebrospinal fluid of human and non-human individuals after intranasal OT. In fact, OT receptors are also widely expressed in peripheral organs, such as the heart, and local effects of OT on these organs may indirectly effect on brain and behaviour. However, studies examining the extent to which changes in brain function after intranasal OT may alternatively result from OT signalling in peripheral territories or minor amounts of plasmatic OT and/or its metabolites crossing the BBB are lacking. Herein we examine the effects of intranasal OXT on whole-brain resting-state functional connectivity, comparing 2 methods of intranasal administration: a standard spray vs the PARI GmbH *SINUS* nebulizer (expected to maximize OXT deposition in the olfactory region - putatively involved in direct nose-to-brain transport). We further compare intranasal administration to intravenous administration to examine the extent to which intranasal effects might be solely explained by peripheral signalling or result from a privileged route of transport to the brain.

Methods:
17 healthy males were recruited for a double-blind, within-subject, placebo-controlled, crossover study evaluating the effects of OXT administration (intranasal spray, nebuliser or intravenous) on whole-brain functional connectivity. Each participant received 40 IU of OXT intranasally (through a spray or a nebulizer), 10 IU of OXT intravenously, as well as placebo in 4 pseudo-randomly allocated visits in a triple dummy design. For each session, resting-state fMRI was acquired 60 min after last drug administration using a multi-echo EPI sequence in a 3T scanner. Blood samples for plasma OXT quantification were collected before and at several time-points after drug administration. Resting-state fMRI images were pre-processed with AFNI(Cox 1996). Then, the three echoes were optimally combined(Posse, Wiese et al. 1999) and the resulting images were de-noised using the ME-ICA approach implemented in AFNI(Kundu, Inati et al. 2012, Dipasquale, Sethi et al. 2017). WM and CSF signals were regressed out and a high-pass temporal filter (cut-off 0.005 Hz) applied. The resulting images were normalized to MNI space and then uploaded in the CONN toolbox for a whole-brain exploration of ROI-ROI functional connectivity across 132 anatomical regions. Connectivity matrices were compared between sessions using T-contrasts. Statistical significance was defined for $p<0.05$, FDR-corrected across all possible ROIs connections.

Results:
OXT spray resulted in widespread significant changes in functional connectivity across different brain areas, involving mostly decreases in the connectivity of the medial temporal gyrus, the lingual gyrus and the temporal and frontal poles. Increased functional connectivity could be observed between the supramarginal gyrus and the superior frontal gyrus, two areas assumed to be involved in salience attribution. Despite identical pharmacokinetic profiles, nebulized OXT only produced increases in connectivity, involving mostly an increase in the connectivity between the precuneus and the paracingulate cortex, two core nodes of the mentalizing network. Importantly, intravenous OXT did not explain the pattern of changes in connectivity observed for the spray or the nebulizer. Instead, intravenous OXT was associated almost exclusively with increases in connectivity, involving mainly the occipital fusiform gyrus and the superior temporal gyrus.

Conclusion:
We mapped the macroscale functional substrates engaged by intranasal OXT and provided new evidence supporting the hypothesis of a direct nose-to-brain pathway underlying intranasal OXT effects in the human brain. We also show two different methods of intranasal administration result in distinct changes in connectivity despite producing similar changes in plasmatic OXT. This observation raises the hypothesis that the two intranasal methods may differ in the provided bioavailability of oxytocin in the brain.

References:
Cox, R. W. (1996). "AFNI: software for analysis and visualization of functional magnetic resonance neuroimages." Comput Biomed Res **29**(3): 162-173.
Dipasquale, O., et al. (2017). "Comparing resting state fMRI de-noising approaches using multi- and single-echo acquisitions." Plos One **12**(3): e0173289.
Kundu, P., et al. (2012). "Differentiating BOLD and non-BOLD signals in fMRI time series using multi-echo EPI." Neuroimage **60**(3): 1759-1770.
Posse, S., et al. (1999). "Enhancement of BOLD-contrast sensitivity by single-shot multi-echo functional MR imaging." Magn Reson Med **42**(1): 87-97.

OP27
Intranasal Naloxone Rapidly Occupies Brain mu-opioid Receptors in Human Subjects

Jarkko Johansson[1,2], Jussi Hirvonen[1,3], Zsófia Lovró[4,5], Laura Ekblad[1], Valtteri Kaasinen[6], Olli Rajasilta[5], Semi Helin[1], Jouni Tuisku[1], Saija Sirén[5], Mirka Pennanen[4], Arvind Agrawal[7], Roger Crystal[7], Petri J. Vainio[5], Hannu Alho[8,9], Mika Scheinin[4,5]

[1] Turku PET Centre, University of Turku, Turku, Finland. [2] Department of Radiation Sciences, Umeå University, Umeå, Sweden. [3] Department of Radiology, University of Turku, Turku, Finland. [4] Clinical Research Services Turku CRST Ltd., Turku, Finland. [5] Institute of Biomedicine, University of Turku and Unit of Clinical Pharmacology, Turku University Hospital, Turku, Finland. [6] Division of Clinical Neurosciences, University of Turku and Turku University Hospital, Turku, Finland. [7] Opiant Pharmaceuticals Inc., Santa Monica, CA, USA. [8] National Institute for Health and Welfare, Helsinki, Finland. [9] Abdominal Center, University Hospital of Helsinki, Helsinki, Finland.

Introduction:
Naloxone is a well-established product for the reversal of respiratory depression in the management of opioid overdose. Intranasal (IN) delivery of naloxone was recently approved by the FDA based on its high bioavailability (~50 %) and ease of delivery compared to intravenous or intramuscular administration. The time-course of naloxone mu-opioid receptor (MOR) occupancy, however, has not been characterized in humans. Pharmacokinetic studies have indicated rapid absorption of naloxone from the nasal cavity in humans (Krieter *et al.*, 2016; Tylleskar *et al.*, 2017), while an earlier PET study has suggested high MOR occupancy by naloxone in non-human primates (Saccone *et al.*, 2016), without, however, specifying the time-course of occupancy development. Here, we used [^{11}C]-carfentanil PET in young, healthy volunteers (n=14) to probe the time-course and level of MOR occupancy after IN naloxone. In a subgroup of participants (n=8), naloxone was delivered in-scan, rather than pre-scan, allowing assessment of the initial MOR occupancy time-course.

Materials and Methods:
The study was double-blind and placebo-controlled, including two [^{11}C]-carfentanil scans for each participant in a counter-balanced order. Plasma naloxone concentrations were followed from 0 to 360 min after drug administration. PET scans were conducted using HRRT (Siemens, Knoxville, USA) and high molar activity [^{11}C]-carfentanil injections. T2-weighted brain MRI scans were acquired for anatomical reference and automated region-of-interest (ROI) generation (Johansson *et al.*, 2017). Primary PET analyses were made within an automatically generated grey-matter ROI including regions with high MOR availability. Time-activity-curve (TAC) data were fitted using a simplified reference-tissue model (SRTM) and by using the linearized-parametric neurotransmitter-PET approach (lp-ntPET, Normandin *et al.*, 2012). The occipital cortex was used as a reference region (Hirvonen *et al.*, 2009). Low-volume (0.1 mL) IN doses of naloxone (2 mg, n=7; 4 mg, n=7) or inactive placebo were delivered in-scan (20 min from radiotracer administration, n=8) or 300 min prior to PET scanning (n=6). Bayesian information criteria (BIC) and Akaike weights were used to choose the model with the best fit in each experiment, and binding potential (BP_{ND}) was considered as the main outcome parameter. Receptor occupancy (RO) estimates were calculated as $RO(t)=100\%(1-BP_{ND}^{naloxone}(t)/BP_{ND}^{placebo})$, where t=0, 1, 2, …, 60 min, or t=330 min relative to naloxone delivery in the in-scan and pre-scan experiments, respectively.

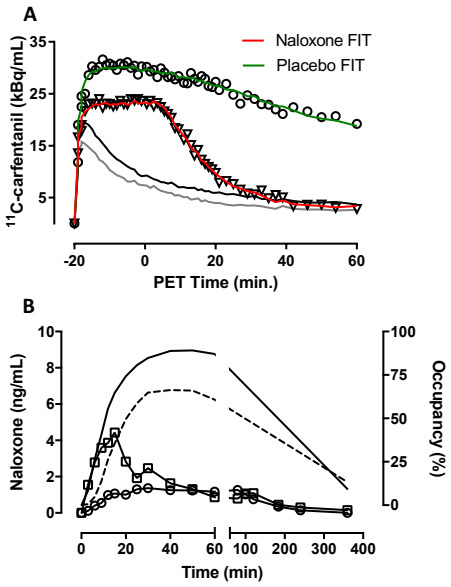

Results:

Akaike weights indicated no effect of placebo in the in-scan experiments, while a clear indication of MOR occupancy was observed in the naloxone experiments (data not shown, but c.f. Fig. 1A). Hence, the subsequent analyses of in-scan naloxone data were conducted using lp-ntPET, while other experiments were analyzed using conventional SRTM. Rapid appearance of naloxone in plasma was observed in a dose-dependent manner (Fig. 1B), associated with rapid onset of MOR occupancy, which peaked somewhat later compared to the observed C_{max}, reflecting competition with [^{11}C]-carfentanil. Residual occupancy of approximately 1/8 of the peak occupancy was observed at 330 min (see Fig. 1B), suggesting an approximately 100 min half-life of naloxone occupancy.

Fig. 1 A: [^{11}C]-carfentanil-derived TAC data following IN administration of placebo (circles) and naloxone (triangles) in one individual. **B**: Mean plasma naloxone concentrations after IN naloxone (2 mg, n=7, circles, and 4 mg, n=7, squares), and the corresponding mean occupancy (%) estimates (2 mg, broken line, 4 mg, solid line).

Discussion:

The availability of IN naloxone is aimed to alleviate the morbidity and mortality related to the present opioid epidemic. Other possible uses of IN naloxone include anti-addiction treatments similar to oral opioid antagonists in alcoholism. Indeed, at present, targeted use of IN naloxone is investigated in the treatment of gambling disorder, a “behavioral addiction”. The possible efficacy of IN naloxone in such use is determined by the extent and time-course of the achieved MOR occupancy; rapid onset of action is desirable, while a short duration of action might also be beneficial for targeted anti-addiction use. The present results support the amenability of IN naloxone for anti-addiction use in terms of rapid onset and relatively short duration of MOR occupancy. The observed short half-life of MOR occupancy is in concordance with the re-narcotization of opioid overdose patients sometimes observed in the clinic.

References:

Hirvonen J, Aalto S, Hagelberg N, Maksimow A, Ingman K, Oikonen V, *et al.* (2009). Measurement of central μ-opioid receptor binding in vivo with PET and [^{11}C]carfentanil: A test-retest study in healthy subjects. *Eur J Nucl Med Mol Imaging* **36**: 275–286.

Johansson J, Ajalin R, Tuisku J, Karjalainen T, Joutsa J, Scheinin H (2017). Quantification of mu-opioid receptor binding with ^{11}C-Carfentanil PET: a comparison of ROI-methods using test-retest analysis. *Suppl issue J Cereb Blood Flow Metab* .

Krieter P, Chiang N, Gyaw S, Skolnick P, Crystal R, Keegan F, *et al.* (2016). Pharmacokinetic properties and human use characteristics of an FDA approved intranasal naloxone product for the treatment of opioid overdose. *J Clin Pharmacol* **56**: 1243–1253.

Normandin MD, Schiffer WK, Morris ED (2012). A linear model for estimation of neurotransmitter response profiles from dynamic PET data. *Neuroimage* **59**: 2689–2699.

Saccone PA, Lindsey AM, Koeppe RA, Zelenock KA, Shao X, Sherman P, *et al.* (2016). Intranasal opioid ddministration in Rhesus monkeys: PET imaging and antinociception. *J Pharmacol Exp Ther* **359**: 366–373.

Tylleskar I, Skulberg AK, Nilsen T, Skarra S, Jansook P, Dale O (2017). Pharmacokinetics of a new, nasal formulation of naloxone. *Eur J Clin Pharmacol* **73**: 555–562.

OP28
Molecular signatures of psychiatric disorders: A volumetric meta-analysis of human neurotransmission imaging studies

Lauri Nummenmaa[1,2], Lauri Tuominen[1], Jussi Hirvonen[1,3], & Enrico Glerean[1]

[1]Turku PET Centre, Turku, Finland, [2]Department of Psychology, University of Turku, Finland, [3]Department of Radiology, University of Turku, Finland

Introduction:

Psychiatric diagnoses are traditionally based on categories of clinical symptoms ranging from behavior to subjective sensations (1), yet functional and structural MRI studies have failed to establish consistent, condition-specific alterations at the neural level (2). Unlike MRI, nuclear medicine imaging techniques such as PET and SPECT have high biological resolution and allow targeting specific neurotransmitter systems, thus providing information about disease mechanisms and potential drug targets. Here we provide the first large-scale volumetric meta-analysis of human neuroreceptor and neurotransmitter changes across a wide spectrum of psychiatric disorders.

Materials and methods:
We analyzed 470 studies measuring neuroreceptor and neurotransmitter level changes across common psychiatric disorders using PET or SPECT. We encoded study details and coordinates or names of the regions of interest were altered neurorceptor or transmitter levels were found in patients versus controls. We then used automatic semantic matching algorithm to remap the ROI / coordinate-level changes into “pseudo-t contrast” maps in the MNI space. Voxelwise effect size maps were then computed separately for each disorder (averaging over target molecules) as well as for each disorder and target molecule separately. Mean similarity matrix for the effect size maps was constructed and subjected to t-distributed Stochastic Neighbor Embedding (t-SNE; 3). Resulting similarities were projected over a two-dimensional space to evaluate the molecule-level similarity structure of the psychiatric conditions in the brain

Results:
Alterations in midbrain and striatum were common to all conditions, and thalamic and fronto-cingular alterations were observed in all conditions except major depressive disorder. Changes in amygdala were found in anorexia nervosa, anxiety disorders, borderline personality disorder and post-traumatic stress disorder (**Fig 1**). The t-SNE solution revealed a clear two-dimensional structure, with depression – schizophrenia division on the X axis and anxiety on Y-axis (**Fig 2**).

Conclusions:
Our findings provide a first proof-of-concept demonstration of mapping ROI-level data back to the volumetric level for meta-analysis, and demonstrate regionally specific alterations of neurotransmission across different psychiatric conditions. A priori disorder categories however formed multiple clusters or lacked clear cluster structure, contradicting one-to-one mapping between disorders and regional alterations in specific neurotransmitter systems.

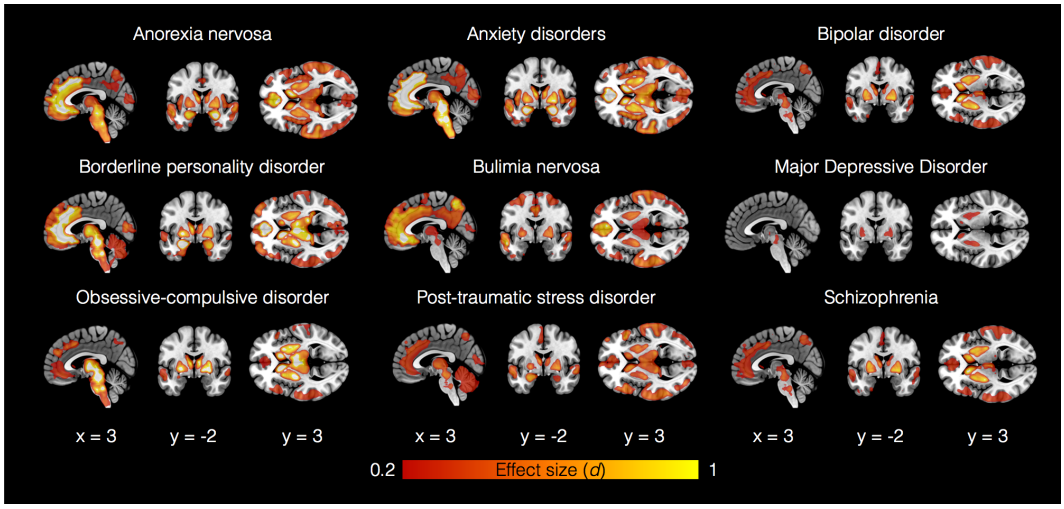

Figure 1. *Brain regions showing consistent alterations (averaged across molecular targets) in the nine major psychiatric conditions. Colourbar shows the effect size.*

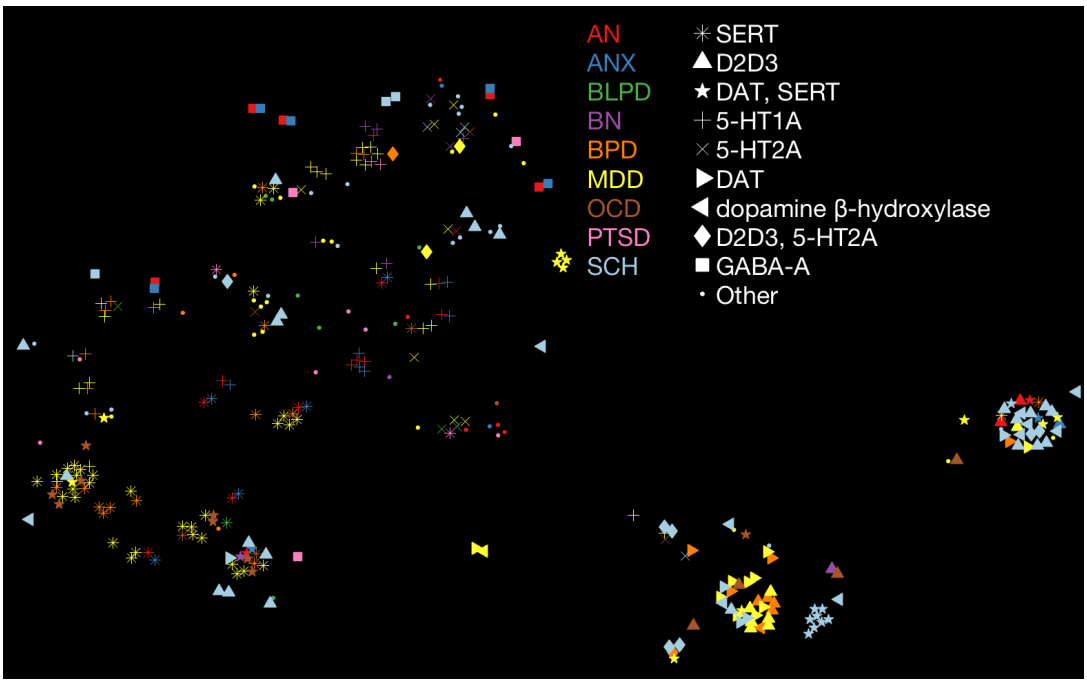

Figure 2. *Similarity structure of psychiatric conditions based on neurotransmission imaging. Each marker represents one study, colouring indicates the condition and shape the targeted molecule. AN = Anorexia Nervosa, ANX = Anxiety disorders, BLPD = borderline personality disorder, BPD = Bipolar disorder, MDD = Major depressive disorder, OCD = Obsessive-compulsive disorder, PTSD = Post-traumatic stress disorder, SCH = Schizophrenia.*

Acknowledgements:
This work was supported by the Academy of Finland (grant #294897 to LN) and Sigrid Juselius Foundation.

References

1. Fischer BA (2012) A Review of American Psychiatry Through Its Diagnoses The History and Development of the Diagnostic and Statistical Manual of Mental Disorders. *J. Nerv. Ment. Dis.* 200(12):1022-1030. 2. Goodkind M, *et al.* (2015) Identification of a Common Neurobiological Substrate for Mental Illness. *JAMA Psychiatry* 72(4):305-315. 3. van der Maaten L & Hinton G (2008) Visualizing Data using t-SNE. *J. Mach. Learn. Res.* 9:2579-2605.

OP29

A novel ^{18}F-labeled radiotracer for imaging 11β-HSD1: Synthesis and evaluation of ^{18}F-AS2471907 in non-human primates

Yiyun Huang[1], Songye Li[1], Zhengxin Cai[1], Wenjie Zhang[1], Daniel Holden[1], Evan Baum[1], Nabeel Nabulsi[1], Jim Ropchan[1], Hong Gao[1], Mike Kapinos[1], Sherry McKee[2], and Kelly Cosgrove[2]

[1]PET Center, Department of Radiology and Biomedical Imaging, Yale University, New Haven, CT 06520, USA; [2]Department of Psychiatry, Yale University, New Haven, CT 06520, USA

Introduction:

The 11β-hydroxysteroid dehydrogenase-1 (11β-HSD1) is an important enzyme in the regulation of stress and stress response, as it catalyzes the conversion of cortisone to the "stress hormone" cortisol. Accumulating evidence has implicated 11β-HSD1 in a wide range of diseases including neurodegenerative diseases, metabolic disorders, stress-related disorders, and neuroinflammation. Development of PET imaging agents to probe 11β-HSD1 *in vivo* will enable the investigation of this enzyme's involvement in the pathophysiology of diseases. Further, PET imaging with 11β-HSD1-specific radioligands can be used to assess target engagement and correlate target occupancy, dose exposure and therapeutic response of 11β-HSD1 inhibitors current in clinical trials, and thus facilitate the development of novel therapeutic agents. We have previously developed ^{11}C-AS2471907 as a PET radioligand to image 11β-HSD1 in non-human primates and humans[1,2]. However, the current method for its production is low-yielding and unreliable, as three regioisomers are formed in the process, with the desired isomer (^{11}C-AS2471907) as minor product. Fortuitously, the molecule can also be radiolabeled with fluorine-18 with no formation of regioisomers. Therefore, we developed a method for the radiosynthesis of ^{18}F-AS2471907 and evaluated this new ^{18}F-labeled radioligand in non-human primates.

Materials & Methods:

^{18}F-AS2471907 was produced using iodonium ylides as precursor (**Figure 1**). PET imaging experiments with ^{18}F-AS2471907 were carried out on the Focus-220 scanner in rhesus monkeys. Blocking scans were also conducted with administration of two separate 11β-HSD1 inhibitors (ASP3662 and a Merck ligand) at 10 min before ^{18}F-AS2471907 injection, to assess binding specificity of the radioligand. Arterial blood samples were drawn during each PET scan for HPLC analysis of radioactive metabolites in plasma and measurement of the arterial input function. Time-activity curves in brain regions were analyzed with the 1-tissue compartment (1TC) model to estimate regional volume of distribution (V_T). Target occupancy by blocking drugs and the non-displaceable volume of distribution (V_{ND}) were determined from the occupancy plots. Regional binding potential (BP_{ND}) values were calculated from baseline V_T and V_{ND} obtained from the blocking scans. Comparison of ^{18}F-AS2471907 with ^{11}C-AS2471907 was also made.

Results:

^{18}F-AS2471907 was prepared in >98% radiochemical purity and 4.9 ± 2.4 % radiochemical yield (decay-uncorrected, n = 17) at the end of synthesis. Metabolism of ^{18}F-AS2471907 was slow, and similar to that of ^{11}C-AS2471907, with parent fraction of 94 ± 4% at 30 min post-injection (n = 7). Plasma free fraction was 5 ± 2% (n = 7). Uptake of ^{18}F-AS2471907 in the rhesus monkey brain was high (peak SUV of 5.2), and similar to that of ^{11}C-AS2471907

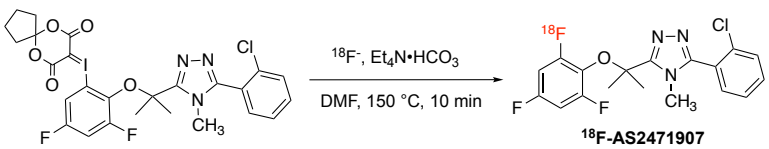

Figure 1. Radiosynthesis of ^{18}F-AS2471907

(**Figure 2**). Tissue kinetics was fast, with peak uptake between 10 and 25 min post-injection. Brain regional time activity curves were fitted well by the 1TC model to provide reliable regional V_T estimates, which were similar to those of ^{11}C-AS2471907 (**Table 1**). Pretreatment with ASP3662 (0.3 mg/kg) or a Merck 11β-HSD1 inhibitor (1 mg/kg) reduced uptake in all brain regions to almost homogeneous levels and produced target occupancies of 94 % and 99 %, respectively. Estimated V_{ND} was 3.18 and 2.82 mL/cm^3, respectively, for the two blocking scans in two separate monkeys. Regional BP_{ND} values ranged from 0.4 to 3.0 (**Table 1**), indicating high levels of specific binding for ^{18}F-AS2471907 *in vivo*.

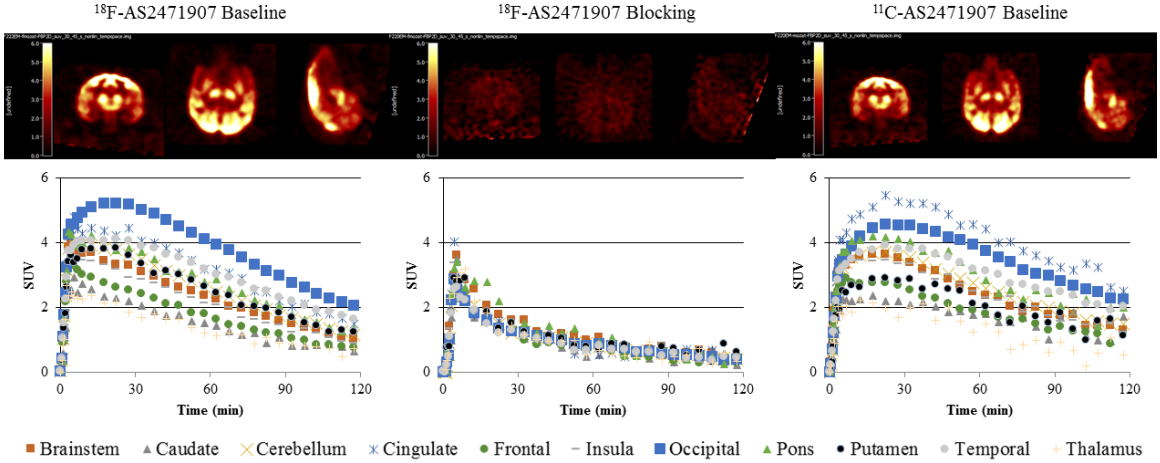

Figure 2. PET SUV images summed from 30-45 min after radioligand injection (top) and time-activity curves (bottom) from a baseline scan with ^{18}F-AS2471907, a blocking scan with pre-administration of AS3662 (0.3 mg/kg) and a baseline scan with ^{11}C-AS2471907 (from left to right).

Discussion/Conclusion:

We developed ^{18}F-AS2471907 as the first ^{18}F-labeled radioligand for 11β-HSD1 and evaluated its pharmacokinetic and imaging characteristics in rhesus monkeys. ^{18}F-AS2471907 displayed the same attractive properties as ^{11}C-AS2471907: slow metabolism, high brain uptake, appropriate tissue kinetics, and high levels of specific binding signals. We conclude that ^{18}F-AS2471907 is a highly promising PET radioligand to image 11β-HSD1 and have translated it to PET imaging evaluation in humans.

Table 1. 1TC-derived regional V_T (mL·cm^{-3}) values from ^{18}F-AS2471907 baseline scans, a blocking scan with ASP3662 (0.3 mg/kg), and ^{11}C-AS2471907 baseline scans, as well as regional BP_{ND} estimates of ^{18}F- AS2471907.

ROI	V_T			BP_{ND}
	^{18}F-AS2471907 Baseline (n = 4)	^{18}F-AS2471907 AS3662 Blocking	^{11}C-AS2471907 Baseline (n = 4)	^{18}F-AS2471907 (n = 4)
Brainstem	7.7 ± 1.2	4.3	8.3 ± 0.8	1.4 ± 0.4
Caudate	4.9 ± 0.9	3.4	5.7 ± 1.1	0.5 ± 0.3
Cerebellum	8.3 ± 1.3	3.6	10.7 ± 4.5	1.6 ± 0.4
Cingulate cortex	11.8 ± 1.1	3.5	8.8 ± 1.5	2.7 ± 0.3
Frontal cortex	5.7 ± 0.9	3.1	5.4 ± 0.4	0.8 ± 0.3
Insula	7.0 ± 1.0	3.3	7.4 ± 1.0	1.2 ± 0.3
Occipital cortex	12.7 ± 2.1	3.5	12.2 ± 2.9	3.0 ±0.7
Pons	9.4 ± 1.3	4.5	9.2 ± 0.9	2.0 ± 0.4
Putamen	7.9 ± 1.7	3.9	7.9 ± 1.3	1.5 ± 0.5
Temporal cortex	10.0 ± 1.7	3.3	8.1 ± 1.5	2.2 ± 0.6
Thalamus	4.5 ± 0.9	3.6	5.5 ± 0.7	0.4 ± 0.3

References:

1. Iwashita A *et al*. [2016] *J. Nucl. Med.* 57(Suppl. 2):1050.

2. Huang Y *et al.* [2016] *J. Nucl. Med.* 57(Suppl. 2):580

OP30
Strategies for Simplified ^{11}C-UCB-J PET Quantification: Ratio and Reference Tissue Methods

Mika Naganawa[1], Jean-Dominique Gallezot[1], Sjoerd J. Finnema[1], David Matuskey[1,2], Ming-Kai Chen[1], Adam Mecca[2], Nabeel B. Nabulsi[1], Yiyun Huang[1], Christopher H. van Dyck[2], Richard E. Carson[1]

[1]PET Center, Department of Radiology and Biomedical Imaging, Yale University, New Haven, CT, USA; [2]Department of Psychiatry, Yale University, New Haven, CT, USA

Introduction:
The synaptic vesicle protein 2A (SV2A) PET radiotracer ^{11}C-UCB-J, used to quantify synaptic density, has high brain uptake and fast kinetics in humans. The one-tissue compartment (1TC) model derived ^{11}C-UCB-J distribution volume (V_T) has excellent test-retest reproducibility (3-9%) [1]. However, the 1TC model requires arterial blood sampling and a dynamic PET scan of 60-90 min. To simplify or eliminate blood sampling from the scan protocol, we explored two strategies. The first approach used a ratio method (tissue-to-plasma (TTP), tissue-to-reference (TTR)) and the second approach applied a reference tissue model. The estimated parameters were evaluated against the gold standard V_T and binding potential (BP_{ND}) in Alzheimer's disease (AD) and healthy controls (HC).

Materials and Methods:
A total of 17 PET scans (HC:*n*=8, AD:*n*=9) were acquired for 90 min on the HRRT scanner. Arterial blood sampling and metabolite analysis were conducted to obtain the input function to compute 1TC model parameters as gold standard values for the neocortices, striatum, hippocampus, and centrum semiovale (CS). Static TTP and TTR values were calculated at 60-90 min after injection. Simplified reference tissue model (SRTM) and SRTM2 were applied to generate BP_{ND} parametric images. Regional TTR and BP_{ND} values were determined using CS as a reference region. In SRTM2, the values of k_2 and k_2' (the efflux constants for target ROIs and the reference region) are similar for this tracer, and the k_2/k_2' ratio should be different from unity to reduce statistical error in k_2' [2]. Therefore, for SRTM2, k_2' was determined using the following two methods: (Method-1) The population average $k_{2(1TC)}$ value in CS was used as k_2'. (Method-2) The difference between the $k_{2(1TC)}$ of CS and the $k_{2(1TC)}$ of ~100 regions were computed. Then, regions where the difference was more than 40% on average across all subjects were selected. SRTM2 coupled fits were subsequently applied to the time-activity curves (TACs) of the selected regions to obtain k_2'. The % differences of TTP and TTR-1 were computed for comparison with gold standard values. Additional analyses were performed to compare disease-specific changes in the hippocampus using 1TC, TTR, and SRTM2. Between-group differences were compared using *t*-test.

Results:
TTP overestimated V_T (TTP=1.69×$V_{T(1TC)}$+0.42, R^2=0.82, P<0.0001), with similar % difference between TTP and $V_{T(1TC)}$ among the examined regions (CS:74±20%; gray matter:72±20%). Regional TTR-1 was similar to $BP_{ND(1TC)}$ (TTR-1=0.98×$BP_{ND(1TC)}$-0.04, R^2=0.95, P<0.0001) and the difference between TTR-1 and $BP_{ND(1TC)}$ was very close to zero (-1%±7%) because there was a similar overestimation with TTP between the target and reference regions. Hippocampus TTR-1 matched well with $BP_{ND(1TC)}$ (TTR-1=1.00×$BP_{ND(1TC)}$–0.07, R^2=0.98, P<0.0001). $BP_{ND(1TC)}$ in hippocampus was 1.45±0.29 for HC and 0.82±0.57 for AD. The group average of TTR-1 in hippocampus was similar to that of $BP_{ND(1TC)}$ (1.45±0.34 for HC and 0.87±0.59 for AD). The HC-AD group difference was significant using both $BP_{ND(1TC)}$ and TTR-1 (TTR-1:P=0.028, $BP_{ND(1TC)}$:P=0.013).
Simulations were performed to assess whether the excellent agreement between TTR-1 and $BP_{ND(1TC)}$ was time-dependent. PET TACs were simulated using the fitted 1TC model

parameters and an extrapolation of the metabolite-corrected plasma curve using a final mono-exponential washout rate β (~0.010 /min). Transient equilibrium [3] was reached at ~5 h post-injection. Then, TTR-1 overestimated $BP_{ND(1TC)}$ by ~36% (TTR-1=1.36×$BP_{ND(1TC)}$+0.36). This simulation result indicates the overall excellent agreement between TTR-1 and $BP_{ND(1TC)}$ is time-dependent.

SRTM produced noisy images with many outliers close to gray matter voxels. For SRTM2, k_2' using Method 1 was 0.028 (min^{-1}). The $k_{2(1TC,CS)}$ from ROI TAC analyses was similar between subjects (0.028±0.004 /min, n=17). In Method 2, 11 ROIs were selected, including frontal and temporal cortical regions. The k_2' values from Method 2 were 0.031±0.007 /min. The regression line between $BP_{ND(SRTM2)}$ (y) and $BP_{ND(1TC)}$ (x) was computed for each scan and both k_2' determination methods. Figure 1 shows a scatter plot of the slope of these regression lines vs. % differences between $k_{2(1TC,CS)}$ and k_2'. When k_2' was underestimated, $BP_{ND(SRTM2)}$ was overestimated. The difference between $BP_{ND(SRTM2)}$ and $BP_{ND(1TC)}$ was 8%±9% (Method 1) and 6%±13% (Method 2). The HC-AD group difference in hippocampus was significant using both methods (Method 1, P=0.013; Method 2, P=0.006).

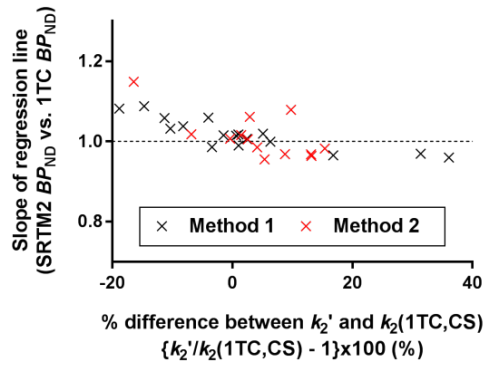

Figure 1 Scatter plot of the slope of regression lines and % differences between k_2' and 1TC k_2 in the CS

Discussion:

TTR-1 from 60-90 min matched extremely well with $BP_{ND(1TC)}$, suggesting that a short scan after tracer injection without arterial sampling may be sufficient for accurate quantification of ^{11}C-UCB-J specific binding. However, since the agreement between TTR-1 and $BP_{ND(1TC)}$ is time-dependent, careful validation of ratio methods should be performed in each patient cohort. As SRTM images were too noisy, SRTM2 was used to reduce image noise. For SRTM2 parametric imaging, the method for selection of k_2' is important and the k_2' determination method should be assessed using different patient cohorts.

Acknowledgements 1R01NS094253-01, 1R01AG052560-01A1, Dana Foundation and ADRC P50AG047270

References

[1] Finnema et al, [2017], J Cereb Blood Flow, epub.
[2] Ichise et al, [2008], J Cereb Blood Flow, 28:420-430.
[3] Carson et al, [1993], J Cereb Blood Flow Metab, 13:24-42.

OP31
$A\beta_L$ – a more sensitive biomarker for amyloid imaging

Alex Whittington[1,2], John Seibyl[1], Roger N. Gunn[1,2,3]

1. *Invicro*
2. *Division of Brain Sciences, Imperial College London, UK*
3. *Institute of Biomedical Engineering, University of Oxford, Oxford, UK*

Introduction:
Visual assessment and standardised uptake value ratio (SUVr) have been used to date for classification of PET amyloid scans and their assessment in clinical trials of novel therapeutics in Alzheimer's disease (AD). In this work, we present the novel biomarker, amyloid load ($A\beta_L$) along with an automated algorithm for its calculation and demonstrate that it has a substantial increase in power over previous approaches for cross-sectional analysis, longitudinal analysis and classification of scans into Aβ- or Aβ+.

Materials & Methods:
Spatially normalised [^{18}F]-Florbetapir SUVr (grey matter cerebellum reference) images were effectively modelled using a linear combination of previously derived canonical images for the non-specific binding **NS** and carrying capacity **K** (Equation 1).

$$\mathbf{SUVr_{fit}} = ns\mathbf{NS} + A\beta_L\mathbf{K} \qquad (1)$$

$A\beta_L$ is calculated from a single [^{18}F]-Florbetapir SUVr scan and a structural T1 MR image using the $IQ_{A\beta}$ algorithm (Figure 1). PET images are spatially normalised to MNI152space using DARTEL[1] and the associated MR image before an image based regression is performed to determine the parameters ($A\beta_L$, ns). The $\mathbf{SUVr_{fit}}$ image and a difference image showing the residuals between the spatially normalised SUVr image and $\mathbf{SUVr_{fit}}$ are also calculated.

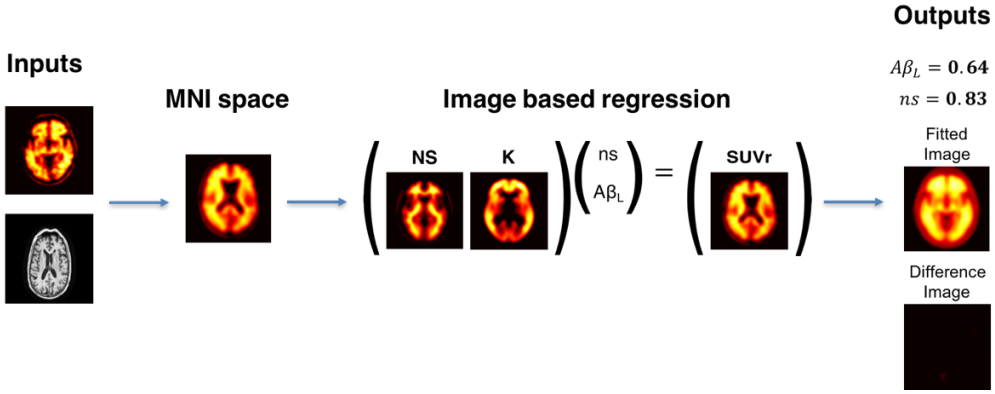

Figure 1

$A\beta_L$ and mean cortical SUVr were calculated on a cross-sectional dataset consisting of 769 subjects (211 healthy controls (HC), 223 early mild cognitive impairment (EMCI), 204 late mild cognitive impairment (LMCI), 132 AD) and a two-year follow-up (mean 1.96 ±(0.12) years) scans for 147 EMCI subjects. 672 images from the cross-sectional dataset were classified as positive or negative using visual assessment (343 Aβ- and 329 Aβ+). Effect sizes (hedges' g) were calculated for both $A\beta_L$ and mean cortical SUVr between different ADNI classifications in the cross-sectional data and between baseline and follow-up for the longitudinal data. Receiver operated characteristic (ROC) curves were produced for $A\beta_L$ and

mean cortical SUVr using visual read outcome as the gold standard from which optimum thresholds were determined.

Results:

In cross-sectional data, $A\beta_L$ produced greater effect sizes (hedges g) between all ADNI disease classifications when compared to mean cortical SUVr (Figure 2) with the mean increase being 56%.

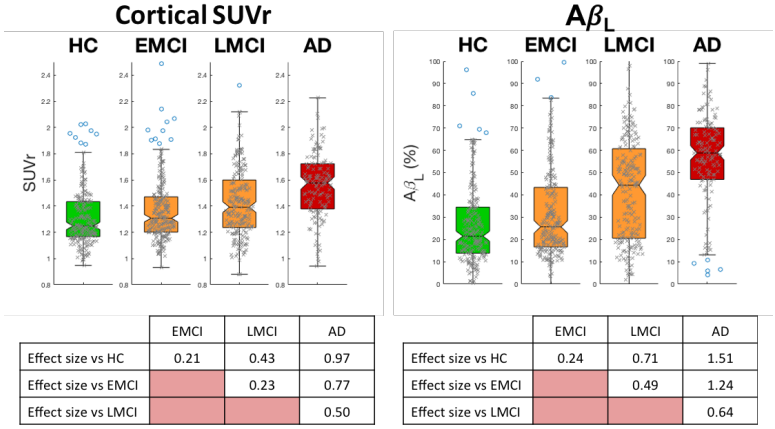

	EMCI	LMCI	AD
Effect size vs HC	0.21	0.43	0.97
Effect size vs EMCI		0.23	0.77
Effect size vs LMCI			0.50

	EMCI	LMCI	AD
Effect size vs HC	0.24	0.71	1.51
Effect size vs EMCI		0.49	1.24
Effect size vs LMCI			0.64

Figure 2

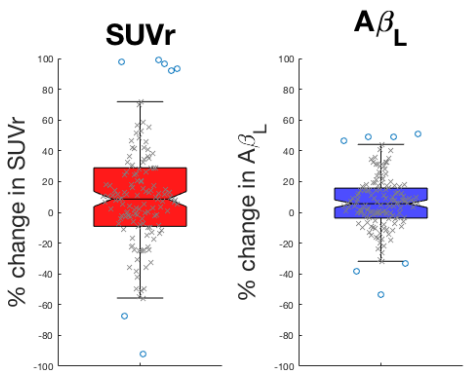

Figure 3

The effect size between baseline and follow-up in longitudinal data was 0.35 using mean cortical SUVr and 0.49 using $A\beta_L$ (Figure 3) representing a 40% increase.

For classification of scans, the ROC curve for $A\beta_L$ showed an optimum threshold of 32% with an accuracy of 93.5% and AUC of 0.98 which was better than mean cortical SUVr (Accuracy = 82.7%, AUC=0.89) (Figure 4). At the optimum threshold, $A\beta_L$ had 19 false negatives and 25 false positives.

Discussion/Conclusion:

We have shown that the novel biomarker $A\beta_L$ has greater power than mean cortical SUVr to detect differences in the Aβ from [^{18}F]-Florbetapir scans in both cross-sectional and longitudinal data. Further, $A\beta_L$ has a higher agreement with visual reads for [^{18}F]-Florbetapir scans that opens up the possibility of automating the reading process. With the fully automated $IQ_{A\beta}$ algorithm, $A\beta_L$ may provide a sensitive, accurate and cost-efficient biomarker to quantify the Aβ in the brain.

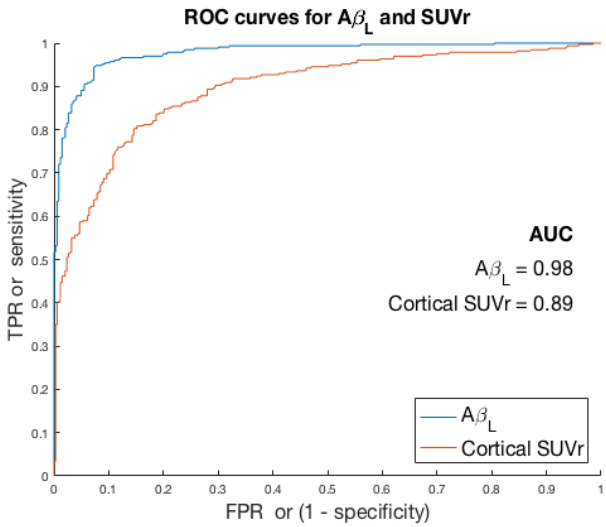

Figure 4

References

1. Ashburner J.*Neuroimage* **38,**95–113(2007)

OP32
Is intranasal radiotracer delivery feasible for PET imaging?

N Singh[1,2], M Veronese[1], T Sementa[2], J O'Doherty[3,4], S Bongarzone[2], D Cash[1], C Simmons[1], M Arcolin[1], P Marsden[3], A Gee[2,3], F Turkheimer[1]

1. *Centre for Neuroimaging Sciences, IoPPN, KCL, De Crespigny Park, London SE 5 8AF*
2. *Imaging Chemistry and Biology, St Thomas' Hospital, KCL, London SE1 7EH*
3. *PET Imaging Centre Facility, St Thomas' Hospital, London SE1 7EH*
4. *Department of Molecular imaging, Sidra Medicine, Doha, Qatar*

Introduction:
Although the intranasal (IN) route has been frequently used for drug delivery to the brain[1], it has not yet been exploited for brain PET imaging. In this study we aimed to establish whether or not the IN route is a viable option for radiotracer delivery in PET imaging. The development of clinically useful tracers for PET imaging is enormously challenging and expensive. If the intranasal pathway is a viable option, it extends the PET imaging field by increasing the number of tracers available for human use. This study was designed to evaluate the pharmacokinetics and the radiation exposure expected using two different ^{18}F-labelled radiotracers, [^{18}F]FDG and [^{18}F]Fallypride via the intranasal route.

Methods:
Male, Sprague-Dawley rats were anaesthetised, and arterial and venous cannulas were surgically placed in the femoral artery and vein, respectively. Rats were dosed with either [^{18}F]FDG or [^{18}F]Fallypride via the IN or the intravenous (IV) administration route. Arterial blood samples were collected at different time intervals, centrifuged to extract plasma and gamma counted. In case of [^{18}F]Fallypride, the plasma samples were further processed to separate the parent fraction from metabolites. Image acquisition was carried out using a BioScan nanoPET-CT^{Plus} scanner and images were analysed using using VivoQuant 2.0 software and PMOD version 3.7. Standardised uptake values (SUV) (g/cc) was calculated by dividing the image derived concentration with the ratio of the injected dose to the body weight.

Results:
Measurable uptake in brain through IN administration
In both cases [^{18}F]FDG and [^{18}F]Fallypride, we obtained quantifiable images through the IN route.

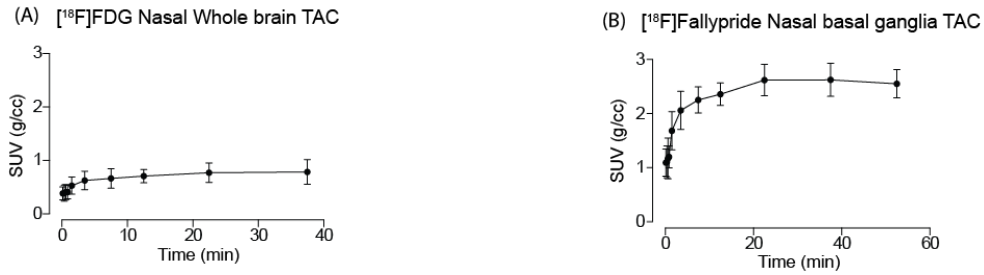

Figure 1. SUV for intranasally administered [^{18}F]FDG (A) and [^{18}F]Fallypride (B)

In case of [^{18}F]FDG we do not see a comparable uptake into the whole brain via the IN route. Interestingly though, the olfactory bulb region shows a much higher radiotracer uptake compared to the rest of the brain. For [^{18}F]Fallypride the uptake in the basal ganglia for IN administration was comparable to IV administration, However, the highest uptake was still observed in the olfactory region.

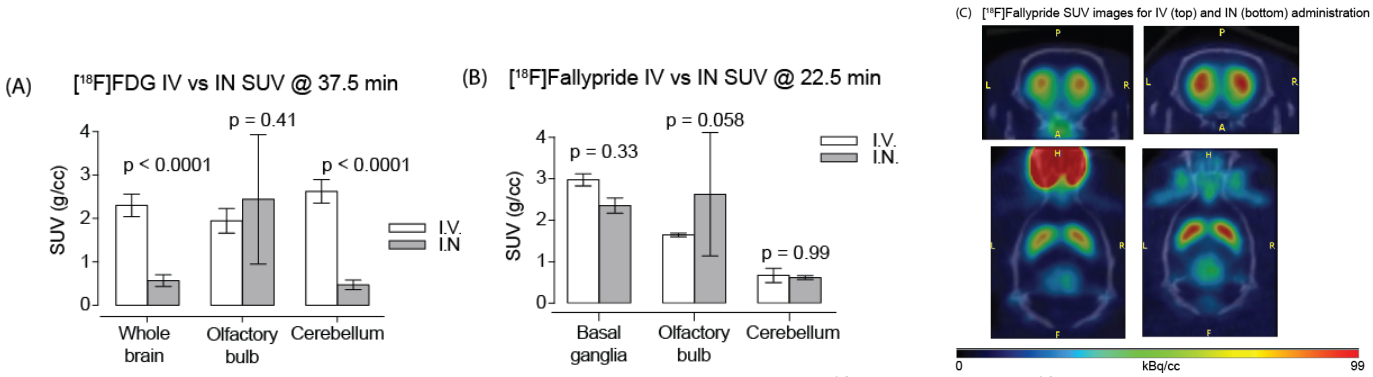

Figure 2. SUV comparisons for three brain regions for [^{18}F]FDG (A), [^{18}F]Fallypride (B). SUV images for IN and IV [^{18}F]Fallypride (C).

Ratio [tissue] : [plasma] to show comparison between different brain regions

In both cases, the only region that showed higher fractional uptake was the olfactory bulb ($p<0.0001$ for both [^{18}F]FDG and [^{18}F]Fallypride). No other significant differences were observed between any other brain regions.

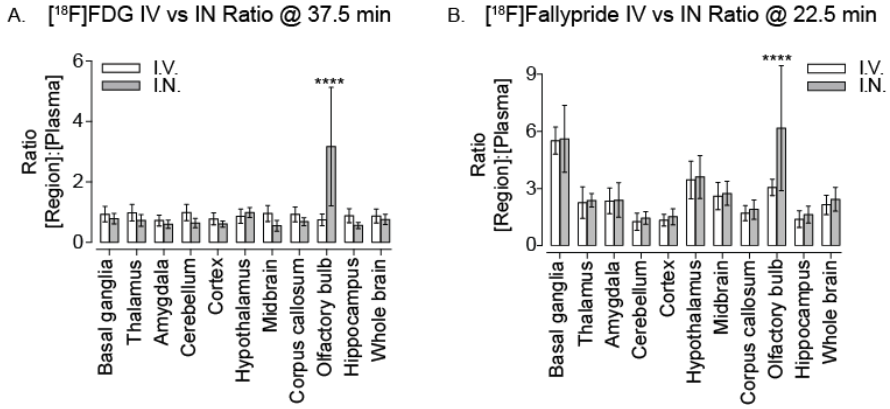

Figure 3. Comparison of IV and IN [Tissue]: [Plasma] ratios for [^{18}F]FDG (A) and [^{18}F]Fallypride (B)

Conclusion:

Based on the results, it appears that the IN pathway would not be suitable for quantitative PET imaging. Even though the images are quantifiable, it appears that in both cases, [^{18}F]FDG and [^{18}F]Fallypride show a higher uptake only in the olfactory region for IN administration, which suggests that the radiotracer moves into the olfactory bulb, but then does not progress further into other brain regions. Additionally, as the nasal cavity has a small surface area, dosimetry limitations and higher variability limit its utility. Therefore, we conclude that the IN route of administration for radiotracers is not a viable route for PET imaging.

Acknowledgments

This work was funded by Medical Research Council (MRC, MR/K022733/1) and an Independent Researcher award to Dr Singh (RIC, King's College, London).

References

1. Lochhead, J. J. & Thorne, R. G. *Advanced Drug Delivery Reviews* **64,** 614–628 (2012).

OP33
Prediction of the human whole-brain transcriptome for integrative analysis in brain imaging

Gregor Gryglewski[1], René Seiger[1], Gregory Miles James[1], Godber Mathis Godbersen[1], Arkadiusz Komorowski[1], Jakob Unterholzner[1], Paul Michenthaler[1], Andreas Hahn[1], Wolfgang Wadsak[2,3], Markus Mitterhauser[2,4], Siegfried Kasper[1], Rupert Lanzenberger[1]

1 Department of Psychiatry and Psychotherapy, Medical University of Vienna, Austria
2 Department of Biomedical Imaging and Image-guided Therapy, Division of Nuclear Medicine, Medical University of Vienna
3 Center for Biomarker Research in Medicine (CBmed), Graz, Austria
4 Ludwig Boltzmann Institute Applied Diagnostics, Vienna, Austria

Introduction:
The study of mRNA expression in the cerebral cortex provides novel insights into brain function. The Allen Human Brain Atlas (AHBA) provides extensive post-mortem mRNA microarray data of the human brain transcriptome [1]. However, the abundance of different genes, probes of varying sensitivity and the fact that a different sampling scheme was applied to each brain hamper the integration of this data in multimodal analysis of imaging results. We developed a method to predict mRNA expression on the entire surface of the cerebral cortex for each gene. The models of spatial dependence of gene expression devised for this end provide further insight on the nature of cerebral gene expression.

Materials & Methods:
MRI and microarray data from the AHBA website were downloaded. Cortical surface reconstruction was carried out in FreeSurfer 5.1. mRNA samples from each of the 6 post-mortem brains were registered to the fsaverage surface [2]. 18 686 genes with signal significantly different from background and associated with Entrez ID were processed separately. Microarray probes associated with each gene were averaged and excluded step-wise if they were found to negatively affect relative structured variability (RSV) of expression. RSV is a measure of spatial dependence derived from variogram modelling and expresses the percentage of the variance in the difference in expression between locations that can be expressed as a function of their distance. Gaussian process regression was used to calculate best linear unbiased estimates of gene expression for each point on the cortical surface in R using the gstat package [3]. Leave-one-out validation was performed to obtain correlation of predicted and observed data.
For the serotonin 1A receptor, surface-based quantification of binding potentials (BP_{ND}) using multilinear reference tissue modeling was carried out on PET data obtained using the specific tracer [*carbonyl*-^{11}C]WAY-100635 in 30 healthy subjects [4,5]. Predicted comprehensive *HTR1A* gene expression and discrete samples were correlated with BP_{ND} in surface space.

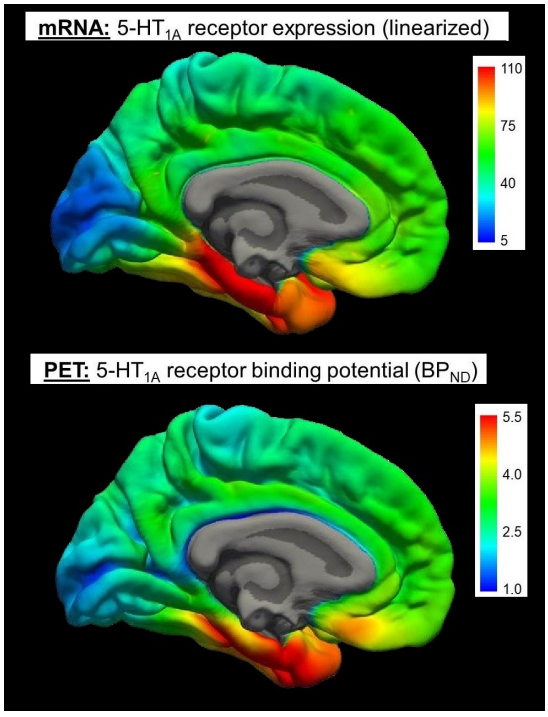

Figure 1: Top: Predicted expression of *HTR1A* gene on the surface of the left cerebral hemisphere, medial view. mRNA data was linearized for display purposes. Bottom: 5-HT_{1A} BP_{ND} after surface-based quantification using MRTM.

Results:
816 genes had a high RSV of >50% indicating high spatial dependence of their expression on the cortical surface. There was a strong relationship (r=0.91) between RSV and validity of prediction (based on Pearson's correlation coefficient in leave-one-out analysis). Bias indicated in leave-one-out analysis was minimal (±0.016 log2 intensity). Correlation of *HTR1A* expression with BP_{ND} was ρ=0.55 (Spearman's correlation coefficient) for discrete samples and ρ=0.72 for predicted data.

Discussion:
Prediction of comprehensive mRNA expression data allows for direct integration of transcriptome data in analysis of imaging data. Furthermore, intuitive viewing of these results may aid hypothesis generation for research and development in psychopharmacology. The RSV metric obtained from spatial modeling constitutes a rationale for the decision whether or not a process exhibits a robust topological pattern.

Acknowledgements:
G. Gryglewski is recipient of a DOC Fellowship of the Austrian Academy of Sciences at the Department of Psychiatry and Psychotherapy, Medical University of Vienna.

References
[1] Hawrylycz MJ, Lein ES, Guillozet-Bongaarts AL et al. [2012] Nature 489: 391–399
[2] Fischl B, Sereno MI, Tootell RB et al. [1999] Hum. Brain Mapp. 8: 272-284
[3] Pebesma EJ, Wesseling CG [1998] Comp. Geosci. 24: 17–31
[4] Ichise M, Liow JS, Lu JQ et al. [2003] J. Cereb. Blood Flow Metab. 23: 1096–1112
[5] Greve DN, Svarer C, Fisher PM et al. [2014] Neuroimage 92: 225–236

OP34:
A methodology study to assess binding kinetics and test-retest repeatability of the PDE4B PET radioligand [^{18}F]PF-06445974 in healthy subjects

Ryosuke Arakawa[1], Per Stenkrona[1], Andrea Varrone[1], Akihiro Takano[1], Sangram Nag[1], Kevin P. Maresca[2], Thomas A. Chappie[2], Zoe Hughes[2], Ye Tan[2], Lei Zhang[2], Christopher Schmidt[2], Timothy McCarthy[2], Christer Halldin[1]

1. Department of Clinical Neuroscience, Centre for Psychiatry Research, Karolinska Institutet and Stockholm County Council, Stockholm SWEDEN
2. Worldwide Research & Development, Pfizer Inc., Cambridge, MA, USA

Introduction:
[^{18}F]PF-06445974 is a promising PET radioligand for the PDE4B enzyme in the human brain. Potential clinical application of this developing PET ligand could include measurements of the target engagement/occupancy of therapeutic PDE4B inhibitors and PET studies including potential patient populations. Thus, it is important to investigate [^{18}F]PF-06445974 quantitatively, and to evaluate its test-retest repeatability. The aim of this study is to evaluate several kinetic models and the test-retest repeatability of [^{18}F]PF-06445974 in healthy human subjects.

Materials & Methods:
Five healthy male subjects were included in the study. PET measurements were performed with the ECAT EXACT HR (Siemens) system. The radioligand [^{18}F] PF-06445974 was administered intravenously as a bolus injection and the PET measurement lasted up to 123 minutes for the first two subjects, and 234 minutes including two breaks for the remaining three subjects. The radioactivities in whole blood and plasma, and the amount of unchanged [^{18}F]PF-06445974 in plasma of arterial blood were also measured. Regions of interest (ROI) were defined using the Anatomical Automatic Labeling (AAL) template. As the main outcome measure, the total distribution volume (VT) defined as K1/k2 by one tissue compartment (1TC) model, (K1/k2)×(k3/k4+1) by two tissue compartment (2TC) model and Logan graphical analysis (GA) was calculated with metabolite corrected plasma radioactivity as the input function. The test-retest repeatability of VT was expressed by the difference between the first and second PET measurements relative to the mean of the two values. To evaluate the time stability of both VT and test-retest repeatability with the duration of PET measurements, the PET data was truncated down to 63 minutes from the full length of measurements.

Results:
The injected radioactivity (n=10) of [^{18}F]PF-06445974 was 191.6 ± 26.5 (158 – 226) MBq. The molar activity at the time of injection was 35.6 ± 15.5 (22 – 73) GBq/μmol, and the injected mass was 2.12 ± 0.77 (1.02 – 3.46) μg. The peak uptake was 2-3 %ID (1-1.5 SUV) at around 20 minutes. The washout was relatively slow, and that was the reason for extending the scan duration. The thalamus and putamen showed high uptakes, and hippocampus showed low uptake. VTs were high for the thalamus and putamen, and low in hippocampus (Table 1). The VT values determined by 1TC were slightly lower than those employing 2TC. The average of absolute test-retest repeatability of VT showed 9.4-19.9% in 2TC and 6.6-23.0% in GA. Even though 234 minutes data was used, VT did not show a plateau, continuing to rise throughout the measurement. The repeatability of VT truncated to 123 minutes was better than that of 234 minutes data, with 63 minutes truncated data demonstrating instability.

Discussion/Conclusion:
Moderate repeatability of VT, below 20%, was observed using 2TC. Shorter acquisition data such as 2 hours showed better repeatability, but also underestimation of VT. [^{18}F]PF-

06445974 is a good PET radioligand for measurement of PDE4B activity in human brain, although careful interpretation of calculated VT is needed (e.g. the study of target occupancy).

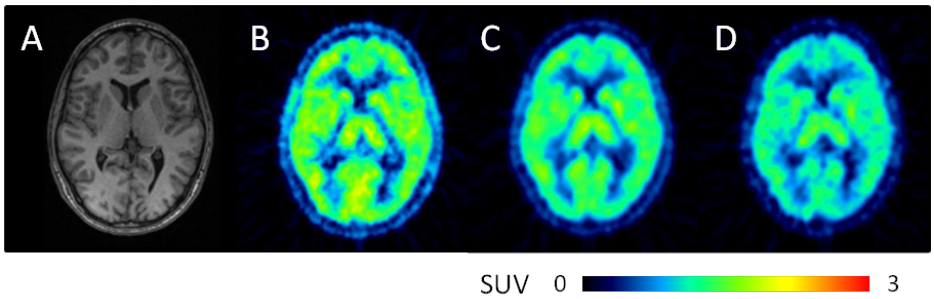

Figure 1. Representative images of A) MRI, B) 0-63min, C) 90-144min, and D) 180-234min of [^{18}F]PF-06445974

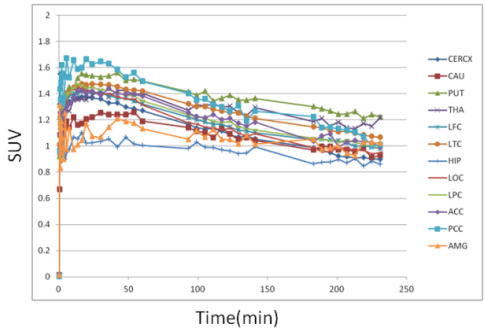

Figure 2. Regional TACs of [^{18}F]PF-06445974 (same measurement of Figure 1)

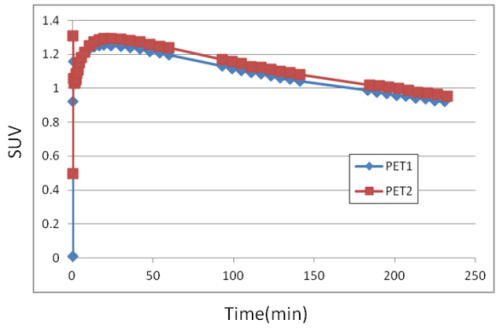

Figure 3. Whole brain TACs of test and retest measurements (same subject of Figure 1)

Table 1. VT values (Mean ±SD), absolute test-retest and differences between the 1TC and 2TC models in three brain regions

	1TC			2TC			GA			2TC-1TC PET 1
	PET 1	PET 2	TRT (%)	PET 1	PET 2	TRT (%)	PET 1	PET 2	TRT (%)	Mean(CI 95%)
THA	12.7±2.5	13.4±3.0	11.1±3.8	16.6±2.6	16.5±3.1	20.9±8.0	17.2±2.5	17.4±2.9	16.5±9.5	3.9(2.0,5.8)
PUT	12.5±2.3	13.1±2.7	7.6±6.4	16.8±0.9	17.8±2.3	7.9±6.7	15.6±2.2	16.8±3.7	15.9±11.7	4.4(3.0,5.7)
HIP	8.8±2.1	9.5±2.8	11.9±7.1	12.2±3.2	12.4±3.0	19.1±15.3	13.0±2.7	13.4±3.4	15.7±11.4	3.4(1.0,5.8)

Acknowledgements:
The study was supported by Pfizer Inc.

References

Zhang L, Chen L, Beck EM, et al. [2017], J Med Chem, 60(20):8538-8551.

OP35:
Clinical Correlates of Complementary Spatial Patterns in [11]C-DTBZ, [11]C-MP, [11]C-RAC, and [11]C-DASB PET Images Revealed by Multiset Canonical Correlation Analysis in Parkinson's Disease

Jessie Fanglu Fu[1], Ivan S Klyuzhin[3], Elham Shahinfard[2], Jess McKenzie[2], Nicole Neilson[2], Tobias R Baumeiser[2], Siobhan McCormick[2], Ju-Chieh Kevin Cheng[1,2], Andre C Felicio[2], Martin J McKeown[2], A Jon Stoessl[2], Vesna Sossi[1]

1. *Department of Physics and Astronomy, University of British Columbia, Vancouver, BC, Canada*
2. *Pacific Parkinson's Research Center, Vancouver, BC, Canada*
3. *Department of Medicine, University of British Columbia, Vancouver, BC, Canada*

Introduction:
In Parkinson's disease (PD), while dopaminergic deficit plays a major role in motor manifestations, serotonergic alterations may contribute to non-motor symptoms. Additionally, interaction between the serotonergic and dopaminergic systems may lead to abnormal dopamine release, a major contributor to treatment-induced motor complications. Here we used a joint multimodal analysis to explore whether complementary dopaminergic, serotonergic and dopamine release spatial patterns can be identified in PD, and their relationships with motor and non-motor clinical measures.

Methods and Materials:
14 early PD subjects (disease duration 3.3±2.8 years) were scanned with: a) [11]C-DTBZ (a vesicular monoamine transporter type 2 marker) and [11]C-MP (a dopamine transporter marker) to assess dopaminergic integrity; b) [11]C-DASB to examine serotonergic integrity; c) [11]C-RAC (postsynaptic D2 receptor marker), one scan at baseline and another after levodopa administration to estimate dopamine release. All subjects were scanned on the High Resolution Research Tomograph (HRRT) and underwent an additional anatomical MRI scan. Non-displaceable binding potential (BP_{ND}) values were calculated with either Logan plot [1] in 10 striatal ROIs (caudate, putamen and ventral striatum) for DTBZ, MP and RAC; or the simplified reference tissue model [2] for DASB to estimate BP_{ND} in 43 ROIs. The reference regions were the occipital cortex for DTBZ and MP and cerebellum for RAC and DASB. To extract the most highly correlated *subject profiles* (canonical variates) among different datasets, multiset canonical correlation analysis (MCCA) [3] was applied to BP_{ND} normalized to age-matched controls (DTBZ, MP and RAC), percentage dopamine release expressed as $\left(^{RAC\ BP_{ND}\ baseline - RAC\ BP_{ND}\ intervention}/_{RAC\ BP_{ND}\ baseline} * 100\right)$, DASB BP_{ND} values, and clinical measures (disease duration, UPDRS in the off-drug state, Montreal Cognitive Assessment (MoCA), Beck Depression Inventory (BDI) and The State-Trait Anxiety Inventory (STAI) scores). MCCA loadings (*ROI weights*) were used to visualize the spatial patterns for each tracer. Permutation tests and leave-one-out cross validation were used to examine the robustness of the obtained patterns.

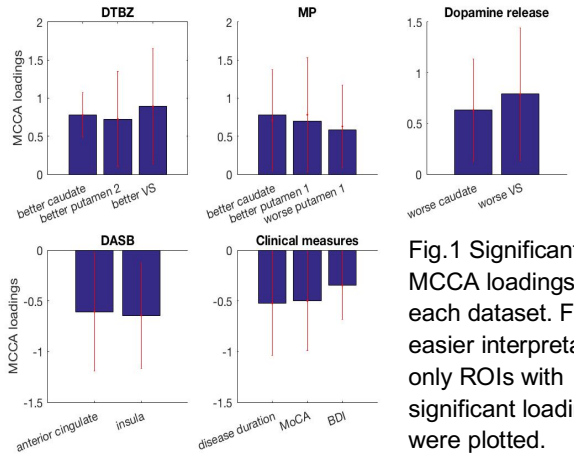

Fig.1 Significant MCCA loadings for each dataset. For easier interpretation, only ROIs with significant loadings were plotted.

Results:

Using a permutation test, the first canonical variates (subject profiles) were found to be significantly correlated among DTBZ, MP, baseline RAC, dopamine release, DASB and clinical measures, with an average correlation coefficient 0.78±0.08 (*p*-value = 0.016). These correlated subject profiles were defined by significant positive MCCA loadings in the less affected (better) caudate, better medial putamen and better ventral striatum for DTBZ binding; positive loadings in the better caudate and dorsal putamen for MP binding; positive loadings in the more affected (worse) caudate and worse ventral striatum for dopamine release estimates; and negative loadings in anterior cingulate and insula for DASB binding [4]; and negative loadings for disease duration, MoCA and BDI (**Fig1)**. **Fig2** shows explicitly the correlation strength (not sign) between subject profiles of the tracer spatial patterns and clinical measure patterns.

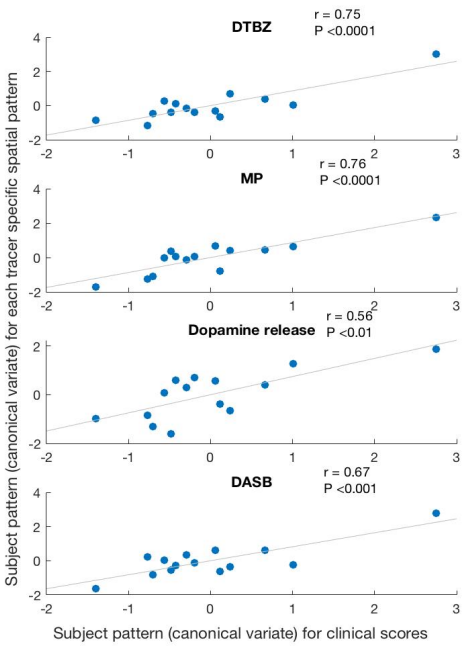

Fig.2 Subject profiles of each tracer patterns correlated with the subject profile of clinical measures pattern. Subject profiles contain subject-specific expression of the tracer-specific spatial or clinical patterns. Only correlation strength (not sign) is presented here.

Discussion/Conclusion:

Joint multimodal analysis demonstrated that deterministic spatial patterns of involving the dopaminergic binding, dopamine release and serotonergic binding can be identified in early PD subjects. Preliminary interpretation of the results may indicate that disease duration is negatively correlated with dopaminergic integrity despite the relatively narrow range of disease duration; higher dopamine release in the more affected caudate and ventral striatum, and lower DASB binding in the anterior cingulate and insula (indicative of impaired serotonergic function) closer to the time of disease onset may contribute to the worse cognitive performance and depression scores in early PD, even with preserved dopaminergic functions and less severe non-motor symptoms (**Fig1**). This observation might reflect the interaction between the serotonergic and dopaminergic systems, which may be associated to non-motor symptoms of PD; it is more prominent at early disease and decreases as all systems become significantly affected. Full analysis leading to a robust interpretation of the data is still undergoing. In addition, follow-up clinical studies on these subjects are now being performed to examine this pattern in a longitudinal context. While these results are preliminary, joint multimodal analysis appears to be a promising method to obtain new insights into the interactions between different neurotransmitter systems.

Acknowledgement:

This work is supported by Canadian Institute of Health Research.

References:

1. Logan, J., Fowler, J.S., Volkow, N.D., Wolf, A.P., Dewey, S.L., Schlyer, D.J., MacGregor, R.R., Hitzemann, R., Bendriem, B., Gatley, S.J., others, [1990]. Graphical Analysis of Reversible Radioligand Binding from Time—Activity Measurements Applied to [N-11C-Methyl]-(-)-Cocaine PET Studies in Human Subjects. J. Cereb. Blood Flow Metab. 10, 740–747.

2. Gunn RN, Lammertsma AA, Hume SP, Cunningham VJ: Parametric imaging of ligand-receptor binding in PET using a simplified reference region model. Neuroimage [1997], 6(4):279-287.
3. Yi-Ou Li, Adali, T., Wei Wang, Calhoun, V.D., [2009]. Joint Blind Source Separation by Multiset Canonical Correlation Analysis. IEEE Trans. Signal Process. 57, 3918–3929.
4. Christopher, L., Koshimori, Y., Lang, A.E., Criaud, M., Strafella, A.P., [2014]. Uncovering the role of the insula in non-motor symptoms of Parkinson's disease. Brain.

OP36
GABAergic Dysfunction and Socio-communicative Deficits in Adults with Autism Spectrum Disorder

Lawrence K Fung, Ryan Flores, Rachel Schuck, Leila Chew, Meng Gu, Daniel Spielman, Frederick Chin, Antonio Hardan
Stanford University, Stanford, California, USA.

Introduction:
Dysfunction of the GABA neurotransmission system is one of the most accepted pathophysiologic mechanisms for autism spectrum disorder (ASD). New imaging technologies allow for *in vivo* determination of GABA levels by magnetic resonance spectroscopy (MRS) and determination of $GABA_A$ receptor densities by [^{18}F]flumazenil-positron emission tomography ([^{18}F]FMZ-PET). Due to the dynamic nature of neurotransmission systems in general, studying both $GABA_A$ receptor densities and GABA levels at the same time in individuals with ASD is highly desirable. In the present investigation, we report the *first* such attempt to simultaneously measure GABA levels and $GABA_A$ receptor densities in the brains of individuals with ASD using a state-of-the-art hybrid PET-MR neuroimaging system. The goal of this study is to examine the effects of $GABA_A$ receptor densities and GABA levels in the left dorsolateral prefrontal cortex (DLPFC), thalami, and cerebellum on socio-communicative abilities.

Materials and Methods:
Participants. Individuals with ASD and typically developing (TD) controls aged 18 to 55 years. *Image acquisition.* Subjects were scanned on GE SIGNA PET/MR (Waukesha, WI). PET data were acquired in list mode (0-60min), dynamically reconstructed into 27 time-frames (12×15s, 3×1min, 3×3min, 9×5min). For the MRS measurement of GABA, the Improved MEGA-SPECIAL[1] was performed on the left dorsolateral prefrontal cortex (DLPFC) and bilateral thalami. *Neuropsychological testing.* Stanford Binet, 5th edition (SB5), Social Responsiveness Scale (SRS-2), Autism Quotient (AQ), Autism Diagnostic Observation Schedule (ADOS), Autism Diagnostic Inventory – Revised (ADIR), Sensory Profile Questionnaire (SPQ), and Berkeley Expressivity Questionnaire (BEQ). *Image and data analysis*. The dynamic PET and structural MR data were normalized to MNI (Montreal Neurological Institute) space (PMOD 3.8, Switzerland). Time-activity curves were extracted using pre-defined volumes-of-interest (VOIs) based on the Hammers atlas. A reference tissue model (MRTM0) was used to calculate binding potentials (BP_{ND}) with pons as the reference region. The Improved MEGA-SPECIAL edited spectrum was obtained by subtracting the editing OFF spectrum from the editing ON spectrum. GABA levels were estimated from the integrated 3ppm peak area in the edited spectrum divided by the sum of the creatine (Cr) and phosphocreatine (PCr) peak areas and the water peak area. Student t tests were performed to determine group differences in GABA/(Cr+PCr) and BP_{ND}'s in various VOIs (thalami, left DLPFC, cerebellum) between ASD and TD groups. Correlation analyses were conducted to examine relationships between neuroimaging markers and behavioral measures.

Table 1. Demographic and behavioral measures.

	ASD	TD
Age (yr)	27.0±8.7	27.4±7.4
Male/Female	16M/9F	17M/9F
FSIQ	103±18	113±12
AQ	30.8±9.1	17.9±8.6
RAADS-total	128±35	50±42
SRS-total	68.1±9.8	51.0±9.8

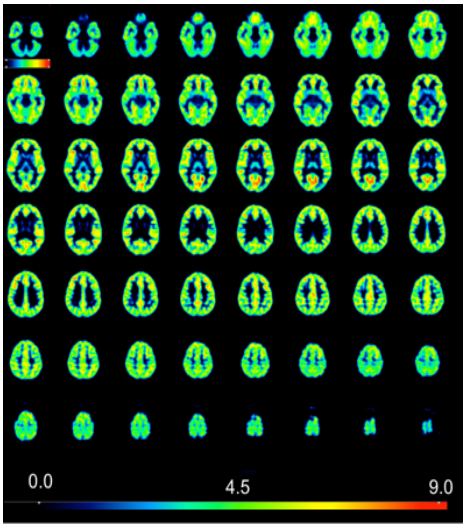

Figure 1. Representative [^{18}F]FMZ-PET images in a male participant.

Results: Twenty-five adults with ASD and 26 healthy volunteers were scanned. Behavioral measures are summarized in Table 1. The highest uptake of [^{18}F]FMZ was observed in the neocortical regions and limbic system, intermediate in the cerebellum, thalami and basal ganglia, and low uptake in the brainstem (Figure 1). Comparing the ASD and TD groups, the [^{18}F]FMZ BP_{ND}'s of all VOIs were found to be statistically indistinguishable. However, the left DLPFC GABA/water ratio for ASD participants was 31% higher than that for TD participants (p=.039). When only male participants were included, this group difference became larger. Both GABA/(Cr+PCr) and GABA/water in the left DLPFC of the ASD group were higher than the TD group by 61% (p=.030) and 66% (p=.007), respectively. In contrast, the GABA/(Cr+PCr) and GABA/water in the thalami of male ASD participants were lower than the TD group by 16% (p=.015) and 14% (p=.039), respectively. Correlation analyses revealed significant relationships between social interaction measures and [^{18}F]FMZ BP_{ND} values in the cerebellum in both ASD and TD groups (Table 2). In the ASD group, higher cerebellar BP_{ND} was associated with more deficits in social cognition and social motivation. On the contrary, in the TD group, higher cerebellar BP_{ND} corresponded to better and broader socio-communicative function. ^{1}H-MRS data revealed that GABA levels in the thalami correlated positively with social cognition, shared enjoyment and RRBs in the ASD group but not the TD group. Furthermore, GABA levels in the left DLPFC correlated negatively with overall ASD symptoms (AQ) in the ASD group. In contrast, GABA levels in the thalami and left DLPFC of the TD were found to correlate negatively with measures of social phobia and social cognition, respectively.

Discussion/Conclusion: This is the first report of GABAergic dysfunction in the thalamo-cortico-cerebellar network of high-functioning adults with ASD. Compared to TD males, ASD males displayed higher GABA levels in the left DLPFC but lower levels in the thalami. The correlations between the PET-MRS data and social interaction measures support that the GABAergic system is associated with social interactions, but this relationship in the ASD group appears to be distinctly different from the TD group.

Acknowledgements: This study was supported by the NIMH (K08MH111750; PI: Fung), AACAP (Pilot Research Award; PI: Fung), Mosbacher Family Fund for Autism Research (PI: Fung), and GE Healthcare. We thank Harsh Gandhi, and Dawn Holley for technical assistance.

Table 2. Correlations between GABAergic function & social interaction measures.		
	ASD	**TD**
$GABA_A$ Receptor Densities / $[^{18}F]$FMZ BP_{ND}		
Thalami	No correlations.	No correlations.
Left MFG	No correlations.	No correlations.
Cerebellum	AQ (R=.482, p=.015) SRS-SC (R=.424, p=.035) SRS-SM (R=.400, p=.048)	SRS-SA (R=-.414, p=.035) SRS-SC (R=-.435, p=.026) SRS-SMT (R=-.414, p=.036) SRS-RRB (R=-.548, p=.004) SRS-SCI (R=-.442, p=.024) SRS-Total (R=-.468, p=.016)
GABA/(Cr+PCr) or GABA/water		
Thalami	SRS-SC (R=-.545, p=.029)^{Cr} SRS-RRB (R=.558, p=.025)^{Cr} (R=.551, p=.027)^{W}	SPAI-Social Phobia (R=-.536, p=.032)
Left DLPFC	AQ (R=-.569, p=.027)^{W}	SRS-SC (R=-.595, p=.019)
Abbreviations: CI, circumscribed interest; Cr, creatine; FSIQ, full scale intelligence quotient; L, language; MFG, middle frontal gyrus; NVIQ, non-verbal intelligence quotient; RRB, Restricted and Repetitive Behavior; SA, Social Awareness; SC, Social Cognition; SCI, Social Communication Impairment; SM, sensorimotor; SMT, social motivation; SR, Social Relatedness; SS, Sensory Seeking; VIQ, verbal intelligence quotient; W, water.		

References:

1. Gu M, Hurd R, Noeske R, Baltusis L, Hancock R, Sacchet MD, Gotlib IH, Chin FT, Spielman DM. GABA editing with macromolecule suppression using an improved MEGA-SPECIAL sequence. *Magn Reson Med.* 2018;79(1):41-47.

OP37
Epigenetic dysregulation in schizophrenia revealed by human histone deacetylase PET imaging and stem cell-derived neuronal modeling

T.M. Gilbert[1], N.R. Zürcher[1], W.-N. Zhao[2,3], P.S. Chindavong[2,3], C.J. Wu[1], A. Bhanot[1], B.G. Hightower[1], M.M. Riley[1], M. Kim[1], D.S. Albrecht[1], H.-Y. Wey[1], F.A. Schroeder[1], Anais Rodriguez-Thompson[1], T.M. Morin[1], K.L. Hart[3], A. Pellegrini[3], C. Wang[1], S.M. Stufflebeam[1], D.J. Holt[1,2], M.L. Loggia[1], R.H. Perlis[2-4], H.E. Brown[2], J.L. Roffman[1,2], S.J. Haggarty[2,3], J.M. Hooker[1]*

[1]Athinoula A. Martinos Center for Biomedical Imaging, Department of Radiology, [2]Department of Psychiatry, [3]Center for Genomic Medicine at Massachusetts General Hospital, Harvard Medical School, Charlestown, MA 02129, USA.[4]Stanley Center for Psychiatric Research, Broad Institute of MIT and Harvard, Cambridge, MA 02142, USA.

Introduction:
Epigenetic mechanisms have been associated with cognitive function through postmortem human and preclinical studies, but no direct associations have been made in living humans, because until recently, epigenetic neuroimaging tools did not exist. Of the epigenetic enzymes that can profoundly influence gene transcription and behavior, histone deacetylases (HDACs) have emerged as potential targets for therapeutic interventions. Here using [^{11}C]Martinostat, an HDAC radiotracer, we measure relative [^{11}C]Martinostat uptake across the cognitively impaired brain, comparing subjects with schizophrenia (SCZ) to healthy controls. To interrogate the underlying biochemical basis of [^{11}C]Martinostat signal and better understand the role of HDACs in cognition, we generated stem cell-derived neuronal models of subjects who were imaged with [^{11}C]Martinostat.

Materials & Methods:
Subjects with SCZ (n=14, ages 22-65) were matched with controls (n=14, ages 23-65) on the basis of age, sex, smoking status, and parental socioeconomic status. Subjects with SCZ were administered the PANSS interview and all subjects underwent the MATRICS battery to assess symptom severity and cognitive function, respectively. Images were acquired on a 3T Siemens TIM Trio with a BrainPET insert. A T1-MPRAGE sequence was collected and reconstructed with FreeSurfer v6.0. Dynamic PET image acquisition was initiated with IV bolus injection of ~185 MBq [^{11}C]Martinostat (controls 185.7± 10.7; SCZ 186.5 ± 10.4; P= 0.89) and binned into 6, 5min frames spanning 60-90min post-injection. PET data were reconstructed using the 3D OP-OSEM algorithm in the units of SUV, motion-corrected, and processed with FreeSurfer and FSL. SUV images were intensity normalized to a whole-brain mean of 1 ($SUVR_{60\text{-}90min}$) and spatially smoothed at 8mm. *A priori* ROI analysis of the dorsolateral prefrontal cortex (DLPFC) and whole-brain voxel-wise analysis using FSL's FEAT with OLS mixed-effects modeling (Z> 2.3, $P_{cluster}$< 0.05) were performed. Induced pluripotent stem cells (iPSCs) were generated from subjects imaged with [^{11}C]Martinostat (control n=1; SCZ n=2), differentiated into post-mitotic neurons (n=3 replicates per subject), and treated for 24 hrs with a pharmacologic dose of Martinostat (2.5μM). Protein levels of an HDAC substrate (histone H3 lysine 9 acetylation: H3K9ac) and mRNA levels of an HDAC-regulated gene associated with SCZ-risk (early growth factor 1: *EGR1*) were measured by western blotting and qPCR, respectively.

Results:
Subjects with SCZ had moderate symptom severity (PANSS total 71±21) and scored significantly lower than controls on MATRICS subdomains including working memory (controls 47.4±12; SCZ 37.5±12; *P= 0.035). We previously determined that postmortem *HDAC2* mRNA levels were significantly decreased in the DLPFC of donors with SCZ compared to controls. In accordance with our postmortem data, $SUVR_{60\text{-}90min}$ in the DLPFC

was significantly decreased in subjects with SCZ (Fig.1A/B). $SUVR_{60\text{-}90min}$ in the DLPFC positively correlated with cognitive performance scores across groups, including social cognition (r=0.53, ***P*=0.0023). Cortical thickness measurements within the DLPFC showed no significant differences between groups (controls 2.34±0.03mm; SCZ 2.27±0.04mm; *P*= 0.18). Exploratory voxel-wise analysis revealed that $SUVR_{60\text{-}90min}$ was significantly decreased in the DLPFC, dorsomedial prefrontal cortex, and orbitofrontal gyrus, and significantly increased in the fusiform gyrus and cerebellum of subjects with SCZ compared to controls (Fig.1C). H3K9ac and *EGR1* levels were significantly increased by Martinostat treatment in all subject lines, demonstrating HDAC engagement and downstream modulation of a gene important for cognition in a model of [^{11}C]Martinostat-imaged subjects (Fig.1D).

Discussion/Conclusion:

Our study provides evidence of neuroepigenetic dysregulation in SCZ through *in vivo* neuroimaging and stem cell-derived neuronal modeling, and sets the foundation to use [^{11}C]Martinostat PET to study the role of HDACs in human cognition.

Acknowledgements:

This research received funding from the Martinos Center, Brain and Behavior Foundation, Massachusetts General Hospital, and the Bluefield Project to Cure FTD.

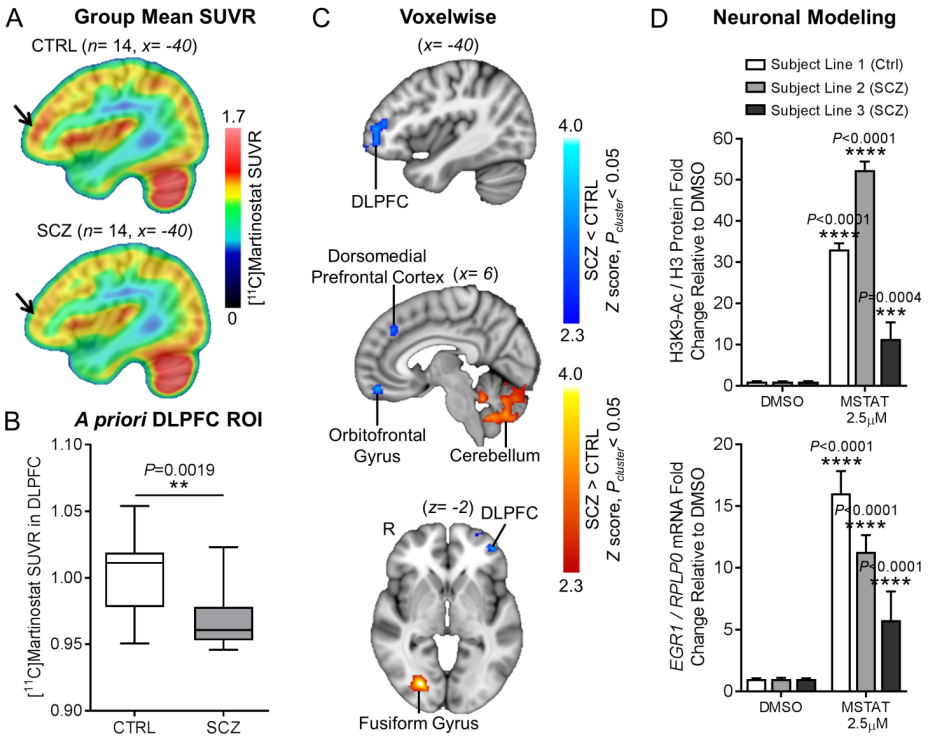

Fig. 1 (A) [^{11}C]Martinostat $SUVR_{60\text{-}90min}$ mean images for *n*=14 subjects with SCZ and *n*=14 matched controls are overlaid onto the MNI template. (B) Boxplots (median; min/max) depict $SUVR_{60\text{-}90min}$ extracted from the *a priori* DLPFC ROI. (C) *Z* score maps are overlaid onto the MNI template. Blue represents regions decreased and red represents regions increased, in subjects with SCZ compared to controls. (D) Neurons derived from a control (line 1) and subjects with SCZ (lines 2 and 3) were treated with unlabeled Martinostat (*n*=3 replicates per line). Levels of H3K9ac protein and *EGR1* mRNA were compared between treated and untreated cells (mean ± *SD*).

OP38

Cannabinoid 1 receptor dysregulation in first episode psychosis: a positron emission tomography study

FR Borgan [1, 2, 3,] M Veronese [2], T Reis Marques [3], T Dahoun[3], M Rogdaki.[1,2,3], F Turkheimer[2], OD Howes [1, 3]

[1] Psychosis Studies Department, Institute of Psychiatry, Psychology and Neuroscience, King's College London, London, England
[2]Centre for Neuroimaging Sciences, Institute of Psychiatry, Psychology and Neuroscience, King's College London, London, England
[3]MRC London Institute of Medical Sciences, Faculty of Medicine, Imperial College London, England

Introduction:
There has been a recent surge of interest in investigating the cannabinoid 1 receptor in psychosis based on evidence that cannabis, a cannabinoid 1 receptor agonist (1), increases the relative risk of onset (2) and relapse of psychosis (3). In this context, we aimed to investigate the cannabinoid 1 receptor in first episode psychosis, for the first time as far as we're aware.

Method:
Forty volunteers including 20 first episode psychosis patients (17 un-medicated, 3 medicated) and 20 matched healthy volunteers underwent a dynamic positron emission tomography scan using a cannabinoid 1 receptor selective, reversible radiotracer [^{11}C]MePPEP (4) with arterial blood sampling.

Results:
Relative to healthy volunteers, first episode psychosis patients showed a significantly lower volume of distribution (V_T) in the anterior cingulate (Hedge's g=0.8), thalamus (Hedge's g=0.7) and hippocampus (Hedge's g=0.7). Cannabinoid 1 receptor availability (V_T) in the anterior cingulate was positively correlated with WAIS IQ scores (p=0.006).

Conclusion:
We showed evidence of cannabinoid 1 receptor dysregulation in the early stages of psychosis across key neural circuits implicated in cognition. We also showed that cannabinoid 1 receptor availability was linked to cognition. Future studies should investigate whether cannabinoid 1 receptor modulation can ameliorate cognitive impairments in schizophrenia.

Ackowledgments:
METSY EU consortium

References:
1. Laaris N, Good CH, Lupica CR. Δ 9 -tetrahydrocannabinol is a full agonist at CB1 receptors on GABA neuron axon terminals in the hippocampus. [cited 2017 May 27]; Available from: https://www.ncbi.nlm.nih.gov/pmc/articles/PMC2882293/pdf/nihms200194.pdf
2. Arseneault L, Cannon M, Witton J, Murray RM. Causal association between cannabis and psychosis: examination of the evidence. Br J Psychiatry [Internet]. The Royal College of Psychiatrists; 2004 Feb 1 [cited 2017 Sep 27];184(2):110–7. Available from: http://www.ncbi.nlm.nih.gov/pubmed/14754822
3. Schoeler, T., Petros, N., Di Forti, M., Klamerus, E., Foglia, E., Ajnakina, O., Gayer-

Anderson, C., Colizzi, M., Quattrone, D., Behlke, I., Shetty, S., McGuire, P., David, A., Murray, R., Bhattacharyya S. Effects of continuation, frequency, and type of cannabis use on relapse in the first 2 years after onset of psychosis: an observational study. The Lancet Psychiatry [Internet]. Elsevier; 2016 Oct 1 [cited 2017 Sep 27];3(10):947–53. Available from: http://www.sciencedirect.com/science/article/pii/S2215036616301882

4. Yasuno F, Brown AK, Zoghbi SS, Krushinski JH, Chernet E, Tauscher J, et al. The PET radioligand [11C]MePPEP binds reversibly and with high specific signal to cannabinoid CB1 receptors in nonhuman primate brain. Neuropsychopharmacology [Internet]. 2008 Jan [cited 2016 May 31];33(2):259–69. Available from: http://www.ncbi.nlm.nih.gov/pubmed/17392732

OP39
Evaluation of the alpha7 nicotinic acetylcholine receptor inrecent onset of psychosis using [^{18}F]ASEM PET

Jennifer M. Coughlin,[a,b] Yong Du,[b] Jeffrey Crawford,[a] Andrew Horti,[b] David J. Schretlen,[a] Dean F. Wong,[a,b] Akira Sawa,[a] Martin G. Pomper[a,b]

[a]*Department of Psychiatry and Behavioral Sciences,* [b]*Russell H. Morgan Department of Radiology and Radiological Science, Johns Hopkins Medical Institutions, Baltimore, MD, USA.*

Introduction:
Low availability of the α7 nicotinic acetylcholine receptor (α7-nAChR) in the hippocampus of patients with schizophrenia has been suggested from study of postmortem tissue.[1] Recent development of novel medications that aim to amplify signaling through the α7-nAChR failed to show cognitive benefit in patients.[2-4] Receptor densensitization and/or the low availability of the α7-nAChR in the hippocampus in non-affective psychosis (NP) may have contributed to these outcomes, although the latter has yet to be evaluated *in vivo*. Our group developed the radiotracer, [^{18}F]ASEM,[5] for estimating the availability of the α7-nAChR with positron emission tomography (PET) in the human brain.

Materials and Methods:
Eleven patients with recent (within five years) onset of psychosis and 15 well-matched healthy controls (HCs) completed PET with [^{18}F]ASEM. Participants were non-smokers. Patients were grouped into those with NP or affective psychosis (AP). Treatment was restricted to current monotherapy (lithium, atypical antipsychotic). The majority of patients were not taking any medication. Participants also underwent neuropsychological testing and structural neuroimaging. Total distribution volume (V_T) in hippocampus was estimated using Logan analysis with metabolite-corrected arterial input function.[6] V_T from partial volume-corrected images[7,8] was also estimated as a secondary outcome measure.

Results:
Among the 26 participants who completed [^{18}F]ASEM PET, 10 patients and 12 HCs completed neuropsychological testing due to its late addition. Patients with recent onset of NP (N=5) performed worse than those with recent onset of AP (N=5) or Hcs in all six cognitive domains. There was no difference in hippocampal volume between the three cohorts (NP, AP, HC). A one-way ANOVA model with three groups (NP, AP, HC) revealed a significant group effect ($F(2,23)= 8.75$, $P = 0.001$) on [^{18}F]ASEM V_T in hippocampus. Secondary analysis controlling for age did not change the results ($P < 0.005$). A Tukey post hoc test revealed that the [^{18}F]ASEM V_T in hippocampus was significantly lower in NP (12.77 ± 1.10) as compared to HC (17.68 ± 2.34, $P = 0.001$) or AP (16.37 ± 2.73, $P = 0.039$). After partial volume correction, [^{18}F]ASEM V_T in hippocampus remained lower in NP compared to each other cohort (AP, HC).

Discussion:
[^{18}F]ASEM PET is a promising tool for assessing the hypothesized low availability of the α7-nAChR in hippocampus of non-smoker patients with recent onset of NP *in vivo*. Further study of the lower availability of the α7-nAChR in NP versus AP or health, and its relationship to cognitive deficits in psychosis is ongoing.

Acknowledgements:
This work was supported by the Henry N. Wagner, Jr. Endowment (MGP), the Alexander Wilson Schweizer Fellowship (JC), a Johns Hopkins Innovation Award (JC), a Johns Hopkins Doris Duke Early Clinician Investigator Award (JC), and the National Institutes of Health [R01 MH107197 (DFW and AH), Shared Instrument Grants S10RR023623 (DFW), S10RR017219 (DFW)].

References:

1. Freedman R, Hall M, Adler LE, Leonard S. [1995], Biological psychiatry. Evidence in postmortem brain tissue for decreased numbers of hippocampal nicotinic receptors in schizophrenia, 38(1):22-33.
2. Haig GM, Bain EE, Robieson WZ, Baker JD, Othman AA. [2016], The American journal of psychiatry. A Randomized Trial to Assess the Efficacy and Safety of ABT-126, a Selective alpha7 Nicotinic Acetylcholine Receptor Agonist, in the Treatment of Cognitive Impairment in Schizophrenia, 173(8):827-835.
3. Keefe RS, Meltzer HA, Dgetluck N, et al. [2015], Neuropsychopharmacology. Randomized, Double-Blind, Placebo-Controlled Study of Encenicline, an alpha7 Nicotinic Acetylcholine Receptor Agonist, as a Treatment for Cognitive Impairment in Schizophrenia, 40(13):3053-3060.
4. Lieberman JA, Dunbar G, Segreti AC, et al. [2013], Neuropsychopharmacology. A randomized exploratory trial of an alpha-7 nicotinic receptor agonist (TC-5619) for cognitive enhancement in schizophrenia, 38(6):968-975.
5. Horti AG. [2015], Biochemical pharmacology. Development of [^{18}F]ASEM, a specific radiotracer for quantification of the alpha7-nAChR with positron-emission tomography, 97(4):566-575.
6. Coughlin JM, Du Y, Rosenthal HB, et al. [2018], NeuroImage. The distribution of the alpha7 nicotinic acetylcholine receptor in healthy aging: An in vivo positron emission tomography study with [(18)F]ASEM, 165:118-124.
7. Muller-Gartner HW, Links JM, Prince JL, et al. [1992], Journal of cerebral blood flow and metabolism. Measurement of radiotracer concentration in brain gray matter using positron emission tomography: MRI-based correction for partial volume effects,12(4):571-583.
8. Meltzer CC, Zubieta JK, Links JM, Brakeman P, Stumpf MJ, Frost JJ. [1996], Journal of cerebral blood flow and metabolism. MR-based correction of brain PET measurements for heterogeneous gray matter radioactivity distribution, 16(4):650-658.

OP40

Combining mu-opioid receptor availability and endogenous opioid release with functional MRI measures of reward anticipation in alcohol and gambling addiction.

Turton S[1], Myers J[1], Paterson LM[1], McGonigle J[1,2], Wilkinson C[1], Lan C[1], Mick I[1], Limbrick-Oldfield[3] E, Rabiner E[2], Gunn RJ[2], Bowden-Jones H[4,5], Clark L[3], Nutt DJ[1], Lingford-Hughes A[1]

(1)Neuropsychopharmacology Unit, Imperial College London, UK, (2)Imanova, London, UK, (3)Centre for Gambling Research, University of British Columbia, Canada, (4)National Problem Gambling Clinic, CNWL NHS Foundation Trust, UK, (5)Department of Medicine, Imperial College London, UK

Introduction:

Endogenous opioid signalling plays a key role in reward processing and hedonic responses. There is evidence of dysregulated opioid signalling in both alcohol dependence (AD) and gambling disorder (GD), including blunted endogenous opioid release (Mick 2016, Williams 2009). However, the mechanisms by which this modulates behaviours in addiction and relapse are not well understood. In AD there are deficits in fronto-striatal responses during financial reward processing (Nestor 2017), whilst in GD, where money is a salient reward, the findings are less consistent. To explore if there is an association between mu-opioid receptor (MOR) availability, endogenous opioid release and reward responses in addiction we have combined within-subject non-simultaneous [^{11}C]carfentanil positron emission tomography (PET) and functional magnetic resonance imaging (fMRI) data in individuals with AD, GD and healthy controls (HC). We hypothesise that higher MOR availability and/or endogenous opioid release, indicating higher MOR tone, will be associated with higher fMRI brain reward responses.

Materials & Methods:

Functional MRI and [^{11}C]carfentanil PET data were collected on separate study visits from n=13 HC, n=15 GD (DSM-IV) and n=13 AD (DSM5, >4weeks abstinent) participants. All participants received two [^{11}C]carfentanil PET scans, one before and one 3-hours following a 0.5mg.kg^{-1} oral dexamphetamine challenge. Participants completed an fMRI protocol which included a monetary incentive delay (MID) task (win or lose £0.50 and neutral trials) (McGonigle 2017).

10 ROIs were selected due to their importance in addiction, opioid signalling and reward: medial prefrontal cortex, amygdala, hippocampus, thalamus, hypothalamus, ventral pallidum, caudate, putamen, nucleus accumbens and ventral tegmental area. [^{11}C]carfentanil time-activity data were sampled from each ROI and binding potential (BP_{ND}) values quantified using the simplified reference tissue model with occipital lobe as the reference region. Post-amphetamine ΔBP_{ND} values were calculated for each ROI (ΔBP_{ND} = *Post-amphetamine*BP_{ND} – *Pre-amphetamine*BP_{ND}*)/Pre-amphetamine*BP_{ND}). fMRI data were pre-processed as previously described (McGonigle 2017). The contrast of interest in the MID task was win anticipation>neutral anticipation. Percent signal change in blood-oxygen-level dependent (Δ%BOLD) values for each ROI were extracted with FSL Featquery.

For each ROI, Pearson correlations were calculated between Δ%BOLD and the two PET measures, creating two 10x10 matrices ($p<0.05$ uncorrected) for each group. These associations were explored further at a whole-brain level by using BP_{ND} or ΔBP_{ND} values from ROIs with significant correlations as covariates in the model (FMRIB's Local Analysis of Mixed Effects FLAME-1, cluster threshold; $Z>2.3$, $p<0.05$).

Results:
There were no significant correlations between Δ%BOLD and BP_{ND} in HC participants. In GD there were significant negative correlations between ventral pallidum [^{11}C]carfentanil BP_{ND} and Δ%BOLD in the thalamus, caudate and putamen. In AD putamen [^{11}C]carfentanil BP_{ND} was negatively correlated with Δ%BOLD in the hippocampus, thalamus, ventral pallidum, caudate and nucleus accumbens. In the whole-brain FEAT analyses, GD participants had BOLD clusters with significant negative correlations with ventral pallidum BP_{ND}. In AD participants there were clusters with significant negative correlations with putamen BP_{ND}, with the exception of a single cluster with positive correlations in the frontal cortex.
There were no significant correlations between Δ%BOLD and ΔBP_{ND} in AD or HC participants. In GD there were significant negative correlations between ΔBP_{ND} in the amygdala, hippocampus, thalamus and ventral pallidum with Δ%BOLD in regions including medial frontal cortex, amygdala and hippocampus (uncorrected $p<0.05$). Whole brain FEAT analyses in GD showed significant BOLD clusters with negative correlations with amygdala, putamen, thalamus and ventral pallidum ΔBP_{ND}.

Discussion/Conclusion:
Contrary to our hypotheses, higher MOR availability may be associated with lower reward anticipation BOLD responses in AD and GD. In GD higher BOLD brain responses may be associated with lower opioid release to the amphetamine challenge. These findings indicate there is a relationship between opioid signalling and reward responses in addiction, although further understanding of this association is needed to inform how treatment with opioid receptor antagonists modulates these neural pathways.

Acknowledgements:
This abstract presents independent research funded by MRC Grant and supported by the NIHR CRF at Imperial College Healthcare NHS Trust. The views expressed are those of the authors and not necessarily those of the MRC, the NHS, the NIHR or the Department of Health

References:
McGonigle J, Murphy A, Paterson LM *et al.* [2017] Psychopharmacol, 31:3-16.
Mick I, Myers J, Ramos A, *et al.* [2016] Neuropsychopharmacology, 41:1742-50.
Nestor LJ, Murphy A, McGonigle J, *et al.* [2017] Addict Biol, 22:1576-1589.
Williams TM, Davies SJ, Taylor LG, *et al.* [2009] Eur Neuropsychopharmacol, 19:740-8

OP41

α7-nAChR: Brain imaging of [^{18}F] ASEM with reproducibility, specific binding, and changes in schizophrenia

Dean F. Wong, MD, PhD[1,2,3,4], Hiroto Kuwabara MD, PhD[1], Andrew G. Horti, PhD[1], Joshua Roberts, PhD[1], Ayon Nandi, MS[1], James Brasic MD, MS[1], Akira Sawa, MD, PhD[2], Heather Valentine, BS[1], David Schretlen[2], PhD, Gary Wand, MD[2,5], Nicola Casella, MD[6], William Kem, PhD[7], Robert Freedman MD[8], Albert Gjedde, MD, DSc[1,9,10]

[1] Russell H Morgan Department of Radiology and Radiological Sciences, [2] Department of Psychiatry and Behavioral Sciences, [3] Solomon Snyder Department of Neuroscience, [4] Department of Neurology, [5] Department of Medicine (Affiliations 1-6: Johns Hopkins University School of Medicine, Baltimore, MD) [6]Sheppard-Pratt Hospital, Baltimore, MD; [7] Department of Pharmacology and Therapeutics, University of Florida, Gainesville, FL [8] Department of Psychiatry, University of Colorado, Aurora Co. [9] Department of Clinical Research, University of Southern Denmark, Odense, Denmark, [10] Department of Nuclear Medicine, Odense University Hospital, Odense, Denmark

Introduction:

Recent evidence has implicated the α7-nAChR nicotinic acetylcholine receptor subtype in normal brain physiology, as well as in neuropsychiatric disorders. The α7-nAChR subtype is primarily distributed in the cerebral cortex, compared to the α4β2-nAChR subtype that has more subcortical distribution. The cortical distribution suggests a role of α7-nAChR in cognition.

Materials and Methods:

Expanding on the first-in-human PET imaging of α7-nAChR with [^{18}F] ASEM, Wong et al (2014), a total of 21 healthy non-smoking volunteers have now been studied. In addition, six male patients with schizophrenia participated in a feasibility study as part of the project. All subjects completed one or two PET sessions with HRRT dynamic imaging for 90 minutes with 30 time points and simultaneous radial arterial sampling and HPLC metabolite detection at 7 time points. Subjects received an average dose of 14 mCi of [^{18}F] ASEM (specific activity 56,000 Ci/mmol). ***Test-retest:*** Twelve healthy volunteers (HC) were retested with [^{18}F] ASEM imaging approximately five weeks (mean 41.2 days) later. ***Blocking studies:*** Additionally, five healthy subjects participated in blocking studies with two PET scans, one at baseline and a second after oral administration of 150 mg of the partial agonist DMXB-A (also known as GTS21), forty minutes before the PET tracer injection. Plasma concentration DMXB-A were obtained at 70, 100, and 130 minutes post-dose, and determined using the method of Kem et al., 2004. ***Feasibility study of patients with schizophrenia:*** Six male patients with DSM-5 criteria for schizophrenia (SCZ) on stable antipsychotic medication, other than clozapine, had PET and were tested with Brief Psychiatric Rating Scores (BPRS) and other neuropsychological tests (part of the CNSS battery, Schretlen et al) appropriate for schizophrenia. ***PET Quantification:*** Regional V_T values were determined as previously reported (Wong et al. 2014). Analysis of occupancy with the Extended Inhibition Plot (EIP) (Phan et al 2017) proceeded as presented in companion abstract (Gjedde et al NRM18).

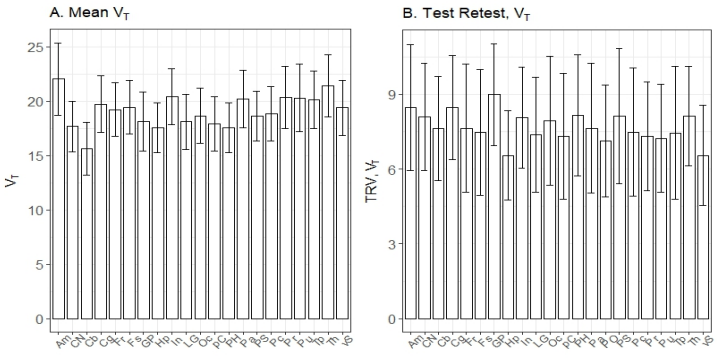

Figure *1*: Mean V_T in controls (n=21) and test-retest variability of V_T (n=8).

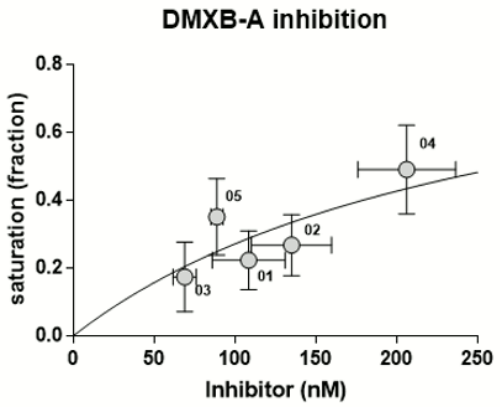

Figure *2*: Inhibition of [^{18}F] ASEM by DMXB-A

Results:

Test-retest: Estimates of V_T were highly reproducible (>90%, variability ≤ 7%) in eight healthy volunteers who completed test-retest and where usable plasma metabolite data was available. (**Figure 1A-B**). ***Blocking studies:*** Using the Extended Inhibition Plot (Phan et al. 2017), the dose-dependent occupancy of α7-nAChR by DMXB-A was estimated at 17-49% for plasma concentrations at 60-200 nM DMXB-A **(Figure 2).** ***Schizophrenia (SCZ):*** The six patients with schizophrenia had a lower group median V_T than healthy volunteers in the same age range (**Figure 3**). However, one patient was a potential outlier. That subject had a V_T value that was higher than the third quartile by more than one and a half times the inter-quartile range (ie, Q3 + 1.5xIQR; Hoaglin, 2003). Without the outlier, the difference in median V_T was significant in cingulate and frontal cortices, and hippocampus, ($P < 0.02$, Mann-Whitney test, corrected for multiple comparisons). Values of V_T correlated positively with BPRS symptom scores, and there was evidence of positive correlation with the cognitive domain score for attention and visual memory. ***Effect of antipsychotics and other potential confounds:*** One patient was studied before and after discontinuing Risperidone, for clinical reasons. This patient did not show any significant differences in V_T. A biodistribution study in rodents also confirmed that antipsychotics (including Risperidone, Olanzapine, and Aripiprizole) had no significant effects on [^{18}F] ASEM binding as compared to placebo. The menstrual cycle did not affect binding, as female subjects in the luteal and follicular phases revealed no pattern of effect.

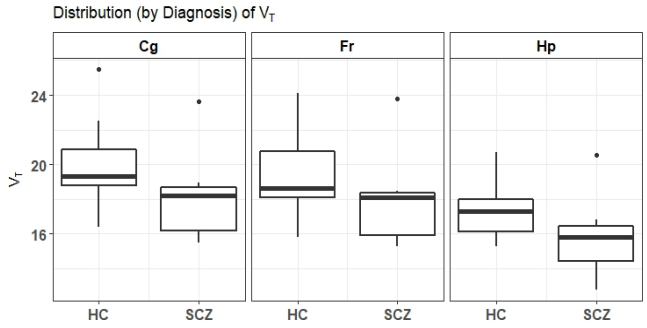

Figure *3*: Boxplots showing distribution of V_T in SCZ vs HC. Five out of the six patients had lower V_T than the mean V_T controls. The 6th patient had a much higher V_T and is a potential outlier (higher than Q3 + 1.5xIQR).

Discussion/Conclusions:

Tracer [^{18}F] ASEM demonstrated excellent reproducibility in test-retest studies and revealed specific displacement in humans by the partial agonist, DXMB-A. Preliminary results show an overall reduction of binding in patients with schizophrenia that is unlikely to be due to antipsychotic treatment. Interestingly, values of V_T in patients tended to be correlated with psychiatric symptoms and cognitive functions, but these findings will be tested in a larger sample. The radiolgand [^{18}F] ASEM has specific binding that revealed changes in schizophrenia in the present feasibility study. Planned larger studies with SCZ with full behavioral and cognitive testing will allow interrogation of the heterogeneity in V_T in vivo that cannot be revealed by prior post-mortem studies and aid in understanding mechanisms of cognitive deficits and potential improved SCZ treatments.

Acknowledgements:
Funding by **PHS** NIH grant 2R01 MH107197

References: Hoaglin DC, [2003], Statistical Sciences:18:311–318.; Kem WR, Mahnir VM, Prokai L, et al. [2004] Molecular pharmacology 65:56-67.; Phan J, Landau A, Jakobsen S, Gjedde A [2017] Scientific Reports 7(1):15979.; Wong DF, Kuwabara H, Pomper M, *et al*. [2014] Mol Imaging Biol (5):730-8.

OP42

Brain mapping of dopaminergic and serotoninergic pathways in non depressed Parkinson's disease patients: a high resolution PET study with [^{18}F]FE-PE2I and [^{11}C]MADAM

Patrik Fazio (MD, PhD)[1], Per Svenningsson (MD, PhD)[2], Zsolt Cselényi (MD, PhD)[1,3], Christer Halldin, PhD[1], Lars Farde (MD, PhD)[1,3] and Andrea Varrone (MD, PhD) [1]

1. *Department of Clinical Neuroscience, Centre for Psychiatry Research, Karolinska Institutet and Stockholm County Council, Stockholm, Sweden.*
2. *Department of Clinical Neuroscience, Centre for Molecular Medicine, Karolinska Institutet, Stockholm, Sweden.*
3. *PET Science Centre, Precision Medicine and Genomics, IMED Biotech Unit, AstraZeneca, Karolinska Institutet, Sweden*

Introduction:
Dopaminergic and serotoninergic systems are involved in the pathophysiology of motor and non motor impairments in Parkinson's disease (PD). Monoaminergic systems are functionally organized so that the origins of the axonal projections are located in the brainstem where the cell bodies are situated. The dopamine and serotonin transporter (DAT and SERT) are relevant imaging targets for examining *in vivo* the monoaminergic pathways in the brain. With the help of the high-resolution research tomograph (HRRT) and the radioligand [^{18}F]FE-PE2I we have examined the DAT along the whole nigrostriatal pathway in PD patients (1). Recently, we also reported a methodology that enables a detailed mapping of the SERT in the brainstem of healthy subjects using [^{11}C]MADAM (2). The main objective of this study was to examine the availability of SERT in the brainstem nuclei of early-stage non-depressed PD patients vs. control subjects. A secondary objective was to compare the differences in SERT availability between PD patients and controls in the serotoninergic projection areas relative to the brainstem nuclei. The loss of SERT was also compared to the loss of DAT in the substantia nigra vs. the striatal regions as a relative index of dopaminergic degeneration in the cell bodies vs.axonal terminals.

Materials & Methods:
Twenty non depressed PD patients (15M/5F, 62±8y, range 47-74y, disease duration 2.8±2.6y;
UPDRS-m:21.1±5.9) and 20 age and gender-matched control subjects were included in the study (15M/5F, 62±7y, range 50-72y). PET measurements were performed with [^{18}F]FE-PE2I (DAT) and [^{11}C]MADAM (SERT) using the HRRT system. Binding potential (BP_{ND}) images were generated with the wavelet-aided parametric imaging software using the Logan Graphical analysis. For each target, afunctional PET template of DAT and SERT availability was generated to support the delineation of volumes of interest (VOIs) on the substantia nigra (DAT) and on subdivisions of the raphe nuclei (SERT). For [^{18}F]FE-PE2I, the definition of striatal VOIs was obtained with an in-house DAT template whereas for [^{11}C]MADAM were obtained by applying the AAL template. T-tests for independent-samples were conducted comparing BP_{ND} values of [^{18}F]FEPE2I and [^{11}C]MADAM between PD patients and control subjects. Bonferroni's correction was used to correct for the multiple comparison in the four VOIs (substantia nigra, caudate, putamen and ventral striatum for DAT and dorsal and median raphe nuclei, caudate and putamen for SERT) with alpha threshold of 5%.

Results:
All subjects underwent MRI and PET imaging successfully. One PD subject was excluded from the SERT analysis because the injected activity of [^{11}C]MADAM was too low. In the substantia nigra, DAT availability was 30 % lower ($p<0.001$) in PD patients compared with control subjects. On the other hand the differences in SERT availability between PD patients

and controls were only 4% in the dorsal raphe and 1.8% in the median raphe (not significant, Fig. 1). In the projection areas, DAT availability was reduced by 70% in the putamen and by 40 % in the caudate ($p<0.001$) in PD vs control subjects whereas SERT availability was reduced by 25 % in the caudate and putamen, but the difference was significant after Bonferroni correction only in the putamen ($p<0.01$) (Fig.1).

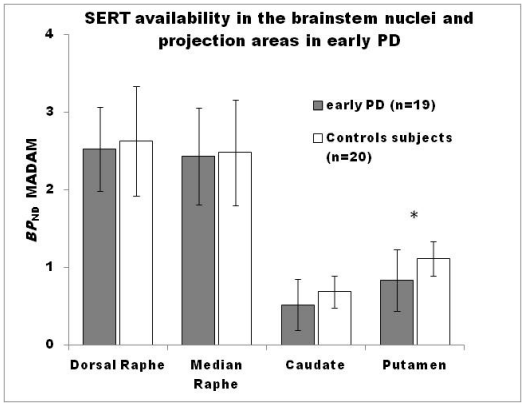

Discussion/Conclusions:

The findings of this study indicate that in non-depressed PD patients, at an early stage of the disease, the SERT availability in the brainstem nuclei is apparently not impaired, whereas a moderate decrease is observed in the striatum, relatively to control values. A more pronounced loss of DAT vs. SERT was observed both in the brainstem and in the projection areas. Overall, the findings of this study suggest that the serotonin system is less impaired than the dopaminergic system.

Fig.1 Bar graphs describing the differences between PD patients and healthy controls in the different volumes of interest (Dorsal and caudal raphe, caudate and putamen) . * $p<0.0125$.

Acknowledgments

This study has been supported by funds from the Swedish Foundation for Strategic Research and the Swedish Parkinson disease Foundation and by a grant from the AstraZeneca Translational Science Centre at Karolinska Institutet.

References:

1. Fazio P, Svenningsson P, Cselényi Z,Halldin C., Farde L, Varrone A. Nigrostriatal dopamine transporter availability in early Parkinson´s disease. Movement disorders. 2018;
2. Fazio P, Schain M, Varnäs K et al. Mapping the distribution of serotonin transporter in the human brainstem with high resolution PET: Validation using post- mortem autoradiography data. Neuroimage. 2016; 113:313-320.

OP43
α_2 Adrenoceptors: Down-regulation in Parkinson's disease

Adjmal Nahimi,[1] Karen Østergaard,[2] Martin B. Kinnerup[1], Jeppe Lund Schaldemose[1], Michael Wintherdahl,[1] Tatyana Fedorova,[1] Steen Jakobsen,[1] Michael Sommerauer,[1] Per Borghammer,[1] and **Albert Gjedde**[3–6].

[1]Department of Nuclear Medicine and PET Centre, Aarhus University Hospitals, Denmark,
[2]Department of Neurology, Aarhus University Hospital, Denmark,
[3]Department of Radiology and Radiological Science, Johns Hopkins University, Baltimore, MD, USA,
[4]Department of Neurology, McGill University, Montreal, QC, Canada,
[5]Department of Clinical Medicine, University of Southern Denmark, Odense, Denmark
[6]Department of Nuclear Medicine, Odense University Hospital, Odense, Denmark

Introduction:
Previously, we showed that [^{11}C]yohimbine, is a suitable ligand for positron emission tomography (PET) of central α2-adrenoceptors (α2R) in the human brain (Nahimi et al. 2015). The role of α2R in Parkinson's disease (PD) has been uncertain since the first findings that lesions of fibers from locus coeruleus (LC) may cause their function to decline (Cash et al. 1984) or rise (Chopin et al. 1989). Here, we tested the hypothesis that values of binding potential relative to non-displaceable binding (BP_{ND}) would change in the direction consistent with up- or down-regulation of α2R in patients compared to healthy control subjects.

Material and Methods:
All PD patients (N=19) and HC subjects (N=13)) underwent 90-minute PET with [^{11}C]yohimbine at baseline. Patients with PD had no medication overnight and were in the "off" state. The [^{11}C]yohimbine steady-state volumes of distribution V_T and binding potentials (BP_{ND}) were determined as described previously with arterial blood concentrations as input and corpus callosum as reference (Nahimi et al., 2015). We used a novel Receptor Availability Plot (RAP) to obtain estimates of the reduction of receptor availability, using the equation,

$$V_{T(PD)} = \left(A \left[\frac{V_{ND(PD)}}{V_{ND(HC)}} \right] \right) V_{T(HC)} + (1 - A)\, V_{ND(PD)} \quad (1)$$

where A is the receptor availability fraction, equal to 1-s, the fractional saturation, and V_T and V_{ND} have their familiar meaning in patients (PD) and healthy controls (HC).

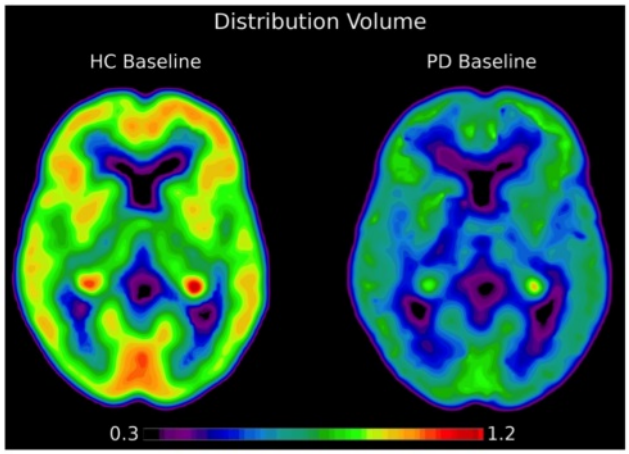

Figure 1 shows parametric images of [^{11}C]yohimbine in healthy controls and in patients with Parkinson´s disease.

Results:
We present a parametric image of values of V_T of [^{11}C]yohimbine in Figure 1. We observed global reduction of the value of V_T of [^{11}C]yohimbine (see Figure 2A), but the values of BP_{ND} of [^{11}C]yohimbine calculated with corpus callosum as reference revealed non-significant reductions in PD (Figure 2B). In contrast, the RAP revealed reduction of α2R availability to 89±5% in patients with PD compared to HC (see Figure 3).

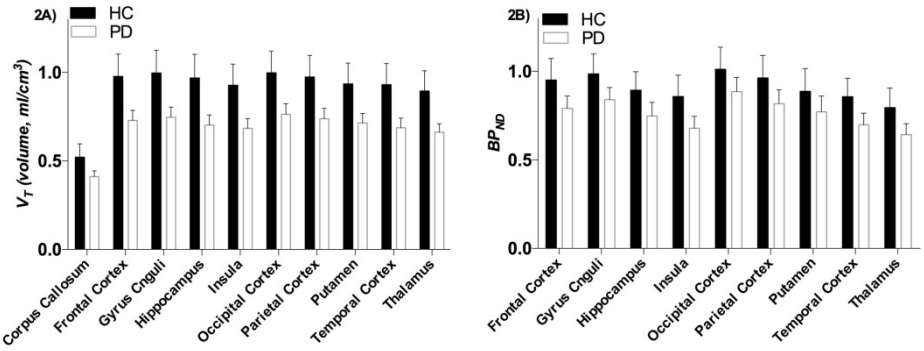

Figure 2A and 2B show volume of distribution and non-displaceable binding potential of [^{11}C]yohimbine, respectively, in patients with Parkinson´s disease (PD) and healthy controls (HC). The volume of distribution was reduced in several brain regions (multiple t-tests) and the binding potential was numerically reduced.

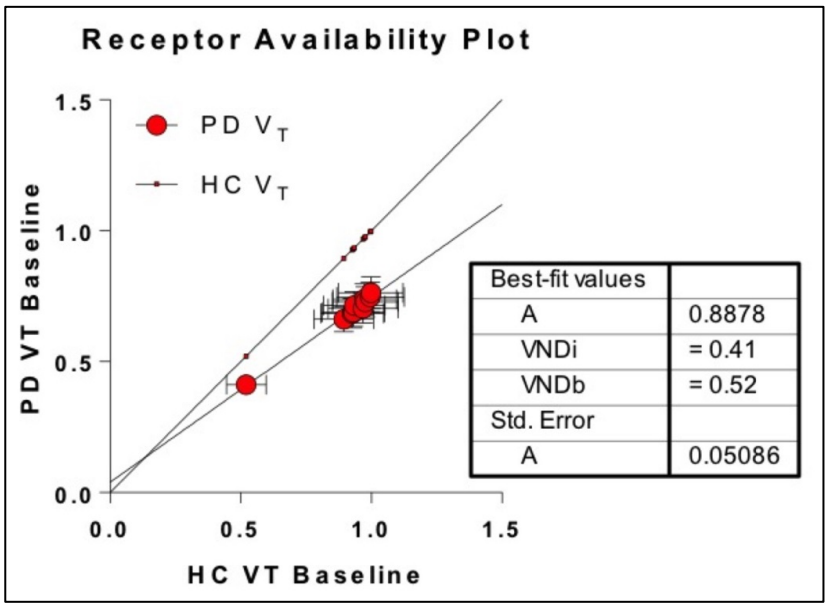

Figure 3 shows the receptor availability plot where the VNDi ($V_{ND(PD)}$) and VNDb ($V_{ND(HC)}$) are constrained to volumes of distribution in corpus callosum in PD patients and healthy controls, respectively.

Discussion/Conclusion:

The findings in the current study indicate that values of V_T and BP_{ND} of [^{11}C]yohimbine are reduced in brain regions with dense noradrenergic innervation. The RAP revealed a loss of α2R availability of 11% across all brain regions. This finding agrees with the results of previous measurements of α2R in post-mortem brains of PD patients. The limitations of the study include the lack of a reference region that is completely devoid of α2R, as corpus callosum also revealed down-regulation of V_T of [^{11}C]yohimbine in the PD patients.

References:

Cash R, et al. "Adrenergic receptors in Parkinson's disease." Brain research (1984) 269-275.

Chopin P, et al. "Effects of alpha-2 adrenoceptor agonists and antagonists on circling behavior in rats with unilateral 6-hydroxydopamine lesions of the nigrostriatal pathway." Journal of Pharmacology and Experimental Therapeutics (1999) 798-804.

Nahimi A, et al. "Mapping α2 adrenoceptors of the human brain with 11C-yohimbine." Journal of Nuclear Medicine (2015) 392-398.

OP44
AADC and NET: Noradrenergic mechanisms in Parkinson's disease

Martin B. Kinnerup[1], Michael Sommerauer[1], Karen Østergaard[2], Jan Jacobsen[1], Anna Schacht[1], Per Borghammer[1], and Adjmal Nahimi,[1-3] **Albert Gjedde**[4-7]

[1]Department of Nuclear Medicine and PET Centre, Aarhus University Hospitals, Denmark,
[2]Department of Neurology, Aarhus University Hospital, Denmark,
[3]Department of Neurophysiology, Aarhus University Hospital, Denmark.
[4]Department of Clinical Research, University of Southern Denmark, Odense, Denmark
[5] Department of Nuclear Medicine, Odense University Hospital, Odense, Denmark
[6]Department of Radiology and Radiological Science, Johns Hopkins University, Baltimore, MD, USA,
[7]Department of Neurology and Neurosurgery, McGill University, Montreal, QC, Canada,

Introduction:

Patients with Parkinson´s disease (PD) suffer from a wide range of non-motor symptoms that may be related to loss of noradrenaline (NA) and noradrenergic mechanisms. We tested the hypothesis that loss of noradrenergic tone would follow changes of NA synthesis or reuptake or both. To do so, we quantified noradrenaline transporter (NET) binding potentials and aromatic amino acid decarboxylase (AADC) activity with [^{11}C]MeNER and [^{18}F]FDOPA PET in the same subjects with PD to reveal possible compensatory mechanisms of noradrenergic neurotransmission, compared to healthy control subjects.

Figure 1:

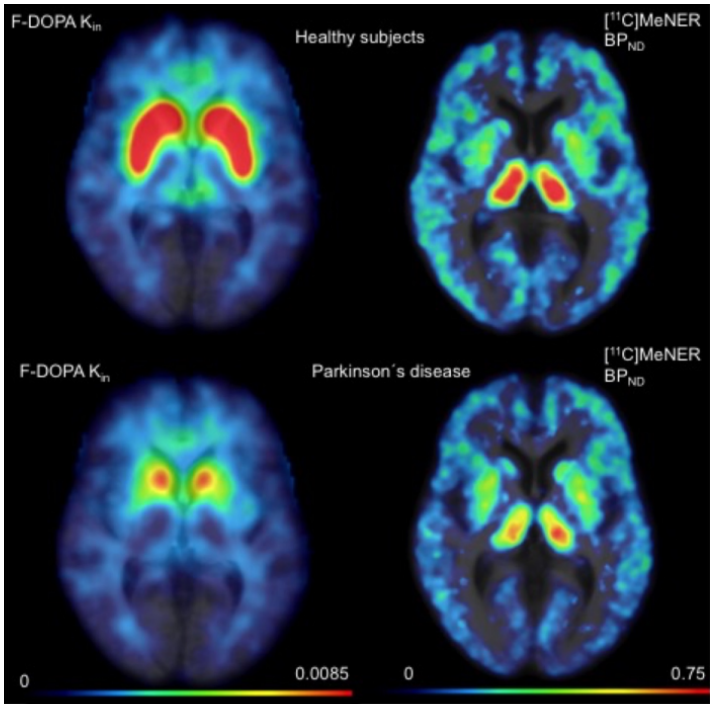

Method and materials:
We obtained PET images of the two tracers (Figure 1). We estimated specific binding potentials (BP_{ND}) of [^{11}C]MeNER in patients (n=11) and control subjects (n=8) as previously described (Nahimi et al, 2017), with caudate nucleus as reference region. The net rate of fluorodopamine formation (k_{in}) from [^{18}F]FDOPA was estimated by the Gjedde-Patlak plot with cerebellum as reference region. In addition, to test the interaction, we computed the [^{11}C]MeNER/[^{18}F]FDOPA BP_{ND} /k_{in} ratios were calculated using normalized [^{11}C]MeNER and [^{18}F]FDOPA values to compare degrees of combined malfunction.

Results:

The PET images revealed declines both of AADC and NET values of the tracer binding. Significant decline of [^{11}C]MeNER binding potentials to about 80% was determined in all regions of patients with PD (Figure 2). Estimates of [^{18}F]FDOPA k_{in} in patients were reduced by 10% on average, with some variability within the regions examined (Figure 3).We also noted that the [^{11}C]MeNER/[^{18}F]FDOPA ratios of patients were decreased by 30% on average in the regions tested (Figure 4), but by 60% in dorsal raphe.

Figure 2: MeNER BP_{ND}

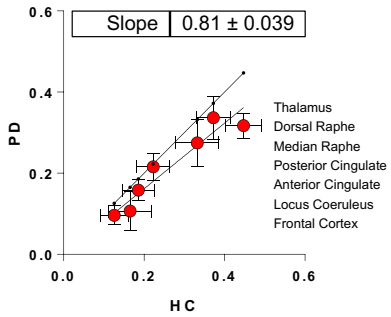

Figure 3: FDOPA k_{in}

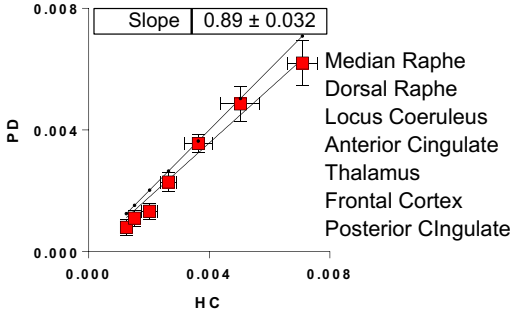

Figure 4: MeNER/FDOPA Ratios

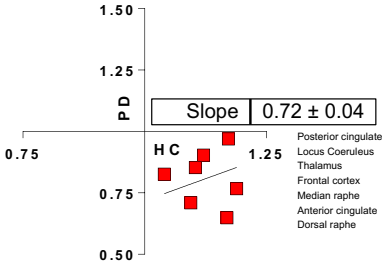

Discussion/Conclusion:

AADC activity remained the least affected or not decreased in areas of the brain with dense noradrenergic projections, in line with previous evidence of unaffected or even increased AADC activity in frontal cortex of early stage PD patients (Brück et al., 2005). Compared to AADC activity, the noradrenergic reuptake sites were down-regulated to a higher degree, to 20% in dorsal and median raphe, as evidenced also by the 60% reduction of the [^{11}C]MeNER/[^{18}F]FDOPA ratio in dorsal raphe of patients, in line with previous reports of compensatory down-regulation of NET in median and dorsal raphe of PD patients.

References

1. Brück A, Aalto S, Nurmi E, Bergman J, Rinne JO. Cortical 6-[18F]fluoro-L-dopa uptake and frontal cognitive functions in early Parkinson's disease. Neurobiol Aging. 2005 Jun;26(6):891-8.
2. Nahimi A, Sommerauer M, Kinnerup MB, Østergaard K, Winterdahl M, Jacobsen J, Schacht A, Johnsen B, Damholdt MF, Borghammer P, Gjedde A. Noradrenergic deficits in Parkinson's disease imaged with (11)C-MeNER. J Nucl Med. 2017 Aug 28. pii: jnumed.117.190975. doi: 10.2967/jnumed.117.190975.

OP45

[*Carbonyl*-^{11}C]*N*-(5-(((*2S*,*4S*)-4-(6-fluoropyridin-2-yloxy)-2-methylpiperidin-1-yl)methyl)thiazol-2-yl)acetamide ([^{11}C]OGA1) is an effective PET radioligand to image brain *O*-linked-□-*N*-acetyl-glucosamine hydrolase in monkey

Shuiyu Lu[1], Jeih-San Liow[1], Cheryl Morse[1], Sami Zoghbi[1], Aneta Kowalski[1], Robert Gladding[1], Vanessa Barth[2], Susan DuBois[2], Kevin Ruley[2], Nicolas Dreyfus[3], Jeremy Gilmore[3], Hugh Nuthall[3], Cynthia Jesudason[2], Robert Innis[1] and Victor Pike[1]

(1) Molecular Imaging Branch, NIMH, NIH, Bethesda, MD 20892 USA; (2) Eli Lilly & Co, Indianapolis, IN 46285 USA; (3) Eli Lilly & Co, Windlesham, GU20 6PH, UK

Introduction:
O-linked-□-*N*-acetyl-glucosamine hydrolase (*O*-GlcNAcase) is a potential biomarker for elucidating tauopathy and a therapeutic target for treating Alzheimer's Disease because of its involvement in *O*-GlcNAc modification of tau proteins.[1,2] To develop a PET radioligand for *O*-GlcNAcase, we labeled *N*-(5-(((*2S*,*4S*)-4-(6-fluoropyridin-2-yloxy)-2-methyl-piperidin-1-yl)methyl)thiazol-2-yl)acetamide (LSN3316612, OGA1), a selective high-affinity inhibitor for this enzyme, with carbon-11. PET imaging of [^{11}C]OGA1 in monkey demonstrated that it is an effective radioligand to image *O*-GlcNAcase in vivo.

Materials and Methods:
[^{11}C]OGA1 was synthesized using a two-stage procedure starting with Pd(0)-mediated insertion of ^{11}CO into iodomethane in THF, followed by treatment with an amine partner.[3] A male rhesus monkey (9.8 kg), anesthetized with ketamine (10 mg/kg) and maintained in anesthesia with 1.5% isoflurane underwent two PET scans. At baseline, [^{11}C]OGA1 (163 MBq; 86 GBq/μmol) was injected i.v. as a bolus. For a preblocked condition three hours later, thiamet-G, a selective *O*-GlcNAcase inhibitor of different chemotype (10 mg/kg), was administered i.v. at 45 min before a second bolus injection of [^{11}C]OGA1 (218 MBq; 43 GBq/μmol). PET images of the brain were acquired on a microPET Focus 220 scanner for 120 min with full arterial input function measurement.

Results:
Under baseline condition [^{11}C]OGA-1 showed good brain penetration (**Fig. 1A**) in monkey. Regional brain radioactivity uptakes reflected *O*-GlcNAcase distribution obtained with autoradiography. All brain regions, such as frontal cortex (FC), striatum (ST), hippocampus (HP), and thalamus (TH), continued to accumulate radioactivity; only cerebellum (CE) showed slow wash-out after radioactivity peaked at around 45 min. Uptake of all brain regions decreased significantly and were indistinguishable after thiamet-G blockade (**Fig. 1B**).
Total volume of distribution (V_T) were 25.8 and 25.7 in enzyme-rich frontal cortex and striatum, and 10.4 in cerebellum. After blockade with thiamet-G, V_T in all regions decreased to ~1.6, representing a greater than 90% reduction (**Fig. 2A**). At baseline, the two-tissue compartmental model showed that V_T values reach within 10% of the terminal values (2 h) after 60 min. The stable V_T values indicate unlikely radiometabolites accumulation in the brain (**Fig. 2B**).

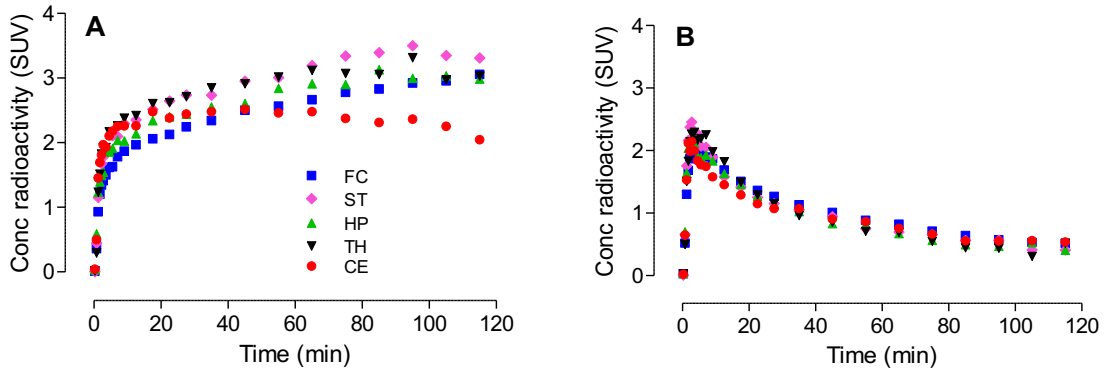

Fig. 1. Brain time-activity curves of a rhesus monkey injected with [^{11}C]OGA1 at baseline (A), and after preblock of *O*-GlcNAcase with thiamet-G (10 mg/kg) (B).

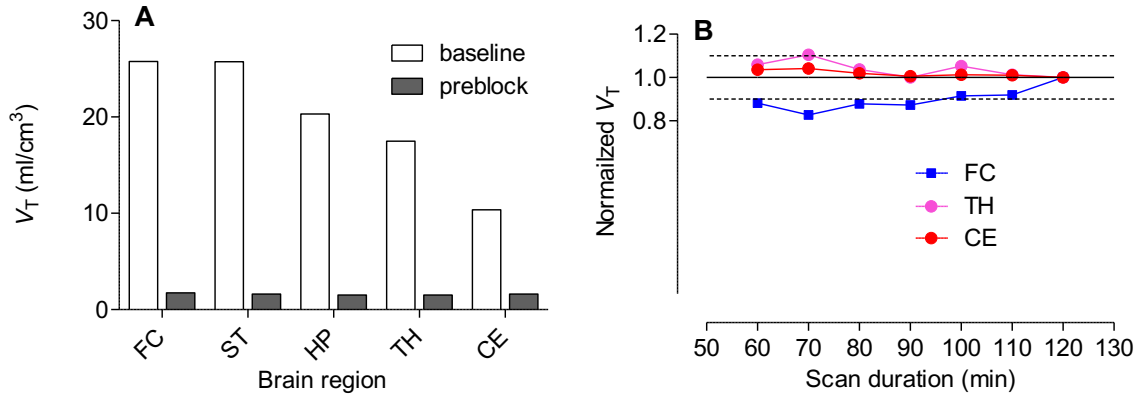

Fig. 2. [^{11}C]OGA1 V_T under baseline and preblock conditions (A). Normalized V_T as a function of scan duration (B).

Conclusion:
[^{11}C]OGA1 is an effective PET radioligand to image and quantify brain *O*-linked-□-*N*-acetyl-glucosamine hydrolase in monkey.

Acknowledgements:
This work was supported by the Intramural Research Program of the National Institutes of Health (ZIA-MH002793 and ZIA-MH002795) and by a CRADA with Eli Lilly & Co.

References:
[1]. Bond MR, Hanover JA [2015] J. Cell Biol. 208: 869-880. [2] Yuzwa SA, Vocadlo DJ [2014] Chem. Soc. Rev. 43: 6839-6858. [3]. Haskali M, Lu S, Morse C, Barth V, DuBois S, Ruley K, Dreyfus N, Gilmore J, Jesudason C, Pike V [2017] J. Nucl. Med. 58 (suppl 1): 128.

OP46

Abstract withdrawn

OP47

Abstract withdrawn

OP48

Measuring synaptic density in Parkinson's disease: Preliminary results from a PET imaging study of SV2A with ^{11}C-UCB-J

David Matuskey[1,2,3], Mark Dias[1], Sjoerd J. Finnema[1], Mika Naganawa[1], Shannan Henry[1], Jim Ropchan[1], Nabeel Nabulsi[1], Yiyun Huang[1], Sule Tinaz[3], Richard E. Carson[1]

[1] PET Center, Department of Radiology and Biomedical Imaging, Yale University, New Haven, CT, United States. [2] Department of Psychiatry, Yale University, New Haven, CT, United States [3] Department of Neurology, Yale University, New Haven, CT, United States.

Introduction:

Parkinson's disease (PD) is a neurodegenerative disease with motor and non-motor symptoms. Mounting evidence points to neurodegeneration beginning decades before clinical symptoms appear. Synaptic changes are critical in this process and understanding the pathogenesis of synaptic degeneration has more recently become a focus in PD research [1]. Recent work has elucidated synaptic changes in both animal models and in patients with PD post-mortem and provided evidence that neurodegeneration in PD is most likely to start at the synapse [1-3]. Moreover, α-synuclein, along with several other PD-associated proteins (e.g., LRRK2, parkin, DJ-1, PINK1) mainly involve synaptic machinery, adding weight to the hypothesis that presynaptic dysfunction, not neuronal loss, is the key event of the pathological process in PD [1].

Thus, the ability to assess synaptic changes *in vivo* in PD might improve early diagnoses and more accurately monitor potential disease-modifying therapies. We have recently developed an *in-vivo* imaging technique to measure synaptic density in humans, using positron emission tomography (PET) with the radiotracer ^{11}C-UCB-J. This tracer binds to synaptic vesicle glycoprotein 2A (SV2A) [4], which is an essential vesicle membrane protein present in virtually all synapses and a validated biomarker for synaptic density. Here we present preliminary data from ^{11}C-UCB-J PET imaging of synaptic density in PD.

Materials & Methods:

PD subjects (N=2) were recruited via the Movement Disorders Clinic at Yale New Haven Hospital and through ongoing partnerships with local support groups. The subjects were 50 and 43 years old females with clinical onset 10 and 4 years ago, respectively. These clinically established PD subjects were compared to matched healthy controls (HC) taken from recent ^{11}C-UCB-J studies (56 and 42 rears old females). All subjects were in good physical health and excluded for signs of dementia (Montreal Cognitive Assesment score < 21) or other conditions (e.g., severe depression, anxiety, excessive daytime sleepiness, psychosis, or adverse effects of medication). Any PD or psychotropic medications were held during scan day to avoid potential confounds.

Subjects received a MRI and then underwent a 120-min PET scan with ^{11}C-UCB-J using a high resolution research tomograph (HRRT). ^{11}C-UCB-J has been shown to be an excellent tracer with good test/retest reliability [5]. Arterial blood sampling and radiometabolite analysis were conducted to obtain a plasma input function. Primary regions of interest (ROI) were defined based upon a MR template and included areas of the striatum (caudate and putamen), substantia nigra (SN) and cortical regions. Secondary regions were included for exploratory analysis. As in previous work, regional time-activity curves were analyzed with the 1-tissue (1T) compartment model to estimate volumes of distribution (V_T) [5]. In order to account for possible partial volume effects, a binary grey matter mask was employed (with the exception of the SN due to the small ROI). Regional BP_{ND} values were also obtained using the centrum semiovale (a white matter rich area) as a reference region. Parametric V_T maps were generated using the 1T model.

Results:
In PD subjects compared with controls, there were ^{11}C-UCB-J V_T reductions across all brain regions examined (**Figs. 1 and 2**), with the most pronounced reductions found in cortical regions (19%-23% decreases) and in the SN and putamen (19% and 15% decreases, respectively). BP_{ND} values were also similarly reduced with decreases of 16%-20% in cortical regions and 33% and 16% decreases in the SN and putamen respectively.

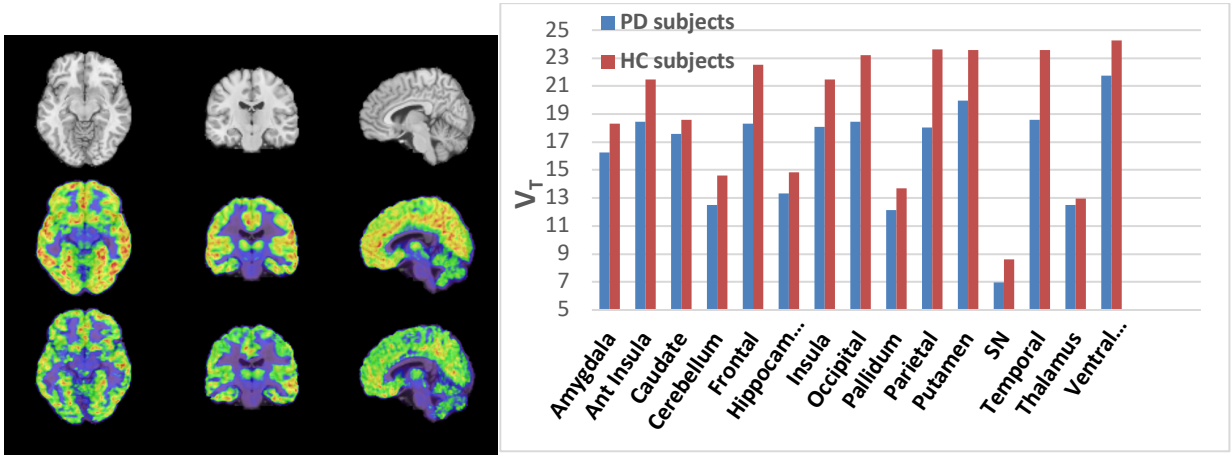

Fig 1. (left image), Template MR images (top row) and parametric V_T maps for HC (middle row) and PD representative subjects (bottom row).
Fig 2. (right image), V_T values were decreased across all brain regions between the PD subjects and HC subjects.

Discussion/Conclusion:
These data suggest that SV2A binding is dramatically altered in PD subjects throughout the brain with large decreases in areas specifically known to be involved in the disease process. These preliminary data should be interpreted with caution, however, due to the very small subject size and lack of a full partial volume correction. This work is currently being expanded to include an additional 20 PD subjects and updated data will be included when possible.

Acknowledgements:
We would like to thank the Connecticut Advocates for Parkinson's for their invaluable support, UCB Pharma for providing the tracer precursor, and AbbVie for supporting the expansion of this study.

References:
1.) Bellucci, A., et al., (2016) *Review: Parkinson's disease: from synaptic loss to connectome dysfunction.* Neuropathol Appl Neurobiol, **42**(1): p. 77-94.
2.) Schulz-Schaeffer, W.J., (2010) *The synaptic pathology of alpha-synuclein aggregation in dementia with Lewy bodies, Parkinson's disease and Parkinson's disease dementia.* Acta Neuropathol, **120**(2): p. 131-43.
3.) Picconi, B., G. Piccoli, and P. Calabresi, (2012) *Synaptic dysfunction in Parkinson's disease.* Adv Exp Med Biol, **970**: p. 553-72.
4.) Finnema, S.J., et al., (2016) *Imaging synaptic density in the living human brain.* Sci Transl Med, **8**(348): p. 348ra96
5.) Finnema, S.J., et al., (2017) Kinetic evaluation of [^{11}C]UCB-J, a novel radioligand for PET imaging of synaptic vesicle glycoprotein 2A in humans. *Journal of Cerebral Blood Flow and Metabolism,* Jan 1:27 1678X17724947. doi: 10.1177/0271678X17724947.

OP49

Abstract withdrawn

OP50
Imaging multiple sclerosis by PET: development of a PET radioligand for K^+ channels to image demyelination

P. Brugarolas[1]*, J. Sánchez-Rodríguez[1], H.M. Tsai[1], F. Basuli[2], S.H. Cheng[1], X. Zhang[2], A.V. Caprariello[3], J. Lacroix[1], R. Freifelder[1], D. Murali[4], O. DeJesus[4], R.H. Miller[3], R.E. Swenson[2], C.T. Chen[1], P. Herscovitch[2], D.S. Reich[2], F. Bezanilla[1], B. Popko[1]

University of Chicago, National Institutes of Health, Case Western Reserve University, University of Wisconsin - Madison

* Massachusetts General Hospital – Harvard Medical School
55 Fruit St, Bulfinch 051, Boston, MA 02114, U.S.A.

Introduction:
Central nervous system (CNS) demyelination represents the hallmark of multiple sclerosis (MS) and contributes to other neurological conditions including traumatic brain injury, brain ischemia and Alzheimer's disease. A tool to image and quantify demyelination is needed to fully understand how much it contributes to these conditions and develop better therapies. Currently, MRI is the gold standard for imaging demyelinating diseases and, even though it can clearly show lesions, it cannot distinguish demyelination from inflammation or axonal loss. PET, on the other hand, has the potential to provide a quantitative and specific measure of demyelination.
Current tracers for demyelination like [^{11}C]PIB or [^{11}C]CIC bind to myelin and thus demyelination correlates with decreases in signal, which can be problematic for small lesions due to partial volume effects. It would be advantageous to have a tracer that positively correlates with demyelination. Upon demyelination, axonal K^+ channels, which are normally buried beneath the myelin sheath, become exposed and increase in expression. This prevents neurons from propagating action potentials and causes neurological symptoms such as difficulty walking, vision problems, numbness or tingling or pain. 4-aminopyridine (4AP, dalfampridine) is an approved drug for MS that when it binds to the exposed K^+ channels on demyelinated axons restores conduction. Here, we used a ^{18}F-labeled analog of 4AP, [^{18}F]3F4AP, to image demyelination.

Materials and Methods:
Autoradiography after *in vivo* administration was used to visualize the distribution of [^{14}C]4AP and [^{14}C]3F4AP in the brains of demyelinated mice. [^{18}F]3F4AP was produced using standard radiolabeling methods. MicroPET/CT imaging was used to evaluate the tracer in rats with chemically induced demyelination. PET/CT was used to evaluate the brain and whole-body distribution of [^{18}F]3F4AP in rhesus monkeys.

Results:
Autoradiography studies showed that 4AP as well as its fluorinated derivative, 3F4AP, preferentially bind to non-myelinated areas and demyelinated areas in mouse models of MS. Radiochemical synthesis of [^{18}F]3F4AP was accomplished by two different methods: i) radiofluorination of a pyridine N-oxide followed by hydrogenation[1,2], and ii) fluorination of a nicotinic acid derivative followed by Curtius rearrangement[3]. MicroPET studies in rats showed that [^{18}F]3F4AP gets into the brain (SUV_{peak} ~4), that it does not undergo defluorination *in vivo* and that it can be used to detect chemically induced demyelination (**Fig. 1A**)[4]. Finally, PET/CT studies in healthy rhesus monkeys confirmed that the tracer goes into the brain, liver, kidneys and eyes. Within the brain of healthy primates, [^{18}F]3F4AP preferentially binds to non-myelinated areas where the K^+ channels are exposed (**Fig. 1B**)[4].

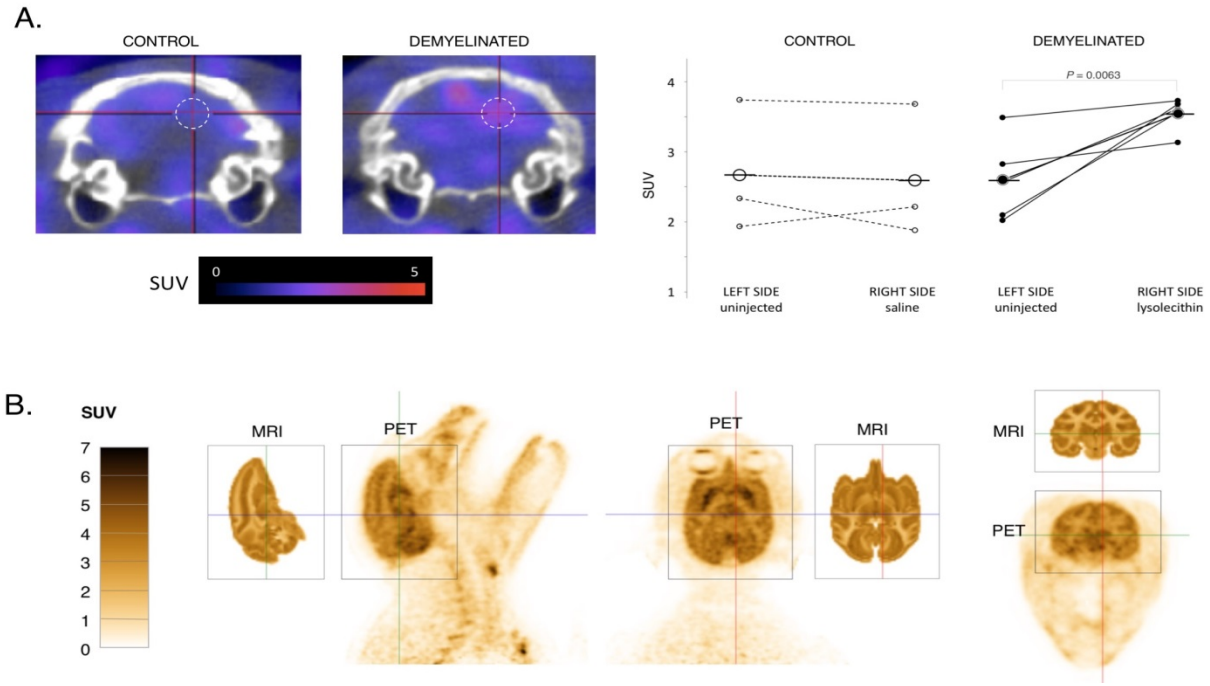

Fig. 1. PET imaging with [^{18}F]3F4AP. A. PET/CT coronal images of the cerebellum of control and demyelinated rat. **B.** PET images of healthy rhesus monkeys next to images from a reference atlas (adapted from ref. #4)

Discussion:
Based on an approved drug for MS, the tracer developed here binds to K^+ channels in demyelinated axons and provides a positive readout of demyelination. Quantitative non-invasive imaging of demyelination may provide a useful measure for diagnosing demyelinating diseases as well as monitoring therapies designed to revert demyelination.

Acknowledgements:
NMSS, NIH/NINDS, NIH/NIBIB, and the Adelson Foundation

References:
1. Brugarolas P, Freifelder, R., Cheng S.-H. and DeJesus, O. Synthesis of meta-substituted [^{18}F]3-fluoro-4-aminopyridine via direct radiofluorination of pyridine N-oxides. Chem Commun 52, 7150-2 (2016).
2. Brugarolas P, Bhuiyan M.B., Kucharski A, Freifelder, R. Automated radiochemical synthesis of [^{18}F]3F4AP: a novel PET tracer for imaging demyelinating diseases. J Vis Exp, 123 (2017).
3. Basuli F, Zhang X, Brugarolas P, Reich DS, Swenson RE. An efficient new method for the synthesis of [18F]3-fluoro-4-aminopyridine via Yamada-Curtius rearrangement. J. Labelled. Comp. Radiopharm. (2017).
4. Brugarolas P*, Sánchez-Rodríguez J, Tsai HM, Basuli F, Cheng SH, Zhang X, Caprariello AV, Lacroix J, Freifelder R, Murali D, DeJesus O, Miller R, Swenson RE, Chen CT, Herscovitch P, Reich DS, Bezanilla F, Popko P. Development of a PET radioligand for potassium channels to image CNS demyelination. Sci Rep 8, 607 (2018)

OP51

Patients with migraine have high brain 5-HT levels: A PET neuroimaging study of the 5-HT_4 receptor in chronic and episodic migraine patients

Marie Deen, MD,[1, 2, 3] Anders Hougaard, MD, PhD,[1] Hanne D. Hansen, PhD,[2] Claus Svarer, PhD,[2] Hans Eiberg, MSc,[4] Scabolzs Lehel,[5] Gitte M. Knudsen, MD, DMSc,[2, 3*] Messoud Ashina, MD, PhD, DMSc,[1, 3*]

[1]Danish Headache Center and Department of Neurology, Rigshospitalet Glostrup, Denmark.
[2]Neurobiology Research Unit and NeuroPharm, Department of Neurology, Rigshospitalet, Denmark.
[3]Faculty of Health and Medical Sciences, University of Copenhagen, Denmark.
[4]Department of Cellular and Molecular Medicine, Faculty of Health and Medical Sciences, University of Copenhagen, Denmark.
[5]PET- and Cyclotron Unit, Rigshospitalet, Denmark.

*These authors contributed equally to the work.

Introduction:
Chronic and episodic migraine are distinguished by an arbitrary frequency limit of 15 headache days pr. month[1]. High brain 5-HT levels have recently been found in episodic migraine patients compared to controls[2], but whether 5-HT is involved in the conversion from episodic to chronic migraine is unknown. Here, we investigated brain 5-HT levels in chronic migraine patients using PET neuroimaging of the 5-HT_4 receptor, which is inversely related to brain 5-HT levels[3], and compared them to both healthy controls and episodic migraine patients. We also evaluated whether 5-HT_4 receptor binding is associated with migraine frequency.

Materials and Methods:
Sixteen chronic migraine patients (age 30±9) underwent a two-hour dynamic PET scan using the HRRT scanner after a 20 seconds bolus injection of [^{11}C]SB207145, a specific 5-HT_4 receptor radioligand. PET data from 15 episodic migraine patients (age 30±10) and 16 controls (age 29±10) from a previous study[2] were included for comparison. Regional non-displaceable binding potentials (BP_{ND}) were estimated using the SRTM with cerebellum as reference region. A volume-weighted neocortical BP_{ND} was calculated by volume weighting grey matter segmented BP_{ND}s from 11 cortical brain regions. The BP_{ND}s were adjusted for mass dose effects using a population-based ID_{50}[4].

Results:
After adjusting for appropriate covariates (sex, age and 5-HTTLPR genotype), we found that chronic migraine patients had 8.6% lower binding of the 5-HT_4 receptor compared to controls (95% CI: [-16%; -1.0%], p = 0.042) (figure 1A). There was no difference in 5-HT_4 receptor binding between chronic and episodic migraine patients (p = 0.46) (figure 1B). When pooling data from chronic and episodic migraine patients we found no association between number of monthly migraine days and 5-HT_4 receptor binding.

Discussion:
Using 5-HT_4 receptor binding as a proxy of brain 5-HT levels, we found that chronic migraine patients have higher brain 5-HT levels than controls. Further, our results indicate that there is no difference in brain 5-HT levels between chronic and episodic migraine patients and that migraine frequency is not related to brain 5-HT levels. Thus, high brain 5-HT levels may be an inherent trait of the migraine brain– rendering subjects more susceptible to migraine induction – rather than a risk factor involved in conversion from episodic to chronic migraine.

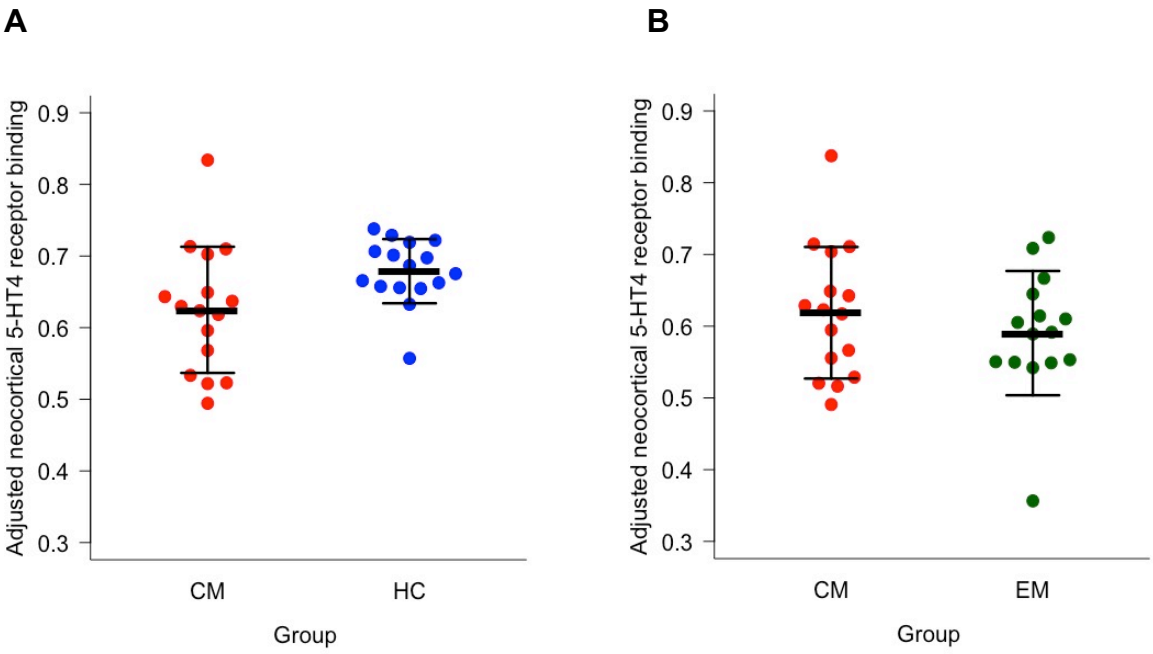

Figure 1. Chronic migraine patients have lower 5-HT_4 receptor binding compared to controls (mean BP_{ND}±SD 0.62±0.09 vs. 0.68±0.04) (**A)**, but do not differ from episodic migraine patients (0.62±0.09 vs. 0.59±0.09) (**B**). CM = Chronic migraine. HC = Healthy controls. EM = Episodic migraine. Black bars represent mean±SD.

Acknowledgements:
We thank all participants for volunteering to this study. Brice Ozenne is gratefully acknowledged for statistical counseling and Bente Dall, Lone Ibsgaard Freyr, Martin Korsbak Madsen, Erik Perfalk and Gerda Thomsen are gratefully acknowledged for their excellent technical assistance. The John and Birthe Meyer Foundation is gratefully acknowledged for sponsoring the HRRT scanner. The study was funded by the Migraine Research Foundation, the Lundbeck Foundation (R180-2014-3398), Innovation Fund Denmark, the A.P. Møller Foundation for the Advancement of Medical Science, and the Cool Sorption Foundation.

References:

1. Third Headache Classification Committee. The International Classification of Headache Disorders, 3rd edition. [2018], Cephalagia, 38:1–211.
2. Deen M, Hansen HD, Hougaard A, et al. [2018], NeuroImage Clinical, 18:97–102.
3. Haahr ME, Fisher PM, Jensen CG, et al. [2014], Molecular Psychiatry, 19:427-432.
4. Madsen K, Marner L, Haahr M, et al. [2011], Nuclar Medicine and Biology, 38:1085–1091.

OP52
Comparison of In vivo and Ex vivo SV2A Density in Human Brain: A ^{11}C-UCB-J PET Study in Temporal Lobe Epilepsy

Takuya Toyonaga[1], Tore Eid[2], Ketaki Deshpande[2], Kamil Detyniecki[3], Kun Wu[2], Jean-Dominique Gallezot[1], Mika Naganawa[1], Yiyun Huang[1], Nihal C. DeLanerolle[2], Amedeo Rapuano[2], Finnema J. Sjoerd[1], Yihuan Lu[1], Mark Dias[1], Dennis D. Spencer[2], Richard E. Carson[1]

1. *PET Center, Department of Radiology and Biomedical Imaging, Yale University, New Haven, CT*
2. *Department of Neurosurgery, Yale University, New Haven, CT*
3. *Department of Neurology, Yale University, New Haven, CT*

Introduction:
PET imaging of synaptic vesicle glycoprotein 2A (SV2A) has the potential to become a general biomarker for synaptic density evaluation based on our data obtained using the novel SV2A tracer ^{11}C-UCB-J. One tissue compartment modeling of ^{11}C-UCB-J PET data provides high quality images of the volume of distribution (V_T) and tracer delivery (K_1). In our previous baboon study, *in vivo* V_T values were well correlated with *ex vivo* measures of synaptic density biomarkers [1, 2]. However, to date, this comparison has not been made in the human brain. In this study, we correlated *in vivo* imaging results and *ex vivo* biological results in brain samples from mesial temporal lobe epilepsy (MTLE) patients. Such samples were resected during epilepsy treatment surgeries.

Materials & Methods:
Five medically refractory MTLE patients were included in this study. All of them underwent unilateral anteromesial temporal lobectomy (AMTL) for treatment of their epilepsy. ^{18}F-FDG and ^{11}C-UCB-J PET scans were performed less than 1 year before surgery (median: 36 days, range: 11 - 246 days). For ^{11}C-UCB-J, a 90-min dynamic scan was performed and data from four subjects were analyzed with one tissue compartment modeling to estimate V_T and K_1. BP_{ND} was calculated from (V_T/V_{ND})-1, using centrum semiovale as a reference region. One subject's BP_{ND} was estimated with simplified reference tissue model 2 (SRTM2), since the input function was not available. For ^{18}F-FDG, subjects underwent a 10-min static scan one hour after injection, and the image was normalized by body weight and injected dose and expressed as standardized uptake value (SUV). Regional measurements in the hippocampus and temporal cortex were made using the AAL template in MNI space. Additionally, we applied a 5-mm spherical ROI in unilateral temporal lobe to be representative of white matter in that region. From brain surgery, two samples were made available per subject, one from the lateral temporal lobe, and the other from hippocampus. A neuropathologist (T.E.) dissected lateral temporal lobe tissues into gray and white matter. All brain samples were homogenized and analyzed by Western blotting to quantify SV2A density.

Results:
The *in vivo* V_T mean ± standard deviation (SD) in hippocampus of the four patients was 10.8 ± 0.56 mL/cm^3, significantly lower than the lateral temporal gray matter V_T values of 18.0 ± 3.02 ($p = 0.006$). Similarly, BP_{ND} in hippocampus was significantly lower than that in lateral temporal gray matter (hippocampus vs. lateral temporal gray matter: 1.33 ± 0.37 vs. 2.97 ± 0.52, $p < 0.0001$). The western blot results also showed different optical density (OD) values between brain regions. The OD values of lateral temporal white matter, hippocampus, lateral temporal gray matter were 0.12 ± 0.08, 0.38 ± 0.11, 0.75 ± 0.25 (mean ± SD), respectively. The hippocampus OD values were significantly different from those of the lateral temporal white matter or gray matter ($p = 0.005$ vs. white matter, $p = 0.03$ vs. gray matter). V_T values

of the four subjects with arterial data from 3 regions (hippocampus, lateral temporal white and gray matter) were well correlated with western blot results (Figure A). The R^2 was 0.69 and p value was <0.001. Note that K_1 from ^{11}C-UCB-J also showed similar results (R^2 = 0.77 for K_1; Figure B). FDG SUV had a lower correlation values with western blot results (R^2 = 0.38). BP_{ND} values in hippocampus and lateral temporal gray matter showed a trend of correlation with Western blot results, but it was not significant in this small sample (p=0.10; Figure C).

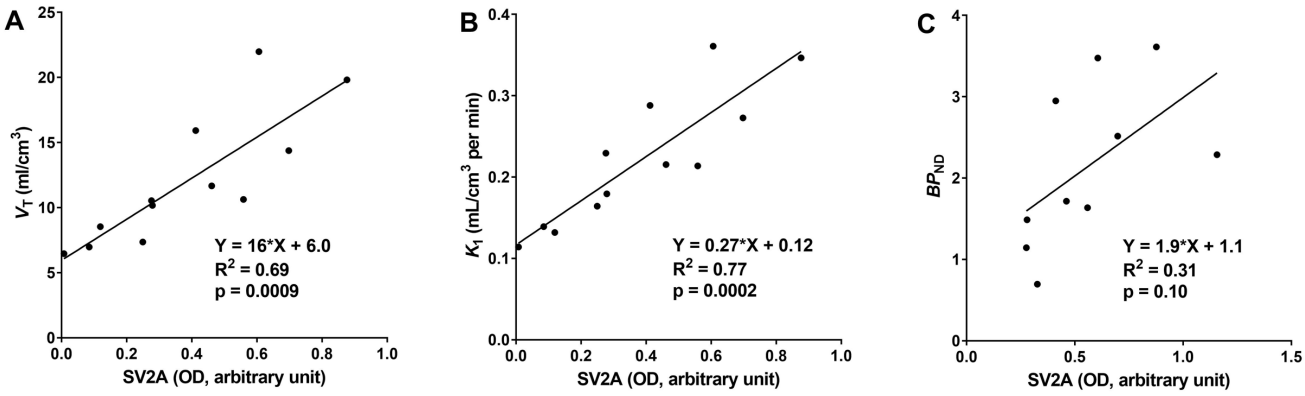

Figure. The scatter plots with *in vivo* imaging results with ^{11}C-UCB-J and *ex vivo* western blot results. V_T (A) and K_1 (B) significantly correlated with ex vivo SV2A density measures. Although there was no significance for BP_{ND} values, there was a similar trend (C).

Discussion/Conclusion:

The distribution volume from ^{11}C-UCB-J PET was well correlated with SV2A measured by Western blot in samples surgically resected from patients with mesial temporal lobe epilepsy. These results further support the validity of ^{11}C-UCB-J as an *in vivo* SV2A biomarker in humans. In addition, ^{11}C-UCB-J K_1 and FDG SUV showed similar results, consistent with the expected correlation of synaptic density (and function) with blood flow and glucose metabolism.

References:

1. Nabulsi NB, Mercier J, Huang Y, et al. [2016] JNM 57:777-84
2. Finnema SJ, Nabulsi NB, Carson RE, et al. [2016] Sci. Transl. Med. 8(348):348ra96

OP53
Measuring NMDA-receptor activation in focal epilepsy using [^{18}F]GE-179 PET

Marian Galovic, Kjell Erlandsson, Ben Thomas, Hasan Sari, Sarah McQuaid, Kris Thielemans, Brian Hutton, Kerstin Sander, Erik Arstad, Colm McGinnity, Fiona Heeman, Bianca De Blasi, Ilaria Boscolo Galazzo, Alaleh Rashidnasab, William Trigg, Sajinder Kaur Luthra, Jo Stevens, Tim Fryer, Young T. Hong, Jonathan Coles, Simon Eaglestone, David Brown, Ana Barnes, Ashley Groves, John Duncan, Matthias J Koepp

Department of Clinical and Experimental Epilepsy, Institute of Nuclear Medicine, and Department of Chemistry, University College London, UK
MRI Unit, Chalfont Centre for Epilepsy, UK
Department of Neurology, Kantonsspital St. Gallen, Switzerland
Division of Imaging Sciences & Biomedical Engineering, King's College London, UK
GE Healthcare plc, The Grove Centre, Amersham, UK
Division of Anaesthesia and Wolfson Brain Imaging Centre, University of Cambridge, UK

Introduction:
N-methyl-D-asparate (NMDA) receptors are involved in generating and sustaining seizures and play a role in the development of epilepsy (epileptogenesis). A pilot study found globally increased NMDA receptor activation in the brain of people with epilepsy [1]. We measured activation of NMDA receptors using [^{18}F]GE-179 positron emission tomography (PET) in people with focal epilepsy and determined its value in lateralizing and localizing the epileptic focus for presurgical evaluation of epilepsy.

Materials and Methods:
Twenty-five consecutive people with focal epilepsy undergoing comprehensive presurgical evaluation and nine healthy controls matched for age and gender received a [^{18}F]GE-179 PET scan. GE-179 is a novel ligand that selectively binds to the open (i.e. activated) NMDA receptor, which is thought to be overactive in epilepsy. Subject-wise comparisons of standardized uptake value (SUV) images were calculated using statistical parametric mapping (SPM) and compared with (i) visual analysis without a fixed threshold and (ii) a prespecified statistical threshold ($p<0.001$, uncorrected). Group-wise comparisons were performed in pre-defined regions of interest.

Results:
Visual inspection of threshold-free statistical maps indicated correct lateralization of the epileptic focus in 92% (23/25 cases, $p<0.001$) and correct localization in 84% (21/25 cases, $p<0.001$). Two example cases are shown in Figure 1. There was substantial agreement with the conclusions of pre-surgical investigations (Cohen's kappa 0.85 and 0.83 respectively). Using a fixed statistical threshold ($p<0.001$), significant signal-abnormalities co-localized with results of pre-surgical investigations in 68% (17/25) cases. A group-level analysis in people with temporal lobe epilepsy (n=18) compared to healthy controls (n=9) showed significant ($p<0.05$) signal increase in the bilateral parahippocampal gyrus, contralateral amygdala, and bilateral orbitofrontal cortex (Figure 2A). The group with mesial temporal lobe epilepsy (n=9) had significant ($p<0.05$) signal increases in areas known to be highly involved in epileptic seizure generation, including the bilateral temporal neocortex, contralateral hippocampus and amygdala, bilateral thalamus, ipsilateral cingulate cortex, and bilateral orbitofrontal cortex (Figure 2B).

Discussion:
[^{18}F]GE-179 PET might help characterize the network involved in generating epileptic seizures. This instrument could be helpful for evaluating the lateralization and localization of the epileptogenic focus.

Figure 1

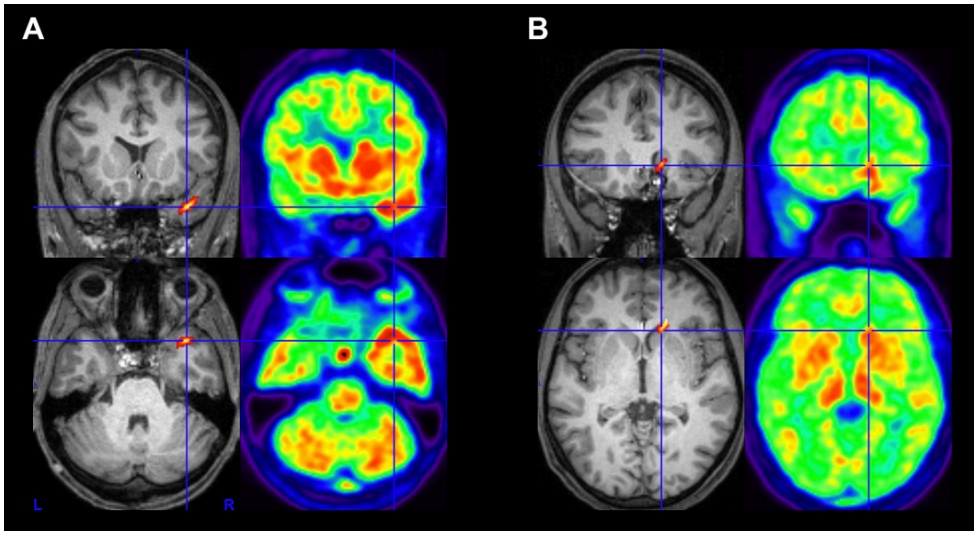

Figure 2

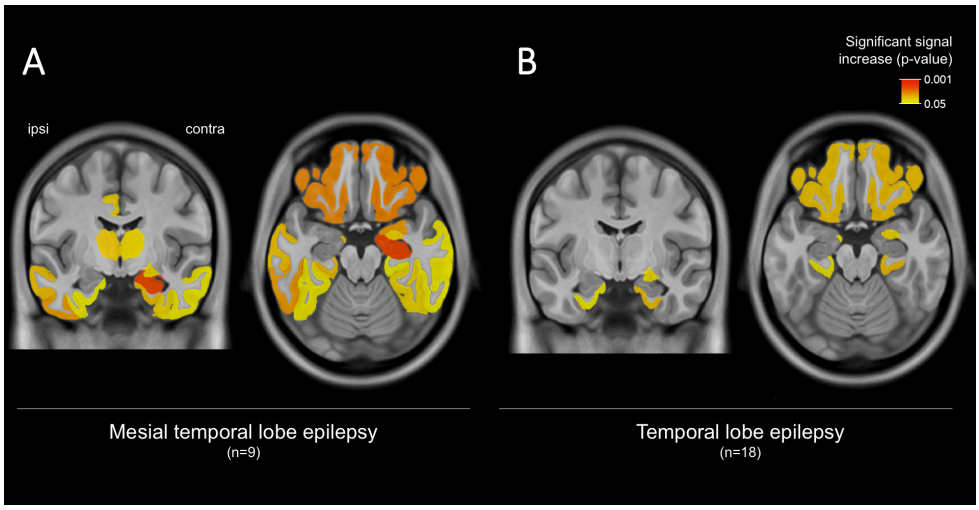

Acknowledgments:
This study was funded by the UK Medical Research Council grant MR/L013215/1.

References:
1. McGinnity CJ, Koepp MJ, Hammers A, Riaño Barros DA, Pressler RM, Luthra S, et al. NMDA receptor binding in focal epilepsies. J Neurol Neurosurg Psychiatr 2015; 86: 1150–1157.

OP54
Frontolimbic connectivity mediates the link between neuroinflammation and depressive symptoms in human chronic pain

Albrecht DS[1], Kim M[1], Akeju O[2], Torrado-Carvajal A[1], Edwards RR[3], Zhang Y[2], Bergan C[1], Protsenko E[1], Kucyi A[1,4], Hooker JM[1], Napadow V[1], Loggia ML[1]

[1]A.A. Martinos Center for Biomedical Imaging, Massachusetts General Hospital, Harvard Medical School (MGH/HMS), Boston MA
[2]Department of Anesthesia, Critical Care and Pain Medicine, MGH / HMS, Boston MA
[3]Department of Anesthesiology, Perioperative and Pain Medicine, Brigham and Women's Hospital, HMS, Boston, MA
[4]Department of Neurology, Stanford University Medical Center, Stanford, California

Introduction:
The experience of chronic pain is intimately linked with negative affect, which can significantly complicate presentation, clinical course and treatment response[1]. Unfortunately, little is known about the pathophysiology of pain-related negative affect, including depression. Using integrated positron emission tomography/magnetic resonance imaging (PET/MRI) and [^{11}C]PBR28, we recently demonstrated elevated brain levels of the translocator protein (TSPO) in chronic low back pain (cLBP) patients[2]. As TSPO is a marker of glial activation, this study provided a link between neuroinflammation and chronic pain. Here we further our understanding of the clinical significance of brain TSPO elevation in chronic pain, and tested the hypothesis that, in certain regions, elevated TSPO may be associated with pain-related depressive symptoms, providing support to a neuroinflammatory hypothesis of negative affect[3]. Moreover, because glial activation has been suggested to modulate functional connectivity between brain regions involved in affective processing[4], we evaluated whether inflammation could be associated with regional connectivity changes in pain-related depressive symptoms.

Material and Methods:
25 cLBP patients and 27 healthy control subjects received [^{11}C]PBR28 PET/MRI scans. Standardized uptake value ($SUV_{60\text{-}90min}$) images, normalized by whole brain (SUVR), were used as a PET outcome metric. We first tested for an association between [^{11}C]PBR28 SUVR and Beck Depression Inventory (BDI) scores using a region of interest (ROI) approach, focused on regions previously identified as potentially relevant for depression (insula, prefrontal and anterior cingulate cortex [PFC, ACC])[3]. These analyses were followed up by whole-brain voxelwise regression analysis. From regions demonstrating a statistically significant association between PET signal and BDI, average SUVR was compared between cLBP patients with high BDI (≥10; n=7), patients with low BDI (<10; n=18), and controls. Using resting-state functional MRI data (TR/TE=2sec/30ms, flip angle=90°, voxel size=3.1x3.1x3mm, 37 slices) collected simultaneously to the PET data, we tested the hypothesis that BDI was associated with differential connectivity in regions showing depression-related neuroinflammation. To this end, we performed a whole brain voxelwise seed-based functional connectivity analysis, utilizing a $3mm^3$ sphere from regions demonstrating a significant association between regional SUVR and BDI from the voxelwise analysis (pregenual and anterior middle cingulate cortices [pgACC, aMCC]; see Results). Functional connectivity analyses included motion parameters and cardiorespiratory noise (estimated using CompCor) as nuisance regressors. Associations between connectivity, PET signal, and BDI scores were assessed with Pearson correlations. Finally, we constructed a mediation model to test the hypothesis that altered connectivity mediated the association between cortical neuroinflammation and depressive symptoms. When appropriate, analyses were conducted controlling for the Ala147Thr *TSPO* polymorphism (which predicts binding affinity to [^{11}C]PBR28)[5].

Results:
In cLBP patients, BDI scores were significantly positively associated with [^{11}C]PBR28 signal in all a priori ROIs: ACC, PFC, and insula (p's<0.033). In follow-up voxelwise regression analyses, a positive relationships between BDI and [^{11}C]PBR28 signal was significant in pgACC and aMCC (**Figure 1**). Average PET signal in pgACC and aMCC was significantly higher in "high BDI" cLBP patients compared to controls (p's<0.003), and no different between "low BDI" cLBP patients and controls (p's>0.137). The pgACC also demonstrated functional connectivity to the dorsolateral PFC (dlPFC) that was correlated with both BDI (p<0.000) and [^{11}C]PBR28 signal in the pgACC (p=0.007; **Figure 2**). The mediation analysis determined that pgACC-dLPFC connectivity was a significant mediator of the association between pgACC PET signal and BDI (**Figure 3**).

Discussion:
These results suggest that neural communication between dlPFC and pgACC, two regions involved in emotional regulation and implicated in the pathophysiology of depression, may mediate the link between neuroinflammation and depressive symptoms in chronic pain. These observations support the existence of a neuroinflammatory component underlying negative affect in pain disorders, suggesting that glial cells may be therapeutic targets for chronic pain and related comorbidities, such as major depressive disorder.

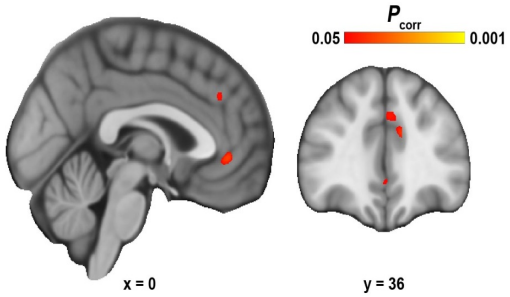

Figure 1. Voxel-wise correlations between SUVR and BDI in cLBP patients (n=25).

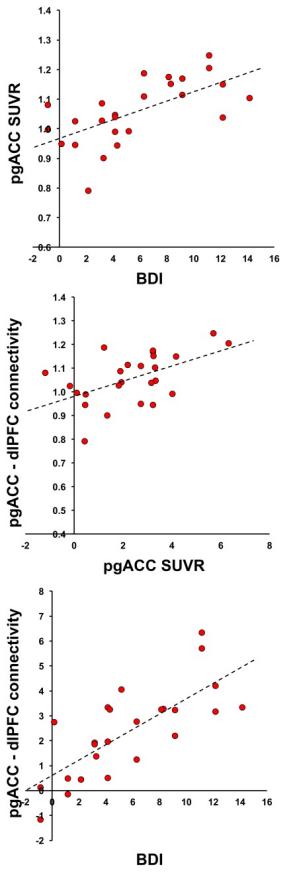

Figure 2. Associations between pgACC SUVR, pgACC-dlPFC connectivity, and BDI

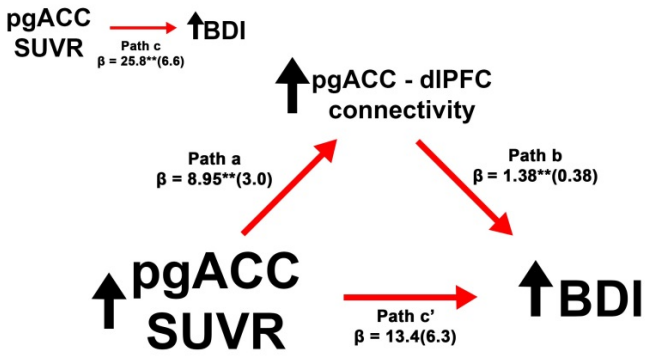

Figure 3. Mediation analysis between pgACC SUVR (IV), BDI (DV), and pgACC-dlPFC connectivity (mediator).

Acknowledgments:
Support: 1R21NS087472-01A1/1R01NS095937-01A1(MLL).

References:
[1] Leo RJ. [2005] Curr Treat Options Neurol 7(5):403-12.
[2] Loggia ML, Chonde D, Akeju O, et al. [2015] Brain 138(Pt 3):604-15
[3] Setiawan E, Wilson A, Mizrahi R, et al. [2015] JAMA Neurol 72(3):268-2752
[4] Colasanti A, Guo Q, Giannait P, et al. [2016] Biol Psych 80:62-72.
[5] Owen DR, Yeo AJ, Gunn RN, et al. [2012] JCBFM 32:1-5.

OP55
Dynamic PET shows cerebral spinal fluid flow alterations in Alzheimer's disease and multiple sclerosis

Julia J Schubert[1], Mattia Veronese[1], Livia Marchitelli[1], Benedetta Bodini[2], Matteo Tonietto[2], Bruno Stankoff[2], Zhen Fan[3], David J Brooks[3], Paul Edison[3], Federico Turkheimer[1]

[1]Centre for Neuroimaging Sciences, Institute of Psychiatry (PO89), London, UK
[2]Sorbonne Universités, UPMC Paris 06, Institut du Cerveau et de la Moelle épinière, ICM, Hôpital de la Pitié Salpêtrière, Inserm UMR S 1127, CNRS UMR 7225, Paris, France
[3]Imperial College London, London, UK

Introduction:
The clearance of solutes and maintenance of fluid homeostasis in the brain parenchyma may be largely accomplished by the newly discovered glymphatic system[1]. This system is thought to be analogous to the peripheral lymphatic system with the additional involvement of glial cells and relies on the normal flow of cerebrospinal fluid (CSF) in the brain[1]. Results from previous studies consistently suggest that alterations of CSF flow contribute to development and progression of neuroinflammatory diseases such as Alzheimer's disease[2,3] (AD) and multiple sclerosis[4,5,6] (MS). Early detection of diminished glymphatic clearance could serve a vital role in the prevention and early diagnosis of inflammatory neurological disorders[7]. However, non-invasive in vivo methods for measuring glymphatic function are limited and the majority of existing data has been collected using animal models[2,6,8]. Dynamic ^{11}C-PiB PET has been used to quantify CSF clearance in humans[3] and could serve as a measure for in-vivo investigation of the glymphatic system. The aims of the current work are to 1) replicate the previous results in AD[3], 2) extend the method to mild cognitive impairment (MCI) patients as well as MS patients, and 3) use these results to make appropriate interpretations about CSF clearance and glymphatic function in healthy and diseased populations.

Materials and Methods:
To investigate differences in CSF clearance in AD and MS, analysis was performed on two separate datasets. One dataset included 12 AD patients, 12 MCI patients, and 12 age- and sex-matched HC[9] and a second dataset included 20 relapsing-remitting MS patients and 8 age- and sex- matched HC[10]. All subjects underwent ^{11}C-PiB PET scanning. One AD and one MCI subject were later excluded from the analysis due to image artifacts. For the AD/MCI dataset, preprocessing was performed and time activity curves (TACs) were calculated using a MIAKAT™ (http://www.imanova.co.uk) pipeline. A priori designated regions of interest (ROIs) were used for the cerebellar cortex reference region and a gray matter ROI. Manual lateral ventricle ROIs were generated for all subjects from both datasets using the ITK-SNAP[11] (www.itksnap.org) snake tool. Standardized uptake value ratios (SUVR) were calculated for each subject from both datasets using cerebellum or cortical gray matter as reference respectively for AD and MS. For consistency with a previous study conducted by de Leon et al.[3], area under the curve (AUC) was calculated for 27 subjects in the AD/MCI dataset due to missing body weight data of 7 subjects. AUC was also calculated for all subjects in the MS dataset. Statistical analysis was performed in SPSS.

Results:
Analysis of variance revealed significant group differences in SUVR across the AD, MCI, and HC groups ($p=0.002$). Additional pairwise comparisons revealed significantly lower magnitude of ventricular PiB, as measured by SUVR, in AD compared to HC ($p<0.001$) and in AD compared to MCI ($p=0.026$). No significant difference in SUVR was observed between MCI and HC ($p=0.217$). Magnitude of ventricular PIB, as measured by SUVR, was

significantly lower in MS than in HC (p=0.009). AUC_{35-80} was significantly lower in AD than in HC (p=0.006). There were no other significant differences in AUC_{35-80} between groups.

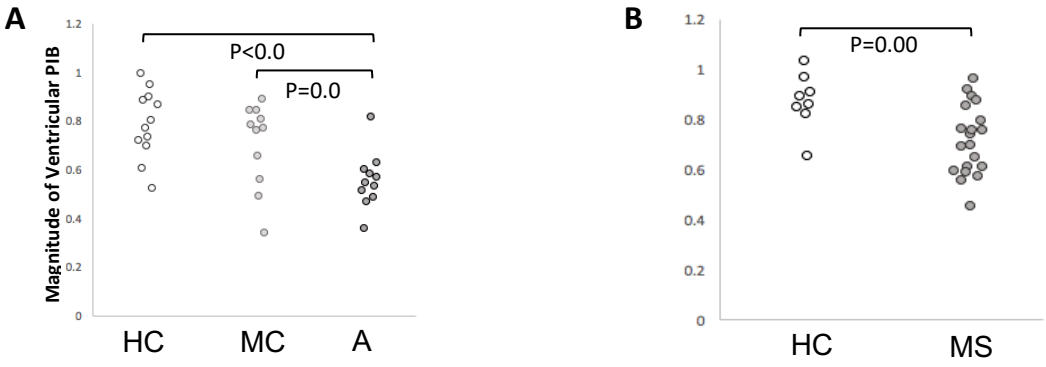

Figure 1. Magnitude of ventricular PIB measured by SUVR in **A.** healthy controls (HC), mild cognitive impairment (MCI) and Alzheimer's disease (AD) and **B.** in HC and multiple sclerosis (MS).

Discussion:

The observation of decreased signal in the ventricular ROIs could indicate reduced tissue-to-CSF clearance in both AD and MS compared to HC, consistent with our hypothesis. Our results in AD are consistent with a previous study conducted by de Leon et al. The MCI cohort has SUVR and AUC values between those of HC and AD. Reduced CSF clearance in AD and MS likely contributes to accumulation of toxic substances in the brain, which could be a contributing factor in the development of disease. Additional information is required to determine potential causes for a decrease in CSF flow and whether decreased CSF flow precedes the development of disease. To further understand the CSF clearance system it may also be important to determine a technique to appropriately control for differences in ventricle size and tissue atrophy between patient and healthy control groups in future analyses. Further analysis is required to determine if CSF clearance may be indicative of clinical status and whether MCI conversion to AD can be predicted with SUVR and/or AUC values.

Acknowledgements

The original MS study received funding from the European Leukodystrophy Association, INSERM-DHOS, Assistance Publique des Hôpitaux de Paris, and the "Investissements d'avenir" ANR-10-IAIHU-06 grant. We also graciously acknowledge Hammersmith Imanet for provision of radiotracers and scanning facilities used for acquiring the AD/MCI dataset.

References

1. Iliff JJ, Wang M, Liao Y et. al. [2012] Sci.Transl.Med 4: 147ra111
2. Peng W, Achariyar TM, Li B et. al. [2016] Neurobiol.Dis 93: 215-25
3. de Leon MJ, Li Y, Okamura N et. al. [2017] J.Nucl.Med 58: 1471-6
4. Magnano C, Schirda C et. al. [2012] J.Magn.Reson.Imaging 36: 825-34
5. ElSankari S, Balédent O et. al. [2013] J.Cereb.Blood.Flow.Metab 33: 1314-21
6. Wolburg-Buchholz K, Mack AF et. al. [2009] Acta.Neuropathol 118: 219-33
7. Jessen N, Munk A, Lundgaard I et. al. [2015] Neurochem.Res 40: 2583-99
8. Iliff JJ, Lee, Lee H, Yu M et. al. [2013] J.Clin.Invest 123: 1299-1309
9. Edison P, Archer HA, Hinz R et. al. [2007] Neurology 68: 501-508.
10. Bodini B, Veronese M, García-Lorenzo D et al. [2016] Ann.Neurol. 79: 726-38
11. Yushkevich PA, Piven J, Hazlett HC et. al. [2006] Neuroimage 31: 1116-28

OP56
Suitability of [^{18}F]FAZA to Measure Hypoxia in Glioblastoma Using PET

David Gorman[1], Natale Quartuccio[1], Daniel Lewis[1,3], Erjon Agushi[1], Georgios Krokos[1], Ibrahim Djoukhadar[4], David Coope[2,3], Alan Jackson[1], Marie-Claude Asselin[1]

[1] *Wolfson Molecular Imaging Centre, Division of Informatics, Imaging and Data Sciences, The University of Manchester, Manchester, UK.*
[2] *Division of Neuroscience and Experimental Psychology, The University of Manchester, Manchester, UK.*
[3] *Department of Neurosurgery, Salford Royal NHS Foundation Trust, Manchester, UK*
[4] *Department of Neuroradiology, Salford Royal NHS Foundation Trust, Manchester, UK*

Introduction:

Insufficient oxygen supply, termed hypoxia, within solid tumours encourages malignant progression and metastatic spread, and is associated with poor treatment response. PET with radiolabelled nitroimidazoles such as [^{18}F]MISO and [^{18}F]FAZA can measure tumour hypoxia non-invasively. In glioblastoma multiforme (GBM), however, the potential for blood-brain barrier (BBB) disruption to confound hypoxia-specific accumulation of [^{18}F]FAZA has yet to be fully characterised [1]. This work aims to combine multi-modal MRI with sequential dynamic [^{15}O]H_2O and [^{18}F]FAZA PET to assess the suitability of [^{18}F]FAZA to identify hypoxic areas in GBM.

Materials and Methods:

To date, five patients with suspected GBM have been recruited. Subsequent histopathological examination confirmed the radiological diagnosis except for patient 4 who was re-classified as transforming pilocytic astrocytoma. Prior to surgery, three dynamic PET scans were acquired on a Siemens HRRT with arterial blood sampling. Patients were first administered with a bolus injection of [^{15}O]H_2O (529-576 MBq) and scanned for 5 min to measure cerebral perfusion. Ten minutes later, a bolus injection of [^{18}F]FAZA (413-556 MBq) was administered with emission data collected for 0-60 min (early scan) and 90-150 min (late scan) p.i. Complimentary T_2-weighted fluid-attenuated inversion recovery (FLAIR) and T_1-weighted (T_1W) MR images before and after Dotarem administration were acquired on a 1.5T Philips Achieva MR scanner. A 6.0-mm or 4.9-mm FWHM Gaussian filter was applied to the dynamic [^{15}O]H_2O and [^{18}F]FAZA PET images, respectively. Fixed size (116 mm^3) regions of interest (ROI) were manually positioned [2] on the necrotic core, tumour on the enhancing rim of the contrast-enhanced T_1W image, tumour outside of the enhancing rim that exhibited high [^{18}F]FAZA uptake, and on contralateral grey and white matter (**Figure 1a**). Patients were given pimonidazole prior to image-guided surgery and targeted biopsies were taken for biological validation.

Results:

[^{18}F]FAZA readily enters erythrocytes as revealed by a constant plasma-to-blood ratio of 0.95±0.03. [^{18}F]FAZA also crosses the BBB as indicated by the tissue-to-plasma ratio of 0.24±0.05 and 0.11±0.02 at 120-150 min p.i. for grey and white matter, respectively. However, the radiotracer may not have reached equilibrium by 150 min (**Figure 1b**). On this low background, accumulation of [^{18}F]FAZA is clearly observed within the enhancing rim for all GBM patients (**Figures 1c** and **2**). Patients 1 and 2 additionally exhibit areas of high [^{18}F]FAZA uptake in suspected tumour tissue outside of the enhancing rim. For patient 1, cerebral perfusion was abnormally low (**Figure 1d**) with similar perfusion observed in the grey matter and within the enhancing rim. Higher perfusion was observed in the non-enhancing tumour area with high FAZA uptake (**Figure 1e**). Extra-tumoral perfusion was normal in patient 5 but not available for the other three patients due to technical difficulties.

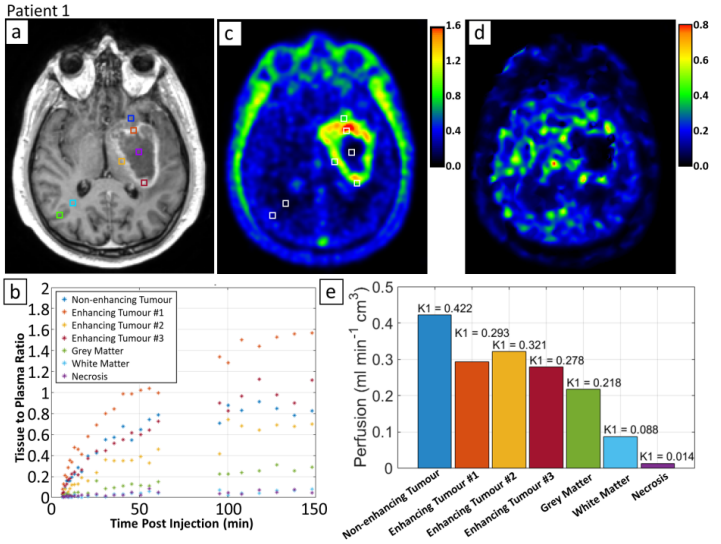

Figure *1*: Preliminary analysis of patient with glioblastoma, a) contrast- enhanced T_1W MR image showing ROIs, b) time course of [^{18}F]FAZA tissue-to-plasma ratio c) map of [^{18}F]FAZA tissue-to-plasma ratio at 120-150 min p.i., d) perfusion map from [^{15}O]H_2O scan, and e) mean perfusion for individual ROIs (colour coded).

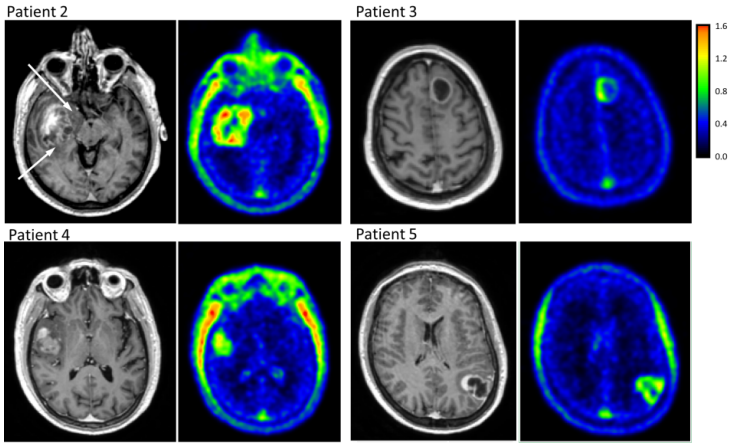

Figure 2: Contrast-enhanced T_1W MR images (grey) and [^{18}F]FAZA tissue-to-plasma ratio maps at 120-150 min (colour) for patients with GBM (2, 3, 5) and transforming pilocytic astrocytoma (4). Regions of notable discordance between the MR and PET images are indicated by arrows.

Conclusion:

Relative to plasma, [^{18}F]FAZA uptake in tumour is comparable to published values for the more lipophilic tracer [^{18}F]FMISO [3] but lower in the brain. The extent to which the uptake represents hypoxia will be further investigated with pharmacokinetic analysis of the PET data and histological assessment. Recruitment is ongoing.

References:

1. Postema EJ, McEwan AJB, Riauka TA, *et al*. [2009]. Eur J Nucl Med Mol Imaging 36:1565-73.
2. Preibisch C, Shi K, Kluge A, *et al*. [2017]. NMR Biomed 30: doi: 10.1002/nbm.3775.
3. Valk PE, Mathis CA, Prados MD, *el al*. [1992] J Nucl Med 33: 2133-37.

OP57

The expression of inflammatory markers and their potential influence on efflux transporters in drug-resistant mesial temporal lobe epilepsy tissue

Lora D. Weidner[1,2], Pavitra Kannan[3], Nicholas Mitsios[2], Sun J. Kang[4], Matthew D. Hall[5], William H. Theodore[6], Robert B. Innis[1], Jan Mulder[2]

[1]*Molecular Imaging Branch, National Institute of Mental Health, NIH, Bethesda, MD*
[2]*Department of Neuroscience, Karolinska Institutet, Stockholm, Sweden*
[3]*CRUK/MRC Oxford Institute for Radiation Oncology, University of Oxford, Oxford, UK*
[4]*Statistical Genomics and Data Analysis Core, National Institute of Mental Health, NIH, Bethesda, MD*
[5]*Chemical Genomics Center, National Center for Advancing Translational Sciences, NIH, Bethesda, MD*
[6]*Clinical Epilepsy Section, National Institute of Neurological Disorders and Stroke, NIH, Bethesda, MD*

Introduction:
It is unclear what type of role neuroinflammation plays in mesial temporal lobe epilepsy (MTLE). Animal models of epilepsy have shown increases in the inflammatory enzymes cyclooxygenase (COX)-1, and -2. COX-1 and -2 convert arachidonic acid into prostanoids [1]. Which prostanoids are produced is dependent on the type of cell in which this pathway is activated. Therefore, knowing the cellular expression of COX-1 and COX-2 is important for understanding their function. Only two studies have investigated the expression of COX-2 in epilepsy, but there are no reports on COX-1. We therefore sought to measure the expression of COX-1, COX-2, and TSPO (an inflammatory biomarker included as a positive control) in brain tissue samples from patients with drug-resistant MTLE.
Since a high portion of MTLE patients are drug resistant, we also investigated whether a correlation exists between ABC transporter expression and inflammation. Upregulation of the ABC transporters P-glycoprotein (P-gp) and breast cancer resistance protein (BCRP) at the blood-brain barrier is thought to contribute to drug-resistant epilepsy (DRE) [2]. Increased P-gp expression has been reported in brain tissue samples from subjects with DRE; however, such studies traditionally suffer from a lack of appropriate control tissue. Previous animal studies have shown that certain inflammatory proteins upregulate ABC transporter expression [3], but this relationship needs to be elucidated in human tissue. Therefore, we also measured the levels of expression of P-gp and BCRP, to see whether they correlated with COX-1, COX-2, or TSPO immunoreactivity.

Materials and Methods:
Formalin-fixed, paraffin-embedded surgical brain tissue was obtained from patients with drug-resistant MTLE (n = 31). We used multiplex immunofluorescence and in-situ hybridization protocols to quantify expression and distribution of COX-1, COX-2, and TSPO amongst microglia, astrocytes, and neurons within the tissue. We also stained for P-gp and BCRP expression within glucose transporter positive capillaries.

Results:
We found that COX-1 is expressed in microglia, while COX-2 and TSPO are expressed in microglia and neurons. In-situ hybridization confirmed a higher expression of all three proteins in microglia over astrocytes. BCRP density was significantly correlated with TSPO density, suggesting a potential relationship between inflammatory markers and efflux transporters. No other correlations between BCRP or P-gp and COX-1, COX-2, or TSPO were observed.

Discussion:
Knowing the cellular localization of the inflammatory proteins COX-1 and COX-2 is important for understanding their function. To the best of our knowledge, this is the first study to measure the cellular expression of COX-1, COX-2, and TSPO amongst microglia, astrocytes, and neurons in surgical brain tissue samples from patients with drug-resistant MTLE. Further research is needed to determine the effects of the COX inflammatory pathway in epilepsy. In addition, we observed a positive linear correlation between BCRP and TSPO. This finding warrants further investigation to understand the relationship between inflammation and drug-resistance in the context of epilepsy.

Acknowledgements:
This work was supported by Intramural Research Programs of the National Institute of Mental Health, the National Institute of Neurological Disorders and Stroke, and by Karolinska Institutet. We thank Dr. Yin Yao for statistical assistance. We also thank Drs Sara Inati and Susumu Sato for evaluation of the patients, and Drs John Heiss and Kareem Zaghloul who performed the resective surgeries.

References:
[1] Aid, S., Bosetti, F., Targeting cyclooxygenases-1 and -2 in neuroinflammation: therapeutic implications. *Biochimie* **93**, 46-51 (2011).
[2] Kwan, P., Schachter, S. C., Brodie, M. J., Drug-resistant epilepsy. *N. Engl. J. Med.* **365**, 919-926 (2011).
[3] Bauer, B. *et al.*, Seizure-induced up-regulation of P-glycoprotein at the blood-brain barrier through glutamate and cyclooxygenase-2 signaling. *Mol. Pharmacol.* **73**, 1444-1453 (2008).

RF1
Optimized protocol for quantification of task-specific glucose metabolism and comparison to functional MRI

Lucas Rischka[1], Gregor Gryglewski[1], Sarah Pfaff[2], Thomas Vanicek[1], Marius Hienert[1], Manfred Klöbl[1], Markus Hartenbach[2], Wolfgang Wadsak[2,3], Markus Mitterhauser[2,4], Marcus Hacker[2], Siegfried Kasper[1], Rupert Lanzenberger[1], Andreas Hahn[1]

[1] *Department of Psychiatry and Psychotherapy, Medical University of Vienna, Austria*
[2] *Department of Biomedical Imaging and Image-guided Therapy, Division of Nuclear Medicine, Medical University of Vienna, Austria*
[3] *Center for Biomarker Research in Medicine (CBmed), Graz, Austria*
[4] *Ludwig Boltzmann Institute Applied Diagnostics, Vienna, Austria*

Introduction:
The brain's energy demands in glucose and oxygen can be readily assessed with PET and functional MRI (fMRI), respectively. The introduction of combined PET/MRI systems now enables the simultaneous acquisition of both modalities and multimodal analyses. The recently introduced approach of functional PET (fPET) with constant infusion of [^{18}F]FDG offers the quantification of task-specific changes in glucose metabolism (CMRGlu) in a single measurement [1,2]. Since fPET is still in its infancy, we aimed to enhance the procedure with an initial bolus application, an evaluation if automatic blood sampling was required and a multimodal separation between task and baseline metabolism. Additionally, we investigated the association of task-specific changes in glucose and oxygen demands.

Materials & Methods:
Twenty healthy subjects underwent one measurement on a fully-integrated PET/MRI system. The radioligand [^{18}F]FDG was administered 1 min as a bolus of 20% followed by constant infusion. During the examination, the subjects completed two tasks in four blocks for fMRI (4x30 s blocks) and for fPET (4x10,5,2 or 1 min). The tasks consisted of finger-tapping, where the thumb of the right hand was repeatedly moved towards the fingers, and simultaneously watching landscape movies. The blocks were separated by a baseline condition where subjects observed a black cross on grey background and let their thoughts wander.
To separate task from baseline metabolism a general linear model analysis was carried out with baseline, task and movement regressors. The baseline term was defined with three different approaches: i) multimodal, where all task-relevant voxels were excluded as determined by the individual fMRI analysis, ii) atlas-based, where presumably task-specific regions were removed and iii) model-based, where all grey matter voxels were fitted with exponential functions. To capture the initial peak of the input function, arterial blood samples were drawn automatically for the first 5 mins and manually thereafter. Finally, the Patlak plot was applied to assess task-specific changes in CMRGlu.

Results:
A high correlation between CMRGlu quantified with and without arterial blood sampling was achieved ($r=0.9996$, $n=13$). The multimodal baseline definition provided better model fits than the other tested approaches ($p<0.001$).
Significant changes in primary motor and visual cortices were found with fPET and fMRI. However, higher peak t-values were achieved with fPET (t_{M1} = 18.7 and t_{V1} = 18.3) as compared to fMRI (t_{M1} = 16.0 and t_{V1} = 17.6, $p<0.05$ FWE-corrected, Figure 1) as well as higher percent signal change (~18 to 27% with fPET vs ~2% with fMRI). Additional active regions were found with fMRI in the supplemental motor area, secondary visual and

contralateral motor cortex. The association between task-specific CMRGlu and fMRI was not significant (r=0.26).

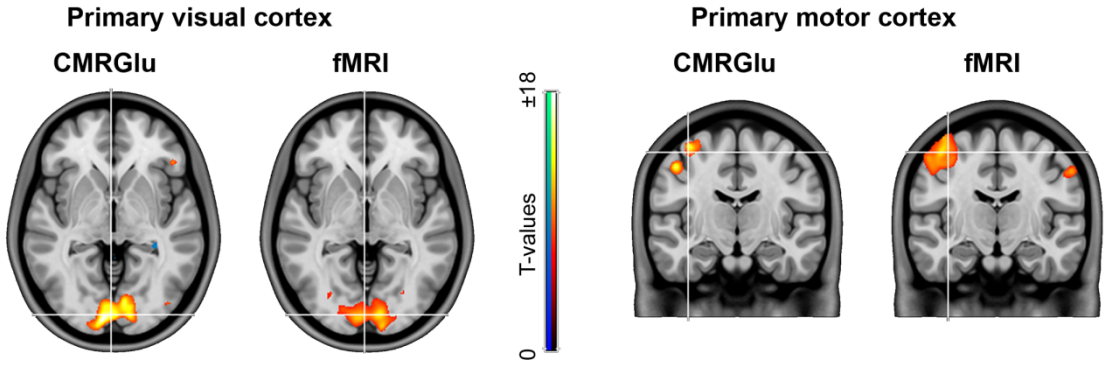

***Figure 1**: Task-specific changes were found in the primary visual and motor cortices with fMRI and fPET with higher peak t-values for the latter (p<0.05 FWE-corrected).*

Conclusion:
The protocol of an initial bolus of 20% followed by constant infusion does not require automatic blood sampling, increases the PET signal-to-noise ratio and leaves a sufficient amount of radioligand to determine task-specific changes in CMRGlu. The ideal approach for a reliable baseline definition and hence, identification of task-specific effects, was to exclude voxels which were active in the individual fMRI analysis. Although task-specific changes could be found with fPET and fMRI, the non-significant correlation, the different activation patterns and the divergence of percent signal change suggest that the two modalities capture complementary physiological aspects of brain energy metabolism.

Acknowledgements:
This research was supported by a grant from the Austrian Science Fund to A.Hahn (FWF KLI 610). L.Rischka, G.Gryglewski and M.Klöbl are recipients of DOC Fellowships of the Austrian Academy of Sciences at the Department of Psychiatry and Psychotherapy, Medical University of Vienna.

References:
[1] Villien M, Wey H-Y, Mandeville JB et al. [2014] NeuroImage 100:192-199.
[2] Hahn A, Gryglewski G, Nics L et al. [2016] J.Nucl.Med 57:1933-1940.

RF2

Lower levels of the glial marker TSPO in psychosis patients – an individual participant data meta-analysis

Pontus Plavén-Sigray[1], Granville J. Matheson[1], Karin Collste[1], Abhishekh H. Ashok[2,3,4], Jennifer M. Coughlin[5,7], Oliver D. Howes[2,3,4], Romina Mizrahi[6], Martin G. Pomper[5,7], Pablo Rusjan[6], Mattia Veronese[8], Yuchuan Wang[7], **Simon Cervenka[1]**

[1]Department of Clinical Neuroscience, Center for Psychiatry Research, Karolinska Institutet and Stockholm County Council, SE-171 76 Stockholm, Sweden
[2]IoPPN, King's College London, De Crespigny Park, London, SE5 8AF, UK
[3]MRC London Institute of Medical Sciences, Hammersmith Hospital, London W12 0NN
[4]Institute of Clinical Sciences (ICS), Faculty of Medicine, Imperial College London, Du Cane Road, London W12 0NN
[5]Department of Psychiatry and Behavioral Sciences, Johns Hopkins Medical Institutions, Baltimore, MD, USA
[6]University of Toronto, Department of Psychiatry, Toronto, Canada
[7]Russell H. Morgan Department of Radiology and Radiological Science, Johns Hopkins Medical Institutions, Baltimore, MD, USA
[8]Department of Neuroimaging, Institute of Psychiatry, Psychology & Neuroscience, King's College London, London, UK

Introduction:
Accumulating evidence suggests that the immune system may have a role in the disease mechanism in schizophrenia. Using Positron emission tomography (PET) and radioligands binding to the translocator protein (TSPO), which is expressed on glial cells, brain immune function can be assessed in vivo. Thus far, PET TSPO studies in schizophrenia have been inconclusive. However, sample sizes have been limited, and most patients have been on antipsychotic medication which may be a confounding factor. We conducted an individual participant data meta-analysis of all TSPO PET studies performed in psychosis or schizophrenia using second-generation radioligands, where Total distribution volume (V_T) was included as the outcome measure. The primary objective was to evaluate the hypotheses of 1) an increase or 2) a decrease or 3) no difference in V_T between patients and healthy control subjects. A secondary objective was to assess the effects of antipsychotic medication on TSPO binding.

Materials and Methods:
Individual participant data were obtained from all PET studies that 1) used a second-generation TSPO radioligand, 2) reported distribution volume (V_T) values in brain in patients with psychosis as compared to healthy controls (HC), and 3) reported TSPO affinity type of all participants. The outcome measure was V_T in frontal cortex (FC), temporal cortex (TC) and hippocampus (HIP). Bayes factors (BF) were applied to examine the relative support for higher, lower or no-change of TSPO levels in patients as compared to healthy controls.

Results:
Five studies were included, amounting to 75 patients with first-episode psychosis or schizophrenia and 77 healthy control subjects (1-5). In all regions investigated, BF for lower V_T in patients was >32 (indicating that a decrease is 32 times more likely relative to no-change), and >422 relative to an increase. From the posterior distributions, mean patient-control differences in standardized V_T values were -0.48 for FC (95% credible interval (CredInt)=-0.88 to -0.09), -0.47 for TC (CredInt=-0.87 to -0.07) and -0.63 for HIP (CredInt=-1.00 to -0.25). The mean of the posterior over the change in standardized V_T due to medication was 0.009 for FC (CredInt95% -0.384 to 0.401), -0.013 for TC (CredInt95% -0.407 to 0.381) and -0.040 for HIP (CredInt95% -0.423 to 0.343).

Discussion:
To our knowledge, this is the first individual participant data metaanalysis in clinical PET research. Using Bayesian linear-mixed-effect modeling statistics, strong support was found for a reduction of TSPO in psychosis patients compared to control subjects. No support was found for an effect of antipsychotic drug treatment on TSPO levels. Lower TSPO binding could indicate a compensatory mechanism to a pro-inflammatory signal or altered function of glial cells such as abnormal energy utilization, both hypotheses that need to be addressed in future studies.

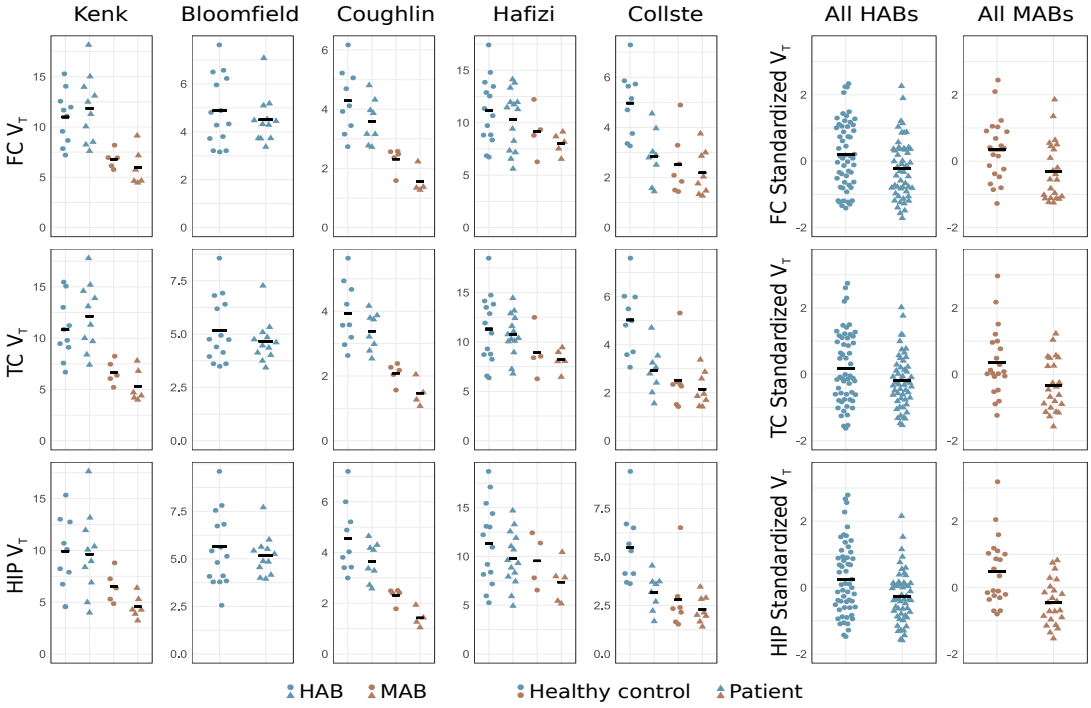

Fig 1. Individual participant raw data showing TSPO binding (estimated using V_T) in patients with psychosis disorder and healthy controls, from all five included studies, from frontal cortex (FC), temporal cortex (TC) and hippocampus (HIP). The black bars denote the group means. For each region, subjects' V_T values have been z-scored within study, and within TSPO genotype, in order to produce the pooled plots of all High Affinity Binders (HABs) and Mixed Affinity Binders (MABs).

References:

1. Bloomfield PS, Selvaraj S, Veronese M et. al. [2015] Am. J. Psychiatry 173:44-52
2. Kenk M, Selvanathan T, Rao N et. al. [2015] Schizophr. Bull. 41: 85–93.
3. Coughlin JM, Wang Y, Ambinder EB et. al. [2016] Transl. Psychiatry 12; 6:e777
4. Hafizi S, Tseng HH, Rao N et. al. [2017] Am. J. Psychiatry 174: 118–124.
5. Collste K, Plavén-Sigray P, Fatouros-Bergman H et. al. [2017] Mol. Psychiatry 22: 850–856.

RF3

Multi-delay arterial spin labeling MRI accurately identifies hypoperfusion in Moyamoya disease: comparison with a normative PET/MRI database

Audrey P. Fan[1], Mohammad M. Khalighi[2], Jia Guo[1], Yosuke Ishii[1], Mirwais Wardak[1], Jun-Hyung Park[1], Bin Shen[1], Dawn Holley[1], Harsh Gandhi[1], Prachi Singh[1], Tom Haywood[1], Gary K. Steinberg[2], Frederick T. Chin[1], Greg Zaharchuk[1]

[1]Radiology, Stanford University, Stanford, CA, United States;
[2]GE Healthcare, Menlo Park, CA, United States, [3]Neurosurgery, Stanford University, Stanford, CA, United States

Introduction:

Despite recent efforts[1] to standardize arterial spin labeling (ASL) MRI for perfusion imaging, typical ASL protocols often fail in patients with long arterial transit times (ATTs). In Moyamoya disease, patients benefit from cerebral blood flow (CBF) assessment to decide on surgical revascularization, but are prone to ASL inaccuracies due to extremely long ATT[2]. Furthermore, ASL lacks validation with a gold standard (PET), since natural fluctuations in brain perfusion render comparisons between different modalities challenging. This study uses simultaneous PET/MRI to compare multi-delay and standard ASL to [^{15}O]-water PET in Moyamoya patients; and investigates whether ASL and PET identify similar areas of pathophysiology relative to a normative database from healthy volunteers. We hypothesized that multi-delay ASL outperforms standard ASL because it directly estimates ATT with a kinetic model and uses this information to correct CBF measures.

Methods:

Simultaneous time-of-flight 3T PET/MRI (GE Healthcare Signa) was acquired in 15 healthy volunteers (ages 27-62 yrs, 8 female) and 15 patients with Moyamoya disease (ages 25-52 yrs, 11 female). Four patients had unilateral disease and the rest had bilateral stenosis or occlusion. PET imaging of CBF with injection of [^{15}O]-water (550-925 MBq) was performed simultaneously with standard ASL (single post-label delay, 2025ms) and sequential multi-delay ASL (5 delays, 700-3000ms). ASL scan parameters included pseudo-continuous labeling with label duration of 1450ms in standard-delay and 2000ms in multi-delay; echo time=10.7ms; bandwidth=62.5kHz; and 3D stack-of-spiral readout. All healthy volunteers and 12 patients underwent immediate repeat scans. Dynamic [^{15}O]-water PET frames were reconstructed (30x1s, 10x3s, 12x5s, 12x10s). An image-derived input function was created for each PET scan from the cervical arteries, with correction for spill-over effects based on an MRI angiogram[3]. PET CBF (ml/100g/min) maps were quantified by fitting a one-tissue kinetic model with weighted linear regression in PMOD software.

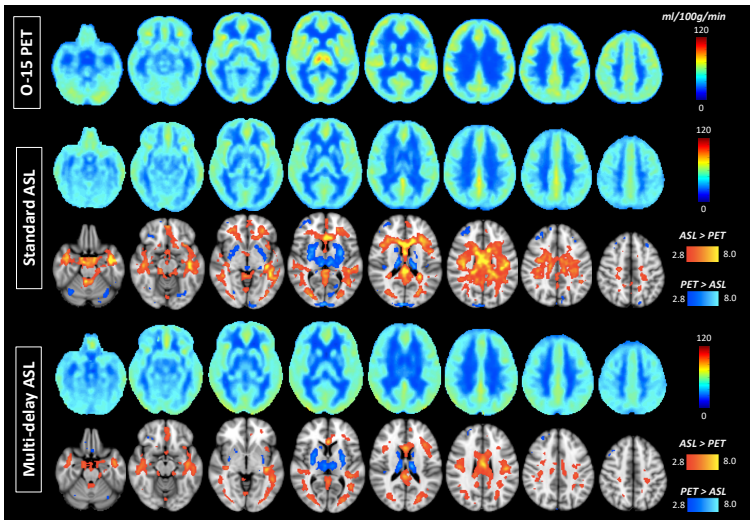

Figure 1. Normative database from healthy volunteers showing mean CBF by [^{15}O]-water PET, standard ASL, and multi-delay ASL. T-statistic maps show areas of overestimation (red) and underestimation (blue) of ASL relative to PET.

ASL CBF maps were quantified with a one-compartment model for standard ASL; and a two-compartment model for multi-delay ASL to correct for estimated ATT. CBF images were registered to the Montreal Neurological

Institute template with use of each individual's T_1-weighted anatomical scan, and voxel-based statistics were calculated in SPM software.

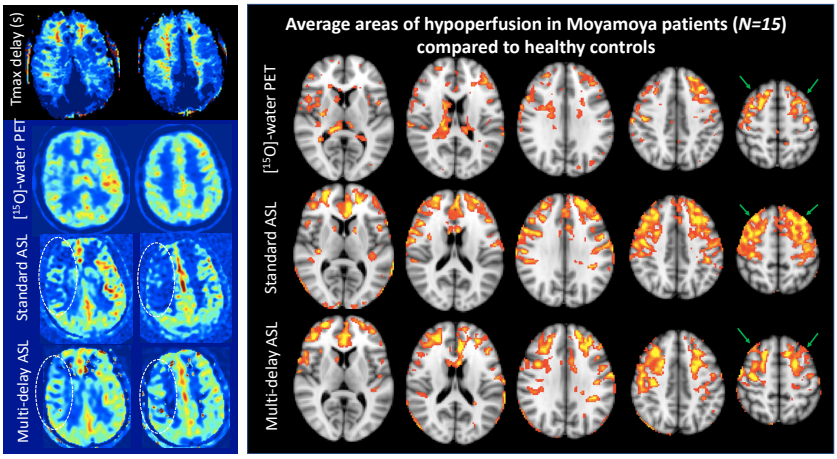

Figure 2 (left). Bilateral Moyamoya case with long time-to-maximum (Tmax) delays in right hemisphere show lack of signal on standard ASL relative to PET that is recovered by multi-delay ASL. Figure 3 (right) shows average areas of hypoperfusion in 15 Moyamoya patients after comparison to the healthy normative database.

Results:

Normative CBF databases including mean CBF and standard deviation (SD) per voxel were generated from the healthy control images (**Figure 1**). In healthy controls, multi-delay ASL reduced the CBF underestimation in deep gray matter and overestimation in white matter. Scan-rescan coefficient of variation across cortical regions was 9.4%, 5.9%, and 6.4% respectively for PET, standard ASL, and multi-delay ASL. **Figure 2** shows representative PET/MRI perfusion images in a 45-year old female patient with bilateral Moyamoya disease. Standard ASL showed areas of reduced CBF (white circle) relative to PET due to long ATTs characteristic of Moyamoya pathology, as well as focal hotspots indicative of slow flow in large vasculature. Multi-delay ASL visually improved the CBF uniformity along the cortex and showed stronger correlation with PET in areas of longer delays (Tmax > 3s).

In each Moyamoya case, after registration to template space, the individual's PET scan was compared to the PET database and each ASL scan was compared to the corresponding ASL database. **Figure 3** shows average areas of hypoperfusion across all patients (*N=15*) relative to healthy controls, defined as 2 SDs below the mean CBF in controls. Standard ASL overestimates the regions affected by Moyamoya disease (bilaterally in the anterior and middle cerebral artery territories) compared to PET; whereas multi-delay is more specific to true hypoperfusion.

Discussion:

CBF quantification with ASL and comparison with a normative database identified regions of hypoperfusion in frontal and parietal regions that are consistent with Moyamoya pathology. Standard ASL overestimated the areas of hypoperfusion compared to PET, suggesting that low ASL signal in standard protocols may be incorrectly interpreted as low CBF. Multi-delay ASL acquisition increased specificity of MRI to true hypoperfusion in Moyamoya disease; and improves CBF correlation with PET for long circulation delays[4]. Despite this improvement, multi-delay ASL still under-estimated CBF in severe cases and requires extended post-label delay range (up to 5s) or alternate velocity-selective strategies[5] to accurately quantify CBF in challenging cases.

Acknowledgements: GE Healthcare, Stanford Neuroscience Institute Interdisciplinary Scholar Award

References: 1. Alsop (2015) *Magn Reson Med* 73. 2. Goetti (2014) *Am J Neuroadiol* 35. 3. Khalighi (2017) *JCBFM* 38. 4. Qiu (2012) *J Magn Reson Imag* 36. 5. Fan (2017) *Stroke* 48.

RF4

Novel COX-2 PET radioligand, [^{11}C]MC1, can detect and quantify COX-2 upregulation during neuroinflammation in rhesus monkeys

Stal Shrestha[1]

[1]*NIH*

Introduction:

The cyclooxygenase (COX) isozymes, COX-1 and COX-2, mediate inflammatory responses, and are targets for nonsteroidal anti-inflammatory drugs (NSAIDs). To study the distribution and function of these COX isozymes in vivo, our laboratory developed two novel PET radioligands: ^{11}C-PS13 and ^{11}C-MC1. PS13 demonstrated potent selectivity for COX-1 (IC_{50} = 1 nM) compared to COX-2 (IC_{50} > 1,000 nM). Conversely, MC1 was potent and selective for COX-2 (IC_{50} = 1 nM) compared to COX-1 (IC_{50} > 1,000 nM). Previously, we showed that ^{11}C-PS13, but not ^{11}C-MC1 shows specific uptake in normal monkey brain. Whether ^{11}C-MC1 exhibits specific binding in conditions that elicit significant densities of COX-2 has yet to be studied. This study sought to examine whether ^{11}C-MC1 could image COX-2 in a model of neuroinflammation via intracerebral injection of lipopolysaccharide (LPS). As a control, we measured COX-1 using ^{11}C-PS13 before and after LPS.

Methods:

To elicit an inflammatory response in monkey brain, LPS (from Escherichia coli O26:B6), was injected into the right putamen of monkeys (n=4). Prior to injection, a T1-weighted MRI was obtained to guide the insertion of the needle. In total, 10 µg of LPS was injected at a concentration of 1 µg/µL and an infusion rate of 0.5 µL/min. Dynamic brain PET scans were acquired for two hours both pre- and post-LPS injection. Approximately 220 MBq of radioligand was injected intravenously into the monkey before each scan. Blocking studies were also conducted with non-radioactive PS13 or MC1 (0.3-1 mg/kg) to confirm the specific uptake of the radioligands in the brain. Full quantitation with arterial sampling was done to measure volume of distribution (V_T) before and after LPS injection.

Results:

In this LPS model of neuroinflammation, ^{11}C-MC1 measured specific binding to COX-2. After the first injection, a widespread, 60% increase of ^{11}C-MC1 uptake was observed in the brain that was displaced by non-radioactive MC1. Following the second injection, there was an even more dramatic, and localized increase (>200%) in ^{11}C-MC1 uptake at the site of injection (Figure 1). As a comparator, we found no increase in COX-1 after LPS injection. ^{11}C-PBR28, a radioligand for translocator protein (TSPO), showed increased uptake, as expected, at the site of injection.

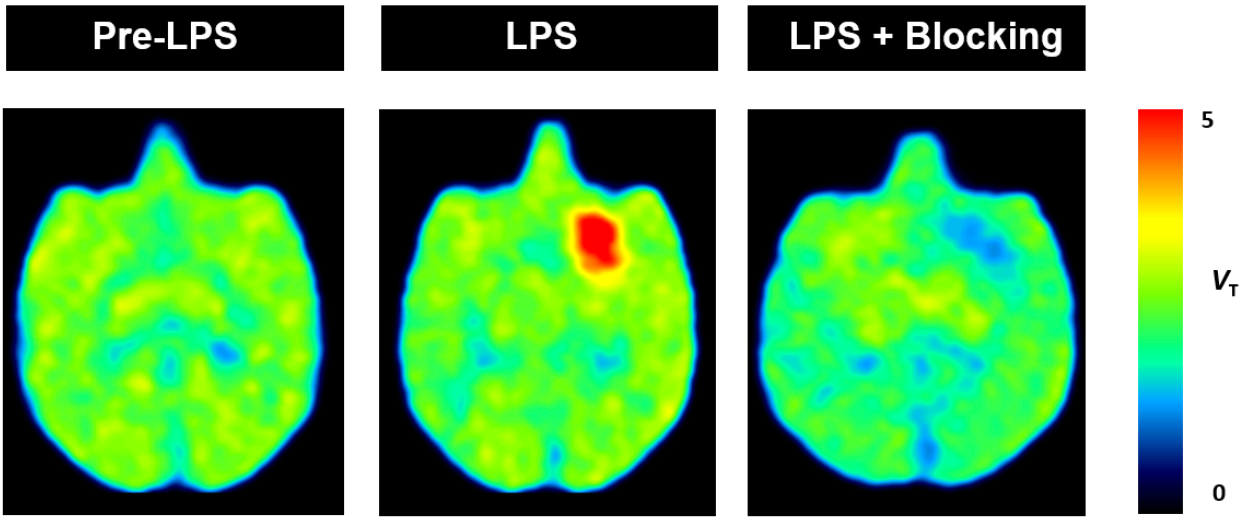

Figure 1. The effect of inflammogen, LPS, on ^{11}C-MC1 uptake in a monkey brain shown as volume of distribution (V_T). In normal brain (pre-LPS), there was no detectable uptake. After the second injection of LPS into right putamen, ^{11}C-MC1 uptake increased by >200% in the area of lesion, and blocked by non-radioactive MC1 (1 mg/kg i.v.).

Conclusions:

^{11}C-MC1 successfully captures COX-2 upregulation in rhesus macaque brain from basal levels to 60% after a single injection and >200% after a second injection. We show that in monkey brain, COX-2 but not COX-1 is upregulated after inflammation, which is consistent with the general notion that expression of COX-2 is inducible and COX-1 is constitutive. Of interest, COX-2 was primarily in neurons, and infiltrating peripheral mononuclear neutrophils. Ongoing first in-human studies will measure COX-1 in healthy conditions, and COX-2 in inflammatory disorders, and can also be used to evaluate the selectivity of NSAIDs, and delivery to brain for the two COX isozymes.

RF5

Striatal dopamine D2/3 receptors and amphetamine-evoked dopamine release in impulsivity and novelty-seeking traits : a SPECT imaging study using [^{123}I]IBZM in rats

Diego Pandolfo[1], Andrea Dimiziani[1], Lidia Bellés[1], Stergios Tsartsalis[1,2], Phillipe Millet[1,2], François Herrmann[3,4], **Nathalie Ginovart[1,2]**

[1]Department of Psychiatry, University of Geneva, Switzerland; [2]Laboratory for Translational Imaging in Psychiatric Neuroscience, Department of Mental Health and Psychiatry, University Hospitals of Geneva, Switzerland; [3]Department of Internal Medicine, Rehabilitation and Geriatrics, University Hospitals of Geneva, Switzerland; [4]Division of Geriatrics, Geneva University Hospitals, Switzerland.

Introduction:

Current research links impulsivity and novelty-seeking to alterations in dopamine (DA) signaling within the mesostriatal system and, notably, to a deficit in striatal DA $D_{2/3}$ receptor ($D_{2/3}R$). However, the vast majority of studies investigating the neurobiological underpinnings of impulsivity and novelty-seeking have focused on post-synaptic $D_{2/3}R$, and few studies have investigated presynaptic aspects of DA signaling, such as presynaptic DA release, albeit it is known to regulate postsynaptic $D_{2/3}R$ expression.

The aim of this study was to get further insight into the DAergic underpinnings of impulsivity and novelty-seeking. To this aim, we investigated, using a within subject design, the associations between impulsivity, novelty-seeking ,the density of striatal $D_{2/3}R$ and amphetamine (AMPH)-induced DA release. We used two strains of rats, the Swiss sublines of Roman high- (RHA) and low- (RLA) avoidance rats, which display divergent phenotypes in terms of impulsivity and novelty-seeking.

Materials & Methods:

Two groups of adult male RHA (n=25) and RLAs (n=24) rat were tested for impulsivity using the 5-choice serial reaction time task (5-CSRTT) and for novelty-seeking using the novelty-induced place preference (NIPP) test. Rats were then scanned with SPECT imaging using [^{123}I]IBZM to measure D2/3R density and AMPH-induced DA release in striatum. Binding potential (BP_{ND}) and gamma (γ) values were quantified as indexes of D2/3R density and AMPH-induced DA release, respectively, using a single scan and the linearized simplified reference region model (LSRRM).

Results:

When compared with RLAs, RHA rats produced a significantly higher number of premature responses in the 5-CSRTT (30±2 vs. 8±1 ; $p<0.001$) and spent significantly more time in the unfamiliar (ie. novel) compartment in the NIPP test (62±3 vs. 38±3 seconds, $p<0.001$), demonstrating that RHAs are both more impulsive and more novelty-seeker than RLAs. Two-way ANOVA revealed a significant interaction effect between the two rat lines and *in vivo* measures of BP_{ND} and gamma ($F_{2,45} = 33.3$; $p<0.0001$). When compared to RLAs, RHAs displayed lower [^{123}I]IBZM BP_{ND} (2.02±0.1 vs. 3.00±0.11; $p<0.001$), but higher AMPH-induced DA release in striatum (γ : 0.0297±0.0022 vs. 0.0137±0.001; $p<0.001$).

Importantly, individual measures of premature responding were negatively correlated ($r = -0.66$, $p<0.001$) with BP_{ND}, but positively correlated with γ ($r=0.62$, $p<0.001$). Similarly, individual measures of novelty-seeking were negatively correlated with striatal [^{123}I]IBZM BP_{ND} ($r = -0.40$; $p<0.001$) and positively correlated with [^{123}I]IBZM γ values ($r = 0.58$; $p<0.001$). Because [^{123}I]IBZM BP_{ND} and γ values were highly correlated ($r = -0.66$: $p<0.0001$), mediation analyses were used to investigate the extent to which [^{123}I]IBZM BP_{ND} accounted for links between γ values and behavioral trait variables. A Sobel test confirmed

that [^{123}I]IBZM BP_{ND} partially mediated the effect of [^{123}I]IBZM γ on impulsivity ($Z = 2.89$; $p < 0.01$). Moreover, multiple regression analysis revealed striatal D2/3R density as the most important correlate of impulsivity. Mediation analysis also revealed a non-significant mediating effect of [^{123}I]IBZM BP_{ND} between [^{123}I]IBZM γ and novelty-seeking ($z = 0.32$; $p=0.747$), suggesting that [^{123}I]IBZM γ uniquely and independently predicted novelty seeking.

Discussion:

This study confirms and extends previous data of an association between striatal D2/3R deficits and impulsivity by showing that presynaptic DA release is also an important factor predicting this personality trait. Moreover, these data suggest that the deficits in striatal $D_{2/3}R$ observed in high impulsive rats may not be constitutive but be consecutive to an heightened presynaptic DA function. Diminished levels of striatal $D_{2/3}R$ allied with an excessive presynaptic tone may represent a unique DA phenotype associated with impulsive action and contributing to increased vulnerability to addiction.

Moreover, although novelty-seeking has been previously associated to impulsivity, both personality traits may not share the exact same neurochemical substrates. Those findings provide further information on the mechanism by which altered transmission at D2/3R may contribute to impulsive behaviours.

Acknowledgements:

This work was supported by the Swiss National Science Foundation.

RF6

Investigating mGluR5 as a biomarker of suicidality in Bipolar Disorder: *in-vivo* and post-mortem evidence

Sophie E Holmes[1], Ansel T Hillmer[1], Margaret T Davis[1], Nicole DellaGioia[1], Jean-Dominique Gallezot[1], Nabeel Nabulsi[1], David Matuskey[1], Neha Pashankar[1], Marina Picciotto[1], Yann Mineur[1], Gustavo Turecki[2], Christopher Pittenger[1], Richard E Carson[1], Irina Esterlis[1,3]

[1]Yale University, New Haven, CT, United States [2]McGill Group for Suicide Studies, McGill University, Montreal, Canada [3]VA National Center for PTSD, West Haven, CT, USA

Introduction:

Suicide continues to be one of the leading causes of death in the US, with rates currently at their highest levels in 3 decades[1]. The need for identifying novel targets for treatment and prevention strategies is therefore critical. Over 90% of suicide attempters have a diagnosed psychiatric disorder, most commonly a mood disorder. Individuals with major depressive disorder (MDD) are 10-20 times more likely to attempt suicide than the general population[2], while those with bipolar disorder (BD) are 30 times more likely[3]. However, the neurobiological mechanisms underlying suicide attempt in these disorders remain unknown. Dysfunction of the glutamate system has been implicated in suicidal behaviour[4-7]. Emerging evidence suggests specific involvement of the metabotropic glutamate receptor 5 (mGluR5), which plays a key role in cognition and emotion[8], in suicidality[9,10,11,12]. To our knowledge, this study is the first to investigate mGluR5 as a potential biomarker of suicide attempt in MDD and BD. Specifically, we used PET and [^{18}F]FPEB to investigate mGluR5 *in vivo* in individuals with MDD and BD. We also conducted autoradiography with [^{3}H]ABP688 to quantify mGluR5 availability post-mortem in a sample of MDD and BD individuals who had died by suicide, and compared to controls.

Materials & Methods:

For the *in*-vivo investigation, 21 individuals with BD consisting of 6 suicide-attempters (SA) (mean age 30.6±2.7; mean MADRS 17.0±4.4; 2 women), and 15 non-attempters (non-SA) (mean age 40.7±12.8; MADRS 12.3±7.9; 10 women), and 26 individuals with MDD consisting of 6 suicide-attempters (mean age 30.7±8.1; MADRS 21.8±7.4; 4 women) and 20 non-attempters (mean age 39.7±13.8; MADRS 21.4±6.8; 12 women) were scanned with the mGluR5 radioligand [^{18}F]FPEB on the HRRT. [^{18}F]FPEB was injected as bolus plus constant infusion and participants were scanned during steady state (90-120mins post-injection). The outcome measure was volume of distribution (V_T: the ratio of activity in tissue relative to that in blood), computed using a venous input function in a composite prefrontal cortex (PFC) region consisting of orbitofrontal cortex, ventromedial and dorsolateral PFC. Autoradiography was performed on tissue obtained from the Douglas-Bell Canada Brain Bank from the dlPFC of 10 individuals with BD (mean age 48.1±14.6 yrs; 5 females) and 10 individuals with MDD (49.3±15.7 yrs; 5 females) who had died by suicide, and 10 HCs (mean age 52.0±18.7 yrs; 5 females) using the mGluR5 radioligand [^{3}H]ABP688. Adjacent sections were incubated in the same solution with the addition of unlabelled mGluR5 antagonist MPEP to determine non-specific binding.

Results:

Within the *in*-vivo BD group, there was significantly higher PFC mGluR5 availability in suicide attempters vs non-attempters, by an average of 22% (univariate ANOVA; $F_{1,19}$=7.40, p=0.014, Cohen's d=1.42). However, there was no difference in PFC mGluR5 availability between suicide-attempters and non-attempters in the MDD group ($F_{1,24}$=0.07, p=0.795). The significance of results was unchanged after controlling for symptom severity (MADRS). Furthermore, there was a trend toward higher mGluR5 availability in BD suicide attempers

as compared to MDD suicide attempters (p=0.10). In the post-mortem sample, we found significantly higher mGluR5 availability or levels in dlPFC tissue in BD compared to HC groups ($F_{1,18}$=8.35, p=0.010, d=1.30), by an average of 38%. However, there was no difference in mGluR5 availability in MDD compared to HC groups ($F_{1,18}$=1.11, p=0.305).

Conclusion:

Our findings point to higher mGluR5 availability in suicide attempters and completers in BD but not MDD, raising the possibility that mGluR5 could represent a biomarker for suicide in BD specifically. PET results were consistent with the post-mortem sample, with [^{3}H]ABP688 binding higher in BD suicide victims as compared to MDD suicide victims and controls. Further research is needed to identify the mechanisms that might underlie the association between mGluR5 and suicide in BD. One possibility is a compensatory upregulation of mGluR5, secondary to abnormal glutamate transmission[13]. Our findings add to the evidence implicating a role for glutamate in suicide, and we propose mGluR5 as a potential new biomarker and therapeutic target for reduction of suicide in BD specifically. Indeed we have previously shown that ketamine, which has anti-suicidal properties[14], leads to a rapid downregulation of mGluR5[15,16]. Further work needs to confirm our preliminary findings, and to explore mGluR5 as a novel biomarker and potential treatment target for suicide in BD.

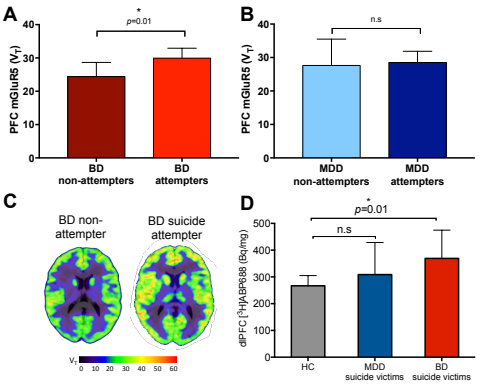

Figure 1. (A) Significantly higher PFC mGluR5 availability in BD suicide attempters vs non-attempters **(B)** No difference between PFC mGluR5 availability in MDD suicide attempters vs non-attempters **(C)** Parametric V_T [^{18}F]FPEB images of representative BD non-attempter (left) and attempter (right) **(D)** Autoradiography results showing significantly higher mGluR5 availability in BD suicide victims, but not MDD victims compared to HCs, in dlPFC post-mortem tissue. Error bars represent SD.

References:

1. Curtin SC, Warner M, Hedegaard H. Increase in Suicide in the United States, 1999-2014. *NCHS data brief.* 2016(241):1-8.
2. Angst J, Angst F, Stassen H. *Journal of clinical psychiatry.* 1999.
3. Potash JB, Kane HS, Chiu YF, et al. *Am J Psychiatry.* 2000;157(12):2048-2050.
4. Sequeira A, Mamdani F, Ernst C, et al. *PloS one.* 2009;4(8):e6585.
5. Bernstein HG, Tausch A, Wagner R, et al. *CNS & neurological disorders drug targets.* 2013;12(7):900-913.
6. Caroline C, Giovanni G, Thomas PW, Sukhwinder SS, Derek KT. *Therapeutic Advances in Psychopharmacology.* 2013;4(2):75-99.
7. Erhardt S, Lim CK, Linderholm KR, et al. *Neuropsychopharmacology.* 2013;38(5):743-752.
8. Krystal JH, Mathew SJ, D'Souza DC, Garakani A, Gunduz-Bruce H, Charney DS. *CNS Drugs.* 2010;24(8):669-693.
9. Chandley MJ, Szebeni A, Szebeni K, et al. *International Journal of Neuropsychopharmacology.* 2014;17(10):1569-1578.
10. Rao S, Leung CST, Lam MH, Wing YK, Waye MMY, Tsui SKW. *Gene.* 2017;603:34-41.
11. Strauss J, McGregor S, Freeman N, et al. *Psychiatry research.* 2012;197(1):49-54.
12. Dean B, Gibbons AS, Boer S, et al. *Australian & New Zealand Journal of Psychiatry.* 2016;50(3):275-283.
13. Jollant F, Near J, Turecki G, Richard-Devantoy S. *Prog Neuropsychopharmacol Biol Psychiatry.* 2016;

14. Reinstatler L, Youssef NA. *Drugs in R&d.* 2015;15(1):37-43.
15. DeLorenzo C, DellaGioia N, Bloch M, et al.. *Biological psychiatry.* 2015;77(3):266-275.
16. Esterlis I DN, Pietrzak RH, Matuskey D, Nabulsi N, Abdalla CG, Yang J, Pittenger C, Sanacora G, Krystal JH, Parsey RV, Carson RE, Delorenzo C. *Molecular Psychiatry:* 2017.

RF7
Estimation of V_{ND} of ^{11}C-UCB-J PET in an SV2A Occupancy Study

Samantha Rossano[1,2], Takuya Toyonaga[2], Mika Naganawa[2], Sjoerd Finnema[2], Steven De Bruyn[3], Christian Otoul[3], Armel Stockis[3], Jean-Marie Nicolas[3], Paul Martin[3], Ralph Paul Maguire[3], Joel Mercier[3], Richard Carson[1,2]

[1]Department of Biomedical Engineering, Yale University, New Haven, CT, [2] Yale PET Center, Department of Radiology and Biomedical Imaging, Yale University, New Haven, CT, [3]UCB Pharma S.A., Brussels, Belgium

Introduction:
^{11}C-UCB-J is a PET radiotracer that specifically binds to the synaptic vesicle glycoprotein 2A (SV2A), which exists in brain presynaptic terminals and is the target for the antiepileptic drugs Levetiracetam (LEV) and Brivaracetam (BRV). Due to this specificity, ^{11}C-UCB-J PET can be used to investigate occupancy of SV2A by LEV or BRV *in vivo*. Receptor occupancy and V_{ND}, the nondisplaceable volume of distribution in tissue (i.e., non-specifically bound + free), can be estimated from the changes in volume of distribution, V_T, between baseline and blocking conditions using multiple regions of interest with the Lassen Occupancy Plot, which assumes that occupancy and V_{ND} are shared across all regions. In order to fulfill assumptions for quantification by reference tissue methods, V_{ND} should equal the baseline V_T of the reference region, which for ^{11}C-UCB-J has been proposed to be the white matter (WM), due to its negligible SV2A concentration in the baboon brain [1]. Apparent displacement in the WM region in human displacement scans [1] is believed to be due in part to lack of convergence of low-uptake regions using Ordered Subset Expectation Maximization (OSEM) algorithms for image reconstruction. The objective of this work is to use occupancy studies with BRV and LEV to estimate V_{ND} and compare V_{ND} to baseline WM V_T at higher OSEM iterations.

Materials and Methods:
13 pairs of baseline and blocking scans with varying doses of BRV (n=8, 50, 100, or 200 mg iv) and LEV (n=5, 1500 mg iv) were performed with 10 healthy volunteers. Images were reconstructed with 2 (standard), 3, and 4 OSEM iterations of 30 subsets. From each of these images, regional V_T values were estimated using a 1 tissue compartment (1TC) model from 60 min of data for 22 cortical and subcortical regions. V_T values were also estimated for the WM within the centrum semiovale, which was based on the average of individual white matter MRI segmentations registered to the AAL template space. Measures of occupancy and V_{ND} were estimated using the Lassen Occupancy Plot.

Results:
A Lassen Occupancy Plot with higher OSEM iterations is shown for a typical subject (Figure 1). The average (±SD) V_{ND} across all occupancy studies increased with increasing OSEM iterations, from 2.76 (±0.60) mL/cm^3 at 2 iterations, to 3.08 (±0.51) mL/cm^3 and 3.10 (±0.52) mL/cm^3 at 3 and 4 iterations, respectively. The baseline white matter V_T decreased with increasing iterations from 4.40 (±0.43) mL/cm^3 at 2 iterations, to 4.02 (±0.52) mL/cm^3 (Table 1). Combined, these changes led to a decrease in the percent difference between baseline WM V_T and estimated V_{ND} from 59.4% at 2 iterations to 29.7% at 4 iterations. The average percent decrease observed between baseline and post-dose WM V_T values also decreased with increasing OSEM iterations, 20.2 (±5.5)% at 2 iterations to 12.3 (±6.3)% at 4 iterations.

Figure 1: Lassen occupancy plots from images reconstructed with 2 (blue), 3 (orange), and 4 (green) OSEM iterations of 30 subsets.

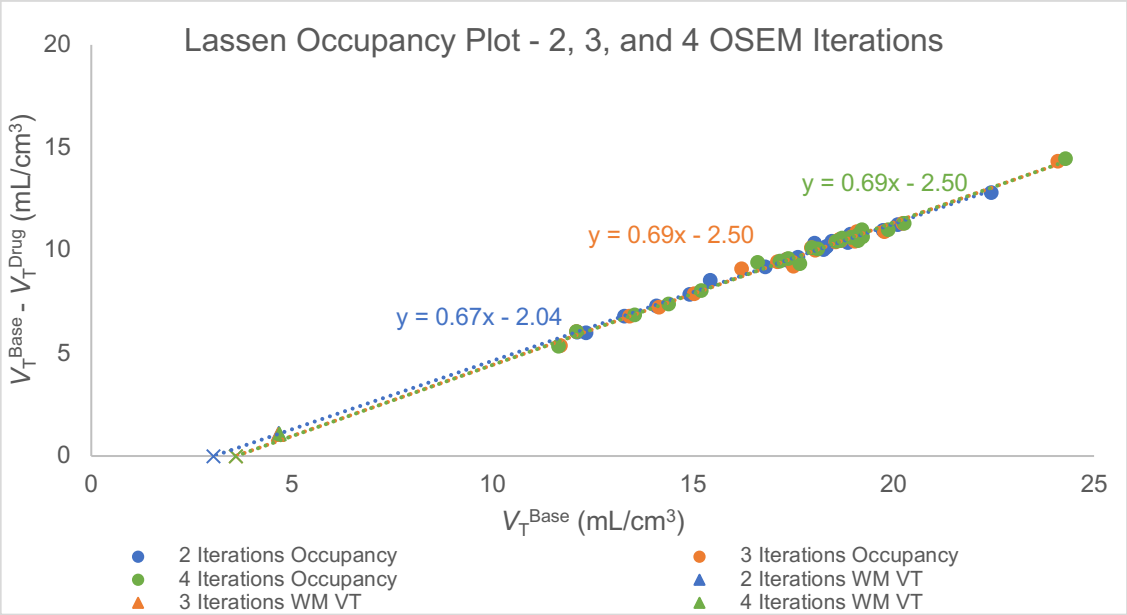

Table 1. Average (±SD, N=13) changes in parameter estimates with Increasing OSEM Iterations of 30 subsets

OSEM Iterations	Occupancy (%)	V_{ND} (mL/cm^3)	Baseline WM V_T (mL/cm^3)	Post-Dose WM V_T (mL/cm^3)
2	75 (±10)	2.76 (±0.60)	4.40 (±0.43)	3.49 (±0.23)
3	76 (±8)	3.08 (±0.51)	4.11(±0.46)	3.49 (±0.31)
4	76 (±8)	3.10 (±0.52)	4.02 (±0.52)	3.51 (±0.33)

Conclusion:

^{11}C-UCB-J is a successful imaging tracer to measure SV2A occupancy levels and V_{ND} estimates. Increasing the number of OSEM iterations decreased the difference between baseline and post-dose WM V_T, as well as decrease the difference between the extrapolated V_{ND} and the baseline white matter V_T; however, the V_T of white matter is larger than the V_{ND} of gray matter by about 30%. White matter V_T may still be a useful although inaccurate measure of nonspecific binding, the effect of white matter reference on occupancy measures needs to be investigated.

Acknowledgements:

Funding Sources: R01 AG052560, R01 NS094253, UCB Pharmaceuticals

References:

1. Finnema, S. J., et al. [2016]. Sci Transl Med **8**(348): 348ra396.

RF8

An open label PET imaging study to evaluate the mGlu5 receptor occupancy following ADX48621 (dipraglurant) administration

Dean F. Wong[1,2], Hiroto Kuwabara[1], Sonia- Maria Poli[3] , Lorena Gapasin[1], Joshua Roberts PhD[1], Kelly Kitzmiller[1], Thierry Duvauchelle[4]

[1]Johns Hopkins University, Department of Radiology, [2]Johns Hopkins University, Department of Psychiatry, [3]Addex Therapeutics, Switzerland, [4]Phaster 1, France

Introduction:

ADX48621 (dipraglurant) is a selective, orally available, small molecule drug candidate which acts as a negative allosteric modulator (NAM) of the metabotropic glutamate receptor 5 (mGlu5 receptor). ADX48621 is selective for the mGlu5 receptor and does not have any significant activity or binding affinity to other mGlu receptors or CNS receptors, including serotonin, GABA and dopamine receptors.

Preclinical profiling of the safety of ADX485621 has been performed *in vitro* and *in vivo* to support up to three months of dosing in humans. ADX48621 is effective in the MPTP macaque model of Parkinson's disease (PD) levodopa induced dyskinesia (LID) and in addition other preclinical pharmacology models of dystonia, anxiety, compulsion, depression, and parkinsonian motor symptom control.

Dipraglurant has been studied in three Phase 1 clinical studies and a Phase 2a LID Proof of Concept (POC) trial in PD patients, where it showed clinically meaningful improvements in LID scores at doses that were generally safe and well tolerated. To date, the clinical studies have enrolled 220 subjects (including 76 PD patients).

A series of PET imaging studies with [^{18}F]-FPEB were previously performed in non-human primates to determine mGlu5 receptor occupancy following intravenous injection of ADX48621. The collected data demonstrated that the receptors occupancy by ADX48621 was dose-dependent

The aims of the study were to: 1) to demonstrate brain penetration and target engagement of brain mGlu5 receptors after single or two oral doses of ADX48621in healthy subjects, using [^{18}F]-FPEB; 2) to assess the relationship between ADX48621 plasma concentration and its brain mGlu5 occupancy

Materials & Methods:

This was an open label, non-randomized, PET study, investigating the mGlu5 receptor occupancy after single or two oral doses of ADX48621 in healthy male subjects using [^{18}F]-FPEB using an adaptive dosing design where the dose administered could be changed after observation of the occupancy after each subject studied. Each subject was scanned using the high-resolution research tomograph (HRRT) 2 mm axial resolution with [^{18}F]-FPEB synthesized at the JHU radiochemistry/PET center. In Part 1, subjects underwent two [^{18}F]-FPEB PET imaging sessions: a baseline scan. then a second scan after treatment with one dose of ADX48621. The second scan was taken at Tmax for ADX48621 (1 hour post dose). In part 2 , the dose that provided sufficient receptor occupancy as determined in Part 1, was studied in Part 2. Subjects received 2 doses of

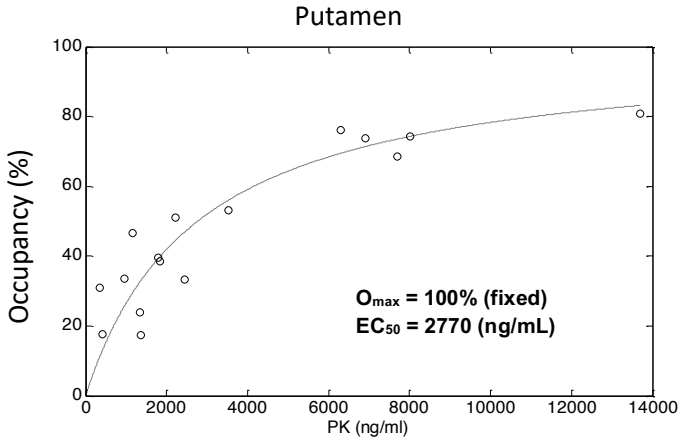

Figure 1: Occupancy-PK plot for Putamen (Pu).

ADX48621 as a single dose on 2 separate days, and underwent three [^{18}F]-FPEB PET imaging sessions: a baseline scan, post dose scan 1 and post dose scan 2.
The plasma reference graphical analysis (PRGA) was used to obtain distribution volume (V_T) values of regions. It was examined that whether V_T values of the cerebellum white matter (CW) remain stable across doses and PK values to evaluate whether CW could serve for reference region in occupancy scans. In parallel, distribution volume of non-displaceable compartment (V_{ND}) was estimated for individual baseline-post-dose scan pairs using the inhibition plot (Gjedde and Wong et al).

Blood samples for PK were collected up to 3.00 hours post dose in Part 1 and up to 4.00 hours post dose in Part 2.

Results:
Twelve subjects were studied. It was noted that V_T values of CW decreased with doses and PK values ($p<0.007$; simple regression), while V_{ND} values remained unchanged across doses (1.5 ± 0.8 mL/mL). Therefore, occupancy values were calculated as follows: Occupancy (%) = ΔVT / (baseline V_T) – V_T)) - 100. Observed PK values ranged from 354 to 13699 ng/mL, while occupancy values ranged from just above 10% to just above 80% across regions. The occupancy-PK plots fitted very well with the first-order Hill equation (occupancy = $PK \cdot O_{max} / (PK + EC_{50})$; O_{max} = 100%) across regions, including data of subjects who had second post-dose scans (n=5; ΔPK range: 655 – 5991 ng/mL). Observed EC_{50} values averaged at 2910 ± 152 ng/mL across regions, and EC70 values averaged at 6791 ± 354 ng/mL.

Discussion/Conclusion:
This study showed that occupancy of ADX48621 of mGluR5s obeys the first-order Hill equation as measured with [^{18}F]-FPEB. Five subjects had two post-dose scans after separate single oral dose of ADX48621. Data points of these subjects existed along the model predicted curves in individual regions whether PK values were close to each other (n=2) or very different (n=3) between the two scans. These findings on double post-dose scans ensured the assertion, compared to the single post-dose scan design.
This study also yielded important findings regarding [^{18}F]-FPEB. It was demonstrated that binding in CW was displaceable in a dose-dependent manner, and about 50% of V_T in CW (slightly above 3 mL/mL) was displaceable, based on observed V_{ND} values (about 1.5 mL/mL). Therefore, drug occupancy studies could be misleading without employing arterial plasma data. In this study, EC_{50} values of tissue reference methods (no blood data) were about 2.5 times higher than EC_{50} values given by PRGA.

Acknowledgements:
This work is supported in part by Addex pharmaceuticals and MJ Fox Foundation.

References:
Gjedde, A. & Wong, D. F. Neuroimage11, 6, S48 (2000).

RF9

A voxel-wise multimodal approach to evaluate the accuracy of simplified methods to quantify changes in TSPO binding using [^{18}F]-DPA-714

Nadja Van Camp, Anne-Sophie Herard, Yaëll Balbastre, Sonia Lavisse, Martine Guillermier, Aurelie Berniard, Pauline Gipchstein, Caroline Jan, Romina Aron-Badin, Thierry Delzescaux, Philippe Hantraye, Gilles Bonvento

CEA/DRF/IBFJ/MIRCen;CNRS, Université Paris-Sud, UMR9199, Neurodegenerative Diseases Laboratory, F-92260 Fontenay-aux-Roses, France

Introduction:

Brain imaging, especially TSPO-PET, is a promising tool to monitor neuroinflammation in many neurodegenerative diseases, allowing to chart their progression and to assess the efficacy of therapies. Due to the burden of arterial blood sampling, semi-quantitative - *standard uptake values (SUV) or SUV-ratios* - or simplified reference approaches - *calculating non-displaceable binding-potentials (BP_{ND}) using the cerebellum as a pseudo-reference region* – are currently used, despite the ubiquitous expression of TSPO in the healthy brain. However, to the best of our knowledge it has never been evaluated which of these simplified methods has the highest sensitivity and predictive value [1] to detect changes in TSPO expression.

In the present study, we aim to identify which out of four simplified quantification methods for [^{18}F]-DPA-714 is the most accurate to detect TSPO expression in a non-human primate (NHP) model of Ciliary Neurotrophic Factor (CNTF)-induced astrocytic activation.

Methods:

Three NHP were injected with a lentiviral vector expressing CNTF [2] in the caudate-putamen. Animals underwent MRI and [^{18}F]-DPA-714 PET imaging at baseline (BL) and 6 months post-injection (6MPI) as previously described [3]. Parametric images were generated from raw PET data using PMOD®3.8 (PMOD-Technologies Ltd., Zürich, Switzerland). The total volume of distribution (V_T, [ml/ccm]) was obtained by the graphical method of Logan using a metabolite-corrected arterial input function (mcAIF). Non-displaceable binding potentials (BP_{ND}) were calculated by SRTM, MRTM0, and Logan using the cerebellum as a pseudo-reference region. SUV was obtained by normalization for injected dose and bodyweight. Based on the average TSPO baseline level, parametric images at 6MPI were segmented by thresholding, and voxels below the threshold (cut-off) were set at 0. To estimate the impact of the segmentation by thresholding, this step was repeated using different cut-off values (V_T: {8.5, 10, 11.5} ml/cc, BP_{ND}: {0.1, 0.2-0.5}, SUV: {0.9, 1.0, 1.2}). Finally cross-validation between quantification methods was done at a threshold set at [AVERAGE+2*StDEV], using the average and standard-deviation of the whole brain at baseline.

After PET imaging at 6MPI, brains were sectioned and immunostained for CNTF, Vimentine and TSPO. A three-dimensional immunohistological TSPO-density map (TSPO-IHC) was calculated from one NHP brain using a procedure previously described in detail [4, 5]. TSPO-IHC was co-registered to the PET/MR image data for voxelwise comparison. Considering TSPO-IHC as ground truth, each voxel of the segmented TSPO-PET images was scored as false or true (F, T), positive or negative (P, N). We then calculated three accuracy criteria: sensitivity *(=TP/TP+FN*), specificity *(=TN/TN+FP)* and predictive positive value *(PPV=TP/(TP+FP)),* to identify the best TSPO-PET simplified quantification method [1].

Results:

The CNTF vector induced a local and selective activation of astrocytes that was associated with an increased expression of TSPO [2].

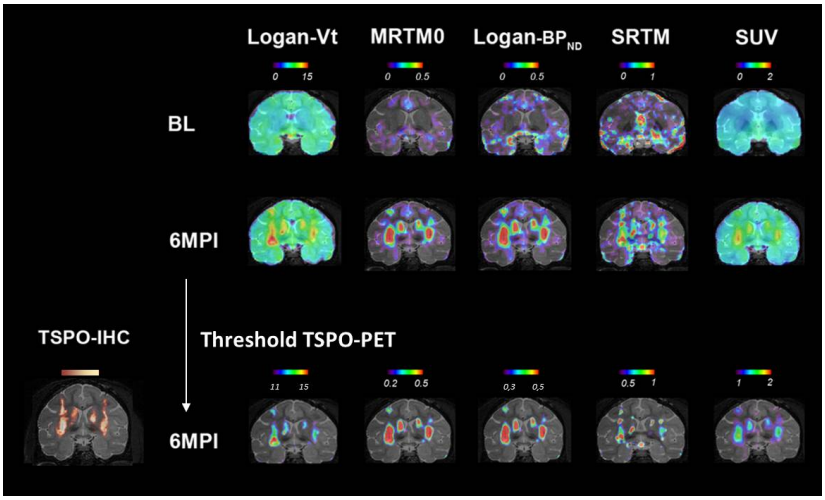

At BL, the BP_{ND} parametric images showed [^{18}F]-DPA-714 uptake along the sulci and ventricles. V_T and SUV images showed a homogenous whole brain uptake and small regional differences. At 6MPI, locally increased TSPO-expression was measured by all quantification methods (*figure*).

V_T had the best PPV and specificity, although a low sensitivity. SRTM and SUV showed a very poor specificity, which improved when increasing the cut-off although with the cost of losing sensitivity. Nevertheless, the PPV of SRTM and SUV was below all other quantification methods. In the same range as V_T, BP_{ND} by Logan obtained optimal results for sensitivity, PPV and specificity, followed by MRTM0.

Conclusions:

Calculation of V_T by mcAIF-Logan was the most accurate measurement, despite a low sensitivity. When arterial sampling is not feasible, Logan using the cerebellum as pseudo-reference region is largely preferable over SUV or SRTM for DPA quantification.

References

1. Šimundić, A.-M., *Measures of Diagnostic Accuracy: Basic Definitions.* EJIFCC, 2009. **19**(4): p. 203-211.
2. Escartin, C., et al., *Activation of astrocytes by CNTF induces metabolic plasticity and increases resistance to metabolic insults.* J Neurosci, 2007. **27**(27): p. 7094-104.
3. Lavisse, S., et al., *[18F]DPA-714 PET imaging of translocator protein TSPO (18 kDa) in the normal and excitotoxically-lesioned nonhuman primate brain.* Eur J Nucl Med Mol Imaging, 2015. **42**(3): p. 478-94.
4. Dauguet, J., et al., *Three-dimensional reconstruction of stained histological slices and 3D non-linear registration with in-vivo MRI for whole baboon brain.* J Neurosci Methods, 2007. **164**(1): p. 191-204.
5. Balbastre, Y., et al., *A Quantitative Approach to Characterize MR Contrasts with Histology*, in *Brainlesion: Glioma, Multiple Sclerosis, Stroke and Traumatic Brain Injuries: First International Workshop, Brainles 2015, Held in Conjunction with MICCAI 2015, Munich, Germany, October 5, 2015, Revised Selected Papers*, A. Crimi, et al., Editors. 2016, Springer International Publishing: Cham. p. 104-115.

RF10

High resolution [^{11}C]ABP688 imaging of mGluR5 in healthy volunteers: sex differences and test-retest variability.

Smart K[1] *, Cox SML[1] *, Scala SG[1], Tippler M[1], Jaworska N[1,2], Boivin M[3], Séguin J[4,5], Benkelfat C[1]†, Leyton M[1,4,6]†.

1. McGill University, Montreal, QC, Canada; 2. University of Ottawa, Institute of Mental Health Research, Ottawa, ON, Canada; 3. Université Laval, QC; 4. CHU Ste-Justine Research Centre, Montreal, QC; 5. Université de Montréal, Montreal, QC; 6. Concordia University, Montreal, QC.
** KS and SMLC contributed equally to this work. † CB and ML contributed equally to this work.*

Introduction:
The positron emission tomography (PET) ligand [^{11}C]ABP688 binds selectively at an allosteric site on the metabotropic glutamate type 5 receptor (mGluR5). This receptor is implicated in mood, anxiety, and substance use disorders [1–3], and drugs targeting the mGluR5 allosteric site are being explored as potential treatments for some of these conditions [4,5].
In humans, the variability in [^{11}C]ABP688 binding has been unexpectedly high. In part, this might reflect sex differences, which have been tentatively identified in some small preliminary studies. Greater binding variability in women than men has also been reported [6,7]. It might also reflect circadian effects since in test-retest studies comparing scans acquired on the same day, binding potential is consistently higher in scans performed in the afternoon compared to the morning [7].
Since these hypothesized sources of [^{11}C]ABP688 binding variation remain poorly understood, the present studies aimed to (i) explore sex differences in a large sample of healthy young adults, and (ii) assess test-retest variability under consistent scanning conditions.

Materials & Methods:
[^{11}C]ABP688 PET scans were acquired in 84 healthy volunteers (32 male, 52 female, mean age 20±2.9 years) using a high-resolution research tomograph (HRRT, CTI/Siemens). Regions of interest were defined on a 3T anatomical MRI acquired for each participant. Mean regional binding potential (BP_{ND}) values were determined using the simplified reference tissue model with cerebellar grey matter as the reference region. A subset of participants (n=8) was scanned a second time 3 weeks after the first, with all scans acquired between 10:00am and 1:30pm. This subgroup reported on subjective mood states after each PET scan and blood samples were drawn for serum cortisol analysis.

Results:
BP_{ND} was correlated with percent of *(E)*-isomer in the tracer product (mean % *(E)*-isomer 92±3.9%; ρ=0.28, p=0.01). This measure was included as a covariate in all subsequent analyses.
Variability in BP_{ND} across the sample was high, with over 3-fold differences in striatal BP_{ND} values between participants (**Figure 1**, mean BP_{ND} 1.1±0.22, range 0.5 to 1.6). No relationship was observed between BP_{ND} and age (r=-0.05, p=0.65). BP_{ND} in the striatum was 20% higher in men compared to women (mean BP_{ND} 1.2±0.24 in men, 1.0±0.19 in women; F=11.0, p=0.001).

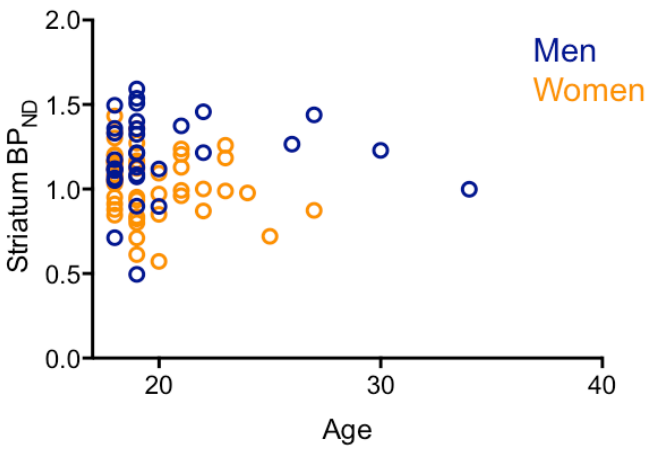

Figure 1. Mean striatal [^{11}C]ABP688 BP_{ND} in 52 women and 32 men.

In the test-retest sample, with scans performed 3 weeks apart, there was no significant change from scan 1 to scan 2. Mean regional variability between scans ranged from 12% in the dorsolateral prefrontal cortex to 23% in the hippocampus. Intraclass correlation values ranged from 0.30 in the associative striatum to 0.61 in the amygdala, indicating poor to fair reliability. While anxiety ratings were higher following scan 1 than scan 2 (mean [0-10] rating scan 1, 2.9±1.5; mean rating scan 2, 1.4±1.3; t=3.6 p=0.002), there was no relationship between BP_{ND} and anxiety ratings (r=-0.45, p=0.20) or serum cortisol levels (r=-0.33, p=0.35). BP_{ND} did not differ between women scanned in luteal vs. follicular menstrual phase (F=0.33, p=0.59) and was not related to scan start time (r=-0.48, p=0.16).

Discussion:

This study presents [^{11}C]ABP688 binding data from a large sample of healthy young adults. Controlling for the effects of *(E)*-isomer content, striatal BP_{ND} values were significantly higher in men compared to women. Test-retest reliability was low to moderate across various brain regions. Variability was lower than has been reported in same-day test-retest studies, and no systematic change was observed from first to second scan.

Future studies using [^{11}C]ABP688 should consider sex differences, and the functional effects of these differences should be explored further. Clinical and pharmacological studies using this ligand should take into account the considerable variability in binding between scans and account for the time of scan as a potential confound.

References:

1. Deschwanden, A. *et al.* [2011] *Am. J. Psychiatry* **168:** 727–734.
2. Esterlis, I. *et al.* [2017] *Mol. Psychiatry*, Epub ahead of print.
3. Milella, M. S. *et al.* [2014] *NeuroImage* **98:** 195–202.
4. Caprioli, D., Justinova, Z., Venniro, M. & Shaham, Y. [2017] *Biol. Psychiatry*, Epub ahead of print.
5. Foster, D. J. & Conn, P. J. [2017] *Neuron* **94:** 431–446.
6. Akkus, F. *et al.* [2017] *Schizophr. Res.* **183:** 95–101.
7. DeLorenzo, C. *et al.* [2017] *J Cereb. Blood Flow Metab.* **37(8):** 2716-2727.

RF11
Simultaneous PET/MR imaging of 5-HT_{1A} receptor 'biased' agonists

Benjamin Vidal[1], Sylvain Fieux[1], Jérôme Redouté[2], Dider Le Bars [2,3], Adrian Newman-Tancredi [4], Nicolas Costes [2], **Luc Zimmer** [1,2,3]
[1]Université Claude Bernard Lyon 1, Lyon Neuroscience Research Center, INSERM, CNRS, Lyon, France
[2]CERMEP-Imaging Platforme, Bron, France
[3]Hospices Civils de Lyon, Lyon, France
[4]Neurolixis Inc, Dana Point, CA, USA

Introduction:
In pharmacology, the recent concept of 'biased agonism' implies the capacity of highly specific agonists to target specific intracellular pathways in specific brain areas. In the context of serotonin pharmacotherapy, 5-HT_{1A} receptor biased agonists can be of interest to optimize pharmacological treatments of several neuropsychiatric disorders. The aim of this study was to bring additional support to this concept thanks to simultaneous functional MRI and PET molecular imaging (PET-MRI). We compared a highly selective 5-HT_{1A} receptor agonist, F13640 (a drug-candidate for the treatment of L-DOPA-induced dyskinesia) with a 5-HT_{1A} receptor biased agonist, F15599 (a drug-candidate for the treatment of breathing deficits in Rett syndrome), at different doses, in anaesthetized cats. The drug occupancy was measured by PET imaging with [^{18}F]MPPF, a 5-HT_{1A} receptor radiopharmaceutical, after administration of both agonists and was correlated with agonist-induced brain activation patterns.

Materials and Methods:
PET and fMRI data were acquired simultaneously using a Siemens Biograph mMR hybrid camera (CERMEP-Imaging Platform). [^{18}F]MPPF was injected in a 90-min perfusion (bolus followed by a constant infusion) in isoflurane-anesthetized cats (n=4). After a post-injection equilibrium period of 50 min, F13640 or F15599 was injected i.p. The 5-HT_{1A} receptor occupancy was quantified by comparing [^{18}F]MPPF binding potential values, before and after the pharmacological challenge. Thirty minutes after the beginning of the PET acquisition, continuous T2*EPI MRI acquisitions were performed to measure the Blood Oxygen Level Dependence (BOLD) signal. The fMRI session was divided into 20 minutes of baseline and 20 minutes after drug injection. A voxel based analysis of the fMRI data was performed at an individual level, followed by a second-level analysis. This PET-MRI protocol was replicated for each cat with increasing doses of F13640 and F15599 (0.04, 0.08, 0.16 mg/kg ip). Finally, to compare the multimodal data, a correlation analysis was performed between 5-HT_{1A} receptor occupancy (PET data) and BOLD signal variations (fMRI data) at each voxel using the toolbox Biological Parametric Mapping (BPM).

Results:
PET and fMRI data, taken together, showed clear differences between the two agonists in terms of binding and subsequent activation patterns. 5-HT_{1A} receptor occupancy was found to be dose-dependent for both agonists, but differed in magnitude and spatial distribution at equal doses with distinct BOLD activation or inhibition patterns. Voxel-based correlations analyses between PET and fMRI data suggested that F13640 stimulates both 5-HT_{1A} pre-synaptic and post-synaptic receptors, whereas F15599 preferentially stimulates post-synaptic cortical heteroreceptors. In cingulate cortex, the agonists induced opposite BOLD signal changes in response to 5-HT_{1A} occupancy.

Discussion/Conclusion:
These data constitute the first simultaneous exploration of 5-HT_{1A} receptor occupancy and its consequences in terms of brain activation and demonstrates differential signalling by two selective 5-HT_{1A} receptor biased agonists. PET/MRI represents a powerful tool in neuropharmacology and opens new ways to address *in vivo* the concept of functional selectivity by translational approaches.

Acknowledgements:
This work was supported in part by the Fondation Neurodis and the French national program 'Investissement d'Avenir' Programs (LILI – Lyon Integrated Life Imaging: hybrid MR-PET ANR-11-EQPX-0026), the hospital University Institut CESAME (Brain and Mental Health ANR-10-IBHU-0003) and the Lyon Neuroscience Research Center.
This work was performed within the framework of the LABEX PRIMES (ANR-11-LABX-0063) of Université de Lyon, within the program "Investissements d'Avenir" (ANR-11-IDEX-0007) operated by the French National Research Agency (ANR).

References:
Luttrell LM, Maudsley S, Bohn LM [2015] Mol. Pharmacol. 88:579-588.
Kenakin T, Christopoulos A [2013] Nat. Rev. Drug Discov. 12:205-216.
Becker G, et al. [2016] Sci. Reports 6:26633.

RF12

Kinetic modelling for endogenous neurotransmitter discharge characterization using PET imaging: optimization of lp-ntPET

Inés Mérida[1], Flora Olivier[1], Alexander Hammers[2], Jérôme Redouté[1], Anthonin Reilhac[3], Nicolas Costes[1], Zacharie Irace[1]

[1]CERMEP-Imagerie du vivant, Lyon, France, [2]King's College London & Guy's and St Thomas' PET Centre, Division of Imaging Sciences and Biomedical Engineering, Kings' College London, UK, [3]CIRC, Singapore, Singapore

Introduction

Data analysis techniques have been developed in the last years to detect and characterize neurotransmitter release during dynamic PET imaging with a displaceable radio-tracer (Alpert et al., 2003), in response to a stimulus or a pharmaceutical challenge. In this work, we propose a new variant of the parameter estimation method lp-ntPET (Normandin et al., 2012) by estimating the model parameters in two steps. We also introduce a new robust macro parameter (the Displacement Ratio) to characterize a transient endogenous neurotransmitter release.

Materials and Methods

Model and parameters estimation

In the lp-ntPET model (Normandin et al., 2012), the kinetics C_T of a target region are defined relatively to the kinetics C_R of a reference region according to *(Eq. 1),* where h_i characterises the endogenous neurotransmitter discharge *(Eq. 2).* In the original study, a least squares method is used to estimate the parameters (R_1, k_2, k_{2a}, γ) all at once, for each h_i chosen from a set of basis functions. However, in this method, results are possibly biased due to interdependence between the parameters.

$$C_T(t) = \boldsymbol{R_1} C_R(t) + \boldsymbol{k_2} \int_0^t C_R(u)du - \boldsymbol{k_{2a}} \int_0^t C_T(u)du - \boldsymbol{\gamma} \int_0^t C_T(u) h_i(u)du \quad \textit{(Eq. 1)}$$

$$h_i(u) = \left(\frac{u-\boldsymbol{t_D}}{\boldsymbol{t_p}-\boldsymbol{t_D}}\right)^{\boldsymbol{\alpha}} exp\left(\boldsymbol{\alpha}\left[1-\frac{u-\boldsymbol{t_D}}{\boldsymbol{t_p}-\boldsymbol{t_D}}\right]\right) \quad \textit{(Eq. 2)}$$

Here, we propose to estimate the parameters in two steps. First (Step 1), the least squares estimation of kinetic parameters R_1, k_2 and k_{2a} is obtained from the first part of the TAC (from the beginning of the scan to the stimulation time t_D) with the MRTM model (Ichise et al., 2003) (*Eq. 3*). The set of parameters (R_1, k_2, k_{2a}) can be estimated without risk of being altered by parameters in h_i. Then (Step 2), for each parameter set (α, t_D, t_P), and with the parameters (R_1, k_2, k_{2a}) already estimated, the whole TAC is used to estimate γ with a least squares algorithm. Parameters that yield the best fit to the observed data are selected.

$$C_T(t) = R_1 C_R(t) + k_2 \int_0^t C_R(u)du - k_{2a} \int_0^t C_T(u)du \quad \textit{(Eq. 3)}$$

Displacement ratio

We introduce a macro parameter (Displacement Ratio, DR) to measure the percentage of tracer displaced by the endogenous release. For this, a pseudo placebo curve ($C_{T\_placebo}$) is extrapolated for C_T from t_D until the end of the scan (t_{end}), according to the MRTM equation (*Eq. 3*) with estimated parameters R_1, k_2, k_{2a}. We compute the DR as follows (*Eq. 4*):

$$DR = \frac{\int_{t_D}^{t_{end}} C_{T\_placebo} - \int_{t_D}^{t_{end}} C_{T\_stimulation}}{\int_{t_D}^{t_{end}} C_{T\_placebo}} \times 100 \quad \textit{(Eq. 4)}$$

Simulated PET data

To reproduce a bolus-infusion [^{11}C]raclopride protocol, realistic dynamic brain PET data were simulated for 21 subjects using PET-SORTEO (Reilhac et al., 2016). Emission and attenuation phantoms were created for each subject, from MRI and CT data. Fifteen regions of interest (ROI) were defined. A 90-minute input time-activity-curve, derived from real PET/CT data, was associated to each ROI, with a stimulation at 40 min, of four magnitudes (0, 5, 10 and 25%, respectively named placebo, stim05, stim10, stim25).

Results

With classic lp-ntPET, the accuracy of estimated kinetic parameters R_1, k_2, k_{2a} was affected by the increasing magnitude of the stimulation (mean absolute bias 1.6% at placebo and 11.7% at stim25), whereas with 2-step lp-ntPET, estimated kinetic parameters were reproducible across conditions, and close to the theoretical values (mean absolute bias 0.2% at placebo and 1.8% at stim25) (*Figure 1*).

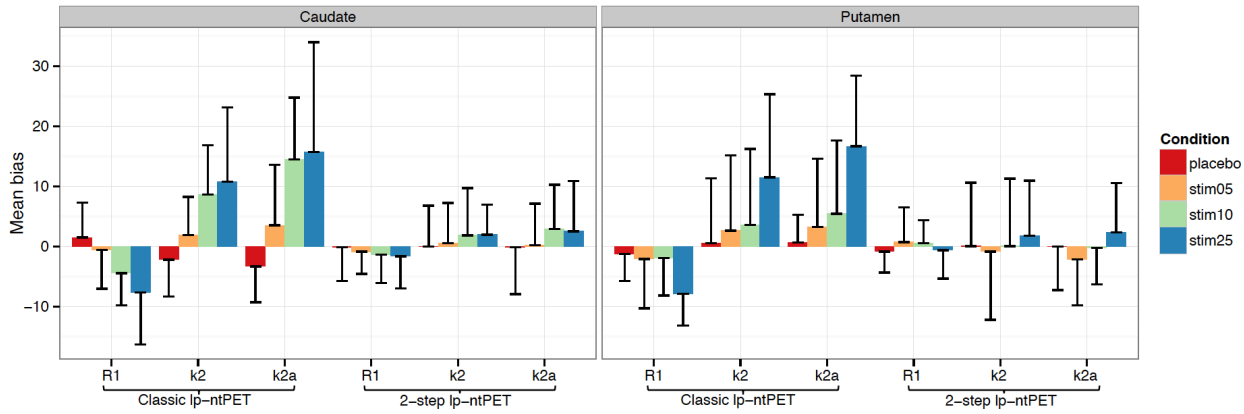

Figure 1: Mean absolute bias for kinetic parameters R_1, k_2 and k_{2a} estimated with classic and 2-step lp-ntPET methods, per stimulation condition and region.

Differences in DR versus placebo were statistically significant for all three conditions with the 2-step lp-ntPET approach, for both caudate and putamen (*Figure 2*). In contrast, the classic lp-ntPET approach only distinguished stim10 and stim25 from placebo for putamen, and only stim25 for caudate.

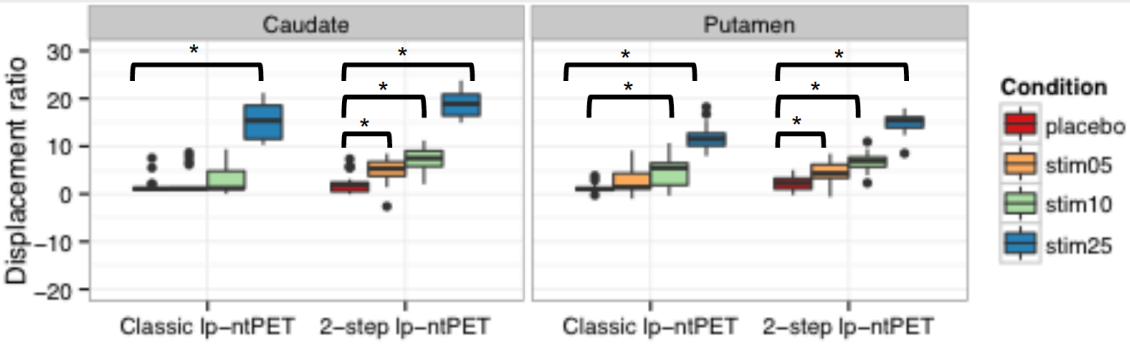

*Figure 2: Displacement ratio estimated with classic and 2-step lp-ntPET methods, per stimulation condition and region. * p<0.05 corrected for multiple comparisons. Only differences with placebo are shown.*

Conclusion and outlook

The new proposed method allowed a better estimation of kinetic parameters independently from the magnitude of the release. Displacement ratios allowed better detection of even low amplitudes of neurotransmitter discharge. The 2-step lp-ntPET method is now being implemented at a voxel level. Further work will integrate MRI information to constrain the PET kinetic model.

References

Alpert, N.M., Badgaiyan, R.D., Livni, E., Fischman, A.J., 2003. Neuroimage 19, 1049–1060. doi:10.1016/S1053-8119(03)00186-1

Ichise, M., Liow, J.-S., Lu, J.-Q., Takano, A., Model, K., Toyama, H., Suhara, T., Suzuki, K., Innis, R.B., Carson, R.E., 2003. J. Cereb. Blood Flow Metab. 23, 1096–1112. doi:10.1097/01.WCB.0000085441.37552.CA

Normandin, M.D., Schiffer, W.K., Morris, E.D., 2012. Neuroimage 59, 2689–2699. doi:10.1016/j.neuroimage.2011.07.002

Reilhac, A., Soderlund, T., Thomas, B., Irace, Z., Mérida, I., Villien, M., Redouté, J., Costes, N., 2016. PSMR. pp. 1–2.

RF13
Pharmacokinetic modeling of sigma-1 radioligand [^{18}F]FTC-146 binding in brain

Samantha T. Reyes[1], Geoffrey I. Warnock[2], Scarlett G. Guo[1], Jessa B. Castillo[1], Jun Hyung Park[1], Bin Shen[1], Christopher R. McCurdy[3], and Frederick T. Chin[1]

1. *Department of Radiology, Stanford University School of Medicine, Stanford, CA 94305, USA;*
2. *PMOD Technologies LLC, Zurich, Switzerland*
3. *Department of Medicinal Chemistry, College of Pharmacy, University of Florida, Gainesville, FL, 32610, USA.*

Introduction:
Sigma-1 receptors (S1Rs) are implicated in a variety of neurologic conditions including Alzheimer's Disease,[1,2] addiction,[3] and neuropathic pain.[4] Thus, positron emission tomography (PET) imaging of S1Rs using the selective radioligand [^{18}F]FTC-146, could serve important clinical applications. To further evaluate [^{18}F]FTC-146 as a diagnostic tool, we performed fully quantitative PET with [^{18}F]FTC-146 in rats, using continuous arterial sampling to obtain the arterial input function. In further studies, we will perform test-retest reliability, and dose-response challenge experiments.

Materials and Methods:
Sprague Dawley female rats (n=4) weighing 250-270g, anesthetized with isoflurane, were used for 60-minute dynamic PET imaging with [^{18}F]FTC-146. Femoral arterial and venous catheters were implanted and an arteriovenous shunt with coincidence detector (Swisstrace Twilite) was used to measure the arterial whole blood input function. [^{18}F]FTC-146 was injected intravenously (41.87±11.41 MBq/1.13±0.31 mCi) via the arteriovenous shunt. Separate rats of equal weight (n=3) were used to derive the whole blood to plasma ratio and parent fraction for metabolite correction. Femoral arterial and venous catheters were similarly implanted and the rats were injected intravenously with a bolus of [^{18}F]FTC-146 (121.13±32.86 MBq/3.27±0.90 mCi) for our radiometabolite studies. Blood was collected every 5 minutes for an hour. Two-tissue compartment kinetic modeling was performed in four brain regions (frontal cortex, right striatum, cerebellum and brain stem) using PMOD 3.7.

Results:
The two-tissue compartment model was successfully fitted to the 60-min dynamic rat brain PET data for [^{18}F]FTC-146 (**Figure 1**). The whole blood input function was well described by a bi-exponential model starting from the peak, and the parent fraction was well described by a single exponential model. After 5 min, 27% of counts in plasma could be attributed to the parent compound, dropping to 15% after 10 min. The data suggested a fixed correction (whole blood:plasma ratio = 1:1.135) for whole blood counts to plasma. The mean delay due to external measurement of the input function was 30 seconds. Model macro parameters are summarized in **Table 1**. The molar activity at time of injection was 177.3±118.0 TBq/□mol (4793±3189 Ci/□mol).

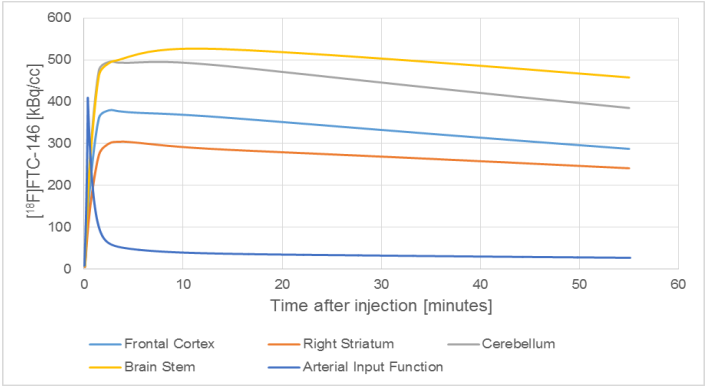

Figure 1. Two-tissue compartment model of [^{18}F]FTC-146 fitted for a 60-minute dynamic PET scan with arterial input function.

Table 1. Summary of two-tissue compartment model macro parameters.

Brain Region	Average V_S	Average V_T	Average k_3/k_4
Frontal Cortex	64.4±11.2	73.6±11.4	7.3±2.2
Right Striatum	56.2±15.0	63.3±17.6	9.1±3.8
Cerebellum	82.4±12.0	89.8±12.4	11.0±1.1
Brain Stem	114.6±19.6	123.0±21.0	13.8±1.4

Discussion:
Our results indicate that [^{18}F]FTC-146 binding can be fully quantified using a 2-tissue compartment model, given a detailed arterial input function with necessary corrections. Further studies will be performed to evaluate the reproducibility of binding macro parameters between measurements. Pilot studies have indicated that it is feasible to perform test-retest studies, including arteriovenous shunt, in the same rats. This will be useful to gauge the utility of [^{18}F]FTC-146 in the clinic. Dose-response studies will also be performed to evaluate the usefulness of [^{18}F]FTC-146 in occupancy studies.

Acknowledgements:
This research was supported in part by NICHD R01 HD084214 and the Ben & Catherine Ivy Foundation. We would like to thank PMOD Technologies LLC and Swisstrace for their invaluable support for this research. We would also like to thank the Small Animal Imaging Facility at Stanford.

References:
1. Uchida N, Ujike H, Tanaka Y, et al. [2005], Am J Geriatr Psychiatry, 13:1062-1066
2. Jansen KL, Faull RL, Storey P, Leslie RA. [1993], Brain Res, 623:299-302
3. Narayanan S, Mesangeau C, Poupaert JH, McCurdy CR. [2011], Curr Top Med Chem, 11:1128-1150
4. De la Puente B, Nadal X, Portillo-Salido E, et al. [2009,] Pain, 145:294-303
5. Warnock G, et al. [2014], J Nucl Med, 55:1336-1341

RF14
Imaging considerations for dynamic and static PET imaging of tau pathology with [^{18}F]MK-6240

Tobey J. Betthauser[1]; Karly A. Cody[1]; Matthew D. Zammit[1]; Alexandra H. DiFilippo[1]; Dhanabalan Murali[1]; Alexander K. Converse[1]; Todd Barnhart[1]; Charles K. Stone[1]; Howard A. Rowley[1]; Sterling C. Johnson[1]; Bradley T. Christian[1]

1 University of Wisconsin, School of Medicine and Public Health, Madison, USA;

Introduction:
[^{18}F]MK-6240 has shown promise for in vivo PET imaging of neurofibrillary tau tangles in Alzheimer's disease (AD)(1). Investigation of in vivo quantification strategies and characterization of potential off-target binding sites is needed for implementation of this tracer in multi-center and longitudinal human studies. This work investigates the in vivo kinetics properties of target (i.e. tau) and off-target binding and consideration for PET scanning protocols for [^{18}F]MK-6240 in humans from young controls to probable AD.

Materials and Methods:
Fifty-one participants underwent [^{18}F]MK-6240 PET and T1-weighted MRI scans (3 young controls, 33 older controls, 6 longitudinal cognitive declining, 2 MCI, 7 probable AD). Amyloid status was determined based on [^{11}C]PiB PET imaging. [^{18}F]MK-6240 PET scans consisted of a nominal 370 MBq bolus injection followed by dynamic acquisition from injection (n=19) or after a 60-minute uptake period (n=32) for up to 120 minutes post-injection. The reconstructed PET time series was realigned and coregistered to native space T1-w MRI. Off-target binding regions (e.g. meninges, sinuses) were identified by averaging parametric MK-6240 standard uptake value ratio (SUVR, 70-90 min, inferior cerebellum reference region) images across controls in MNI space. Time-activity-curves (TACs) were extracted in T1-w MRI space from inverse warped AAL and manually segmented regions of interest (ROIs). Graphical Logan and MRTM2 reference tissue methods were investigated for estimation of distribution volume ratios (DVRs), which were compared by linear regression to SUVR estimates using stepwise 20-minute windows beginning 40 minutes post-injection. Stability of DVR estimates using shortened scan durations was also investigated. SUV and Target-to-reference (TTR) TACs in target and off-target regions were compared to identify the kinetic dependence of potential off-target spill in to target regions.

Results:
SUV TACs in the inferior cerebellum and the pons peaked 2-4 minutes after bolus injection (SUV_{max} = 2 to 5) and indicated similar clearance across all subjects. TTR TACs in regions associated with neurofibrillary tau in AD stabilized around 70 minutes with the exception of high binding AD subjects, which were still increasing at 90 minutes (Figure 1). Logan DVR estimates (t*=35 min, k_2'=0.04 min^{-1}) were slightly lower (mean difference -0.02±0.05) than MRTM2 (t* = 30 min) when using the entire dynamic scan duration. Sixty-minute scans were suitable for Logan DVR estimation, whereas MRTM2 indicated higher variability and regression parameters further from unity (Table 1) when scan durations were shortened. Regression of stepwise SUVR on MRTM2 or Logan DVR indicated fits near unity for 60-80 and 70-90 minute windows. TTR TACs in regions that included bone marrow (clivus, ethmoid sinus, spenotemporal buttress) and in the meninges were increasing throughout the entire 120-minute scan duration and spilled over into adjacent cortex in some cases. Minor off-target binding was also observed in the pineal gland, superior cerebellum, superior anterior vermis, and in the substantia nigra. TTR TACs in these regions plateaued by 60 minutes with the exception of the substantia nigra, which was decreasing after 40 minutes. Similarly, TTR TACs in the striatum were also decreasing after 40 minutes. MK-6240 specific

binding patterns observed in amyloid positive subjects recapitulated Braak hierarchical staging of neurofibrillary tau.

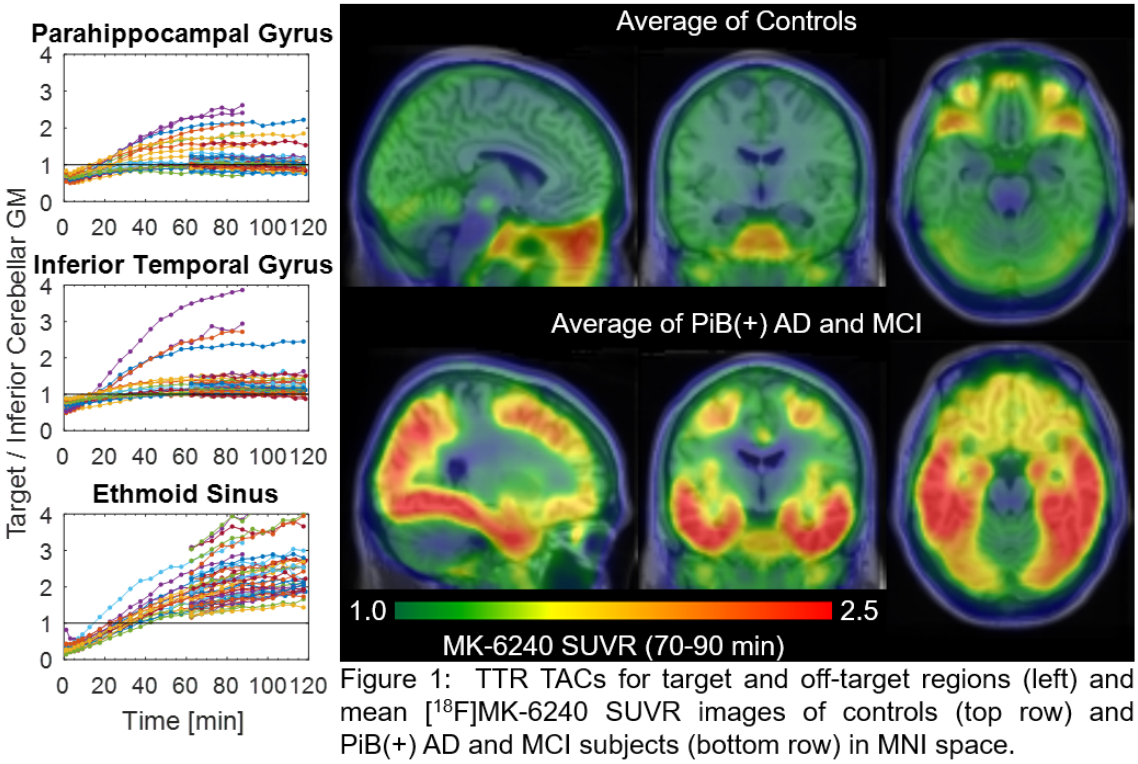

Figure 1: TTR TACs for target and off-target regions (left) and mean [^{18}F]MK-6240 SUVR images of controls (top row) and PiB(+) AD and MCI subjects (bottom row) in MNI space.

Discussion/Conclusion:

These results indicate reference tissue methods produce stable DVR estimates when using scan durations as short as 60 minutes and the inferior cerebellum as a reference region. SUVR quantification from 70-90 minutes post-injection provides accurate binding estimates while simultaneously reducing spill-in from off-target binding regions outside the brain. Agreement with neuropathological staging of AD neurofibrillary tau combined with reduced off-target binding in the brain compared to other tau PET ligands indicate [^{18}F]MK-6240 will be suitable for in vivo evaluation of neurofibrillary tau in AD.

Method	Scan Duration [min]	Mean Bias ± sd [%]	Slope	Intercept	R^2
Logan	50	-0.5 ± 4.5	0.98	0.02	0.98
Logan	60	-0.3 ± 3.0	0.99	0.01	0.99
Logan	70	-0.3 ± 1.9	0.99	0.01	1.00
Logan	80	-0.1 ± 1.1	0.99	0.01	1.00
MRTM2	50	-2.2 ± 8.3	0.84	0.15	0.97
MRTM2	60	-0.3 ± 6.2	0.96	0.04	0.97
MRTM2	70	0.0 ± 4.5	0.95	0.05	0.99
MRTM2	80	0.4 ± 4.9	0.96	0.04	0.99

Table 1: Within-method regression of DVR estimates derived from shortened scan duration against DVRs derived from at least 90-minute acquisitions and the average bias.

Acknowledgements:

We would like to acknowledge the UW-Madison Cyclotron Group, Waisman PET Group, the Wisconsin Alzheimer's Disease Research Center for their contributions to this work and Cerveau Technologies for providing chemical precursor and MK-6240 reference standard. Funding for this work was provided by NIH T32 CA009206, NIH R01 AG021155, NIH R01 AG027161, NIH-NIA P50 AG033514, and NICHD U54 HD090256.

References:

1. Hostetler ED, Walji AM, Zeng Z, Miller P, Bennacef I, Salinas C, Connolly B, Gantert L, Haley H, Holahan M, Purcell M, Riffel K, Lohith TG, Coleman P, Soriano A,

Ogawa A, Xu S, Zhang X, Joshi E, Della Rocca J, Hesk D, Schenk DJ, Evelhoch JL. [2016] J Nucl Med, 57(10):1599-606.

RF15
Synthesis of [^{11}C]NR2B-Me and its derivatives for evaluation as PET radioligands for NR2B subunits in NMDA receptors

Lisheng Cai, Jeih-San Liow, Cheryl L Morse, Riley Davies, Robert B Innis, Victor W Pike.

Molecular Imaging Branch, National Institute of Mental Health, NIH, Bethesda, Maryland, USA.

Objectives: NR2B is the most studied NMDA receptor subunit within the NMDA complex, and its expression is largely limited to forebrain regions and dorsal horn of the spinal cord [1]. NR2B is considered to be a therapeutic target for schizophrenia, stroke, and neurodegenerative diseases, especially neuro-pain. Therapeutics targeting NR2B rather than the NMDA channel have fewer side-effects [1]. The quantification of NR2B subunits within NMDA receptors could help to elucidate the contribution of this receptor to neuropsychiatric disorders and also assist in drug develoment [2]. Currently, no PET radioligand is available for such quantification [3]. Here, within a broader medicinal chemistry campaign, we designed and synthesized a number of derivatives based on 7-methoxy-2,3,4,5-tetrahydro-1H-benzo[*d*]azepin-1-ol (MTB) and discovered 7-methoxy-3-(4-(4-methylphenyl)butyl)-2,3,4,5-tetrahydro-1*H*-benzo[*d*]azepin-1-ol (NR2B-Me), which shows affinity for NR2B in the nM range, moderate computed lipophilicity (clog*D* = 3.4), and amenability to labeling with carbon-11. We therefore prepared [^{11}C]NR2B-Me from an boronic ester precursor for evaluation as an NR2B PETradioligand in rat.

Methods: A total of about 20 derivatives, based on MTB were synthesized in 1−4 steps in up to 40% overall yields. All were evaluated for binding to the NR2B site and other neuro-targets by The NIMH Psychoactive Drug Screening Program (PDSP). The precursor for labelling [^{11}C]NR2B-Me, namely 7-methoxy-3-(4-(4-(4,4,5,5-tetramethyl-1,3,2-dioxaborolan-2-yl)phenyl)butyl)-2,3,4,5-tetrahydro-1*H*-benzo[*d*]azepin-1-ol, was synthesized in 4 steps. Treatment of this precursor (0.5 mg, 1.1 μmol) with cesium fluoride in methanol (1 M, 20 μL, 20 μmol), palladium catalyst (0.4 mg, 1:2 mixture of $Pd_2(dba)_3$, *tris*(2,4-dimethylphenyl)phosphine), and [^{11}C]MeI in MeOH (400 μL) at 80 ^{o}C for 5 min gave [^{11}C]NR2B-Me, which was purified with HPLC on a Waters X-Bridge C18 column (250 × 10 mm) eluted with 0.1% TFA in H_2O/MeOH (50:50 v/v), and then formulated for intravenous injection. PET imaging of brain was performed after intravenous administration of [^{11}C]NR2B-Me to rats at baseline and after displacement with the NR2B-selective ligand Ro 25 6981 (at 0.01−3 mg/kg, i.v. at 10 min after radioligand injection).

Results: Structure-activity relationship for derivatives based on MTB showed that the binding affinity of these compounds for the NR2B site is quite sensitive to substituents on the remote aryl group, either on the ring or attached. The groups most detrimental to binding are hydrophilic, such as pyridinyl. However, binding affinity does increase with molecular weight. Overall, the binding affinity versus calculated clogD tends to follow an exponential curve, with other variables also affecting the binding. The tether length between the tertiary amine and the remote aryl group plays a critical role, with the optimal length being 4 methylene groups, as shown previously [4]. Even other polar groups, such as ether, non-polar groups, such as thioether, or bulky groups, such as ketal, cannot be tolerated. [^{11}C]NR2B-Me was obtained in 20% yield from cyclotron-produced [^{11}C]CO_2 and with a radiochemical purity of >99% and a mean molar activity of 180 GBq/μmol. PET imaging of [^{11}C]NR2B-Me in rats at baseline revealed very high brain radioactivity uptake, reaching 3.0 SUV at 5 min followed by a slow washout over 90 min. Ro 25 6981 displacement accelerated brain radioactivity washsout in a dose-dependent manner.

Table. Structure-activity relationship for derivatives based on 7-methoxy-2,3,4,5-tetrahydro-1H-benzo[d]azepin-1-ol (MTB).

#	Structure	Mw	cLogD	*K*i (nM), automatic	*K*i (nM), manual	σ_1 receptor at 10 µM (%)	σ_2 receptor at 10 µM (%)
1	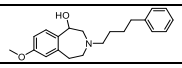	439.48	3.1	43.5	9.8	89.1	87.8
					5.4±0.4 [4]	182±38 [4]	554±127 [4]
2	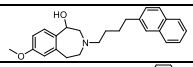	489.54	4.3	22.7	7.3	84.4	94.0
3	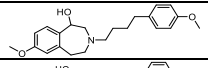	469.50	2.9	44.0	8.7	94.0	91.4
4	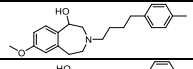	453.50	3.4	31.3	4.9	89.7	90.7
5	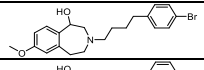	518.37	3.7	26.7	2.5	83.7	90.0
6	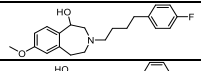	457.47	3.1	28.0	3.7	57.9	76.9
7	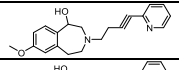	436.43	1.9	493.0	97	66.4	74.2
8	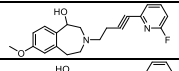	454.42	2.0	583.5	129	40.8	56.4
9	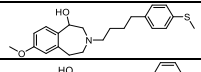	485.56	3.7	20.0			
10	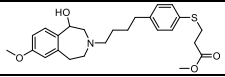	557.63	3.6	42.0			
11	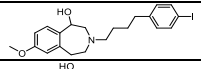	565.37	4.0	21.0			
12	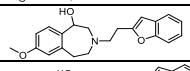	451.44	2.9	119.8			
13	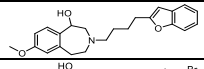	479.50	3.5	44.0			
14	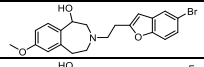	530.34	3.7	66.3			
15	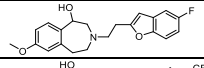	469.43	3.0	53.7			
16	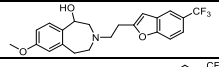	519.44	3.7	48.7			
17	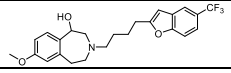	547.49	3.9	19.3			

Figure 1. Calculated clog*D* vs. K_i values follows an exponential curve.

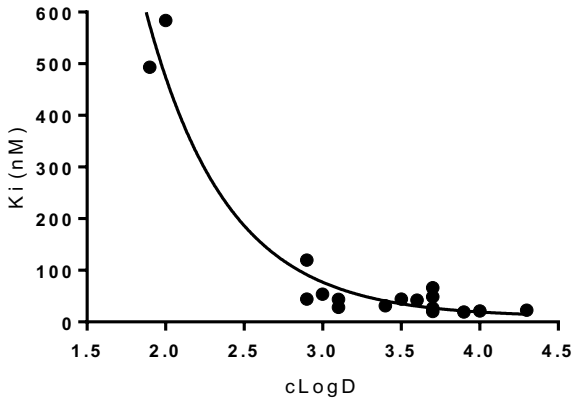

Figure 2. Displacement of [11C]NR2B-Me by Ro 25 6981 at different doses.

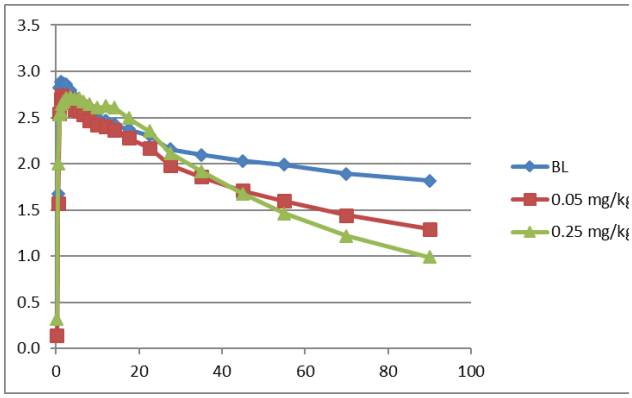

Conclusions: Structure-activity relationships were established for MTB derivatives. The most important factors for binding affinity are hypophilicity and the length of the tether between the tertiary amine and the remote aryl group. The nature of the aryl ring also played a role. [^{11}C]NR2B-Me was readily synthesized, and showed high brain uptake in rat, which could be displaced by Ro 25 6981. Further study is required to characterize the nature of the specific binding of [^{11}C]NR2B-Me in rat brain and its utility in brain research. These studies are ongoing.

Research Support: Intramural Research Program of the National Insitutes of Health (NIMH).

References:

[1] Zhuo M, *Neuropharmacology*, **2017**, *112*, 228.
[2] Kassenbrock A, Vasdev N, Liang SH. Curr*. Top. Med. Chem*. **2016**, *16*, 1830.
[3] Krämer SD *et al*.,*J. Nucl. Med.* doi:10.2967/jnumed.117.200451.
[4] Tewe B et al., *ChemMedChem* **2010**, *5*, 687

RF16

Abstract Withdrawn

RF17

Synthesis and biological evaluation of novel F-18 labelled peripheral benzodiazepine receptor PET radioligand: [^{18}F]fluorovinpocetine.

S. Nag[1], R. Krasikova[1,2], A. Airaksinen[3], B. Gulyas[1,4], and C. Halldin[1]

[1]Karolinska Institutet, Department of Clinical Neuroscience, Stockholm, Sweden
[2]N.P. Bechtereva Institute of Human Brain Russian Academy of Sciences, St.-Petersburg, Russia; [3]Department of Chemistry, University of Helsinki, FInland
[4]Lee Kong Chian School of Medicine, Nanyang Technological University, Singapore

Introduction:
Vinpocetine, a synthetic ethyl ester of apovincamine is structurally related to the Vinca minor alkaloid vincamine. Since 1978, Vinpocetine is prescribed as a drug for the prevention and treatment of various cerebrovascular diseases. It effectively increases the cerebral blood flow and cerebral glucose metabolism. Vinpocetine has previously been labeled with carbon-11 and applied in preclinical and clinical PET studies as peripheral benzodiazepine receptor radioligand[1]. Carbon-11 labeled compounds are less suitable for longer PET scanning time as well as for the distribution to external clinics because of its relatively short half-life. In this project our aim was to develop a fast and efficient synthetic method for labeling novel vinpocetine analogues with fluorine-18 and to evaluate its biological activity *in-vivo* and *in-vitro* as peripheral benzodiazepine receptor ligand.

Method:
The precursor apovincaminic acid was bought from commercial source and the reference standard cold fluorovinpocetine was synthesized by one-step organic synthesis. Radiolabeling was achieved in two steps. In the first step, the radioactive intermediate 2-[^{18}F]fluoroethyl bromide ([^{18}F]FEtBr) was synthesized via one step nucleophilic substitution followed by the alkylation of the acid precursor. [^{18}F]fluorovinpocetine was tested in human whole hemisphere autoradiography experiments. Two baseline PET experiments were performed in rhesus monkeys using HR (Siemens) PET scanner. Radiometabolites were measured in monkey plasma using gradient HPLC.

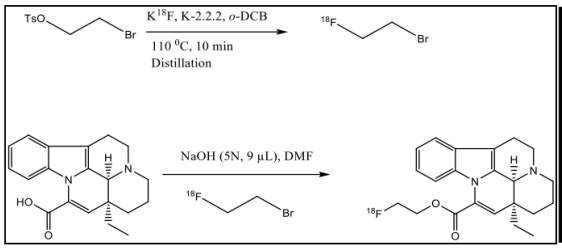

Figure 1: Synthesis scheme.

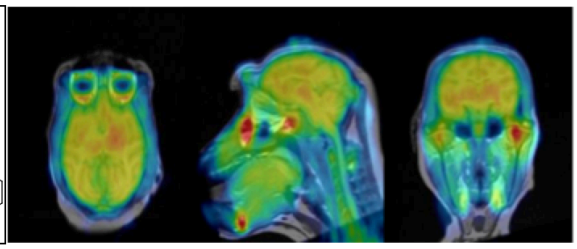

Figure 2: PET image.

Results and discussion:
Radiolabeling was accomplished successfully with an radiochemical yield >15%. The radiochemical purity was higher than 99% and the molar radioactivity was >170 GBq/µmol at the time of administration. In the autoradiography assay, [^{18}F]fluorovinpocetine binding was observed in all grey matter regions. Co-incubation with, cold vinpocetine, led to reduced in vitro radioligand binding. *In-vivo*, there were high uptake in the monkey brain (>4% id) at 4 min (Fig. 2) with higher amounts in the thalamus compared to the cortex and cerebellum. The time activity curves looked similar to what was obtained by 11C-labelled vinpocetine. Metabolite studies demonstrated 10% unchanged radioligand at 120 min post injection.

Conclusion:
A fast and efficient synthetic method to produce [^{18}F]fluorovinpocetine was developed. [^{18}F]Fluorovinpocetine displays favorable properties for in vivo imaging of peripheral

benzodiazepine receptor; including, high blood-brain-barrier permeability, regional uptake, and fast washout from the NHP brain and is a potential candidate for human PET studies.

Reference:

1. Gulyas, B.; Halldin, C.; Vas, A.; Banati, R. B.; Shchukin, E.; Finnema, S.; Tarkainen, J.; Tihanyi, K.; Szilagyi, G.; Farde, L. *Journal of the Neurological Sciences* **2005,** 229, 219-223.

RF18
Synthesis and *in vivo* characterization of [^{11}C]Ro 04-5595 for PET imaging of NR2B subtype NMDA receptors

Jimmy E. Jakobsson[a], Marthe F. Fjelldal[a], Shivashankar Khanapur[a], Ragnhild E. Paulsen[a] and Patrick J. Riss[abc]

[a]Realomics SFI, Kjemisk Institutt, Universitetet i Oslo, Sem Sælands vei 26, Kjemibygningen, 0371 Oslo, Norway. [b]Klinik for Kirurgi og Nevrofag, Oslo Universitets Sykehus HF-Rikshospitalet, Postboks 4950 Nydalen, 0424 Oslo, Norway. [c]Norsk Medisinsk Syklotronsenter AS, Gaustad, Postboks 4950 Nydalen, 0424 Oslo, Norway.

Introduction:
NMDA (*N*-methyl-D-aspartate) receptors are glutamate gated ion channels essential in the central nervous system. NMDA receptors are comprised of different subunits.[1] Regions rich in NR2B subunits are cerebral cortex, hippocampus, striatum and thalamus.[2,3] NMDA Receptors play an important role in neuroplasticity, learning and memory formation.[4] Dysfunction of NMDA receptors are associated with severe neurological disorders such as Parkinson's disease and Alzheimer's disease.[5] The involvement in disease states and its regional distribution make NR2B receptors a highly attractive imaging target for radiotracer development. An NR2B selective radiotracer could facilitate drug discovery, serve as a tool compound for elucidating the connection between NR2B expression and disease states and have use in diagnostic imaging.

Materials and Methods:
We envisioned Ro 04-5595 developed by F. Hoffmann-La Roche[6] with a reported K_D of 20±3 nM[7] and high selectivity towards subtype NR2B[6] a promising PET radiotracer candidate (Figure 1). synthesised [^{11}C]Ro 04-5595 via routine radiosynthesis starting from [^{11}C]MeI and the N-desmethylated precursor. The radiotracer was evaluated in rat (Sprague Dawley SD, 8-10 weeks, 250-320 g) using PET imaging. We further characterised the radioligand via autoradiography using [^{3}H]Ro 04-5595 synthesised via catalytic [^{3}H]-hydrogenation of the corresponding alkene.

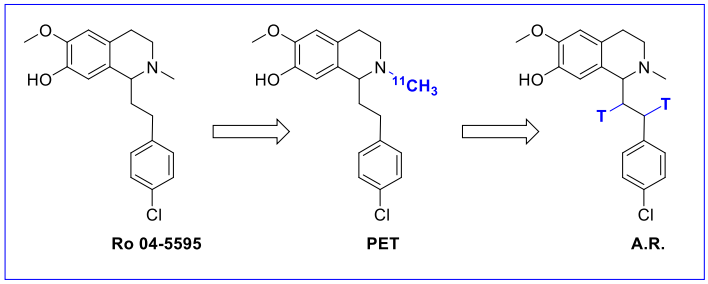

Figure 2: PET Tracer development process.

Results:
The radiotracer showed rapid brain uptake followed by washout over the duration of a 90 minute PET scan. Summed images obtained from early frames show characteristic, high uptake into cortex, striatum, thalamus, midbrain and hippocampus, in line with NR2B distribution in the rat brain. Autoradiography using [^{3}H]Ro 04-5595 provided high resolution images showing strong binding in cortex and hippocampus with some accumulation observed in striatum, thalamus and midbrain. As expected very little binding was found in for example cerebellum. Increasing concentration of Ro 04-5595 diminished the signal, which demonstrates tissue saturability.

Discussion/Conclusion:
Experimental results using [^{11}C]Ro 04-5595 in PET imaging show very promising results. The radiotracer shows good brain uptake without problematic metabolites. Coupled with the tritiated analogue, we were able to assess NR2B binding *in vivo* and, with excellent resolution, *in vitro* with little off target binding. Further work aims to evaluate the radioligand

in non-human primates and to provide a tool compound for additional biological investigations *in vitro*.

Acknowledgements:
This study was funded by the faculty of Mathematics and Natural Sciences, the Department of Chemistry, University of Oslo (startup grant to PJR), the Realomics SFI and NFR ES 231553.

References
[1] Paoletti P., Neyton J., [2007], *Curr. Opin. Pharmacol,* 7:39-47. [2] Monyer H., Burnashev N., Laurie D., [1994], *Neuron*, 12:529-540. [3] Rigby M., Le Bourdellès B., Heavens R.P., [1996], *Neuroscience,* 73:429-447. [4] Cull-Candy S., Brickley S., Farrant M., [2001], *Curr. Opin. Neurobiol.* 3:327-335. [5] Furukawa H., Singh S. K. Mancusso R., [2005], *Nature,* 438:185-192. [6] EP 0787493 A1. [7] Mutel V., Buchy D., Klingelschmidt A., [1998], *J. Neurochem.* 70:2147-2155.

RF19

Abstract withdrawn

RF20

An approach for minimally-invasive quantification of 18F-FEPPA PET in clinical populations using venous-metabolite correction and PET/MR-image derived input function.

Udunna C Anazodo[1], Esther Warnert[2], Qi Qi[1], Lumeng Cui[3], Matt Kewin[1], Linshan Liu[1], Pablo Rusjan[4], Justin Hicks[1], Raju Poolacherla[5], Jonathan D Thiessen[1], Lena Palaniyappan[6], Frank S Prato[1], Elizabeth Finger[7], Keith S St Lawrence[1].

[1]Lawson Health Research Institute, Medical Biophysics, Western University, London, Ontario. [2]Department of Radiology, Erasmus MC, Rotterdam, the Netherlands. [3]Department of Biomedical Engr. University of Saskatchewan. [4]Research Imaging Centre, Centre for Addiction and Mental Health, Toronto, Ontario. [5]Department of Anesthesia & Perioperative Medicine, Western University, London, Ontario. [6]Department of Psychiatry, Western University, London, Ontario. [7]Clinical Neurological Sciences, Western University, London, Ontario.

Introduction:

Chronic microglia activation triggered by brain injury or inflammation is associated with neurodegeneration[1] and may contribute to the pathogenesis of several psychiatric disorders[2]. PET ligands that bind to translocator proteins (TSPO) over expressed by activated microglia offer a means for *in vivo* assessment of inflammation-mediated neurodegeneration. Accurate quantification of TSPO PET require invasive arterial blood sampling for metabolite-corrected plasma input function (pIF), which limits clinical application of TSPO PET. To eliminate serial blood sampling, semi-quantitative methods using reference tissue regions have been proposed. However the absence a brain region free of TSPO expression makes reference-based methods challenging[3]. Recently, the feasibility of using a population-based pIF calibrated by a single arterial sample was assessed for 18F-FEPPA[4], a high-affinity TSPO PET ligand. In this study, we introduce a minimally-invasive, individualized approach for measuring the pIF where a PET/MR image-derived input function (IDIF)[5] is metabolite-corrected using venous blood, negating the need for specialized and invasive arterial line placement. A validation study comparing measurement of 18F-FEPPA in venous and arterial plasma samples was performed in a porcine model. Clinical feasibility of this approach is illustrated by generating pIF and estimating 18F-FEPPA distribution volume (V_T) in a frontotemporal dementia (FTD) patient and a healthy control.

Materials & Methods:

Validation study; manual arterial and venous samples (4 to 10 ml/sample) were collected in 10 pigs (~20 kg) at 2.5, 7, 12, 20, 30, 45, 60, 90, 120 and 180 minutes after injection of 18F-FEPPA (5 MBq/kg) and analyzed according to Rusjan et al[6]. Blood samples were centrifuged to extract plasma. The parent fraction (PF) in plasma was estimated using solid-phase extraction chromatography. Radioactivity concentrations in total blood, plasma, PF, and radioligand metabolite samples were counted in a high-purity germanium well counter. Blood-to-plasma ratios (BPR) and PF samples were fitted with a biexponential function. Linear regression, Bland-Altman and area-under-the-curve (AUC) were used to evaluate agreement between arterial- and venous-based BPR and PF. Four to six venous samples from 0-90 min were compared to arterial samples at 0-180 and 0-90 min to evaluate the feasibility of shorter acquisition with fewer venous sampling.

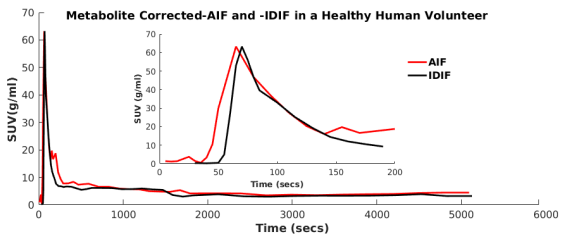

Clinical application; 90 min PET/MRI scans from 1 FTD patient and 2 controls (Biograph mMR; Siemens Healthcare, Erlangen, DE) acquired immediately after 18F-FEPPA injection

(5 MBq/kg) were corrected for attenuation[7], decay and scattering, and reconstructed (OSEM-PSF algorithm) to 51 time frames of variable lengths. IDIF was obtained from PET in carotid vessels guided by time-of-flight MRI[5] and corrected for radioligand metabolites, to generate individual pIF. To validate our PET/MR IDIF approach in humans, 1 control received arterial line placement and the IDIF was compared to automated sampled arterial IF corrected for delay and dispersion, as shown in the *figure to the right*.

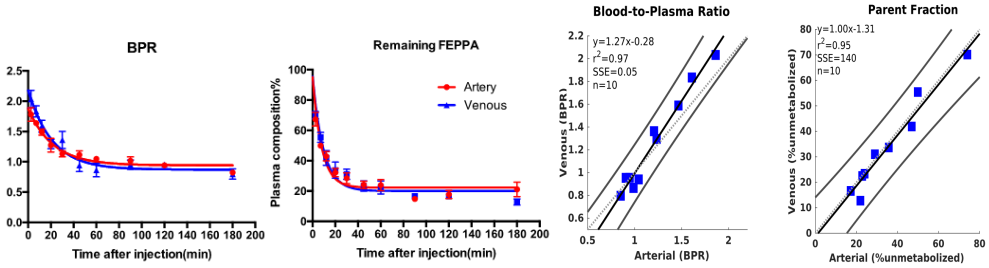

Results:
A good agreement between venous and arterial sampling in 10 pigs were observed in BPR (r^2 = 0.97) and PF/remaining FEPPA (r^2 = 0.95) measures (see time-activity and regression plots below), even when fewer venous samples are used, as shown in the table below.

Table: Comparison of venous to arterial samples. AUC-Ratio (0-90min) = AUC venous / AUC arterial.

	Parent Fraction (PF) in Plasma				Blood to Plasma Ratio (BPR)			
Fitting Results	Arterial	Venous	Venous (6)	Venous (4)	Arterial	Venous	Venous (6)	Venous (4)
Goodness of Fit (R-square)	0.85	0.89	0.92	0.97	0.76	0.78	0.80	0.80
Intercept	93.38	93.93	96.43	99.99	1.96	2.17	2.21	~ 2.64
Plateau	22.51	21.69	22.41	22.20	0.94	0.89	0.89	0.93
K	0.10	0.09	0.11	0.18	0.05	0.05	0.05	~ 0.19
AUC-Ratio (arterial short)		1.05	1.40	1.51		0.98	0.97	1.02

The higher FEPPA V_T in the FTD patient *(top panel)* compared to control, particularly around atrophied regions seen on T1-MR images, illustrate the clinical utility of our approach. *Note mean regional V_T in controls are within reported values*[4,6].

Discussion and Conclusion: We demonstrated that PET/MR-derived IDIF corrected using as few as 4 venous samples could be a suitable alternative for absolute quantification of 18F-FEPPA in clinical populations particularly in longitudinal studies where patient discomfort can be minimized. Inclusion of PET partial volume correction using T1-MR can further improve quantification. This proposed method is being used to investigate neuroinflammation in FTD patients and patients with major depressive disorders.

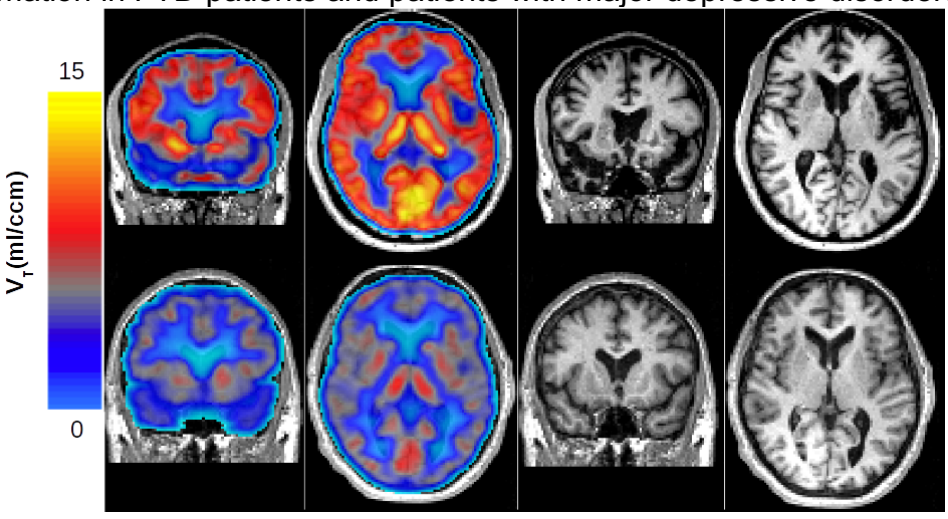

References:

[1]. Lull, ME. & Block, ML. [2010], Neurotherapeutics, 7(4):345-365. [2]. Réus GZ., Fries GR., Stertz L., et al., [2015], Neurosci. 300:141-54 [3]. Feeney C., Scott G., Raffel J., et al., [2016], EJNMMI, 43(12): 2201-2210. [4]. Mabrouk R., Strafella AP., Knezevic D., et al., [2017] *PLoS One,* May 17 2017. [5]. Anazodo U., Kewin M., Finger E., et al. [2015], EJNMMI Physics, 2(S1):A80. [6]. Rusjan PM., Wilson AA., Bloomfield PM., et al. [2011] JCBFM, 31, 1807-1816. [7]. Ladefoged CN., Benoit D., Law I., et al. [2015] PMB, 60, 8047-8065.

P1
Likelihood Estimation of Drug Occupancy for Brain PET Studies

Martin Schain[1], Francesca Zanderigo[1,2], R Todd Ogden[1,2,3]

[1]*Department of Psychiatry, Columbia University, New York, NY, USA*

[2]*Molecular Imaging and Neuropathology Division, New York State Psychiatric Institute, New York, NY USA*

[3]*Department of Biostatistics, Mailman School of Public Health, Columbia University, New York, NY, USA*

Introduction:

The established procedure to estimate the occupancy using PET data both acquired at baseline and after administration of a competitor is via linear regression analysis, which forms the basis for the so-called Lassen plot[1]. Simple linear regression analysis is not entirely appropriate for analyzing these data, since the usual assumptions are not generally satisfied. Here, we propose the use of Likelihood Estimation of Occupancy (LEO) in such a situation. Similar to the Lassen plot, LEO uses the total distribution volume (V_T) estimates at baseline and at block condition in multiple brain regions as input, but estimates the non-displaceable distribution volume (V_{ND}) and fractional occupancy (Δ) via direct maximum likelihood estimation.

Methods:

Central to the performance of LEO is specification of the covariance structure of the data, which, if accurately done, can improve the accuracy and precision of the estimates of Δ and V_{ND}. If a test-retest dataset is available, it can be used to estimate the covariance matrix. LEO's performance in estimating Δ and V_{ND} in relation to the Lassen Plot was evaluated via two separate simulation experiments.

Simulation 1: A test-retest dataset[2] with [^{11}C]DASB was used to define a "true" covariance structure. One thousand instances of new test-retest and blocking data with known values for Δ and V_{ND} following this covariance structure were simulated. LEO and Lassen plot were then used to estimate Δ and V_{ND}, and their agreement with the true values was investigated. Simulation settings included varying the number of simulated test-retest subjects (100, 10, and 5), true value for Δ (0.25, 0.5, and 0.75), and noise level (100%, 110% and 125% of realistic values). Several procedures to estimate the covariance matrix from the simulated test-retest data were evaluated, including non-linear shrinkage[3] and diagonal approximations.

Simulation 2: A test-retest dataset[4] with [^{11}C]WAY-100635 was used to define a "true" covariance structure. Using this covariance matrix, V_T values simulating a blocking study in which a hypothetical drug (K_i = 25 ng/ml, $\Delta^{max} = 100\%$) were administered at various doses prior to the second scan were generated. The Lassen plot and LEO were then used to estimate corresponding values for Δ, which were used to estimate K_i and Δ^{max}.

Application to real data: LEO and Lassen plot were evaluated on a dataset[5] acquired with [^{11}C]WAY-100635, in which sertraline was used as a blocking agent. Δ estimated with Lassen plot and LEO were compared to that obtained from $\Delta = 1 - BP_p^{block} / BP_p^{baseline}$,

where the binding potential BP_p was calculated using the cerebellar white matter as a reference region.

Results:

Simulation 1: For reasonable options for the covariance matrix, LEO always resulted in higher accuracy and precision in estimates of Δ and V_{ND} than did the Lassen plot. Figure 1 shows the results obtained with 10 test-retest subjects, 50% occupancy, and 100% noise.

Simulation 2: Using LEO resulted in improved precision in the estimates of K_i and Δ^{max} for the hypothetical compound (Figure 2).

Application to real data: Δ estimated with LEO was in closer agreement to those derived using a reference region than those obtained using Lassen plot (Figure 3).

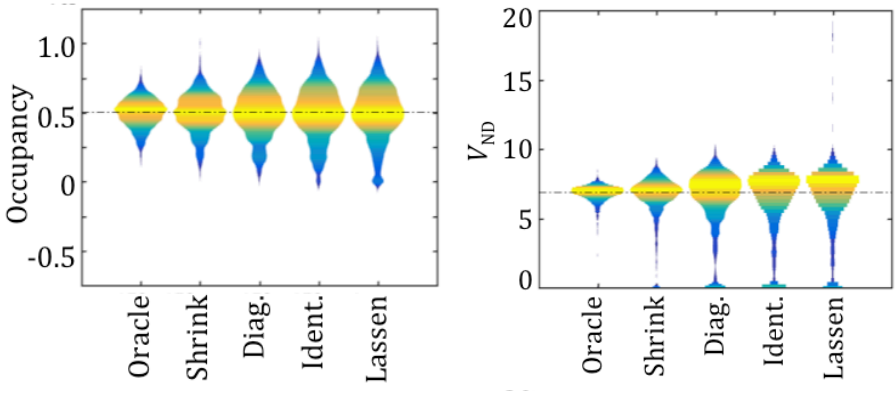

Figure 1: Distribution of estimated Δ and V_{ND} from simulation 1, using LEO with different methods to estimate the covariance matrix (Non-linear shrink[3], Diagonal, and Identity matrices). Dashed black lines show the true values. "Oracle" refers to when the true covariance matrix was used in LEO.

Discussion:

The results show that, particularly when a rest-retest dataset is available from which the covariance matrix can be estimated, LEO provides better estimates than the Lassen plot, possibly since the limitations intrinsic to linear regression are avoided[6].

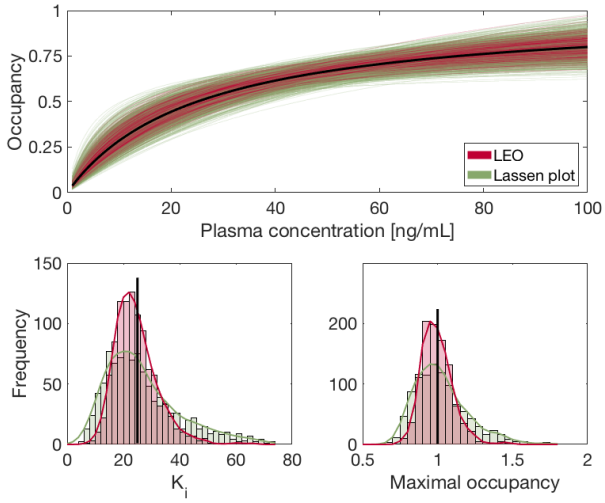

Figure 2 Results from Simulation 2. Top panel show occupancy plots obtained with LEO and Lassen plot (each line represents one simulation), using 10 simulated test-retest subjects, with covariance matrix estimated with shrink[3]. Bottom panels show distributions of estimates of K_i and Δ^{max}. Black lines correspond to true values.

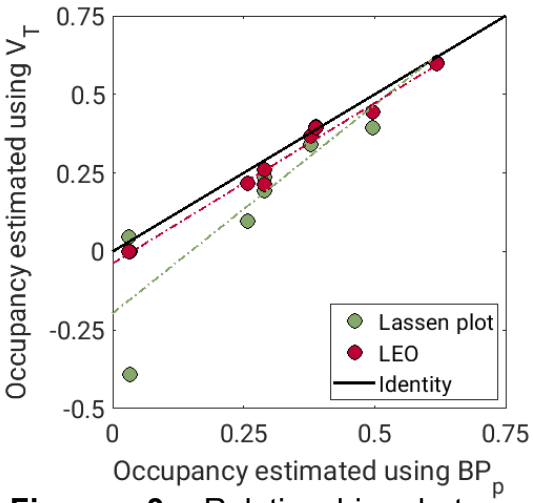

Figure 3 Relationship between Δ estimated using a reference region and either LEO (5 test-retest subjects and the shrink method) or Lassen plot, using real [^{11}C]WAY100635 data

References:

[1]Cunningham VJ, Rabiner EA, Slifstein M et al., [2010], J Cereb Blood Flow Metab.30:46-50
[2]Ogden RT, Ojha A, Erlansson K, et al., [2007], J Cereb Blood Flow Metab.27:205-17
[3]Ledoit O, Wolf M, [2015] J Multivariate Anal. 139:360-84
[4]Parsey RV, Slifstein M,Hwang DR, et al, [2000], J Cereb Blood Flow Metab.20:1111-33
[5]Martinez D, Hwang D, Mawlawi O, et al., [2001], Neuropsychopharmacology.24:209-29
[6]Naganawa M, Gallezot JD, Rossano S, et al., [2017], Bull Math Biol.In press

P2
Evaluation of [^{18}F]-FEOBV in rats

A. Schildt[1,2], E.F.J. de Vries[1], A.T.M. Willemsen[1], R.E. Moraga-Amaro[1], B. Lima-Giaccobo[1], J.W.A. Sijbesma[1], V. Sossi[2], R.A.J.O. Dierckx[1], J. Doorduin[1]

[1]*Department of Nuclear Medicine and Molecular Imaging, University of Groningen, University Medical Center Groningen, Groningen, the Netherlands*

[2]*Department of Physics and Astronomy, University of British Columbia, Vancouver, Canada*

Introduction:

The vesicular acetylcholine transporter (VAChT) is a marker of the cholinergic system and the target for the PET radioligand [^{18}F]-FEOBV. [^{18}F]-FEOBV has been used in rodents and has been validated for use in humans.[1,2] However, no modeling of the pharmacokinetic behavior of [^{18}F]-FEOBV in rodents has been reported yet. In the present study, we therefore determined if [^{18}F]-FEOBV can be used for imaging changes in VAChT availability in rats. For this purpose, we explored the pharmacokinetic behavior of [^{18}F]-FEOBV in rats and the influence of unlabeled FEOBV (partial blocking due to its toxicity), raclopride (D_2-receptor block) and haloperidol (D_2- and σ-receptor block).

Methods:

Male Wistar rats underwent a 90-min dynamic PET scan with blood sampling from the femoral artery to generate a metabolite corrected input function. Rats were injected with DMSO (control, n=4), 1 mg/kg raclopride (n=4) or 10 mg/kg haloperidol (n=3) at 45 min, or 10 µg/kg unlabeled FEOBV (n=3) at 15-10 min before the injection of [^{18}F]-FEOBV and start of the PET scan. Kinetic analysis was performed for eight volumes of interest (VOIs) (cerebellum, frontal cortex, cortex, hypothalamus, hippocampus, thalamus, striatum, whole brain) using one- (1TCM) and two-tissue compartmental models (2TCM) and Logan graphical analysis with plasma input for 60 and 90 min acquisition time. Differences in V_T between treatment groups and control were compared for each VOI using one way analysis of variance (ANOVA).

Results:

The 1TCM was not able to describe [^{18}F]-FEOBV kinetics for 90 or 60 min acquisition time. Modeling with a reversible 2TCM for the 90-min acquisition time in control rats, revealed very small k_4 values in all brain regions with a large variability between rats (e.g. striatum k_4 = 0.008 ± 0.005 min^{-1}, coefficient of variation (CoV) 71%). As a result, a large variability was found in V_T between rats (e.g. striatum: V_T = 57 ± 41 mL·cm^{-3}, CoV 71%) and BP_{ND} (e.g. striatum: BP_{ND} = 8.4 ± 3.3, CoV 39%). The irreversible 2TCM was explored, but showed slightly higher AIC values compared to the reversible 2TCM. Lower AIC values, and a decrease in V_T and in the V_T variability were found when shortening the acquisition time from 90 to 60 min (e.g. striatum V_T = 28 ± 6 mL·cm^{-3}, CoV 23%; BP_{ND} = 4.4 ± 1.0, CoV 22%). Nevertheless, the estimation of k_4 was still unreliable (>30% standard error in 3 rats). For 60-min acquisition time, Logan graphical analysis with blood input showed a similar variability in V_T (striatum: V_T = 22 ± 6 mL·cm^{-3}, CoV 26%) and good correlation with 2TCM (Pearson r = 0.82).

In the pretreatment groups the best results were also found for an acquisition of 60 min, similar to the control group. The variability in V_T and BP_{ND} decreased in rats pretreated with unlabeled FEOBV but increased in the haloperidol and raclopride groups compared to control animals. Similar to the control group, Logan with plasma input function showed the lowest CoV of V_T in the striatum in the pretreatment groups (24-32% compared to 34-200% for reversible 2TCM).

Using the V_T obtained from Logan analysis, it was found that treatment with raclopride increased V_T in striatum by 36 %, when compared to control rats, but did not affect V_T in the cerebellum. Blocking with unlabeled FEOBV decreased V_T in the striatum by 50% and cerebellum by 32%, whereas other regions showed a decrease of 40 %. Haloperidol treatment decreased VT by 10% in the striatum and by 74% in the cerebellum, while the other brain regions showed a decrease between 50% and 78%. Despite the large average changes in V_T between groups, no statistically significant differences were found, likely due to the small sample size and large within-group variability.

Conclusion:

Our results show that [^{18}F]-FEOBV can be used as a radioligand for VAChT PET imaging in rats. [^{18}F]-FEOBV showed a similar behavior in rats as in humans in the control group with poorly estimated, very low k_4 values and large variation in macroparameters for 2TCM.[1] Logan with plasma input estimated V_T with higher precision than 2TCM, especially for a 60-min acquisition time, and showed the most reliable V_T values in both control and pretreated rats. Furthermore, our results suggest that the use of the cerebellum as tissue input should be explored with caution. The changes in V_T by treatment with the D_2- and σ-receptor blocker haloperidol indicate that effects of intervention on the reference region could influence the outcome parameters of reference tissue models.

References :

1. Petrou, M. *et al.* [2014], *J. Nucl. Med.*, **55**:396–404.

2. Kilbourn, M. R. *et al.* [2009], *Nucl. Med. Biol.*, **36**:489–493.

P3
Comparisons of Biased and Non-biased μ-Opioid Receptor Agonists using PET/MRI

Hsiao-Ying Wey[1], Michael S. Placzek[1], Jacob M. Hooker[1], Bruce R. Rosen[1], Joseph B. Mandeville[1]

[1]*Athinoula A Martinos Center for Biomedical Imaging, Department of Radiology, Massachusetts General Hospital, Harvard Medical School, Charlestown, MA 02129, USA*

Introduction:

μ-Opioid receptor (MOR) agonists are the most effective analgesics for pain management. However, MOR agonists also elicit adverse effects such as respiratory depression. Upon agonist binding, MOR activates G-protein to induce downstream signaling [1]. In addition, β-arrestins are recruited to regulate receptor activity by desensitizing and internalizing MORs [1]. Emerging evidence from pharmacological and genetic animal studies suggests that selective activation of the G-protein but not the β-arrestin pathway may lead to effective analgesia without undesired side-effects [2, 3]. Therefore, biased agonism at the MORs has become a promising new direction for therapeutic development [3]. However, the *in vivo* action mechanisms of biased MORs remain to be shown. TRV130 (Oliceridine) is the first G-protein biased MOR agonist currently in late phase clinical trials [4]. The purpose of this study is to measure drug-receptor occupancy and drug-induced functional MRI responses of TRV130 and compare the results with the prototypical MOR agonist – morphine – using simultaneous PET/MRI.

Materials and Methods:

PET and MR images were acquired from two male macaques using a 3T Siemens BrainPET with a μ-opioid selective radiotracer, [^{11}C]carfentanil (~296 MBq; specific activity: >111 GBq/μmol), given as bolus-infusion for 100 min. PET data were binned into 1-min frames. Cerebral blood volume (CBV) fMRI was measured following an iron oxide (10 μg/kg, i.v.) injection. Graded doses of TRV130 (0.3, 0.5, and 1.0 mg/kg) and morphine (0.5 and 1.0 mg/kg) were given intravenously at 35 min post radiotracer administration. PET data was analyzed for binding potentials referenced to a non-displaceable compartment (BP_{ND}) using the simplified reference tissue model. A gamma-variate function was used to model the PET/fMRI temporal response to drug challenge.

Results:

Under baseline condition, PET BP_{ND} maps showed a high-level of specific binding in the thalamus, caudate, putamen, frontal cortex (Fig 1a). Baseline time activity curves (TACs) reached a steady-state with bolus/infusion of [^{11}C]carfentanil (Fig 1b). Apparent increases in TACs in high-binding regions following morphine injection were observed (Fig 1b and 1c) suggesting a potential increase in ligand-target affinity due to receptor trafficking. Percent increases in BP_{ND} ranged from ~25–65%. In contrast, TRV130 caused a dose-dependent reduction in BP_{ND} ranging from ~20–50% (Fig 1b and 1d). Because MORs are inhibitory, it was anticipated that MOR agonism would induce negative fMRI responses. We observed a global reduction of CBV in response to morphine and TRV130 (Fig 2) as expected. In addition, subtle spatial differences between the morphine and TRV130 fMRI responses were noticed. TRV130-induced stronger %CBV changes in the brainstem and the (orbital-)frontal

cortex than other brain regions, while morphine-induced a more uniform %CBV change across the whole brain.

Discussion/Conclusion:

The primary finding of this study is that morphine and TRV130 elicit similar fMRI but different PET responses. Both morphine and TRV130 induce negative CBV-fMRI responses confirming activations of the inhibitory MORs. The discrepancy of PET BP_{ND} could potentially be due to the G-protein biased property of TRV130. Specifically, TRV130 does not trigger β-arrestin-mediated receptor desensitization and internalization that potentially affect receptor affinity. Therefore, TRV130 caused a robust reduction in [^{11}C]carfentanil BP_{ND} in accordance to the classic occupancy model. Conversely, a morphine-induced increase in PET BP_{ND} cannot be attributed to drug-radiotracer competition. An alternative explanation is that morphine induces MOR desensitization. Desensitized MORs have recently been shown to have higher binding affinity [5]. [^{11}C]carfentanil is an agonist radiotracer, therefore, it is capable of detecting a change in receptor affinity. Our study demonstrated that biased agonists interact with MORs differently from conventional, non-biased MOR agonists even if fMRI responses are similar. In addition, our results suggest that agonist-induced MOR desensitization could be detected as an increase in BP_{ND} suggestive of an increase in affinity. Future studies using β-arrestin knout-out mice could help validate our hypothesis and facilitate the development of neuroimaging tools for measuring receptor desensitization and internalization.

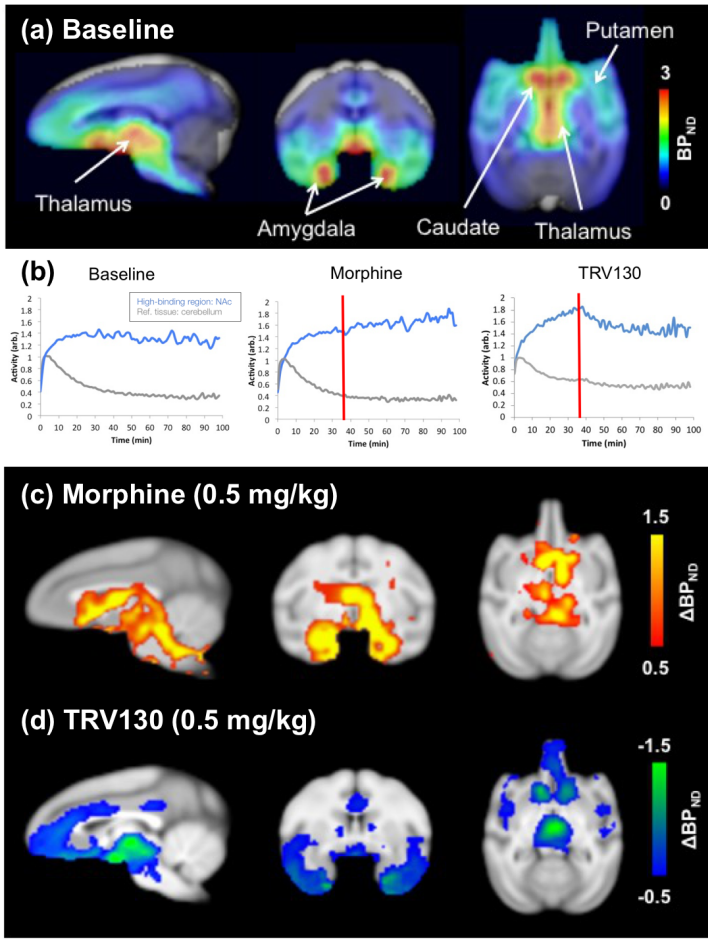

Fig 1. PET. (a) Baseline [^{11}C]carfentanil binding potential (BP_{ND}) maps show the availability of mu-opioid receptors. (b) Time-activity curves from 1 animal. Morphine causes an increase in BP_{ND} (c) while TRV130 causes a reduction in BP_{ND} (d).

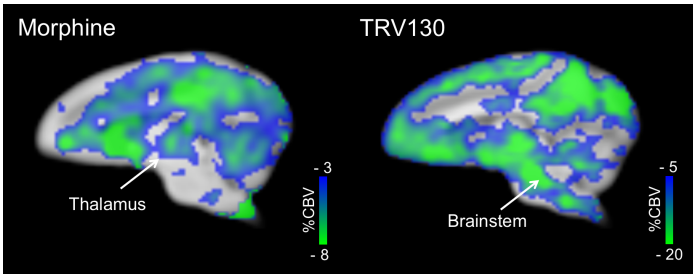

Fig 2. Agonist-induced fMRI responses. Averages %CBV maps from two animals (all doses) in response to morphine (left) and TRV130 (right) challenges.

Acknowledgements:

This research is support by NIH R00DA037928.

References:

1. Birdsong WT, et al. [2013] J Neurosci. 33: 4118–27.
2. Williams JT, et al. [2013] Pharmacological Reviews. 65: 223–54.
3. Bohn LM, et al. [1999] Science. 286: 2495–8.
4. Violin JD, et al. [2014] Trends Pharmacol Sci. 35: 308–16.
5. Soergel DG, et al. [2014] Pain. 155: 1829–35.

P4
GABAA Receptors and Executive Function in Fragile X Syndrome

Soujanya Gade[1], Trine Hjoernevik[2], Jun Hyung Park[1], Bin Shen[1], Jaeho Jung[3], Byung Chul Lee[4], Sang Eun Kim[4], Scott Hall[5] and Frederick T. Chin[1]

[1]*Molecular Imaging Program at Stanford, Department of Radiology, Stanford University School of Medicine, Stanford, CA, USA.*

[2]*Department of Diagnostic Physics, Oslo University Hospital, Oslo, Norway*

[3]*Bio Imaging Korea Co., Ltd, Seoul, Republic of Korea.*

[4]*Department of Nuclear Medicine, Seoul National University College of Medicine, Seoul National University Bundang Hospital, Seongnam, Republic of Korea.*

[5]*Psychiatry & Behavioral Sciences, Stanford University School of Medicine, Stanford, CA, USA.*

Introduction:

Fragile X syndrome (FXS) is an ideal condition to study cognitive disabilities due to its underlying neurological and neurogenetic functions.[1] FXS is the result of a mutation on the FMR1 gene and is the leading heritable cause of cognitive disability. Investigating biophysiological processes can lead to better prognosis in neurodevelopmental disorders. Currently, pharmacological agents and behavioral intervention are focused on symptomatic treatment. Recently, research has implicated the gamma-aminobutyric acid (GABA) system in the role of learning and memory.[2] Specifically, GABAergic dysfunction has been examined in autism and shown to play a key role in normal neuronal function.[3,4] Evidence indicates $GABA_A$ receptors are involved in the inhibitory mechanisms in the brain that give rise to the behavioral symptoms that can be observed in autism.[5] To date, there have been animal studies investigating $GABA_A$ in FXS however there been minimal development of information regarding the $GABA_A$ receptor availability in human adults with FXS. Understating the differences in neuro-mechanisms in relation to the behavioral symptomology can serve to be useful in understanding the etiology of the disorder as well as tailoring targeted treatments for patients with FXS.

Materials and Methods:

Given that males with a diagnosis of FXS are affected to a significantly greater degree than females, only males were included in this study. A total of 13 participants (age 24.6 ± 2.7 years) enrolled in the study, 8 young adult males with FXS and 5 young adult males with idiopathic intellectual delay (matched on age and IQ). A comprehensive neuropsychology battery of assessments for cognitive function (Stanford-Binet Intelligent Scales), adaptive skills (Vineland-II) and autism spectrum symptoms (ADOS-2) were completed. Clinical-grade [^{18}F]flumazenil was synthesized at on-site. Following intravenous injection of [^{18}F]flumazenil (182.8 ± 9.4 MBq/4.9 ± 0.3) participants were dynamically scanned on a hybrid PET/MR system (Signa, GE Healthcare, Waukesha, WI) for 60 mins. Simultaneously, MEGA-SPECIAL GABA-editing sequence, Diffusion Tensor Imaging (DTI), and structural MR data was acquired. PET images were reconstructed into 27 time-frames and spatially normalized to MNI space in PMOD 3.7 using the individual T1w MRI data. Time-activity curves were extracted using pre-defined volumes-of-interest (VOIs) for thalamus, caudate and pons and a reference tissue model (Ichise model; MRTM0) was used to calculate binding potentials (BP_{ND}) with pons as the reference region[6]. Pearson correlations were

computed to examine the relationship between Stanford-Binet Intelligence scores and BP_{ND} values for 13 participants.

Results:

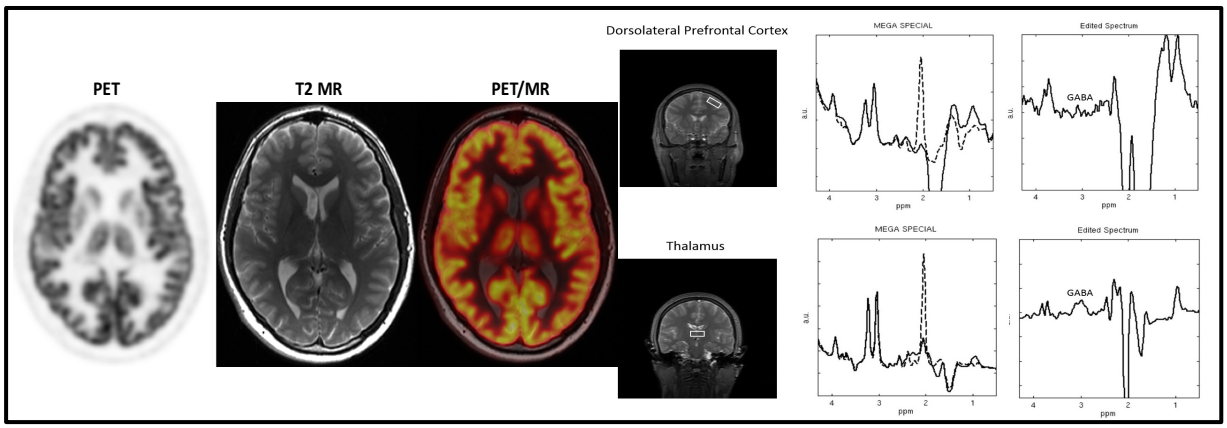

Figure 1. A) Selected transverse PET, MR, and fused PET/MR images of a participant with FXS. PET data were reconstructed with attenuation correction. **B)** MEGA-SPECIAL sequence TE= 80ms, TR=2s, 2 min water referencing

Selected axial PET, MR, and fused PET/MR brain images of one participant with FXS are shown in Figure 1A. Representative 1H-MRS data on the GABA editing are shown in Figure 1B. Results suggest a relationship between the BP_{ND} of thalamus ($r(13)=.702$, $p<0.026$) and caudate ($r(13)=.87$, $p<0.012$) and IQ scores. In general, results suggest that adults with lower $GABA_A$ receptor expression tend to demonstrate lower IQ scores than adults with higher $GABA_A$ receptor expression.

Discussion:

This study is a first of its kind to quantify neuronal information in the population of FXS. This could prove to be groundbreaking in the efforts to move toward quantifying FXS on a molecular level. Further analysis to include future participant data is underway. Concurrent analysis will include MRS, DTI and volumetric measurements.

Acknowledgements:

This research was supported in part by NICHD R01 HD084214 and the Ben & Catherine Foundation. We are also thankful to GE Healthcare, PMOD Technologies LLC, the Stanford Cyclotron and Radiochemistry facility for their kind assistance.

References:

1. Coffee, B., et. al. [2009], The American Journal of Human Genetics, 85(4):503-514
2. Mihalek, R. M., et. al. [1999], Proceedings of the National Academy of Sciences, 96(22):12905-12910
3. Chao, H.-T., et. al. [2010], Nature, 468(7321):263–269
4. Ma, D. Q., et. al. [2005], The American Journal of Human Genetics, 77(3):377–388
5. Coghlan, S., et. al. [2012], Neuroscience and Biobehavioral Reviews, 36(9):2044–2055
6. Odano I., et. al. [2009], *Neuroimage,* 45(3):891-902

P5
Development of brain penetrant P2ry12 ligands towards microglia specific PET radiotracers

Placzek MS [1,2,3], Stransky N [1,2], Dahl K [2], Vasdev, N [2,3], Butovsky O [3,4], Weiner HL [3,4], Hooker JM [1,2,3]

[1] A. A. Martinos Center for Biomedical Imaging, Charlestown, MA, USA, [2] Massachusetts General Hospital, Boston, MA, USA, [3] Harvard Medical School, Boston, MA, USA, [4] Ann Romney Center for Neurologic Diseases at Brigham and Women's Hospital, Boston, MA, USA

Introduction:

Under normal physiological conditions, microglia play an important role in maintaining homeostasis within the brain. In many neurodegenerative diseases (NDDs), microglia adopt an altered molecular phenotype and there is emerging evidence that microglia play an important role in some of the earliest pathological events, including synaptic loss [1]. Currently, there is no way to study how these distinctive molecular signatures evolve throughout disease in the living human brain. One specific receptor, P2ry12, which is only expressed on microglia in the brain, appears to signify (and be mechanistically involved in) the change of microglia from homeostasis to other 'active' phenotypic states [2]. P2ry12 expression is lost in microglia during disease progression in mouse models and human multiple sclerosis, amyotrophic lateral sclerosis and Alzheimer's disease. Towards our ultimate goal of developing microglia-specific PET radiotracers for studying microglia dysregulation in NDD, we have designed, synthesized, and characterized brain penetrant P2ry12 ligands.

Materials and Methods:

Five novel P2ry12 radiotracers were synthesized and evaluated for brain uptake *in vivo* with PET in Sprague-Dawley rats. [^{11}C]MP3-21 and [^{11}C]MP3-30 were synthesized from their corresponding aryl bromides and radiolabeled via Pd-catalyzed cyanation with [^{11}C]HCN. [^{11}C]MP4-28, [^{11}C]NS-21, and [^{11}C]NS-14 were radiolabeled by $^{11}CO_2$-fixation from their decoupled amines to form the corresponding [^{11}C]urea. Each radiotracer was purified by reverse-phase HPLC, reformulated in 10% ethanol / 90 % saline, and sterile filtered to afford an injectable solution. Male Sprague-Dawley rats were anesthetized under isoflurane with oxygen carrier and received a radiotracer bolus (i.v.), followed by a 60 minute dynamic PET brain scan and computed tomography scan on a GammaMedica Triumph PET/SPECT/CT small animal scanner. Reconstructed images were co-registered to a rat brain atlas with PMOD 3.3 and time activity curves were generated using a whole brain region of interest.

Results:

MP3-21 and MP3-30 (and corresponding bromo precursors), as well as, MP4-28, NS-21, and NS-14 (and corresponding piperazine precursors) were synthesized according to methods previously published [3,4]. [^{11}C]MP3-21 displayed low brain uptake (SUV = 1.1 at peak) and rapid washout kinetics in the rat brain (likely attributed to the acidic acyl sulfonamide linker). To test whether removing this linker would increase brain uptake, we synthesized the corresponding phenethylamide, [^{11}C]MP3-30. This compound exhibited increased brain uptake (SUV = 1.5 at peak) with slower wash out kinetics, but failed to demonstrate saturable binding when blocked with its C-12 isotopologue, indicating high nonspecific binding. [^{11}C]MP4-28 exhibited low brain uptake (SUV = 0.85 at peak), possibly due to its high molecular weight (416.9 g/mol) and lipophilicity (cLogP 4.24). [^{11}C]NS-21,

exhibited increased brain uptake (SUV = 1.5 at peak), but allyl [^{11}C]NS-14 had high brain uptake (SUV = 4.2 at peak) and good kinetics likely attributed to its favorable physicochemical properties (Mol. Wt. 366.85 g/mol, cLogP 3.3, tPSA 74).

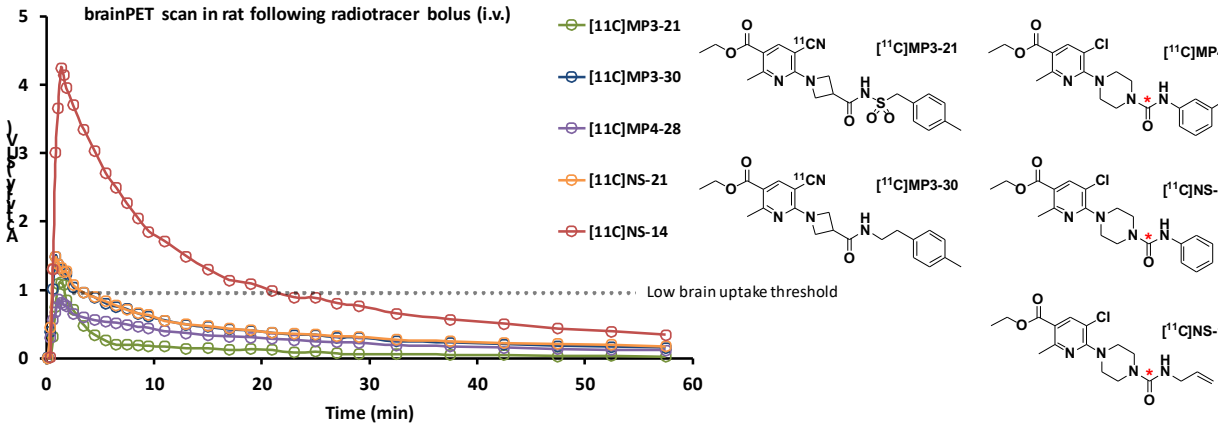

Figure 1. Chemical modifications of existing P2RY12 ligands led to higher brain uptake in rats measured *in vivo* with PET.

Discussion/Conclusion:

AstraZeneca reported a series of ethyl 6-aminonicotinates as potent antagonists at P2RY12. Several compounds in this series had potencies in the low nanomolar range and contained functional groups which could be substituted for a positron-emitting isotope (C-11). In addition, a few derivatives exhibited physicochemical properties close to typical CNS PET radiotracers, warranting experiments to test radiochemical feasibility and brain uptake. In a pilot study, we synthesized a set of compounds from two scaffolds reported by AstraZeneca, including radiolabeling precursors. MP3-21 was originally reported by AstraZeneca and displayed potent affinity at P2ry12 (IC_{50}: 6 nM). Unfortunately, this compound exhibited low brain uptake and failed to demonstrate saturable binding in rats. Replacing the acyl sulfonamide linker with phenethylamide [^{11}C]MP3-30 resulted in slightly higher brain uptake but showed a decrease in affinity at P2ry12. In parallel, we synthesized three piperazinyl ureas and evaluated brain uptake. In an effort to lower the cLogP of MP4-28, we replaced the tolyl substituent with phenyl (NS-21), then allyl (NS-14). [^{11}C]NS-14 displayed high uptake in rat brain. Unfortunately, binding results indicated a decrease in affinity compared to its tolyl and phenyl derivatives, warranting further development. We are currently designing a larger chemical library of novel ligands optimized for high binding affinity and brain uptake as P2ry12 PET radiotracers.

References:

1. Keren-Shaul H, Spinrad A, Weiner A et. al. Cell. Elsevier Inc.; 2017;169: 1276–1290.e17.

2. Butovsky O, Jedrychowski MP, Moore CS, et. al. Nat Neurosci. 2014;17: 131–143.

3. Bach P, Boström J, Brickmann K, et. al. Bioorganic Med Chem Lett. Elsevier Ltd; 2011;21: 2877–2881.

4. Bach P, Antonsson T, Bylund R, et. al. J Med Chem. 2013;56: 7015–7024.

P6
Steps toward Promoting Reproducible Research Practices in PET through Open Data and Open Code

Granville J. Matheson[1], Zsolt Cselényi[2], Christer Halldin[1], Lars Farde[2], Simon Cervenka[1]

[1]*Department of Clinical Neuroscience, Centre for Psychiatry Research, Karolinska Institutet and Stockholm Health Care Services, Stockholm County Council, Stockholm, Sweden*

[2]*Personalised Healthcare and Biomarkers, AstraZeneca PET Science Centre, Karolinska Institutet, Stockholm, Sweden*

Introduction:

Neuroimaging data are highly complex, containing information in different formats from different sources arranged in different ways. Collection, storage, analysis and sharing of data and results are therefore high idiosyncratic between or even within groups, and communication of all steps taken through scientific publications is not always feasible. This complicates replication efforts and thereby retards scientific progress. This has led to calls for computational reproducibility, or more broadly 'reproducible research' (RR), as a minimum standard for assessment of scientific claims, i.e. that researchers share analysis data and code such that all steps are recorded, allowing an independent researcher to reproduce the results and assess their veracity (1). RR practices further accelerate scientific progress, as novel methods can be readily validated, applied and extended by other researchers using the shared code. The Brain Imaging Data Structure (BIDS) has recently been introduced for MRI data (2), and has now been extended to PET, to provide a standard, machine-readable way to structure data to generalise both data storage and image processing pipelines. This structure is already supported by numerous software packages (SPM, FSL, FreeSurfer etc.), which can be implemented 'out-of-the-box' due to the standardised structure, and can further be employed with little to no installation or setup as so-called BIDS Apps (3). In this way, RR practices can improve research quality, quality assessment, as well as accelerate progress in neuroimaging. We present two ongoing projects which will assist PET researchers to embrace RR practices.

Materials and Methods:

We are assembling a large, open-access PET dataset consisting of raw image data from four previously published test-retest studies according to BIDS specifications. These studies include two measurements from each participant measured using [^{11}C]SCH23390 (n=15), [^{11}C]AZ10419369 (n=8), [^{11}C]PBR28 (n=12) and [^{11}C](R)-PK11195 (n=6). The latter two studies will also include all blood data. We also present *kinfitr*, a software package for performing kinetic modelling using the open-source R language. The R community has a strong culture of RR, and the language consists of numerous tools which allow both effective and easy sharing and communication of analysis code. Further, the package is written in such a way as to allow analytical flexibility during modelling, with 14 different kinetic models currently implemented using a consistent syntax, as well as to allow for this flexibility to be effectively and transparently communicated. The package makes use of tidyverse principles (4), which have been designed to optimise readability for non-experts, as well as ease of learning for beginners. The R language also contains powerful tools for statistical analysis and data visualisation, such that results of kinetic analysis do not need to be exported before analysis. We have previously shared full analysis notebooks which can be easily modified for new analyses.

Results:

The dataset of raw 4D PET data according to BIDS specification will be uploaded in full to OpenfMRI website, from which it can be freely downloaded and used without requiring explicit permission. The *kinfitr* package is available on GitHub (5) with installation instructions as well as time activity curve data and example analyses to demonstrate its use.

Discussion/Conclusion:

PET is a resource-intensive methodology, requiring extensive expertise both for measurement and analysis. Sharing data alone has the potential for considerable financial savings, and sharing of analysis code and software will improve the quality of research and accelerate the application and development of new methods. We hope that this dataset specifically will accelerate the development of new software which can automatically read and digest data in BIDS. Further, by sharing test-retest data specifically, this will allow for new methods and tools to be tested and evaluated using this dataset. Finally, by providing open-source tools for kinetic modelling, including documentation and examples, we hope to extend access to methodology for research groups lacking software engineering expertise, as well as simplify transparent and reproducible reporting. We hope that our sharing this data and software will help the PET community to develop new analytical methods, write and share reproducible analysis code for kinetic and statistical modelling, but also encourage others to start sharing their own data and code.

Acknowledgements:

We thank the staff of the PET group at Karolinska Institutet for their assistance.

References

1. Sandve, GK, Nekrutenko A, Taylor J et al., (2013) PloS Comput Biol 9(10)
2. Gorgolewski KJ, Auer T, Calhoun VD et al., (2016) Scientific Data 3
3. Gorgolewski KJ, Alfaro-Almagro F, Auer T. et al., (2017) PLoS Comput Biol 13(3)
4. Wickham, H. (2017) The tidyverse style guide
5. *https://github.com/mathesong/kinfitr*

P7
Reducing the duration and amount of task blocks in [^{18}F]FDG functional PET

Andreas Hahn[1], Lucas Rischka[1], Gregor Gryglewski[1], Sarah Pfaff[2], Thomas Vanicek[1], Marius Hienert[1], Manfred Klöbl[1], Markus Hartenbach[2], Markus Mitterhauser[2,3], Wolfgang Wadsak[2,4], Marcus Hacker[2], Siegfried Kasper[1], Rupert Lanzenberger[1]

[1]*Department of Psychiatry and Psychotherapy, Medical University of Vienna, Austria*
[2]*Department of Biomedical Imaging and Image-guided Therapy, Division of Nuclear Medicine, Medical University of Vienna, Austria*
[3]*Ludwig Bolzmann Institute Applied Diagnostics, Vienna, Austria*
[4]*Center for Biomarker Research in Medicine (CBmed), Graz, Austria*

Introduction:

Constant infusion protocols for [^{18}F]FDG enable the assessment of task-specific changes in the cerebral metabolic rate of glucose (CMRGlu) in a single PET measurement [1,2]. Previous studies mostly used blocks of 10min duration for detection of task-related changes. This implies long scan durations, which include disadvantages of increased movement and habituation effects, directly influencing estimates of task CMRGlu. We evaluated the possibility to reduce the duration and the amount of task blocks in fPET imaging.

Materials and Methods:

Twenty healthy subjects (26.3±4.1 years, 9 female) underwent one PET/MR scan (Siemens mMR) with bolus plus constant infusion of [^{18}F]FDG (4.5-5.6MBq/kg). The paradigm included right finger tapping during the presentation of landscape movies in 4 blocks. Block durations were kept constant within a scan but varied across subjects (10, 5, 2 and 1min with n=5 per duration).

PET images were reconstructed with frame durations of 60, 30, 12 and 6s, respectively. Attenuation correction was carried out with a database approach using the individual structural T1-weighted image [3]. Image preprocessing included motion correction, spatial normalization and smoothing with SPM12.

Task-specific glucose metabolism was quantified with arterial blood samples as described previously [2]. A general linear model (GLM) was used to separate task effects from baseline metabolism, while correcting for movement artifacts. The different number of task blocks was evaluated by including all 4 or only 3, 2 and 1 blocks in the GLM. The Patlak plot was used to compute task-specific CMRGlu.

Overall task-specific changes in CMRGlu for the full paradigm (i.e., all 4 task blocks) were assessed by ANOVA across all subjects with a factor to adjust for the different task durations. Post-hoc t-tests were used to evaluate the different task durations. Reducing the amount of task blocks was assessed by absolute percent signal change as compared to the full paradigm (i.e., 3, 2 and 1 vs 4 blocks). Furthermore, the individual t-values of the GLM analysis were used as a measure of the ability to robustly detect task-specific effects.

Results:

For the full paradigm, task-specific changes in CMRGlu were observed in the primary visual (V1, Fig.1A) and motor cortices (M1, $p<0.05$ FWE corrected). All different block durations showed significant task effects in both regions, except for 1min in V1. This was also reflected in the model fits of the task-specific time activity curves (Fig.1B) and the individual t-values obtained from the GLM (black boxplots in Fig.1D).

Reducing the amount of task blocks showed increasing variability in CMRGlu as compared to all 4 blocks in V1. Here, absolute values of signal changes were beyond 10% for all task durations, except when using 3 (5.7±4.7%) or 2 blocks (8.0±5.5%) for task duration of 5min (Fig.1C). GLM t-values markedly decreased when reducing the amount of blocks for 2 and 1 min task durations (Fig.1D). Interestingly, even a task duration of 10min exhibited generally lower CMRGlu as well as increased variance and lower t-values when reducing the amount of task blocks.

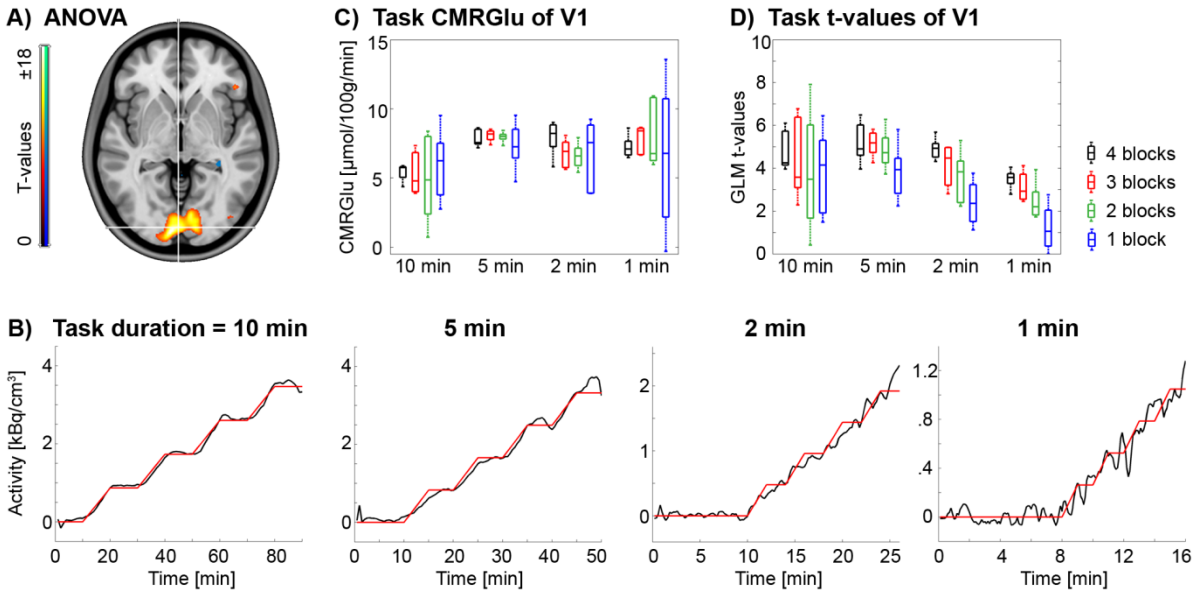

***Figure 1**: Task-specific effects in V1. A) CMRGlu changes for the full paradigm and across all subjects. B) Average time activity curves (black) and GLM (red) with n=5 for each task duration. C) CMRGlu and D) t-values for different durations and amount of task blocks.*

Discussion:

Reducing the task block duration to 5min seems to be the best tradeoff between measurement time and robust identification of task-specific changes. The amount of task blocks could be further reduced from 4 to 2 with minor differences in CMRGlu and task identification.

The design with 2min task duration and 4 blocks appears promising for direct comparison with fMRI, but further adaptations to increase identifiability are required.

In contrast, a task duration of 10min does not seem favorable due to the long scan time and the variation across task blocks. Protocols with 1min task duration do not yet yield a robust signal for quantification of task-specific CMRGlu.

Acknowledgements:

This research was supported by a grant from the Austrian Science Fund to A.Hahn (FWF KLI 610). L.Rischka, G.Gryglewski and M.Klöbl are recipients of DOC Fellowships of the Austrian Academy of Sciences at the Department of Psychiatry and Psychotherapy, Medical University of Vienna.

References:

1. Villien et al. [2014] NeuroImage 100:192-199.

2. Hahn et al. [2016] J.Nucl.Med 57:1933-1940.

1. Burgos et al. [2014] IEEE.Trans.Med.Imaging 33:232-2341.

P8
Assessment of a statistical arterial input function extraction technique from [^{18}F]fluortriopride PET images

Robert Doot, Jacob Dubroff[1], Chris Ward[2], Kyle Labban[1], Jenny Cai[1], Shihong Li[1], Hsiaoju Lee[1], Erin Schubert[1], Robert Mach[1], and Finbarr O'Sullivan[3]

[1]*Dept. of Radiology, Perelman School of Medicine, University of Pennsylvania, Philadelphia, PA USA*

[2]*Dept. of Anesthesiology and Critical Care Medicine, Children's Hospital of Philadelphia, PA USA*

[3]*School of Mathematical Sciences, University College Cork, Ireland*

Introduction:

Dopamine D3 receptors are thought to represent principal neural substrates in the dopaminergic mesolimbic circuit, the primary reward pathway in the mammalian brain. D3 receptor dysfunction has been implicated in many diseases including drug addiction, Parkinson's disease, and schizophrenia. In anesthetized non-human primates, [^{18}F]fluortriopride ([^{18}F]FTP) binding was sensitive to levels of endogenous dopamine [1] but reflected the distribution of D3 receptors as determined by autoradiography [2]. The purpose of this study was to assess whether using a statistical image-extraction technique [3] to inform fitting of an arterial input function from both [^{18}F]FTP PET images and 4 measures from blood samples would improve 2-compartmental kinetic analyses of [^{18}F]FTP uptake in the D3 receptor-rich thalami.

Materials & Methods:

Participants provided informed consent for the studies according to guidelines of University of Pennsylvania Institutional Review Board. Following the bolus intravenous administration of 6.87 ± 0.22 mCi of [^{18}F]FTP, 10 healthy adults, 6 males (31.8 ± 9.8 years) and 4 females (26.3 ± 6.2 years) underwent 120 minutes of dynamic PET brain imaging on a Philips Ingenuity TF PET/CT instrument. Each participant also underwent MRI T1 imaging with isotropic voxels for co-registration. Integrated Data Analysis Environment [4] software was used to perform the segmentation of MRI images, co-registration of PET images, and generation of regional brain time activity curves (TACs). The [^{18}F]FTP uptake in thalami was selected as a representative region due to their relatively high concentration of D3 receptors and large compact volumes relative to other D3-rich regions, which minimize partial volume effects. The original bloodAIF method used Pmod's (Pmod v3.7) 3-exponential model to fit blood activity concentrations from 20 arterial blood samples and Pmod's sigmoidal fit parent fraction measurements from 7 arterial blood samples. The imageAIF method used in-house statistical recovery software to extract the arterial input curve (AIF) and parent radioligand fraction function from dynamic PET images of the entire head with results scaled based on the activity concentrations of [^{18}F]FTP in arterial blood sampled at 5, 30, 60, and 120 minutes after radiotracer injection [3]. Thalami TACs were combined with either bloodAIF or imageAIF AIFs and corresponding parent fraction functions as input for kinetic image analyses of [^{18}F]FTP uptake via a 2-compartment model [5]. The difference between chi-squared values for fits by the two methods of thalami [^{18}F]FTP uptake was examined using a 2-tailed, paired Student t-test. P-values less than 0.05 were considered significant.

Results:

The original method for estimating the AIF (bloodAIF) had an average chi-squared value of 0.855 ± 0.742 (±SD) while the method for image-extracted AIF (imageAIF) had an average chi-squared value of 0.590 ± 0.528 for fits of [^{18}F]FTP uptake in human brain thalami. A paired t-test of the bloodAIF and imageAIF chi-squared values found a significant difference between the methods (p=0.035). The average individual improvement in chi-squared values was 26.1% ± 27.8%. The Bland-Altman plot in Figure 1 compares chi-squared values for the two methods.

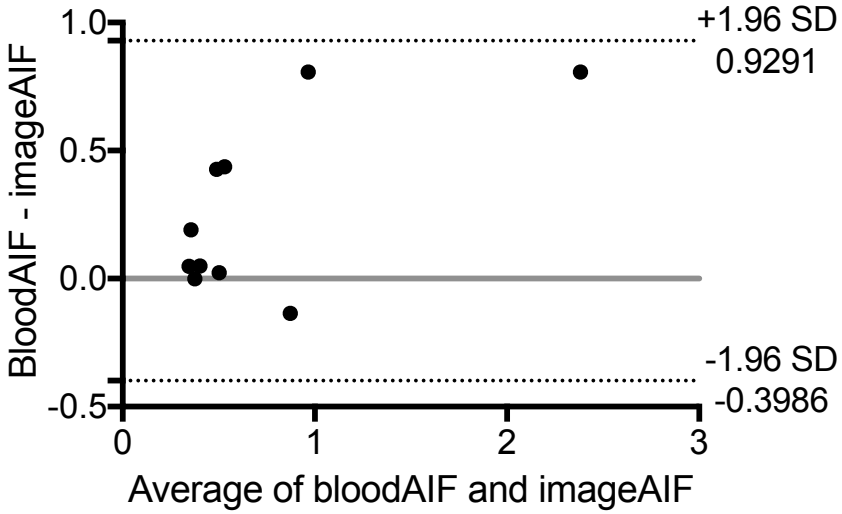

Fig 1. Bland-Altman plot of chi-squared values of fits of [^{18}F]FTP uptake in human thalami (n=10)

Conclusion:

The Bland-Altman plot and formal paired analysis found a significant difference (p=0.035) between the chi-squared values for fits of [^{18}F]FTP uptake in the thalami using the two methods. On average, we find a 26.1% ± 27.8% improvement in fit when using the statistical arterial input function extraction from PET images technique.

Acknowledgements:

Authors appreciate research support provided by K01DA040023-01A1 (RD), K23DA038726 (JD), R01DA029840-06A1 (RM), UPenn McCabe Pilot Award (JD), UPenn Center for Magnetic Imaging and Spectroscopy (JD). The authors thank Dean Wong and Hiroto Kuwabara for sharing their IDAE analysis software, as well as Catherine Hou, Regan Sheffer, Kuiying Xu, and Alex Schmitz for their assistance in conducting these studies.

References:

[1] Mach R et al. [2011] Synapse 65: 724-32
[2] Sun J et al. [2012] PLoS One 7: e49483
[3] O'Sullivan F et al. [2018] J Med Imaging 5: 011010
[4] Kuwabara H et al. [2014] NRM Abstract Book p133
[5] Innis R et al. [2007] J.Cereb.Blood.Flow.Metab 27: 1533-9

P9
Targeting brain HDAC6 using [^{18}F]Bavarostat

Johanna Rokka[1], Martin G. Strebl[1], Frederick A. Schroeder[1], Jacob M. Hooker[1]

[1]*Athinoula A. Martinos Center for Biomedical Imaging, Department of Radiology, Massachusetts General Hospital, Charlestown, Massachusetts 02129, United States*

Introduction:

[^{18}F]Bavarostat is the first positron emission tomography (PET) tracer that selectively binds histone deacetylase 6 (HDAC6) [1]. Abnormal expression of HDAC6 has been shown to be related to several neurological diseases such as Rett syndrome, Alzheimer's disease and Charcot-Marie-Tooth disease as well as various types of cancer [1,2]. In this ongoing study [^{18}F]Bavarostat is evaluated in mouse and baboon in order to better understand the properties of the imaging tool before exploring HDAC distribution and density in models of disease. A key aim is to evaluate the uptake and binding properties in brain and major peripheral organs in rodents and non-human primates, expanding on recently published results [1]. Our translational work strongly supports that [^{18}F]Bavarostat is a suitable tracer for HDAC6 brain PET-imaging.

Materials & Methods:

Baseline uptake of [^{18}F]Bavarostat was compared with homologous and heterologous blocking studies and [^{18}F]Bavarostat metabolite profiles were evaluated in plasma, brain and liver. Whole body distribution of [^{18}F]Bavarostat was evaluated in two scans of an anesthetized, female baboon. Scans were completed with and without pretreatment of non-radioactive Bavarostat (1 mg/kg, dosed 5 min before tracer injection). Imaging sessions each lasted 2 hours starting with a 90-minute dynamic PET scan of the thorax and upper abdominal area and following by three 10-minute static scans of the head and neck area, thorax and upper abdominal, and lower body area. Anatomical magnetic resonance images were acquired simultaneously. During each scan, blood samples were collected and the plasma metabolite profile of [^{18}F]Bavarostat was analyzed. Baboon brain metabolites were studied *in vitro* by incubating [^{18}F]Bavarostat in baboon brain homogenate at 37 °C.

In mice, [^{18}F]Bavarostat whole body distribution was studied *in vivo* and *ex vivo*. The metabolite profile of [^{18}F]Bavarostat of mouse brain and liver was analyzed using *ex vivo* tissue samples. Healthy C57BL/6J male mice were pretreated with a single dose of non-radioactive Bavarostat (0.01 – 2 mg/kg i.p.) 1.5 or 4 hours prior to [^{18}F]Bavarostat injection. The distribution of radioactivity was studied in anesthetized animals with a PET scan lasting 30 minutes. Mice were then euthanized and tracer uptake in brain was immediately measured by *ex vivo* autoradiography of cryostat-sectioned tissue. Healthy C57BL/6J female mice were treated with three doses of non-radioactive Bavarostat (2 mg/kg i.p.) or ACY-775 (5 mg/kg i.p.) at 23 hours, 3 hours, and 30 min prior [^{18}F]Bavarostat injection. Brain radioactivity distribution was studied using *ex vivo* autoradiography 1 hour after injection of [^{18}F]Bavarostat. Animal studies were approved by the IACUC at the Massachusetts General Hospital.

Results:

[^{18}F]Bavarostat has high brain uptake in baboon and mouse. In baboon, evidence of blocked binding was seen in brain as well as in heart and pancreas. Metabolite analyses of baboon plasma samples and mouse brain and liver samples indicate that [^{18}F]Bavarostat has only

one highly hydrophilic radioactive metabolite. The amount of intact [^{18}F]Bavarostat in baboon plasma samples was 40% 2 hours after [^{18}F]Bavarostat injection. In baboon brain homogenate ~90% of radioactivity was intact [^{18}F]Bavarostat after 2 hours of incubation. *Ex vivo* tissue metabolite analysis showed that in mouse brain > 95% of radioactivity was intact [^{18}F]Bavarostat whereas in liver, only ~30% remained present 30 minutes after [^{18}F]Bavarostat injection. In separate assays measuring liver microsome and hepatocyte stability, non-radiolabled Bavarostat was efficiently metabolized in samples from rat and mouse, with marginally better stability in human.

Dose-dependent homologous blocked binding of [^{18}F]Bavarostat was seen in mouse brain *in vivo* and *ex vivo* and was observed 1.5 and 4 hours after blocking dose administration. Multi-dosing treatment using non-radioactive Bavarostat or ACY-775 effectively blocked [^{18}F]Bavarostat binding in the mouse brain.

Discussion/Conclusion:

[^{18}F]Bavarostat has robust uptake in brain with evidence of specific binding (via blocked binding). Only a small amount of the radioactive metabolite of [^{18}F]Bavarostat is seen in experimental animal brain *in vitro* and *ex vivo*, indicating that metabolites do not contribute significantly to the signal of [^{18}F]Bavarostat in brain imaging studies.

We are in the process of further evaluating the brain binding kinetics of [^{18}F]Bavarostat in baboon and mouse and studying the role of HDAC6 in biological processes related to neurological diseases using several HDAC6 inhibitors as heterologous blocking agents and [^{18}F]Bavarostat as an imaging tool.

In conclusion, these results confirm [1] that [^{18}F]Bavarostat is a useful and specific tracer for HDAC6 PET imaging, particularly for neuroimaging studies.

Acknowledgements:

Project funding to J. Rokka, Sigrid Jusélius fellowship and to J. Hooker, NINDS grant #1R01NS099250-01A1.

References:

1. Strebl M, Campbel AJ, Zhao W-N et al. [2017] ACS Cent Sci. 3:1006-1014, [2] Ganai S [2017] Curr. Med. Chem. 24:1-17

P10

Abstract withdrawn

P11
In vivo measurement of brain exposure and distribution of [^{11}C]osimertinib in human subjects using positron emission tomography (PET)

Andrea Varrone,[1] Katarina Varnäs,[1] Aurelija Jucaite,[1, 2] Zsolt Cselényi,[1, 2] Peter Johnström,[1, 2] Magnus Schou, [1, 2] Ana Vazquez-Romero,[1] Mohammad Mahdi Moein,[1] Christer Halldin,[1] Andrew P Brown,[3] Karthick Vishwanathan,[4] Lars Farde[1, 2]

[1]Department of Clinical Neuroscience, Centre for Psychiatry Research, Karolinska Institutet and Stockholm County Council, Stockholm, Sweden; [2]PET Science Centre, Precision Medicine and Genomics, IMED Biotech Unit, AstraZeneca, Karolinska Institutet, Sweden; [3] Global Medicines Development Oncology, AstraZeneca, UK; [4]Quantitative Clinical Pharmacology, Early Clinical Development, IMED Biotech Unit, AstraZeneca, USA

Introduction:
PET measurements are routinely used to diagnose diseases, assess treatment responses and furthermore, to understand the distribution of labeled compounds in the regions of interest. Typically, this approach has been used in neuroscience to understand receptor binding and activation. The utility of this approach in neuro-oncology to diagnose brain tumors is well known and currently, the understanding of compound distribution in the tumor regions is growing. Osimertinib is a potent tyrosine kinase inhibitor of the mutated epidermal growth factor receptor (EGFR), used for treatment of patients with locally advanced and metastatic non-small cell lung cancer (NSCLC). In clinical trials, the efficacy of osimertinib was similar in patients with or without brain metastases.

Aim:
The aim of this PET study was to measure brain exposure of [^{11}C]osimertinib administered intravenously in healthy volunteers with an intact blood-brain barrier.

Methods:
[^{11}C]Osimertinib was produced at high radiochemical purity >99% and at high molar radioactivity (141±23 GBq/µmol). Eight male healthy volunteers (age 52±8 years) underwent one PET measurement with [^{11}C]osimertinib (radioactivity: 347±51 MBq, injected mass: 1.26±0.12 µg) using the HRRT system. Arterial blood sampling was performed to obtain a metabolite-corrected plasma input function for the quantitative analysis of [^{11}C]osimertinib. The fraction of unchanged drug was measured using high-performance liquid chromatography (HPLC). Region-of-interest analysis was done using the Automated Anatomical Labeling template. Quantification of [^{11}C]osimertinib brain exposure was performed using two-tissue (2T) and one-tissue (1T) compartment models (CM). The outcome measure was the total distribution volume (V_T). The pharmacokinetic parameters $C_{max\ (brain)}$, $T_{max\ (brain)}$ and $AUC_{0\text{-}90\ min\ brain/blood\ ratio}$ were calculated.

Results:
[^{11}C]Osimertinib was rapidly distributed to the brain, with mean T_{max} of 13 min (range 5-30 min), time at which 2.2±0.2% of injected radioactivity was in brain. The C_{max} was 1.4±0.3 SUV (range 1-1.8), $AUC_{0\text{-}90\ min\ brain/blood\ ratio}$ was 3.8±0.3 (range 3.3-4.1). [^{11}C]Osimertinib brain uptake was highest in putamen followed by thalamus, frontal cortex, temporal cortex, caudate, cerebellum and white matter (Figure 1). The HPLC analysis was performed up to 30 min due to very low radioactivity concentration in the plasma samples. The fraction of the parent in plasma at 30 min was 73±8%. The input function was generated with a population

based approach using Hills-Richard mixed model. 2TCM was better than 1TCM in all regions except the white matter. Mean V_T of the whole brain was 14 mL*cm^{-3} (range 11-18). V_T was highest for the putamen (17 mL*cm^{-3}, range 13-24) and lowest for the cerebellum (13 mL*cm^{-3}, range 10-16). Mean V_T of the white matter was 7 mL*cm^{-3}, range 5-12.

Conclusions:

This study demonstrates the utility of PET analysis to understand the regional distribution of compounds in brain and provides evidence that [^{11}C]osimertinib penetrates the intact blood-brain barrier in healthy volunteers. This PET approach is a simple way to assess brain exposure of compounds of interest.

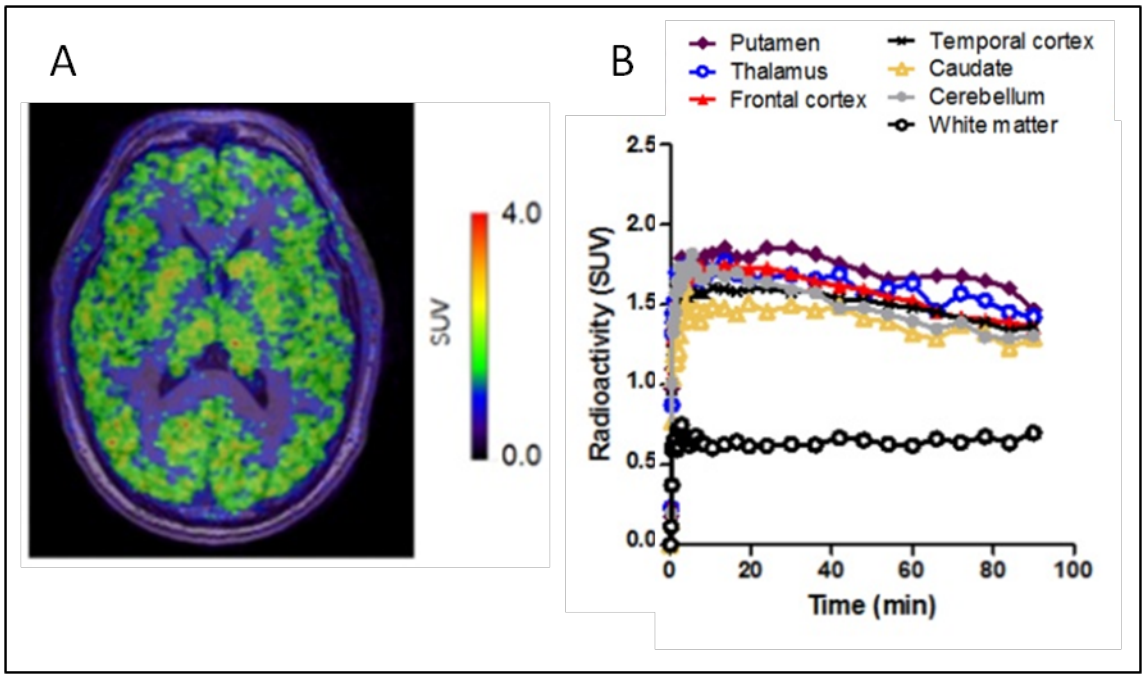

Figure 1. A) A representative PET image of [^{11}C]osimertinib overlaid on MRI is displayed with B) corresponding time activity curves of [^{11}C]osimertinib in different brain regions.

P12
Improved measurement of serotonin 1A receptor density with a novel image reconstruction technique: phantom and human studies

Nandita Joshi[1], Arthur Mikhno[2], Elsa Angelini[3], Mark Slifstein[1], Chuan Huang[1], Paul Vaska[1], Steve Weise[4], Georges El Fakhri[4], Ramin V. Parsey[1], Christine DeLorenzo[1]

[1]Stony Brook University, Stony Brook, NY, USA [2]Independent Researcher, Princeton, NJ, USA [3]Imperial College London, UK [4]Gordon Center for Medical Imaging, Boston, MA, USA

Introduction:

Major Depressive Disorder (MDD) is a chronic recurrent illness and second leading cause of global disease[1]. Measuring serotonin 1A receptor density within the raphe, the principal site of the serotonergic system is challenging, given its size[2]. However, accurate quantification of the activity within the raphe may be an objective biomarker for MDD. With image reconstruction techniques such as Filtered Back Projection (FBP), Maximum Likelihood Expectation Maximization (MLEM), and point-spread-function (PSF) model within MLEM (PSF-MLEM), the raphe nuclei are difficult to identify due to noise corruption, over-enhancement, and convergence issues[3]. This study assesses the qualitative and quantitative performance of a novel reconstruction technique, Gradual PSF MLEM (GPSF-MLEM)[4], in order to improve PET-based biomarker performance for identifying MDD versus controls.

Materials & Methods:

GPSF-MLEM was initialized with 20 iterations of MLEM, and 380 iterations with a PSF of gradually decreasing isotropic full-width-half-maximum (FWHM)-10mm to 4.5mm.

Phantom: A Hoffman brain phantom was injected with [^{18}F]FDG. ECAT HR+ scans were reconstructed with FBP, MLEM, PSF-MLEM, and GPSF-MLEM and co-registered to the 3D Hoffman Digital Reference Object (DRO)[5]. A small region of interest (ROI), similar in volume to the raphe, was drawn on the DRO. Qualitative and quantitative assessment using hot contrast recovery (CR) and background standard deviation (BSD) measures[6] were performed with all four techniques.

Human: [^{11}C]WAY-100635 imaging data were obtained for 35 male subjects(20 controls,15 MDD)[7]. FBP and GPSF-MLEM reconstructed images were motion-corrected and MRI coregistered using a PET-derived raphe atlas[8]. Time-activity curves were extracted and BP_F quantified using a 2-tissue compartment constrained (2TCC) model (cerebellar white matter reference: one-tissue compartment fit) and a metabolite corrected arterial input function. One control subject deemed an outlier due to a reconstruction issue was excluded. Classification performance was assessed with both FBP and GPSF-MLEM.

Results:

Phantom: In Fig. 1, quantitatively, the peak CR obtained with GPSF-MLEM was 67% and 4% higher as compared to MLEM and PSF-MLEM, respectively. GPSF-MLEM yielded the highest value of maximum CR at the lowest BSD across reconstruction techniques. Qualitatively, the FBP image displays typical radial streak artifacts, and hot activity regions are not clearly discernible. At the respective maximum CR values, the MLEM image is largely corrupted by noise, the PSF-MLEM image is dominated by noise and hot-spots. The GPSF-MLEM image appears more uniform, with clearly defined cortical structures, and reduced noise/hot-spots.

Human: In Fig. 2, receiver operating characteristic (ROC) area under the curve for diagnostic classification of controls versus MDD was 0.92 with FBP and 0.98 with GPSF-MLEM reconstructions. The sensitivity(%)|specificity(%)|accuracy(%) at balanced and high-specificity BP_F cutoffs were: 87|79|82 and 53|100|79 with FBP, and 93|89|91 and 87|100|94 with GPSF-MLEM reconstructions.

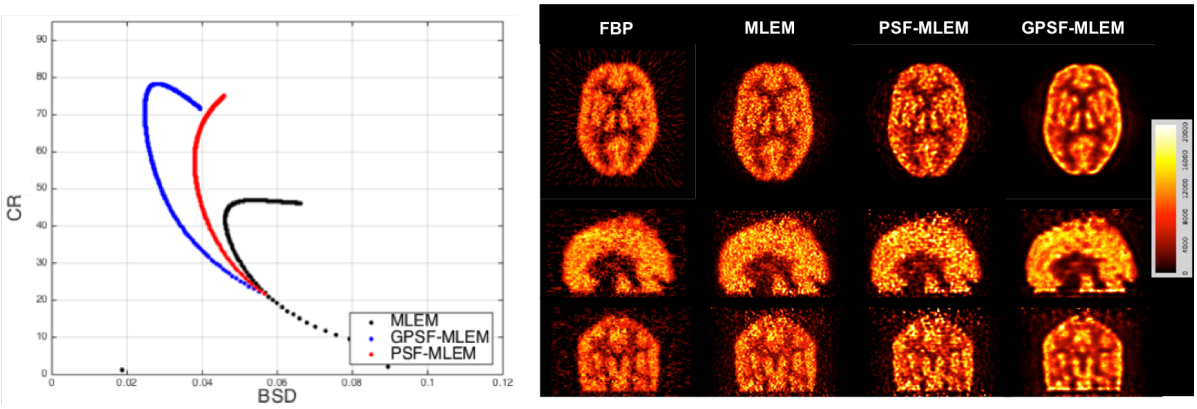

Fig. 1: (Left) Contrast recovery (CR) versus background standard deviation (BSD) for the three iterative reconstruction methods. (Right) Visual comparison of PET images at maximum CR in axial, sagittal, and coronal views, reconstructed with FBP, MLEM, PSF-MLEM, and GPSF-MLEM.

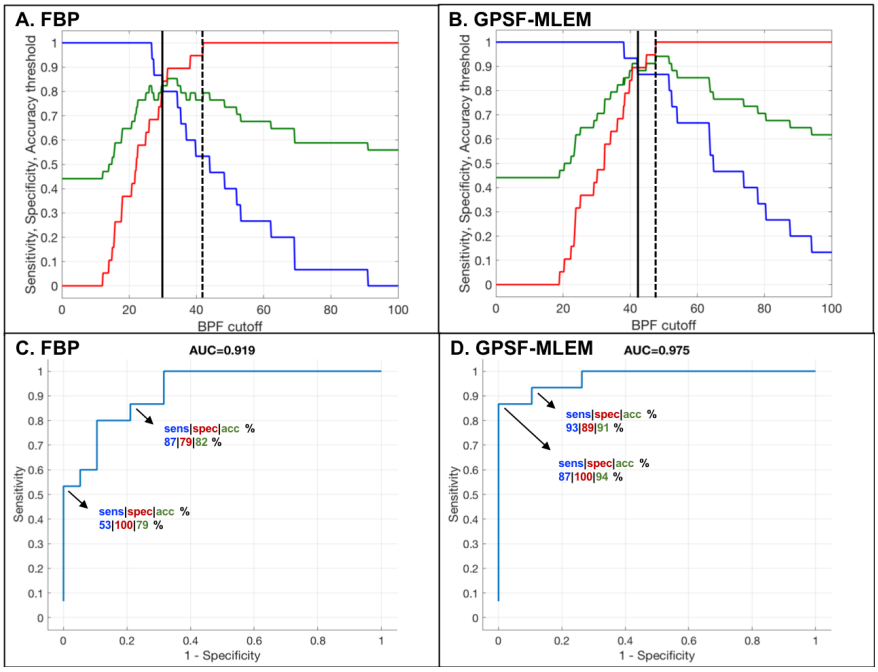

Fig. 2: MDD versus controls classification using raphe BP_F. (A,B) Sensitivity (blue), specificity (red), and accuracy (green) characteristics for FBP and GPSF-MLEM reconstruction methods. Black dotted and solid lines denote sensitivity and accuracy at a high-specificity (100) and balanced BP_F cutoffs, respectively. (C,D) ROC curves for FBP, GPSF-MLEM. The marked points denote high-specificity and balanced BP_F cutoffs as shown by the vertical lines in (A,B).

Conclusion:

GPSF-MLEM PET image reconstruction may provide better resolution recovery as compared to MLEM and PSF-MLEM in smaller structures, both qualitatively and quantitatively; potentially improving quantification of clinical PET scans. Measuring raphe signal from GPSF-MLEM reconstructed PET images improved identification of MDD versus controls in male subjects as compared to FBP, aiding the development of a biomarker for MDD that could improve diagnosis and treatment. Further validation of GPSF-MLEM on additional scanners and tracers is the subject of future work.

Acknowledgements: This work was partially supported by NIMH grants MH40695, MH62185, R01 MH074813-01 and grants through The Stanley Medical Research Institute and American Foundation for Suicide Prevention.

References: 1. Collaborators GBoDS. [2015], Lancet, 386(9995):743-800.
2. Kranz GS, Hahn A, Savli M et al. [2012], Proc. Natl. Acad. Sci. U.S.A., 109(29):E2000.
3. Rahmim A, Qi J and Sossi V. [2013], Med. Phys., 40(6):064301.
4. Mikhno A. [2014], Columbia University, PhD Thesis
5. Harrison RL, Elston BF, Byrd DW et al. [2013], Proc. IEEE NSS/MIC
6. Rapisarda E, Bettinardi V, Thielemans K et al. [2010], Phys. Med. Biol., 55:4131-4151.
7. Kaufman J, Sullivan GM, Yang J et al. [2015], Neuropsychopharmacology, 40:1692-1699.
8. DeLorenzo C, Delaparte L, Thapa-Chhetry B et al. [2013], Fron. Psych., 4(5).

P13
Validation of V_{ND} estimates derived from Inhibition, Saturation and Occupancy plots of [^{11}C]raclopride binding in healthy human brain

Jenny-Ann Phan[1,2], Dean F. Wong[3,4], Albert Gjedde[5,6]

[1]*Department of Biomedicine, Aarhus University, Aarhus, Denmark,*

[2]*Department of Nuclear Medicine and PET Centre, Aarhus University Hospital, Aarhus, Denmark,*

[3]*Department of Radiology and Radiological Sciences, Division of Nuclear Medicine, and*

[4]*Department of Psychiatry , Neurosciences and Neurology, Johns Hopkins Medical Institutions, Baltimore, USA*

[5] *Department of Clinical Research, University of Southern Denmark, Odense, Denmark*

[6]*Department of Nuclear Medicine, Odense University Hospital, Odense, Denmark*

Introduction:

Radioligands with a wide distribution in the brain have been applied more frequently in recent years, leading to more complicated analysis due to the lack of a real reference region. For instance, the radioligand [^{18}F]ASEM of α7-nicotinic acetylcholine receptors, [^{11}C]PBR28 for the translocator protein and [^{11}C]yohimbine of α_2 adrenoceptors are a few examples of radioligands lacking such an apparent reference region. In this case, a mathematical reference distribution volume, V_{ND}, is estimated by means of a linear regression of receptor occupancy at two different levels. Three linear models have been derived yielding the V_{ND}, including the Inhibition, Saturation (Lassen), and Occupancy plots that we collectively call the ISO Plots. The accuracy of the V_{ND} value is important, because this value influences the calculation of the binding potential. Therefore, the aim of this study is to test the accuracy of the V_{ND} estimated from the respective ISO plots, using [^{11}C]raclopride data in healthy humans, where a real reference volume is assumed to exist in the cerebellum.

Materials and Methods:

We included [^{11}C]raclopride acquisitions with plasma input from healthy human subjects (n=19) at baseline and at challenge with non-radiolabeled raclopride in this study. The volumes of distribution, V_T , were obtained by the Logan plot with a plasma input function. The time frames of V_T estimation automatically were identified as those with the greatest R^2 values of iterative linearization (Phan et al. 2017)(1). The V_{ND} values were estimated by ISO plots, the derivation of which started from the receptor availability,

$$1 - s = \frac{BP_{ND(i)}}{BP_{ND(b)}}, \qquad (1)$$

indicating that the available fraction of receptors (1-*s*) in presence of a competitor equals the ratio of the binding potential at inhibition condition ($BP_{ND(i)}$) with pharmacological challenge relative to baseline condition ($BP_{ND(b)}$) in absence of the competitor. The binding potentials can be expressed in terms of the partition volumes,

$$BP_{ND(i)} = \frac{V_{T(i)} - V_{ND(i)}}{V_{ND(i)}} \quad \text{and} \quad BP_{ND(b)} = \frac{V_{T(b)} - V_{ND(b)}}{V_{ND(b)}} \qquad (2)$$

Then, the relative receptor availability is obtained by combination of eqs. 1 and 2,

$$1 - s = \frac{V_{T(i)} - V_{ND}}{V_{T(b)} - V_{ND}}, \quad (3)$$

which is the common equation that the respective ISO Plot are derived from the Inhibition Plot(2), derived from isolation of the volume of distribution at inhibition condition $V_{T(i)}$,

$$V_{T(i)} = (1 - s)\, V_{T(b)} + s\, V_{ND}, \quad (4)$$

where the distribution volumes at baseline and inhibition condition are plotted against each other and

the V_{ND} is solved from the intercept of the plot and the line of identity. The Saturation plot (also known as the Lassen plot(3)) is derived by isolation the $дV_T$, which is the difference between the volumes of distribution at baseline and inhibition condition, from eq. 3,

$$\Delta V_T = s\, V_{T(b)} - s\, V_{ND} \quad (5)$$

where V_{ND} is solved from the y-intercept. Finally, the Occupancy plot(4) is obtained by isolation of the volume of distribution at baseline from eq. 5,

$$V_{T(b)} = \frac{1}{s} \Delta V_T + V_{ND} \quad (6)$$

where V_{ND} is solved from the x-intercept.

Results:

Figure 1

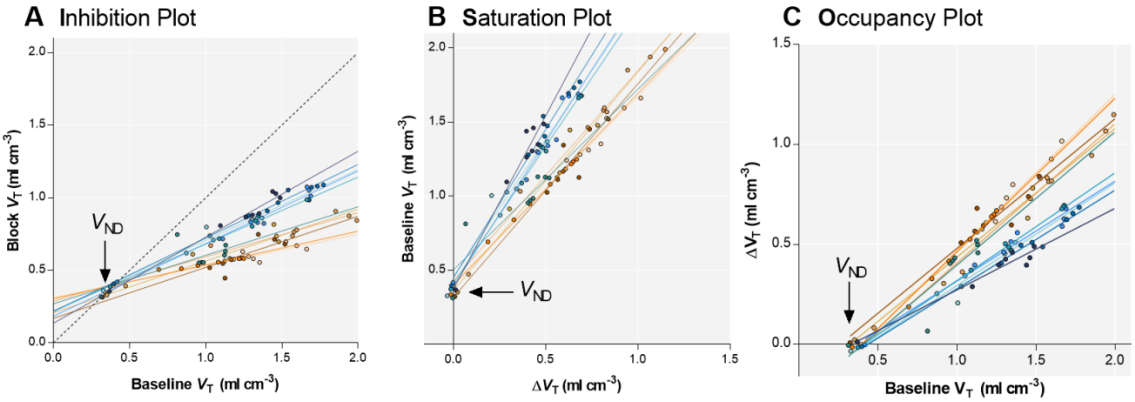

Figure 1A-C show the individual ISO Plots of subjects in the age range 18-30, and the arrows indicate the V_{ND} estimates.

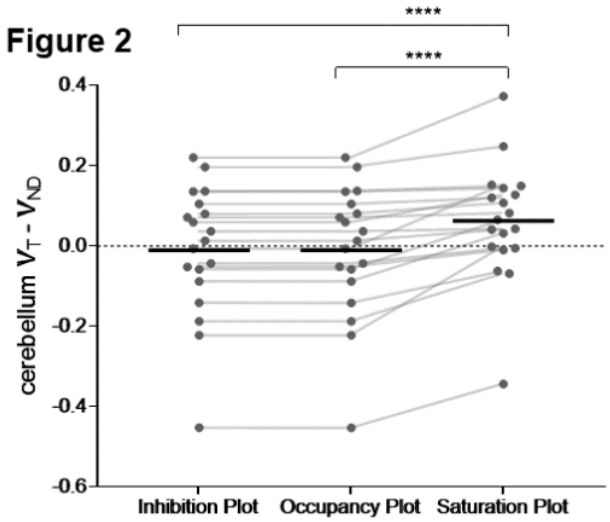

Figure 2 illustrates the difference between the V_{ND} estimates and the real reference volume, V_T in cerebellum, demonstrating V_{ND} estimates from the Inhibition and Occupancy plots are identical, and the error is distributed equally on both sides of zero. In contrast, the Saturation plot displayed a tendency to overestimate V_{ND}.

Conclusion:

The use of [^{11}C]raclopride enabled us to directly compare the V_{ND} estimates with the measured V_T in cerebellum. The analysis showed that the output from the Inhibition and Occupancy plots were identical, and the V_{ND} values obtained from these two plots had greater accuracy than the Lassen plot.

References:

1. Phan JA, Landau AM, Jakobsen S, Gjedde A. 2017 Sci Rep.Radioligand binding analysis of alpha 2 adrenoceptors with [(11)C]yohimbine in brain in vivo: Extended Inhibition Plot correction for plasma protein binding.7(1):15979.
2. Gjedde A, Wong DF. 2000 Neuroimage.Receptor occupancy in absence of reference region.11:S48.
3. Lassen NA, Bartenstein PA, Lammertsma AA, Prevett MC, Turton DR, Luthra SK, et al. 1995 J Cereb Blood Flow Metab.Benzodiazepine receptor quantification in vivo in humans using [11C]flumazenil and PET: application of the steady-state principle.15(1):152-65.
4. Cunningham VJ, Rabiner EA, Slifstein M, Laruelle M, Gunn RN. 2010 J Cereb Blood Flow Metab.Measuring drug occupancy in the absence of a reference region: the Lassen plot re-visited.30(1):46-50.

P14
Target occupancy study and whole body dosimetry with a MAGL PET ligand [^{11}C]PF-06809247 in nonhuman primates

Ryosuke Arakawa[1], Akihiro Takano[1], Sangram Nag[1], Zhisheng Jia[1], Nahid Amini[1], Kevin P. Maresca[2], Lei Zhang[2], Edmund J. Keliher[2], Christopher R. Butler[2], Justin Piro[2], Tarek Samad[2], Deborah Smith[2], Deane Nason[2], Steve O'Neil[2], Patrick Trapa[2], Kari R. Fonseca[2], John Litchfield[2], Timothy McCarthy[2], Christer Halldin[1]

1. Department of Clinical Neuroscience, Centre for Psychiatry Research, Karolinska Institutet and Stockholm County Council, Stockholm SWEDEN

2. Worldwide Research & Development, Pfizer Inc., Cambridge, MA, USA

Introduction:

Monoacylglycerol lipase (MAGL) is a serine hydrolase highly expressed throughout the brain, and it regulates the tone of endocannabinoid signaling. MAGL PET ligand candidate, PF-06809247, was successfully radio-labelled with C-11. To further develop [^{11}C]PF-06809247 into a clinically usable PET ligand, we assessed the relationship between MAGL target occupancy in the brain and the plasma exposure for a MAGL inhibitor in nonhuman primate (NHP). Additionally, we measured the whole body distribution of [^{11}C]PF-06809247 in NHPs and estimated the human effective radiation doses based on the NHP data.

Materials & Methods:

For target occupancy study, five cynomolgus monkeys were used. PET measurements were conducted using the High Resolution Research Tomograph (HRRT) (Siemens Molecular Imaging). A MAGL inhibitor, PF-06818883, was administrated intravenously with bolus infusion of different doses (0.01-0.42 mg/kg) approximately one hour before the PET measurement. The [^{11}C]PF-06809247 was administered intravenously as a bolus injection and the PET measurement lasted up to 63 minutes for 16 measurements (eight sets of baseline and pretreatment). Radioactivities in whole blood and plasma, and the amount of unchanged [^{11}C]PF-06809247 in plasma of arterial blood were also measured. Regions of interest (ROI) were defined manually using the MRI of the individual NHP. Based on the assumption of irreversible binding of [^{11}C]PF-06809247, k4 was set as 0, and kinetic parameters as K1, k2 and k3 were estimated by two tissue compartment (2TC) model using metabolite corrected plasma radioactivity as the input function. As the main outcome measures, Ki defined as (K1 × k3) / (k2 + k3) and Patlak slope were calculated. The target occupancy was calculated as %decrease of Ki between baseline and pretreatment conditions. For whole body dosimetry, two cynomolgus monkeys were used. Whole-body PET measurements were conducted using a GE Discovery PET/CT 710 (GE healthcare) for 100 min immediately after i.v. injection of [^{11}C]PF-06809247. The effective dose was estimated with the OLINDA/EXM software using the adult male model.

Results:

For target occupancy study, the brain uptake of [^{11}C]PF-06809247 was approximately 3%ID at peak under baseline conditions). Kinetic analysis by 2TC with k4=0 was relatively well fitted and Ki value showed good correlation to Patlak slope, supporting the irreversible property of [^{11}C]PF-06809247. The uptake of [^{11}C]PF-06809247 decreased in all brain regions with administration of PF-06818883 (Figure 1 and 2). The target occupancy range by Patlak slope was 23.4% – 99.5%, and increased in a concentration dependent manner with increasing dosing of PF-06807893 (active metabolite of PF-06818883). For whole body dosimetry, high uptakes were shown in the liver, small intestine, kidney, and brain. The effective dose is about 0.0043 mSv/MBq.

Discussion/Conclusion:

The NHP brain occupancy measured with [^{11}C]PF-06809247 showed concentration dependency with dosing of the MAGL inhibitor. This data suggests that [^{11}C]PF-06809247 can estimate the MAGL activity, specifically in NHP brain in vivo. The effective dose of [^{11}C]PF-06809247 is just below the median of other reported C-11 PET radioligands (0.0047 mSv/MBq). [^{11}C]PF-06809247 is a promising PET ligand for estimating MAGL activity in human brain upon further evaluations.

Acknowledgements:

The study was supported by Pfizer Inc.

References:

Zanotti-Fregonara P, Innis RB. [2012], Eur J Nucl Med Mol Imaging, 39(3):544-7

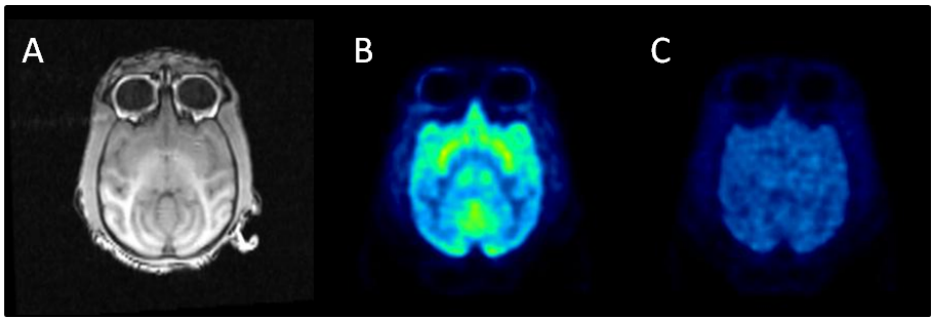

Figure 1. Representative images of A) MRI, B) baseline, and C) pretreatment conditions of [^{11}C]PF-06809247.

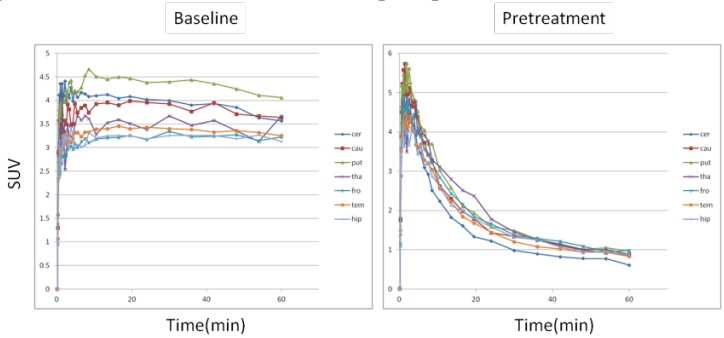

Figure 2. Regional TACs of [^{11}C]PF-06809247 under baseline and pretreatment conditions (same NHP as shown in Figure 1.)

P15
Serotonin 1B receptor mapping in the human brainstem using Positron Emission Tomography and Autoradiography

Emma Veldman, Andrea Varrone, Katarina Varnäs, Marie Svedberg, Johan Lundberg - *Karolinska Institutet, Department of Clinical Neuroscience, Stockholm Centre for Psychiatry Research, Stockholm, Sweden*

Introduction:

The serotonin 1B (5-HT_{1B}) receptor receives increasing interest in studies of psychopathology. For example, anti-depressive treatment seems to reduce 5-HT_{1B} receptor availability in the dorsal brainstem [1]. However, test-retest metrics show low reliability in this region [2]. This is likely attributed to the poor visibility of brainstem nuclei on Magnetic Resonance Imaging (MRI). As individual MR images typically are used to guide the delineation of volumes of interest (VOIs) on dynamic Positron Emission Tomography (PET) images, quantification of 5-HT_{1B} receptor availability in the brainstem is challenging. Two methods have previously been developed to more precisely define brainstem VOIs based on the serotonin transporter distribution visualized on parametric images of binding potential (BP_{ND}): Schain et al. [3] created a method which uses individual data to estimate VOIs, while the method by Fazio et al. [4] is based on template data. To our knowledge, similar approaches for the quantification of 5-HT_{1B} receptor availability in the brainstem have not been evaluated. The aim of the current study was therefore to develop an improved method for PET quantification of 5-HT_{1B} receptor binding in brainstem regions.

Materials & Methods:

The previously developed individual and template-based methods were tested, compared and adjusted for 5-HT_{1B} receptor density quantification in the brainstem. An atlas guided manual VOI of the dorsal part of the brainstem, as published by Nord et al. [2], was used as comparison. Test-retest PET data of 8 healthy subjects examined with the HRRT and the 5-HT_{1B} radioligand [^{11}C]AZ10419369 was used. BP_{ND} maps were created with wavelet-aided noise reduction [5]. Regions for quantification were chosen based on *post mortem* findings of 5-HT_{1B} receptor availability in literature [6]. For the template-based method, a [^{11}C]AZ10419369 PET template was created by averaging all parametric BP_{ND} images. Estimated VOIs were manually drawn on the template and eroded based on BP_{ND} thresholding to volumes defined in literature [7] (Figure 1). Subsequently, the eroded VOIs were applied to the individual parametric BP_{ND} images. For the individual-based method, estimated VOIs were directly drawn and eroded on each individual parametric image.

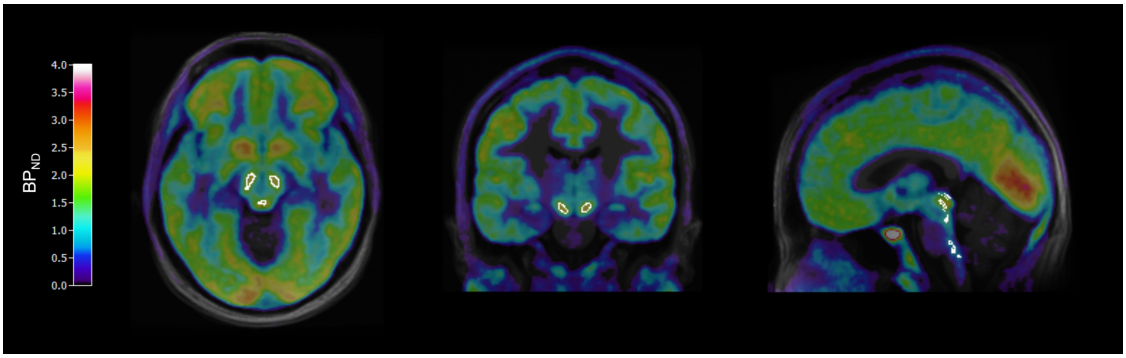

***Figure 1**: Template VOIs (white) superimposed on the template [^{11}C]AZ10419369 parametric BP_{ND} image, overlaid on an average of the corresponding MR images*

An adjusted template-based method was also developed, which included an adjustment of the VOI based on BP_{ND} distribution at individual level, before average BP_{ND} values were determined for each ROI. Test-retest metrics were calculated for brainstem VOIs and regional BP_{ND} values throughout the brain were compared to whole hemisphere [^{3}H]AZ10419369 autoradiography (ARG) specific binding values.

Results:

The distribution of 5-HT_{1B} receptors in the brainstem nuclei obtained with the three methods was consistent with *post mortem* ARG data and facilitated the delineation of VOIs. ICC values increased with all three methods compared with the manual VOI [2] in the dorsal brainstem (Figure 2). APD was not found to be significantly altered.

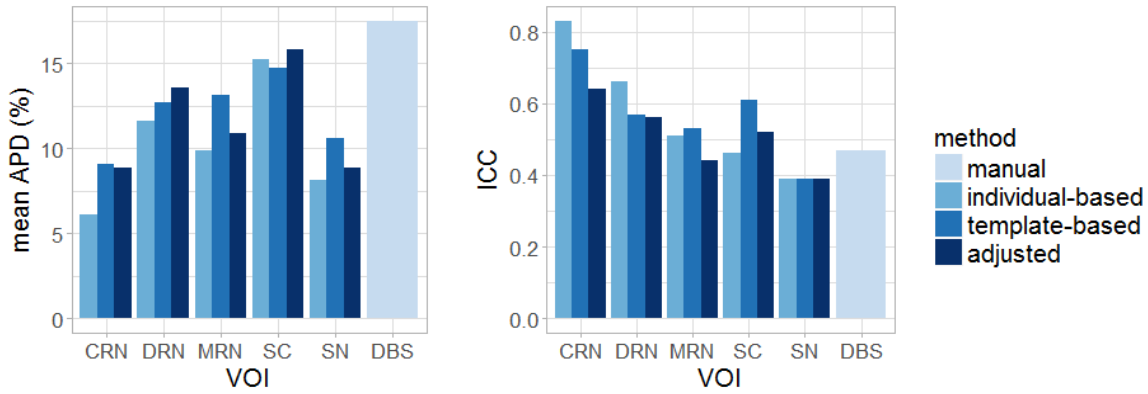

***Figure 2**: Mean absolute percentage differences (APD, left graph) and intraclass correlation coefficients (ICC, right graph) for brainstem VOIs achieved with different methods. CRN: caudal raphe nuclei; DRN: dorsal raphe nuclei; MRN: median raphe nuclei; SC: superior colliculi; SN: substantia nigra; DBS: dorsal brainstem (manual VOI incl. DRN and MRN [2]).*

Discussion/Conclusion:

Both the individual-based method and the template-based method showed improved reliability compared with manual VOIs. The template-based method performed best in VOIs with low BP_{ND} values (CRN and SC). However, overlap of VOIs was seen after

transformation from template to individual data, probably due to the continuous distribution of 5-HT_{1B} receptor binding and spill-over effects. This could only be partly reduced with the adjusted template-based method. Alternative VOIs are therefore desired for 5-HT_{1B} receptor density quantification. To improve the definition of the VOIs on the brainstem nuclei and to overcome spill-over effects, the 5-HT_{1B} receptor distribution is currently studied in higher resolution, by creating a 3D ARG model.

References:

1. Tiger M, Rück C, Forsberg A, Varrone A, Lindefors N, Halldin C, Farde L and Lundberg J. [2014], Psychiatry Res. 2:164-170

2. Nord M, Finnema SJ, Schain M, Halldin C and Farde L. [2014], Eur J Nucl Med Mol Imaging, 2:301-307

3. Schain M, Tóth M, Cselényi Z, Arakawa R, Halldin C, Farde L and Varrone A. [2013], Eur J Nucl Med Mol Imaging, 2: 228-37

4. Fazio P, Schain M, Varnäs K, Halldin C, Farde L and Varrone A. [2016], Neuroimage 133:313-320

5. Cselényi Z, Olsson H, Farde L and Gulyás B. [2002], Neuroimage, 1:47-60

6. Varnäs K, Halldin C and Hall H. [2004], Human Brain Mapping, 3:246-260

7. Hornung JP. [2012] Raphe Nuclei, in: The Human Nervous System. Eds: Mai JK & Paxinos G, 401–424

P16
Modelling arterial input functions using data acquired with an MR- compatible sampler: a validation study using [^{18}F]GE-179

Barbara Santangelo[1,2], Joel Dunn[3], Katherine Beck[1], Colm J. McGinnity[3], Matteo Tonietto[4], Federico Turkheimer[2], Oliver Howes[1], Mattia Veronese[2]

1 Psychosis Studies Department, Institute of Psychiatry, Psychology & Neuroscience, King's College London, London, UK

2 Department of Neuroimaging, Institute of Psychiatry, Psychology & Neuroscience, King's College London, London, UK

3 School of Biomedical Engineering & Imaging Science, King's College London, UK, and King's College London/Guy's & St Thomas' PET Centre, St Thomas's Hospital, London, UK

4 Sorbonne Universités, UPMC Paris 06, Brain and Spine Institute, ICM, Hôpital de la Pitié Salpêtrière, Paris, France

Introduction:

Full quantification of dynamic position emission tomography (PET) data often requires the knowledge of the tracer concentration in the arterial blood and plasma measured as a function of time. In bolus-injection PET experiments, blood samples are typically acquired automatically for approximately 15 minutes after the tracer injection by using a continuous blood sampling device, where blood is pumped at a constant rate through a well-shielded radiation detector (*1*). These blood measures need to be fitted with multi-exponential models to generate a time-continuous noise-free curve that is used as blood-to-tissue delivery function for the data quantification (*2*). In simultaneous PET-MR scanners, accurate measures of automatic blood data are particularly challenging due to the complication of working in a strong magnetic field which leads to noisier data in comparison to standard acquisition with PET/CT (*3*). This work aims to extend the use of an existing pipeline for modelling arterial input function (AIF) to noisy blood datasets measured with PET-MRI compatible blood samplers. For the validation, we used two independent datasets of [^{18}F]GE-179 PET data that were acquired on PET-CT and PET-MR scanners, respectively.

Materials & Methods:

Datasets. We considered two different datasets of simulated and measured arterial blood data. All datasets were calibrated and corrected for the radiotracer decay and background (kBq/mL). For the simulation, 1000 simulations of continuous whole blood noisy data (from 0 to 16 minutes) were generated with Poisson noise consistent with a typical PET-CT continuous blood sampler ("Allogg" AB, Mariefred, Sweden) and with a PET-MR compatible continuous blood sampler (Swisstrace "Twilite", Menzingen, Switzerland). Due to the high background of the Twilite system, background correction was simulated 3 different ways, as a constant (ground truth background) and as the mean taken from 900 and 3600 seconds of simulated data, respectively. The ground truth was based on a representative [^{18}F]GE-179 PET study (*4*). Measured data comprised two datasets of 1) dynamic [^{18}F]GE-179 PET scans of 9 healthy volunteers acquired with a PET-CT scanner (automatic blood sampling using "Allogg") (*4*) and 2) 10 healthy volunteers acquired with a Siemens simultaneous PET-MR scanner (automatic blood sampling using "Twilite"), respectively.

Methods. Simulated and measured data were fitted with Multiblood, a robust and flexible pipeline that allowed the estimation of both radiometabolites and parent concentration models from the raw blood measurements (*5) (https://github.com/MatteoTonietto/MultiBlood*). The software returns a model description for both whole blood (yCb) and parent plasma (yCp). In the simulation, we compared the modelled data with the ground truth values, by using the relative difference of the area under the AIF curve (AUC) as performance index. In measured data analysis, we compared AUCs for PET-CT derived AIFs with those of PET-MR derived AIFs, by using two-way ANOVA analysis (*IBM SPSS statistics 24*). To account for those differences, we measured AIFs with standardized uptake value (SUV).

Results:

Simulated data: for both whole blood and parent plasma, the AUC mean relative difference obtained from the two blood samplers were negligible (from -2.58% to 0.24%). The performance of Multiblood was not affected by background noise (*Table*). *Measured data*: there was no significant difference between the yCp AUC, calculated at different time-points, obtained by the fitted continuous whole blood data measured with "Allogg" and the ones measured with "Twilite" (F=0.402, p=0.535) (*Figure*).

Table

AUC mean relative difference	**Whole Blood** Mean (SD)	**Parent Plasma** Mean (SD**)**
Allogg	0.83% (0.46)	0.24% (0.66)
Twilite (ground truth background)	-0.78% (1.05)	-1.67% (2.18)
Twilite (900 seconds background)	-1.22% (1.75)	-2.58% (3.08)
Twilite (3600 seconds background)	-0.83% (1.21)	-1.86% (2.37)

Figure

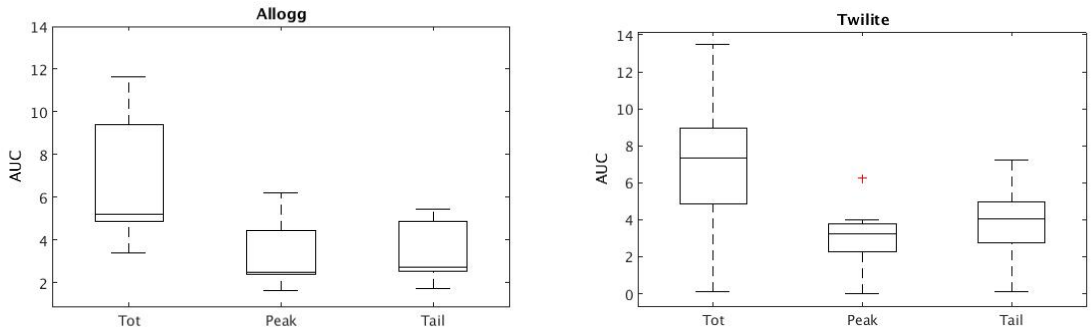

On the left yCp AUC measured with 'Allogg', on the right yCp AUC measured with 'twilite' at different time-points (Tot=total scan duration – 90 minutes, Peak = 0 – 5 minutes from the tracer injection, Tail = 5-90 minutes from the tracer injection)

Discussion:

By applying Multiblood and a PET-MR sampler we obtained results that are consistent with the ones achieved with PET-CT, despite the higher noise level. The flexibility of this method allows it to be used with other PET tracers.

References:

1 Eriksson, L. et al (1995). IEEE Transactions on Nuclear Science, 42(4).
2 Tonietto, M., et al (2015). Conf Proc IEEE Eng Med Biol Soc, 2015, 2247-2250. doi:10.1109/EMBC.2015.7318839.
3 Muzic, R. F., et al. (2014). Semin Roentgenol, 49(3), 242-254. doi:10.1053/j.ro.2014.10.001
4 McGinnity, C. J., et al (2014). J Nucl Med, 55(3), 423-430. doi:10.2967/jnumed.113.130641
5 Tonietto et al. (under review, IEEE - Transactions on Biomedical Engineering).

P17
Selective imaging of phosphodiesterase-4 subtype D in monkey brain

Masahiro Fujita[1], Sanjay Telu[1], Maarten Ooms[1], Cheryl Morse[1], Sami S. Zoghbi[1], Robert L. Gladding[1], Richard Nugent[2], Xuesheng Mo[2], Mark E. Gurney,[2] Victor W. Pike[1], and Robert B. Innis[1].

[1]National Institute of Mental Health, Bethesda, MD, USA and

[2]Tetra Discovery Partners Inc., Grand Rapids, MI, USA.

Introduction:

The signal transduction cascade of 3',5'-cyclic adenosine monophosphate (cAMP) is important in a number of pathologies, including depression, cognitive impairment, substance abuse, and inflammation. In the brain, phosphodiesterase-4 (PDE4) selectively metabolizes cAMP to the inactive monophosphate. PDE4 inhibition increases signal transduction from cAMP and is expected to show antidepressant and anti-inflammatory effects, as well as cognitive improvement. In human, the prototypical PDE4 inhibitor rolipram had antidepressant effects but caused unacceptable emesis, possibly due to rolipram's lack of selectivity among the four PDE4 subtypes (A, B, C, and D). Our laboratory previously used positron emission tomography (PET) to image PDE4 with ^{11}C-(*R*)-rolipram and found that this radioligand reflected cAMP cascade activity[1, 2]. We further identified downregulation of the cAMP cascade in unmedicated patients with major depressive disorder[3], which was partially normalized by selective serotonin reuptake inhibitors (SSRIs)[4]. Building on our previous works, the current study sought to develop a PET ligand capable of selectively imaging PDE4 subtype D (PDE4D), which could be used to evaluate PDE4D-selective therapeutic agents.

Materials and Methods:

We developed two ^{11}C-labeled ligands, T-1650 and T-1660. For both, in vitro experiments showed selective binding to PDE4D relative to PDE4B. In the current studies, PET scans were performed in monkeys to assess whether T-1650 and T-1660 had specific binding to PDE4D in vivo. A pair of baseline and blocked scans was conducted for each of ^{11}C-T-1650 and ^{11}C-T-1660; rolipram (1 mg/kg) was used as the blocking agent. For ^{11}C-T-1650, specific binding to PDE4D was also examined by administering BPN14770—which has been tested in healthy human subjects as a cognitive enhancer—as a blocking agent (three pairs of baseline and blocked scans). For each scan, binding (V_T) of the radioligand was measured by Logan plot and radiometabolite-corrected arterial input function. Specific-to-nondisplaceable ratio BP_{ND} was measured using V_T and Lassen occupancy plot.

Results:

Both ^{11}C-T-1650 and ^{11}C-T-1660 showed modest levels of peak brain uptake (3-4 SUV) that was washed out to half that level in two hours. Binding of both ^{11}C-T-1650 (Figs. 1 and 2) and ^{11}C-T-1660 was blocked by rolipram and also by BPN14770 (for T-1650). Both showed a quick decline in percentage of parent in plasma decreasing to < 50% between five and 10 minutes and dropping to < 10% at 90 minutes. V_T ranged from 5-10 across brain areas, with slightly greater values for ^{11}C-T-1650. ^{11}C-T-1650 had a BP_{ND} of 0.7-1.2. The single blocking experiment with ^{11}C-T-1660 showed a BP_{ND} of 0.7. For both radioligands, the analysis under

various data lengths showed that longer durations produced greater V_T values, which is consistent with radiometabolites entering the brain. V_T from the 90-minute data was ~20% smaller than V_T from the 120-minute data.

Discussion/Conclusion:

We developed two radioligands to selectively image PDE4D in brain. Overall, ^{11}C-T-1650 showed slightly better performance. Selective imaging of PDE4D will allow us to study PDE4D changes in unmedicated patients with depression or cognitive impairment and also to link binding site occupancy of BPN14770 and its therapeutic effects.

References:

1. *J Nucl Med*. 2009; 50:749. 2. *Synapse*. 2010; 64:172. 3. *Biol Psychiat*. 2012; 72:548. 4. *Mol Psychiat*. 2017; 22:754.

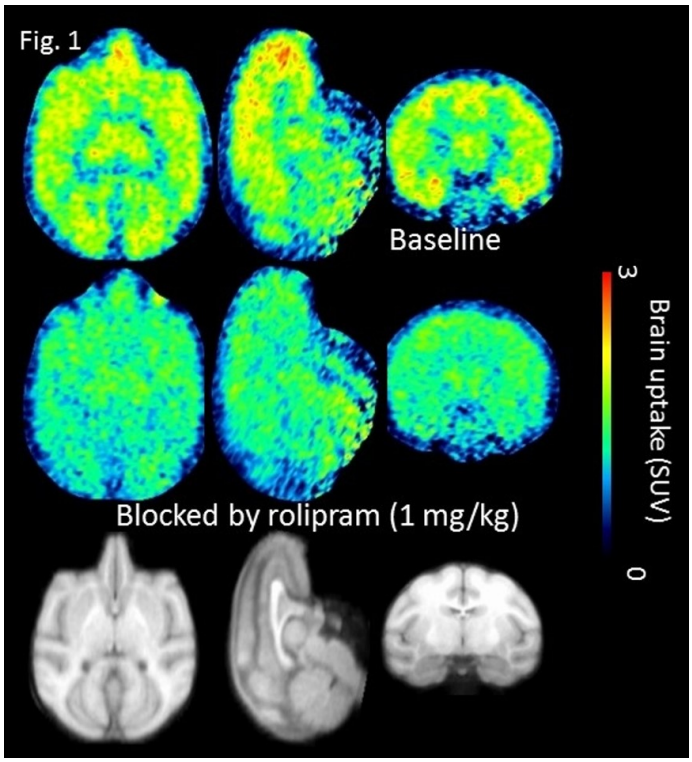

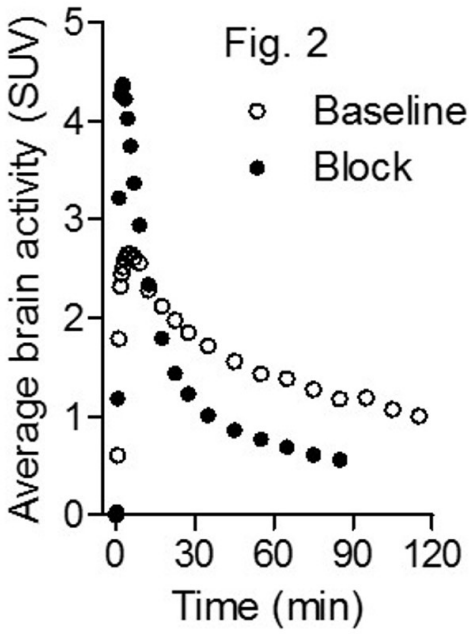

P18
Improved quantification of [^{18}F]flortaucipir uptake in the hippocampus after partial volume correction

Sandeep SV Golla[1*], Emma Wolters[1,2*], Tessa Timmers[1,2], Rik Ossenkoppele[1,2], Chris W.J. van der Weijden[1], Philip Scheltens[2], Lothar Schwarte[3], Mark A Mintun[4], Michael Devous[4], Robert C Schuit[1], Albert D Windhorst[1], Frederik Barkhof[1,5], Maqsood Yaqub[1], Adriaan A Lammertsma[1], Bart NM van Berckel[1,2], Ronald Boellaard[1]

Departments of [1]Radiology & Nuclear Medicine, [2]Neurology & Alzheimer Center, and [3]Anaesthesiology, Amsterdam Neuroscience, VU University Medical Center, Amsterdam, the Netherlands, [4]Avid Radiopharmaceuticals, Inc., United States [5]Institutes of Neurology & Healthcare Engineering, UCL, London, United Kingdom

Introduction:

In Alzheimer's Disease (AD), the hippocampus is one of the first brain regions affected by tau pathology[1]. Given the close proximity of the hippocampus to the choroid plexus (CP), off-target binding in the CP may cause spill-in of [^{18}F]flortaucipir activity, potentially leading to overestimation of tau binding in the hippocampus. The purpose of this study was to assess the impact of CP activity on quantification of hippocampal uptake and to correct for this spill-in using partial volume correction (PVC).

Materials & Methods:

130 minutes dynamic PET scans, including arterial sampling, were performed in 10 AD patients and 10 healthy controls. A combination of HYPR denoising[3] and Van Cittert iterative deconvolution was used to generate PVC PET images[2]. Regions of interest (ROI) were defined in two different ways for hippocampus by 1) using T1 weighted MRI, Hammers template and PVElab (complete ROI), 2) an eroded hippocampal ROI (eroded ROI), to correct for spill-in from the CP. The CP was drawn manually on PVC PET images and an MRI flair image was used to evaluate the ROI definition. Hippocampal distribution volume (V_T) for complete and eroded ROI with/without PVC were correlated with CP V_T.

Results:

For controls, the relationship between hippocampus and CP uptake was significantly reduced when using an optimized ROI in combination with PVC (r^2=0.59, slope=0.80 without PVC versus r^2=0.15, slope=0.15 with PVC; p for interaction <0.05) (figure 1). A similar, even stronger, trend was observed for AD patients indicating that the dependence of hippocampal V_T on CP uptake can be decreased by PVC and VOI adjustment regardless of subject group (p <0.01) (figure 2).

Conclusion:

After PVC and optimized hippocampal ROI delineation, only a weak correlation remained between hippocampal and CP V_T. The proposed PVC method significantly improves accuracy of hippocampal V_T values and should be used when investigating the relationship between *in vivo* tau binding in the hippocampus and both clinical and pathophysiological markers of AD.

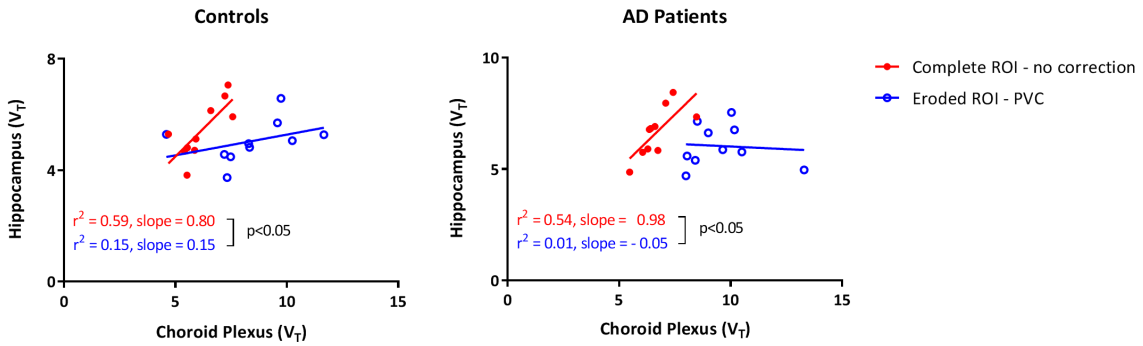

Figure 1: Scatter plots illustrating the relationship between hippocampal V_T and choroid plexus V_T before and after PVC in combination with erosion of the hippocampal ROI in both controls (left) and AD patients (right).

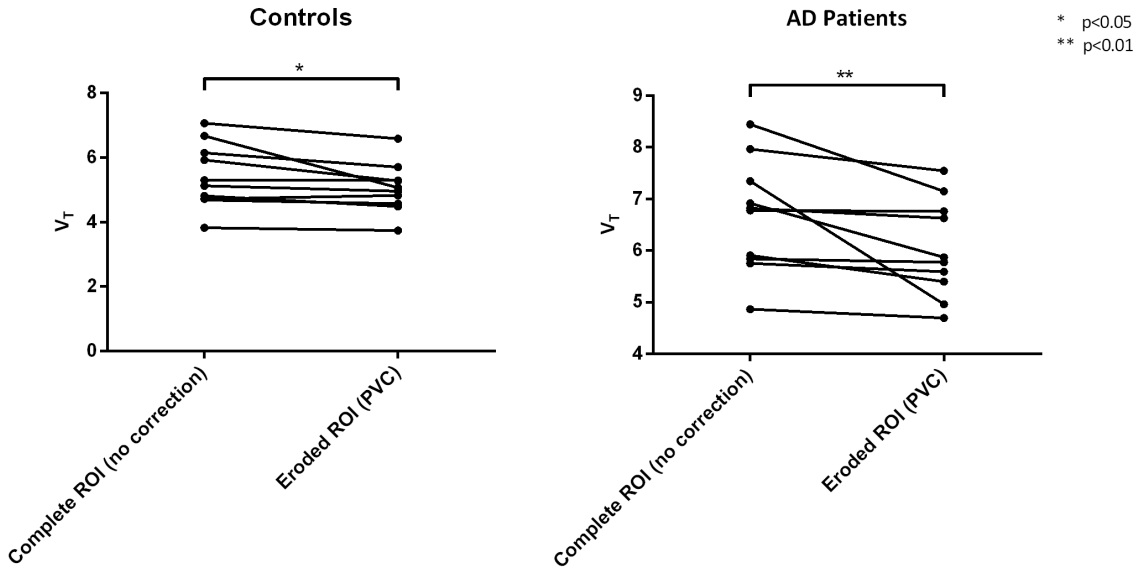

Figure 2: Hippocampal V_T before and after PVC in combination with erosion of the hippocampal ROI in both controls (left) and AD patients (right).

References:

1. Braak H, Braak E, *Neuropathological stageing of Alzheimer-related changes.* Acta neuropathologica, 1991. **82**: 239-59.
2. Golla SSV, et al., *Partial volume correction of brain PET studies using iterative deconvolution in combination with HYPR denoising.* EJNMMI Res, 2017. **7**: 36.
3. Christian BT, et al., *Dynamic PET denoising with HYPR processing.* J Nucl Med, 2010. **51**: 1147-54.

P19
False positive rates in positron emission tomography

Melanie Ganz[1,2], Martin Nørgaard[1,3], Vincent Beliveau [1,3], Douglas Greve[4], Gitte M Knudsen[1,3]

[1]Neurobiology Research Unit, Rigshospitalet, Copenhagen, Denmark
[2]Department of Computer Science, University of Copenhagen, Copenhagen, Denmark
[3]Faculty of Health and Medical Sciences, University of Copenhagen, Copenhagen, Denmark
[4]Athinoula A. Martinos Center for Biomedical Imaging, Department of Radiology, Massachusetts General Hospital & Harvard Medical School, Boston, MA, USA

Introduction:
In this work we seek to investigate the false positive rate (FPR) of positron emission tomography (PET) studies. This topic has recently received significant attention in the functional magnetic resonance imaging (fMRI) [Eklund 2016] as well as the structural MRI community [Greve 2017], however the effects on PET neuroimaging analyses are largely unknown. We evaluated the FPR using real PET data under group assignments that should yield no significant results using common corrections for multiple comparisons (MC) in regional as well as surface-based voxel-wise analyses.

Methods:
We evaluated the FPR similarly as presented in [Eklund 2016] and [Greve 2017]. In this work, we used PET data from 159 healthy controls imaging either the serotonin transporter ([^{11}C]DASB; N = 100) or the 5-HT$_4$ receptor ([^{11}C]SB207145; N = 59), [Beliveau 2016]. Subjects were tested for global or regional effects of age and gender and none were found. Using this null data, we estimate the FPR at a regional level by performing 1000 group analyses with either N = 10, 20, 30 or 40 subjects randomly assigned to each group, and for each tracer. The regional analyses were performed on 16 subcortical regions and 34 cortical regions (left hemisphere only) using a parametric t-test and a non-parametric Mann-Whitney test at a significance level of 0.05, following Bonferroni correction for MC. We do not expect any real group differences, so any positive regional outcome ($P < 0.05$) was interpreted as a false positive. We also extended the analysis to the cortical surface (left hemisphere only) consisting of 163142 vertices [Beliveau 2016]. For each vertex, a two-group GLM analysis was performed, and corrected for MC using Monte Carlo simulations. Clusters were formed by thresholding the vertex-wise maps at cluster forming thresholds (CFT) of 0.05, 0.01 and 0.001. A false positive was declared if one or more clusters with a cluster wise p-value were less than 0.05.

Results:
Our analysis showed that for random group studies of regional binding potentials of group sizes N = 10, 20, 30 and 40 the FPR for both tracers was far below the nominal 5% level (0-4%) when correction for MC with Bonferroni. The FPR was also stable across group sizes. This was irrespective of the use of a parametric or non-parametric test for the statistical analysis. The surface-based analysis yielded the results shown in Figure 1A and 1B. For the most liberal CFT of 0.05, the FPR was inflated above the nominal 5% level (up to 24%) for both [^{11}C]DASB and [^{11}C]SB207145, but not at the same level as reported for fMRI [Eklund 2016] and structural MRI data [Greve 2017]. This could be caused by a heavier-than-Gaussian spatial autocorrelation [Eklund 2016] [Greve 2017], violating the parametric assumptions in the MC correction (Figure 1C). Additionally, the parametric MC assumes a uniform smoothness. We found that the smoothness of the residuals of the GLM analysis was highly non-stationary (Figure 1D), but that the global smoothness estimate was slightly

overestimated (see inset histogram). This would improve the performance of the parametric MC slightly since it assumes a smoother noise model. For the common CFT of 0.01, the FPR was maximally 10% and using a CFT of 0.001 was too conservative. Again, the FPR was relatively stable across group size.

Discussion:

For regional analyses, the FPR is well controlled when the statistics are appropriately conducted and a correction for MC performed. For surface-based analysis, surprisingly the false positive rates are not as poor as reported for fMRI and structural MRI, but they are nonetheless inflated. Hence, either a conservative CFT or more appropriately non-parametric corrections for MC such as permutations should be performed.

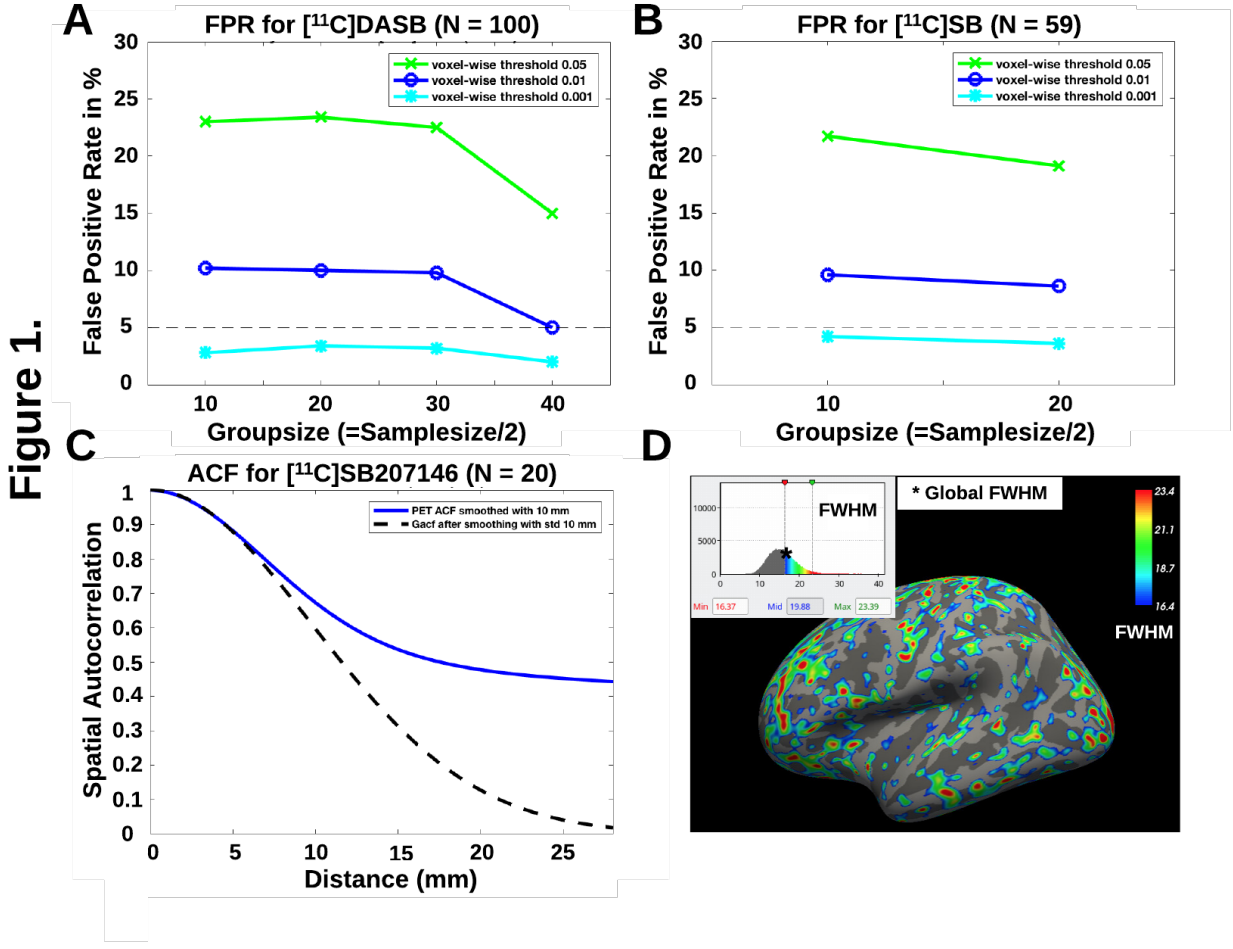

Figure 1.

References:

Beliveau, V., Ganz, M., Feng, L., Ozenne, B., Højgaard, L., Fisher, P.M., Svarer, C., Greve, D.N. and Knudsen, G.M. [2017]. Journal of Neuroscience, 37(1):120-128.

Eklund, A., Nichols, T.E. and Knutsson, H. [2016] Proceedings of the National Academy of Sciences, 113(28):7900-7905.

Greve, D.N. and Fischl, B. [2018] NeuroImage, 171:6-14.

P20
Optimization of the k_2' parameter for the pharmacokinetic modelling of dynamic PIB scans using SRTM2

Débora E. Peretti[1], Fransje E. Reesink[2], Janine Doorduin[1], Bauke M. de Jong[2], Rudi A.J.O. Dierckx[1], Peter P. De Deyn[2,3], Ronald Boellaard[1], David Vállez García[1]

[1] *University of Groningen, University Medical Centre Groningen, Department of Nuclear Medicine and Molecular Imaging, The Netherlands*

[2] *University of Groningen, University Medical Centre Groningen, Department of Neurology, Alzheimer Research Centre, The Netherlands*

[3] *University of Antwerp, Institute Born-Bunge, Laboratory of Neurochemistry and Behaviour, Belgium*

Introduction:

In Alzheimer's disease (AD), quantitative measures of amyloid-β (Aβ) deposition in the brain can be assessed by the analysis of dynamic ^{11}C-labelled Pittsburgh Compound B (PIB) scans. To this end, pharmacokinetic modelling of the data is required, with the most frequent approach being the simplified reference tissue model 2 (SRTM2). However, this method was originally developed for the analysis of neuroreceptor binding, thus it expects a well-defined receptor-rich region. This assumption might be violated in the case of PIB, especially in healthy subjects, which are not expected to have Aβ deposition. Therefore, the aim of this study was to explore the consequences of violating this assumption and, if possible, to define an optimal brain region for estimating k_2' (i.e. transfer of the tracer from the reference tissue back to plasma), which is used and fixed in the second iteration of SRTM2.

Materials and Methods:

Thirty subjects underwent a dynamic PIB PET scan and were then classified by visual inspections as PIB positive (+) or PIB negative (-), with a total of fifteen per group. A set of regions were used to estimate the median value of the k_2' parameter for SRTM2: seven anatomical regions derived from the Hammer's atlas (grey matter, frontal lobe, parietal lobe, temporal lobe, white matter, brainstem, and the combination of white matter and brainstem), one SPM voxel-based comparison of statistical differences between the groups, and three using different binding potential (BP_{ND}) thresholds (0.01, 0.05, 0.1). A sensitivity analysis was also made by fixing a range of k_2' values (from 0.03 to 0.09) and assessing the effects of these changes on estimated BP_{ND}.

Results:

The different regions used to estimate k_2' resulted in distinct values for this parameter. In general, values from grey matter and statistical regions showed a larger difference between the groups, an average difference of 32%. The method that presented the smallest difference was the one where the brainstem was used for the estimation (2% difference between groups), but the estimated median values were, in general, higher than for the other methods. Distribution of median k_2' values showed that the most common estimation is 0.05 for this set of subjects. The method that presented the lowest difference between groups and was the closest to this estimated value was the threshold approach using BP_{ND} equal to 0.1. Sensitivity analysis of the effects of different k_2' estimation on BP_{ND} showed that the larger the k_2' value, the smaller the change in BP_{ND}.

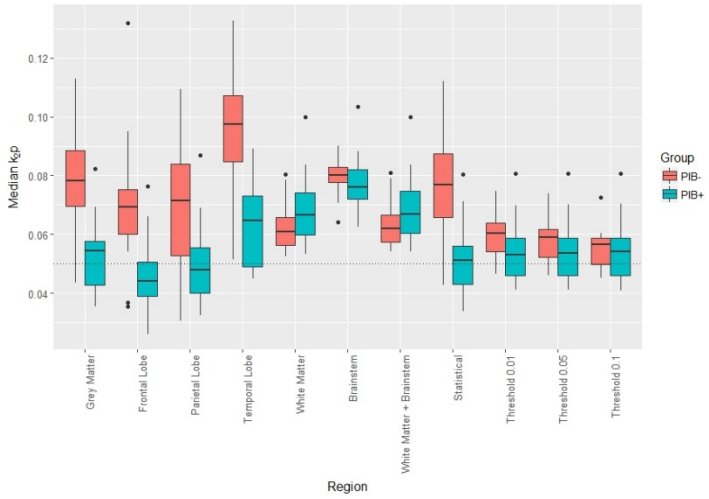

Figure 1: Estimated values of k2' for the different methods of estimation.

Discussion

The large difference between k_2' estimations between groups suggests that grey matter VOI based methods and the one based on statistical differences between groups might not be acceptable. Threshold based approaches guarantee that only regions with some binding will be considered when estimating k_2'. Preliminary analysis of the data showed that since the relationship between k_2' and BP_{ND} is not linear, an overestimation of k_2' value might result in a smaller bias in BP_{ND} estimation than an underestimation. Therefore the best method for estimating the k_2' is by using a threshold on the BP_{ND}.

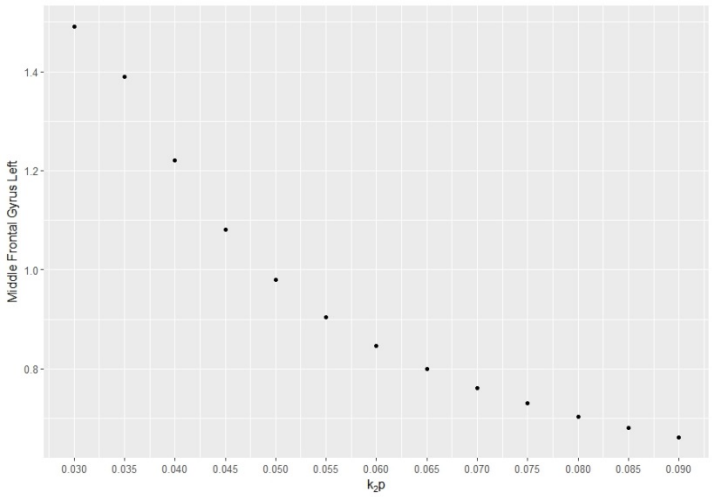

Figure 2: Representative plot of the sensitivity analysis of BP_{ND} estimation in the middle frontal gyrus left for a range of k2' values of a typical AD patient.

References:

Klunk WE, Henriksen G, Wester HJ et al. [2005] Eur.J.Nucl.Med.Mol.Imaging 32: 486-510

Tolboom N, Yaqub M, Boellaard R et al. [2009] Eur.J.Nucl.Med.Mol.Imaging 36: 1629–1638

Yaqub M, Boellaard R, Kropholler MA et al. [2006] Phys.Med.Biol. 51: 4217–4232

Wu Y, Carson RE [2002] J.Cereb.Blood Flow Metab. 22: 1440–1452

P21
Evaluation of the new PET radiotracer ^{18}F-FC024 in the *h*CB_2-AAV rat model of human cannabinoid type 2 receptor local overexpression.

Bala Attili[1], Fabien Caillé[2], Guy Bormans[1] and Bertrand Kuhnast[2]

[1]*Laboratory for Radiopharmaceutical Research, Department of Pharmaceutical and Pharmacological Sciences, KU Leuven , Campus Gasthuisberg, O&N2, Herestraat 49, Box 821, 3000 Leuven, Belgium.*

[2]*UMR 1023 IMIV, Service Hospitalier Frédéric Joliot, CEA, Inserm, Université Paris Sud, CNRS, Université Paris-Saclay, Orsay, France.*

Introduction:

Upregulation of the cannabinoid type 2 receptors (CB_2R) unveils pathological processes such as neuroinflammation in multiple sclerosis, Alzheimer's or Parkinson's diseases. Positron emission tomography (PET) is a highly sensitive approach to image the CB_2R for which we have recently described a promising fluorine-18 labeled radiotracer, **^{18}F-FC024**.[1] In the course of translating this tracer to clinical trials, we report herein both in vitro autoradiography and a in vivo µPET imaging study in an *h*CB_2-AAV local overexpressed rat model.

Material and Methods:

Animal model. Female Wistar rats were stereotactically injected with an adeno-associated viral (AAV) vector serotype 2/7 encoding *h*CB_2 (D80N), in the right striatum under control of a CaMKII promoter. A control AAV2/7 vector expressing the enhanced green fluorescent protein (eGFP) under control of a CaMKII promoter was injected in the left striatum at the contralateral side. [2] The developed rat model was validated by injection of the well-characterized CB_2R radiotracer ^{11}C-NE40. [3]

Autoradiography. Brain slices of *h*CB_2-AAV rats (n = 4) were incubated for 15 min with **^{18}F-FC024** (18.5 Kbq/section) alone or in the presence the CB_2-specific compound NE40 (100 µM), exposed to a high performance phosphor storage screen for 1 hour (Super resolution screen; Perkin Elmer, Waltham, USA). The screens were read using a Cyclone Plus system (Perkin Elmer) and data were analyzed using Optiquant software (Perkin Elmer).

µPET imaging. hCB_2-AAV rats (n = 3) were injected *i.v.* with **^{18}F-FC024** (33 MBq) and scanned on a Focus™ 220 PET scanner. The standardized uptake values (SUV) were recorded in the right striatum (ipsilateral) and in the left striatum (contralateral). Blocking studies were performed with *i.p.* injections of NE40 (1 mg/kg, n = 3 and 10 mg/kg, n = 3) 30 min prior to injection of **^{18}F-FC024**.

Results:

Autoradiography. An 8-fold increase of the signal was observed in the right relative to the left striatum of *h*CB_2-AAV rat brain sections. A 91% reduction in the signal was observed in right striatum of *h*CB_2-AAV rats compared to control when blocking with NE40.

µPET imaging. The SUV in the of *h*CB_2-AAV rats at 30 min *p.i* was much higher in the right striatum (average $SUV_{20\text{-}120\ min}$ = 5.9±0.2) and also higher than ^{11}C-NE40 concentration in the right striatum (average $SUV_{20\text{-}90\ min}$ = 1.5±0.2) in same rats. Blocking with 1 mg/kg of

NE40 decreased the SUV in the right striatum (average SUV $_{0\text{-}120\ min}$ = 3±0.1). Using a dose of 10 mg/kg of NE40 for the blocking experiment further decreased the SUV in the right striatum (Average SUV $_{0\text{-}120\ min}$ = 1.2±0.1).

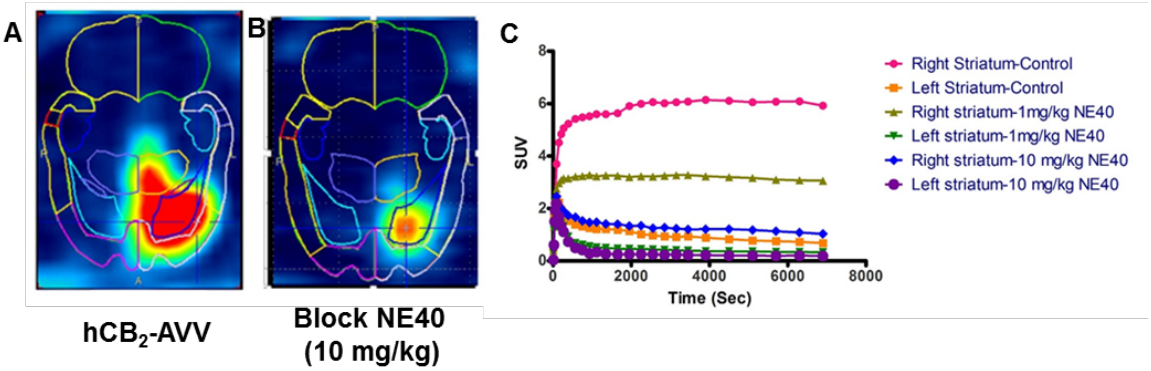

Fig 1. µPET imaging of *h*CB_2-AAV rats with **^{18}F-FC024** (A) and blocking experiments with NE40 (1 and 10 mg/kg) (B) and time-activity curves in both ipsi and contralateral striata (C).

Discussion:

µPET imaging showed that **^{18}F-FC024** is able to cross the blood brain barrier (BBB) and bind to the *h*CB_2R in the ipsilateral right striatum of *h*CB_2-AAV rats with a 4-fold increase compared to the CB_2R reference tracer ^{11}C-NE40. Time-activity curves showed uptake and fast wash-out of the tracer in the contralateral left striatum whereas a maximal uptake of SUV=6 was reached after 30 min *p.i.* in the ipsilateral region, underlining strong binding of **^{18}F-FC024** to the *h*CB_2R. Autoradiography studies with brain slices of control rats showed 27% blocking effect from coincubation with NE40 (100 µM) indicating tracer binding to rat brain CB_2R. Self-blocking experiments with **FC024** and blocking experiments with a CB_1-selective compound still need to be performed to evaluate a potential off-target binding.

^{18}F-FC024 is therefore a very promising tracer to image the CB_2R *in vivo* in the brain with PET. Both a brain radiometabolite analysis study and PET experiments in non-human primates are currently ongoing to fully characterize this tracer before performing a first-in-man study in patients with neurodegenerative diseases.

Acknowledgments:

The authors thank the InMiND research consortium (HEALTH-F2-2011-278850) for financial support.

References:

[1] Caillé F, Cacheux F, Peyronneau M-A et. al. [2017] Mol. Pharm. 14: 4064-4078

[2] Vandeputte C, Evens N, Toelen J et. al. [2011] Nucl. Med. 52(7): 1102-1109

[3] Evens N, Vandeputte C, Coolen C et. al. [2013] Nucl. Med. Biol. 39: 389-399

P22
Application of a reference region-free HYbrid DEConvolution Approach for quantifying PET binding potentials in the absence of blood samples

Francesca Zanderigo[1,4], Martin Schain[1], J. John Mann[1,2,4], R. Todd Ogden[1,2,3]

[1]Department of Psychiatry, [2]Department of Radiology, [3]Department of Biostatistics, Columbia University, New York, NY, USA [4]Molecular Imaging and Neuropathology Division, New York State Psychiatric Institute, New York, NY, USA

Introduction:

Estimation of PET binding potentials (BP_P, BP_{ND})[(1)] in absence of both a measured arterial input function (AIF) and a valid reference region is challenging. Estimating BP_{ND} with a reference region and a reference region-based approach[(2)] is not appropriate for many targets that are present throughout the brain, and using an invalid reference region can cause BP_{ND} underestimation[(3)]. We have proposed simultaneous modeling across multiple brain regions to quantify BP_P and BP_{ND} when no reference region is available[(4)], and have extended the approach to quantification of BP_{ND} in the absence of both blood data and a reference region[(5)]. These approaches[(4-5)], while performing accurately for some tracers (e.g., [^{11}C]WAY100635, [^{11}C]CUMI101), perform poorly for others (e.g., [^{11}C]DASB, [^{11}C]harmine). We have also proposed, and applied to [^{11}C]DASB, a HYbrid DEConvolution Approach (HYDECA)[(6)] that quantifies BP_P and BP_{ND} in absence of a reference region. HYDECA, however, still requires an AIF. Here we combine HYDECA with a noninvasively derived AIF to estimate BP_P and BP_{ND} in the absence of both blood samples and a reference region.

Material and Methods:

In 13 human subjects, imaged with the serotonin transporter tracer [^{11}C]DASB at baseline and then again after administration of sertraline[(7)], we computed the non-displaceable distribution volume (V_{ND}) using the Lassen plot[(8)] ($V_{ND-Lassen}$). Using only the baseline data and 7 regions of interest for [^{11}C]DASB (midbrain, ventral striatum, amygdala, dorsal caudate, hippocampus, temporal lobe, cerebellar gray matter, CGM), we then computed:

$$BP_P = V_T\left(LEGA_{AIF}\right) - V_{ND-Lassen}$$

$$BP_{ND} = \left[V_T\left(LEGA_{AIF}\right) - V_{ND-Lassen}\right] / V_{ND-Lassen}$$

where $V_T\left(LEGA_{AIF}\right)$ is the total distribution volume (V_T) calculated using Likelihood Estimation in Graphical Analysis (LEGA)[(9)].

In each subject we used HYDECA[(6)] to compute: 1) $V_{ND}\left(HYDECA_{AIF}\right)$ using the AIF; 2) $V_{ND}\left(HYDECA_{SIME-AIF}\right)$ using a simultaneously estimated AIF[(10)] (SIME-AIF), which only requires one blood sample to be used as anchor point (50 minutes post-injection for [^{11}C]DASB[(10)]); and 3) $V_{ND}\left(HYDECA_{SIME-AIF-ARB}\right)$ using an AIF simultaneously estimated[(10)] with an arbitrary anchor α (SIME-AIF-ARB). In order to investigate the effect on estimating binding potentials when applying HYDECA with a less-invasive AIF, SIME-AIF, (one blood sample vs. full sampling), and a blood-free AIF, SIME-AIF-ARB (no blood required), we then calculated:

$$BP_P(HYDECA_{AIF}) = V_T(LEGA_{AIF}) - V_{ND}(HYDECA_{AIF})$$
$$BP_P(HYDECA_{SIME-AIF}) = V_T(LEGA_{SIME-AIF}) - V_{ND}(HYDECA_{SIME-AIF})$$

$$BP_{ND}(HYDECA_{SIME-AIF}) = BP_P(HYDECA_{SIME-AIF}) / V_{ND}(HYDECA_{SIME-AIF})$$

$$BP_{ND}(HYDECA_{SIME-AIF-ARB}) = \left[V_T(LEGA_{SIME-AIF-ARB}) - V_{ND}(HYDECA_{SIME-AIF-ARB})\right] / V_{ND}(HYDECA_{SIME-AIF-ARB})$$

where $V_T(LEGA_{SIME-AIF})$ and $V_T(LEGA_{SIME-AIF-ARB})$ are V_T calculated via LEGA[9] using SIME-AIF and SIME-AIF-ARB, respectively. Similarly to[5], while calculation of BP_P carries no utility when an arbitrary anchor was used, BP_{ND} calculation should be unaffected, since $V_{ND}(HYDECA_{SIME-AIF-ARB})$ and $V_T(LEGA_{SIME-AIF-ARB})$ are proportionally biased by the same factor. BP_{ND} was also calculated with the simplified reference tissue model (SRTM)[11] with CGM as reference region ($BP_{ND}(SRTM)$).

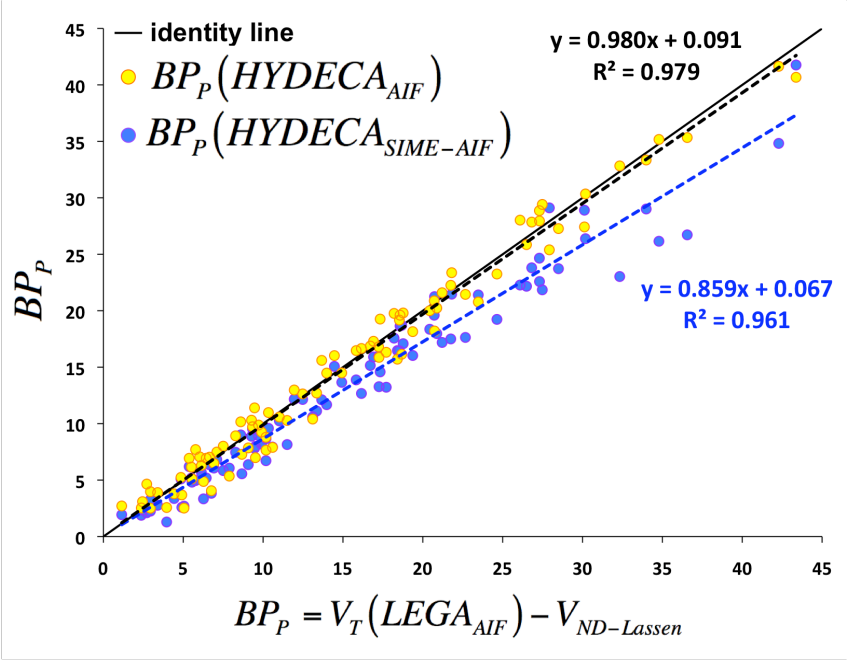

Figure 1. Lassen plot-based vs. HYDECA-based BP_P values obtained with AIF and SIME-AIF. All subjects and regions are reported.

Results:

HYDECA-based BP_P values obtained using either AIF or SIME-AIF are highly correlated and close to those obtained using AIF and Lassen plot (**Figure 1**). HYDECA-based BP_{ND} values obtained using either SIME-AIF or SIME-AIF-ARB are very similar to each other, and tend to be closer to, and more correlated with, values based on AIF and Lassen plot than SRTM (**Figure 2**).

Discussion:

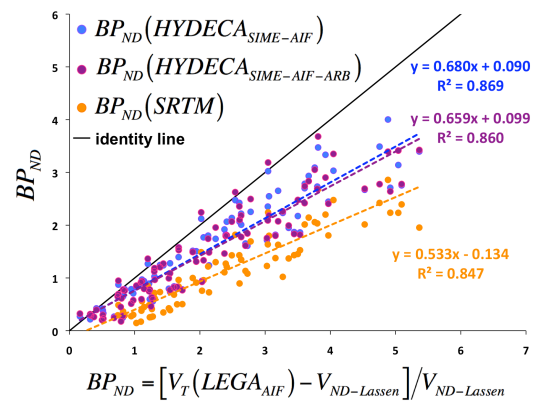

Figure 2. Lassen plot-based vs. SRTM vs. HYDECA-based BP_{ND} values, obtained with both SIME-AIF and SIME-AIF-ARB. All subjects and regions are reported, besides CGM for SRTM.

HYDECA can quantify reference region-free BP_P values for [^{11}C]DASB using a minimally-invasive SIME-AIF, provided that accurate sampling of one arterial blood sample at 50 minutes post-injection, and parent fraction analysis on such sample, can be obtained. In the absence of any blood data, HYDECA combined with simultaneous estimation can also provide BP_{ND} values that are more accurate than those from SRTM. We also explore sensitivity of results to HYDECA settings[6], investigate whether estimation changes by combining HYDECA with a population-based AIF instead of simultaneous estimation, and assess test-retest properties of blood-free HYDECA.

References:

1) Innis RB, Cunningham VJ, Delforge J et al. [2007] J Cereb Blood Flow Metab 27(9): 1533-9; **2)** Zanderigo F, Ogden RT, Parsey RV [2013] J Cereb Blood Flow Metab 33(6): 888-97; **3)** Salinas CA, Searle GE, Gunn RN [2015] J Cereb Blood Flow Metab 35(2): 304–11; **4)** Ogden RT, Zanderigo F, Parsey RV [2015] NeuroImage 108: 234-42; **5)** Schain M, Zanderigo F, Mann JJ et al. [2017] NeuroImage 146: 121-31; **6)** Zanderigo F, JJ Mann, Ogden RT [2017] PLoS One12(5):e0176636; **7)** Parsey RV, Kent JM, Oquendo MA et al. [2006] Biological psychiatry 59(9): 821–8; **8)** Cunningham VJ, Rabiner EA, Slifstein M et al. [2010] J Cereb Blood Flow Metab 30(1): 46–50; **9)** Ogden RT, Ojha A, Erlandsson K et al. [2007] J Cereb Blood Flow Metab 27(1): 205-17; **10)** Ogden RT, Zanderigo F, Choy S et al. [2010] J Cereb Blood Flow Metab 30: 816-26; **11)** Lammertsma AA, Hume SP [1996] NeuroImage 4(3 Pt 1): 153-8.

P23
[^{11}C]PBR28 PET imaging reveals decreased regional brain expression of translocator protein (TSPO) in young adult males with autism

Zürcher NR[a,b,c], Loggia ML[a,b,c], Mullett JE[b,d], Bhanot A[a,b], Richey L[a,b], Hightower B[a,b] Wu C[a,b] Butterfield RI[a,b], Chonde D[a,b], Izquierdo-Garcia D[a,b,c], Wey HY[a,b,c], Catana C[a,b,c], Hadjikhani N[a,b,c], McDougle CJ[b,c,d], Hooker JM [a,b,c]

[a] A. A. Martinos Center for Biomedical Imaging, Charlestown, MA, USA, [b] Massachusetts General Hospital, Boston, MA, USA, [c] Harvard Medical School, Boston, MA, USA, [d] Lurie Center for Autism, Lexington, MA, USA

Introduction:

Despite 1 in 68 school-aged children being affected by autism spectrum disorder (ASD), the neurobiological basis for this disorder remains unknown and currently no drug effectively treats the core symptoms. While a single etiology is unlikely, recent work suggests that numerous ASD risk genes converge onto astrocytic, microglial and immune markers.[1] Although microglia and astrocytes are known to play essential roles in neuroimmune cross-talk and synaptic pruning, they are strikingly understudied in ASD. Translocator protein 18 kDa (TSPO), is a protein whose expression depends on glial activity states and is expressed on both microglia and astrocytes. The aim of our study here was to assess whether individuals with ASD can be characterized by abnormal *in vivo* brain expression of TSPO using [^{11}C]PBR28 PET imaging.

Materials and Methods:

Twelve male participants with ASD (24.8 years ± 5.9 (mean ± SD)) and 18 healthy age-matched control male participants (CON) (25.5 years ± 5.8,) underwent simultaneous magnetic resonance (MR) and positron emission tomography (PET) imaging on a hybrid MR-PET scanner consisting of a 3 Tesla Siemens Tim Trio with an integrated PET camera. Only mixed and high affinity binders, as identified based on Ala174Thr TSPO polymorphism (ala/thr and ala/ala, respectively), were included; TSPO polymorphism was statistically controlled for in the analyses. [^{11}C]PBR28 was injected as a slow intravenous bolus, with a mean administered dose of 518.7 MBq ± 21.4 for ASD and 509.9 MBq ± 44.2 for CON, *n.s.* Attenuation correction was conducted using validated MR-based methods. [2,3] Standardized uptake value (SUV) images were created for radioactivity in the field of view 60-90 min post-radioligand injection. $SUV_{60–90}$ images were then registered to MNI space, spatially smoothed (6mm FWHM), and intensity-normalized to a whole brain mean of 1 ($SUVR_{60-90}$), following previously published methods.[4,5] Voxelwise whole brain comparisons were conducted between ASD and CON groups (Z>2.3, $p_{cluster}$ <0.05). In order to assess longitudinal stability, a subset of subjects (6 ASD, 10 CON) were rescanned after 3-5 months and [^{11}C]PBR28 $SUVR_{60-90}$ extracted from FreeSurfer derived regions of interest (ROI) were compared across time points.

Results:

Voxelwise whole brain analysis showed that [^{11}C]PBR28 binding was significantly decreased in the insular cortex, superior temporal gyrus, angular gyrus and posterior cingulate/precuneus cortex in individuals with ASD compared to matched CON (Z>2.3, $p_{cluster}$ <0.05), Figure 1. [^{11}C]PBR28 uptake was stable over a period of 3-5 months, with a

region such as the fusiform cortex showing test-retest variability of -2.3 % signal change ± 1.5 (mean ± SD) in ASD and -0.2 % signal change ± 2.6 in CON, *n.s.*

Discussion/Conclusion:

[^{11}C]PBR28 uptake was significantly decreased in male adults with ASD compared to CON males. Altered TSPO expression could be attributed to changes in neuroimmune processes, but could also reflect changes in cell metabolism, mitochondrial respiration/energy production, or oxidative stress.[6]

Studies aimed at exploring the significance of decreased TSPO expression are ongoing. Reduction in TSPO expression has previously been reported in schizophrenia, another neurodevelopmental disorder.[7]

Given the difficulty of performing an MR-PET scan in non-sedated individuals with ASD, this pilot study was conducted using $SUVR_{60\text{-}90}$. Future work using arterial sampling will focus on determining a suitable pseudo-reference region in this population, an approach that has been successfully applied and validated for [^{11}C]PBR28 for other disease populations. [8,9]

Acknowledgements:

We wish to thank the physicians Christopher Keary and Michelle Palumbo for obtaining informed consent, Dr. Lisa Nowinski for neuropsychological assessments, and nuclear medicine technologists Shirley Hsu and Grae Arabasz for radiotracer injection and assistance with MR-PET scans, as well as Judit Sore and the radiopharmacy team for radioligand production. Funding for this study was provided by the Robert E. and Donna Landreth Fund for the Study of Neuroinflammation in Autism, as well as by a Meixner Translational Postdoctoral Fellowship # 9258 from Autism Speaks awarded to Nicole Zürcher.

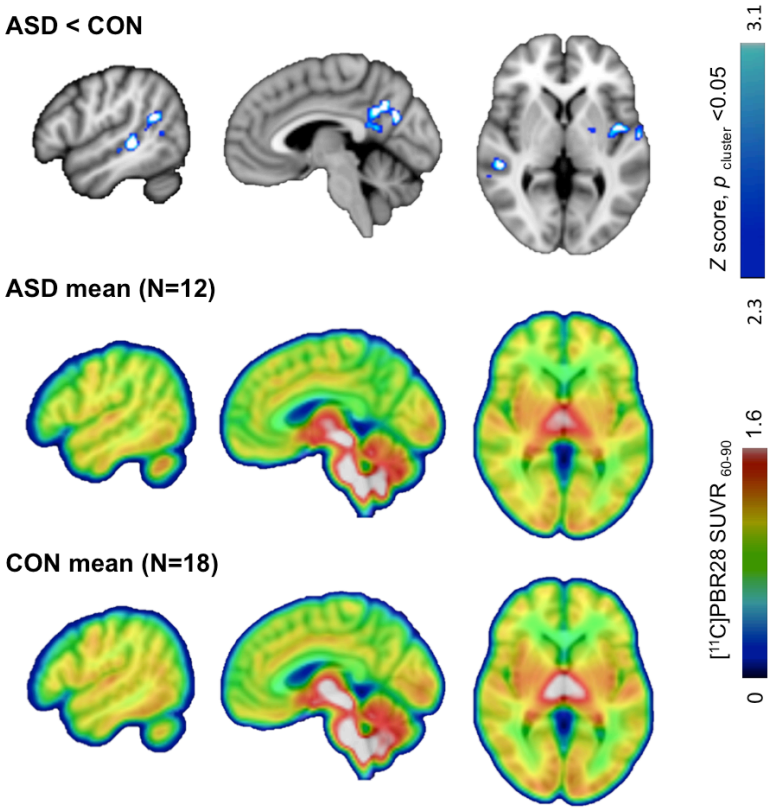

Figure 1: Statistical maps for between group comparison showing areas with decreased TSPO expression in males with ASD (top), mean [^{11}C]PBR28 $SUVR_{60\text{-}90}$ maps in adult males with ASD (middle) and in CON males (bottom).

References:

[1] Voineagu et al. [2011] *Nature* 474(7351):380-4, [2] Izquierdo-Garcia et al. [2014] *Journal of Nuclear Medicine*, 55(11):1825–1830. [3] Ladefoged et al. [2017] *Neuroimage* 147:346-359 [4] Loggia et al. [2015] *Brain*, 138(Pt 3):604-15 [5] Zurcher et al. [2015] *NeuroImage Clinical*, 7:409-14 [6] Notter et al. [2017] *Molecular Psychiatry*. 23(1):36-47 [7] Collste et al. [2017] *Molecular Psychiatry* 22, 850–856 [8] Albrecht et al. [2017] *Journal of Nuclear Medicine* 59(1):107-114 [9] Lyoo et al. [2015] *Journal of Nuclear Medicine* 56(5):701-6.

P24
Dopamine D1 receptor availability is not associated with delusional ideation measures of psychosis proneness

Granville J. Matheson[1], Pontus Plavén-Sigray[1], Anaïs Louzolo[2], Predrag Petrovic[2], Simon Cervenka[1]

1. *Department of Clinical Neuroscience, Centre for Psychiatry Research, Karolinska Institutet and Stockholm Health Care Services, Stockholm County Council, Stockholm, Sweden*
2. *Department of Clinical Neuroscience, Karolinska Institutet, Stockholm, Sweden*

Introduction:

The dopamine system is centrally implicated in the pathophysiology of schizophrenia. There is a wealth of evidence for elevations of presynaptic dopamine levels in striatum (1), including in at-risk populations prior to onset (2). The role of the dopamine D1 receptor (D1R) in this condition is not well understood, and there have only been a handful of studies reported showing inconsistent results. A parsimonious interpretation of these studies is that the D1R may be increased in unmedicated patients, and decreases following antipsychotic treatment. One study suggests that D1R elevations may even be present in those at high genetic risk for the disorder (3). Psychosis proneness can be measured as a continuous trait in the general population, for which the Peters Delusion Inventory (PDI), measuring delusional ideation, is a reliable, valid and commonly used psychometric instrument (4). We therefore investigated whether D1R availability is associated with delusional ideation in healthy controls.

Materials and Methods:

The dataset consists of three cohorts of individuals from four separate data collections. 76 individuals were measured with PET using [^{11}C]SCH23390, examining BP_{ND} in dorsolateral prefrontal cortex (DLPFC) and striatum, calculated using the simplified reference tissue model with cerebellar grey matter as reference. 69 of these individuals completed the PDI (4). 184 individuals completed the Temperament and Character Inventory (TCI), of whom 52 also underwent PET measurements (5). This study consisted of an exploratory and a confirmatory component. In the exploratory component, we created a new measure of psychosis proneness from items of the spiritual transcendence subscale of the TCI (TCI-ST-DP), and evaluated its psychometric reliability, convergent validity and association with D1R availability. In the confirmatory component, we performed a replication study of the association between the TCI-ST-DP and D1R availability observed in the exploratory analysis, and evaluated the association of PDI scores and [^{11}C]SCH23390 BP_{ND} in two cohorts. For the confirmatory studies, we made use of Bayesian inference, allowing for more nuanced conclusions than a traditional analysis might allow.

Results:

The TCI-ST-DP scale was found to show acceptable reliability (Cronbach's α=0.76), and convergent validity was demonstrated by its association with PDI scores (r=0.64). In a sample of 24 individuals, we showed a strong negative association between TCI-ST-DP and BP_{ND} in both ROIs (standardised beta=0.5 for DLPFC; 0.6 for striatum). In the confirmatory studies, we first performed a replication study of the former TCI-ST-DP results in a new cohort, finding moderate to strong evidence in favour of the null hypothesis compared to the previous estimates for both DLPFC (BF_{0R}=5.5) and striatum (BF_{0R}=10.5). Comparing BP_{ND}

with PDI scores in one cohort, we found moderate to strong evidence in favour of the null hypothesis (BF_{01}>6), and parameter estimation suggested little to no association between BP_{ND} and PDI scores. We performed Bayesian parameter updating to evaluate this hypothesis in the other cohort, leading to results consistent with this interpretation. Final parameter estimates showed that across the entire PDI scale, DLPFC BP_{ND} would be expected to change by only 6.5%.

Discussion/Conclusion:

Although our original exploratory analysis showed promising results, subsequent confirmatory analyses provide strong evidence that there is little to no association between delusional ideation measures of psychosis proneness and D1R availability in healthy controls. If an increase in D1R can be confirmed in schizophrenia patients, our results suggest that this increase may occur at the onset of the disorder, or may be associated with specific behavioural or genetic aspects of psychosis proneness other than delusional ideation.

Acknowledgements:

We thank the staff of the PET group at Karolinska Institutet for their assistance during this study.

References

1. Howes OD, Kambeitz J, Kim E et al. [2012] Arch. Gen. Psychiatry 69:8.
2. Howes OD, Montgomery AJ, Asselin M et al. [2011] Arch. Gen. Psychiatry 66:1.
3. Hirvonen J, van Erp TGM, Huttunen J et al. [2006] Am. J. Psychiatry 163:10
4. Peters E, Joseph S, Day S et al. [2006] Schiz Bulletin 30:4
5. Cloninger CR, Svarakic DM and Pyrzbeck TR [1993] Arch. Gen. Psychiatry 50:12

P25
Elevated raphe 5-HT$_{1A}$ binding is associated with gray matter diffusion entropy changes in temporal and frontal lobes.

Karl D Spuhler[a], Mala Ananth[b], Elizabeth Bartlett[a], Christine DeLorenzo[b], Ramin Parsey[b], Chuan Huang[a,b,c]

[a] Stony Brook University Department of Biomedical Engineering; [b] Stony Brook University Medical Center Department of Psychiatry; [c] Stony Brook University Medical Center Department of Radiology

Introduction:

A rich system of projections from the raphe nuclei supplies serotonin to higher brain regions, including the frontal and temporal lobe areas widely implicated in mood disorders. Previously published PET studies suggest that differences in raphe 5-HT$_{1A}$ binding can serve as biomarkers of both bipolar[1] and major depressive disorders[2], as well as a moderating factor in treatment response[3,4].

Recently, we published diffusion tensor imaging (DTI) MRI data which suggest that patients with bipolar disorder exhibit micro-organizational changes in cortical regions of the temporal lobe[5]. Therein, diffusion entropy, a measure of heterogeneity in a distribution of values, was found to be markedly lower in patients with bipolar disorder than in age- and sex-matched controls.

Previous studies have demonstrated morphological changes in gray matter related to serotonergic transport in various pathologies[6-8]. Here, we provide evidence for a connection between our gray matter findings and the implicated role of raphe 5-HT$_{1A}$ in mood disorders. We show that elevated binding to the raphe 5-HT$_{1A}$ receptor is correlated with reduced diffusion entropy throughout the gray matter regions of the temporal and frontal lobes.

Materials & Methods:

Data for this retrospective analysis were obtained from our concluded PET and MRI study of bipolar disorder neurophysiology. Selection criteria for this specific analysis were: available BP$_F$ data, an MRI scan obtained on the same Siemens Trio 3T scanner, and PET and MRI scans having been performed within 30 days. Data from 18 individuals (6 bipolar patients and 12 healthy controls) were included.

120-minute dynamic [11C]-CUMI PET data were acquired on a Siemens ECAT HR+ scanner. Raphe region of interests were determined by thresholding, after registering subject scans onto a mean binding map consisting of 52 previously scanned healthy subjects[9]. PET data were binned into 21 frames, motion-corrected and co-registered to the reference MRI scan. BP$_F$ data were estimated using likelihood estimation in graphical analysis[10] with input functions determined using either repeated arterial sampling or a validated simultaneous estimation algorithm[11], making use of a single blood sample. A 64-direction DTI sequence was used to determine diffusion entropy in the frontal and temporal lobe gray matter (segmented using FreeSurfer 5.3).

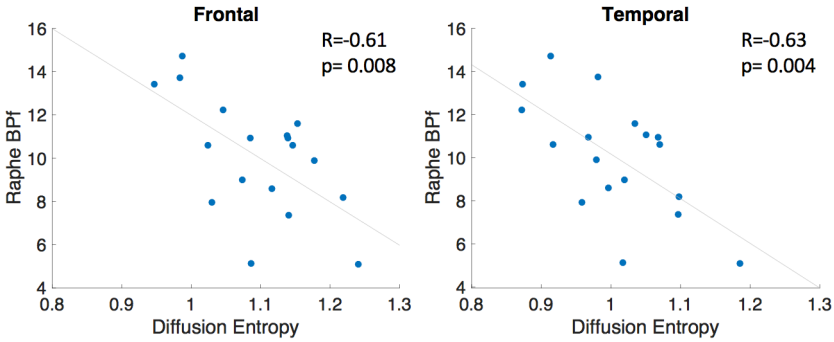

Pearson correlation was performed in SPSS to assess the relationship between diffusion entropy and raphe 5-HT_{1A} BP_F.

Results:

We observed statistically significant correlations between raphe 5-HT_{1A} binding and diffusion entropy in the frontal and temporal lobe gray matter (Figure 1). Partial correlation correcting for age and sex yielded similar results (frontal: p=0.024; temporal p=0.033). In both instances, greater raphe 5-HT_{1A} binding was correlated with lower diffusion entropy, agreeing with our previous findings of lower gray matter entropy[5] and elevated 5-HT_{1A}[1] in bipolar disorder.

Discussion:

Our data are an interesting addition to published findings of serotonin-related changes in gray matter. While 5-HT_{1A} receptors are expressed both pre- and post-synaptically, those found in the raphe are overwhelmingly pre-synaptic[3], acting to limit serotonin transmission. Diffusion entropy is a novel metric and reflects the homogeneity of voxel-wise diffusion values in the region considered. In this sense, a lower entropy is indicative of a more homogenous structure, while a higher entropy indicates larger structural variations.

We previously reported that diffusion entropy is significantly lower in patients with bipolar disorder in comparison to matched controls[5] which we speculate is indicative of altered fine-scale organization of cortical matter. In this work, we show evidence, in a combined population of patients with bipolar disorder and healthy controls, that such changes throughout the frontotemporal brain are associated with elevated 5-HT_{1A} binding in the raphe. While published data have demonstrated changes in gray matter volume in relation to pathology, this finding is the first DTI-predicated analysis of gray matter to suggest possible anatomical and functional differences that relate to serotonergic transmission.

References:

1. Sullivan GM, Ogden RT, Oquendo MA, et al. 2009. *Biological psychiatry.*66(3):223-230.
2. Kaufman J, Sullivan GM, Yang J, et al. 2015. *Neuropsychopharmacology.*40(7):1692-1699.
3. Parsey RV, Olvet DM, Oquendo MA, et al. 2006. *Neuropsychopharmacology.* 31(8):1745-1749.
4. Lan MJ, Hesselgrave N, Ciarleglio A, et al. 2013. *Synapse.*67(11):773-778.
5. Spuhler K, Bartlett E, Ding J, et al. 2018. Synapse. 72(2)
6. Frodl T, Koutsouleris N, Bottlender R, et al. 2008. *Molecular psychiatry.* 13(12):1093-1101.
7. Wassink TH, Hazlett HC, Epping EA, et al. 2007. *Archives of General Psychiatry.*64(6):709-717.
8. Pillai RL, Malhotra A, Rupert DD, et al. 2018. *Human brain mapping.*.
9. DeLorenzo C, Delaparte L, Thapa-Chhetry B, et al. 2013 *Frontiers in psychiatry.*4:5.
10. Parsey RV, Ogden RT, Mann JJ. 2003. *Journal of Cerebral Blood Flow & Metabolism.*23(12):1471-1478.
11. Ogden RT, Zanderigo F, Choy S, et al. 2010. *Journal of Cerebral Blood Flow & Metabolism.*30(4):816-826.

P26
Evaluation of [^{18}F]-FEPPA as neuroinflammation PET radiotracer in a LPS injected mice model.

Nicolas Vignal[1,2], **Carine San[2]**, Fortune Hontonnou[2], Thibaut Gelé[2], Xavier Declèves[1,3], Laure Sarda-Mantel[4,5], Salvatore Cisternino[1,6], Benoît Hosten[1,2], Nathalie Rizzo-Padoin[1,2]

[1]Variabilité de Réponse aux Psychotropes, Université Paris Descartes, Inserm UMR-S 1144, Paris, France ; [2]Unité Claude Kellershohn, Hôpital Saint-Louis, Assistance Publique – Hôpitaux de Paris (AP-HP), Paris, France ; [3]Hôpital Cochin, AP-HP, Paris, France ; [4]Médecine nucléaire, Hôpital Lariboisière, AP-HP, Paris, France ; [5] Biomarqueurs cardiovasculaires, Université Paris Diderot, Inserm UMR-S 942, Paris, France ; [6]Hôpital Necker – Enfants Malades, AP-HP, Paris, France.

Introduction:

[^{18}F]-FEPPA is a second generation radioligand of 18kDa translocator protein (TSPO) used in PET (Positron Emission Tomography) imaging as a biomarker of neuroinflammation. Neuroinflammation is known as a major factor in the pathophysiology of many neurodegenerative diseases. Indeed, TSPO PET studies have been conducted and showed an increase in TSPO signal in patients with Alzheimer disease, Parkinson disease or multiple sclerosis. To our knowledge, [^{18}F]-FEPPA has been already used to study neuroinflammation in humans and rats studies [1] but not in mice. The aim of the study was to evaluate [^{18}F]-FEPPA in mice with neuroinflammation induced by intraperitoneal injection of lipopolysaccharide (LPS).

Materials and Methods:

[^{18}F]-FEPPA was prepared as previously described in the literature [1] with minor changes to optimize the process. 12-week-old C57Bl/6 mice (n = 11) were used in the study and were divided in two groups (controls and LPS). To induce neuroinflammation, the LPS group (n = 6) received an intraperitoneal injection of *Salmonella enterica* serovar Typhimurium LPS (5 mg/kg) 24 hours prior to CT/PET imaging. All mice received a dynamic scan of 2 hours after injection of [^{18}F]-FEPPA (9.9 ± 1.5 MBq) in the tail vein. Mice brain and blood were then extracted to evaluate TSPO expression by western blot and to study metabolism of [^{18}F]-FEPPA. Arterial input function was computed from plasma sampling and corrected for metabolism of the parent ligand. Time-activity curves (TAC) of the whole brain region were obtained after co-registration to an MRI-based atlas of the mice brain. TAC were then fitted to two-tissue compartment model (2TCM) and to two-tissue compartment model with vascular trapping (2TCM-1K) [2] to estimate kinetic parameters and total distribution volume for the radioligand. One-sided t-test was used to test the difference between the LPS mice and controls.

Results:

[^{18}F]-FEPPA was obtained in high chemical and radiochemical purity. The radiosynthesis time has been shortened to 49 min with a non-decay corrected yield at 28.8 ± 3.6 %. Metabolism study showed a faster metabolism in blood (60% of the parent fraction at 30 min) than in brain (85% of the parent fraction at 90 min). Also, only one radiometabolite has been detected in blood and in brain. TSPO is significantly overexpressed in whole brain of LPS injected mice (mean TSPO/GAPDH LPS: 0.93 vs. controls: 0.43; p = 0.004). Based on

the Akaike criterion, the 2TCM-1K provided a better fit than 2TCM. We observed in the whole brain of LPS mice a significant increase of V_T (LPS: 3.77 ± 0.41 vs. controls: 2.25 ± 0.44; p = 0.0001) and AUC (LPS: 15940 ± 1226 vs. controls: 11910 ± 934; p = 0.0032).

Discussion/Conclusion:

The increase of V_T and AUC can be explained by the elevation of TSPO expression in brain, suggesting that specific binding to TSPO is significantly higher in LPS group. These results demonstrate that [^{18}F]-FEPPA may be a useful tool to evaluate neuroinflammation in mice. Besides, single intraperitoneal injection of *Salmonella enterica* serovar Typhimurium LPS in mice provides a simple, non-invasive and reproducible neuroinflammation model.

References

[1] A. A. Wilson, A. Garcia, J. Parkes *et al.*, [2008], Nuclear Medicine and Biology, 35:305–314.

[2] G. Rizzo, M. Veronese, M. Tonietto *et al.*, [2014], J Cereb Blood Flow Metab, 34:1060–1069.

P27

Blood glucose levels interact with dopamine $D_{2/3}$ receptor availability at baseline and in presence of d-amphetamine inversely in patients with schizophrenia and in healthy volunteers. A [^{11}C]-(+)-PHNO PET study.

Sauerzopf U[1], Weidenauer A[1], Bauer M[1,2], Bartova L[1], Meyer B[1], Nics L[3], Philippe C[3], Pfaff S[3], Mitterhauser M[3,4], Lanzenberger R[1], Kasper S[1], Pezawas L[1], Wadsak W[3,5], Praschak-Rieder N[1], Willeit M[1]

(1) Medical University of Vienna, Department of Psychiatry and Psychotherapy, Division of General Psychiatry
(2) Medical University of Vienna, Department of Clinical Pharmacology
(3) Medical University of Vienna, Department of Biomedical Imaging und Image-guided Therapy, Division of Nuclear Medicine

(4) Ludwig-Boltzmann-Institute Applied Diagnostics, Vienna

(5) Center for Biomarker Research in Medicine CBmed, Graz

Introduction:

Patients with schizophrenia show increased insulin resistance in both, treated and medication-naïve states (Takayanagi et al. 2012; Chen et al. 2013). It has been suggested that deficiency of insulin receptors on dopaminergic midbrain neurons may play a role in the development of psychosis in schizophrenia (Caravaggio et al. 2015a), and that antipsychotic compounds prone to increase peripheral insulin resistance (Allison et al. 1999) confer part of their antipsychotic action via modulating of insulin signalling.

We have explored the relationship between blood glucose levels and dopaminergic neurotransmission with [11C]-(+)-PHNO and positron emission tomography (PET) in healthy volunteers and patients with schizophrenia.

Materials and Methods:

Eighteen (13m, 5f) young medication-naïve first episode patients with schizophrenia and 27 (14m, 13f) young healthy volunteers without prior exposure to psychostimulant drugs underwent an [^{11}C]-(+)-PHNO PET scan at baseline and a second scan approximately 1.5 hours after ingestion of 0.4 mg/kg bodyweight d-amphetamine sulfate. Non-displaceable [^{11}C]-(+)-PHNO binding potential (BP_{ND}) values were derived employing the simplified reference tissue model (SRTM2) using the cerebellar cortex as a reference region. Parametric maps (SPM) have been calculated employing PMOD 2.6. Utilizing a linear mixed effects model, we have analysed the dependency of radioligand BP_{ND} values on blood glucose measured at start of the PET Scan, disease status, and amphetamine ingestion.

Results:

Blood glucose levels were significantly higher in medication-naïve patients with schizophrenia than in healthy volunteers, at baseline as well as after d-amphetamine administration ($p < 0.0005$) indicating some degree of metabolic dysfunction in the patient collective. Administration of amphetamine had no significant effects on blood glucose levels in either group.

SPMs revealed two significant clusters in the left head of the caudate nucleus, comprising some of the ventral striatum, and the right substantia nigra / ventral tegmental area (SNVTA) (FDR corrected p-values < 0.01) indicating dependency of [^{11}C]-(+)-PHNO BP_{ND} values on the independent variables. At baseline, healthy volunteers displayed a positive relationship between blood glucose levels and [^{11}C]-(+)-PHNO BP_{ND} values ($p < 0.01$) which shifted to a negative relationship during the amphetamine-challenged condition ($p < 0.01$). In patients, however, at baseline, higher blood glucose levels were related to lower [^{11}C]-(+)-PHNO BP_{ND} values ($p < 0.01$). In the amphetamine condition, higher blood glucose levels were associated with higher [^{11}C]-(+)-PHNO BP_{ND} values.

In an uncorrected correlation, healthy volunteers displayed a moderate positive relationship between blood glucose levels and [^{11}C]-(+)-PHNO BP_{ND} values in the left head of the caudate (r: 0.48 $p < 0.05$) and the right SNVTA (r: 0.66, $p < 0.001$). No significant correlations were observed in the patient cohort or amphetamine challenged condition. However, changes in the direction of the correlations (as shown in the full mixed effects model) were observed.

Discussion:

[^{11}C]-(+)-PHNO BP_{ND} has been shown to be highly sensitive to changes in endogenous dopamine levels (Willeit et al. 2008), with some evidence that variance in unstimulated[^{11}C]-(+)-PHNO BP_{ND} values is in part reflecting endogenous dopamine levels (Caravaggio et al. 2014). In a previous study in healthy volunteers, insulin resistance was associated with higher [^{11}C]-(+)-PHNO BP_{ND} values, indicating lower levels of the endogenous ligand, dopamine (Caravaggio et al. 2015b). The negative correlation of blood glucose levels with [^{11}C]-(+)-PHNO BP_{ND} values in our patients (instead of positive correlations in healthy subjects) corroborates the hypothesis an alteration in the functional link between dopamine signalling and insulin functions in the SNVTA in psychosis.

References

Allison, D; Mentore, JL; Heo, M; Chandler, LP; Cappelleri, JC; Infante MC and Weiden PJ (1999). *Antipsychotic-Induced Weight Gain: A Comprehensive Research Synthesis*, American Journal of Psychiatry 156 : 1686-1696.

Chen, S.; Broqueres-You, D.; Yang, G.; Wang, Z.; Li, Y.; Wang, N.; Zhang, X.; Yang, F. and Tan, Y. (2013). *Relationship between insulin resistance, dyslipidaemia and positive symptom in Chinese antipsychotic-naive first-episode patients with schizophrenia*, Psychiatry Research 210 : 825 - 829.

Caravaggio, F.; Hahn, M.; Nakajima, S.; Gerretsen, P.; Remington, G. and Graff-Guerrero, A. (2015a). *Reduced insulin-receptor mediated modulation of striatal dopamine release by basal insulin as a possible contributing factor to hyperdopaminergia in schizophrenia*, Medical hypotheses 85 : 391-396.

Caravaggio, F.; Borlido, C.; Hahn, M.; Feng, Z.; Fervaha, G.; Gerretsen, P.; Nakajima, S.; Plitman, E.; Chung, J. K.; Iwata, Y.; Wilson, A.; Remington, G. and Graff-Guerrero, A. (2015b). *Reduced Insulin Sensitivity Is Related to Less Endogenous Dopamine at D(2/3) Receptors in the Ventral Striatum of Healthy Nonobese Humans*, International Journal of Neuropsychopharmacology 18 : pyv014-.

Caravaggio, F.; Nakajima, S.; Borlido, C.; Remington, G.; Gerretsen, P.; Wilson, A.; Houle, S.; Menon, M.; Mamo, D. and Graff-Guerrero, A. (2014). *Estimating Endogenous Dopamine Levels at D(2) and D(3) Receptors in Humans using the Agonist Radiotracer ((11)C)-(+)-PHNO*, Neuropsychopharmacology 39 : 2769-2776.

Willeit, M.; Ginovart, N.; Graff, A.; Rusjan, P.; Vitcu, I.; Houle, S.; Seeman, P.; Wilson, A. A. and Kapur, S. (2008). *First Human Evidence of d-Amphetamine Induced Displacement of a D2/3 Agonist Radioligand: A [11C]-(+)-PHNO Positron Emission Tomography Study*, Neuropsychopharmacology 33 : 279-289.

P28
Brain glucose uptake is modulated by the interaction between microglial activation and amyloid load: a longitudinal microPET study

Min Su Kang[1,2,3], Monica Shin[1,2], Maxime J. Parent[1], Sulantha Mathotaarachchi[1,2], Tharick A. Pascoal[1,2], Andrea L. Benedet[1], Joseph Therriault[1], Mira Chamoun[1], Melissa Savard[1], Antonio Aliaga[3], Gassan Massarweh[3], Jean-Paul Soucy[3], Serge Gauthier[1,2], A. Claudio Cuello[4], Pedro Rosa-Neto[1,2,3]

Translational Neuroimaging laboratory - McGill Centre for Studying in Aging[1], Brain Imaging Centre – Douglas Research Centre[2], McConnell Brain Imaging Centre – McGill University[3], Department of Pharmacology – McGill University[4],

Background:

The decline in regional brain metabolism in Alzheimer's disease (AD) has been evident in individuals with high level of abnormal aggregates of amyloid-beta proteins. In particular, the spatial agreement in amyloid plaque deposition and hypometabolism and longitudinal studies suggest that amyloidosis lead to hypometabolism. However, recent evidence suggests that neuroinflammation plays an intimate role in propagating the amyloidosis effects in the downstream cascade of AD pathophysiology. The new generation of positron emission tomography (PET) tracer specific for mitochondrial translocator protein (TSPO) in activated microglia allows precise investigation of neuroinflammation. Here, we employed 3 PET tracers, [^{18}F]AZD4694, [^{18}F]FDG, and [^{18}F]PBR06 for amyloidosis, metabolism, and neuroinflammation, respectively. We aim to study the effects of amyloidosis and neuroinflammation on brain metabolism in McGill-R-Thy1-APP transgenic (Tg) rat model of AD[1]. This model is unique to display full AD-like amyloid pathology without neurofibrillary tangles (NFTs) or cell deaths that are invariantly present in AD patients. Such platform using Tg animal model and imaging technique allows us to study the effects of amyloidosis and neuroinflammation on brain metabolism without confounding NFTs or cell deaths. Here, we hypothesize that amyloidosis and neuroinflammation have synergistic effects on brain metabolism in McGill-R-Thy-APP Tg compared to wild type (WT) animals.

Methods:

A total of age and gender matched 7 WT and 7 Tg rats was used. Each animal underwent longitudinal PET [^{18}F]AZD4694, [^{18}F]FDG, [^{18}F]PBR06, and MRI at 10 and 17 months old. All images were registered to individual MRI with lsq6. Then, they are normalized into sample average template using lsq12 with nonlinear transformations. [^{18}F]AZD4694 and [^{18}F]PBR06 images were acquired for 60 minutes emission scan with a concomitant bolus injection, which was followed by 10 minute transmission scan. [^{18}F]FDG image was acquired 50 minutes post-bolus injection for 20 minutes. [^{18}F]AZD4694 and [^{18}F]PBR06 binding potential map (BP_{ND}) using cerebellar grey matter as a reference region were generated using Simplified Reference Tissue Method (SRTM). [^{18}F]FDG SUVR was generated using pons as a reference region. For statistical analysis, we performed voxel-wise analysis using VoxelStats[2] to show the effect of [^{18}F]PBR06 BP_{ND} on [^{18}F]FDG SUVR using following model in each group. [^{18}F]FDG SUVR ~ [^{18}F]PBR06 BP_{ND}. Furthermore, [^{18}F]AZD4694 and [^{18}F]PBR06 interaction model was applied in Tg to investigate the synergistic effect of amyloidosis and neuroinflammation on brain metabolism: [^{18}F]FDG SUVR ~ [^{18}F]AZD4694 BP_{ND} * [^{18}F]PBR06 BP_{ND}.

Results:

WT showed only positive association between neuroinflammation and brain metabolism in neocortex and piriform cortex. Tg only showed negative association between neuroinflammation and brain metabolism in frontal cortex, cingulate cortex, temporal cortex, and dorsal entorhinal cortex at 10 months old. This association was present in somatosensory cortex, cingulate cortex, dorsal and ventral entorhinal cortex, perirhinal cortex, basal lateral amygdaloid nucleus at 17 months old. Furthermore, the interaction model revealed a negative synergistic effect between amyloidosis and neuroinflammation in neocortex driving the metabolic decline while positive synergistic effect was found in striatum and nucleus accumbens.

Conclusion:

Our results show that healthy aging display positive association between neuroinflammation and brain metabolism in neocortex. However, neuroinflammation is negatively associated with brain metabolism in the presence of amyloidosis in neocortex while positively associated in striatum and nucleus accumbens. Our study suggests that amyloidosis and neuroinflammation drive the metabolic decline in AD.

Figure1.

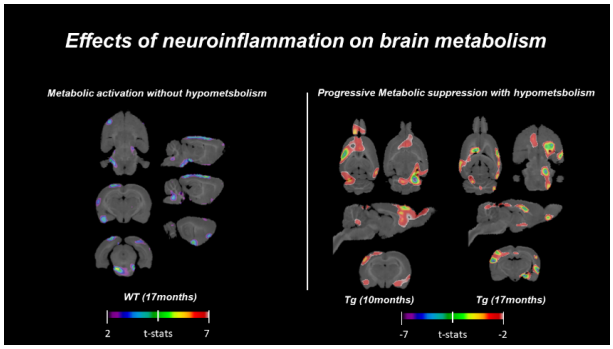

Figure2.

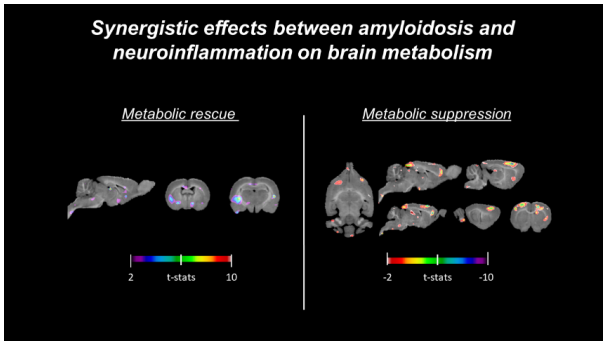

References:

4. Leon, Wanda Carolina, et al. [2010] "A novel transgenic rat model with a full Alzheimer's-like amyloid pathology displays pre-plaque intracellular amyloid-β-associated cognitive impairment." *Journal of Alzheimer's Disease* 20.1: 113-126.
5. Mathotaarachchi, Sulantha, et al. [2016] "VoxelStats: a MATLAB package for multi-modal voxel-wise brain image analysis." Frontiers in neuroinformatics 10: 20.

P29
Parametric maps of TSPO expression in a mouse model of epilepsy

Catriona Wimberley[1], Loc Nguyen[1], Charles Truillet[1], Raphael Boisgard[1], Viviane Bouilleret[1], Irène Buvat[1]

[1]Imagerie Moléculaire In Vivo (IMIV), UMR 1023 Inserm/CEA/Université Paris Sud - ERL 9218 CNRS, CEA/I2BM/SHFJ, Orsay, France

Introduction:

The translocator protein (TSPO) is of great interest as a biomarker for the study of diseases that have a component of neuroinflammation, such as epilepsy or Alzheimer's disease. TSPO-PET imaging can follow neuroinflammation using 18F-DPA714 (1), but for imaging in the mouse brain there are quantification challenges due to the small size of the structures causing partial volume effects. The small blood volume in the mouse makes it near impossible to do arterial sampling and there is always a low level of TSPO expression, so no reference region is available. Recently, a method to extract an image derived input function (IDIF) using factor analysis (FA) was developed for the mouse (2). The aim of this study was to investigate the impact of applying resolution recovery and noise removal followed by parameter estimation using a FA derived IDIF on regional and voxel wise parameter estimates for PET scans in a longitudinal study of a mouse model of epilepsy.

Materials and methods:

The model was induced by injection of kainic acid (KA) into the right dorsal hippocampus of adult male C57/Bl6 mice (n=7) (3). A dynamic 18F-DPA714 PET/CT (60 min) was performed at 4 time points: (i) baseline scan (BL, n=7), (ii) 7 days (KA7d, n=5), (iii) one month (KA1m, n=6) and (iv) 6 months (KA6m, n=7) after KA injection. Images were reconstructed using OSEM 2D. A 4D iterative deconvolution (15 iterations) and a temporal regularisation process (12 basis functions) were performed (4,5). The images were registered to an MRI atlas (6) and regional TACs extracted. FA was applied to each raw image (before resolution recovery and noise removal) (PIXIES, http://www.apteryx.fr/) (7) with 4 factors. Constraints were applied: (i) one factor with a similar shape to the IDIF derived from presaturation scans, (ii) all factors should be positive and (iii) have only one maximum (2). The extracted factors were converted to radiotracer concentration by normalising the sum of the factors against the activity in the whole scan. The factor showing the earliest peak was used as the IDIF.

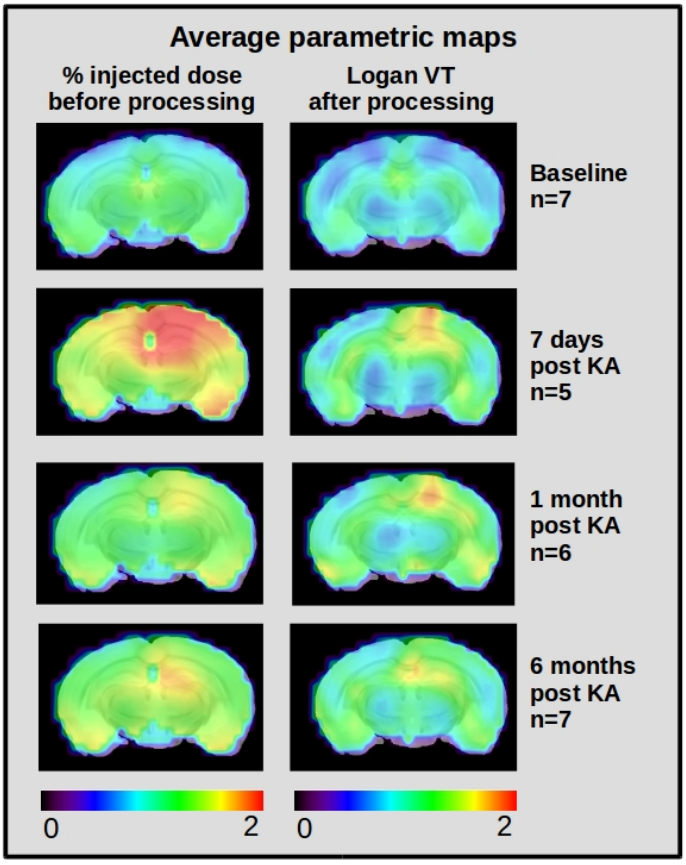

***Figure 1**: Average parametric maps for %ID before processing (left) and Logan VT using the IDIF with processed images (right).*

The IDIF was used in a Logan analysis of the processed images to estimate the total volume of distribution (VT) regionally and voxel wise for parametric maps. For comparison, the percent injected dose (%ID) was calculated. For the %ID maps, each raw dynamic image was summed from 22.5-60 minutes and normalised to the ID. For regional %ID values, extracted TACs were summed (0-60 minutes) and normalised to the ID. For both the VT and %ID, regional estimates were averaged over the animals at each time point, as were the maps. A student t-test was applied regionally between the post KA time points and baseline.

Results:

Figure 1 shows average parametric maps at each time point. The left hand column shows the %ID without partial volume correction or noise removal. The right hand column shows VT maps after resolution recovery and noise removal. Table 1 shows the regional values with significant differences ($p<0.05$) between each time point and baseline in yellow.

%ID	Amygdala L	Amygdala R	Cer cortex L	Cer cort R	Occipital L	Occipital R	Pons	Hipp L	Hipp R
Baseline	1.5 (0.15)	1.5 (0.16)	1.6 (0.13)	1.6 (0.15)	1.0 (0.13)	1.0 (0.11)	1.6 (0.17)	1.3 (0.15)	1.3 (0.11)
7 days	1.8 (0.17)	1.9 (0.16)	2.0 (0.2)	2.0 (0.18)	1.6 (0.18)	1.9 (0.20)	1.8 (0.16)	1.9 (0.18)	1.7 (0.17)
1 month	1.5 (0.35)	1.6 (0.33)	1.6 (0.3)	1.7 (0.31)	1.3 (0.22)	1.5 (0.23)	1.6 (0.28)	1.5 (0.22)	1.4 (0.20)
VT	**Amygdala L**	**Amygdala R**	**Cer cortex L**	**Cer cort R**	**Occipital L**	**Occipital R**	**Pons**	**Hipp L**	**Hipp R**
Baseline	0.7 (0.13)	0.8 (0.11)	1.0 (0.11)	1.0 (0.15)	0.7 (0.11)	0.7 (0.09)	0.7 (0.11)	0.6 (0.08)	0.6 (0.08)
7 days	0.7 (0.04)	0.9 (0.11)	1.0 (0.06)	1.0 (0.06)	0.9 (0.10)	1.1 (0.21)	0.7 (0.05)	0.8 (0.13)	1.0 (0.04)
1 month	0.8 (0.11)	0.9 (0.16)	1.0 (0.08)	1.1 (0.11)	0.8 (0.11)	0.91 (0.13)	0.7 (0.05)	0.8 (0.08)	0.9 (0.07)

***Table 1**: Regional parameter estimates: top %ID and bottom VT: mean (SD).*

Discussion and conclusions:

The voxel wise maps in Fig 1 show that partial volume effects have been greatly reduced after processing and it is possible to see the location of neuroinflammation more precisely. On top of that, using the %ID without any image processing shows a significant difference of tracer uptake in unexpected regions (Table 1), especially at 7 days (no pathology in the cerebellum or pons expected in this model), which is not observed when using the IDIF for VT estimation. This is reflected in the %ID image at 7 days that shows a global increase of tracer uptake. For PET studies in the mouse brain, resolution recovery, noise removal and kinetic modelling greatly enhance regional and voxel wise mapping of parameter estimates, and considerably facilitate longitudinal studies.

Acknowledgements:

Catriona Wimberley is supported by the CEA-Enhanced Eurotalents: FP7 Marie Sklodowska-Curie COFUND Program: 600382

References:

1. James M, Belichenko N, Nguyen TV et al. [2015] J. Nucl. Med., 56:311-6

2. Wimberley C, Nguyen L, Fontyn Y et al. [2017] IEEE-MIC

3. Bouilleret V, Ridoux V, Depaulis A et al. [1999] Neuroscience, 89:717-29

4. Reilhac A, Charil A, Wimberley C et al. [2015] Neuroimage, 118:484-93

5. Wimberley C, Nguyen L, Fontyn Y et al. [2016] IEEE-MIC

6. Dorr A, Lerch JP, Spring S, et al., Neuroimage [2008] 42:60-9

7. Frouin F, DeCesare A, Bouchareb Y, et al. [1996] Phys. Med. Biol., 44:2289

P30
[^{11}C]-(*R*) PK11195 uptake in sporadic vestibular schwannoma and a comparison of two referencing approaches

D Lewis[1, 2], R Hinz[1], E Agushi[1, 2], O Pathmanaban[2], A Jackson[1], AT King[2], D Coope[1, 2]

[1]Wolfson molecular imaging Centre, University of Manchester; [2]Manchester centre for clinical neurosciences (MCCN)

Introduction:

Previous studies have utilised the simplified reference tissue model (SRTM) to demonstrate specific binding of the TSPO PET ligand [^{11}C]-(R)PK11195 within CNS tumours such as glioma[1]. Total cerebellum or cerebellar grey matter (GM) has been used as a 'pseudo-reference' input, on the assumption that the cerebellum is devoid of specific binding[1, 2], but there has been no comparative study investigating [^{11}C]-(*R*)PK11195 specific binding within cerebellopontine angle tumours such as sporadic vestibular schwannoma, which are anatomically adjacent to the cerebellum itself. It is unclear in this tumour group whether use of the cerebellum or an internally derived reference region obtained through a supervised cluster analysis[2] is most appropriate. The purpose of this pilot study was to assess tracer uptake kinetics and specific binding of [^{11}C]-(*R*) PK11195 within sporadic vestibular schwannoma, and to compare the specific binding potential (BP_{ND}) values derived using either a cerebellar GM or supervised cluster analysis reference input.

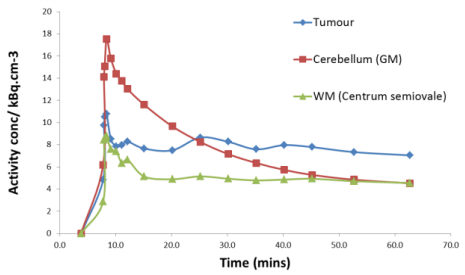

Figure 1: Decay corrected tissue time-activity curves (TACs) from tumour ROI (blue), cerebellar GM (red) and WM of centrum semiovale (green) in a patient with a large left sided VS.

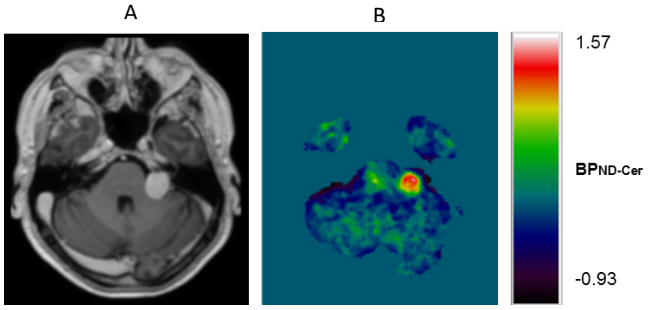

Figure 2: a) Post contrast T1W MRI displaying large left sided VS**; b)** Parametric map of $BP_{ND\text{-}Cer}$ from same patient.

Materials and methods:

Nineteen patients with sporadic VS of different tumour sizes underwent contrast-enhanced structural MRI and dynamic [^{11}C] -(*R*) PK11195 PET. Tissue time-activity curves (TACs) were extracted from the tumour ROI as defined on the post-contrast MR, cerebellar GM and a ROI placed within the centrum semiovale bilaterally. Parametric maps of specific binding potential (BP_{ND}) were then generated using either an atlas defined grey matter reference input region ($BP_{ND\text{-}Cer}$) or an internally derived reference region($BP_{ND\text{-}Sup}$) obtained using a supervised cluster analysis. Derived values of BP_{ND} within the tumour ROI calculated using the two methods were compared, and a pixelwise comparison was also undertaken for voxels both within the tumour and normal brain through Bland–Altman analysis. To determine if BP_{ND} values within the cerebellum showed variability across the cohort of patients, $BP_{ND\text{-}Sup}$ values for both ipsilateral and contralateral cerebellar GM region were extracted and compared using a ROI based analysis.

Results:

TAC analysis demonstrated that all tumours displayed WM type uptake kinetics (See Figure 1). Bland Altman analysis demonstrated that the mean difference between derived $BP_{ND\text{-}Cer}$ and $BP_{ND\text{-}Sup}$ within the tumour ROI was 0.042 (95% CI -0.024 to 0.108), and both referencing approaches demonstrated increased BP_{ND} with increasing tumour size (see Figure 2 and 3).

Pixel-wise Bland-Altman analysis demonstrated that in 10/19 patients the cerebellum pseudo-reference region derived ($BP_{ND\text{-}Cer}$) estimates closely matched the $BP_{ND\text{-}Sup}$ values. Whilst in four patients there was a small systematic underestimation of $BP_{ND\text{-}Cer}$ relative to $BP_{ND\text{-}Sup}$, and within five patients there was a small systematic overestimation of $BP_{ND\text{-}Cer}$ compared to use of the internally derived reference region; these differences did not change the overall size related increase in tumour BP_{ND}.

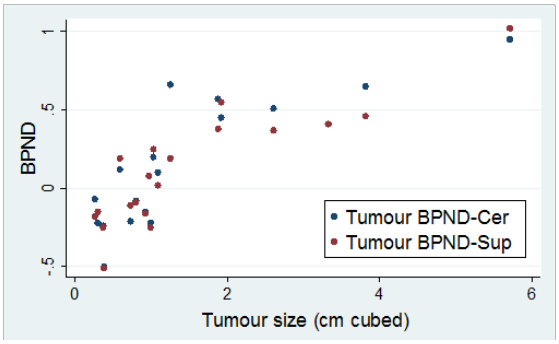

Figure 3: Scattergraph showing correlation of tumour size with mean tumour $BP_{ND\text{-}Cer}$ (Rho=0.83, p<0.001) and $BP_{ND\text{-}Sup}$ (Rho=0.85, p<0.001).

Discussion:

This pilot study has demonstrated for the first time that there is uptake of [11C] -(R) PK11195 within sporadic vestibular schwannoma, and that these tumours display WM type uptake kinetics. Our analysis suggests that a cerebellar input region can be used when investigating pathology within the cerebellopontine angle, but that derived specific binding values should be cross-validated where possible using either an internally derived reference region or an arterial input function analysis.

Acknowledgements: Thank you to Cancer research UK (CRUK) for their financial support.

References:

1. Su Z, Roncaroli F, Durrenberger PF, et al (2015) The 18-kDa mitochondrial translocator protein in human gliomas: an 11C-(R)PK11195 PET imaging and neuropathology study. J Nucl Med 56(4):512–7

2. Turkheimer FE, Edison P, Pavese N, Roncaroli F, Anderson AN, Hammers A, Gerhard A, Hinz R, Tai YF, Brooks DJ (2007) Reference and target region modeling of [11C]-(R)-PK11195 brain studies. J Nucl Med 48(1):158–67

P31
Title: Effects of Lithium Monotherapy on 5-HT1A [^{11}C]-CUMI-101 Binding in Bipolar Depression

Elizabeth Bartlett[1], Mala Ananth[2], Chuan Huang[3,4], R. Todd Ogden[5], Christine DeLorenzo[3], Ramin V. Parsey[3]

1. Biomedical Engineering, Stony Brook University; 2. Neurobiology & Behavior, Stony Brook University; 3. Psychiatry; Stony Brook University. 4. Radiology; Stony Brook University. 5. Biostatistics; Columbia University

Introduction:

Despite being the first line of therapy for bipolar depression (BPD), little is known regarding lithium monotherapy's therapeutic mechanism of action. Of the systems potentially implicated in lithium's effects, the serotonin-1A receptor (5-HT1A) is thought to play a critical role in the antimanic and antidepressant effects of lithium.[1] Rodent studies suggest that lithium monotherapy decreases 5-HT1A receptor densities in the frontal cortex and hippocampus,[1-4] but not in the dorsal raphe nucleus,[5] suggesting that lithium treatment has a specific effect on post-synaptic 5-HT1A receptors, but not somatodendritic 5-HT1A receptors. Here we examined for the first time to our knowledge, the *in vivo* impact of lithium on 5-HT1A binding with [^{11}C]-CUMI-101 in humans. Additionally, we investigated the relationship between the change in 5-HT1A binding with lithium treatment and clinical response. Our primary hypothesis was that the previously reported effect of upregulated 5-HT1A binding in patients with BPD relative to controls[6-8] would normalize in post-synaptic regions (e.g. the frontal cortex and hippocampus), while somatodendritic 5-HT1A binding in the raphe nucleus would remain unchanged. That is, 5-HT1A binding would downregulate post-synaptically, but not somatodendritically, in response to lithium. Further, we hypothesized that lithium-induced post-synaptic 5-HT1A downregulation would also associate with better response to treatment.

Materials & Methods:

120-minute [^{11}C]-CUMI-101 scans were obtained from 21 medication-free patients with BPD in a current depressive episode (9 female) on a Siemens ECAT HR+ scanner. Patients then underwent eight weeks of lithium monotherapy, where 14 BPD patients completed treatment and were given a second [^{11}C]-CUMI-101 scan, post-treatment. Arterial sampling was performed to generate metabolite-corrected input functions[10] or a validated simultaneous estimation algorithm was used to compute the arterial input function using a single venous or arterial blood sample.[9] Likelihood estimation in graphical analysis (LEGA)[11] was used to obtain reference region free estimates of BP_F (B_{max}/K_D) in the 19 pre-treatment and 13 post-treatment scans in the patients with BPD where arterial sampling was successfully performed. The simplified reference tissue method (SRTM) was also applied to obtain blood-free estimates of BP_{ND} (V_T-V_{ND}/V_{ND}) with cerebellar grey matter as the reference region[10] in the full 21 pre-treatment BPD patient, 14 post-treatment BPD patient sample. Lithium treatment response was assessed using the percentage change from pre-to-post treatment in 24-item Hamilton Depression Rating Scale (HDRS-24) scores.[12] In a model with sex as a covariate, the raphe nucleus was examined first as an *a priori* region of interest and then 12 additional post-synaptic regions were considered.[6]

Results:

Post-lithium-treatment BP_F or BP_{ND} was not significantly different from the pre-treatment scans in patients with BPD in the raphe nucleus or in post-synaptic regions (Figure 1). Further, we did not find a significant relationship between the change in [^{11}C]-CUMI-101 BP_F or BP_{ND} pre-to-post treatment and lithium treatment response in any region.

Discussion:

Contrary to our primary hypotheses, our findings indicate that lithium did not significantly alter post-synaptic 5-HT1A binding levels in bipolar depression; and that post-synaptic 5-HT1A binding alterations during treatment were not found to associate with treatment responses. Despite pre-clinical evidence implicating cortical 5-HT1A downregulation in chronic lithium monotherapy,[2-4] in this sample of patients with bipolar depression, lithium does not appear to act through modulation of post-synaptic 5-HT1A densities. However, concordant with our somatodendritic 5-HT1A hypothesis and the preclinical literature,[5] raphe nucleus 5-HT1A binding was unaltered by lithium treatment and did not associate with the treatment's antidepressant effect. Future studies with increased sample sizes are needed to corroborate these findings and better understand the 5-HT1A receptor's role in the lithium mechanism of action.

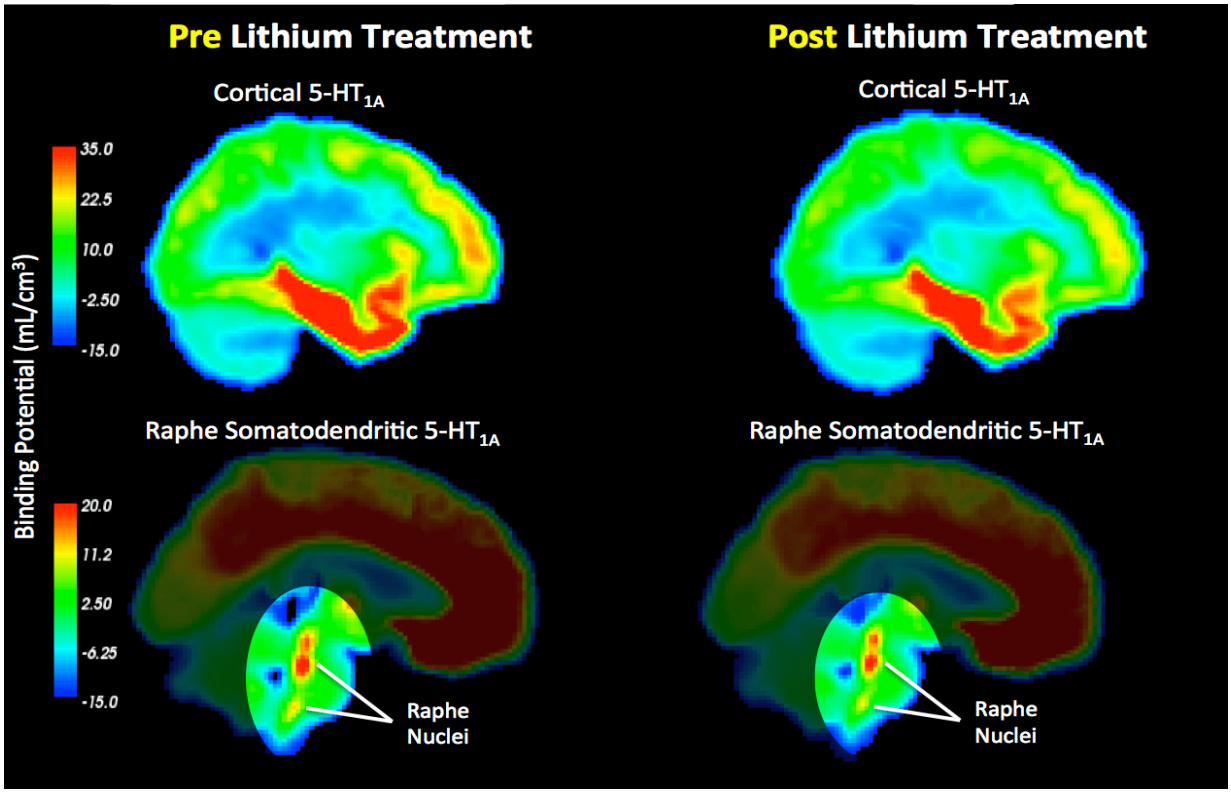

Figure 1: Group-wise averaged BP_F voxel maps displaying lithium effect on [11C]-CUMI-101 5-HT1A binding, where pre-treatment is in left pane and post-treatment is in right pane.

Acknowledgements:

The National Institute of Mental Health provided funding for this study (R01MH090276, PI: Ramin Parsey, MD, PhD). We would like to thank the Yale PET Center for their work in radiotracer synthesis, PET scanning, and blood analysis. We would also like to thank the Center for Understanding Biology using Imaging Technology (CUBIT) image analysts at Stony Brook University for their work in data importing, analysis, and quality control.

References:

1 Bauer M, Adli, M, Baethge C, *et al*. [2003], *The Canadian Journal of Psychiatry,* **7**:440-448
2 Hotta I, Yamawaki S, and Segawa T. [1986], *Neuropsychobiology,* **1**:19-26
3 Mizuta T and Segawa T. [1988], *Jpn J Pharmacol,* **2**:107-113
4 Odagaki Y, Koyama T, Matsubara S, *et al.* [1990], *Journal of psychiatric research,* **3**:271-277
5 McQuade R, Leitch M, Gartside E & Young, A. H. [2004], *J Psychopharmacol,* **4**:496-501
6 Sullivan G, Ogden R, Oquendo M, *et al.* [2009], *Biological psychiatry,* **3**:223-230
7 Parsey R, Ogden R, Miller J, *et al.* [2010], *Biological psychiatry,* **2**:170-178
8 Hesselgrave N and Parsey R. [2013] *Phil. Trans. Series B, Biological sciences,* **1615**:20120004
9 Ogden R, Zanderigo F, Choy S, *et al*. [2010] *JCBFM,* **4**:816-826
10 Milak M, DeLorenzo C, Zanderigo F, *et al.* [2010], *JNM* **12**:1892-1900
11 Ogden R, Parsey R and Mann J. [2002] NeuroImage **16**:73.
12 Hamilton M [1960]. *Journal of neurology, neurosurgery, and psychiatry,* **1**:56-62

P32
Effects of Lithium Monotherapy on [^{11}C]DASB Binding to the Serotonin Transporter in Bipolar Depression

Mala Ananth[1], Elizabeth Bartlett[2], Francesca Zanderigo[3], Chuan Huang[4,5], R. Todd Ogden[6], Christine DeLorenzo[4], Ramin V. Parsey[4]

1. Neurobiology & Behavior: Stony Brook University; NY; 2. Biomedical Engineering; Stony Brook University; NY; 3. Psychiatry; Columbia University, NY; 4. Psychiatry: Stony Brook University, NY; 5. Radiology; Stony Brook University, NY; 6. Biostatistics; Columbia University, NY.

Introduction:
Abnormalities of the serotonergic system are thought to play a critical role in mood disorders including bipolar depression (BPD). Lithium is the first line of therapy and one of the few effective treatments in BPD. It has been hypothesized that lithium works by enhancing serotonergic transmission[1-3]. Whether these mechanisms are via increases in serotonin (5-HT) release (through the 5-HT$_{1A}$ receptor) or changes to the 5-HT transporter (5-HTT) uptake remain to be seen. Preclinical studies have shown increases in 5-HTT density (B_{max}) in cortical regions following chronic lithium treatment[3], but not in subcortical regions known to be affected in BPD and major depression, including midbrain and amygdala[4-6]. Here we examined the effects of lithium monotherapy on 5-HTT *in vivo* binding potential in BPD. Additionally, we investigated whether there was a relationship between change in 5-HTT binding following lithium treatment and clinical response. We hypothesized that: a) lithium monotherapy would increase cortical binding towards control levels[4,6], and b) lithium-induced upregulation in 5-HTT binding would associate with better clinical response.

Materials and Methods:
16 medication-free patients with BPD (7 females) currently in a depressive episode were imaged using the 5-HTT tracer [^{11}C]DASB. BPD subjects then received eight weeks of standardized monotherapy with lithium. Twelve subjects completed therapy and were imaged again using [^{11}C]DASB. Scans were acquired on a Siemens ECAT HR+ scanner for 90 minutes after tracer injection. Arterial blood samples[7] were collected to calculate the metabolite-corrected arterial input function, or a validated simultaneous estimation algorithm was used to compute the arterial input function using a single venous or arterial blood sample[8]. Time activity curves were fit with likelihood estimation in graphical analysis (LEGA)[9] to calculate [^{11}C]DASB total distribution volume (V_T), from which the outcome measure V_T/f_P was calculated using the tracer plamsa free fraction f_P (BPD pre-treatment = 16, BPD post-treatment = 12), as it has been shown that no brain region is completely devoid of [^{11}C]DASB binding[10]. To determine reference region-free estimates of the binding potential (BP_F ($(V_T-V_{ND})/f_P$) and BP_{ND} ($(V_T-V_{ND})/V_{ND}$); BPD pre-treatment = 12, BPD post-treatment = 10) we used a novel data-driven hybrid deconvolution approach (HYDECA)[11] that, with the full input function and PET data, determines subject-specific V_{ND} (non displaceable distribution volume) estimates. Lithium treatment response was determined using the 24-item Hamilton Depression Rating Scale (HDRS-24)[12]. In models, midbrain, amygdala and anterior cingulate cortex were examined as a priori regions of interest. The parcellation of these regions are based on separately acquired MRI images.

Results:
The data revealed no significant differences between pre- and post-lithium treatment scans using V_T/f_P, BP_F, or BP_{ND} in any regions. Additionally, we found no significant relationship between change in 5-HTT binding (V_T/f_P, BP_F, and BP_{ND}) pre-to-post lithium treatment and treatment response.

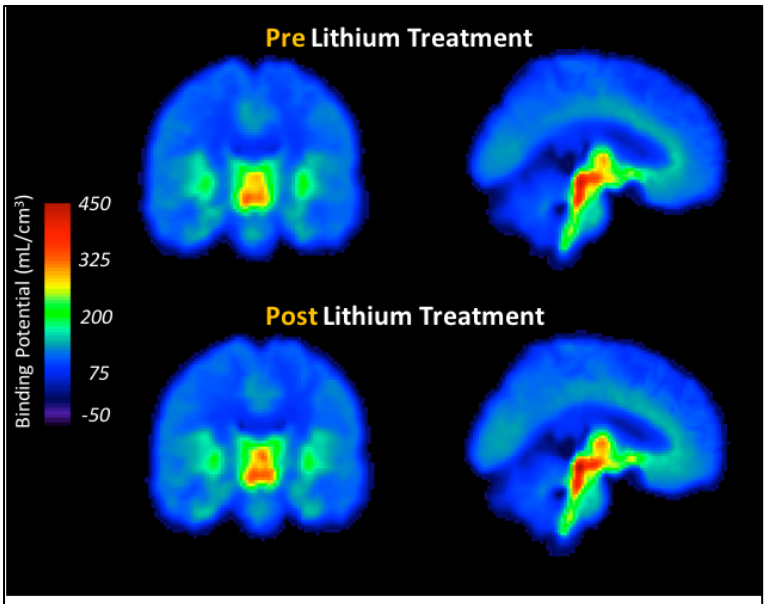

Figure 1: Groupwise averaged V_T/f_P voxel maps displaying effects of lithium on 5-HTT [^{11}C]DASB binding

Discussion/Conclusion:

To our knowledge, this is the first report of the effects of lithium on the serotonergic system, *in vivo.* These findings suggest that lithium does not directly act on 5-HTT to mediate treatment response. It is possible that lithium's primary mechanism of action is via other serotonergic proteins, or that its effects remain distinct from the serotonergic system. Future studies with increased sample sizes are needed to further corroborate these findings and better understand the effect of lithium on the serotonergic system.

Acknowledgements:

The National Institute of Mental Health provided funding for this study (R01MH090276, PI: Ramin Parsey, MD, PhD). We would like to thank the Yale PET Center for their work in radiotracer synthesis, PET scanning, and blood analysis. We would also like to thank the Center for Understanding Biology using Imaging Technology (CUBIT) image analysts at Stony Brook University for their work in data importing, analysis, and quality control.

References:

1. Bauer M, Adli M, Baethge C, et al. [2003]. Canadian J of Psych. 48(7):440-448.
2. Carli M, Afkhami-Dastjerdian S, Reader TA. [1997] Neurochem Res. 22(4):427-435.
3. Carli M, Reader TA. [1997] Synapse. 27(1):83-89.
4. Miller JM, Everett BA, Oquendo MA, Ogden RT, Mann JJ, Parsey RV. [2016] Synapse. 70(1):24-32.
5. Miller JM, Hesselgrave N, Ogden RT, et al. [2013] Biol Psych. 74(4):287-295.
6. Oquendo MA, Hastings RS, Huang YY, et al. [2007] Arch Gen Psych. 2:201-208.
7. Ogden RT, Ojha A, Erlandsson K, et al. [2007] J Cereb Blood Flow Metab. 1:205-217.
8. Ogden RT, Zanderigo F, Choy S. et al. [2010] J of Int. Soc of Cereb Blood Flow. And Metab. 4:816-826.
9. Ogden RT. [2003]. Stat Med. 22(22):3557-3568.
10. Parsey RV, Kent JM, Oquendo MA, et al. [2006] Biol Psych. 9:821-828.
11. Zanderigo F, Mann JJ, Ogden RT. [2017] PloS one. 5:e0176636.
12. Hamilton M. [1960] J Neurol Neurosurg Psych. 1:56-62.

P33
Radioisotope Specific Resolution Kernel Improves Estimation Of Cerebral Perfusion From Dynamic [^{15}O]H_2O-PET Images In Patients With Glioblastoma

Georgios Krokos[1,2], Jose Anton-Rodriguez[1], Ibrahim Djoukhadar[1], Ethan Du-Crow[1], Matthew Walker [1,3], Neil Thacker[1], Julian Matthews[1], Alan Jackson[1], Marie-Claude Asselin[1]

[1] *Wolfson Molecular Imaging Centre (WMIC), Division of Informatics, Imaging and Data Sciences, The University of Manchester, Manchester, UK*.

[2] *School of Imaging Sciences & Biomedical Engineering, Faculty of Life Sciences and Medicine, King's College London, London, UK*.

[3] *Department of Clinical and Experimental Neurology, Institute of Neurology, London, UK.*

Introduction:

Radiotracer delivery to the brain depends on cerebral perfusion which is best measured using [^{15}O]H_2O-PET. The accuracy and noise of PET images can be improved by using i) complementary frame reconstruction (CFR) [1] and ii) resolution modelling (RM). The positron range for ^{15}O is four times longer than for ^{18}F. In this work, we assessed the synergistic effects of using an ^{15}O specific resolution kernel for RM [2] in combination with CFR on dynamic [^{15}O]H_2O-PET images from an Esser phantom and of the brain of healthy volunteers and patients with glioblastoma.

Methods:

The ^{15}O specific resolution kernel was theoretically estimated from published data [3] and measurements of printed ^{18}F point sources [2] using a method experimentally validated using ^{68}Ga. A modified Esser phantom was filled with [^{15}O]H_2O at a 4:1 contrast and scanned on the HRRT PET scanner. The list-mode data were reconstructed using OP-OSEM with RM using the default ^{18}F kernel or the estimated ^{15}O kernel for both the conventional independent frame reconstruction (IFR) and CFR for up to 20 iterations. Dynamic data from six healthy volunteers and four patients with glioblastoma acquired on the HRRT for 5 min after bolus injection of [^{15}O]H_2O (357-606 MBq) were also reconstructed using both algorithms and kernels. Pharmacokinetic analysis was performed using the single-tissue compartment model with the sampled arterial blood input function assuming negligible blood volume.

Results:

CFR improved the accuracy of low count phantom images over IFR at the expense of increasing noise (**figure 1**). Reconstruction with the^{15}O kernel further improved accuracy in the hot cylinders by 12% for CFR and 30% for IFR compared to the^{18}F kernel. Accuracy in the cold cylinder remained unchanged for CFR but improved by 15% for IFR. Noise was also reduced when using the ^{15}O kernel, especially for CFR. The four reconstructions yielded similar perfusion estimates for whole grey and white matter, with subtle improvements in contrast (**figure 2**). In the necrotic core perfusion decreased by up to 31% for IFR and 8% for CFR when using the ^{15}O kernel.

Conclusion:

Compared to the ^{18}F kernel, reconstruction of [^{15}O]H_2O-PET images using an ^{15}O kernel resulted in more accurate radioactivity concentrations and perfusion images with lower noise. The improvements were more pronounced for IFR but CFR with the ^{15}O kernel provided the most accurate images.

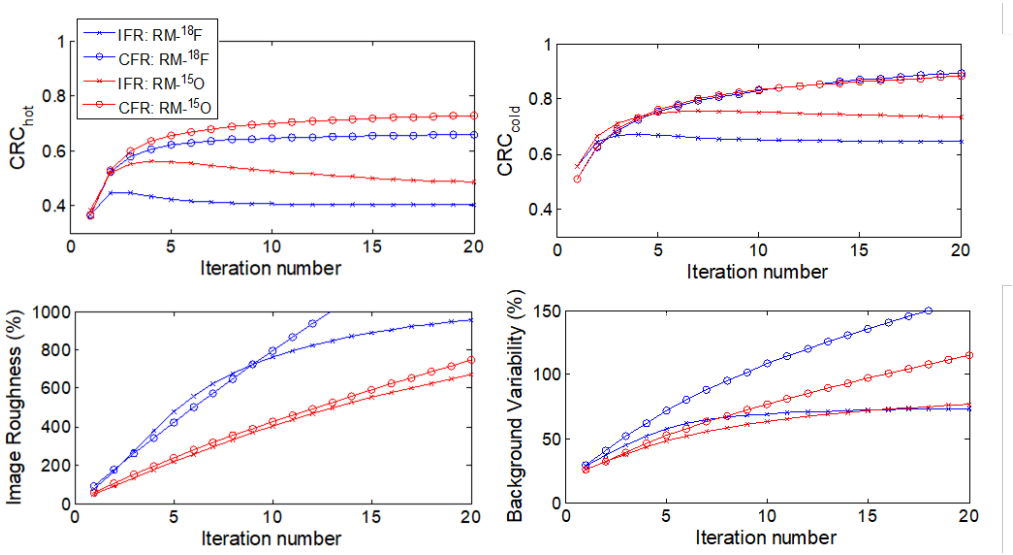

Figure 1: Contrast recovery coefficient (CRC) in the 16-mm hot cylinder (top left) and 25-mm cold cylinder (top right) of the Esser phantom, and background noise defined by image roughness (bottom left) and background variability (bottom right) against number of iterations for the 4 different reconstructions. Early 5-sec frame with 0.9-M counts plotted.

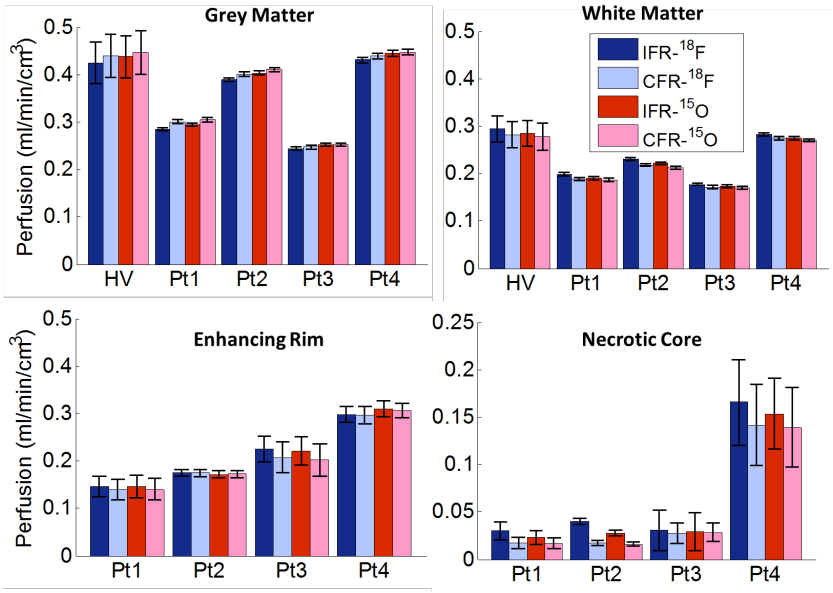

Figure 2: Perfusion estimates from the regional analysis in 6 healthy volunteers and 4 glioblastoma patients. *Error bars* indicate the standard deviation between volunteers and the standard error on the parameter estimate for the patients. *12th iteration* used.

Acknowledgements

To Maria Feldmann, Matthias Koepp, Gerard Thompson, Natale Quartuccio and Erjon Agushi for acquisition of the clinical [^{15}O]H_2O-PET data and to the CRUK and EPSRC Cancer Imaging Centre in Cambridge and Manchester and EURIPIDES for financial support.

References

[1] Hong I., Cho S. Michel CG *et. al.* [2014] Phys. Med. Biol. 59(18): 5441-55.
[2] Kotasidis F.A., Angelis G.I., Anton-Rodriguez J. *et. al.* [2014] Med. Phys. 41(5): 052503.
[3] Cal-González J., Herraiz J.L., España S. *et. al.* [2013] Phys. Med. Biol. 58(15): 5127-52.

P34
TSPO imaging in High Grade Glioma - a multitracer PET, MRI and neuropathology study

E Agushi[1,2], R Hinz[1], D Lewis[1,2], F Roncaroli[1,2], A Jackson[1], D Coope[1,2]

[1]Wolfson molecular imaging Centre, University of Manchester; [2]Salford Royal NHS Foundation Trust, Manchester Centre for Clinical Neurosciences (MCCN)

Introduction:

High grade gliomas (HGG) continue to have a poor survival outcome despite substantial efforts and modern advances in surgery, radio- and chemotherapy. The mean survival is 11.1-14.6 months for tumours of WHO grade IV, post-surgical resection and Stupp protocol and yet, tumour recurrence is still the norm. [1]

HGG have a disrupted blood-brain barrier (BBB) which causes contrast enhancement (CE) on conventional MR scan, although aggressive tumour phenotype has also been found extending beyond the CE, raising questions about how far the surgical resection should extend. The disrupted BBB in the very heterogeneous HGGs may also impact on the reliability of brain PET imaging, although specific tracers with high diffusivity and affinity binding to tumoural cells can overcome these difficulties.

The translocator protein (TSPO) is an 18 kDa mitochondrial molecule (previously known as Peripheral Benzodiazepine Receptor), largely studied in neuroinflammation disorders and recently of growing interest in neuro-oncology [2,3]. Its role and function remain still to be elucidated but it certainly plays a crucial role in steroidogenesis, porphyrine metabolism and complex cellular mechanisms [4]. The aim of our study is to investigate whether uptake of [11C](R)-PK11195 (a PET radiotracer for TSPO) can predict the site of tumour recurrence in HGG and whether [11C]Methionine can offer a better delineation of tumour margin for resection.

Methods:

Eleven patients (mean age 60 ± 16, M/F=5/6) with lesions suspicious of HGG on clinical MRI were recruited. All patients underwent contrast-enhanced structural and diffusion tensor MR imaging as well as dynamic [11C]-(R)PK11195 and [11C]Methionine PET scans before treatment. Parametric maps of [11C]-(R)PK11195 binding potential (BP) were generated using simplified reference tissue modelling with cerebellar grey matter as reference tissue. BP parametric maps were co-registered to post-contrast T1, fractional anisotropy(FA) and apparent diffusion coefficient (ADC) maps, and finally to [11C]Methionine summed image. Tumour was delineated as a T/N threshold above 1.4 on co-registered [11C]Methionine PET scans and a further regions delineating gadolinium enhancement and necrosis within the tumour were manually delineated. Co-registered MR/PET images were used to guide targeted tumour biopsies which were used to compare directly with histology.

Results:

All confirmed HGG patients demonstrated a vivid uptake of [11C](R)-PK11195 (mean BP of whole tumour delineated using 1.4 [11C]Methionine threshold: 2.95 range 1.7-4.1; maximal BP: 4.12 range 2.1-6.2). [11C]Methionine uptake extended beyond gadolinium enhancement almost in all HGG cases, and regions of higher uptake did not spatially

correlate to hottest [11C](R)-PK11195 areas (Figure 1). A significant correlation was found instead between increased [11C]Methionine uptake and mean diffusivity values (pairwise correlation coeficient = 0.69, $p<0.01$).

TSPO antibody stain of hot TSPO targeted biopsies showed clearly higher values on optical density(OD) measurements, compared to cold uptake targeted areas within the tumour, confirming the correlation of [11C](R)-PK11195 PET imaging and histology (hot biopsies mean OD 4.3% vs 1.3% cold, $p<0.001$) (Figure 2). Further 3D histology modelling, colouring with multiple antibodies (Iba1, IDH1 and CD31) showed the localisation of TSPO in tumour hottest regions is mainly in the neoplastic cells rather than microglia or endothelium.

Tumour recurrence was found to coincide with the regions of higher [11C](R)-PK11195 uptake in 2 of the patient's clinical MR scans.

Discussion:

[11C]-(R)PK11195 has the potential to detect early recurrence and provides information complimentary to perfusion metrics in early detection of recurrence. Methionine offers a better tumour delineation which could lead to more extensive surgical resections and better chances for survival.

Figure 1. A. Post-contrast MR scan showing enhancing lesion (yellow arrow) B. Co-registered [11C](R)-PK11195 parametric map C. Co-registered [11C]Methionine add image D. Delineation of the hottest areas on [11C](R)-PK11195 (yellow) and [11C]Methionine (red).

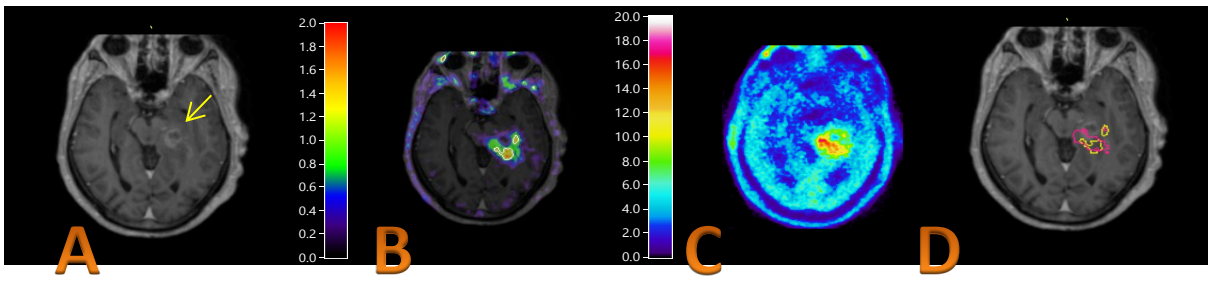

Figure 2. Scatter plot of cold (blu circles) and hot (red squares) biopsies showing the mean BP of the 7 voxel VOI region where biopsy was taken (x-axis) and OD of TSPO quantification expressed in % of the overall surface (y-axis).

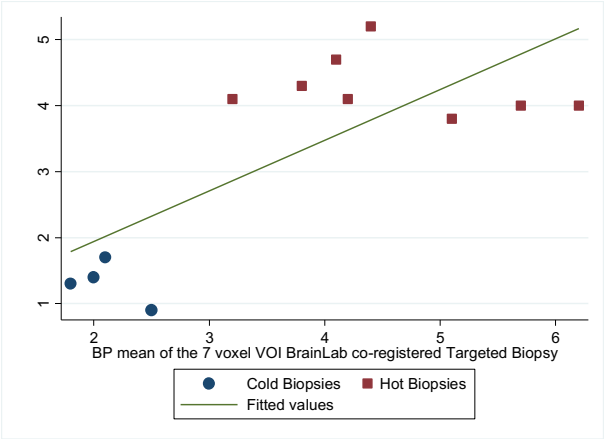

References

1. Stupp R, Mason WP, van den Bent MJ et-al. N. Engl. J. Med. 2005;352 (10): 987-96.
2. Papadopoulos V, Baraldi M, Guilarte TR et-al. Trends Pharmacol Sci. 2006 Aug;27(8):402-9
3. Su, Z.; Roncaroli, F.; et al. (2015) J. Nucl. Med. 56: 386-391
4. Roncaroli F, Su Z, Herholz K et-al. Clin Transl Imaging. 2016;4:145-156.

P35
[^{11}C]*(R)*-PK11195 PET imaging of microglial activation in recent onset and chronic schizophrenia

Catherine J Gregory[1,2], Silke Conen[1,2], Rainer Hinz[1], Jose Anton-Rodriguez[1], Bill Deakin[2], Peter S Talbot[1]

[1]Wolfson Molecular Imaging Centre and [2]Neuroscience and Psychiatry Unit, Division of Neuroscience and Experimental Psychology, School of Biological Sciences, Faculty of Biology, Medicine and Health, University of Manchester, Manchester Academic Health Science Centre, Manchester, UK

Introduction:

Neuroinflammation may be implicated in the pathophysiology of schizophrenia[1] and can be studied *in vivo* with positron emission tomography (PET) using radioligands specific for the 18kDa translocator protein (TSPO) which is upregulated in activated brain microglia. Recent studies have shown a lack of clear evidence for elevated TSPO in schizophrenia, and even suggest reductions in drug-free patients.[2,3] In the present study, we aimed to determine if there are differences in TSPO across illness stages using PET with [^{11}C]*(R)*-PK11195 in recent onset and chronic schizophrenia compared to healthy controls.

Materials and Methods:

Mostly-medicated patients (27 male, 14 female), with DSM-IV schizophrenia, schizoaffective or schizophreniform disorders were recruited with either recent onset (<5 yr; n=20; age 24.2±5.1 yr) or chronic (>10 yr; n=21; age 46.3±6.4 yr) illness. Age- and sex-matched healthy control groups were recruited contemporaneously (n=9 and n=10, respectively). All underwent a 60 minute dynamic PET scan with [^{11}C](*R*)-PK11195 (704±60 MBq) using a High Resolution Research Tomograph (Siemens/CTI). A grey matter cerebellum input function was used to generate parametric maps of BP_{ND} using the SRTM. A maximum probability brain atlas was applied to the parametric brain maps to provide mean BP_{ND} in anterior cingulate (ACC), prefrontal (PFC), orbitofrontal (OFC) and parietal cortices, putamen, brainstem and thalamus.

Results:

Chronic patients were significantly older than recent onset patients. The two groups were well matched for sex, smoking status, PANSS positive (15±6 vs 15±6) and negative (12±4 vs 13±5) scores. We found no significant difference in BP_{ND} between patients and controls either in the ACC (2-way ANOVA, main effect of diagnostic group $F_{1,56}$ = 0.121, p=0.730) or across all ROIs ($F_{1,56}$=0.821, p=0.369). A significant main effect of age group ($F_{1,56}$ = 13.492, p=0.001) but no significant age group*diagnostic group interaction ($F_{1,56}$ = 0.641, p=0.427) confirmed that the higher BP_{ND} in chronic patients (Figure 1) is due to their older age rather than illness stage.

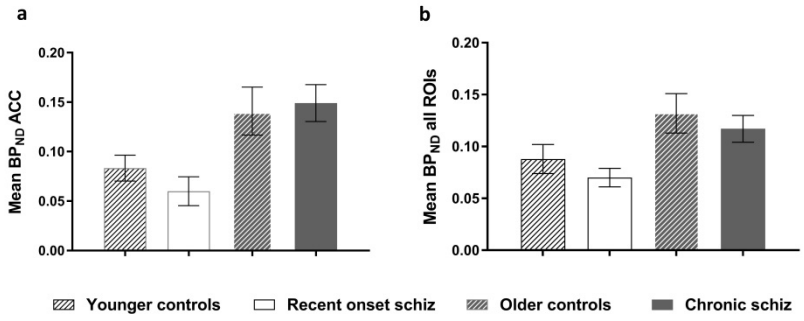

Fig 1. [^{11}C]*(R)*-PK11195 BP_{ND} in recent onset and chronic schizophrenia compared to separate age- and sex- matched controls. **(a)** Mean BP_{ND} in the ACC; **(b)** Mean BP_{ND} across all ROIs

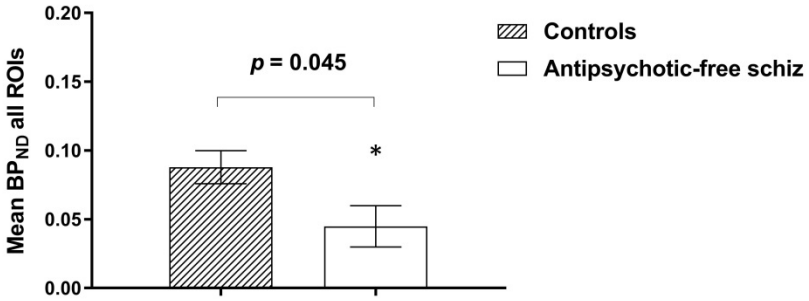

Figure 2: Mean [^{11}C]*(R)*-PK11195 BP_{ND} across all ROIs in antipsychotic-free recent onset schizophrenia (n=6) compared to age- and sex-matched controls (n=9)

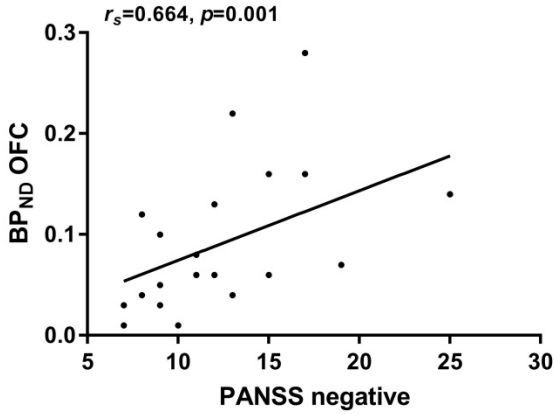

In a subgroup of antipsychotic-free recent onset patients (n=6), mean BP_{ND} across all ROIs was significantly lower compared to controls (n=9) ($F_{1,13}$=4.935, p=0.045; Figure 2).

In chronic patients, there was a significant positive correlation between PANSS negative score and BP_{ND} in the PFC (r_s=0.533, p=0.013) and OFC (r_s=0.664, p=0.001) (Figure 3), with a trend in the ACC (r_s=0.404, p=0.070). There was no correlation between PANSS negative score and BP_{ND} in recent onset patients.

Discussion:

We found no evidence for elevated TSPO in mostly-medicated patients with schizophrenia or related disorders compared to healthy controls or across illness phases. Our finding of lower BP_{ND}, suggestive of lower microglial activation, in antipsychotic-free recent onset patients is consistent with recent studies.[2,3] It may represent an underactive immune response in schizophrenia, which is ameliorated by antipsychotic medication. Our results also show an association between microglial activation in frontal regions and negative symptoms in chronic schizophrenia, which could indicate a harmful immune response in those with chronic illness. However, the possibility of pseudo-negative symptoms induced by antipsychotic medication in these patients cannot be excluded.

Acknowledgements:

The study was funded by a Medical Research Council Experimental Medicine Challenge Full Grant (MR/K020803/1).

References:

[1]Muller N, Weidinger E, Leitner B et al. [2015], Front. Neurosci., 9:372

[2]Collste K, Plaven-Sigray P, Fatouros-Bergman H et al. [2017], Mol. Psychiatry, 22:850-6

[3]Di Biase MA, Zalesky A, O'Keefe G et al. [2017], Transl. Psychiatry, 7, e1225

P36
Volumetric measures in selected areas of the prefrontal cortex are associated with amphetamine-induced dopamine release: Implications for psychosis research.

Matthäus Willeit (1), Ana Weidenauer (1), Ulrich Sauerzopf (1), Martin Bauer (1,2), Lucie Bartova (1), Sarah Pfaff (3), Bernhard Meyer (1), Markus Mitterhauser (3,4), Siegfried Kasper (1), Pablo Rusjan (5), Lukas Pezawas (1), Rupert Lanzenberger (1), Nicole Praschak- Rieder (1)

(1) Medical University of Vienna, Department of Psychiatry and Psychotherapy, Division of General Psychiatry
(2) Medical University of Vienna, Department of Clinical Pharmacology
(3) Medical University of Vienna, Department of Biomedical Imaging und Image-guided Therapy, Division of Nuclear Medicine

(4) Ludwig Boltzmann Institute Applied Diagnostics, Vienna, Austria

(5) PET Imaging Centre, Centre for Addiction and Mental Health, University of Toronto, Canada

Introduction:
It is long known that patients with schizophrenia exhibit and increase in the behavioural and neurochemical response to dopamine-releasing agents such as d-amphetamine. Much less is known on pathogenic elements leading to this hypersensitivity. Repeated administration of d-amphetamine to healthy subjects elicits an increase in the behavioural response to the drug. This phenomenon, known as 'sensitization', is paralleled by an increase in d-amphetamine-induced reductions in dopamine $D_{2/3}$ receptor radioligand binding, a semi-quantitative measure of the amount of dopamine released into the extracellular space as a response to the drug. In view of the parallels to findings in psychotic states, it has been proposed that d-amphetamine-induced sensitization may serve as a model for alterations in brain dopamine transmission in schizophrenia. We tested this model by studying in parallel d-amphetamine-induced dopamine release in drug-naïve patients with first episode psychosis and healthy volunteers prospectively undergoing d-amphetamine sensitization. Since it is known that the prefrontal cortex is an important physiological regulator of subcortical dopamine function, we analyzed prefrontal cortical volumetric measures for their relationship to d-amphetamine-induced changes in $D_{2/3}$ receptor binding.

Materials and Methods:

Measures of amphetamine-induced dopamine release were obtained using the dopamine $D_{2/3}$ receptor agonist radioligand [^{11}C]-(+)-PHNO positron emission tomography (PET). [^{11}C]-(+)-PHNO binding potential (BP_{ND}) values were derived in dopamine-rich regions of interest (ROIs) using the simplified reference tissue model (SRTM2) as implemented in PMOD analysis software. ROIs were drawn manually and by using the analysis software ROMI. [^{11}C]-(+)-PHNO BP_{ND} values measured in scans without intervention were compared to those measured in scans performed 90 to 120 min after ingestion of 0.04 mg/kg bodyweight d-amphetamine. Relative changes in BP_{ND} values were calculated as $(BP_{ND}^{baseline} - BP_{ND}^{amphetamine}) / BP_{ND}^{baseline} * 100$). The study sample consisted of medication-naïve (or minimally exposed and drug free) and patients with first episode schizophrenia and healthy subject who underwent prospective sensitization to d-amphetamine by repeated (four to five times) ingestion of the drug. Volumetric measures were derived from T1-magnetic resonance (MR) images using Freesurfer 6.0. analysis software. Data were analyzed using analysis of variance and Pearson product moment correlation coefficients.

Results:

Data showed significantly larger d-amphetamine-induced changes in patients with schizophrenia when compared to healthy volunteers before sensitization. No differences were found to schizophrenia patients after healthy volunteers had been sensitized to d-amphetamine. Analysis of variance showed significant interactions between diagnostic group and selected areas of the prefrontal cortex (mainly those forming the inferior frontal gyrus) and d-amphetamine induced changes [^{11}C]-(+)-PHNO BP_{ND} values in substantia nigra / ventral tegmental area (SN/VTA). These interactions were mainly explained by strong inverse correlations between inferior frontal gyrus volume and d-amphetamine effects on dopamine release in healthy volunteers before sensitization. These correlations disappeared (or became slightly positive) in sensitized healthy volunteers and were not found in patients with schizophrenia.

Discussion:

Our data strongly support the validity of d-amphetamine-induced sensitization as an experimental tool for studying the pathogenesis of schizophrenia. Further, they lend strong support to the hypothesis that a dysfunction in prefrontal cortical regulation of subcortical dopamine function constitutes an important element in the pathogenesis of hyper-dopaminergic states in schizophrenia. Our data would have profited from a prospective approach on volumetric data in sensitization. Still, for the first time to our knowledge, they identify a specific mechanism in a specific neuronal pathway – inhibition of SN/VTA by thee inferior prefrontal gyrus – as a plausible candidate mechanism for hyperdopaminergic states in schizophrenia.

Ackowledgements:

This study was funded by the Austrian Science Fund [FWF P23585-B09], the Anniversary Fund of the Austrian National Bank [ONB 16723], the Medical Scientific Fund of the Mayor of Vienna (Medizinisch-Wissenschaftlichen Fonds des Bürgermeisters der Bundeshauptstadt Wien) [BMF 15189], and the Vienna Science and Technology Fund [WWTF CS15-033] granted to M.W.

References:

Laruelle M [2000] Brain Res Brain Res Rev 31(2-3):371-84

Willeit M, Ginovart N, Graff A et. al. [2008] Neuropsychopharmacology 33(2):279-89

Weidenauer A, Bauer M, Sauerzopf U et.al. [2017] Int J Neuropsychopharmacol. 20(1):1-10

P37

Abstract withdrawn

P38
Oxytocin modulation of resting state regional cerebral blood flow: comparing the effects of intranasal and intravenous methods of administration

Y. Paloyelis[1], F. Zelaya[1], N. Mazibuko[1], S. Maltezos[2], U. Schuschnig[3], S. Williams[1]

[1] *King's College London, Department of Neuroimaging, Institute of Psychiatry, Psychology and Neuroscience, London, UK*

[2] *King's College London, Department of Forensic and Neurodevelopmental Science, Institute of Psychiatry, Psychology and Neuroscience, London, UK*

[3] *PARI GmbH, Gräfelfing, Germany*

Introduction:

Animal and human studies highlight the role of the central oxytocin (OT) system in social cognition and behaviour and the potential of synthetic OT to treat social impairment in neuropsychiatric disorders.[1,2] Yet the translational potential of efforts to evaluate the therapeutic efficacy of synthetic OT is impeded by a lack of sufficient understanding of its central actions and of the pathways though which it may exert its effects in the living human brain. Human studies rely almost exclusively on nasal sprays, assuming a privileged nose-to-brain route of transport, despite the lack of direct or indirect evidence to this effect. In this study, we compared two methods of intranasal administration: a standard spray vs the PARI *SINUS* nebulizer (expected to maximize OT deposition in the olfactory region - putatively involved in direct nose-to-brain transport). We further compared intranasal administration to intravenous administration to examine the extent to which intranasal effects might be solely explained by peripheral signalling or result from a privileged route of transport to the brain.

Materials and Methods:

Sixteen healthy young male adults were recruited for a double-blind, within-subject, placebo-controlled, crossover study. We visualized and quantified OT-induced changes in regional cerebral blood flow (rCBF)[3], and hence neuronal activation, while participants rested, eyes open, in a 3T scanner. We used pulsed-continuous arterial spin labelling to obtain a series of eight 8-min CBF maps (in standard physiologic units - mL blood/100 g tissue/min) spanning about 100 min post OT administration. Each participant received 40 IU of OT intranasally (through a spray or a nebulizer), 10 IU of OT intravenously, as well as placebo in 4 pseudo-randomly allocated visits in a triple dummy design. Blood samples for plasma OT quantification were collected at baseline and throughout the observation period. CBF maps were processed using previously described methods,[3] and we mapped the distribution of effects of synthetic OT at each time point using mass univariate voxel-by-voxel analysis in a series of paired sample t-tests on, allowing inferences regarding local regions. We used a cluster forming threshold: $P<.005$ and conducted cluster level inference using FWE correction $P<.05$.

Results:

The intranasal administration methods did not differ in their pharmacokinetic profiles in any of the parameters (C_{max}, T_{max}, AUC, k^h-1, $t_{1/2}$). As expected, when administered through the IV route, plasma OT levels were significantly elevated throughout the observation period, compared to the intranasal methods. Preliminary analyses demonstrated that despite the similar pharmacokinetic profiles, the two intranasal administration methods resulted in markedly different patterns of increases in rCBF (intranasal spray: anterior insula, superior frontal gyrus, superior temporal gyrus; nebuliser: robust increases in rCBF at the precuneus at multiple time points). These increases in rCBF could not be accounted by plasma levels of synthetic OT. However, administration of synthetic OT via intranasal sprays also resulted in significant decreases in rCBF over the amygdala and dorsal ACC, which could be explained by increases in plasma OT.

Discussion/Conclusion:

We provide new evidence supporting the hypothesis of a direct nose-to-brain pathway underlying intranasal OT effects in the human brain, as well as evidence suggesting that some of the effects of intranasal synthetic OT may be due to peripheral signalling. The different patterns of increases in rCBF between the two intranasal methods suggest that they may differ in the achieved bioavailability of OT in the brain. Higher OT deposition in the olfactory region might have resulted in an increased amount of OT reaching the brain. Our findings help illuminate the mechanisms of absorption of intranasal OT in humans and the identification of potentially more efficient intranasal administration methods compared to nasal sprays.

References:

1. Hammock, E. A. and Young, L. J. (2006). Oxytocin, vasopressin and pair bonding: implications for autism. *Philos Trans R Soc Lond B Biol Sci*., **361**(1476):2187-98.

2. Zink C.F. and Meyer-Lindenberg A. (2012). Human neuroimaging of oxytocin and vasopressin in social cognition. *Horm Behav.,* **61**(3):400-409.

3. Paloyelis, Y., Doyle, O., Zelaya, F., Maltezos, S., Williams, S., Fotopoulou, A., Howard, M. (2016). A spatiotemporal profile of in vivo cerebral blood flow changes following intranasal oxytocin in humans. *Biological Psychiatry*, **79**(8):693-705.

P39
First assessment of the P-glycoprotein substrate PET tracer [^{11}C]metoclopramide in healthy volunteers

Martin Bauer[1], Nicolas Tournier[2], Sylvain Auvity[2], Verena Pichler[3], Lukas Nics[3], Eva-Maria Klebermass[3], Marcus Hacker[3], Maria Weber[1], Markus Zeitlinger[1], Oliver Langer[1,3]

(1) *Medical University of Vienna, Department of Clinical Pharmacology, Vienna, 1090, Austria*

(2) *Imagerie Moléculaire In Vivo, IMIV, CEA, INSERM, CNRS, Universite Paris Sud, Université Paris Saclay, CEA SHFJ, Orsay, France*

(3) *Medical University of Vienna, Department of Biomedical Imaging and Image-guided Therapy, Division of Nuclear Medicine, Vienna, 1090, Austria*

Background:

At the human blood-brain barrier (BBB), the ATP-binding cassette (ABC) transporter ABCB1 (P-glycoprotein) limits brain distribution of diverse drugs. ABCB1 function at the BBB may change over age and is altered in cancer and neuropsychiatric disorders. Currently available PET tracers to study ABCB1 activity are high-affinity ABCB1 substrates with low brain uptake, while many drugs, such as metoclopramide, are weak ABCB1 substrates with sufficiently high passive permeability to cross the BBB.[1] There is a lack of knowledge on the impact of ABCB1 on the neuropharmacokinetics of such weak ABCB1 substrates.

Materials and Methods:

Five drug free, healthy volunteers (mean age: 27 ± 3 years, body weight: 76 ± 7 kg) underwent 60 min PET scans with [^{11}C]metoclopramide before and during a 2 hour infusion of the ABCB1 inhibitor cyclosporine A at a dose of 2.5 mg/kg body weight/hour.[2] In parallel to PET imaging arterial blood sampling was performed. Plasma concentrations of [^{11}C]metoclopramide and its radiolabelled metabolites were determined with HPLC to derive a metabolite-corrected arterial input function. For PET data analysis, the adult brain maximum probability map (“Hammers_mith atlas”; n30r83) was used to define the individual MR based, whole brain grey matter region of interest. The PMOD Kinetic Modeling tool (PKIN) Version 3.6 was used to analyze the PET data employing a reversible 1-tissue-2-rate constant compartmental model. In addition, the elimination rate constant of radioactivity from the brain (k_{el}) was determined by linear regression analysis of the log-transformed PET data from 15 to 60 min after radiotracer injection.

Results:

In baseline scans, [^{11}C]metoclopramide showed appreciable brain uptake (total volume of distribution V_T: 2.00 ± 0.12 mL/cm^3). During cyclosporine A infusion, there was a marked and significant decrease in radioactivity elimination from the brain (change in k_{el}: -43 ± 22%, $p < 0.05$, Wilcoxon matched pairs test). Moreover, K_1 was increased by +14 ± 8%, k_2 was decreased by -10 ± 4% and V_T was increased by +26 ± 8% (for all: $p < 0.05$). Forty minutes after radiotracer injection, 60 ± 8% and 57 ± 5% of total radioactivity in plasma consisted of unchanged parent tracer in scan 1 and scan 2, respectively.

Discussion:

Using a validated protocol for ABCB1 inhibition at the human BBB,[2] we found a significant increase in brain distribution of [^{11}C]metoclopramide under conditions of ABCB1 inhibition, which confirms that [^{11}C]metoclopramide is transported by ABCB1 at the human BBB. In contrast to currently available high-affinity ABCB1 substrate radiotracers ((*R*)-[^{11}C]verapamil, [^{11}C]*N*-desmethyl-loperamide), ABCB1 inhibition led to a decrease in radiotracer elimination from the brain, which suggests that ABCB1 exerts a pharmacokinetically different impact on brain distribution of weak as compared with strong ABCB1 substrates.

References:

[1] Pottier G, Marie S, Goutal S et al. [2016] J.Nucl.Med. 57: 309-14

[2] Sasongko L, Link JM, Muzi M et al. [2005] Clin.Pharmacol.Ther 77: 503-14

P40
Greater dopamine D3 receptor availability in males than females as determined by [^{18}F] Fluortriopride, a D3 receptor selective radiotracer

Jacob Dubroff[1], Robert Doot[1], Christopher Ward[2], Kyle Laban[1], Jenny Cai[1], Hsiaoju Lee[1], Erin Schubert[1], Finbarr O'Sullivan[3], and Robert Mach[1]

1 Department of Radiology, University of Pennsylvania USA

2 Department of Anesthesiology, Children's Hospital of Philadelphia USA

3 School of Mathematical Sciences, University College Cork IRL

Introduction:

Gender differences can influence the brain's response to drugs of abuse(*1*). The dopamine D2-like receptors (including D2 and D3 receptors) are important in reward and motivation behaviors; their dysfunction has been in implicated in addiction, Parkinson's disease and schizophrenia. The D3 dopamine receptor, specifically, is considered critical to the mesolimbic circuit. [^{18}F]Fluortriopride (FTP) is a new radiotracer that demonstrates high specificity for D3 vs D2 receptors (>160-fold) with some affinity for the serotonin 5-HT$_{1A}$ receptor. (*2-4*) We examined gender differences in baseline dopamine D3 receptor availability using this new radiotracer.

Materials & Methods:

Following the bolus intravenous administration of 6.87 mCi (+/-0.22) of [^{18}F]FTP, 10 healthy adults, 6 males (31.8 years +/-9.8) and 4 females (26.3 years +/-6.2) underwent 120 minutes of dynamic PET brain imaging. Each participant also underwent MRI T1 imaging with isotropic voxels for co-registration. Participants provided informed consent for the studies according to guidelines of University of Pennsylvania Institutional Review Board. Integrated Data Analysis Environment (*5*) software was used to perform the segmentation of MRI images, co-registration of PET images, and generation of regional brain time activity curves (TACs). Statistical recovery software was used to extract the arterial input curve from early dynamic PET images of the entire head with the result scaled based on the activity concentrations of [^{18}F]FTP in arterial blood sampled at 5, 30, 60, and 120 minutes after radiotracer injection (*6*). The regional brain TACS, image-extracted and blood scaled arterial input function, and parent fraction function served as input for kinetic image analyses of [^{18}F]FTP uptake via a 2-compartment model to yield total distribution volumes, V_T (Pmod v3.7 software). Because one male participant experienced unanticipated stress during his MRI scanning (claustrophobia) resulting in an unevaluable MRI, his data was excluded. The difference between V_T values from males and females was examined using a 2-tailed, 2-sample Student t-test with equal variances. P values less than 0.05 were considered significant.

Results:

Males demonstrated greater [^{18}F]FTP V(t) in four of the predefined volumes of interest (VOIs) suggesting greater dopamine D3 and/or serotonin 5-HT$_{1A}$ receptors(*7*) availability in these neuroanatomical regions (figure 1). Although the FTP V(t) mean was greater in the ventral striatum (figure 1) as well as other regions (not shown), this relationship was not significant.

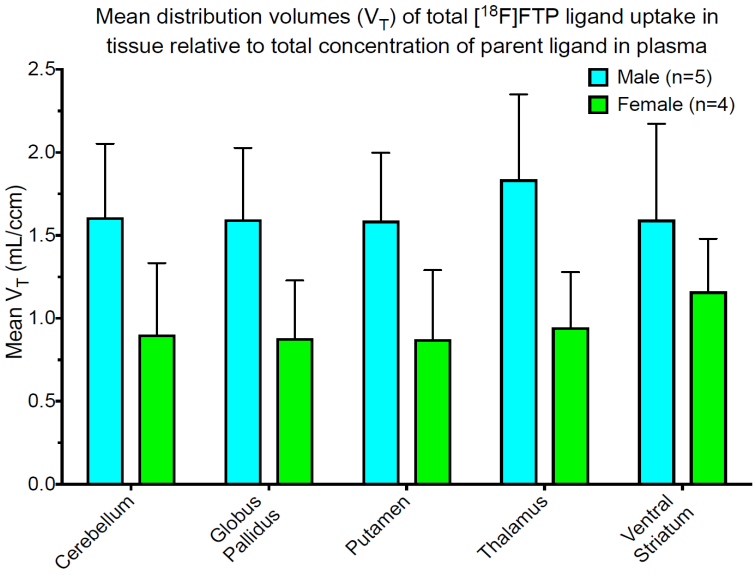

Fig 1. Mean total distribution volumes (V_T) of total [^{18}F] ligand uptake in tissue relative to total concentration of parent ligand in plasma. Uptake significantly differed ($p \leq 0.04$) in all regions except in the ventral striatum.

Discussion/Conclusion:

Prior PET D2-type dopamine receptor studies focused on gender differences in striatal dopamine release elicited by d-amphetamine(*8, 9*) or nicotine(*10, 11*) challenges. No gender difference at baseline in healthy controls has been reported using [^{18}F]fallypride(*11*) or [^{11}C]raclopride(*8*). Our data suggests greater dopamine D3 receptor availability in healthy control males which could explain previously observed differences in striatal dopamine release. Further studies, both challenge and pharmacological blocking, are needed to clarify these differences and evaluate this promising new radiotracer including a recently approved D3 but not serotonin 5-HT$_{1A}$ receptor blocking study.

Acknowledgements:

Research support provided by 5K23DA038726 (JD), R01DA029840-06A1 (RM), K01DA040023-01A1 (RD), UPenn McCabe Pilot Award (JD), UPenn Center for Magnetic Imaging and Spectroscopy (JD). The authors thank Dean Wong and Hiroto Kuwabara for sharing their invaluable analysis software. The authors are grateful to Catherine Hou, Regan Sheffer, and Alex Schmitz for their assistance in conducting these studies.

References:

1. Becker J, McClellan M, Reed B [2017] J Neurosci Res 95:136-47
2. Mach R et al. [2011] Synapse 65: 724-32
3. Rangel-Barajas C et al. [2014] J Neurochem 131: 418-31
4. Tu Z et al. [2011] J Med Chem 54:1555-64
5. Kuwabara H et al. [2014] NRM X, Egmond aan Zee, NL
6. O'Sullivan F et al. [2018] J Med Imaging 5: 011010
7. Beliveau V et al. [2017] J Neurosci 37: 120-8
8. Munro C et al. [2006] Biol Psychiatry 59: 966-74
9. Riccardi P et al. [2006] Am J Psychiatry 163: 1639-41
10. Cosgrove K et al. [2014] J Neurosci 34: 16851-5
11. Okita K et al. [2016] Neuropsychopharmacology 41: 2913-9

P41

Abstract Withdrawn

P42

Abstract Withdrawn

P43
Novel alpha-Synuclein positron emission tomography (PET) Tracers for the Diagnosis of Parkinson's Disease

Francesca Capotosti[1], Elpida Tsika[1], Jerome Molette[1], Luigino Grasso[1], Myriam Ravache[1], Efthymia Vokali[1], Patrick Rodriguez[1], Aurelien Davranche[1], Vincent Darmency[1], Ajay Purohit[2], David Paterson[2], Laurent Martarello[2], Heiko Kroth[1], Jan Stoehr[1], David Lowe[1], Andrea Pfeifer[1], Andreas Muhs[1].

1 AC Immune, EPFL Innovation Park, Building B, 1015 Lausanne Switzerland
2 Biogen, 225 Binney Street, Cambridge, MA 02142, US

Introduction:
The accumulation of aggregated alpha-synuclein in form of Lewy bodies and Lewy neurites is the pathognomonic signature in patients with Parkinson's disease (PD) and other synucleinopathies. Currently, the diagnosis of PD and other synucleinopathies is solely based on the clinical evaluation of symptoms. The direct association between progressive formation of alpha-synuclein inclusions and severity of clinical symptoms supports the development of PET tracers for non-invasive examination of low-density alpha-synuclein aggregates in the human brain as an objective diagnostic tool for clinical applications.

Materials and Methods:
We designed and screened low-molecular-weight compounds, with CNS-PET imaging properties, that selectively bind to aggregated alpha-synuclein. Binding affinities and selectivity were evaluated by fluorescence staining, *in vitro* radiobinding assay, as well as autoradiography with ^{3}H compounds on human PD and Alzheimer's disease (AD) samples. Several compounds were ^{18}F radiolabeled, tested for brain penetration and their general pharmacokinetic (PK) profile in rodent models.

Results:
We identified compounds derived from several different chemical series that showed binding to Lewy bodies and neurites in human PD brain sections with low nanomolar affinities. These compounds were also selective for alpha-synuclein aggregates over amyloid-beta aggregates as measured by autoradiography and radiobinding assays using AD patient-derived samples. Furthermore, pharmacokinetic (PK) profiling in rodents with ^{18}F radiolabeled compounds showed fast brain uptake and washout properties.

Discussion:
We identified several compounds with potential high affinity and selectivity for human PD-derived alpha-synuclein aggregates. Brain uptake and PK profiles are supportive for their further development as PET ligands to allow the direct imaging and possibly diagnosis of synucleinopathies in humans.

P44
Reduced acquisition time amyloid PET quantification: sensitivity analysis

Catherine J Scott[1], Jieqing Jiao[1], Andrew Melbourne[1], Pawel J Markiewicz[1], Jonathan M Schott[2], Brian F Hutton[3], Sebastien Ourselin[1,2]

[1]*Translational Imaging Group, CMIC, University College London, UK*

[2]*Dementia Research Centre, Institute of Neurology, University College London, UK*

[3]*Institute of Nuclear Medicine, University College London, London, UK*

Introduction:
Due to the long acquisition time required for dynamic PET with pharmacokinetic (PK) modelling, the static standardised uptake value ratio (SUVR) is commonly used. However, SUVR is sensitive to blood flow changes which confound longitudinal studies. We have proposed a framework to incorporate cerebral blood flow (CBF) from simultaneous arterial spin labelling (ASL) MRI into the PK modelling to halve the acquisition time from 60 to 30 mins[1]. In this work we perform sensitivity analysis for [^{18}F]-florbetapir data to assess the influence of errors in tracer delivery (R_1) estimation from ASL-CBF on amyloid burden (BP_{ND}) using two different R_1 estimation methods.

Materials & Methods:
The simplified reference tissue model (SRTM) is adapted for reduced acquisition time and applied to 32 subjects from Insight46- a neuroimaging sub-study of the Medical Research Council National Survey of Health and Development[2]. Two methods are used to derive R_1 from ASL-CBF: the linear regression (LR) method[1], and the intensity fusion (IF) method[3]. Both methods require a database of subjects with 60 mins of PET data and ASL, and are evaluated on a leave-one-out basis with 31 database subjects.

The LR method performs LR between R_1 and ASL-CBF on the database and the relationship is applied to an unseen ASL-CBF map. For IF, the local similarity between the unseen ASL-CBF map and those in the database is used to weight the propagation of R_1 database values into the subject's space. Errors in R_1 were calculated on regional and voxel levels and used for the sensitivity analysis (SA). SA was performed on 16 simulated time-activity-curves at 12 noise levels[4] (0.5-30%, 200 realisations).

For comparison, SUVR is calculated using data from 50-60 mins post injection, as this gave the lowest error compared to the gold standard SRTM[5] BP_{ND} estimated from 60 mins of PET data. A cerebellar grey matter reference region was used in all cases.

Results:
Table 1 shows the SA results. Here the regional mean absolute error in BP_{ND} using IF is significantly lower than LR (p<0.05), and for both methods is well below 0.1. This represents a negligible change in amyloid burden. For voxelwise analysis, IF performs significantly better (p<0.05), due to ASL artefacts propagating directly into the R_1 estimation for the LR method. However, the greater noise in the PET data means that errors may increase to a clinically notable level for noisy voxels.

Method (scale)	% R1 error	% noise in PET data											
		0.5	1.2	2.2	2.9	3.9	5.2	7.0	9.3	12.5	16.7	22.4	30.0
IF (region)	0.08	0.0153	0.0326	0.0546	0.0671	0.0781	0.0933	0.1139	0.1345	0.1599	0.1692	0.1692	0.1692
LR (region)	1.7	0.0182	0.0336	0.0552	0.0676	0.0784	0.0936	0.1141	0.1342	0.1599	0.1692	0.1692	0.1692
IF (voxel)	2.5	0.0205	0.0348	0.0559	0.0681	0.0786	0.0939	0.1141	0.1344	0.1600	0.1693	0.1693	0.1693
LR (voxel)	18.6	0.0829	0.0874	0.0928	0.0978	0.1026	0.1136	0.1288	0.1473	0.1677	0.1761	0.1764	0.1764
	Scale:	Regional level				Voxel level				Noisy voxel level			

Table 1. Sensitivity analysis showing mean absolute error in amyloid burden estimation (BP_{ND}) for simulated data fitted using the proposed method on 30 mins of PET data plus fixed R_1 of known % error, compared to the gold standard 60 mins of PET data. Simulated % R_1 errors were taken from errors calculated on real data.

Figures 1 and 2 show the application of the techniques on the real data. Regional analysis shows that both R_1 estimation methods perform better than SUVR, however, as seen in the SA, IF gives a better estimate of the gold standard BP_{ND}. For the voxelwise analysis, shown in figure 2, again both methods perform better than SUVR and IF has a lower error than LR. However, even when using the IF method, the error in BP_{ND} is higher than that for the regional analysis due to the higher error in R_1 estimation and the increased noise in the PET data.

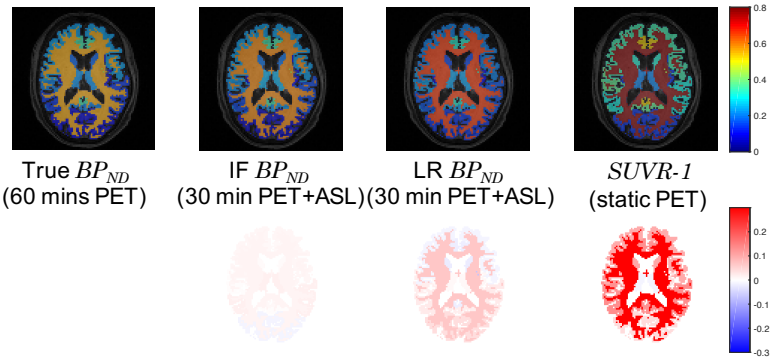

Figure 1**.** Regional example subject. [Top] estimation of amyloid burden, [bottom] difference map relative to the gold standard (true BP_{ND}).

Discussion and Conclusion:

Using the IF based R_1 estimation on ASL-CBF and 30 mins of PET data produces accurate BP_{ND} estimates, which account for blood flow, indicating the method's suitability for regional longitudinal analysis of [^{18}F]-florbetapir data. However, the accuracy of the technique on a voxelwise basis depends on the noise in the PET data and improved R_1 estimation may be required for noisy data.

Combined PET and ASL PK modelling using either R_1 estimation method always outperforms the clinical standard SUVR. This technique can be directly applied to other tracers in which the SRTM has been validated.

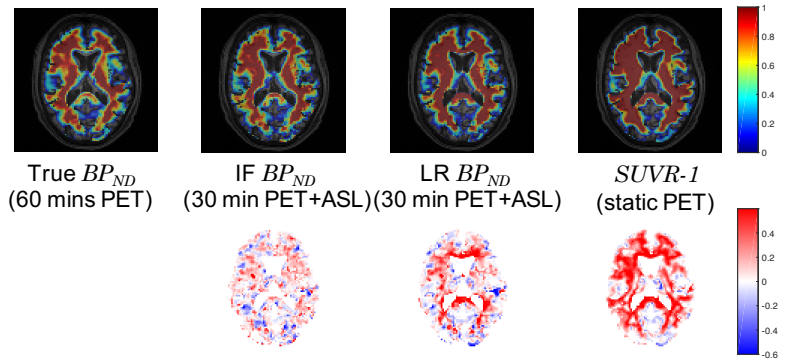

Figure 2**.** Voxelwise example subject. [Top] estimation of amyloid burden, [bottom] difference map relative to the gold standard (true $\boldsymbol{BP_{ND}}$).

Acknowledgements:
This work was supported by the EPSRC UCL Centre for Doctoral Training in Medical Imaging (EP/L016478/1), UCL Leonard Wolfson Experimental Neurology Centre (PR/ylr/18575), EPSRC (EP/H046410/1, EP/J020990/1, EP/K005278), MRC (MR/J01107X/1), NIHR UCLH Biomedical Research Centre (inc. High Impact Initiative, BW.mn.BRC10269). Insight 1946 receives funding from Alzheimer's Research UK (ARUK-PG2014-1946), MRC Dementia Platform UK (CSUB19166) and The Wolfson Foundation, and support from Avid Radiopharmaceuticals, a wholly owned subsidiary of Eli Lilly. We are grateful to the Insight 46 participants for their involvement in this study.

References:

1. Scott CJ, Jiao J, Melbourne A et. al. [2016], LNCS 9902: 406–413
2. Lane C, Parker T, Cash D et. al. [2017], BMC Neurology 17:75
3. Scott CJ, Jiao J, Cardoso MJ et. al. [2017], LNCS 10434: 737-744
4. Ichise M, Liow J, Lu J et. al. [2003], J Cereb Blood Flow Metab 23: 1096–1112
5. Gunn RN, Lammertsma AA, Hume SP et. al. [1997], Neuroimage 6:279-287

P45
[^{18}F]Florbetapir specific binding in relation to cognition in subjective cognitive decline

Tessa Timmers[1,2], Sander C.J. Verfaillie[2], Linda M.P. Wesselman[2], Rosalinde E. R. Slot[2], Niels D. Prins[2], Chris W.J. van der Weijden[1], Maqsood Yaqub[1], Adriaan A. Lammertsma[1], Ronald Boellaard[1], Rik Ossenkoppele[2,3], Wiesje M. van der Flier[2,4], Bart N.M. van Berckel[1]

[1]Department of Radiology & Nuclear Medicine, Amsterdam Neuroscience, VU University Medical Center, Amsterdam, The Netherlands
[2]Alzheimer Center, Department of Neurology, Amsterdam Neuroscience, VU University Medical Center, Amsterdam, The Netherlands
[3]Clinical Memory Research Unit, Lund University, Lund, Sweden
[4]Department of Epidemiology and Biostatistics, VU University Medical Center, Amsterdam, The Netherlands

Background:

Subjective cognitive decline (SCD) is associated with an increased risk of dementia and might reflect the earliest changes related to Alzheimer's disease. The aim of this study was to investigate the relationships between specific [^{18}F]florbetapir binding at baseline and concurrent and longitudinal cognitive performance in SCD.

Methods:

106 subjects with SCD (age 64±8, 44% female, MMSE 29±1, 23% amyloid positive on visual assessment) were recruited from the SCIENCe study, an ongoing prospective memory clinic cohort study on SCD. All underwent 90 minute dynamic [^{18}F]florbetapir PET scans at baseline. Receptor parametric mapping (RPM) with cerebellar gray matter as reference tissue was used to calculate [^{18}F]florbetapir binding potential (BP_{ND}) in parietal, temporal, occipital, frontal and global regions. Neuropsychological tests, covering memory, language, executive function and attention domains, were performed at baseline and for a subset at follow up (n=65 at follow up year 1, n= 12 at follow up year 2). Linear mixed models, adjusting for age, sex and education, were used to assess the relationships between [^{18}F]florbetapir BP_{ND} and neuropsychological scores.

Results:

Significant main effects of [^{18}F]florbetapir showed that higher BP_{ND} in global neocortex, and frontal, temporal and parietal regions were related to lower baseline MMSE ($p<0.05$, Table-1, figure 1A). Significant interactions with time indicated that higher [^{18}F]florbetapir BP_{ND} was associated with steeper annual decline on Visual Association Test, Digit Span forward and Trail Making Test-B (figure 1B-D).

Conclusion:

SCD subjects with higher specific [^{18}F]florbetapir binding demonstrated somewhat lower global cognitive performance at baseline. Moreover, higher amyloid load predisposed for faster decline in memory, attention and executive functioning. These data are in line with the notion that amyloid positivity in cognitively normal individuals increases the risk of subsequent cognitive decline.

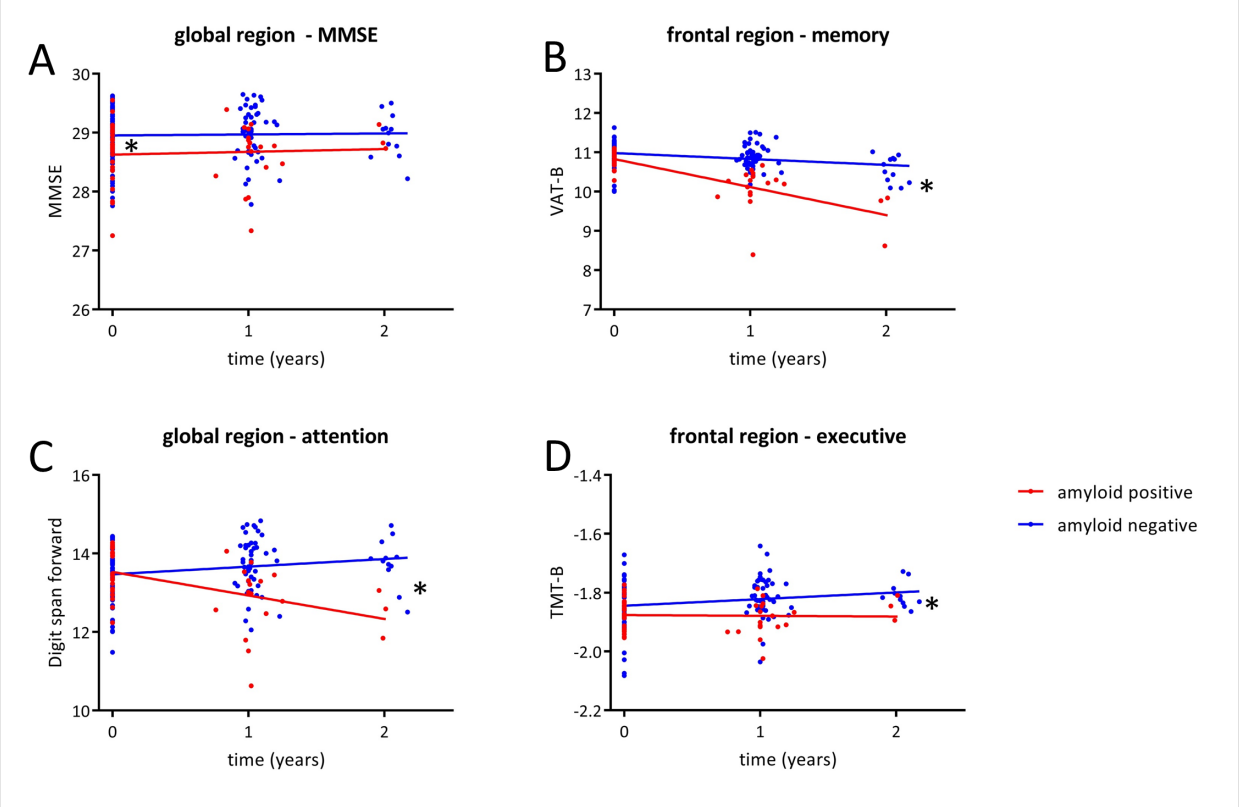

Figure 1: Cross sectional (panel A) and longitudinal (panel B-D) relationships between global amyloid load (left) or frontal amyloid load (right) and cognitive functioning. *Results of linear mixed models with global BP_{ND} or frontal BP_{ND}, time, age, gender and global BP_{ND} * time or frontal BP_{ND} * time as predictor and neuropsychological tests as dependent variable. For visualization purposes, results are binarized for amyloid positive and amyloid negative subjects.*
Abbreviations: VAT = Visual Association Test, TMT = Trail Making Test, MMSE = Mini Mental State Examination. TMT-B scores are inversed and log transformed
** $p < 0.05$*

P46
Amyloid Staging Models: Semi-Quantitative versus Quantitative Measures

Lyduine E. Collij,[1] Fiona Heeman,[1] Elles Konijnenberg,[2] Anouk den Braber,[3] Maqsood Yaqub,[1] Pieter Jelle Visser,[2] Alle Meije Wink,[1] Philip Scheltens,[2] Ronald Boellaard,[1] Bart N.M. van Berckel,[1] Mark Schmidt,[4] Frederik Barkhof,[1,5] and Isadora Lopes Alves[1]

[1]Dept. of Radiology and Nuclear Medicine, VU University Medical Center, Amsterdam, The Netherlands; [2]Alzheimer Center and Dept. of Neurology, VU University Medical Center, Amsterdam, The Netherlands; [3]Dept. of Biological Psychology, VU University Amsterdam, The Netherlands. [4]Janssen Pharmaceutica, Beerse, Belgium; [5]Institute of Neurology and Healthcare Engineering, University College London, London, United Kingdom.

Background:
Recently, Grothe and colleagues explored the feasibility of developing an *in-vivo* amyloid staging model (ASM) using PET and showed a highly consistent regional hierarchy of [^{18}F]florbetapir PET-evidence amyloid deposition across cognitively normal subjects (*N* = 179, mean age 73.8 y), using semi-quantitative standard uptake value ratios (SUVR). However, it has been shown that SUVR is influenced by both flow and wash-out effects, resulting in a biased measure compared to a non-displaceable binding potential (BP_{ND}), derived from dynamic PET acquisition. We aim to investigate the effect of using fully quantitative measures when defining a spatial-temporal amyloid staging model.

Material & Methods:
Dynamic [^{18}F]flutemetamol PET acquisition using the coffee-break protocol (0-30 and 90-110 min. scan) was performed in 190 cognitively healthy participants (mean age 70.4 years, 60% female, mean MMSE score 29). Standard uptake value ratio (SUVR) and non-displaceable binding potential (BP_{ND}) parametric images with cerebellar grey matter as a reference region were generated and regional values were obtained using the Hammers atlas. A global cut-off was computed based on the majority visual read of the parametric images and used to determine regional positivity. The frequency of regional amyloid positivity was used to construct the ASM. All participants were classified according to the model and classifications were associated with clinical measures.

Results:
The spatial-temporal ordering of cortical brain regions was highly consistent between our SUVR-based and BP_{ND}-based models, with the first four brain regions being the anterior and posterior cingulate cortex, orbitofrontal cortex, and middle frontal gyrus in both models. The main difference between the two models was the ordering of the thalamus and striatum, which were both earlier in the BP_{ND}-based model.
Following the proposed method for stage definition resulted in one cortical region in stage-I of the SUVR-based model and required optimization. Furthermore, the BP_{ND}-based model displayed a more continuous distribution of amyloid positivity compared to the SUVR-based model. Visual optimization of both models, resulted in a 4-staging model when using SUVR and a 5-staging model when using BP_{ND}. Both resulted in a plausible distribution of stage classification in our cohort (**Figure 1 & 2**). Two cases could not be classified based on the BP_{ND} model as they showed amyloid positivity in regions corresponding to stage-II, but not to stage-I.
Comparison between the ASM-classification and the majority visual read showed that for SUVR, 100% of stage-0, 90% of stage-I and 79% of stage-II were read as negative, while all stage-III/IV participants were read as positive. For BP_{ND}, all stage-0/I/II participants were read as negative and 60% of stage-III, 94% of stage-IV, and 100% of stage-V participants were read as positive.

Both the SUVR- and BP_{ND}-ASM-classifications showed a positive effect of age ($p < .05$), but no relationship with APOE ε4 carriership and visual scores of global cortical atrophy and white matter hyperintensities. BP_{ND}-based stage-III participants had a higher hippocampal atrophy visual score than stage-0/I/II participants, which was not observed for the SUVR-ASM-classifications. For both models, there was not relationship with CSF $A\beta_{42}$ levels, but BP_{ND}-based stage-IV participants had a significantly lower $A\beta_{40}/A\beta_{42}$ ratio compared to stage-0/I.

Conclusions:

Our amyloid staging models showed high spatial-temporal consistency between them, suggesting high robustness of methodology used for the development of the models. Optimization resulted in a 4-stage model for SUVR and 5-stage model for BP_{ND}. Classification based on the 5-stage BP_{ND}-model showed a more continuous relationship with majority visual read and associations with 3 other clinical measurements, while classification based on the 4-stage SUVR-model only showed an association with 1 other clinical measurement. Further work is being done to assess the following potential limitations: 1) applying a global cut-off to regional values, 2) effect of gender and age on positivity cut-offs, and 3) using improved AD-related regions by applying the Harvard-Oxford atlas.

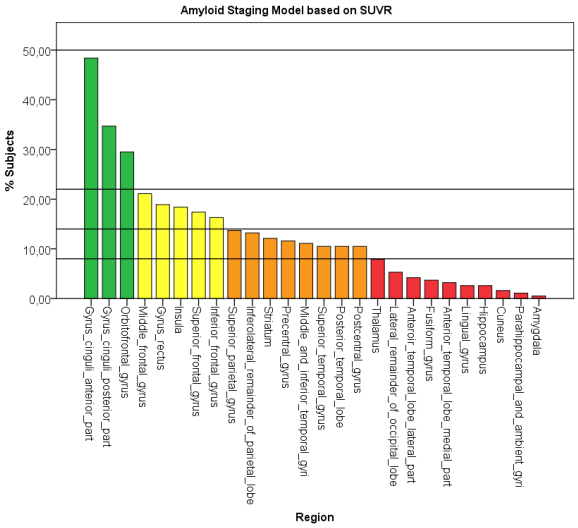

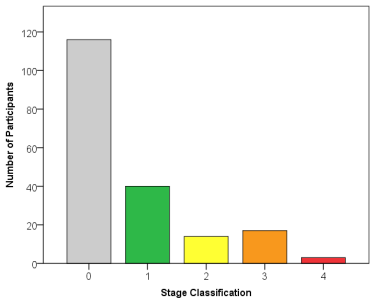

Figure 1. Amyloid Staging Model based on SUVR in a control population.
Left) Spatio-temporal distribution of cortical brain regions defined based on the Hammers atlas.
Right) Distribution of stage classification of our cohort.

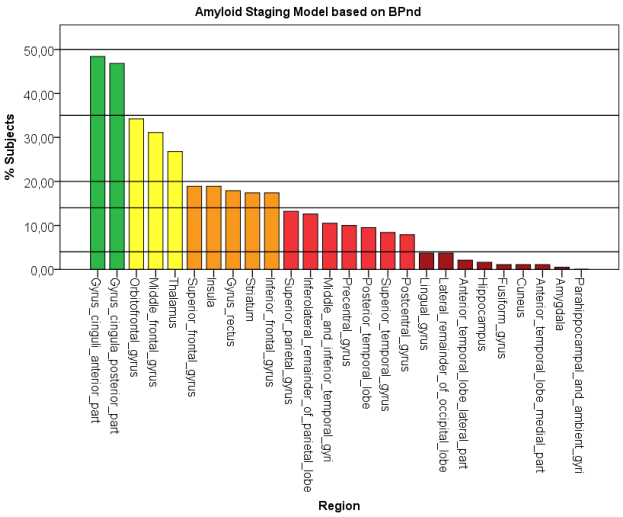

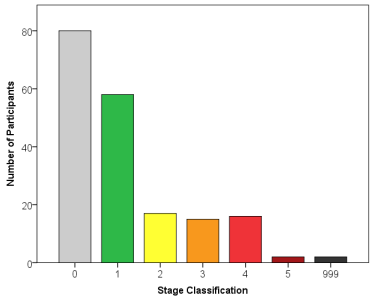

Figure 2. Amyloid Staging Model based on BP_{ND} in a control population.
Left) Spatio-temporal distribution of cortical brain regions defined based on the Hammers atlas.
Right) Distribution of stage classification of our cohort.

P47
Parametric imaging of [^{18}F]florbetapir: a test-retest study in healthy subjects and patients with Alzheimer's disease

Sander CJ Verfaillie[1,2*], Sandeep SV Golla[1*], Chris WJ van der Weijden[1], Tessa Timmers[1,2], Patrick Schober[3], Robert C Schuit[1], Albert D Windhorst[1], Philip Scheltens[2], Wiesje M van der Flier[2,4], Adriaan A Lammertsma[1], Bart NM van Berckel[1], Ronald Boellaard[1]

Departments of [1]Radiology & Nuclear Medicine, [2]Neurology & Alzheimer Center, [3]Anaesthesiology, and [4]Epidemiology & Biostatistics, VU University Medical Center, Amsterdam, Netherlands. All authors are affiliated with Amsterdam Neuroscience

*authors contributed equally

Background:

Accumulation of amyloid beta (Aβ) is one of the pathological hallmarks of Alzheimer's disease (AD), which can be visualized using [^{18}F]florbetapir positron emission tomography (PET). Accurate quantification of Aβ is important for monitoring both disease progression and response to disease modifying therapies. The aim of this study was to evaluate various parametric methods for voxel-by-voxel quantification of [^{18}F]florbetapir binding and to assess their test-retest (TRT) reliability.

Methods:

Eight AD patients (age: 67±6) and eight controls (age: 63±4) were included. Two 90 minutes dynamic PET scans (Philips Ingenuity PET/CT), including arterial sampling, were acquired (~4 weeks apart) after a bolus injection of 293±15 MBq [^{18}F]florbetapir (specific activity: 4 µg/mL). Parametric images were generated using several linearization and basis function approaches (reference region: cerebellum grey matter). Logan and Spectral Analysis (SA) were used to generate volume of distribution (V_T) images. Receptor parametric mapping (RPM), simplified reference tissue model with fixed k_2' (SRTM2), reference Logan (RLogan) and standardized uptake value ratios ($SUV_{r(50-70)}$) were used to obtain binding potential (BP_{ND}) and $SUV_{r(50-70)}$ images. Regional BP_{ND}+1 and V_T values were compared with corresponding DVR estimates derived from non-linear regression analysis using the plasma input two-tissue compartment (2T4k_V_B) model (n=68 ROIs). TRT values (%) were obtained for both optimal parametric and $SUV_{r(50-70)}$ images.

Results:

RPM (BP_{ND}+1) showed the least bias (r^2=0.92; slope=0.91) compared to 2T4k_V_B derived values. In addition, Logan (r^2=0.94; slope=0.85) and RLogan (r^2=0.92; slope=0.88), and SRTM2 (r^2=0.92; slope=0.88) correlated well with their 2T4k_V_B counterparts. Lower correlations were obtained for SUVr (r^2=0.74; slope=0.90) and SA (r^2=0.60; slope=0.81) with 2T4k_V_B DVR and V_T values. RPM (BP_{ND}+1) and $SUV_{r(50-70)}$ showed a TRT variation of 4.2% (controls: 2.6%, AD: 5.4%) and 8.8% (controls: 8.8%, AD: 8.9%), respectively.

Conclusions:

RPM was the parametric method of choice for [^{18}F]florbetapir, combining the highest accuracy (lowest bias) with the best TRT reliability. Performance of the semi-quantitative SUVr approach was substantially poorer, especially with regards to TRT variability.

P48
Sulfate conjugation of [^{11}C]PBB3, a Tau imaging agent, in the brain

Tatsuya Kikuchi, Maki Okada, Hideki Ishii, Nobuki Nengaki, Maiko Ono, Toshimitsu Okamura, Takafumi Minamimoto, Makoto Higuchi, Ming-Rong Zhang

National Institutes for Quantum and Radiological Sciences and Technology

Introduction:

[^{11}C]PBB3, a Tau imaging agent, is rapidly metabolized to form a sulfate conjugate ([^{11}C]PBB3-sulfate) in peripheral tissues by sulfotransferase (SULT).[1] After the administration of [^{11}C]PBB3 to mice, [^{11}C]PBB3-sulfate was observed also in the brain. The previous report concluded that it was due to the influx of [^{11}C]PBB3-sulfate from blood to brain. However, it is known that SULT is expressed in the brain and [^{11}C]PIB which possesses 6-hydroxybenzothiazole as a fundamental structure (Fig 1) is sulfated in the rat brain.[2] It was therefore expected that [^{11}C]PBB3, a [^{11}C]PIB derivative, would be sulfated in the brain. In this study, the sulfate conjugation of [^{11}C]PBB3 in the brain was investigated because the conjugation might affect the kinetic analysis of Tau imaging with [^{11}C]PBB3. In addition, the hydrolysis of [^{11}C]PBB3-sulfate to form parent [^{11}C]PBB3 in the brain was investigated as sulfate conjugates can be hydrolyzed by sulfatase which is expressed in the brain.

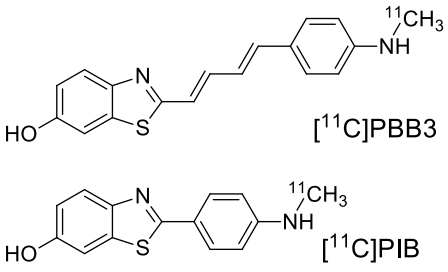

Fig 1. Structure of [^{11}C]PBB3 and [^{11}C]PIB

Materials & Methods:

Sulfate conjugation of [^{11}C]PBB3 in the brain was evaluated by adding [^{11}C]PBB3 and a sulfate donor, 3'-phosphoadenosine-5'-phosphosulfate (PAPS) to the brain homogenate sample. In mice samples (cerebrum, C57BL/6, 8 wo, n=3), reactions were carried out at 37°C for 30 min. In samples of a rhesus monkey (frontal cortex, *Macacca mulatta*, male, 23 yo), reactions were carried out at 37°C and the conjugates generated were analyzed at 5, 15, 30 min after starting reaction. In addition to the crude homogenate (around 0.2 g/mL for mice, 0.16 g/mL for monkey), the sulfate conjugation in the supernatant of homogenate was investigated. The conjugation was analyzed using radio-TLC. Similarly, [^{11}C]PBB3-sulfate, which was prepared by *O*-sulfation of [^{11}C]PBB3 using sulfur trioxide pyridine complex, was incubated in the mice brain homogenate at 37°C for 30 min to evaluate its hydrolysis.

Results:

The sulfate conjugation of [^{11}C]PBB3 was observed in the mice brain samples with 30 min reaction time, and only 7.7±0.44% and 9.2±0.30% of [^{11}C]PBB3 was conjugated in the crude homogenate and supernatant, respectively (Fig 2A). Meanwhile, [^{11}C]PBB3-sulfate was slowly hydrolyzed to form [^{11}C]PBB3 in the brain sample (3.1±0.13% in the crude homogenate and 3.7±0.20% in the supernatant, Fig 2B).

The conjugation rates of [^{11}C]PBB3 in the monkey brain samples were much faster than that in the mice brain samples. The conjugation in the crude homogenate of monkey brain followed first order manner (r^2=1.0) up to 91% decrease of [^{11}C]PBB3 and the rate was estimated to be 0.49 $min^{-1}(g/mL)^{-1}$. The first order kinetics suggested that the hydrolysis rate of [^{11}C]PBB3-sulfate in the monkey brain was much slower than the conjugation rate. Indeed, the conjugation rate and the hydrolysis rate in the supernatant prepared from 0.16 g/mL of monkey brain homogenate were estimated to be 0.35 min^{-1} and 0.013 min^{-1}, respectively (Fig 3).

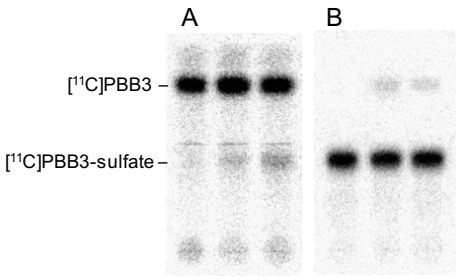

Fig 2. Typical radio-TLC images for the sulfate conjugation of [^{11}C]PBB3 (A) and the hydrolysis of [^{11}C]PBB3-sulfate (B), measured in phosphate buffer (left), in a crude mouse brain homogenate (center), and in the supernatant (right).

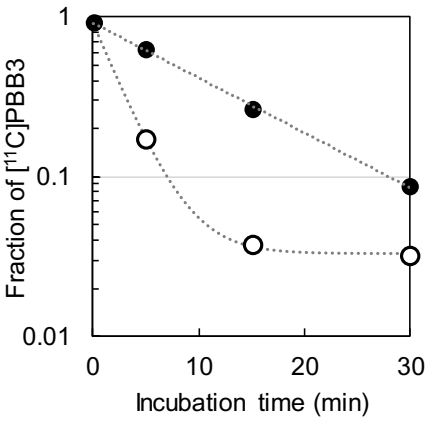

Fig 3. The sulfate conjugation of [^{11}C]PBB3 in the crude monkey brain homogenate (black) and in the supernatant (white). Regression curves are presented as a dotted line.

Discussion:

In mice, [^{11}C]PBB3 slowly but significantly underwent sulfate conjugation in the brain. Therefore, a part of [^{11}C]PBB3-sulfate observed in the mouse brain after [^{11}C]PBB3 administration would be the metabolite generated in the brain. On the other hand, the sulfate conjugation of [^{11}C]PBB3 was quite rapid and apparently irreversible in the monkey brain samples.

In this study, large Interspecies differences regarding the sulfate conjugation of [^{11}C]PBB3 in the brain was observed. Therefore, further investigation about the conjugation of [^{11}C]PBB3 in the human brain would be required.

References:

1. Hashimoto H, Kawamura K, Takei M *et al.* [2015] Nucl. Med. Biol. 42: 905–910
2. Cole GB, Keum G, Liu J *et al.* [2010] Proc. Natl. Acad. Sci. USA 107: 6222–6227

P49
Transgenic rat models of Tauopathy with potential application to PET radiotracer development

Nisha K. Ramakrishnan[1], David J. Williamson[1], Xiaoyun Zhou[1], Steven Kealey[1], Tomáš Smolek[2], Veronika Cubinkova[2], Norbert Žilka[2], Franklin I. Aigbirhio[1]

[1] Molecular Imaging Chemistry Laboratory, Wolfson Brain Imaging Centre, University of Cambridge, [2] Axon Neuroscience R&D Services SE, Bratislava, Slovak Republic

Introduction:

Several novel PET radioligands, selective to the aggregated form of the misfolded protein tau, are under development across groups. We and others have shown that some tau selective imaging probes can bind to tau pathology in transgenic mice in addition to their application in humans[1]. However, rats have distinct advantages over mice for research involving small animal PET imaging; the rat brain is approximately six times larger than the mouse brain, facilitating more accurate radioactivity concentration quantification in brain regions and blood sampling for gold standard blood-based kinetic analysis is feasible. However, imaging tau pathology in a rat model by PET has yet to be achieved. We investigated two rat models of tauopathy with the aim of identifying rat models which are suitable for PET imaging.

Materials & Methods:

Coronal brain slices from two transgenic rat models, SHR24 and SHR72 expressing human truncated tau and their wildtype controls were obtained from Axon Neuroscience. These transgenic rats develop progressive age dependent neurofibrillary degeneration either in the brainstem (SHR72) or in the cortical brain areas (SHR24)[2,3]. Immunofluorescence with AT8 and fluorescence microscopy with T557 (a fluorescent analogue of [^{18}F]AV1451, the current lead compound for imaging Tau) and PBB3 were used to assess the binding of lead compounds to tau in these animals.

Results: The binding of T557 and PBB3 to tau was visualized using fluorescence microscopy. The fluorescence of both these compounds (in green) were co-localized with that of AT8 (in red). SHR24 was found to take up these compounds mainly in the cortex, but also in brainstem to a smaller extend. SHR72 took up these compounds only in the brainstem.

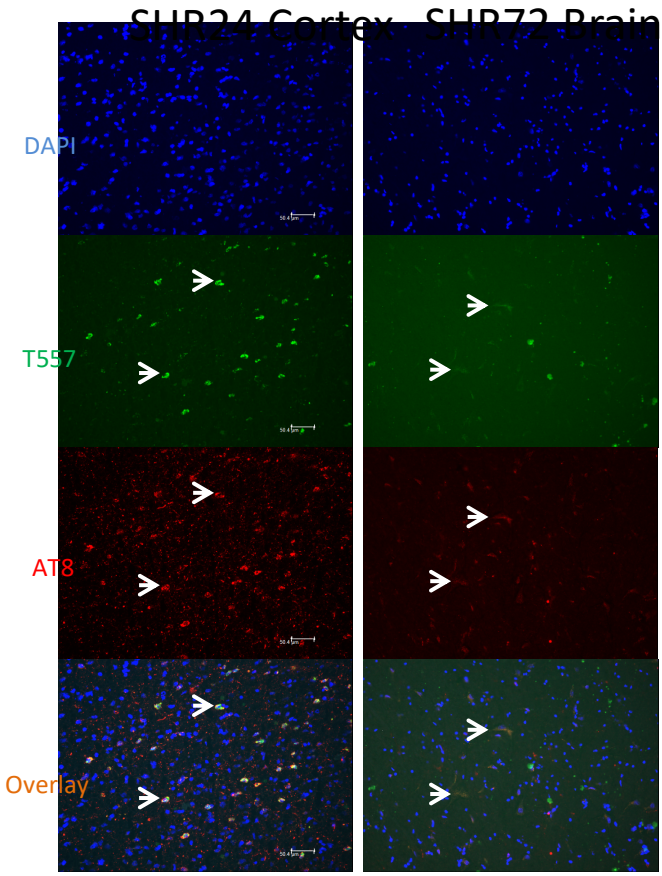

Figure 1: Cortex of SHR24 and brainstem of SHR27 labelled with DAPI (blue; nuclear stain), T557 (green; compound labelling tau), AT8 (red; anti-tau antibody). Arrows indicate a few of the double stained neurons containing NFTs.

Discussion/Conclusion:

The uptake of the lead compounds appeared to be much more abundant in the cortex of SHR24 than in the brainstem of SHR72 in the limited number of samples analysed so far. Further samples are currently being analysed. If a suitable rat model can be identified, this will support their use in the development of PET radiotracers and assessing novel therapeutics.

References:

1. Maruyama *et al*., [2013], Neuron, 6:1094–1108

2. Koson *et al*., [2008], European Journal of Neuroscience, 28: 239–246

3. Filipcik *et al*., [2012], Neurobiology of Aging, 33:1448–1456

P50
Impact of intermittent hypoxia on [^{18}F]CPFPX binding to cerebral A1 adenosine receptors in humans

David Elmenhorst, Judith Fronczek, Andreas Matusch, Tina Kroll, Andreas Bauer

Molecular Neuroimaging, Institute of Neuroscience and Medicine (INM-2)

Forschungszentrum Jülich, 52425 Jülich, Germany

Introduction:

Hypoxic hypoxia induces numerous adaptive changes, e.g., in cerebral blood flow, metabolism and electrical activity. Adenosine, as an inhibitory neuromodulator, is produced in and/or released to the interstitial space during hypoxia and thought to mediate several of these effects. A_1 adenosine receptor (A_1AR) antagonism or knock-out attenuates this synaptic inhibition in mice (Chu *et al.* 2013).

In rodent models inhalation of 8% oxygen (which roughly corresponds to a stay in 6-7 km height in terms of arterial oxygen saturation) led to 2- to 34- fold increases in adenosine in cerebral cortex depending on the method used for determination (cortical cup, microdialysis) (Phillis *et al.* 1993;Zetterstrom *et al.* 1982). In addition, adenosine is involved in neuroprotective effects during hypoxia in ischemia (Borea *et al.* 2016).

In the present pilot study we investigated the impact of acute exposure to normobaric hypoxic hypoxia (8%) on A_1AR availability in the human brain via PET and the highly selective radioligand [^{18}F]CPFPX. This method has been proven suitable for quantifying A_1AR densities in the human brain. A bolus plus constant infusion for steady-state quantification allows investigating acute interventions like the occupancy of A_1AR by a caffeine challenge (Elmenhorst *et al.* 2012).

Materials & Methods:

Four male subjects (22-26 years) underwent a 120 min bolus plus constant infusion [^{18}F]CPFPX PET experiment after caffeine abstinence. Metabolite corrected activity counts of arterial blood samples were used to calculate steady-state distribution volumes (V_T) at baseline (i.e., 50-80 min after start of [^{18}F]CPFPX administration) and after intervention. A hypoxic gas mixture (8% oxygen in nitrogen) was inhaled by two subjects using a sealed breathing mask between 90-105 min and 80-90 min, respectively. Two subjects inhaled normoxic room air as control condition. Changes in A_1AR availability reflected by V_T values were determined using the time spans during and after challenge.

Results:

No change in V_T was found in the control subjects. Hypoxia resulted in a quick reduction in arterial oxygen saturation to 60%-70% after 5 min of exposure, which was restored to 100% after switching back to inhaling room air. In contrast under hypoxia a reduction of A_1AR availability was observed in the range of 10-30% depending on the region of interest. The

nadir of the decrease in V_T was observed ~10 min after start of hypoxia. Subsequent normoxia was followed by an increase in V_T with a delay of ~10 min.

Conclusion:

In this pilot study normobaric hypoxic hypoxia (8%) induces a decrease in A_1AR availability of [^{18}F]CPFPX in the human brain suggesting a transient release of endogenous adenosine in cortical regions which is competing with the radiotracer.

References:

Borea, P. A., Gessi, S., Merighi, S. and Varani, K. Adenosine as a Multi-Signalling Guardian Angel in Human Diseases: When, Where and How Does it Exert its Protective Effects? Trends Pharmacol. Sci., 2016, 37: 419-434.

Chu, S., Xiong, W., Zhang, D.et al. Regulation of adenosine levels during cerebral ischemia. Acta Pharmacol. Sin., 2013, 34: 60-66.

Elmenhorst, D., Meyer, P. T., Matusch, A., Winz, O. H. and Bauer, A. Caffeine Occupancy of Human Cerebral A1 Adenosine Receptors: In Vivo Quantification with 18F-CPFPX and PET. J. Nucl. Med., 2012, 53: 1723-1729.

Phillis, J. W., O'Regan, M. H. and Perkins, L. M. Adenosine 5'-triphosphate release from the normoxic and hypoxic in vivo rat cerebral cortex. Neurosci. Lett., 1993, 151: 94-96.

Zetterstrom, T., Vernet, L., Ungerstedt, U.et al. Purine levels in the intact rat brain. Studies with an implanted perfused hollow fibre. Neurosci. Lett., 1982, 29: 111-115.

P51
In vivo PET evaluation of a potential PDE1 radiotracer – [^{11}C](±)-PF04822163

Steven Kealey, Xiaoyun Zhou, David Williamson, Nisha Kuzhuppilly Ramakrishnan, Franklin I. Aigbirhio.

Molecular Imaging Chemistry Laboratory, Wolfson Brain Imaging Centre, Department of Clinical Neurosciences, University of Cambridge, Cambridge, CB2 0SZ, UK

Introduction:

The phosphodiesterase enzyme (PDE) family play a crucial role in cell signalling by modulating levels of the cyclic nucleotide secondary messengers, cAMP and cGMP. PDE1 has significant CNS expression and is thought to be associated with learning and memory processes, making it a promising therapeutic target for enhancement of cognitive function in a range of disorders. Recently, potent and selective small molecule inhibitors for PDE1 have been described,[1,2] providing the opportunity to design radiolabelled analogues to image this enzyme for the first time using PET. Here we describe the carbon-11 labelling and preliminary in vivo evaluation in rat of PF-04822163, a PDE1 inhibitor reported by Pfizer in 2014 (Figure 1).[1]

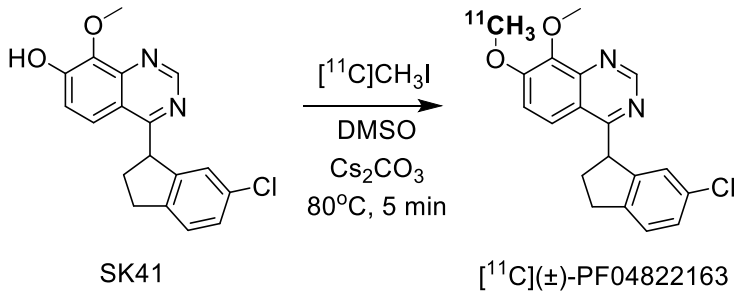

Figure 1. Radiolabelling of [^{11}C](±)-PF04822163

Materials & Methods:

[^{11}C](±)-PF04822163 was radiolabelled using an automated process on a GE TRACERlab FX F-N as follows: A solution of the hydroxyl precursor (SK41), [^{11}C]CH_3I and Cs_2CO_3 in DMSO was heated at 80^{o}C for 5 min, purified by semi-preparative HPLC (Phenomenex Luna C18, 5 µm, 250 x 10 mm; 60% MeCN:40% 50 mM ammonium formate pH 4; 6 mL/min) and reformulated in 10% ethanol-saline using SPE purification (Waters SepPak C18 Light). [^{11}C](±)-PF04822163 (14 MBq) was administered to a male Wistar rat via femoral vein injection and dynamic PET scanning (40 min) was performed using a Focus 120 microPET Scanner. Arterial blood sampling was performed for metabolite analysis by radio-HPLC. LogD was calculated by partition of the tracer between octanol-PBS buffer at pH 7.4.

Results:

[^{11}C](±)-PF04822163 was obtained in high radiochemical purity (>99%) and reasonable molar activity (21 GBq/μmol at end of synthesis) with an isolated radiochemical yield of 10% (from [^{11}C]CH_3I). Log D was measured to be 3.76 ± 0.02.

PET scanning showed that [^{11}C](±)-PF04822163 enters the rat brain (Figure 2); Peak SUV of 7 was observed within a minute, followed by rapid washout in all brain regions. Moderately increased tracer uptake was observed in the striatum compared to the cerebellum (Figure 3). Metabolite analysis showed 45% parent remaining in the blood at 5 min, decreasing to 30% at 10 min, with a single polar metabolite accounting for the remaining radioactivity.

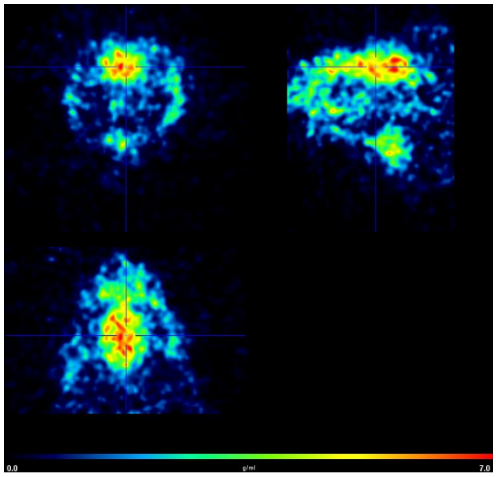

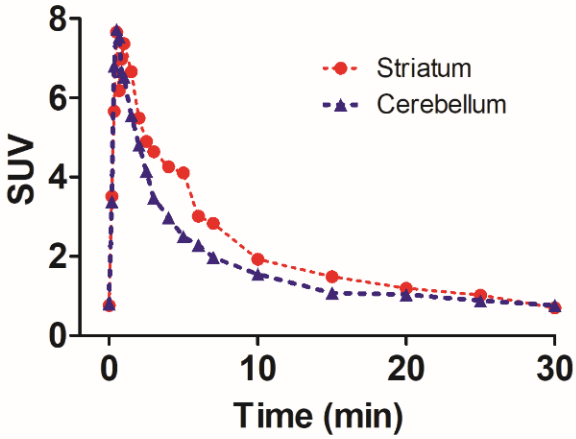

Figure 2. Summed SUV images (0-40 min). **Figure 3**. Time-activity curves of striatum and cerebellum.

Discussion/Conclusion:

Of the PDE1A-C subtypes, PDE1B has the highest CNS levels and is strongly expressed in dopaminergic regions such as the striatum and nucleus accumbens, while all PDE1 subtypes have low expression in the cerebellum.[3] We observed slightly higher uptake of [^{11}C](±)-PF04822163 in the striatum compared to the cerebellum, however the washout in all brain regions was rapid. This washout may be a consequence of the fast metabolism, with only 30% parent remaining after 10 minutes. Later plasma time points were not analysed in our experiments, and are required to fully understand tracer kinetics. Further studies are underway to investigate this tracer under baseline and blocking conditions. Tracers for PDE1 may find application in the study of neuropsychiatric disorders and in the development of therapeutics focussed on this target.

References:

[1] Humphrey J *et al*., [2014], Med. Chem. Comm., 5:1290.
[2] Li P *et al*., [2016], J. Med. Chem., 59:1149.
[3] Lakics V, Karran E. H and Boess F. G, [2010], Neuropharmacology 59:367.

P52

Radiosynthesis and characterization of 3-chloro-4-[^{18}F]fluoro-*N*-(1-(dimethylamino) cyclohexyl)methylbenzamide ([^{18}F]2a) in rats: Hunting for ^{18}F-labelled, selective mu opioid receptor agonists

Waqas Rafique[┼‖*], Julian Ott[‡], Simone Maschauer[‡], Mona M Spilhaug[┼‖], Harald Hübner[#], Peter Gmeiner[#], Olaf Prante[‡], Patrick J Riss[┼‖§]

[┼]*Department of Chemistry, University of Oslo, Postbox 1033, Blindern, 0315 Oslo, Norway.* [‖]*Realomics SFI, Kjemisk Institutt, Universitetet i Oslo, Oslo, Norway.* [‡]*Department of Nuclear Medicine, Molecular Imaging and Radiochemistry, Friedrich Alexander University Erlangen-Nürnberg (FAU), Schwabachanlage 6, D-91054 Erlangen, Germany.* [#]*Department of Chemistry and Pharmacy, Medicinal Chemistry, Emil Fischer Center, Friedrich Alexander University Erlan-gen-Nürnberg (FAU), Schuhstrasse 19, D-91052 Erlangen, Germany.* [§]*Klinik for Kirurgi og Nevrofag, OUS-Rikshospitalet, Oslo, Norway.*

Introduction:

G-protein coupled opioid receptors (OR) are prominent targets for quantitative imaging because of OR involvement in a variety of behavioural and physiological processes.[1] The OR are widely distributed throughout the brain.[2] It has become possible to record the opioid receptor changes caused by endogenously produced opioid peptides, and exogenously administered opioid radioligands, with the help of Positron Emission Tomography (PET).[3] Since all three μ-, κ- and δ-OR share a nearly equal amino acid sequence, the quantification of OR require selective radioligands with marked affinity for one receptor subtype.

On screening the currently available OR PET ligands, three major challenges were encountered: **1)** Most of the validated OR PET radioligands found in literature are antagonists. The complexity of ORs pharmacology limits the utility of antagonists, as agonists are believed to be more sensitive to changes in OR availability in its active state. **2)** The available agonist radioligands have high binding affinity, permitting localisation of radiotracers even in brain regions with very sparse receptor density, which limits their sensitivity in radioligand displacement studies. **3)** Another inherent issue is the lack of receptor selectivity of the PET ligands, which confounds with the imaging study of a single subtype.

The objective of present study was to provide an alternative ^{18}F-labelled μ-subtype selective OR PET radioligand with moderate receptor affinity, thereby allowing the straightforward quantification of the μOR receptor availability in rodent models within 60 minutes p.i.

Material and Methods:

A series of opioid receptor agonists was designed based on the benzamide scaffold 3,4-dichloro-N-(1-(dimethylamino)cyclohexyl)methyl benzamide (AH-7921). The scaffold has an attractive combination of chemical and physical properties, suitable to develop the agonist binding ligands with moderate affinity.[4] In addition; the activated benzoyl moiety allows the direct nucleophilic aromatic substitution applying ^{18}F-fluoride.

Results and Discussion:

Agonist potency, binding affinity and relevant pharmacological profile of synthesized analogues was investigated. *In vitro* studies confirmed full agonist binding, selective for μOR with the desired, moderate binding affinity (K_i **2a** $_{(MOR)}$ = Thl: 79.1 nM; Str: 61.7 nM). [^{18}F]**2a** was obtained through nucleophilic ^{18}F-versus-nitro-substitution in a non-decay corrected radiochemical yield of 23 ± 5% within 60 minutes from EOB in molar radioactivity of 25-40 GBq/μmol.

In vitro and *in vivo* evaluation of [^{18}F]**2a** was achieved using rat brain autoradiography (AR) and small-animal PET imaging. Binding studies have shown high selectivity and pronounced receptor activation for μOR compared to other potential targets (figure – 1). PET imaging

studies in rats revealed specific binding of [^{18}F]**2a** to μOR-rich brain regions, when compared of the time-activity-curves (TACs) obtained in blocking studies with naloxone (1mg/Kg).

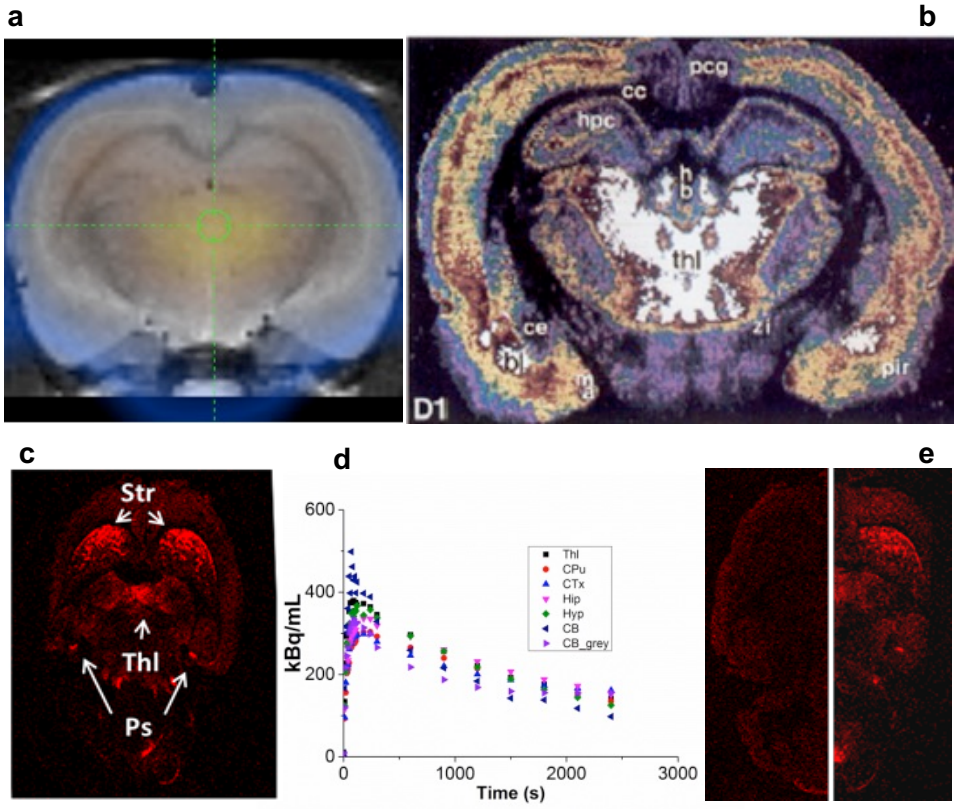

Figure – 1: Direct comparison between the PET image of [^{18}F]**2a** (a) with previously described μOR binding pattern in coronal view[5] (b); AR image of transverse rat brain section obtained through [^{3}H]DAMGO (c), TACs of [^{18}F]**2a** in different regions of the brain (d), AR image showing inhibition in [^{3}H]DAMGO binding using **2a** (1 uM, left) and without **2a** (right) (e).

Conclusion:

We conclude that [^{18}F]**2a** or its analogues have potential as a template to develop selective μOR PET ligands with fast kinetic profile.

Acknowledgement:

This study was funded by the faculty of Mathematics and Natural Sciences, the Department of Chemistry, University of Oslo (startup grant to PJR), the realomics SRI (PJR) and NFR 231553. Part of the study was supported by Deutsche Forschungsgemeinschaft within the framework of DFG Research Training Group under “Medicinal Chemistry of Selective GPCR Ligands” (GRK 1910).

References:

[1]. Pfeiffer A, Pasi A, Mehraein P, Herz A. [1982], Brain Res,248:87–96.
[2]. Dhawan BN, Cesselin F, Raghubir R, Reisine T, Bradley PB, Portoghese PS, Hamon M. [1996], Pharmacol Rev,48(4):567–592.
[3]. Dannals, RF. [2013], J. Label Compd Radiopharm,56(3-4):187-195.
[4] Rafique W, Khanapur S, Spilhaug MM, Riss PJ. [2017], ACS Chem. Neurosci,8(9):1847-1852. [5]. Mansour A, Khachaturian H, Lewis ME, Akil H, Watson SL. [1987], J Neurosci,7:2445-2464.

P53
Age-related dopamine transporter availability measured using [^{11}C]PE2I PET

My Jonasson, Lieuwe Appel, Charles Widström, Tomas Furmark, Torsten Danfors, Jens Sörensen and Mark Lubberink

Uppsala University Hospital, Uppsala, Sweden

Uppsala University, Uppsala, Sweden

Introduction:

[^{11}C]PE2I is a positron emission tomography (PET) ligand with high affinity and selectivity for the dopamine transporter (DAT). Decreased DAT availability is associated with various neurological disorders such as Parkinson's disease. We have recently shown that an 80 min dynamic [^{11}C]PE2I PET scan can be used for differential diagnosis of patients with parkinsonian disorder [1]. For routine clinical application, we have validated the use of shorter acquisition times, with DAT availability estimated using standard uptake value ratio (SUVR)-1 at 30-40 min p.i. [2]. Age-related decline of DAT availability has previously been investigated with PET using [^{18}F]FE-PE2I, showing a reduction of striatal DAT of about 7% per decade as measured with BP_{ND} [3]. The purpose of this study was to investigate the age-related changes of DAT availability measured with [^{11}C]PE2I PET using both BP_{ND} and SUVR-1 estimates.

Materials and Methods:

Thirty healthy controls (HC) were included, age 20-67 years, as given in Table 1. Each subject underwent an 80 min dynamic PET scan after injection of 350-400 MBq [^{11}C]PE2I. Each subject also received a T1-weighted MRI scan, for structural information, to be co-registered to the PET scan. Volumes of interest (VOIs) were defined on the MRI image applying an automated probabilistic VOI template (PVElab).

Table 1: Mean age and numbers of males and females included in each age-group.

Age-group	Number of HC (males / females)	Mean age ± SD
20-30	6 (3 / 3)	24 ± 2
30-40	6 (3 / 3)	33 ± 2
40-50	7 (3 / 4)	44 ± 3
50-60	5 (4 / 1)	54 ± 3
60-70	6 (3 / 3)	65 ± 2

Parametric BP_{ND} images were calculated using receptor parametric mapping (RPM) for the full 80 min data set and SUVR-1 images were calculated for a 30-40 min time window. Cerebellar grey matter was used as reference region. BP_{ND} and SUVR-1 values in caudate and putamen were retrieved from the parametric images by projecting the MRI-based VOIs, mean of left and right side. Relation between the BP_{ND} and SUVR-1 values and age was assessed using linear regression and mean changes per decade were calculated.

Results:

The relationships between age and DAT availability measured with BP_{ND} and SUVR-1 are given in Fig. 1. A decrease of BP_{ND} was found in both caudate and putamen with 7.6 and 2.5 % mean decrease per decade respectively, although the decrease was only significant in caudate ($p<0.05$). A significant decrease was also found for SUVR-1 values in caudate, 6.2 % per decade, while no age-related effect on SUVR-1 values was observed in putamen.

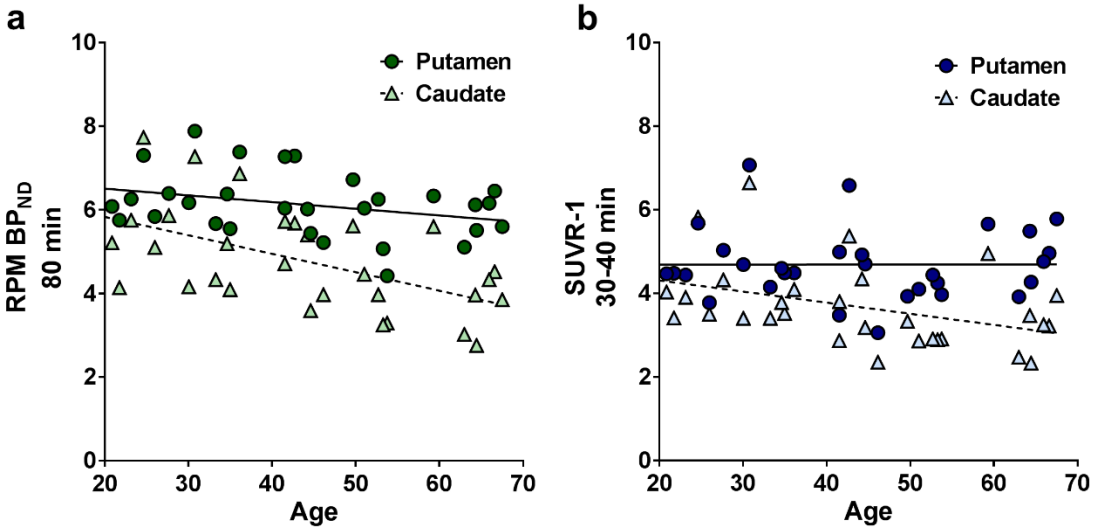

Fig 1: Relationship between age and a) 80 min BP_{ND} and b) 30-40 min SUVR-1, in putamen and caudate.

Discussion:

The decline of 7.6 % of DAT availability per decade in caudate, measured with BP_{ND}, is in line with previous studies. When estimating DAT availability with SUVR-1 on a 30-40 min interval the age-related decrease is lower, which may be explained by the previously demonstrated underestimation of SUVR-1 compared to BP_{ND} which decreases with decreasing BP_{ND} values [2]. Our result regarding the non-significant decline of DAT in putamen deviates from previous studies and needs further investigation. While using these methods for clinical assessment of DAT availability, age effects need to be considered for both BP_{ND} and SUVR-1 values in caudate.

References:

1. Appel, L., *et al.* [2015], J Nucl Med, 56:234-242
2. Jonasson, M., *et al.* [2017], Am J Nucl Med Mol Imaging, 7(6):263-274
3. Shingai, Y., *et al.* [2014], Annl Nucl Med, 28:220-226

P54
The influence of sex hormones on d-amphetamine induced changes in extracellular dopamine: a [^{11}C]-(+)-PHNO positron emission tomography

Nicole Praschak-Rieder (1), Ana Weidenauer (1), Ulrich Sauerzopf (1), Martin Bauer (1,2), Lucie Bartova (1), Verena Pichler (3) Cecile Philippe (3,4), Rupert Lanzenberger (1), Siegfried Kasper (1), Wolfgang Wadsak (3,4), Matthäus Willeit (1)

(1) Medical University of Vienna, Department of Psychiatry and Psychotherapy, Division of General Psychiatry
(2) Medical University of Vienna, Departme nt of Clinical Pharmacology
(3) Medical University of Vienna, Department of Biomedical Imaging und Image-guided Therapy, Division of Nuclear Medicine

(4) Center for Biomarker Research in Medicine CBmed, Graz

Introduction:
Animal studies suggest that behavioral and neurochemical responses to dopamine-releasing agents are modified by the actions of sex hormones. In female rats, estrogen has been shown to enhance the behavioral responses to d-amphetamine (1,2), while progesterone alone does not seem to influence d-amphetamine induced stereotypies. Here we studied the impact of sex hormones on the behavioral and neurochemical response to d-amphetamine in healthy human females using the dopamine $D_{2/3}$ receptor agonist radioligand [^{11}C]-(+)-PHNO and positron emission tomography (PET). Reductions in $D_{2/3}$ receptor radioligand binding are able to provide a semi-quantitative measurement of d-amphetamine induced release of dopamine into the extracellular space.

Materials and Methods:

Ten healthy, stimulant-naïve human females had [^{11}C]-(+)-PHNO PET scans, one without intervention serving as baseline condition, and another one 90 to 120 min after oral administration of 0.04 mg/kg bodyweight d-amphetamine. Relative changes in [^{11}C]-(+)-PHNO binding potential (BP_{ND}) values were calculated as ($BP_{ND}^{baseline} - BP_{ND}^{amphetamine}$) / $BP_{ND}^{baseline}$ * 100). Subjective effects of d-amphetamine were quantified by repeated administration of the drug effects questionnaire (DEQ) and the subjective states questionnaire (SSQ), both dedicated scales for measuring effects of stimulant drugs. Serum levels of follicle stimulating hormone (FSH), luteinizing hormone (LH), estrogen, progesterone, and testosterone were determined the day of the PET scans. [^{11}C]-(+)-PHNO BP_{ND} values were derived in dopamine receptor-rich regions of interest (ROIs; ventral striatum, putamen, caudate, globus pallidus, and substantia nigra/ventral tegmental) delineated manually or with the dedicated software package ROMI using the simplified reference tissue model (SRTM-2) as implemented in PMOD analysis software.

Results:

Subjective responses to d-amphetamine, as measured with DEQ and SSQ, showed direct correlations with serum levels of LH, FSH, and estrogen, with r^2 values reaching values as high as 0.65. No correlations were found between progesterone serum levels and DEQ and SSQ scores. In a preliminary analysis, however, we failed to identify significant relationships between any of the sex hormones and d-amphetamine induced changes in [^{11}C]-(+)-PHNO BP_{ND} values.

Discussion:

Although correlational in nature, our data suggest a relevant impact of serum estrogen levels on the behavioral response to d-amphetamine in healthy females. This finding conforms well to the results obtained in several studies in rodents. Despite showing strong relationship to the subjective response to d-amphetamine, sex hormone-serum levels did not relate to d-amphetamine induced changes in [^{11}C]-(+)-PHNO BP_{ND} values. Our findings thus suggest that there are mechanisms mediating the relationship between sex hormones and the subjective d-amphetamine experience that are unrelated to the subcortical release of dopamine by d-amphetamine.

Ackowledgements:

This study was funded by the Austrian Science Fund [FWF P23585-B09], the Anniversary Fund of the Austrian National Bank [ONB 16723], the Medical Scientific Fund of the Mayor of Vienna (Medizinisch-Wissenschaftlichen Fonds des Bürgermeisters der Bundeshauptstadt Wien) [BMF 15189], and the Vienna Science and Technology Fund [WWTF CS15-033] granted to M.W.

References:

Michanek A, Meyerson BJ [1982] Pharmacol Biochem Behav. 16:875-8799.

Becker JB1, Rudick CN [1992] Pharmacol Biochem Behav. 64:53-57.

P55
JABA: Flexible tool for volumetric meta-analysis of region-of-interest and voxel-based PET neuroimaging data

Enrico Glerean[1], Lauri Tuominen[1], Jussi Hirvonen[1,2], & Lauri Nummenmaa[1,3]

[1]Turku PET Centre, Finland; [2]Department of Radiology, University of Turku, Finland; [3]Department of Psychology, University of Turku, Finland

Introduction:
Meta-analysis has proved an invaluable tool for summarizing results from neuroimaging studies oftentimes suffering from poor statistical power (1, 2). Existing coordinate-based approaches are however not suitable for PET and SPECT literature where most studies report results from a limited set of regions-of-interest (ROIs) and only infrequently report the peak coordinates. Restricting the analysis to specific ROIs would yield a scattered and incomplete representation of the results, given that all possible analyses would have to be run separately for each used ROI. Ideally, analysis should thus be done volumetrically by projecting the ROIs back to MNI volumetric space. Yet, because the nomenclature of the ROIs varies substantially across studies and does not necessary conform with unambiguously defined anatomical structures, and because the studies typically do not provide specific information regarding how the ROIs were generated, remapping between ROIs and MNI space is not straightforward.

Methods:
To resolve this problem, we developed the Just Another Brain Atlas (JABA) pipeline for semantic mapping of regions-of interest to volumetric space (**Fig 1**). We first generated a list of regions of interest based on the AAL (3) and Brodmann atlases derived from the WFU pickatlas tool (4). These were complemented with semantic aliases (e.g. “Brainstem” was mapped to aliases “Midbrain”, “Raphe nucleus” “Substantia nigra” and “locus coeruleus”). To map locations of reported regions with ambiguous anatomical boundaries (such as ventromedial prefrontal cortex) not found in the reference atlases, we also generated a semantic atlas based on the anatomical terms found in *Neurosynth*, the largest collection of meta-analytic data from functional neuroimaging studies (1). For each neuroanatomical term in Neurosynth we extracted the FDR-corrected result image, and restricted the resulting image to a single cluster. Resulting ROIs were subsequently spilt between left and right hemispheres. Because Neurosynth contains labels of the activation foci reported by a large community of neuroscience researchers, these ROIs thus result the net agreement across researchers regarding the region nomenclature.

When conducting a meta-analysis of ROI and coordinate-level results, JABA tool is used to query the reported anatomical regions-of interest in each study in the meta-analysis database against the labels in the reference atlases described above. Mapping is done hierarchically. The algorithm firsts searches for direct matches between nomenclature in the studies and the anatomical labels of AAL and Brodmann atlases. If a direct match is not found, it next queries the Neurosynth-based semantic atlas. This process is repeated iteratively while searching for closest possible match, lowering the semantic similarity criterion on each iteration.

Next, this information is used for reconstructing a 3D “pseudo-contrast map” for each contrast in each study, where voxel intensities quantify the direction of patient-control differences: Each JABA-mapped region where significant difference are reported in each study is filled with 1 for regions having higher and -1 for those having lower values of outcome variable for controls versus patients. If the study reports effects as cluster maxima coordinates in MNI space, Gaussian kernels with 8mm FWHM are generated with similar

directionality and weighting as above. This approach thus maximizes the available spatial information for localizing the effects, and conforms all effects to the same MNI voxel space.

The analytic pipeline was tested using a meta-analysis database of altogether 470 studies measuring neuroreceptor and neurotransmitter level changes in common psychiatric disorders using PET or SPECT, of which some reported patient-control differences as ROIs and others as MNI / Talairach coordinates.

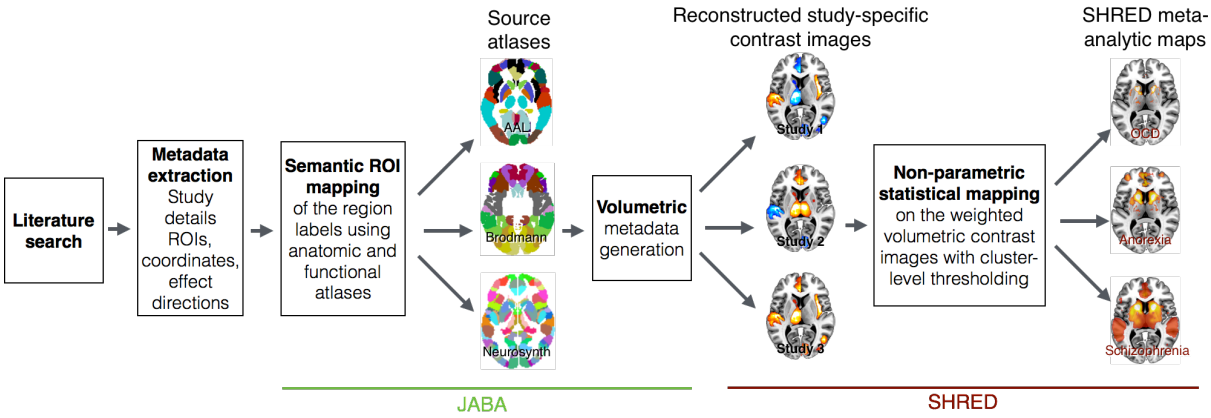

Figure 1. *Overview of the analytic protocol.*

Results and Conclusions:
Optimized JABA tool could retrieve a match for 98% of the terms found in the data, accounting for > 99% of the reported activation foci / ROIs. In second-level analyses, the resulting pseudo-t-contrast maps revealed both common and distinct pathophysiological profiles of specific psychiatric conditions. We conclude that automated semantic mapping of ROIs and coordinates back to the MNI space provides a feasible and potentially powerful way for conducting volumetric meta-analyses of PET and SPECT data.

References:

1. Yarkoni T, Poldrack RA, Nichols TE, Van Essen DC, & Wager TD (2011) NeuroSynth: a new platform for large-scale automated synthesis of human functional neuroimaging data. *Frontiers in Neuroinformatics*.
2. Eickhoff SB*, et al.* (2009) Coordinate-Based Activation Likelihood Estimation Meta-Analysis of Neuroimaging Data: A Random-Effects Approach Based on Empirical Estimates of Spatial Uncertainty. *Human Brain Mapping* 30(9):2907-2926.
3. Tzourio-Mazoyer N*, et al.* (2002) Automated anatomical labeling of activations in SPM using a macroscopic anatomical parcellation of the MNI MRI single-subject brain. *Neuroimage* 15(1):273-289.
4. Maldjian JA, Laurienti PJ, Kraft RA, & Burdette JH (2003) An automated method for neuroanatomic and cytoarchitectonic atlas-based interrogation of fMRI data sets. *Neuroimage* 19(3):1233-1239.

P56
An In vivo Approach to Assess Gut-Microbiome-Brain Axis Determinants of Human Obesity

Swen Hesse[1,2,#], Rima Chakaroun[3,#], S. Kristoffer Forslund[4,5,#], Michael Rullmann[1,2], Julia Luthardt[2], Mandy Drabe[1,2], Yvonne Böttcher[1,6], Georg A. Becker[2], Franziska Zientek[1,2], Philipp M. Meyer[2], Marianne Patt[2], Anja Hilbert[1,7], Michael Stumvoll[1,2], Osama Sabri[1,2]

[1]Integrated Treatment and Research Centre (IFB) AdiposityDiseases, Leipzig University Medical Centre, Leipzig, Germany; [2]Department of Nuclear Medicine, University of Leipzig, Leipzig, Germany; [3]Department of Medicine, University of Leipzig, Leipzig, Germany; [4]Structural and Computational Biology Unit, European Molecular Biology Laboratory, Heidelberg, Germany; [5]Max-Delbrück-Centre for Molecular Medicine, Berlin, Germany; [6]University of Oslo, Institute of Clinical Medicine, Department of Clinical and Molecular Biology, Akershus University Hospital, Lørenskog, Norway; [7]Department of Medical Psychology and Medical Sociology and Department of Psychosomatic Medicine and Psychotherapy, University of Leipzig, Leipzig, Germany; [#]These authors contributed equally to this work.

Introduction:

Among affected axes shaping behaviour, the CNS serotonergic neurotransmission seems to be highly influenced by the gut microbiome composition with consequences towards mental and metabolic health. Here, we investigated in a cohort of individuals with severe obesity, whether central serotonin transporter (*SERT*) availability is associated with overall composition of the gut microbiota, as represented through relative dominance of major clades (ie, firmicutes-, bacteroides-, and prevotella-rich enterotype) (Fig. 1).

Materials and Methods:

Thus far, we have included nine, non-depressed individuals with severe obesity (7 females; age 42.9±11.6 years; body mass index 42.2±4.3 kg/m2, Beck Depression Inventory 6.8±6.4; 0-14), who underwent PET with [^{11}C]DASB (484.1±5.1 MBq; 90-sec bolus infusion, 90 min dynamic scan) to obtain for each the *SERT* binding potential BP_{ND} by applying multi-linear reference tissue model with 2 parameters after co-registration with individual PET-MR data. Gut microbiome signatures were assessed by metagenomic sequencing of faecal specimen to estimate both gene count and Shannon diversity (Forslund et al., 2015). To account for epigenetic variation of the *SERT* gene (ie, early life-stress imprint), we additionally performed analysis of *SERT* gene promoter methylation (Drabe et al., 2017). For behavioural testing, we used the Behavioural Approach System (BAS) Reward Scale.

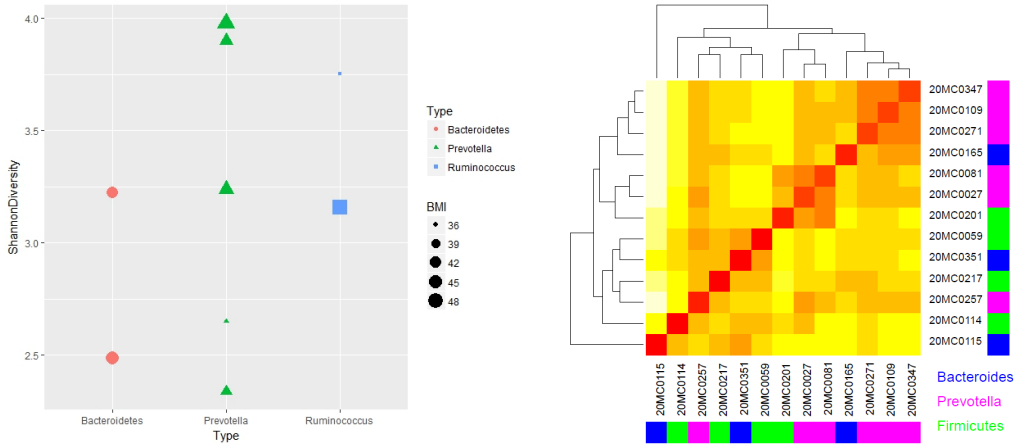

Fig. 1. Alpha-diversity (Shannon diversity) and dominant gut microbiota metagenomic clades in study subjects accounting for body mass index (BMI). Heatmap clusters based on Bray-Curtis dissimilarity between samples with regards to gut taxonomic composition (Genus abundance) reveals enterotype structure as an informative high-level summary of the gut microbiota in these subjects, suggesting utility of its comparison with brain imaging readouts.

Results:

BP_{ND} in the prefrontal cortex (PFC) was positively associated with both gut microbial gene count and diversity (eg, the ventromedial PFC vs. gene count R=0.76; P=0.02; Fig. 2; the dorsolateral PFC vs. gut microbial diversity R=0.71; P=0.03) while there was a negative correlation between BP_{ND} and gut microbial gene count in the hypothalamus (R=-0.70; P=0.03; Fig. 2). Prefrontal BP_{ND} and methylation rates tend towards a negative relationship but this did not reach robust statistical significance (R=-0.66; P=0.05; Fig. 2). Also, BAS Reward (15.8±3.6; 9-20) did not show significant relationship with prefrontal PFC, gut microbial gene count, or Shannon diversity, though there were positive associations between BAS reward and BP_{ND} in the substantia nigra/ventro-tegmental area (R=0.73; P=0.03) and with CpG-methylation (eg, CpG_{12}; R=-0.72; P=0.03).

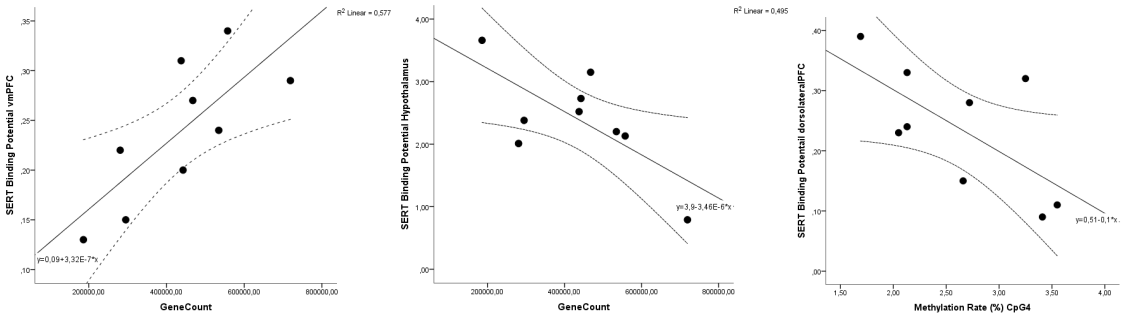

Fig. 2. Relationship between *SERT* binding potential and gut microbial gene count as well as *SERT* gene promoter methylation

Discussion:

These preliminary observational findings hint towards a mechanism integrating a distinct microbiome function and composition, which is associated with differences in the methylation rates and prefrontal *SERT* function in human obesity. Interestingly, these data corroborate other preclinical work that shows changes in prefrontal transcriptome related to the gut microbiota (Hoban et al. 2016). Another putative explanation is that altered prefrontal *SERT* availability represents compensatory changes to lower hypothalamic *SERT* levels. Yet, there is no reliable hint for a relation between reward sensitivity, gut microbiome and prefrontal *SERT* function.

Acknowledgements:

The work is supported by the Federal Ministry of Education and Research (BMBF), Germany, FKZ: 01E01001). We also acknowledge the help of the EU FP7 MetaCardis project (HEALTH-2012-305312) for microbiome analysis methods and metagenome sequencing.

References:

Drabe M, Rullmann M, Luthardt J, et al. [2017] Transl Psychiatry 7: e1167

Forslund K, Hildebrand F, Nielsen T, et al. [2015] Nature 528: 262-266

Hoban AE, Stiling RM, Ryan FJ, et al. [2016] Transl Psychiatry 6: e774

P57
The observation of finger representations in somatosensory area by pressure tactile stimulation

Ji-Hun Jo, Hyung-Sik Kim, Soon-Cheol Chung, Mi-Hyun Choi*

Department of Biomedical Engineering, College of Science and Technology, Konkuk University, Chungju, South Korea

Introduction:

In previous studies, a finger representations was observed in BA 3 by introducing stimulation such as piezoelectric (50 Hz or lower), brush, electric, air, and other means to the fingers [Blankenburg et al., 2003; Westen et al., 2004; Martuzzi et al., 2014; Schweisfurth et al., 2014]. In the previous studies on inter-digit finger representations, results on only the first joint of each finger were reported, and no result has been reported with regard to the finger representations of the second and third joints. Also, no result on the finger representations using pressure stimulation was presented, and no result on the BA 2, which sensitively responds to pressure stimulation, has been reported yet. Using the activation location (peak coordinates) at BA 2 of each finger and joint by pressure stimulation, the finger representations are examined.

Materials and Methods:

Ten normally healthy male participated in the study. None of the participants was reported to have a history of psychiatric or neurological disorders. The functional Magnetic Resonance Image (fMRI) was acquired by applying pressure stimulation with certain strength (8.5 psi) to the three joints [first (p1), second (p2), and third (p3) joints] of the four fingers (index, middle, ring, and little fingers) in the right hand.

The session of fMRI experiments consisted of three blocks: rest phase (30 s), pressure phase (30 s). In the pressure phase, stimulation was randomly applied for 30 s to one of the three joints (p1, p2, or p3) of the selected finger (index, middle, ring, or little finger). Three repetitive experiments were conducted for a selected finger in each session. The experiments were also performed on the other three fingers following the same procedure described above. All subjects participated in a total of 12 sessions for the three repetitive experiments conducted for each finger.

The region-of-interest analysis method was used to observe the activation at Brodmann area 2 (BA 2) only among the entire brain area activated due to the pressure stimulation. The peak coordinates were extracted from the BA 2 activated by stimulation of each finger and joint. The peak coordinates indicated the location of one voxel with the highest intensity (measured by the highest t-value) among the voxels activated at BA 2 into the x, y, and z coordinates. The peak coordinates at BA 2 activated by the application of pressure stimulation to a total of 12 joints were extracted from the group and from each subject.

Results

As a result, the ring finger was excluded from the analysis. Because activation at BA 2 was observed in only three out of the eight subjects during pressure stimulation to the ring finger.

With regard to all joints, peak coordinates appeared from the lateral to the medial direction and from the inferior to the superior direction following the index, middle, and little finger sequence. Also, peak coordinates appeared from the anterior to the posterior direction following the p1, p2, and p3 sequence in all fingers.

Discussion:

When pressure stimulation was applied to the four fingers, no distinctive activation was observed in the ring finger compared with the other fingers. In the previous study [Weinstein, 1962], the sensitivity of the ring finger is lower than that of the other four fingers when the tactile sensitivity of the five fingers is compared. In this study, we determined that consistent result could not be observed when introducing pressure stimulation to the ring finger due to the same reason.

As a result, a finger representations of BA 2 was constructed from the lateral to the medial direction and from the inferior to the superior direction in all joints following the sequence of the index, middle, and little fingers. Although the presented method of stimulation and observed activation area (BA 3 versus BA 2) differed between the previous and the present studies, the pattern of the finger representations by tactile stimulation was shown to be similar. However, no clear trend from the anterior to the posterior direction was observed in the present study.

Acknowledgements:

This research was supported by Basic Science Research Program through the National Research Foundation of Korea(NRF) funded by the Ministry of Education(2017R1D1A1B03029585)

References:

van Westen D, Fransson P, Olsrud J et al. [2004] BMC Neurosci. 5: 28

Blankenburg F, Ruben J, Meyer R et al. [2003] Cereb. Cortex 13: 987-993

Martuzzi R, Zwaag W, Farthouat J et al. [2014] Hum. Brain Mapp. 35: 213-226

Schweisfurth MA, Frahm J, Schweizer R [2014] Front. Hum. Neurosci. 8: 1-14

Weinstein S. [1962] Percept. Mot. Skills 14: 351-354

P58
Stimulation in the VTA is partially driven by dopamine at both D1 and D2 receptors: A multi-modal evaluation with PET/fMRI

Christin Y. Sander[1], John Arsenault[1,2], Wim Vanduffel[1,2], Bruce R. Rosen[1,3] and Joseph B. Mandeville[1]

[1]Athinoula A. Martinos Center, Department of Radiology, Massachusetts General Hospital, Charlestown, MA, [2]Laboratory of Neuro- and Psychophysiology, Medical School, KU Leuven, Belgium, [3]Division of Health Sciences and Technology, Harvard-MIT, Cambridge, MA

Introduction:

The detection of *in vivo* endogenous neurotransmitter release in real time has been of great interest[1]. PET imaging has been previously shown to be sensitive to endogenous dopamine release either using drugs or through behavioral challenges[2,3]. Dopamine release due to deep brain stimulation (DBS) of the ventral tegmental area (VTA) - the primary origin of dopaminergic neurons - has been demonstrated using invasive neuroimaging measurements[4,5]. However, the respective contributions of D1 vs. D2-like receptors, have not been previously explored. The purpose of this study was to dynamically characterize the dopaminergic receptor subtypes that contribute to fMRI activation due to DBS of the VTA and the overall dopaminergic contribution. Simultaneous PET/fMRI together with pharmacological blocking during electrical stimulation was used to decipher the underlying neurotransmitter/receptor contribution due to activation along the mesocorticolimbic circuitry.

Materials & Methods:

An integrated 3T PET/MRI scanner was used to acquire simultaneous [^{11}C]raclopride-PET and fMRI data during acute stimulation of an anesthetized baboon (1.5% isoflurane) with a chronic microstimulation implant in the right VTA. Stimulation was applied through a current of 1mA at 100Hz, in pulse trains of 200ms. Stimulation trains were applied in a nested block design to provide maximum contrast-to-noise for both PET and fMRI, with inter-stimulation intervals of 1-8s over a period of 5-30min. In the PET/fMRI sessions (n=8), [^{11}C]raclopride was administered as a bolus+infusion, with stimulation blocks starting at ~35min. In order to distinguish receptor-specific contributions to the fMRI signal, separate fMRI sessions (n=4) were designed to stimulate before and after a blocking dose of the D1R antagonist SCH23390 (0.03-0.09mg/kg i.v.) and the D2R antagonist prochlorperazine (0.1mg/kg i.v.). Stimulation in these sessions consisted of inter-stimulation intervals of 2s that lasted for 15s and alternated with 93s of rest. This pattern was repeated for 10min. Gradient-echo EPI data were acquired continuously during stimulation and ferumoxytol was used as a contrast agent. fMRI data were analyzed with a standard GLM and converted into cerebral blood volume (CBV) changes. PET data were analyzed with the 2-parameter SRTM[6] and a time-dependent k_{2a} term[7] that was fit during stimulation periods.

Results:

fMRI data from all stimulation sessions showed positive CBV signals in the right (implanted) hemisphere due to repeated stimulations every 1-3s in right caudate (4.5%), nucleus accumbens (3.3%), putamen (2.8%), thalamus (2.4%) and prefrontal cortex. [^{11}C]raclopride-PET data showed mixed results, with single sessions showing an absolute change in BP_{ND} up to 1.3, equivalent to 35% occupancy, during stimulation periods in subregions of the right striatum. However, a group analysis did not show significant displacement during stimulation intervals. Average baseline BP_{ND} values across sessions were 3.8±0.3 (putamen), 2.8±0.3

(caudate) and 2.1±0.1 (nucleus accumbens). There were no significant BP_{ND} differences between left vs. right sides. Comparisons of the fMRI signal due to stimulation before and after pharmacological blocking of D2 receptors (D2R) resulted in a signal increase in all previously activated regions (Fig.1, *upper*). After D2R blocking, the %CBV signal was 1.4, 1.3 and 2.8 times larger than in the pre-drug stimulation condition in putamen, caudate and nucleus accumbens, respectively. Pharmacological blocking of D1 receptors (D1R) showed a drop in CBV magnitude in all previously activated regions (Fig.1, *lower*). After the D1R block, the %CBV signal decreased to 0.5, 0.5 and 0.6 of its pre-drug magnitude. In the D2R blocking condition only, activation was observed in the prefrontal cortex and the contralateral side of the striatum.

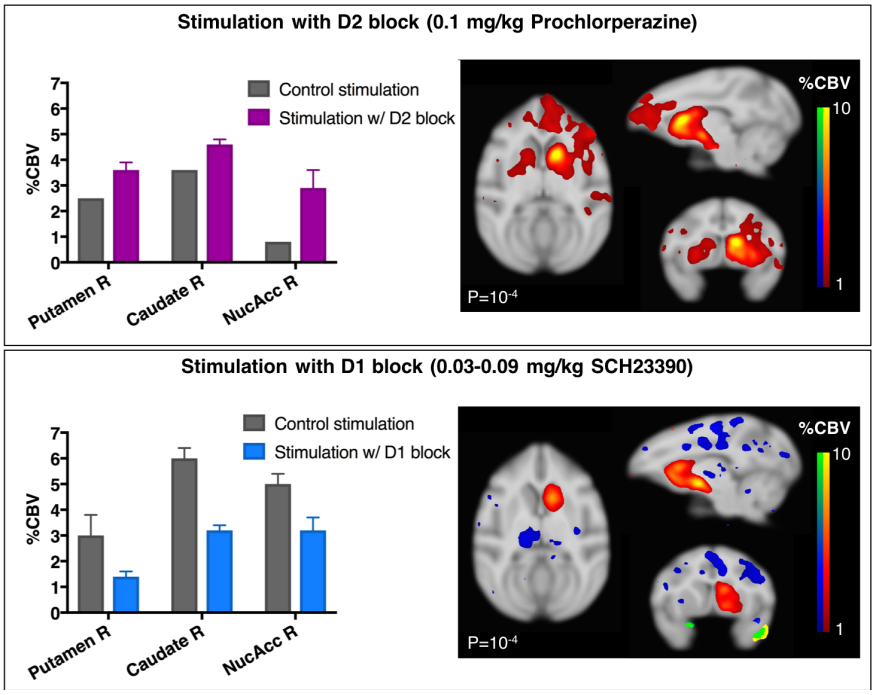

Figure 1.
fMRI data showing overall positive CBV changes due to stimulation in the VTA, relative to baseline (no stimulation). Blocking with a D2R antagonist increases the CBV signal *(upper)*, suggesting suppression of an inhibitory D2R signal. Blocking with a D1R antagonist decreases the CBV signal *(lower)*, consistent with blocking an excitatory D1R contribution. All voxelwise maps show CBV signal changes due to stimulation, relative to baseline (no stimulation).

Discussion/Conclusion:

A robust positive fMRI activation due to stimulation was observed but displacements of [^{11}C]raclopride were not reliably reproducible across sessions. Therefore, we investigated whether fMRI changes were driven by dopamine through a set of blocking studies with D1R and D2R antagonists at doses that have achieved >90% occupancy in separate studies (not shown). The observed CBV increase after blocking D2R suggests that only part of the CBV signal (~31% in putamen, 22% in caudate) is likely to be D2R-mediated, with the CBV increase demonstrating a block of inhibitory D2R signaling. In concordance with that, the D1R block resulted in a CBV decrease, demonstrating a partial excitatory D1R contribution (38% in putamen, 36% in caudate, including an estimated inhibitory D2R signal) that can be suppressed. Yet, the fact that the overall CBV signal remains positive even with a D1R block suggests that a part of the remaining signal (31% in putamen, 42% in caudate) is driven by a non-dopaminergic neurotransmitter/receptor, e.g. glutamate. Since the D2R contribution is likely only ~30% of the overall signal, we estimate D2R-specific signals to be on the order of 1% CBV, which would translate into <10% D2R occupancy by dopamine based upon prior studies[8]. This dopamine contribution is likely to be at the limit of detection in [^{11}C]raclopride-PET. Overall, these results demonstrate that both D1R and D2R signaling are contributing to DBS-induced fMRI signal changes in basal ganglia, but with other neurotransmitters likely playing an important role for VTA stimulation.

Acknowledgements: This work was supported by NIH grants 1K99DA043629, P41EB015896, S10RR026666, S10RR022976, S10RR019933 and S10RR017208, and FWO-Flanders, FG0D5817N, G090714N, and G0007.12.

References:

[1]Arsenault JT, Nelissen K, Jarraya B et al. [2014], *Current Biology,* 77:1174-1186. [2]Badgaiyan R [2014], *Progress in Brain Research* 211:165-182. [3]Shotbolt P, Tziortzi A, Searle G et al. [2012], *JCBFM* 1:127-136. [4]Schluter EW, Mitz AR, Cheer JF et al. [2014], *PLOS ONE* 9:e98692. [5]Lu Y, Driscoll N, Ozden I, et al. [2015], *Neurophotonics* 2:031207. [6]Wu Y and Carson RE [2002], *JCBFM*, 22:1440-1452. [7]Alpert N, Badgaiyan R, Livni E et al. [2003], *NeuroImage* 3:1049-1060. [8]Sander CY, Hooker JM, Catana C, et al. [2015], *Neuropsychopharmacology* 41:1427-1436.

P59
Overcoming major challenges in input-function based PET kinetic modelling

Stefanie D. Krämer[1], Linjing Mu[2], Roger Schibli[1], Simon M. Ametamey[1]

[1] *Radiopharmaceutical Sciences, ETH Zurich, Switzerland;* [2] *Department of Nuclear Medicine,*

University Hospital Zurich, Switzerland

Introduction:

Kinetic modelling with an arterial input function is the gold-standard method in PET compartmental modelling. Determining the blood coincidences with a dedicated coincidence counter provides blood time-activity curves at high temporal resolution. We addressed three major challenges which we encountered in input-function based modelling. These are the estimation of the background counts of the blood-coincidence curve ($\boldsymbol{N_{Bckg}}$), the estimation of the start time of the blood-coincidence curve ($\boldsymbol{t_0}$) and deviations of individual ratios of parent tracer to total radioactivity from averaged representative (reference) data (if not determined individually for each scan).

Material & Methods:

We first simulated the effects of errors in N_{Bckg} and t_0 on the fit parameters and the sum of squared residuals (SSR) of the fit functions of a 2-tissue compartment model. We next used data from rat-brain scans obtained with our recently published NMDA GluN1/GluN2B receptor-targeting tracer [^{11}C]Me-NB1 (ref. 1) and fitted N_{Bckg} and t_0 together with the fit parameters of a 2-tissue compartment model (K_1, k_2, k_3, k_4) and the parameters describing the Logan plot. Simultaneously, a bi-exponential function defining the ratios parent tracer/total radioactivity in plasma was fitted to reference data, allowing individual deviations from the reference data, if this reduced the global (overall) SSR. The sum of weighted SSR of the brain time-activity curve, the Logan plot and the plasma parent tracer/total radioactivity ratios was minimized with a Matlab (MathWorks) solver to determine the optimal fit parameters, including N_{Bckg} and t_0. Both N_{Bckg} and t_0 were subsequently varied to evaluate their influence on the fitted V_T.

Results:

Deviations from the true values of both N_{Bckg} and t_0 increased the SSR in the simulations. Variations in N_{Bckg} had a high impact on V_T, in particular at low signal/noise ratio of the input function (**Fig. 1A-F**). Analysing the experimental data of [^{11}C]Me-NB1 by fitting K_1, k_2, k_3, k_4, the bi-exponential function describing the ratios parent/total radioactivity in plasma, the Logan plot, N_{Bckg}, and t_0 all together revealed a well-defined minimum of the global SSR. An exemplary [^{11}C]Me-NB1 scan and the respective fit function, V_T and V_T from the Logan plot ($V_{T,Logan}$) are shown in **Fig. 1G-I**. We applied this method for the evaluation of rat PET data with [^{11}C]Me-NB1 (ref. 1) and a first-in-human PET study with the mGluR5-targeting tracer [^{18}F]PSS232 (ref. 2). A further refined strategy may include minimizing the difference between V_T and $V_{T,Logan}$ during the fitting procedure.

Discussion/Conclusion:

Major challenges in PET kinetic modelling can be overcome by including N_{Bckg} and t_0 in the fitting procedure and combining the weighted SSR of the non-linear compartmental modelling and the linear Logan Plot. Furthermore, the simultaneous rather than independent fitting of reference parent tracer/total radioactivity ratios in plasma allows individual deviations from the reference data.

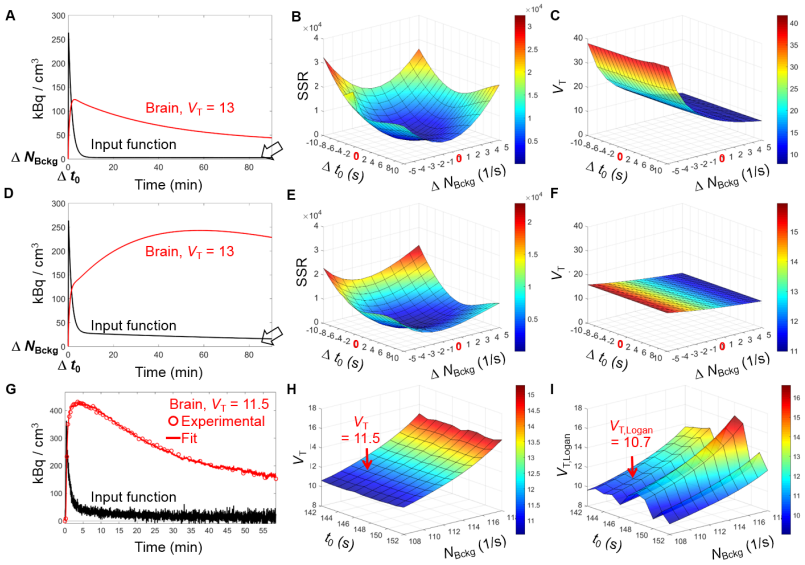

Figure 1. **A-F**) Simulated and **G-I**) experimental data. **A**, **D**) Simulated input functions and time activity curves according to a 2-tissue compartment model with K_1 = 0.6 ml/min/cm^3, k_2 = 0.6 min^{-1}, k_3 = 0.6 min^{-1}, k_4 = 0.05 min^{-1} and V_T = 13 ml/cm^3. Back arrows indicate the differences between **A** and **D** in signal/noise ratio of the input function. **B**, **E**) Corresponding global SSR depending on the deviations in N_{Bckg} and t_0. **C**, **F**) Corresponding fitted V_T, note the influence of N_{Bckg}! **G**) Experimental and fitted time-activity curve of [^{11}C]Me-NB1 in rat whole brain, including as fit parameters besides K_1 to k_4, N_{Bckg}, t_0, Logan plot parameters and the bi-exponential function describing the ratio of parent tracer/total radioactivity in plasma. **H**, **I**) V_T and $V_{T,Logan}$ of the data in **G**, depending on N_{Bckg} and t_0. Red arrows indicate the values at minimal global SSR. The difference between V_T and $V_{T,Logan}$ was not included in the overall SSR in this example.

Acknowledgments:

We thank Bruno Mancosu for tracer production and Claudia Keller for PET scans.

References:

1) Krämer SD, Betzel T, Mu L, Haider A, Herde Müller A, Boninsegni AK, Keller C, Szermerski M, Schibli R, Wünsch B and Ametamey SM [2018] J. Nucl. Med., in press (doi: 10.2967/jnumed.117.200451).
2) Warnock G, Sommerauer M, Mu L, Pla Gonzales G, Geistlich S, Treyer V, Schibli R, Buck A, Krämer SD and Ametamey SM [2018] Eur. J. Nucl. Med. Mol. Imaging, in press (doi: 10.1007/s00259-017-3879-x).

P60
In vivo absolute quantification of striatal and extrastriatal $D_{2/3}$ receptors with [^{123}I]epidepride SPECT

Stergios Tsartsalis[¶], Benjamin B. Tournier[¶], Karl Aoun[¶], Manideep G. Vemula[¶], Nathalie Ginovart[¶§], Philippe Millet[¶§]

[¶]*Division of Adult Psychiatry, University Hospitals of Geneva, Switzerland*

[§]*Department of Psychiatry, University of Geneva, Switzerland*

Introduction:

Molecular imaging of the dopaminergic system with Positron Emission Tomography (PET) and Single Photon Emission Tomography (SPECT) is a powerful tool for the non-invasive study of the living brain in clinical and translational settings. [^{123}I]epidepride is a high-affinity radiotracer that allows imaging of striatal and extrastriatal $D_{2/3}$ sites. Nevertheless, its high-affinity renders their kinetics in the striatum particularly slow, seriously impeding quantification in this region. Here, we describe a partial saturation approach to separately estimate B_{avail} and $appK_d$ in striatal and extrastriatal regions.

Materials and methods:

6 male rats underwent a 180-min SPECT scan in which [^{123}I]epidepride was co-injected with a dose of unlabeled epidepride at a concentration occupying 50-70% of the $D_{2/3}$ receptors. This scanning protocol permits an *in vivo* Scatchard plot to be delineated and B_{avail} and $appK_d$ to be estimated. These results were compared to results of a multi-injection SPECT study (of a total duration of 6.5 hours) performed on a group of three rats by means of linear regression analysis.

Results:

A 120-min SPECT scan is sufficient to estimate B_{avail} and $appK_d$ values of [^{123}I]epidepride with the partial saturation method. These values are comparable and highly correlated to the corresponding values from the multi-injection experiments, as the linear regression analysis demonstrates ($r=0.99$, $p<0.01$ for B_{avail} and $r=0.83$, $p<0.05$ for $appK_d$). No significant difference in the average B_{avail} or $appK_d$ values from the multi-injection and the partial saturation studies was found ($p>0.05$).

Discussion/Conclusion:

Using the partial saturation protocol, *in vivo* imaging of striatal and extra-striatal $D_{2/3}$ receptors is feasible. Given its high-affinity, [^{123}I]epidepride SPECT will allow the separate estimation of B_{avail} and $appK_d$ and may provide information on the receptor concentration and potentially, the presence of endogenous dopamine. This methodology may be directly implemented in preclinical research and has the potential to be used in clinical SPECT studies as well.

References:

Delforge J, Spelle L, Bendriem B et al. [1996] J Nucl Med 37:5-11
Tsartsalis S, Tournier BB, Aoun K et al. [2017] NeuroImage 147:461-72

P61

Increase of ^{11}C-PBR28 binding after a clinical course of Theta Burst Stimulation in Non-Human Primates: a preliminary assessment.

Lucero Aceves-Serrano[1], Jason L Neva[2], Samantha Feldman[3], Lara A Boyd[1,2,3], Doris Doudet[1,4].

[1]Faculty of Medicine, Graduate program in Neuroscience, University of British Columbia, Vancouver, Canada

[2]Department of Physical Therapy, Faculty of Medicine, University of British Columbia, Vancouver, Canada

[3] Faculty of Medicine, Graduate program of Rehabilitation Sciences, University of British Columbia, Vancouver, Canada

[4]Department of Neurology, University of British Columbia, Vancouver, British Columbia, Canada

Introduction:

Theta Burst Stimulation (TBS), a high-frequency type of repetitive Transcranial Magnetic Stimulation (rTMS), has gained attention due to its potential efficiency compared to other rTMS protocols. TBS is administrated in shorter sessions (40-190 seconds) and may lead to longer aftereffects[1] with similar therapeutic outcomes [2]. There is little work investigating whether a clinical course of rTMS induces inflammatory response. Theoretically, TBS has the potential to cause an inflammatory response as result of the high frequencies (50Hz) applied.

Thus, we used ^{11}C-PBR28, a tracer which binds to translocator protein (TSPO) and is considered a marker of activated microglia, to assess the effect of a clinical course of TBS (12-15 sessions) on inflammation in vivo, using positron imaging tomography (PET).

Materials & Methods:

^{11}C-PBR28 scans were acquired in healthy rhesus monkeys before and within 24 hours after a series of 12-15 sessions of either continuous (cTBS) or intermittent TBS (iTBS). Stimulation sessions were administrated daily to the awake animal, Monday to Friday, to mimic a clinical schedule.

Resting motor threshold (TMS) was measured in the anesthetized animal during the first TBS session. Each TBS session consisted of 600 pulses delivered at 90% RMT. Stimulation was administrated over the left motor cortex using a figure-8 shaped coil. Each TBS session was conducted in the awake animal sitting quietly in a primate chair.

For the PBR28 PET studies, the anesthetized animal was scanned for 90 minutes starting at tracer injection. Free fraction was measured in the majority of animals and proved very stable at around 10%. Non displaceable binding potential (BP_{ND}) was obtained using a Logan analysis and white matter as the region of non-specific binding.

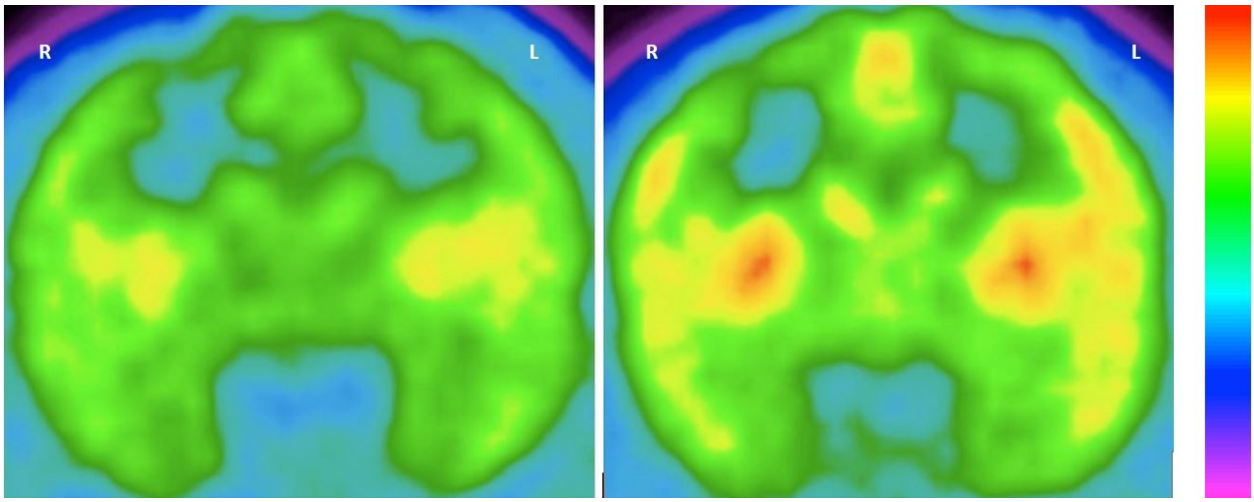

Coronal view of PET scan. Baseline ^{11}C-PBR28 scans is shown in the left side. Post-stimulation scan is shown in the right side. The amount of tracer binding is represented in heat color scale.

Results:

All monkeys showed a significant increase in ^{11}C-PBR28 binding after TBS administration, as compared to sham and with test-retest data. Similar increases were observed following both cTBS and iTBS. We thus averaged the data from the 2 stimulations paradigms. The increase in PBR28 BP_{ND} was greater in all cortical regions compared to the striatum or thalamus.

Discussion/Conclusion:

Here, we demonstrated that a clinical course of TBS could lead to an increase of TSPO binding, a marker of brain immune activation, *as shown by the change of ^{11}C-PBR28 binding.* Increases in markers of inflammation were obsrved in both types of stimulation, suggesting that the immune response could be caused by the high-frequency stimulation rather than a specific pattern of administration (intermittent vs. continous). It is also unknown if this effect is permanent or transient. It is unknown if TSPO binding reflects pro or anti-inflammatory response or a combination of both. These preliminary data will need to be replicated in a larger group of animals.

References:

[1] P. Ragert, M. Camus, Y. Vandermeeren, M. A. Dimyan, and L. G. Cohen, “Modulation of Effects of Intermittent Theta Burst Stimulation Applied Over Primary Motor Cortex (M1) by Conditioning Stimulation of the Opposite M1,” *J. Neurophysiol.*, vol. 102, no. 2, pp. 766–773, 2009.

[2] S. K. Meehan, E. Dao, M. A. Linsdell, and L. A. Boyd, “Continuous theta burst stimulation over the contralesional sensory and motor cortex enhances motor learning post-stroke,” *Neurosci. Lett.*, vol. 500, no. 1, pp. 26–30, 2011.

P62
Radiosynthesis and *in vivo* evaluation of [^{11}C]MPC-6827, the first brain penetrant microtubule PET ligand

J S Dileep Kumar[a], Kiran Kumar Solingapuram Sai[b], Jaya Prabhakaran[a,c], Hakeem R. Oufkir[b], Gayathri Ramanathan[b], Christopher T. Whitlow[b], Hima Dileep[a,c], Akiva Mintz[d], **J. John Mann**[a,c,d]

[a] Division of Molecular Imaging and Neuropathology, New York State Psychiatric Institute, New York; Department of Radiology, [b]Wake Forest School of Medicine, Winston Salem, NC; [c]Department of Psychiatry, Columbia University Medical Center, New York; [d]Department of Radiology, Columbia University Medical Center, New York

Introduction:

Abnormalities of microtubules (MTs) result in misregulation of mitotic spindles and in the pathogenesis of several neurodegenerative disorders, cancers, brain injuries and neuropsychiatric disorders. The role of MTs in mitotic processes has led to new microtubule-targeted agents (MTA) being developed as cancer medications for the past 20 years. More recently, new generation MTAs are undergoing clinical trials for tauopathies. Despite the importance of brain-MT related diseases, no currently available MT PET tracer can penetrate the blood brain barrier (BBB), preventing *in vivo* imaging of MTs in brain. We identified MPC-6827 as a candidate ligand. MPC-6827 (verubulin aka Azixa, IC_{50} = 1.5 nM to MT) was selected based on its high MT affinity, selectivity, optimal pharmacokinetics, pharmacodynamics, and available in vivo preclinical and clinical information.[1,2] In this study, we report the automated radiochemical synthesis of [^{11}C]MPC-6827, its ex vivo biodistribution and *in vivo* PET imaging in rodents.[3]

Materials and Methods:

The radiochemical synthesis of [^{11}C]MPC-6827 was optimized and automated in a GE-FX2MeI/FX2M radiochemistry module by alkylating the corresponding desmethyl-MPC-6827 with [^{11}C]MeI in DMF using NaOH. The binding affinity and selectivity of MPC-6827 was assessed for a large panel of brain targets through NIMH-PDSP. Biodistribution studies of [^{11}C]MPC-6827 (100$\pm$20 µCi) were performed in male white mice (n=4 per time point). Tracer uptake in major organs was measured using a γ-counter and expressed as %ID/g tissue. microPET experiments were performed in anesthetized athymic nude male mice (50$\pm$0.10 µCi n=3) or Sprague-Dawey rats (100$\pm$0.20 µCi, n=2) using a Trifoil PET/CT scanner with 60 minute acquisitions. Blocking experiments (microPET and biodistribution) were performed in white male mice (n=3) 20 min prior to injection of MPC-6827 (5 mg/kg, i. v).

Results:

[^{11}C]MPC-6827 was synthesized with high radiochemical purity (>98%) and high specific activity (2$\pm$0.5 Ci/µmol) with 40$\pm$5% radiochemical yield, decay corrected to EOS (n =20). Except for histamine-4 receptor (H4R, Ki = 155 nM) and sigma-1 receptor (σ1R, Ki =455 nM), MPC-6827 did not show significant affinity (Ki =>1000 µM) for all other tested brain receptors, transporters, enzymes and protein targets. *Ex vivo* biodistribution studies

indicated that [^{11}C]MPC-6827 penetrated the BBB. Blocking experiments at 30 minute demonstrated 70% blockade of radioactivity in brain. The specific uptake ratio of brain is 10 times higher than in muscle, demonstrating an advantage of [^{11}C]MPC-6827 for brain imaging. Apart from brain, muscle, spleen and lungs showed 60%, 42% and 30% specific binding, respectively. Pancreas and heart showed 20% and 16% specific binding, and no significant specific binding was found in other tested regions. MicroPET imaging in mice and rats also confirmed BBB penetration and retention in brain indicated uniform binding across brain regions with no obvious reference region. Specific binding was found with blocking studies using non-radioactive MPC-6827 in mice (Figure 1).

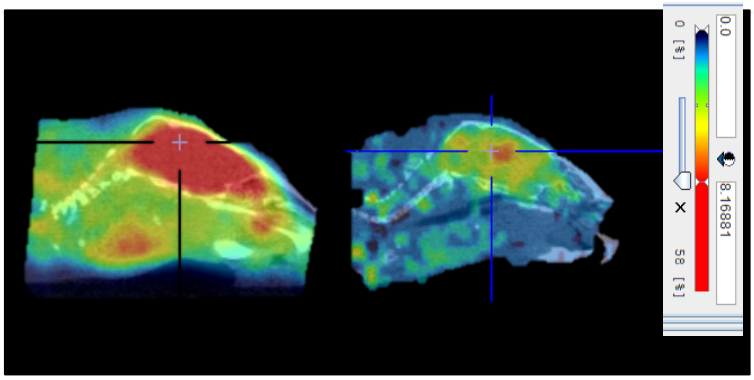

Figure 1. Sum of 0-60 minute emission scan showing PET sagittal images of [^{11}C]MPC-6827 in a representative mouse brain (left: baseline; right: blocking with 5 mg/kg MPC-6827; cross hairs over center of brain).

Conclusions:

We report an automated radiolabeling procedure for [^{11}C]MPC-6827 with high radiochemical yield, purity and specific activity. *In vivo* studies in rodents indicated BBB penetration and binding of the radiotracer in brain and other organs. Combination of favorable kinetics and robust specific binding with excellent brain uptake may make [^{11}C]MPC-6827 a suitable PET ligand for *in vivo* quantification of MT inside and outside the brain. Lack of a suitable reference region is likely to be due to ubiquitous target distribution and not a specific property of this ligand.

Acknowledgement:

Diane Goldberg Foundation (NYSPI/CUMC) and WFSM CTSA TIP (UL1TR001420)

References:

1. Kasibhatla, S.; Baichwal, V.; Cai, S. X.; Roth, B.; Skvortsova, I.; Skvortsov, S.; Lukas, P.; English, N. M.; Sirisoma, N.; Drewe, J.; Pervin, A.; Tseng, B.; Carlson, R. O.; Pleiman, C. M. MPC-6827: a small-molecule inhibitor of microtubule formation that is not a substrate for multidrug resistance pumps. Cancer Res. 2007, 67(12), 5865-71.
2. Grossmann, K. F.; Colman, H.; Akerley, W. A.; Glantz, M.; Matsuoko, Y.; Beelen, A. P.; Yu, M.; De Groot, J. F.; Aiken, R. D.; Olson, J. J.; Evans, B. A.; Jensen, R. L. Phase I trial of verubulin (MPC-6827) plus carboplatin in patients with relapsed glioblastoma multiforme. J. Neurooncol. 2012, 110(2), 257-64.
3. Kumar JSD, Mann JJ. Radiolabeled microtubule compounds and uses thereof, 2017, US 62/578,903.

P63
Head-to-head comparison of ^{11}C-PBR28 and ^{18}F-GE180 for the quantification of TSPO in the human brain

Paolo Zanotti-Fregonara[1], Belen Pascual[1], Gaia Rizzo[2], Meixiang Yu[1], Neha Pal[1], David Beers[1], Randall Carter[3], Stanley H. Appel[1], Nazem Atassi[4], Joseph C. Masdeu[1].

1 Nantz National Alzheimer Center and Houston Methodist Neurological Institute, and Weill Cornell Medicine, Houston, Texas

2 Imanova Ltd., Centre for Imaging Sciences, Hammersmith Hospital, London, UK

3 GE Global Research, Schenectady, New York

4 Neurological Clinical Research Institute, Massachusetts General Hospital, Boston, Massachusetts

Introduction:

^{18}F-GE180 is a new positron emission tomography (PET) tracer to quantify the translocator protein TSPO, a biomarker for inflammation. The aim of this study was to compare head-to-head ^{18}F-GE180 to the well-established TSPO tracer ^{11}C-PBR28, by scanning with either tracer during the same day in the same subjects.

Materials & Methods:

Five subjects underwent a 90-minute PET scan with ^{11}C-PBR28 in the morning and ^{18}F-GE180 in the afternoon. A metabolite-corrected arterial input function was obtained in each subject for both tracers, and the brain uptake was quantified with a two-tissue compartmental model.

Results:

The rate of metabolism of ^{18}F-GE180 in arterial blood was slower than that of ^{11}C-PBR28 (the percentages of unmetabolized parent in plasma at 90 minutes were 74.9 ± 4.15% and 11.2 ± 1.90%, respectively). The plasma free fraction was similar for both tracers: 3.5% ± 1.1 for ^{18}F-GE180 and 4.1% ± 1.1 for ^{11}C-PBR28. The average total volume of distribution (V_T) of ^{18}F-GE180 was about 20 times smaller than that of ^{11}C-PBR28 (0.15 ± 0.03 mL/cm^3 for ^{18}F-GE180 and 3.27 ± 0.66 mL/cm^3 for ^{11}C-PBR28). ^{18}F-GE180 was characterized by a poor transfer from the vascular compartment to the brain (K_1 was about ten times smaller than that of ^{11}C-PBR28). Moreover, kinetic modeling was more difficult with ^{18}F-GE180, as its V_T values were identified with a lower precision than those of ^{11}C-PBR28 and outlying values were more frequent.

Conclusion: The V_T of ^{18}F-GE180 is about 20 times smaller than that of ^{11}C-PBR28, due to a low penetration in the brain from the vascular compartment. In addition, kinetic modeling of ^{18}F-GE180 is more challenging than with ^{11}C-PBR28. Therefore, compared to ^{11}C-PBR28, ^{18}F-GE180 has unfavorable characteristics for TSPO imaging.

P64

Assessment of a new semi-quantitative method "dopamine transporters standardized uptake value (DaTSUV)" in comparison with conventional specific binding ratio (SBR) in [123I] FP-CIT single-photon emission computed tomography (SPECT) (DaTscan).

Yuichi Wakabayashi[1,2], Tomonori Kanda[2], and Kazunari Ishii[3]

1, Kobe University Graduate School of Medicine, Department of Radiology, 7-5-2, Kusunoki-cho, Chuo-ku, Kobe, Hyogo 650-0017, Japan

2, Magnuson Clinical Center, Room B1D43J, MSC 1026, BETHESDA, MD 20814

3, Kindai University Faculty of Medicine, Department of Radiology

Introduction:
We have developed a new analytical method by quantifying dose in the striatal, that was dopamine transporters standardized uptake value (DaTSUV), to evaluate [123I] FP-CIT single-photon emission computed tomography (DaTscan). The purpose of this study is to compare the discriminating ability of the classical SBR and DaTSUV for dopaminergic neurodegenerative diseases (dNDD).

Material and Method:

Seventy-seven consecutive patients underwent DaTscan were included. Patient were divided as dNDD group (n=44 [24 men, 20 women], median age 73 years [interquartile range 67-80.25 years], body weight 52.2 kg [interquartile range 46.5–62.6 kg]) and 33 non-dNDD group (n=33 [14 men, 19 women], median age 75 years [interquartile range 68–77 years], body weight 57.2 kg [interquartile range 46.2–63.2 kg]) based on the clinical diagnosis. Correlation of each methods was evaluated by Pearson's correlation coefficient and t-test. Differences of SBR and DaTSUV in each group were evaluated by t-test. Pairwise comparison of Receiver Operating Characteristic (ROC) curves analysis was performed to compare the discriminating abilities of each methods by standard error of the area under curve (AUC). The significant difference was set to $p<0.05$.

Result:
There was significantly strong correlation between DaTSUV and SBR (r=0.910 [95%CI:0.862-0.942], $p<0.001$). dNDD was significantly lower than non-dNDD with SBR (3.48 [95%CI:3.01-3.94] vs 6.58 [95%CI:6.00-7.16], $p<0.001$) and DaTSUV (4.91 [95%CI:4.14-5.68] vs 8.61 [95%CI:7.59-9.64], $p<0.001$). The discriminating ability of SBR (AUC=0.918) was significantly higher than DaTSUV (AUC:0.838, p=0.0176) (Fig. 1).

Discussion:
SBR using the conventional Bolt method is a method widely used in many facilities and proved that it is a proper quantitative evaluation in DaTscan even though new quantitative method like SUV is devised.

Acknowledgement
No conflict of interests.

Reference
Tossici-Bolt L, Hoffmann SM, Kemp PM, et al. (2006) Quantification of [123I] FP-CIT SPECT brain images: an accurate technique for measurement of the specific binding ratio. Eur J Nucl Med Mol Imaging. 33:1491–9.

P66
Introducing AIVO: A centralized neuroinformatics database for brain-PET data

Tomi Karjalainen[1], Janne Isojärvi[1], Jouni Tuisku[1], Marco Bucci[1], Severi Santavirta[1], Enrico Glerean[1,2], Juha O. Rinne[1], and Lauri Nummenmaa[1,3]

1. *Turku PET Centre, University of Turku, 20520 Turku, Finland*
2. *Department of Neuroscience and Biomedical Engineering (NBE), Aalto University, 00076 AALTO, Espoo, Finland*
3. *Department of Psychology, University of Turku, 20014 Turku, Finland*

Introduction:

Reliability of many neuroimaging findings have been questioned because of low statistical power (Button et al. 2013; Nord et al. 2017). While most of the discussion pertains MRI, many PET studies likely suffer from the same problem. To draw reliable inferences based on PET data, we have begun a local neuroinformatics project at the Turku PET Centre where we i) reprocess all previously obtained brain scans (between the years 1996 and 2016) in standardized fashion and ii) store the outputs with quality control metrics and related metadata from hospital registers into a single database called AIVO. This database will contain approximately 16 000 brain PET studies. Together with our in-house automated brain-PET preprocessing pipeline MAGIA, AIVO enables generation of standardized datasets with significantly higher statistical power than individual PET studies.

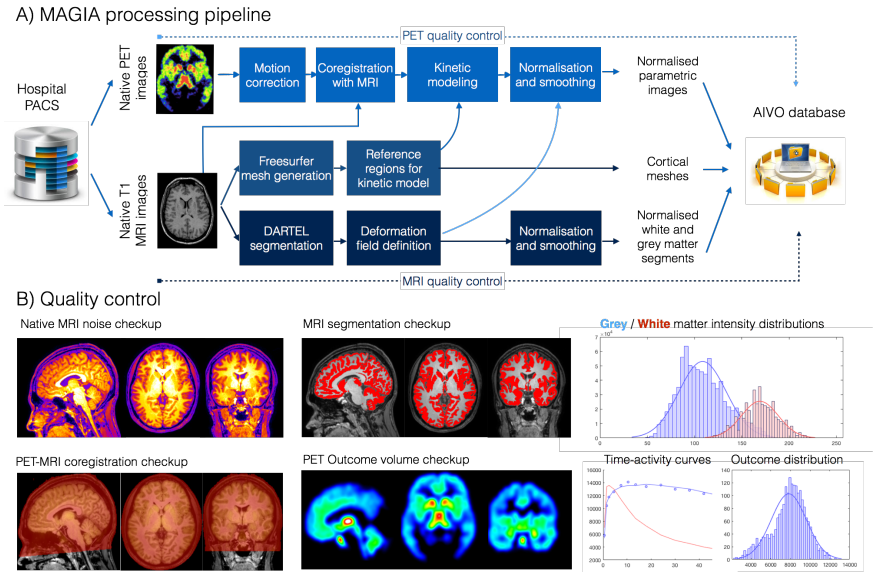

Figure 1. Overall framework for the automated MAGIA data processing pipeline. *The system allows automated data retrieval from hospital PACS, and provides fully automated kinetic modelling of the PET data and morphometric analyses of structural MRI data. Data are stored in the AIVO database allowing analysis and linkage with register data. Visual quality control (B) is complemented with quality control metrics for PET: estimation of signal-to-noise ratio, motion parameters, fit of the input function and SUV time courses against population averages, distribution of outcome measure in reference / target tissue, and comparison of ROI-wise outcome measures against population*

values. For MRI, we use modified MRIQC (Esteban et al., 2017) pipeline including SNR, contrast-to-noise ratio, artefact detection (Mortamet et al., 2009), distribution of WM/GM segment intensities and % overlap. QC metrics are provided at single-subject level and pooled for sample level for every analysis run.

Materials and Methods:

AIVO runs on open-source PostgreSQL (https://www.postgresql.org) on dedicated Ubuntu server "Yngwie". The database contains information about the study protocol, the subject and quality control metrics of the images. AIVO also keeps track of the preprocessing status of each study: preprocessed studies are tagged along with the Git hash of the MAGIA code. The PostgreSQL is complemented with in-house MATLAB functions for reading and writing information in AIVO, enabling automatic processing, and writing quality control metrics to AIVO. We also have a simple MATLAB-based query tool that can be used to select studies that match specified criteria. This allows efficient selection of studies for group-level statistical analyses. All the brain scans stored in AIVO are processed by our automated brain-PET preprocessing pipeline called MAGIA that compiles existing neuroimaging analysis suites SPM12 (http://www.fil.ion.ucl.ac.uk/spm/) and FreeSurfer (http://surfer.nmr.mgh.harvard.edu/). The pipeline allows automated kinetic modeling, normalization of the brains, and generation of cortical meshes and grey/white matter segments from T1 image if that is available. This saves substantial amount of manual labour. The system is currently set up so that any new PET image preprocessed with MAGIA will automatically be stored to AIVO with the required metadata.

Results:

We have now compiled a comprehensive list of all brain PET studies conducted in Turku PET Centre during 1996-2016, and retrieved 7000 images for preprocessing. While the database still has empty fields, we already know 99 % of the participants' ages and tracers used in the studies, as well as over 96 % of the scanners. We have processed over 1000 studies with MAGIA, with average image processing taking 12 hours (due to FreeSurfer cortical mesh generation and T1 image segmentation). We are also gathering project-specific spreadsheets that contain metadata about the studies, allowing us to identify patients from controls and baseline scans from activation scans.

Discussion:

The project has been ongoing for approximately two years. The project has advanced very well thanks to co-operative attitude from several PIs not directly involved in the project. However, we have faced many challenges that we could not anticipate. First, generating a list of all studies conducted at the Centre has been difficult, as we had to merge together information from several uncomprehensive sources. Second, there have been several image storages during the years in Turku PET Centre, and accessing all of them securely has required a lot of work. Third, retrieving metadata from old projects is slow due to lack of standardized digital archives on numerous non-imaging-related variables. However, once the database has been set up and the MAGIA pipeline has been approved for standard

processing system at the Centre, future studies will be easily accessible for “mega-analysis” and discovery science of brain structure and function.

Acknowledgements:

This project was supported by Sigrid Juselius Foundation.

References:

Button KS, Ioannidis JPA, Mokrysz C, Nosek BA, Flint J, Robinson ESJ, Munafò MR. [2013] Nature Reviews Neuroscience, 14:365-376.

Esteban O, Birman D, Schaer M, Koyejo OO, Poldrack RA, Gorgolewski KJ. [2017] PLOS ONE, 12, e0184661.

Mortamet B, Bernsteim MA, Jack CR, Gunter JL, Ward C, Britson PJ. [2009] Magnetic Resonance in Medicine, 62:365-372.

Nord CL, Valton V, Wood J, Roiser JP. [2017] J Neurosci, 37:8051-8061.

P67
Single-subject Correlation Map (SCM): A novel approach to evaluate the pathological interaction in a single subject

Zhen Fan[1], Rainer Hinz[2], Paul Edison[1]

1 – Department of Medicine, Imperial College London, UK

2 – Wolfson Molecular Imaging Centre, University of Manchester, UK

Introduction:

Neuroimaging has been widely applied in the evaluation of the trajectory of neurodegenerative diseases *in vivo*. Neurodegenerative diseases are characterised by multiple pathologies and often the interaction between these pathologies along with genetic and environmental factors lead on to progressive neurodegeneration. In Alzheimer's disease, amyloid-β deposition, neurofibrillary tangles, neuroinflammation, synaptic dysfunction, cortical and sub cortical atrophy and neurodegeneration could readily be measured using different imaging modalities. However, heterogeneity is very common between the individuals and different neurodegenerative diseases. In this study, we present a novel approach to evaluate these pathologies with in a subject: Single-Subject Correlation Map (SCM), which is a voxel-level comparison framework to assess the statistical correlation between different pathological modalities on an individual basis, and how the pathological interaction influence their cognitive performance.

Methods:

In order to investigate the correlation on an individual level, a cluster-unit correlation concept was introduced. The idea is to transform the brain matrix into multiple cluster units, which allows us to run the correlation on individual basis. This new function developed in MATLAB enable the user to customise a desirable cluster unit and to use preferred threshold for the correlation. Initially all images are normalized to a standard space after applying appropriate scaling and smoothing to reduce the noise level. Initially single subject analysis was done where we compared individual patient PET data against the corresponding healthy control cohort using one-way ANOVA, and an individualized SPM-T map was generated to present all clusters with significant tracer uptake compared to healthy controls. A correlation analysis was performed between the two image modalities in the same cluster unit. After applying Shapiro-Wilk test, depending on the normality either Pearson or Spearman correlation were applied in each cluster-unit with the Bonferroni correction. After thresholding for predefined p value, the correlation coefficient (r) value was written onto the single subject correlation map (SCM) for that cluster unit. Lastly, a single-subject Correlation Map (SCM) was generated with the significant Pearson correlation coefficient value for each cluster. An individualized grey and white matter brain mask was applied to calculate the volume of the positive and negative correlated brain regions. Additionally, SCM samples the mean tracer binding of the interactive region for both modalities by applying the correlated atlas to their raw normalized images. Based on the individual SPM-T map in each modality, volume and

average binding potential of the significant clusters were compared with healthy control cohort.

Results:

In the current study, we applied single subject correlations to AD patients with [18F] Flutemetamol and [18F]GE180 PET, which enable us to assess the interaction between the amyloid deposition and neuroinflammation in that patient. Figure 1 has illustrated two SCM maps with positive correlation ($r>0.5$ and $p<0.05$ with Bonferroni correction) between Flutemetamol and [18F]GE180 in two Alzheimer's patients. AD1 revealed a volume of 204,410mm3 (18.8%) positively correlated with amyloid and microglial activation hroughout the brain tissue, while AD2 revealed a positive correlation of 166,085mm3 (15.8%). Additionally, the correlated brain region of amyloid and microglial activation was distributed differently in two patients, AD1 showed more interaction in frontal lobe while AD2 showed more widespread correlated clusters.

Discussion:

Single-Sub Correlation map (SCM) provides a novel way to assess the pathological interaction on an individual basis, and enables a more sophisticated association between individual's neuropathological interactions in the brain to their cognitive and behaviour status. This voxel-wise SCM framework shows potential to evaluate the complex and heterogenous interaction between neuropathological substrates in neurodegenerative disease, and allows the scientists and doctors to evaluate the specific pathological conditions on an individual basis. SCM can has the potential to be used in clinical diagnostic work up to provide insight into pathological interactions.

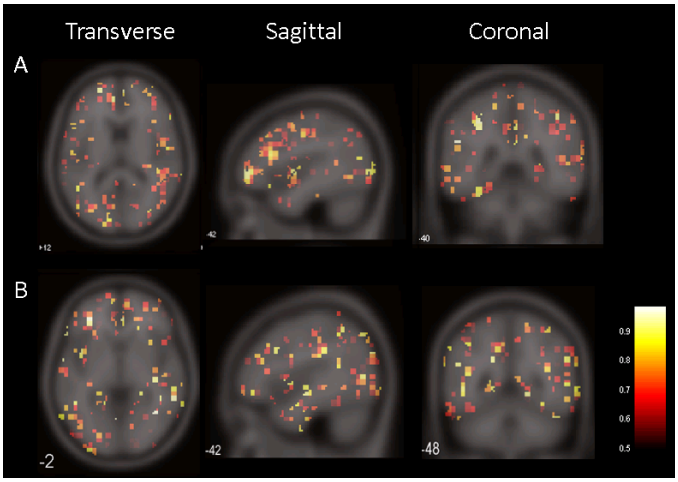

Figures

Figure 1. Single subject correlation maps generated for [18F]GE180 PET and [18F]Flutemetamol PET in two AD subjects, AD1 (A) and AD2 (B). The colour map indicates the correlation coefficient for each significant correlated clusters ($0.5<r<1$).

P68
Radiosynthesis and *In vitro* Evaluation of [^{11}C]FPS-ZM1 as a PET Radiotracer to Quantify the Receptor for Advanced Glycation Endproducts in the Brain

Salvatore Bongarzone,[1,2] Federico Luzi,[1] Vilius Savickas,[1] Nisha Singh,[1,3] Federico E. Turkheimer,[3] Antony D. Gee[1,2]

[1]Division of Imaging Sciences and Biomedical Engineering, King's College London, 4th Floor, Lambeth Wing, St Thomas' Hospital, London SE1 7EH, United Kingdom. [2]PET Imaging Centre Facility, St Thomas' Hospital, London SE1 7EH, United Kingdom. [3]Institute of Psychiatry, Psychology and Neuroscience, Denmark Hill, 16 De Crespigny Park, London SE5 8AF, United Kingdom.

Introduction:
Experimental evidence suggests that the interaction between soluble amyloid beta (Aβ) oligomers and the receptor for advanced glycation endproducts (RAGE) exacerbates the neuronal toxicity of Aβ by increasing amyloid production and by triggering a cascade of neurodegenerative processes such as oxidative stress, inflammation and neurotoxicity.[1] RAGE is up-regulated in the brains of individuals with Alzheimer's disease (AD) compared to healthy controls.[1-3]

N-Benzyl-4-chloro-N-cyclohexylbenzamide (FPS-ZM1) has nanomolar affinity to RAGE (K_i = 25 ± 5 nM, clogP = 5.4) and inhibitory RAGE activity *in vivo*.[4] The aims of this work were: a) to radiolabel FPS-ZM1 with carbon-11 ([^{11}C]FPS-ZM1); and b) to evaluate [^{11}C]FPS-ZM1 *in vitro* using AD model transgenic mice brain tissue.

Materials and Methods:

[^{11}C]FPS-ZM1 was radiosynthesised *via* a palladium-mediated carbonylation using [^{11}C]CO, *N*-benzylcyclohexanamine and 1-chloro-4-iodobenzene (**Fig. 1A**). *In vitro* autoradiography using [^{11}C]FPS-ZM1 was conducted on sagittal brain tissue sections of 8-month-old wild-type (WT) and 17-month-old AD model transgenic mice (Tg2576). Total binding (TB) in the brain was evaluated using [^{11}C]FPS-ZM1 at 5 and 10 nM concentrations and non-specific binding (NSB) determined at 10, 25 and 75 μM concentrations of non-radioactive FPS-ZM1. Images were developed on a phosphor imaging plate followed by the qualitative and quantitative analyses in cerebellar and extracerebellar regions of interest (ROI). Specific binding was obtained by subtracting NSB from TB.

Results:
[^{11}C]FPS-ZM1 was radiosynthesised with a good radiochemical yield (26%), high chemical purity (> 99%) and high radiochemical purity (> 99%). No statistically significant differences in specific binding for RAGE were observed between Tg2576 and WT animals or between the cerebellar and extracerebellar ROIs of either species (**Fig. 1B**).

Discussion:
This exploratory study was successful in combining an effective radiosynthesis method with *in vitro* evaluation of a novel ^{11}C-PET-based RAGE radiotracer. Due to high levels of NSB,

[^{11}C]FPS-ZM1 was not able to discriminate between the RAGE levels in Tg2576 *versus* WT tissues. Future developments of specific RAGE radiotracers will aim to reduce the lipophilicity of this scaffold and increase RAGE affinity/selectivity.

Acknowledgements:
This work was supported by Medical Research Council (MRC, MR/K022733/1), European Commission, FP7-PEOPLE- 2012-ITN (316882, RADIOMI), and Biomedical Research Centre award to Guy's & St Thomas' NHS Foundation Trust.

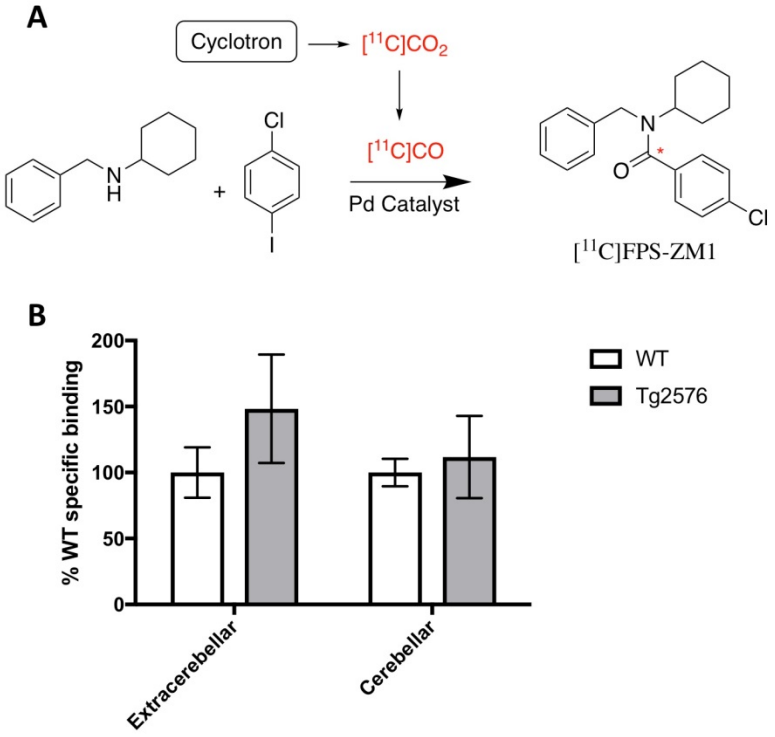

Fig. *1* : ***A.*** Radiosynthesis of [^{11}C]FPS-ZM1. ***B.*** The percentage of specific binding in cerebellar and extracerebellar regions of WT versus Tg2576 mice using 10 nM of [^{11}C]FPS-ZM1 and 75 µM of FPS-ZM1.

References:

1. Bongarzone S, Savickas V, Luzi F and Gee A. D. [2017] J. Med. Chem. 60: 7213-7232

2. Sasaki N, Toki S, Chowei H, Saito T, Nakano N, Hayashi Y, Takeuchi M. and Makita Z. [2001] Brain Res. 888: 256-262

3. Miller M C, Tavares R, Johanson C E, Hovanesian V, Donahue J E, Gonzalez L, Silverberg G. D. and Stopa E. G. [2008] Brain Res. 1230: 273-280

4. Deane R, Singh I, Sagare A P, Bell R D, Ross N T, LaRue B, Love R, Perry S, Paquette N, Deane R. J, Thiyagarajan M, Zarcone T, Fritz G, Friedman A E, Miller B. L. and Zlokovic B. V. [2012] J. Clinical Investig. 122: 1377-1392

P69

Impact of blood-brain barrier disruption induced by focused ultrasounds on the carrier-mediated efflux function: a ^{11}C-erlotinib PET study in rats

Sébastien Goutal[1,2], Matthieu Gerstenmayer[3], Sylvain Auvity[1], Fabien Caillé[1], Sébastien Mériaux[3], Irène Buvat[1], Benoit Larrat[3], **Nicolas Tournier[1]**

1. *Imagerie Moléculaire In Vivo, IMIV, CEA, SHFJ, Orsay, France*
2. *MIRCen, CEA, Fontenay-Aux-Roses, France*
3. *NeuroSpin, CEA, Université Paris Saclay, Gif sur Yvette, France*

Introduction:

The brain permeation of most tyrosine kinase inhibitors (TKIs) through the intact blood-brain barrier (BBB) is limited by efflux transporters such as the P-glycoprotein (ABCB1) and the Breast Cancer Resistance Protein (ABCG2). Improving the delivery of small molecules TKIs such as erlotinib to the tumor and surrounding brain tissue is a prerequisite for molecularly targeted therapy of CNS lesions. Focused ultrasound (FUS)-based strategies have been developed to locally and temporally enhance the delivery of drugs into the brain via the "opening" of the tight junctions and paracellular route (1). FUS-induced BBB disruption was therefore hypothesized to overwhelm and overcome the ABCB1/ABCG2-mediated efflux of erlotinib at the BBB.

Material and Methods:

A large hemispheric BBB disruption was achieved using FUS. Rats were installed in a stereotactic frame. FUS started immediately after microbubbles injection, with continuous waves over the left hemisphere during 5 min. The efficacy and localization of the FUS-induced BBB disruption protocol was first assessed in 2 rats using T1-weighted magnetic resonance imaging (MRI) with gadoteric acid (MW = 558,6 g/mol) as a contrast agent, injected 60 min after FUS. The brain kinetics of erlotinib (MW = 393,4 g/mol) was assessed using ^{11}C-erlotinib PET imaging (37-45 MBq i.v; 30 min acquisition). Animals of the "Baseline" group (n=5) were compared to animals of the "FUS" group (n=5) who received the FUS-induced BBB disruption protocol 10 min before ^{11}C-erlotinib injection. Animals of the "ELA" group received an i.v injection of elacridar 10 mg/kg, a potent ABCB1/ABCG2 inhibitor, 10 min before PET. An ANOVA was performed to statistically compare the brain exposure to ^{11}C-erlotinib, estimated as the area under the time-activity curve (AUC) of the brain kinetics of ^{11}C-erlotinib in volumes of interest (VOI) corresponding to the disrupted (left) and the intact (right) hemispheres. After imaging sessions (MRI and PET), BBB integrity was assessed in all animals using the post-mortem Evan's Blue (EB) extravasation test.

Results:

T1-weighted MR images unveiled that the BBB was permeable to gadoteric acid 60 min after FUS. Images highlighted a large 2mm width stripe from the front of the brain to the cerebellum (Fig. 1). Signal enhancement in the left hemisphere of the rats was increased by 130% and 70% as compared to the contralateral hemisphere. The VOI corresponding to the disrupted BBB covered 41 to 44 % of the volume of the left hemisphere. Compared with baseline ($AUC_{Baseline}$=1.4±0.5 %ID.min), elacridar significantly increased ^{11}C-erlotinib brain exposure to the left hemisphere VOI (AUC_{ELA}=2.2±0.5 %ID.min, p<0.001). Physical BBB disruption did not impact the brain kinetics of ^{11}C-erlotinib in the left hemisphere (AUC_{FUS}=1.2±0.1 %ID.min). AUC_{left} was never significantly different than AUC_{right} in any of the tested conditions (p>0.05). EB extravasation was observed only in animals who received FUS and was consistent in shape and volume to gadolinium-enhanced MR images.

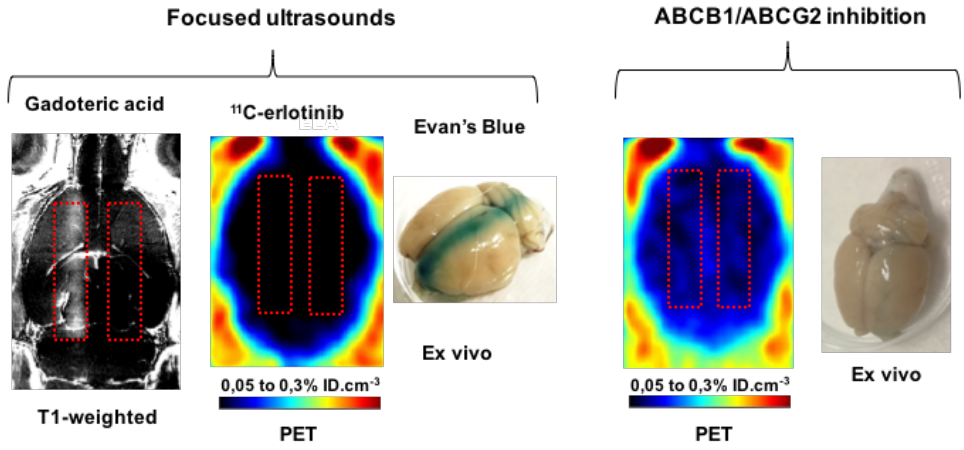

Fig. 1. Impact of focused ultrasounds or ABCB1/ABCG2 inhibition on BBB integrity assessed using Gadolinium T1-weighted MR and Evan's Blue extravasation and corresponding brain distribution of ^{11}C-erlotinib (summed 0-30 min PET images) in rats.

Discussion/Conclusion:

ABC-mediated efflux is the major determinant of erlotinib brain kinetics, thus highlighting the predominance of the "functional" rather than the "physical" component of the BBB in controlling its brain penetration. FUS-induced BBB disruption may not a relevant strategy to transiently overcome ABC-transporter efflux at the BBB in order to improve the brain delivery of erlotinib.

References:

1. Marty B, Larrat B, Van Landeghem M, et al., [2012] J Cereb Blood Flow;32(10):1948–58.

P70
A comparative study of stilbene derivatives repurposed for myelin imaging

Matteo Tonietto[1,*], Sylvain Auvity[2,3*], Fabien Caillé[3], Benedetta Bodini[1], Michel Bottlaender[3], Nicolas Tournier[3], Bertrand Kuhnast[3] and Bruno Stankoff[1].

[1]*Sorbonne Universités, UPMC Paris 06, Brain and Spine Institute, ICM, Hôpital de la Pitié Salpêtrière, Inserm UMR S 1127, CNRS UMR 7225, Paris, France*

[2]*Inserm, U1144, Paris, F-75006, France*

[3]*IMIV, CEA, Inserm, CNRS, Univ. Paris-Sud, Université Paris Saclay, CEA-SHFJ, Orsay, France*

Introduction:

Multiple Sclerosis is the most common demyelinating disease in human, affecting more than 2 million people worldwide. Drugs promoting myelin repair represent a promising therapeutic approach and several candidate molecules are currently being evaluated[1]. A reliable imaging method to specifically quantify myelin in-vivo is crucially needed to test the efficacy of these drugs. PET using the benzothiazole derivative ^{11}C-PiB, repurposed as a myelin biomarker, has been successfully used to quantify myelin content changes in humans[2,3], but it is characterized by a suboptimal signal-to-noise ratio. Another promising class of radiopharmaceutical compounds is the family of stilbene derivatives, such as ^{11}C-BMB and ^{11}C-MeDAS, which have been shown to bind to myelin in animal models[4,5]. Fluorinated analogues ^{18}F-florbetapir and ^{18}F-florbetaben, belonging to the same chemical class, are now commercially available and have the potential to be clinically useful radiotracers for myelin imaging.

The aim of this study was to compare ^{18}F-florbetaben, ^{18}F-florbetapir and ^{11}C-MeDAS with ^{11}C-PiB, with regard to tracer uptake, and scan duration required to derive time-independent estimates in white matter (WM).

Materials & methods:

Four healthy baboons (weight=27.2 ± 2.3 kg) were included in the study and underwent a PET scan for each radioligand, with a minimum rest period of 2 weeks. Dynamic cerebral PET scans were acquired during 90 minutes under propofol anaesthesia after radiotracer injection (244.6 ± 37.8 MBq). For technical reasons, one of the subject did not undergo the ^{11}C-PiB exam. A 3D T1-weighted (T1-w) image was also acquired with a 3T MRI scanner for each subject.

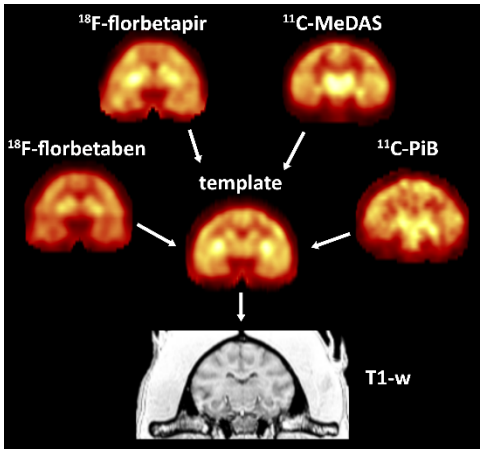

Figure 1: pipeline for PET template construction and registration to the T1-w.

T1-w images were segmented in cerebral spinal fluid, white and grey matter using Atropos[6] and publicly available tissue priors[7]. To minimize intra-subject differences in PET to T1-w registration, all PET images of each subject were firstly aligned to each other to create a subject specific template. Then, this template was registered to the subject T1-w with ANTs (Fig. 1). Derived transformations were then inverted to bring the tissues segmentation to each PET native space.

The tracer uptake in the WM was evaluated using standardized uptake value ratio at 90min ($SUVR_{90}$), and the distribution volume ratio (DVR) calculated with Logan graphical reference method[9]. Cerebellar grey matter was used as reference region for both methods. Scan duration required to derive time-independent estimates in white matter was evaluated by reducing the scan duration up to 60 min with intervals of 5 min and evaluating both SUVR and DVR.

Results:

In white matter, $SUVR_{90}$ of ^{18}F-florbetapir (1.40 ± 0.05) and ^{18}F-florbetaben (1.34 ± 0.07), were higher than that of ^{11}C-MeDAS (1.28 ± 0.03) and ^{11}C-PiB (1.19 ± 0.07) (Fig. 2A). DVR of ^{18}F-florbetapir (1.27 ± 0.03) and ^{18}F-florbetaben (1.26 ± 0.06), were higher than that of ^{11}C-MeDAS (1.16 ± 0.03) and ^{11}C-PiB (1.14 ± 0.02) (Fig. 2B).

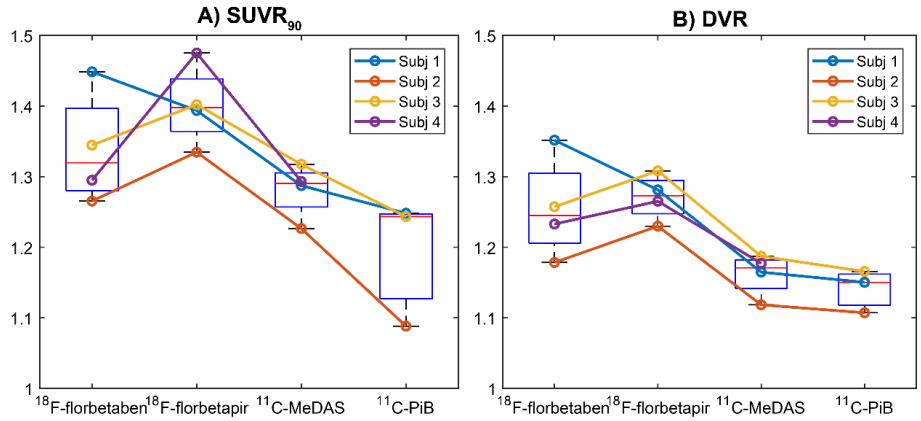

Figure 2 : Boxplot of $SUVR_{90}$ (A) and DVR (B) estimates in WM for the 4 tracers considered. Coloured lines represent different subject.

^{18}F-florbetapir and ^{11}C-PiB reached stability in the estimates of both $SUVR_{90}$ and DVR at 90min (even if the last PET frames of ^{11}C-PiB were noisier), while ^{18}F-florbetaben and ^{11}C-

MeDAS were still increasing at the end of the scan (Fig. 3). However, differences between DVR estimates at 60 and 90 min were less than 5%.

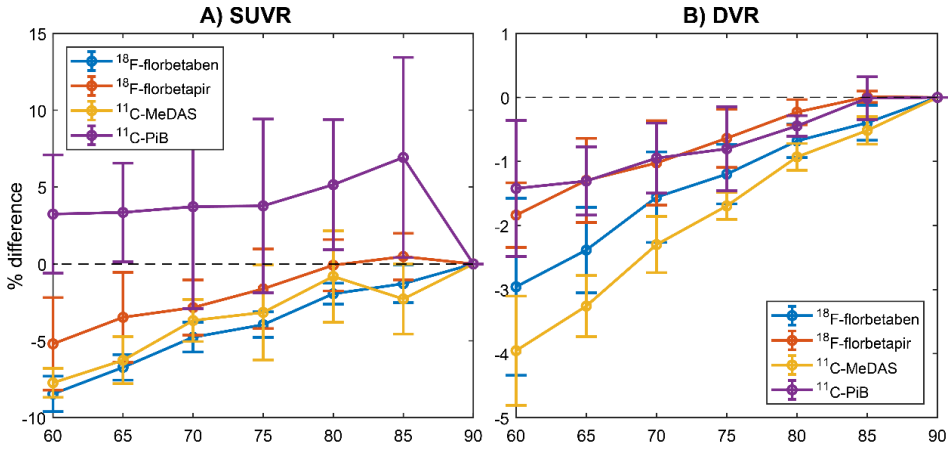

Figure 3: Relation between total duration of scan and estimates of SUVR (A) and DVR (B), expressed as % difference with the estimates obtained at 90min

Conclusion:

All the stilbene derivatives showed a higher WM uptake compared to ^{11}C-PiB. Thanks to their higher DVR and longer half-life, our study indicates that ^{18}F-florbetapir and ^{18}F-florbetaben are promising tracers for clinical application in Multiple Sclerosis and other demyelinating diseases.

References:

1. Plemel *et al.*, *Nat. Rev. Drug Discov.* (2017)
2. Stankoff *et al. Ann. Neurol.* (2011).
3. Bodini *et al.*, *Ann. Neurol.* (2016).
4. Stankoff *et al., PNAS.* (2006).
5. Wu *et al., Bioorg. Med. Chem.* (2010)
6. Avants *et al., Neuroinformatics* (2011).
7. Love *et al., Neuroimage* (2016).
8. Logan *et al., JCBFM.* (1996).

P71
Validation of dopamine D2 receptor density estimations in human brain with TRue EquilibriuM BoLus Estimation (TREMBLE)

Jenny-Ann Phan[1,2], Yoshitaka Kumakura[3], Dean F. Wong[4,5], Albert Gjedde[6,7]

[1]*Department of Biomedicine, Aarhus University, Aarhus,, Denmark,*

[2]*Department of Nuclear Medicine and PET Centre, Aarhus University Hospital, Aarhus, Denmark,*

[3]*Department of Nuclear Medicine, Saitama Medical University, Kawagoe city, Saitama, Japan*

[4]*Department of Radiology and Radiological Sciences, Division of Nuclear Medicine, and*

[5]*Dept of Psychiatry, Neurosciences and Neurology,Johns Hopkins Medical Institutions, Baltimore, MD*

[6]*Department of Clinical Research, University of Southern Denmark, Odense, Denmark*

[7]*Department of Nuclear Medicine, Odense University Hospital, Odense, Denmark*

Introduction:

Identification of a true steady-state of receptor-ligand binding is crucial for accurate and reproducible quantification of receptor density (B_{max}) with PET studies. In particular, radioligands that only approach a transient equilibrium are more subject to variability when binding estimates are not determined at steady-state. Here, we applied a model previously described by Sølling et al.[1] and Wong et al.[2], which yields estimates of binding at true transient equilibrium.

Materials and Methods:

We applied the TREMBLE analysis to [^{11}C]raclopride acquisitions from healthy human subjects (n=19) at baseline and at challenge with non-radiolabled raclopride. The data included in this study is a subset of a larger cohort[3], and were selected based on the availability of plasma input. TREMBLE is a kinetic model consisting of three compartments, m_v representing the plasma compartment, m_e the exchangeable compartment, and m_b the specifically bound partition (**Figure 1**). The change in the measured activity in a region of interest evolves as follows,

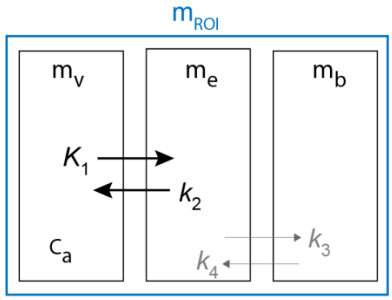

Figure 1.

$$\frac{dm_{\mathrm{ROI}}}{dt} = V_0 \frac{dc_{\mathrm{a}}(t)}{dt} + K_1\, c_{\mathrm{a}}(t) - k_2\, m_e(t), \qquad (1)$$

where V_0 the volume of the vascular bed and c_a(t) is the time-variable plasma concentration. The quantity of ligand in the exchangeable compartment is solved by rearrangement of eq.1,

$$m_e(t) = V_e \left[c_a(t) - \frac{1}{K_1} \left(\frac{dm_{ROI}(t)}{dt} - V_0 \frac{dc_a(t)}{dt} \right) \right], \quad (2)$$

where V_e is the partition volume obtained in a reference region (K_1/k_2). When the quantity of m_e is known, the specifically bound quantity is simply obtained from,

$$m_b(t) = m_{ROI}(t) - m_v(t) - m_e(t) \quad (3)$$

Transient equilibrium is determined at the time, where the first derivative of bound quantity equal zero (db/dt=0). At this exact time point, the steady-state binding potential is defined by the ratio of bound to exchangeable quantity, indicated by upper case symbols,

$$BP_{ND} = \frac{M_b}{M_e} \quad (4)$$

Results:

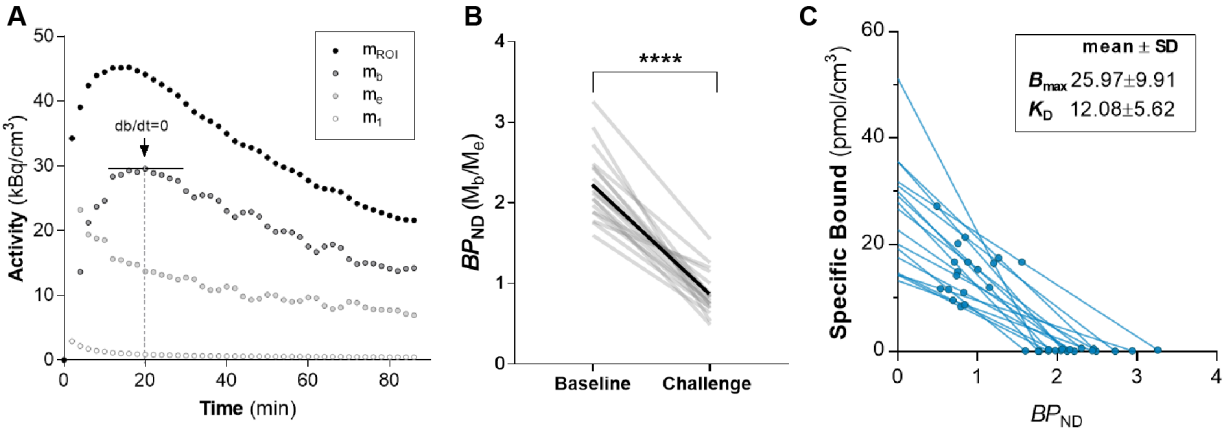

Figure 2A shows the activities in the three compartments in putamen from a representative subject. Db/Dt=0 at time 20 min indicates the true steady-state. The binding potential was calculated as the ratio of bound to exchangeable quantity at this time. As shown in **Figure 2B**, the binding potential decreased significantly upon challenge with non-radiolabeled raclopride (****p<0.0001). The grey lines illustrate the individual estimates in each subject before and after challenge, and black line show the mean. **Figure 2C** illustrates that B_{max} and K_D yielded 25.97±9.91 and 12.08±5.62, respectively.

Conclusion:

We estimated receptor density and affinity using binding estimates at true equilibrium using TREMBLE. The estimates are not unlike estimates from studies of another kinetic model[4-6], but we now proceed to analyze the same data set with the alternative model in order to assess the strengths and limitations of the individual kinetic models.

References:

1 Sølling, T., Brust, P., Cunningham, V., Wong, D. & Gjedde, A. True equilibrium bolus estimation (TREMBLE) confirms rapid transient equilibrium. *Neuroimage* **5**, 29-29 (1997).

2 Wong, D. F., Sølling, T., Yokoi, F. & Gjedde, A. in *Quantitative Functional Brain Imaging with Positron Emission Tomography* 463-468 (Elsevier, 1998).

3 Kuwabara, H. *et al.* Dissociative changes in the Bmax and KD of dopamine D2/D3 receptors with aging observed in functional subdivisions of the striatum: a revisit with an improved data analysis method. *J Nucl Med* **53**, 805-812 (2012).

4 Farde, L. *et al.* D2 dopamine receptors in neuroleptic-naive schizophrenic patients: a positron emission tomography study with [11C] raclopride. *Archives of General Psychiatry* **47**, 213-219 (1990).

5 Hietala, J. *et al.* Striatal D 2 dopamine receptor binding characteristics in vivo in patients with alcohol dependence. *Psychopharmacology* **116**, 285-290 (1994).

6 Pohjalainen, T., Rinne, J. O., Någren, K., SyvÄlahti, E. & Hietala, J. Sex differences in the striatal dopamine D2 receptor binding characteristics in vivo. *American Journal of Psychiatry* **155**, 768-773 (1998).

P72
AADC and NET: Noradrenergic mechanisms in Parkinson's disease

Martin B. Kinnerup[1], Michael Sommerauer[1], Karen Østergaard[2], Jan Jacobsen[1], Anna Schacht[1], Per Borghammer[1], and Adjmal Nahimi,[1-3] **Albert Gjedde**[4-7]

[1]Department of Nuclear Medicine and PET Centre, Aarhus University Hospitals, Denmark,

[2]Department of Neurology, Aarhus University Hospital, Denmark,

[3]Department of Neurophysiology, Aarhus University Hospital, Denmark.

[4]Department of Clinical Research, University of Southern Denmark, Odense, Denmark

[5] Department of Nuclear Medicine, Odense University Hospital, Odense, Denmark

[6]Department of Radiology and Radiological Science, Johns Hopkins University, Baltimore, MD, USA,

[7]Department of Neurology and Neurosurgery, McGill University, Montreal, QC, Canada,

Introduction:

Patients with Parkinson´s disease (PD) suffer from a wide range of non-motor symptoms that may be related to loss of noradrenaline (NA) and noradrenergic mechanisms. We tested the hypothesis that loss of noradrenergic tone would follow changes of NA synthesis or reuptake or both. To do so, we quantified noradrenaline transporter (NET) binding potentials and aromatic amino acid decarboxylase (AADC) activity with [^{11}C]MeNER and [^{18}F]FDOPA PET in the same subjects with PD to reveal possible compensatory mechanisms of noradrenergic neurotransmission, compared to healthy control subjects.

Figure 1:

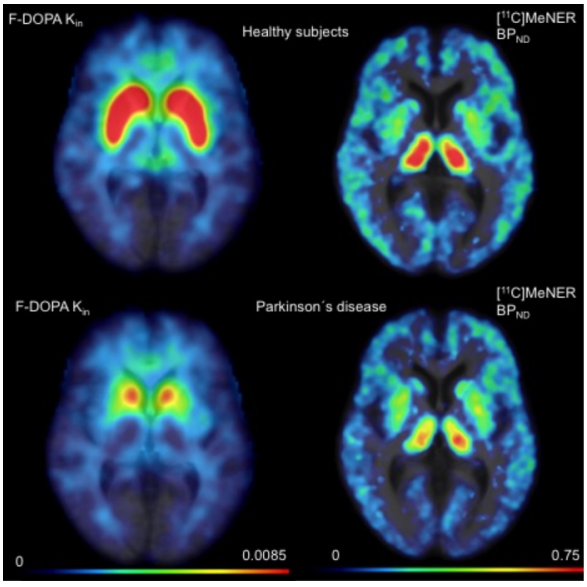

Method and materials:

We obtained PET images of the two tracers (Figure 1). We estimated specific binding potentials (BP_{ND}) of [^{11}C]MeNER in patients (n=11) and control subjects (n=8) as previously described (Nahimi et al, 2017), with caudate nucleus as reference region. The net rate of

fluorodopamine formation (k_{in}) from [^{18}F]FDOPA was estimated by the Gjedde-Patlak plot with cerebellum as reference region. In addition, to test the interaction, we computed the [^{11}C]MeNER/[^{18}F]FDOPA BP_{ND} /k_{in} ratios were calculated using normalized [^{11}C]MeNER and [^{18}F]FDOPA values to compare degrees of combined malfunction.

Figure 2: MeNER BP_{ND}

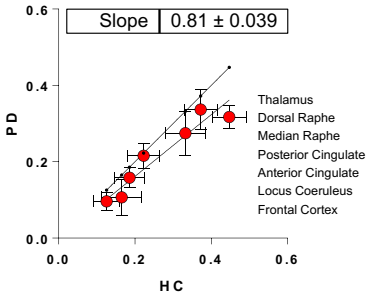

Figure 3: FDOPA k_{in}

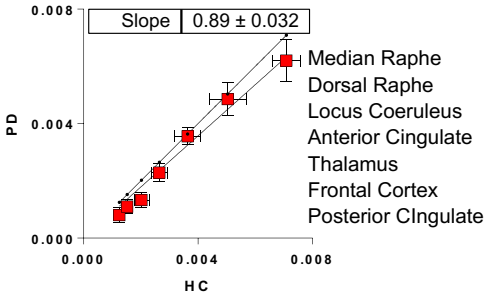

Figure 4: MeNER/FDOPA Ratios

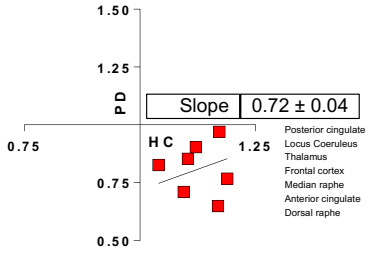

Results:

The PET images revealed declines both of AADC and NET values of the tracer binding. Significant decline of [^{11}C]MeNER binding potentials to about 80% was determined in all regions of patients with PD (Figure 2). Estimates of [^{18}F]FDOPA k_{in} in patients were reduced by 10% on average, with some variability within the regions examined (Figure 3).We also noted that the [^{11}C]MeNER/[^{18}F]FDOPA ratios of patients were decreased by 30% on average in the regions tested (Figure 4), but by 60% in dorsal raphe.

Discussion/Conclusion:

AADC activity remained the least affected or not decreased in areas of the brain with dense noradrenergic projections, in line with previous evidence of unaffected or even increased AADC activity in frontal cortex of early stage PD patients (Brück et al., 2005). Compared to AADC activity, the noradrenergic reuptake sites were down-regulated to a higher degree, to 20% in dorsal and median raphe, as evidenced also by the 60% reduction of the [^{11}C]MeNER/[^{18}F]FDOPA ratio in dorsal raphe of patients, in line with previous reports of compensatory down-regulation of NET in median and dorsal raphe of PD patients.

References:

3. Brück A, Aalto S, Nurmi E, Bergman J, Rinne JO. Cortical 6-[18F]fluoro-L-dopa uptake and frontal cognitive functions in early Parkinson's disease. Neurobiol Aging. 2005 Jun;26(6):891-8.
4. Nahimi A, Sommerauer M, Kinnerup MB, Østergaard K, Winterdahl M, Jacobsen J, Schacht A, Johnsen B, Damholdt MF, Borghammer P, Gjedde A. Noradrenergic deficits in Parkinson's disease imaged with (11)C-MeNER. J Nucl Med. 2017 Aug 28. pii: jnumed.117.190975. doi: 10.2967/jnumed.117.190975.

P73
A convolutional neural network approach for synthesizing patient-specific transmission data using anatomical MRI

Karl D Spuhler[a], Yi Gao[b,c], Christine DeLorenzo[d], Ramin Parsey[d], Chuan Huang[a,d,e]

[a] Stony Brook University Biomedical Engineering; [b] Shenzhen University Biomedical Engineering; [c] Stony Brook Applied Mathematics and Statistics; [d] Stony Brook University Medical Center Psychiatry; e Stony Brook University Medical Center Radiology

Introduction:

Simultaneous PET/MRI scanners are now commercially available from multiple vendors, and are becoming increasingly wide-spread in both clinical and research practice. Simultaneous acquisition offers many exciting opportunities, particularly for neuroimaging research involving quantitative PET. PET/MRI allows for numerous enhancements of PET data, including motion correction, MRI-guided image reconstruction and inherent spatiotemporal registration to anatomical MRI data[1]. In spite of the numerous advantages of PET/MRI, performing accurate attenuation correction of the acquired PET data is a significant challenge. The MRI signal is dependent upon proton density, with no direct connection to the electron density-mediated physics of photon attenuation; this issue is further complicated by the similar dark appearance of air and bone in MRI, along with the sharp boundaries between such spaces in the head.

Whereas recently developed techniques are likely sufficient for clinical PET/MRI attenuation correction[2], there are lingering concerns over their suitability for research predicated upon quantitative PET imaging, where observed changes can be slight and parameter estimation confidence extremely sensitive to variance within the regions analyzed. Current best-performing techniques are based on the derivation of patient-specific CT data, as opposed to transmission data, the historical gold standard for PET attenuation correction. CT data are suboptimal for attenuation correction as they require adjustment for the nearly five-fold energy difference between PET and CT photons; this issue has been shown to lead to significant, yet inconsistent overestimation of radiotracer uptake[3]. Here, we present a novel technique for synthesizing patient-specific transmission data from only anatomical MRI using a fully convolutional network.

Materials & Methods:

We identified 67 patients in our neuroimaging database who received [11C]-WAY PET (Siemens ECAT HR+, transmission scanning used for attenuation correction) as well as T1-weighted anatomical MRI (GE Signa HDx 3.0). This dataset was randomly divided into testing (n=12), validation (n=11) and training (n=44) datasets.

Figure 1: Fully Convolutional Neural Network Architecture

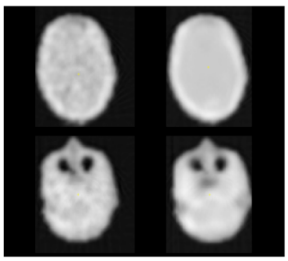

Figure 2: Comparison of ground truth (left) and synthesized (right) attenuation maps for a single subject.

A fully convolutional neural network was implemented in Tensorflow (Figure 1). Feature maps were concatenated between the encoding and decoding legs of the network, as inspired by the uNet architecture which has recently achieved successes in image segmentation tasks[4].

The neural network was trained on pairs of transmission and MRI data. Pseudo-transmission data were synthesized from the MRI data. The network was trained to minimize the L1-error between synthesized and ground truth transmission data.

Following training, synthesized transmission data were determined for all subjects in the testing dataset. 10 minute frames of [11C]-WAY emission data were reconstructed using filtered back projection, with both the ground truth and synthesized attenuation maps. PET reconstructions were masked to only consider voxels with at least 20% of maximal uptake in the ground truth reconstruction. Mean percent errors between synthesized and ground truth attenuation maps and their respective reconstructions are our primary reporting metric. We also report Pearson correlations for reconstructed PET activity.

Results:

Synthesized attenuation maps in the testing set showed a slight negative bias, with a mean percent error of -1.2± 8.3%. Figure 2 shows representative slices of synthesized and ground truth transmission data. This underestimation was reflected by a commensurate positive bias in the reconstructed PET data, which showed a mean percent error of 0.91± 6.53%. All synthetic attenuation map reconstructions showed a strong correlation with their ground truth counterparts, with Pearson's R ranging from 0.953-0.993 ($p<0.0001$, in all cases).

Discussion:

The technique presented here is a novel process which serves as a first step towards optimal PET/MRI radiotracer quantification through the use of genuine gold standard attenuation data. Our fully convolutional neural network approach represents two important improvements of existing techniques: the first of which is its dependence upon gold standard transmission data; secondly, our technique obviates the requirement to register patient MRI data onto a previously acquired atlas. This is a requirement of the currently best performing pseudo-CT methods[2].

Our synthesized attenuation maps exhibited a low bias on average, rivaling the currently best performing pseudo-CT methods, although synthesized transmission data demonstrated a fairly high error standard deviation. To a certain extent this is an unavoidable issue that arises from the noisy nature of ground truth transmission data. The undersestimation of attenuation values is unsurprisingly accompanied by a slight overestimation of radiotracer concentration in the synthesized reconstructions, with mean error again rivaling optimal pseudo-CT techniques.

References:

1. Catana C, Drzezga A, Heiss W-D, Rosen BR. 2012. *Journal of Nuclear Medicine.*53(12):1916-1925.
2. Ladefoged CN, Law I, Anazodo U, et al. 2017. *NeuroImage.*147:346-359.
3. Nakamoto Y, Osman M, Cohade C, et al. 2002. *Journal of Nuclear Medicine.*43(9):1137-1143.
4. Ronneberger O, Fischer P, Brox T. 2015. *International Conference on Medical Image Computing and Computer-Assisted Intervention*.

P74
Optimized coffee-break protocols for quantitative [^{18}F]flutemetamol and [^{18}F]florbetaben studies

Fiona Heeman[1], Maqsood Yaqub[1], Kerstin Heurling[2], Isadora Lopes Alves[1], Juan Domingo Gispert[3], Santiago Bullich[4], Christopher Foley[5], Adriaan A. Lammertsma[1], on behalf of the AMYPAD Consortium

[1]Department of Radiology & Nuclear Medicine, Amsterdam Neuroscience, VU University Medical Center, Amsterdam, The Netherlands; [2]Wallenberg Centre for Molecular and Translational Medicine and the Department of Psychiatry and Neurochemistry, University of Gothenburg, Gothenburg, Sweden; [3]Barcelonaβeta Brain Research Center, Pasqual Maragall Foundation, Barcelona, Spain; [4]Piramal Imaging GmbH, Berlin, Germany; [5]GE Healthcare, Amersham, United Kingdom

Introduction:

[^{18}F]florbetaben and [^{18}F]flutemetamol are established PET tracers for imaging amyloid beta accumulation in the brain. For both tracers, a static scan acquired 90-110 minutes after injection has been approved for diagnostic purposes. For monitoring progression of disease and response to treatment, however, quantification based on a (longer) dynamic scanning protocol may be required to provide higher sensitivity in detecting changes. The scanning time required for the dynamic can be reduced by using a dual time window (coffee-break) protocol, in which a subject is scanned only during early and late phases after tracer injection, with a resting period in between. The aim of this simulation study was to define optimal coffee-break protocols for [^{18}F]florbetaben and [^{18}F]flutemetamol, optimizing patient comfort, whilst maintaining quantitative accuracy.

Materials & Methods:

Based on clinically determined kinetic parameters[1,2], full length (110 min) time-activity-curves (TACs) were simulated using the simplified reference tissue method (SRTM) for the entire range of clinically observed BP_{ND} values and noise levels to represent regional and voxel level data ([^{18}F]flutemetamol, R_1 = 0.827, k_2 = 0.08 & BP_{ND} (DVR-1)=0.003-0.453; [^{18}F]florbetaben, R_1= 0.769, k_2 = 0.075 & BP_{ND} (DVR-1) =0.00001-1.558). Next, TAC data points corresponding to coffee-breaks were removed, ranging from 80 (i.e. 10-90) to 0 (i.e. 90-90=full data set) minutes. The missing data points of the reference region TAC were interpolated using cubic-interpolation (optimized with dynamic [^{18}F]flutemetamol data). Resulting TACs were fitted using both SRTM and its basis function implementation (receptor parametric mapping, RPM). The fitted parameter of interest (BP_{ND}) was assessed and the absolute error was calculated as the subtraction between the simulated value and the corresponding value from the coffee-break intervals. In addition, the resulting error in BP_{ND} for longitudinal measurements was determined and assessed for clinical relevance (error in BP_{ND} > 0.05) based on the known test-retest variability of BP_{ND}[3].

Results:

For both tracers, few extreme outliers (BP_{ND}>2) were present in RPM derived BP_{ND}. For SRTM derived BP_{ND}, extreme outliers were predominantly found for longer coffee-break intervals and at higher levels of (simulated) noise, as expected. Furthermore, a systematic error (COV=0) that increased for longer coffee-breaks, presumably due to failure to interpolate the tracers' kinetics during the coffee-break intervals.

[^{18}F]flutemetamol

The absolute error graphs showed that the largest errors in BP_{ND} and R_1 were found in the 10-90 and 20-90 intervals, even when no noise was added (Fig. 1). For SRTM and RPM, the majority of significant differences in mean were found in the 10-90 and 20-90 minutes intervals, and some in the 30-90 (SRTM,RPM) and 40-90 (RPM) minutes intervals. The errors introduced in longitudinal changes were small (< 0.05) and smaller than the absolute error, for coffee-break intervals of 70 minutes or smaller.

[^{18}F]florbetaben

The absolute error graphs of BP_{ND} revealed a different trend in error distribution and/or larger errors for the 10-90 and 20-90 minutes intervals. At the highest noise level this was also the case for the 30-90 and 40-90 minutes intervals (Fig.1). For SRTM, the majority of significant differences in mean were found in all intervals up to the 60-90 minutes interval. For RPM, significant differences in mean were also found in the 70-90 and 80-90 minutes intervals. The errors introduced in longitudinal changes were small (< 0.05) and smaller than the absolute error, for coffee-break intervals of 60 minutes or smaller (Fig. 2).

Conclusion:

SRTM and RPM provided comparable results when fitting coffee-break interval data. A systematic error was found (COV 0.0) as a function of coffee-break interpolation. Increasing the noise levels and BP_{ND} resulted in additional errors and more outliers. The kinetics of [^{18}F]flutemetamol were easier to interpolate using cubic interpolation during the coffee-break than [^{18}F]florbetaben. However, in longitudinal studies (i.e. AMYPAD) accurate BP_{ND} results can be achieved for both tracers using coffee-break intervals of 60 minutes (i.e. interval of 30-90 minutes) or shorter.

References:

1. Heurling K, Buckley C, Van Laere K et. al. [2015] NeuroImage 121: 184-192.

2. Becker GA, Ichise M, Barthel H et. al. [2013] J. of Nuclear Medicine 54: 723-731.

3. Yaqub, M, Tolboom, N, Boellaard, R et. al. [2008] NeuroImage 42: 76-86.

A

B

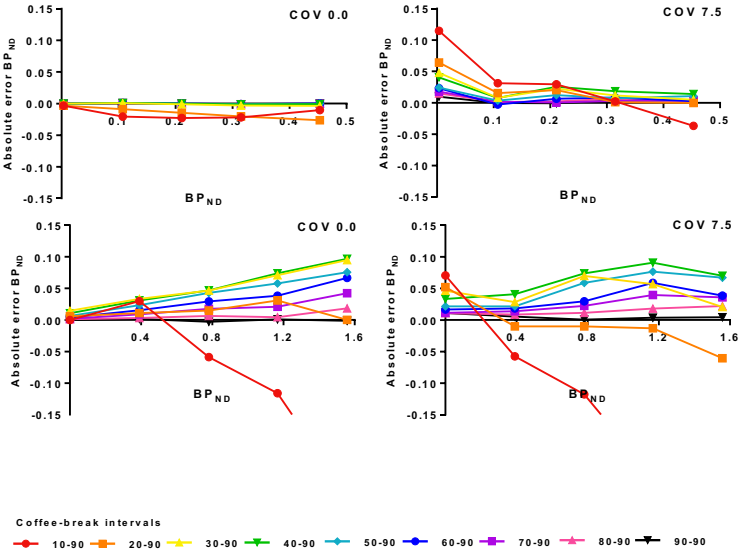

Figure 1. Absolute error in RPM derived BP_{ND} for simulated TACs with different coffee-break protocols for **A)** [^{18}F]flutemetamol **B)** [^{18}F]florbetaben. COV = Coefficient of variation (noise)

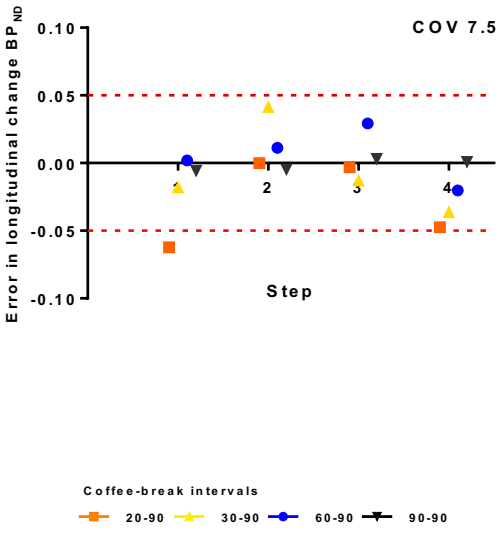

Figure 2. [^{18}F]Florbetaben: error in longitudinal change in RPM derived BP_{ND}

P75

Detecting and Characterizing Dopamine Dynamics in the Cortex with ^{18}F-fallypride PET: A Simulation Study of Time-Varying Models

Heather Liu[1,2], Jenny Ceccarini[3], Bart de Laat[3], Johan Lataster[5], Inez Myin-Germeys[6], Kelly P. Cosgrove[2,4], Evan D. Morris[1,2,4]

1. Dept. Biomedical Engineering, Yale Univ., 2. Dept. Radiology and Biomedical Imaging, Yale Univ., 3. Dept. Nuclear Medicine and Molecular Imaging, KU Leuven, 4. Dept. Psychiatry, Yale University, 5. Fac. Psychology and Educational Sciences, Open University Heerlen, 6. Center for Contextual Psychiatry, Dept. Neurosciences, KU Leuven

Introduction:

The meso-cortico-limbic dopamine (DA) circuitry plays a crucial role in addiction and stress. To explore the meso*limbic* circuit, we already successfully applied the lp-ntPET model[1] to [^{11}C]raclopride data to estimate temporal dynamics of smoking-induced DA release, and discovered a sex difference in the response[2]. Lp-ntPET employs basis functions to estimate voxelwise neurotransmitter release dynamics within a single scan. To explore the meso*cortical* circuit, we seek a model that is sensitive to competition between endogenous DA and a PET tracer in the cortex, where binding of the tracer is ~100x less than in the striatum. There have been promising results using the LSSRM model[3] to describe stress-induced cortical DA release during an [^{18}F]fallypride scan[4]. Like lp-ntPET, LSSRM models the DA component of the PET signal as time-varying. While lp-ntPET is more flexible than LSSRM and makes fewer *a priori* assumptions about the shape of the DA curves, it is possible that lp-ntPET may be over-parametrized for cortical data. To evaluate the validity of extending lp-ntPET to the cortex, we simulated [^{18}F]fallypride uptake kinetics with a DA stimulus occurring mid-scan. We applied both lp-ntPET[3] and LSSRM and compared the ability of the models to detect and characterize simulated DA release.

Methods:

Realistic noisy simulations of [^{18}F]fallypride PET data in the cortex and striatum were performed in the presence of DA competition induced by a stimulus. Simulations were performed using an extended compartmental model[5]. Stimulus-induced DA release was modeled as gamma-variates of differing shapes (e.g. variation in "rise-time" as shown in Fig. 1). Each simulation included a stimulus at 170 min, DA takeoff at 175 min and scan end at 225 min; short time frames were specified during the response and longer ones elsewhere. Amplitude of DA release was varied between 2x and 5x baseline to simulate possible behavioral and pharmacological stimuli. Tracer kinetic parameters for [^{18}F]fallypride were based on literature reports[6]. Population variability, based on a cohort of 12 subjects, was introduced into tracer parameters and also applied to the magnitude of DA release. Within-subject variability was modeled as: $\varepsilon_i = scale \cdot sqrt(PET_i/\Delta t_i)$. ε_i is the standard deviation of the additive error at a time point, *i*, of the TAC, which was all scaled to resemble the variability in experimental cortical[3] and striatal [^{18}F]fallypride data. For all DA release shapes, simulated PET data were fitted with LSSRM and lp-ntPET to estimate the peak DA amplitude above baseline, γ. t-scores for γ (detection sensitivity)

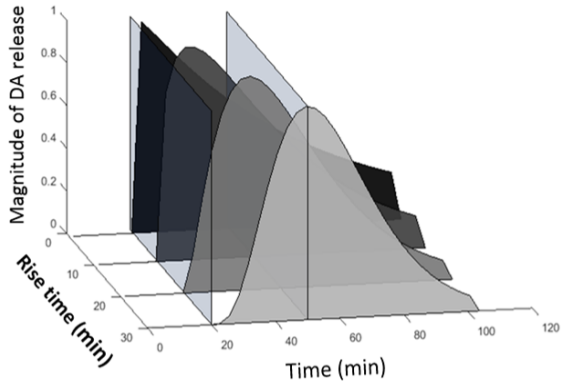

Figure 1: Example gamma-variate DA curves a function of time. The effect of rise time (for responses starting at 20 min, arbitrarily) is illustrated.

were compared between models. Weighted sums of squared residuals (WSSR) measured accuracy of fitting to the PET signal. The χ^2-statistic gauged the ability of the models to recover the true DA curve. The F-statistic was computed to determine if the difference in WSSR between models was significant. DA peak-time predictions were compared as an index of (estimated) DA curve accuracy. WSSR, F-statistic, and χ^2-statistic were computed for data from 10 min before the stimulus until scan end.

Results:

In striatal simulations, LSSRM and lp-ntPET produced similar t-scores (Fig. 2A, D), indicating comparable detection sensitivities. However, lp-ntPET outperformed LSSRM for DA release detection in the cortex, over all simulated DA curve shapes (i.e., uniformly higher t-score). In both the striatum and cortex, WRSS (Fig. 2B, E) and F-tests (not shown) confirm that lp-ntPET fitted the PET data significantly more accurately over the duration of stimulus-induced DA release. In striatal simulations, WRSS of LSSRM degraded with greater rise-time and DA release magnitude, whereas WRSS for lp-ntPET remained stable over all DA shapes (Fig 2B). Lp-ntPET predicted the time of peak DA release (not shown) with greater accuracy than LSSRM in both regions. But, both models suffered biases in the cortex. The χ^2-statistic (Fig. 2C, F) demonstrated the superiority of lp-ntPET over LSSRM in reproducing the *temporal profiles of DA release.* These findings held for both striatal and cortical simulations, and a wide range of DA shapes.

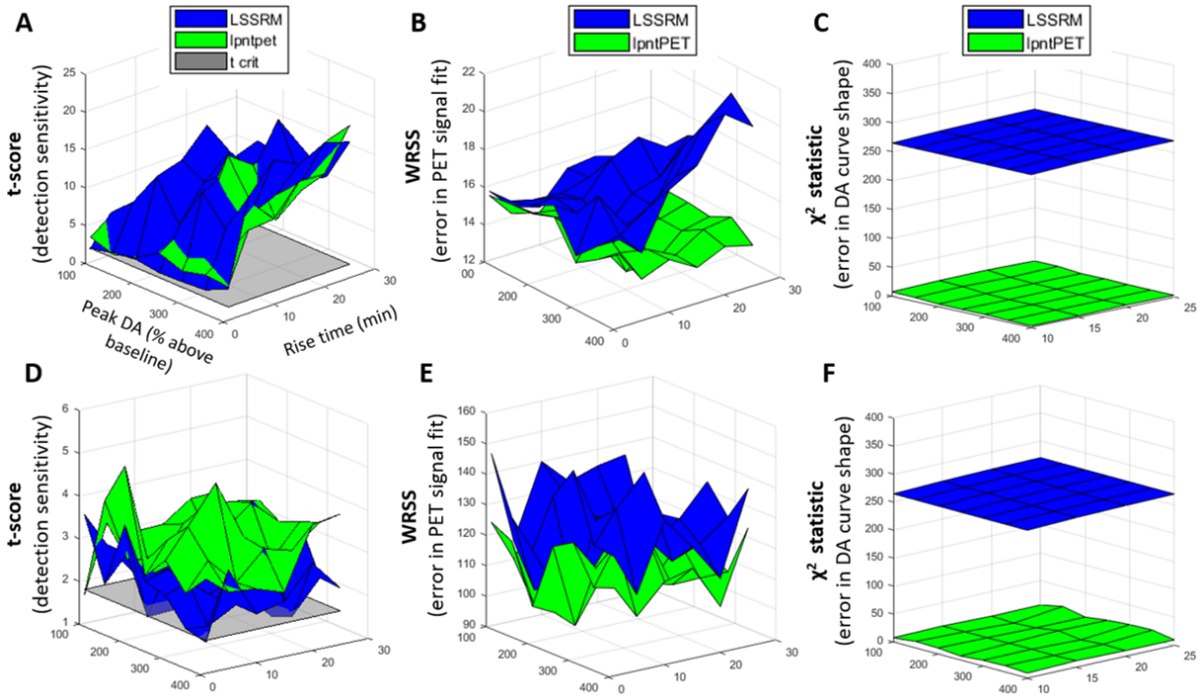

Figure 2: Surface plots for t-score (A, D), WRSS (B, E), and χ^2 statistic for error between estimated basis function and simulated DA response (C, F) in striatum (top row: A, B, C) and cortex (bottom row: D, E, F). X and Y axes, i.e. the simulated DA release parameters, are labeled on top left figure and are the same for all figures.

Conclusion:

lp-ntPET is more sensitive and more accurate than LSSRM for detecting and characterizing DA changes in both striatal and extrastriatal regions. The utility of simulations depends on the validity of the assumptions. Here, we assumed 1) DA responses followed a gamma-variate shape and 2) cohorts were comprised of people with similar DA responses that varied only in magnitude. LSSRM is inflexible; it models DA release as a decaying exponential that peaks instantaneously at the start of stimulus. In contrast, lp-ntPET can accommodate variability in DA start time, peak time, and recovery rate. The greater sensitivity and predictive value (i.e. describing DA over time) of lp-ntPET suggests that it

may be possible to observe the DA transmission timing in the entire mesocorticolimbic circuit using a single PET scan and a high-affinity DA tracer.

Acknowledgements:
Research support provided by 1R01DA038709 (to EDM). HL was supported by the Biomedical Engineering Program at Yale University and Robert E. Apafel Fellowship.

References:
1. Kim et al. [2014], Hum. Brain Mapp. 35(9):4876, 2. Cosgrove and Wang et al. [2014], J Neurosci. 34(50):16851, 3. Alpert et al. [2003], NeuroImage 19(3):1049, 4. Lataster et al. [2011], NeuroImage 58(4):1081, 5. Morris et al. [1996], JCBF&M 16(5):841, 6. Christian et al. [2004], JCBF&M 24(3):309

P76
The Impact of Preprocessing Pipeline Choice on Serotonin Transporter Measurements

Martin Nørgaard[1,2*], Melanie Ganz[1,3], Claus Svarer[1], Douglas N. Greve[5], Stephen C. Strother[4], Gitte M. Knudsen[1,2]

[1] *Neurobiology Research Unit, Copenhagen University Hospital Rigshospitalet, Copenhagen, Denmark*

[2] *Faculty of Health Sciences, University of Copenhagen, Copenhagen, Denmark*

[3] *Faculty of Computer Science, University of Copenhagen, Copenhagen, Denmark*

[4] *Rotman Research Institute at Baycrest, University of Toronto, Toronto, Canada*

[5] *Martinos Center for Biomedical Imaging, MGH, Harvard Medical School, Boston, MA, USA*

Introduction:

Positron Emission Tomography (PET) imaging is a prominent tool to capture the spatiotemporal distribution of neurotransmitters and receptors in the brain. The outcome of a PET study can, however, potentially be obscured by suboptimal and/or inconsistent choices made in complex processing pipelines required to reach a quantitative estimate of radioligand binding. Variations in subject selection, experimental design, data acquisition, preprocessing, and statistical analysis may lead to different outcomes and neurobiological interpretations.

The purpose of this study was to evaluate inter- and intra-scan variability in a test-retest study using high-resolution [^{11}C]DASB PET data for capturing serotonin transporter (5-HTT) binding[1], and to quantify associated preprocessing pitfalls for future group- and longitudinal studies.

Methods:

We examined the effects of 384 different preprocessing choices in 30 female subjects that were all scanned twice[1], spanning five common PET preprocessing steps (Fig. 1); delineation of volumes-of-interest (VOI; 3 choices), motion correction (MC; 2 choices), co-registration (4 choices), partial volume correction (PVC; 4 choices), and kinetic modeling (4 choices). All settings have previously been used in the PET literature. Inter- and intra-scan variability as a function of preprocessing pipeline choice was estimated using measures of within- and between-subject variability, the intraclass-correlation coefficient, and global signal-to-noise ratio[2].

Results:

The results showed a complicated interaction between various preprocessing steps on test-retest performance, particularly; MC, PVC, kinetic modeling and dependence on the region being investigated. We observed a small but consistent negative bias in 5-HTT binding across test and retest in 98% of tested preprocessing pipelines, ranging from 0-6% depending on the choice of preprocessing. In addition, the sample size needed to detect a given effect size interacted with various preprocessing steps, producing up to 80% differences in needed sample size, increasing from 27 subjects (pipeline: without MC, PVC with GTM 4 mm, co-registration with NMI and the average PET image, non-invasive Logan as kinetic modeling) to 49 subjects (pipeline: with MC, PVC with GTM 0 mm, co-registration with NMI and the average image, SRTM as kinetic modeling) in the anterior cingulate cortex, when changing the preprocessing pipeline (Fig. 2).

Discussion:

The reported results indicate, that seemingly small changes within a preprocessing pipeline may have significant impact on the output. We here examine how optimal neuroimaging results can be obtained by making appropriate preprocessing choices depending on the neuroscientific question. In addition, the presented results contribute to a better understanding of methodological uncertainty and variability in preprocessing decisions for future neuroimaging group- and/or longitudinal studies.

References:

1. Frokjaer, V. G., Pinborg, A., Holst, KK, et al. (2015). Biological Psychiatry, 78(8):534–543.

2. Churchill, N. W., Spring, R., Afshin-Pour, B., et al. (2015). *PLoS ONE*, *10*(7), 1–25.

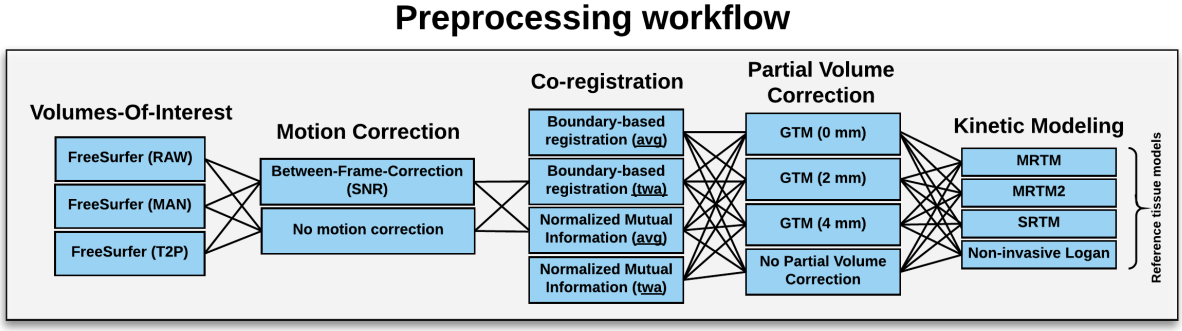

Figure 1: Overview of the various preprocessing steps. Abbreviations; average (avg), time-weighted average (twa), signal-to-noise ratio (SNR), Geometric Transfer Matrix (GTM).

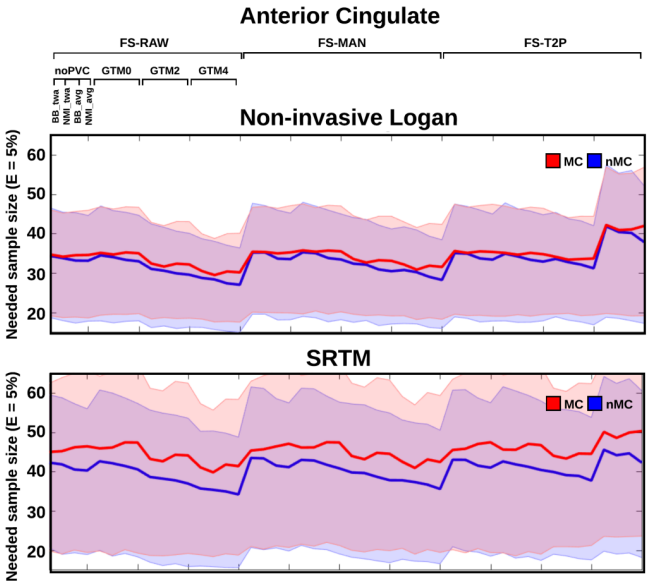

Figure 2: Needed sample size to show and effective change (E) of 5% from the mean BP_{ND}. Abbreviations; Boundary-based (BB), Normalized Mutual Information (NMI), FreeSurfer (FS),
Simplified Reference Tissue Model (SRTM), with/without Motion Correction (MC/nMC), raw VOIs in FS (FS-RAW), manual edits in FS (FS-MAN), T2 pial edits in FS (FS-T2P).

P77
Quantification of [^{11}C]PBR28 using venous blood sampling and population-based input function approach as less invasive method

Ryosuke Arakawa[1], Martin Schain[1], Naoki Kanegawa[1], Katarina Varnäs[1], Aurelija Jucaite[1,2], Christer Halldin[1], Simon Cervenka[1], Lars Farde[1,2], Andrea Varrone[1]

1. *Department of Clinical Neuroscience, Centre for Psychiatry Research, Karolinska Institutet and Stockholm County Council, Stockholm SWEDEN*
2. *PET Science Centre, Precision Medicine and Genomics, Innovative Medicine & Early Development (IMED) Biotech Unit, AstraZeneca, Karolinska Institutet, Sweden*

Introduction:

[^{11}C]PBR28, a PET radioligand for translocator protein (TSPO), has been used to evaluate the immune function in human brain. Several clinical studies have reported changes in [^{11}C]PBR28 binding in patients with Alzheimer's disease, epilepsy, multiple sclerosis, and schizophrenia. However, to quantify binding of this PET radioligand, arterial blood sampling is required, which is a costly and sometimes uncomfortable procedure. The purpose of this study is to examine the possibility to replace the arterial blood measurements with venous blood so as to make the quantification of [^{11}C]PBR28 binding to TSPO less invasive.

Materials & Methods:

Nineteen healthy subjects (2 females and 17 males, age range 43-71 yrs) were included in the study. PET measurements were performed with the HRRT (Siemens) system to obtain the radioactivity of [^{11}C]PBR28 in the brain. The measurement of blood and plasma radioactivity from both arterial and venous blood samples with HPLC analysis was performed. For technical reasons, venous data were not available in two subjects, therefore the comparison between arterial and venous data was performed in 17 subjects. The PET data were analyzed using Logan graphical analysis to derive the total distribution volume, V_T, as outcome measure. Region of interest was defined as gray matter. V_T measured with arterial input function was considered the gold standard. As a population-based approach, V_T was calculated with the following parameters: population-based blood curve, population-based plasma-to-blood ratio, and population-based parent fraction. The population-based parameter was generated by excluding the individual data for the subject that was tested while averaging across remaining subjects (a leave-one-out procedure). Scaling of the population based-parameter was done for each individual using the subject-specific measurement. The correlations of V_T with arterial input function and population-based data were estimated using Pearson correlation coefficient. Additionally, to check the cause of variability, one of the population-based parameters was assessed, while the others used individual data. That is, if the population-based blood curve was used, then the individual plasma-to-blood ratio and the individual parent fraction were used.

Results:

All three population-based parameters (blood curve, plasma-to-blood ratio and parent fraction) scaled by individual arterial data showed good agreement with V_T obtained with measured input function, with $R^2 = 0.95$. A good agreement was also observed when using all three population-based parameters scaled by individual venous data, with $R^2 = 0.86$ (Figure 1). However, scaling with venous measurements resulted in larger variability than when arterial samples were used. While scaling with venous measurements, estimation of the blood curve introduced more variability than estimation of plasma-to-blood ratio and parent fraction.

Discussion/Conclusion:

Our results indicate that venous sampling may be a useful alternative to arterial sampling for quantifying [^{11}C]PBR28 binding. To reduce the variability from the population-based blood curve scaled by venous blood, an image-derived approach such as Mourik´s method or the pair-wise correlation (PWC) analysis will be tested.

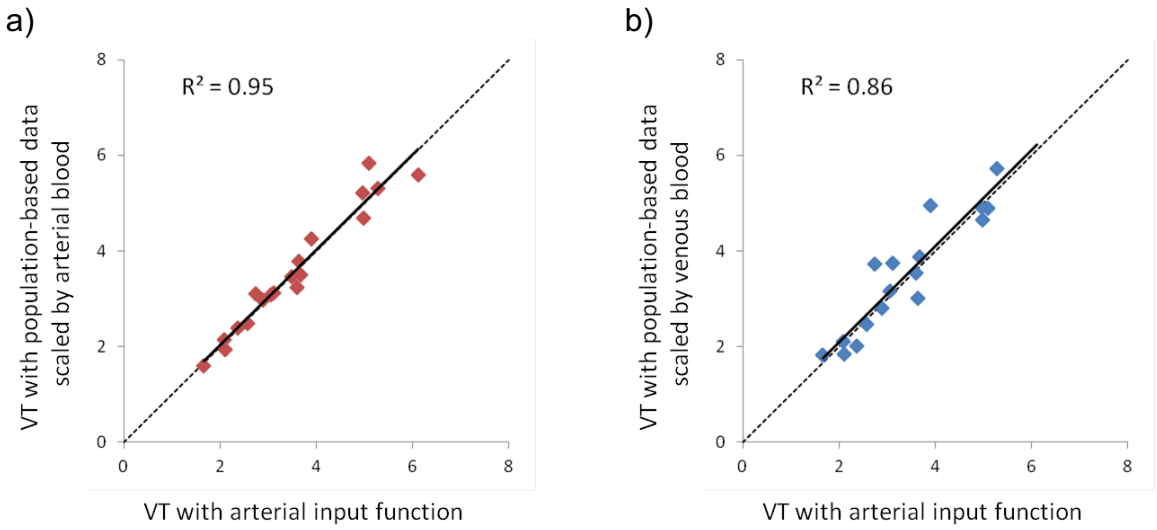

Figure 1. Correlations of V_T with arterial input function and population-based data scaled by a) arterial blood and b) venous blood.

Acknowledgements:

The study has been supported by AstraZeneca and by funds from the EU project INMiND, FP7/2007-2013-no HEALTH-F2-2011-278850 (http://www.uni-muenster.de/InMind).

References:

Collste K, Plavén-Sigray P, Fatouros-Bergman H, et al. [2017], Mol Psychiatry, 22(6):850-6.

Schain M, Benjaminsson S, Varnäs K, et al. [2013], J Cereb Blood Flow Metab, 33(7):1058-65.

P78
Relative cerebral flow from dynamic PIB scans as an alternative for FDG scans in Alzheimer's disease PET studies

Débora E. Peretti[1], David Vállez García[1], Fransje E. Reesink[2], Tim van der Goot[1], Peter P. De Deyn[2,3], Bauke M. de Jong[2], Rudi A.J.O. Dierckx[1], Ronald Boellaard[1]

[1] *University of Groningen, University Medical Centre Groningen, Department of Nuclear Medicine and Molecular Imaging, The Netherlands*

[2] *University of Groningen, University Medical Centre Groningen, Department of Neurology, Alzheimer Research Centre, The Netherlands*

[3] *University of Antwerp, Institute Born-Bunge, Laboratory of Neurochemistry and Behaviour, Belgium*

Introduction:

In Alzheimer's Disease dual-tracer positron emission tomography (PET) studies with 2-[^{18}F]-fluoro-2-deoxy-D-glucose (FDG) and ^{11}C-labelled Pittsburgh Compound B (PIB) are used to assess metabolism and cerebral amyloid-β deposition, respectively. Relative cerebral metabolism and blood flow (rCBF) are closely coupled, both providing an index for neuronal function. Pharmacokinetic modelling of PIB can be used to provide information on amyloid-β deposition, but also an estimation of rCBF. The present study explores the use of PIB-derived rCBF, approximated by the ratio of tracer influx in target regions relative to reference region (R_1), as a surrogate for FDG scans.

Materials and Methods:

Thirty subjects underwent both FDG and PIB scans. Based on visual inspection, they were classified as PIB positive (+) or negative (-). Each group was composed of fifteen subjects. Then, discriminative performance (PIB+ versus PIB-) of R_1 parametric maps, derived from SRTM2, were compared with normalized standardized uptake value FDG uptake (SUVR).

Results:

The resemblance between the R_1 and SUVR images was noticeable, with similar AD patterns. Strong positive correlations were found between R_1 and FDG analysis (0.86 for the PIB+ group, and 0.84 for the PIB-), suggesting that R_1 provides information that is closely related to that seen on FDG scans. Yet, overall higher SUVR values were found. While SUVR had a mean of 0.96 ± 0.15 for the PIB+ patients and 1.01 ± 0.15 for the PIB-, R_1 presented 0.88 ± 0.13 and 0.90 ± 0.11 respectively. Moreover, distinct differences in R_1 and FDG SUVR occur in specific regions such as midbrain and precuneus, which in turn depend on the subject classification, suggesting that R_1 is not entirely an alternative biomarker for FDG SUVR. Voxel-based analysis between groups showed that the main discrepancy between tracers was the size of the clusters, despite that their main core could be seen in both R_1 and SUVR, implying that R1 might not be as sensitive as SUVR (a difference in volume of 7.51% of the total number of voxels).

Discussion:

Pharmacokinetic analysis of dynamic PIB PET studies provides high-quality rCBF images comparable with those obtained by FDG SUVR. The high correlation between R_1 and normalized FDG uptake suggests that the first might be used as an alternative to FDG PET for diagnostic purposes. However, despite the good correlation between SUVR and R_1, the lower sensitivity of the latter may result in difficulties to assess small differences between subjects. Moreover, some distinct differences between R1 and FDG SUVR were seen in the midbrain and the precuneus, depending on amyloid status, suggesting that R1 cannot be considered as an alternative biomarker for FDG SUVR, in particular in studies focussed on studying pathophysiology or drug effects.

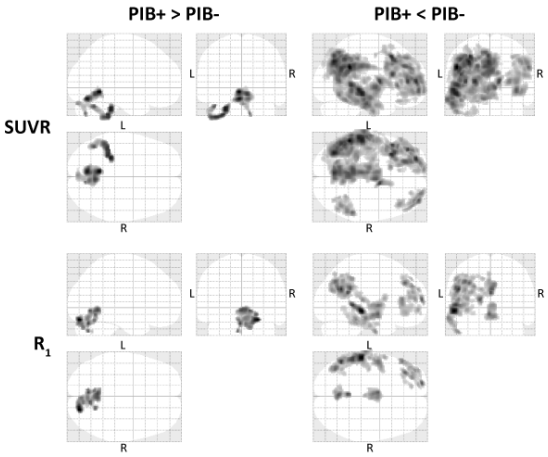

Figure 1: Maximum Intensity Projections derived from the voxel-based analysis showing regions that presented statistically significant differences between PIB+ patients and PIB- subjects.

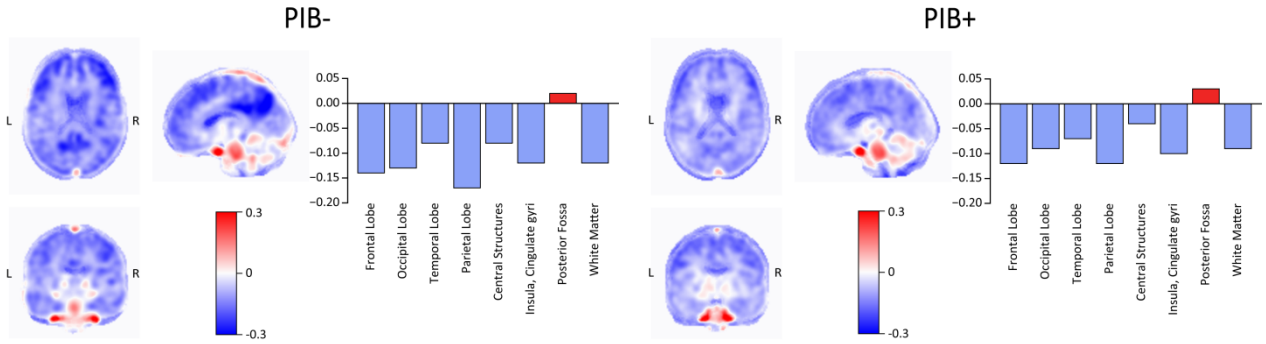

Figure 2: Mean difference images per groups comparing normalized FDG uptake and R_1 parametric maps (R_1 – SUVR). The closer the R_1 and SUVR estimates, the more white the voxel appears. Blue voxels represent voxels where SUVR presented higher values.

References:

Klunk WE, Henriksen G, Wester HJ et al. [2005] Eur.J.Nucl.Med.Mol.Imaging 32: 486-510
Meyer PT, Hellwig S, Amtage F et al. [2011] J.Nucl.Med. 52: 393-400
Mosconi L [2005] Eur.J.Nucl.Med.Mol.Imaging 32: 486-510
Paulson OB, Hasselbalch SG, Rostrup E et al. [2010] J.Cereb. Blood Flow Metab. 30: 2–14.
Yaqub M, Tolboom N, Boellaard R et al. [2008] Neuroimage 42: 76-86

P79
Development of a medium-throughput method to screen the effect of test articles on mouse brain activity using ^{14}C-2-deoxyglucose (^{14}C-2DG) 3D autoradiography

Jenna M. Sullivan[1], Mohammed Qutaish[1], Ildiko Polyak[1], Mark Aldridge[1], Jack Heimann[1], Inna Gertsenshteyn[1], Marc Seaman[1], Paige Czarnecki[1], Matthew D. Silva[1], Jacob Hesterman[1], Andrew Giovanni[2], Sharon Engel[2], Carrie Bowen[2], Ryan Terry-Lorenzo[2], Nina Dedic[2], Larry Hardy[2]

[1] *Invicro, LLC,* [2] *Sunovion Pharmaceuticals Inc.*

Introduction:

The objective of this study was to develop a 3D autoradiographical method for medium-throughput screening of the effect of test articles on ^{14}C-2DG concentration in mouse brain.

Materials & Methods:

One-hundred and eight (108) C57BL/6 mice were separated into twelve groups of nine animals. After an overnight fast, each mouse was administered one of 12 test articles while awake via intraperitoneal injection. Three of the test articles were reference compounds and included water (vehicle), haloperidol, and ketamine. Fifteen minutes after test article administration, each mouse was administered ^{14}C-2DG intravenously. Mice were euthanized at 45-minutes post-injection of ^{14}C-2DG, and their brains were harvested.

Each brain was resected whole and frozen. Frozen brains were embedded in optimal cutting temperature (OCT) compound in two blocks, 54 brains/block, in grid-like configurations for autoradiography. Each block contained radioactive and white light visible fiducial markers. Sagittal, 30-µm thick brain sections were obtained using a cryomacrotome. High resolution optical (white light) images were acquired prior to each section being taken from the block. Sections were exposed to phosphor imaging plates to measure radioactivity in the tissue and to produce autoradioluminograms.

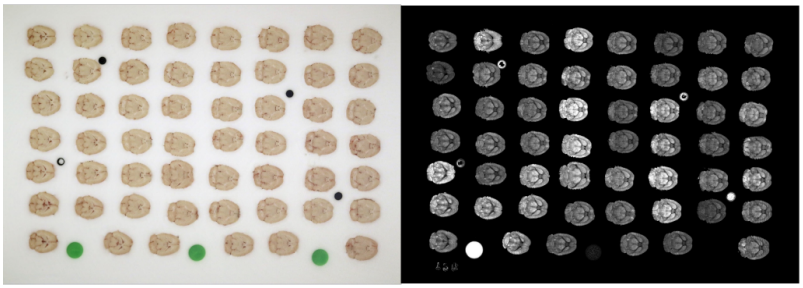

Fig 1. (Left) White light image of one block showing 54 brains being sectioned in the frontal plane. (Right) Autoradioluminogram of the brains shown on the left.

All 2D white light images and autoradioluminograms (~225 per block) were reconstructed into 3D volumes. Individual 3D brain volumes were digitally extracted and all 108 brains

(white light and autoradiography data) were registered to a common space. Qualitative and quantitative statistics (vehicle vs. test articles) were performed on radioactivity concentration normalized to whole brain activity at the voxel-level and the region-level using a custom 67-region brain atlas. Voxel-level parametric maps of significant differences between vehicle and test article after false discovery rate (FDR) correction were produced.

Results:

By collecting every 30-µm thick section, we were able to build 3D brain volumes and analyze the autoradiography data in 3D using conventional *in vivo* image processing methods. The pattern of ^{14}C-2DG distribution agreed with published results for similar ^{14}C-2DG or ^{18}F-FDG studies. Statistical maps demonstrated significant group-level effects. The group that received haloperidol showed significantly higher normalized ^{14}C-2DG signal in the caudoputamen and lateral habenula, and significantly lower normalized ^{14}C-2DG signal in the sensory-motor cortex related part of the thalamus (compared to vehicle group).

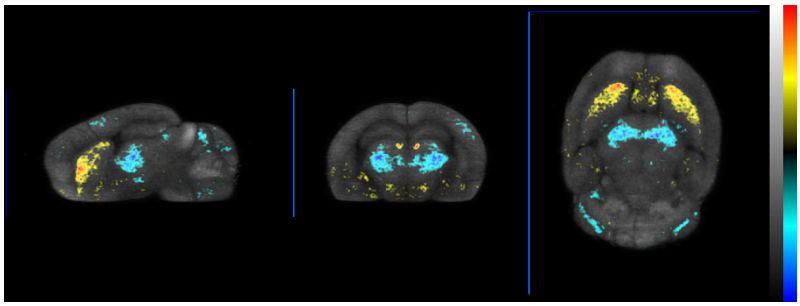

Fig 2. Voxel-level statistical map of significant voxels from comparison of ^{14}C-2DG concentrations normalized to whole brain in haloperidol (n=9) and vehicle (water) groups (n=9). T-stat values in significant voxels (after FDR correction with q = 0.01) are shown in color on top of an autoradiography image from a single brain for anatomical reference. T-stat map has been smoothed with a 0.05 mm gauss filter. Warm colors indicate higher signal in haloperidol group than control and cool colors indicate lower signal in haloperidol group than control.

Discussion/Conclusions:

A medium-throughput 3D autoradiography method was developed and applied to measure the effect of test articles on ^{14}C-2DG radioactivity in the mouse brain. As the resolution of quantitative autoradiography is on the order 100 µm, this method provides a higher-resolution complement to preclinical *in vivo* PET imaging.

Acknowledgements:

None

References:

Barlett EJ, Brodie JD, Simkowitz P, et al. [1994], American Journal of Psychiatry, 151:681-686.

Pizzolato G, Soncrant TT, Holloway HW, et al. [1985], Journal of Neuroscience, (5)11:2831-2838.

P80
Image-derived input functions from heart and vena cava/aorta region for quantification of A1 adenosine receptors in mice brain using [^{18}F]CPFPX and PET

Xuan He, Franziska Wedekind, Tina Kroll, Angela Oskamp, Andreas Bauer, David Elmenhorst

Molecular Neuroimaging, Institute of Neuroscience and Medicine (INM-2) Forschungszentrum Jülich, 52425 Jülich, Germany

Introduction:

Arterial input functions are still the gold standard for quantification of target proteins by means of PET. However, the measurement of arterial input functions is a method of restricted applicability because of the small total blood volume and the related difficulties in withdrawing blood in mice. Therefore, the aim of this study was to select the best region of interest for an image-derived input function (IDIF) for mice by using dynamic positron emission tomography (PET) images. IDIF is an attractive noninvasive alternative method compared with arterial sampling. [^{18}F]CPFPX is a highly selective and specific ligand for A_1ARs and a suitable radioligand for noninvasive PET imaging of A_1ARs in the living brain.

Materials and Methods:

In this study four mice were scanned with [^{18}F]CPFPX for 60 min. Arterial blood samples (n=8 per animal) were collected from the femoral artery and corrected for metabolites. To generate IDIF, three different approaches were selected: volumes of interest (VOIs) were placed over the heart (cube, 12mm) and abdominal vena cava/aorta region (cuboid, 5 x 5 x 15mm). Within these spatial frames only voxels exceeding 50% of the total activity inside the VOI in the first 30 seconds were read out subsequently. Additionally, 1 x 1 x 1mm voxels on 10 consecutive slices (Lanz B, 2014) were manually placed over the abdominal vena cava/aorta region (centered on highest activity spot). An empirical scaling factor of 1.7 was used to correct for e.g. partial volume effects. To calculate IDIF, data reflecting the metabolite-corrected arterial plasma activity, a population-based plasma fraction and metabolite function were used.

In addition to the visual comparison of blood sampling and IDIF whole blood curves, a quantitative analysis was performed by using the mean area under the curve (AUC) ratio between the image-derived and arterial-derived whole-blood curves (Zanotti-Fregonara P et al, 2011). Also, kinetic modelling with a two-tissue compartment model (2 TCM) was used to compare the IDIF/blood mean distribution volume (V_T) ratio in e.g. cortex, hippocampus, and thalamus for each mouse in the different VOIs.

Results:

After comparing the overall shape of the curves, the height of the peaks as well as the slope of the tails with the reference arterial curves, we found the method with VOI over the heart matched slightly better than others. The whole-blood AUC ratio between image-derived and arterial curves of the VOI over heart was 1.03±0.04, which showed the least difference to the arterial method (Table 1). As for the V_T values obtained from 2 TCM modeling, which presented that the manually defined VOI over abdominal vena cava/aorta region was slightly better.

Table 1. IDIF/blood sampling based V_T ratio and AUC ratio (mean ± SD) for each VOI

	Heart (cube)	Vena cava/aorta (cuboid)	Vena cava/aorta (manually defined)
2TCM V_T ratio	0.92±0.11	0.91±0.16	1.02 ±0.40
Whole-blood AUC ratio	1.03±0.04	1.04±0.10	1.23±0.32

Discussion:

The whole-blood curves extracted from the three different VOIs in a **[^{18}F]CPFPX PET study in mice revealed a good performance for calculating the image-derived input function. Moreover,** the method with VOI over the heart matched slightly better comparing with arterial method in visual comparison and AUC ratio of whole blood. **Manually defined vena cava/aorta region had a better performance in** IDIF/blood sampling based V_T ratio. **In future, this input function method might also be transferable to other radioligands and targets.**

References:

Zanotti-Fregonara P, Liow JS, Fujita M et. al. [2011] PLoS One 6(2):e17056

Lanz B, Poitry-Yamate C, Gruetter R [2014] J Nucl Med 55(8):1380-8

P81
Accounting for endothelial binding in the kinetic modeling of [^{18}F]FEPPA, a TSPO radioligand.

Pablo M Rusjan, Tania Da Silva, Romina Mizrahi, Sylvain Houle.

Department of Psychiatry. University of Toronto & PET Centre. Centre for addiction and Mental Health, Toronto, Canada.

Introduction:

It has been claimed that the quantification of some translocator protein (TSPO) radioligands, including [^{11}C]PBR28, [^{18}F]DPA714 and [^{11}C]R-PK11195, are improved by adding an irreversible compartment in parallel to the two-tissue compartmental model (2TCM)[1]. This extra compartment represents endothelial TSPO specific binding (2TCM-1k model). While it is known that these radioligands do not bind irreversibly to TSPO, the supporters of the 2TCM-1k model based the decision in practical considerations about identifiability of the outcome parameters[1], and theoretical arguments related to differences in reactive volumes[2]. [^{18}F]FEPPA is an [^{18}F] radioligand analog to [^{11}C]PBR28, which has shown an affinity 3 times higher for TSPO in rats. As with other second generation TSPO radioligands, the binding of [^{18}F]FEPPA is affected by a polymorphism (rs6971), creating three groups of binders: high affinity binders (HABs), mixed affinity binders (MABs) and low affinity binders (LABs). The 2TCM-1k model has never been tested for the quantification of [^{18}F]FEPPA. Thus, the goal of the present work is to evaluate whether 2TCM-1k can improve the quantification of [^{18}F]FEPPA.

Methods:

Two hour [^{18}F]FEPPA images of 22 healthy subjects (13 HABs, 6 MABs and 3 LABs) were analyzed with the 2TCM and 2TCM-1k. Images were acquired with a High Resolution Research Tomography (HRRT), and arterial blood samples were extracted manually and with an automatic blood sampling system [3]. For a subset of subjects (9 HABs, 3 MABs), 3 hour scan times were available and analyzed independently. Analysis was performed with PMOD 3.9. Data points were weighted based on the length of the frame and the regional uptake. Goodness of fit tests (the Akaike Information Criterium and the Model selection criterion) were compared with paired t-test using a significance level of 0.05. Results are expressed as mean ± standard deviation.

Results:

For MABs and HABs, noise in the TAC, which is associated with the size of the ROI and the regional uptake, predicted the need of an extra parameter in the model. While in big ROIs (temporal, prefrontal, parietal, cerebellar cortices) 2TCM-1k fitted the TACs better than 2TCM, in medium sized ROIs (insula cortex, thalamus), the 2TCM-1k did not improve fittings. In smaller sized ROIs and/or low uptake ROIs, including the putamen, caudate head, anterior cingulate and middle brain, the 2TCM was better than the 2TCM-1k. For the ROIs

where the 2TCM-1k was better, the total distribution volume (V_T) estimation for both models correlated (r~0.6), however the %standard error (%SE) of V_T was higher for 2TCM-1k (~10%) than the 2TCM (~3%). In agreement, the between subjects variability of V_T was higher for 2TCM-1k (HABs=49±4%, MABs=40±6%) than 2TCM (HABs=27±1%, MABs=25±1%). 2TCM-1k was able to deliver a V_T for LABs, with a %SE ranging from 4% to 15%, which is not possible for 2TCM. V_T and the vascular binding rate (K_b) rank order for HABs, MABs and LABs were consistent with the radioligand affinity for TSPO (eg. for the temporal cortex, V_T=4.7±2.2, 3.5±1.5, 0.4±0.2 ml/cm^3 and K_b=0.44±0.17, 0.36±0.08, 0.20±0.08 min^{-1} for HABs, MABs and LABs, respectively). The main findings persisted when analyzing the 3 hour scans. For the ROIs where 2TCM-1k fit better, the %SE of V_T was reduced to ~6% for the 2TCM-1k and <2% for the 2TCM. The correlation of V_T between models also improved slightly (r~0.7).

Discussion:

The 2TCM-1k shows some merit from a goodness of fit perspective, and provides the possibility to quantify LABs. The %SE of 2TCM-1k is unacceptable for 2 hour scans but improves for 3 hour scans. The correlation of V_T between the 2 models, and the lower variability of V_T for 2TCM as compared to 2TCM-1k does not support the need of a more complex modeling approach to the quantification of [^{18}F]FEPPA. However this work does not imply that 2TCM-1k can be discarded as a better model. While the possibility of quantifying LABs using the 2TCM-1k is of particular interest, its validity should be experimentally tested.

References

1. Rizzo G, Veronese M, Tonietto M, Zanotti-Fregonara P, Turkheimer FE, Bertoldo A. (2014): JCBFM Kinetic modeling without accounting for the vascular component impairs the quantification of [(11)C]PBR28 brain PET data. 34(6):1060-9
2. Rizzo G, Veronese M, Tonietto M, Bodini B, Stankoff B, Wimberley C, Lavisse S, Bottlaender M, Bloomfield PS, Howes O, Zanotti-Fregonara P, Turkheimer FE, Bertoldo A. (1017) JCBFM Generalization of endothelial modelling of TSPO PET imaging: Considerations on tracer affinities.
3. Rusjan PM, Wilson AA, Bloomfield PM, Vitcu I, Meyer JH, Houle S, Mizrahi R. (2011) JCBFM Quantitation of translocator protein binding in human brain with the novel radioligand [18F]-FEPPA and positron emission tomography. 31(8):1807-16

P82
Non-invasive estimation of [^{11}C]PBR28 binding potential – application to Alzheimer's Disease

Martin Schain[a], Francesca Zanderigo[a,b], R. Todd Ogden[a,b,c], William C. Kreisl[d,e]

[a] *Department of Psychiatry, Columbia University, New York, NY, USA*

[b] *Molecular Imaging and Neuropathology Division, New York State Psychiatric Institute, New York, NY, USA*

[c] *Department of Biostatistics, Mailman School of Public Health, Columbia University, New York, NY, USA*

[d] *Molecular Imaging Branch, National Institute of Mental Health, Bethesda, MD, USA*

[e] *Taub Institute for Research on Alzheimer's Disease and the Aging Brain, Columbia University, New York, NY, USA*

Introduction:

[^{11}C]PBR28 is a PET radioligand used to estimate densities of the 18 kDa translocator protein (TSPO) *in vivo*. Since there is no suitable reference region, arterial blood sampling during the PET scan is required for full quantification. Here, we evaluate a methodology for full quantification of [^{11}C]PBR28 PET data that does not require either a reference region or blood samples.

Simultaneous estimation (SIME)[1] uses the time-activity curves from several brain regions to estimate the non-displaceable distribution volume (V_{ND}), which in turn can be used to calculate the binding potential (BP_{ND}), a theoretically more sensitive outcome measure than total distribution volume (V_T). SIME can be applied with either a measured arterial input function (AIF)[1] or a template input function (tIF)[2] that has similar shape as the AIF, but with arbitrary amplitude. If a tIF is used, only proportionally biased estimates of V_T and V_{ND} can be estimated. Since the bias is approximately equal, however, it cancels out in the calculation of BP_{ND}, resulting in a theoretically unbiased outcome measure[2].

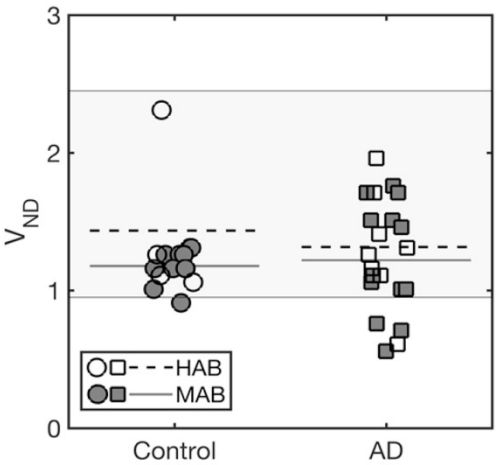

Figure 1 V_{ND} estimated with SIME. The gray box indicates the range of V_{ND} values reported in a previous blocking study[4].

Materials and methods:

We evaluated the ability of SIME to detect group differences in TSPO densities using PET and arterial plasma data from 21 Alzheimer's disease (AD) patients and 15 controls that underwent [^{11}C]PBR28 imaging[3]. tIFs curves were derived in a population-based "leave-one-out" manner, without any scaling with individually acquired blood samples. Regional BP_{ND} obtained with tIFs were compared to those obtained using measured AIFs. Standard kinetic modeling with the two-tissue compartment model was also used for comparison. The sensitivity of each method to detect group differences in TSPO densities was assessed by comparing estimated effect sizes between AD patients and controls. For this purpose, BP_{ND} values estimated in one region with high pathological burden (inferior temporal cortex), and in one region with low pathological burden (cerebellum), were used[3].

Results:

Using SIME and measured AIFs resulted in V_{ND} values that were in a similar range as those reported in a previous [^{11}C]PBR28 blocking study[4] (Figure 1). BP_{ND} estimates obtained with SIME and tIFs were close to identical to those obtained with AIFs (Figure 2, 3.0 ± 21% difference, r^2 = 0.78). In this dataset, the effect sizes between AD patients and controls for both SIME with AIF and SIME with tIF were similar (30.3%, p = 0.001 and 31.0%, p = 0.004, respectively, Figure 3) and both greater than the effect size observed with V_T/f_p (16.1%, p = 0.12). With V_T/f_p, but not with BP_{ND}, there were two apparent outliers in the AD group. None of the tested methods showed difference in TSPO binding in cerebellum.

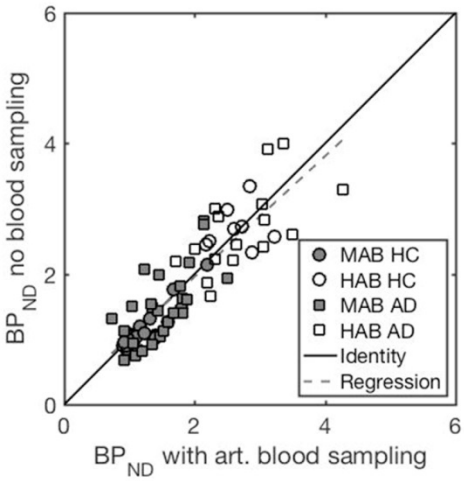

Figure 2. There was a close agreement between BP_{ND} values estimated with AIF and tIF, suggesting that arterial blood sampling may not always be necessary for [^{11}C]PBR28

Discussion:

These results demonstrate that BP_{ND} can be estimated for [^{11}C]PBR28 using SIME, and may be useful in clinical studies. Arterial sampling may not be necessary if tIFs can be reliably estimated.

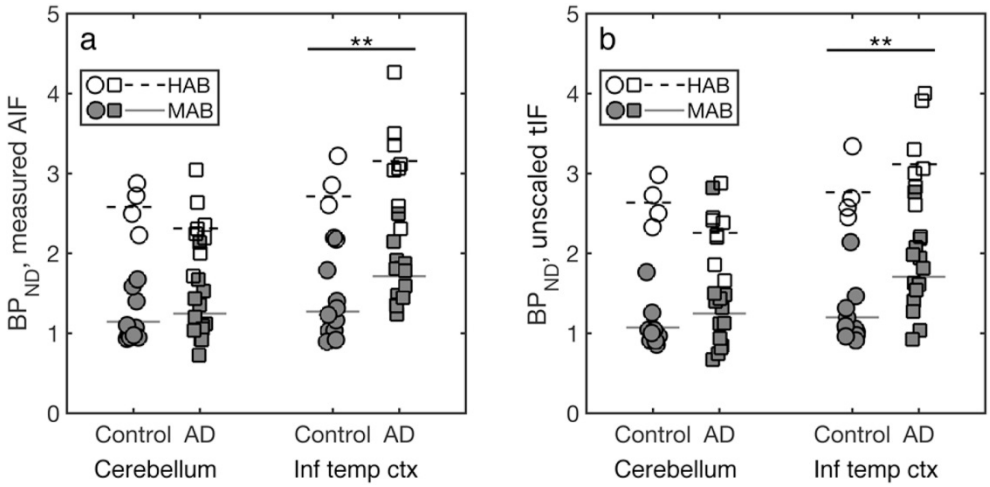

Figure 3 [^{11}C]PBR28 BP_{ND} obtained with measured (a) and population-based (b) input functions. In both cases, a significant different between AD patients were observed in inferior temporal cortex, but not in cerebellum.

References:

[1] Ogden RT, Zanderigo F, Parsey RV, [2015], NeuroImage, 108:234-42

[2] Schain M, Zanderigo F, Mann JJ, et al., [2017], NeuroImage, 146:121-31

[3] Kreisl WC, Lyoo CH, McGwier M, et al., [2013], Brain 136:2228-38

[4] Owen DR, Guo Q, Kalk NJ, et al., [2014], J Cereb Blood Flow Metab. 34:989-94

P83
Test-retest properties and noninvasive quantification of [^{11}C]Harmine binding to brain monoamine oxidase A

Francesca Zanderigo[1,2], Alexandra E. D'Agostino[3], Nandita Joshi[4], Martin Schain[1], Dileep Kumar[2], Ramin V. Parsey[3], Christine DeLorenzo[3], J. John Mann[1,2,5]

[1]Department of Psychiatry, Columbia University, New York, NY, USA [2]Molecular Imaging and Neuropathology Division, New York State Psychiatric Institute, New York, NY, USA [3]Department of Psychiatry, Stony Brook University, Stony Brook, NY, USA [4]Department of Electrical and Computer Engineering, Stony Brook University, Stony Brook, NY, USA [5]Department of Radiology, Columbia University, New York, NY, USA

Introduction:

Monoamine oxidase (MAO) is a mitochondrial enzyme that catalyzes deamination of monoamine neurotransmitters. Inhibition of the isoform A of MAO (MAO-A) is useful in treatment of depression and anxiety disorders. [^{11}C]Harmine is a PET tracer targeting MAO-A that is used to study mood disorders and antidepressant treatment, although its test-retest characteristics have to date only been partially investigated(1). Furthermore, since MAO-A is ubiquitously expressed, no valid reference brain region is available, thus requiring arterial blood sampling during PET scanning for [^{11}C]harmine full quantification. Analytical methods that aim at reducing the need for arterial sampling have not so far been explored for this tracer. Here we investigate [^{11}C]harmine binding measurements test-retest properties; assess effects of using a minimally-invasive input function estimation on binding quantification and repeatability; and explore binding potentials estimation using a reference region-free approach.

Material and Methods:

Five healthy males were imaged twice with [^{11}C]harmine, on the same day. In each scan, arterial blood samples were collected during the acquisitions for measurement of tracer parent fraction and total plasma counts. Each parent fraction curve was fitted with a Hill function, and multiplied by the total plasma counts curve to obtain a metabolite-corrected arterial input function, which was then fitted using a linear interpolation before the peak and the sum of three-decreasing exponentials after the peak. We applied kinetic models (one-, 1TC, and two-, 2TC, tissue compartment) and graphical analyses (Logan plot and Likelihood Estimation in Graphical Analysis, LEGA(2)) to quantify [^{11}C]harmine distribution volume (V_T). Time activity curves were corrected for vascular contribution using a fixed fractional blood volume of 5% before applying each of the quantification approach. The t* for Logan and LEGA was set to 45 min post-injection to allow all considered regions and scans to reach the “linear phase”. We compared repeatability of V_T estimates based on absolute test-retest percent difference (TRPD) and intra-class correlation coefficient (ICC). The optimal quantification procedure was also used with a simultaneously estimated input function(3) in place of the measured curve. Simultaneous estimation(3) (SIME) only requires one blood

sample for identifiability of the metabolite-corrected input function; samples from 4 time points (6, 20, 50, and 95 min post injection) were considered. Lastly, an approach for quantification of binding potentials (BP_P, BP_{ND}) in absence of a reference region[4] was evaluated.

Results:

Both kinetic models provided similar fits, and V_T estimates comparable to those obtained from graphical approaches. V_T estimates quantified using arterial blood and kinetic modeling showed average absolute TRPD values of 7.7% to 15.6%, and ICC values between 0.56 and 0.86, across brain regions (**Figure 1**). TRPD values were numerically higher for Logan and LEGA (range 9.6% to 16.3%). The optimal blood sampling time for SIME was found to be 20 min post injection. Using SIME and 1TC resulted in V_T estimates close to those obtained using arterial input function (r = 0.951, slope = 1.073, intercept = -1.037) (**Figure 2**), with numerically but not statistically higher test-retest difference (range: 16.6% to 22.0%), but with overall poor ICC values, between 0.30 and 0.57. Application of our reference region-free approach[4] for quantification of binding potentials consistently failed to provide a unique solution for [^{11}C]harmine.

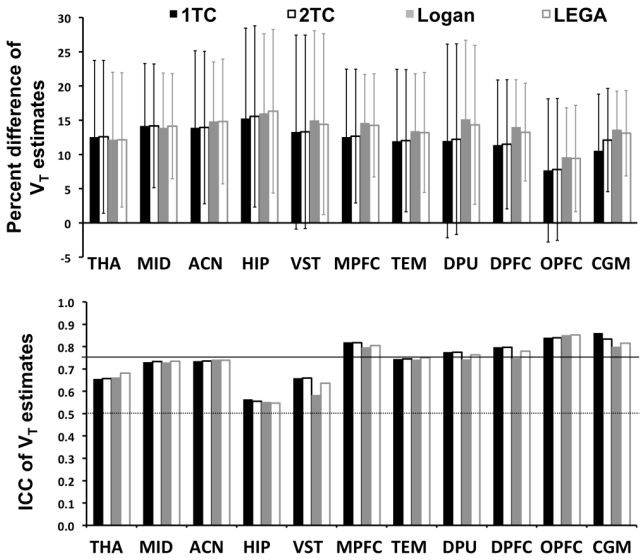

Fig 1. TRPD and ICC values for V_T; horizontal lines indicate ICC = 0.5 (dotted) and ICC = 0.75 (solid). THA: thalamus; MID: midbrain; ACN: anterior cingulate; HIP: hippocampus; VST: ventral striatum; MPFC: medial prefrontal cortex (PFC); TEM: temporal lobe; DPU: dorsal putamen; DPFC: dorsolateral PFC; OPFC: orbital PFC; CGM: cerebellar gray matter.

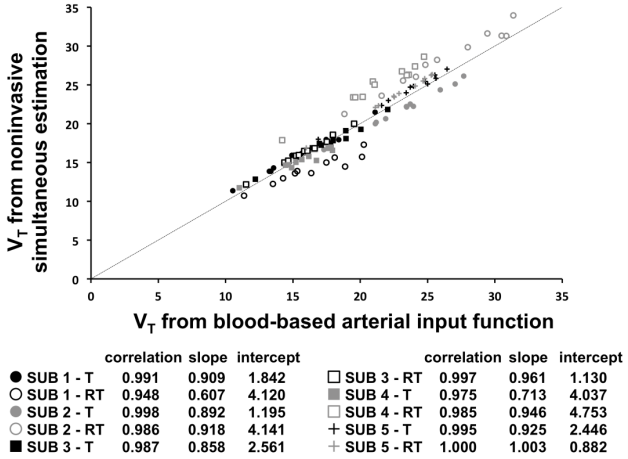

Fig 2. Scatter plot of V_T values obtained using measured arterial input function (x-axis) and SIME-derived input function (y-axis) using the 1TC model. Black dotted line indicates the identity line.

Discussion:

We find the test-retest repeatability of [^{11}C]harmine binding to MAO-A, when quantified using arterial blood sampling and either kinetic compartment models, to be comparable to that of other used PET tracers, thus prospective studies using [^{11}C]harmine are possible. Results with SIME suggest that simplifying acquisition of [^{11}C]harmine data by eliminating arterial catheterization may be possible, provided that accurate sampling of one arterial blood sample at 20 minutes post injection, and parent fraction analysis on such sample, can be obtained. Estimation of [^{11}C]harmine binding potentials remains a challenge that requires further investigation.

Acknowledgements:

The authors would like to thank Dr. Rajan Murthy for his help with the protocol used to acquire the scans. This research was supported by 5P50MH062185, Conte Center: The Neurobiology of Suicidal Behavior (National Institute for Mental Health) (PI: Mann).

References:

1) Ginovart N, Meyer JH, Boovariwala A et al. [2006] J Cereb Blood Flow Metab 26:330-44; 2) Ogden RT [2003] Statistics Med 22: 3557-68; 3) Ogden RT, Zanderigo F, Choy S et al. [2010] J Cereb Blood Flow Metab 30: 816-26; 4) Ogden RT, Zanderigo F, Parsey RV [2015] NeuroImage 108: 234-42.

P84
Evaluation of the novel PET tracer [^{11}C]HACH242 for imaging the GluN2B NMDA receptor in non-human primates

Jasper van der Aart[1], Maqsood Yaqub[1], Esther Kooijman[1], Jaco Bakker[2], Jan Langermans[2], Robert Schuit[1], Mark Hofman[1], Thanos Metaxas[1], Hans Christiaans[1], Adriaan Lammertsma[1], Bert Windhorst[1] Bart van Berckel[1]

[1] *Department of Radiology & Nuclear Medicine, Amsterdam Neuroscience, VU University Medical Center, Amsterdam, The Netherlands*

[2] *Animal Science Department, Biomedical Primate Research Centre, Rijswijk, The Netherlands*

Introduction:

There are currently no PET radiotracers available for the GluN2B (NR2B) binding site of brain *N*-Methyl-D-aspartate (NMDA) receptors. Previous work has shown that the GluN2B antagonist Ro25-6981 reduced binding of N-((5-(4-fluoro-2-[^{11}C]methoxyphenyl)pyridin-3-yl)methyl)cyclopentanamin ([^{11}C]HACH242) in rats with a regional distribution that is consistent both with the expression pattern of GluN2B subunits and the density of [^{3}H]Ro25-6981 binding sites [1]. The current abstract reports on the initial in vivo assessment of [^{11}C]HACH242 PET in non-human primates at baseline and following administration of the potent and selective GluN2B negative allosteric modulator radiprodil.

Materials & Methods:

Eight dynamic [^{11}C]HACH242 PET scans were acquired in 3 male anesthetised rhesus macaques, including a retest session of subject 1. Ninety minute scans were performed on a Philips PET/MRI scanner at baseline and 10 minutes after intravenous administration of radiprodil 10 mg/kg. Standardised uptake values (SUV) were calculated for 8 brain volumes of interest (VOIs) as well as whole-brain grey matter. Discrete arterial blood samples were manually obtained at six time points to characterise the pharmacokinetic profile of [^{11}C]HACH242 in blood and plasma. Reliable input functions for kinetic modelling could not be generated because of variability in the whole blood radioactivity measurement.

Results:

[^{11}C]HACH242 readily entered the brain and displayed a fairly uniform pattern of uptake. The rate of radioligand metabolism in plasma was high, with mean (±SD) parent fractions of 52±16% at 5 mins, 26±10% at 20 mins and 8±5% at 85 mins post injection (p.i.). Polar metabolites constituted 52±10% at 10 mins and 76±8% at 85 mins p.i. The mean nonpolar metabolite fraction was approximately 9% from 10 mins p.i. until the end of the scan. Whole-brain SUV (area under the curve) normalised for plasma radioactivity was 39% to 110% higher in the radiprodil condition, and partly driven by lower parent plasma radioactivity of -

11% to -56%. Radiprodil increased [^{11}C]HACH242 whole-brain SUV in the last 15 minute PET frame by 25%, 1%, 3% and 17% for subjects 1, 2, 3 and retest of subject 1, respectively (figure 1). The pattern of lower radiotracer peak uptake and slower wash-out in the radiprodil condition was most pronounced in the cerebellum and occipital cortex compared with other VOIs.

Discussion/Conclusions:

Results do not indicate that intravenous infusion of radiprodil consistently change brain SUVs that are corrected for plasma parent fraction. The findings may be explained by variations in cerebral blood flow due to pharmacodynamic effects of radiprodil and the anaesthetics, a low fraction of specifically bound tracer, or interactions of the radiotracer with endogenous NMDA receptor ligands at the binding site. In addition, [^{11}C]HACH242 also has affinity for sigma 1 receptors, in line with other GluN2B ligands. The present results show that [^{11}C]HACH242 has a suitable kinetic profile in the brain and low accumulation of lipophilic radiometabolites. Full PET pharmacokinetic modelling with an arterial input function is required for accurate quantification of specific binding. Novel GluN2B blockers that are approved for human use will enable the clinical evaluation of [^{11}C]HACH242 in the near future.

Reference:

[1] Christiaans J, Klein P, Metaxas A, et al. [2014] Synthesis and preclinical evaluation of carbon-11 labelled N-((5-(4-fluoro-2-[^{11}C]methoxyphenyl)pyridin-3-yl)methyl)cyclopentanamine as a PET tracer for NR2B subunit-containing NMDA receptors. Nucl Med Biol 41:670–680

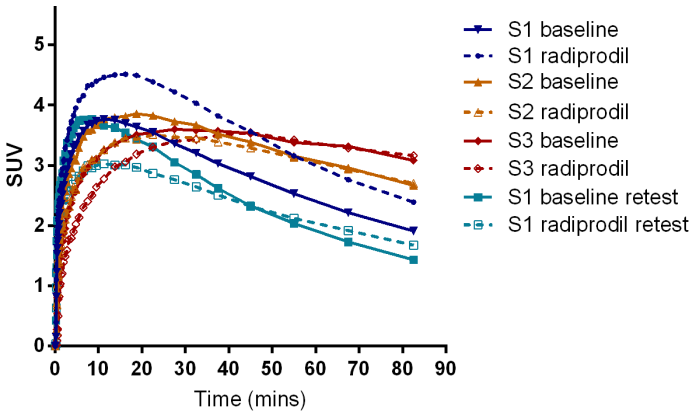

Fig 1. Individual subject [^{11}C]HACH242 SUVs in whole-brain grey matter.

P85
Co-expression of 2 genes with the enzyme monoamine oxidase A quantified by PET in the human brain

Godbersen GM[1], James GM[1], Vraka C[2], Gryglewski G[1], Seiger R[1], Berroterán-Infante N[2], Unterholzner J[1], Komorowski A[1], Hahn A[1], Mitterhauser M[2,3], Wadsak W[2,4], Kasper S[1], Lanzenberger R[1]

1 Department of Psychiatry and Psychotherapy, Medical University of Vienna, Austria

2 Department of Biomedical Imaging and Image-guided Therapy, Division of Nuclear Medicine, Medical University of Vienna

3 Ludwig Boltzmann Institute Applied Diagnostics, Vienna, Austria

4 Center for Biomarker Research in Medicine (CBmed), Graz, Austria

Introduction:

The association of protein distribution assessed by positron emission tomography (PET) and gene expression measured by post mortem analysis based on the Allen Human Brain Atlas (AHBA) can help to generate hypotheses for potentially relevant protein interrelations in the human brain, as previously shown for serotonergic key targets [1]. For the analysis presented here, an approach originating from geostatistics was applied [2]. It allows the prediction of mRNA expression on the entire cerebral cortical surface for the genes provided by the AHBA and further enables the integration of PET data. In this study, we examined the co-expression of different genes with the enzyme monoamine oxidase A (MAOA).

Materials & Methods:

Magnetic resonance imaging and mRNA microarray data of the human brain transcriptome were downloaded from the AHBA and registered to the FreeSurfer surface space for cortical samples. Further, gene expression was predicted on the entire surface based on discrete post mortem samples. For co-analysis, the high-resolution cortical maps of mRNA expression of 18,686 different genes were correlated with the volume of distribution (V_t) map of MAOA (radio tracer [^{11}C]harmine, based on mean values of 32 healthy subjects (17 female; 35.3 $\pm$ 10.5 years)). Measures for the spatial distribution were computed using the R package *gstat* [3], including the relative structured variability (RSV), a measure of spatial dependence that originates from variogram modelling [4], the standard deviation (SD), hinting at cortical spreading, and the Spearman correlation coefficient (ρ). Subsequently, in order to find the highly correlating genes with a high cortical spreading, those were selected that had a SD and a Spearman coefficient above the 99th percentile.

Results:

Two genes survived the statistical thresholds, namely *chromosome 1 open reading frame 187* or C1orf187 (Spearman correlation coefficient ρ=0.49 vertex-wise, SD=0.62, RSV=67.12%) and *transmembrane protein 215* or TMEM215 (ρ=0.53 vertex-wise, SD=0.50, RSV= 11.29%), indicating a high spatial co-expression with MAOA. For mRNA maps see Figure .

Discussion:

As already apparent from the nomenclature [5], little is known about the function of C1orf187. The gene TMEM215 codes for a transmembrane protein of yet unknown purpose. It is highly expressed in bipolar cells in the retina and may play a role in developmental processes [6]. However, in the case of unknown protein function, hypothesizing about potential interrelations is not feasible. Nevertheless, future research on the proteins' function may benefit from the information on their spatial distribution and the co-expression with MAOA in the human brain.

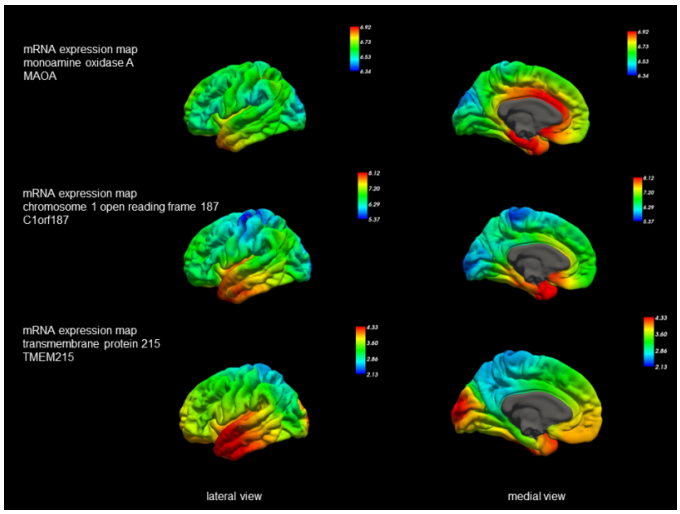

Figure 1: Top: predicted expression of MAOA gene on the surface of the left cerebral hemisphere, left lateral view and right medial view. Middle and below: mRNA maps of the two correlating genes (C1orf187 and TMEM215).

References:

[1] Komorowski A., et al. [2016] *Cerebral Cortex,1:* 1–14
[2] Gryglewski G. et al. [2018] *NRM 2018 abstract*
[3] Pebesma, E et al. [1998] *Computers & Geosciences,* 24:17–31
[4] Schabenberger, O et al. [2001] *CRC press*
[5] Wain, HM et al. [2002] *Genomics,* 79:464–70
[6] Park, K. et al. [2014] *Investigative Ophthalmology & Visual Science*, 55:717–717

Acknowledgements:

Gryglewski G. is recipient of DOC Fellowship of the Austrian Academy of Sciences at the Department of Psychiatry and Psychotherapy, Medical University of Vienna.

P86
Co-expression of fourteen genes with the serotonin-1A receptor quantified by PET in the human brain

Unterholzner J[1], Gryglewski G[1], Philippe C[2], Seiger R[1], James GM[1], Pichler V[2], Godbersen M[1], Komorowski A[1], Hahn A[1], Wadsak W[2,3], Mitterhauser M[2,4], Kasper S[1], Lanzenberger R[1].

1 Department of Psychiatry and Psychotherapy, Medical University of Vienna, Austria

2 Department of Biomedical Imaging and Image-guided Therapy, Division of Nuclear Medicine, Medical University of Vienna

3 Centre for Biomarker Research in Medicine (CBmed), Graz, Austria

4 Ludwig Boltzmann Institute Applied Diagnostics, Vienna, Austria

Introduction:

The identification of biologically relevant protein co-expressions is important for a better understanding of biochemical signalling processes and the optimisation of therapeutic strategies in neuropsychiatric disorders. Different methods and databases, such as the Integrated Interactions Database (IID), have been developed in this regard [1]. Using data from the Allan Human Brain Atlas (AHBA) of the Allen Institute and in house PET binding potential (BP_{ND}) data, we have recently shown a high correlation between predicted mRNA expression and PET data for the serotonin 1A receptor (HTR1A) [2]. Here, we present an exploratory approach to define viable gene co-expressions with the serotonin 1A receptor that might yield new targets for drug development in the future.

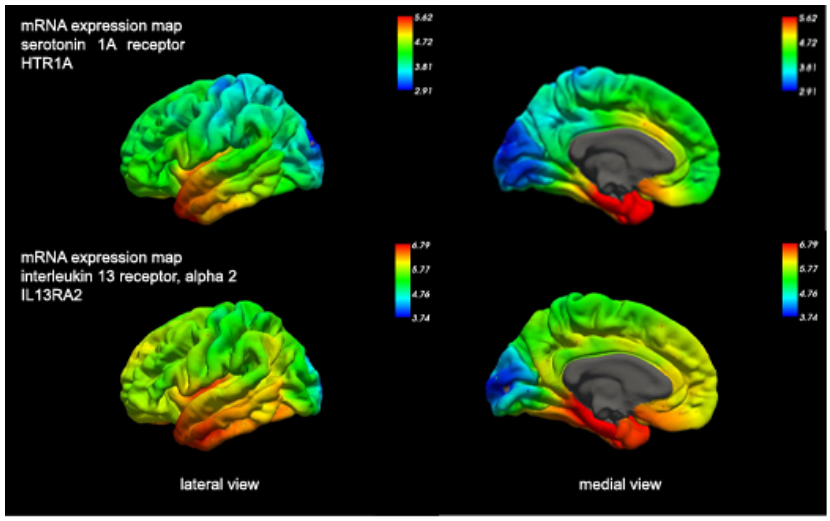

Figure 1: Predicted expression of serotonin 1A receptor gene on the surface of the left hemisphere; Lower: mRNA distribution map of alpha 2 subunit of the interleukin 13 receptor. Left: lateral view, right: medial view.

Methods:

We correlated whole-brain mRNA expression data of 18,686 genes from the AHBA with both the mRNA expression data of the HTR1A of this atlas as well as in-house PET binding potential (BP_{ND}) data for the HTR1A by means of Spearman correlation coefficients. Calculations were done in the R package gstat 1.1-5 utilising a recently developed prediction model for unbiased whole-brain data [3]. Cut-off values for Spearman correlations and standard deviation were set above the 99th percentile.

Results:

Spearman coefficients of predicted mRNA expression data showed 14 genes highly spatially correlated with the BP_{ND} data for the HTR1A (Spearman ρ>0.7 voxel-wise) (Table 1). A relative structured variability (RSV) of >50% indicated high spatial dependence of expression of these genes on the surface of the cortex. Ten of these genes also showed high correlations with the HTR1A mRNA (Spearman ρ>0.8 voxelwise, RSV of >67%).

Entrez ID	Gene name	Gene symbol	LH_RSV	LH_SD	LH_Spearman
260434	PYD (pyrin domain) containing 1	PYDC1	70.22	0.66	0.78
5409	phenylethanolamine N-methyltransferase	PNMT	85.57	0.60	0.77
221421	radial spoke head 9 homolog (Chlamydomonas)	RSPH9	79.22	0.56	0.75
4878	natriuretic peptide A	NPPA	59.83	0.49	0.74
11202	kallikrein-related peptidase 8	KLK8	51.79	0.58	0.73
54550	N-terminal EF-hand calcium binding protein 2	NECAB2	79.44	0.64	0.73
3598	interleukin 13 receptor, alpha 2	IL13RA2	77.59	0.58	0.73
1E+08	uncharacterized protein CXorf49-like	LOC100129291	69.14	0.69	0.73
386618	potassium channel tetramerisation domain containing 4	KCTD4	81.15	0.68	0.72
3350	5-hydroxytryptamine (serotonin) receptor 1A, G protein-coupled	HTR1A	67.48	0.52	0.72
430	achaete-scute complex homolog 2 (Drosophila)	ASCL2	71.92	0.66	0.72
374946	chromosome 1 open reading frame 187	C1orf187	67.18	0.62	0.72
4062	lymphocyte antigen 6 complex, locus H	LY6H	77.24	0.49	0.71
161829	exonuclease 3'-5' domain containing 1	EXD1	70.26	0.70	0.71

Table 1: Genes highly spatially correlated with BP_{ND} data for the HTR1A (Spearman >0.7 voxelwise). Highlighted genes also highly spatially correlated with the mRNA of the HTR1A (Spearman >0.8 voxelwise); LH= left hemisphere, RSV=relative structured variability, SD=standard deviation. Values rounded to

Discussion:

Among the genes highly correlating with BP_{ND} data for the HTR1A was the mRNA of the HTR1A, suggesting validity of our approach. Further, out of these eleven highly spatially correlated genes at least one has already been connected to serotonergic functioning. Interleukin-13 seems to modulate tryptophan hydroxylase 1 activity and thereby influence 5-HT synthesis at both the level of mRNA and protein expression [4]. Eventually, biochemical and cell-based assays could provide functional validation for the co-expression

of the HTR1A with the *interleukin 13 receptor*, *alpha 2* and *PYD (pyrin domain) containing 1*, amongst others, to potentially define new, clinically relevant protein interactions that could in future be used as therapeutic targets.

Acknowledgements

G. Gryglewski is recipient of a DOC Fellowship of the Austrian Academy of Sciences at the Department of Psychiatry and Psychotherapy, Medical University of Vienna.

References

[1] Sokolina K, Kittanakom S, Snider J et al 2017 Molecular Systems Biology 13: 918

[2] Komorowski A, James GM, Philippe C et al 2016 Cerebral Cortex 1: 117-130

[3] Gryglewski G, Seiger R, James GM et al 2018 Neuroimage *submitted*

[4] Manocha M, Shajib MS, Rahman MM et al 2012 Mucosal Immunology 6: 146-55

P87
Cu-catalysed methods for radiolabelling radioligands and radiotracers for neuroreceptors with ^{18}F and ^{11}C

Stephen Thompson[‡], Andrew V. Mossine[‡], So Jeong Lee[‡], Allen F. Brooks[‡], Vadim Bernard-Gauthier[§], Lingyun Yang,[‡] Katarina J. Makaravage[†], Matthew S. McCammant[†], Naoko Ichiishi[†], Xia Shao[‡], Ralf Schirrmacher,[§] Melanie S. Sanford[†], Peter J. H. Scott[‡]

[†]*Department of Chemistry, University of Michigan, 930 North University Avenue, Ann Arbor, Michigan 48109, United States*

[‡]*Department of Radiology, University of Michigan Medical School, 1301 Catherine Street, Ann Arbor, Michigan 48109, United States*

[§]*Department of Oncology, Division of Oncological Imaging, University of Alberta,*

Edmonton, AB T6G 2R3, Canada

Introduction:

The development of radiopharmaceuticals that can cross the blood-brain barrier for imaging of neuroreceptors using positron emission tomography (PET) imaging is critically dependent on the availability of methods to incorporate small, non-metal isotopes such as carbon-11 and fluorine-18 into candidate scaffolds. Currently, incorporation of the desired radioisotope of choice into the majority of PET radiopharmaceuticals for imaging the human brain is accomplished using a very small subset of reactions, including methylation reactions (using [^{11}C]MeI or [^{11}C]MeOTf), and nucleophilic substitution reactions (for [^{11}C]cyanide and [^{18}F]fluoride).[1] Over the last 5-6 years, the advent and maturation of metal-catalysed radiolabelling using [^{11}C]cyanide and [^{18}F]fluoride has greatly expanded the reaction toolbox available to radiochemists.[2] We have begun to see the use of these novel reactions for the synthesis of new radiopharmaceuticals which would otherwise have been inaccessible using more traditional reactions. Herein, we summarise new methods developed in our group for accessing radiotracers and radioligands for brain imaging and demonstrate the utility of these methods through the synthesis of a number of radiotracers for functional neuroimaging.

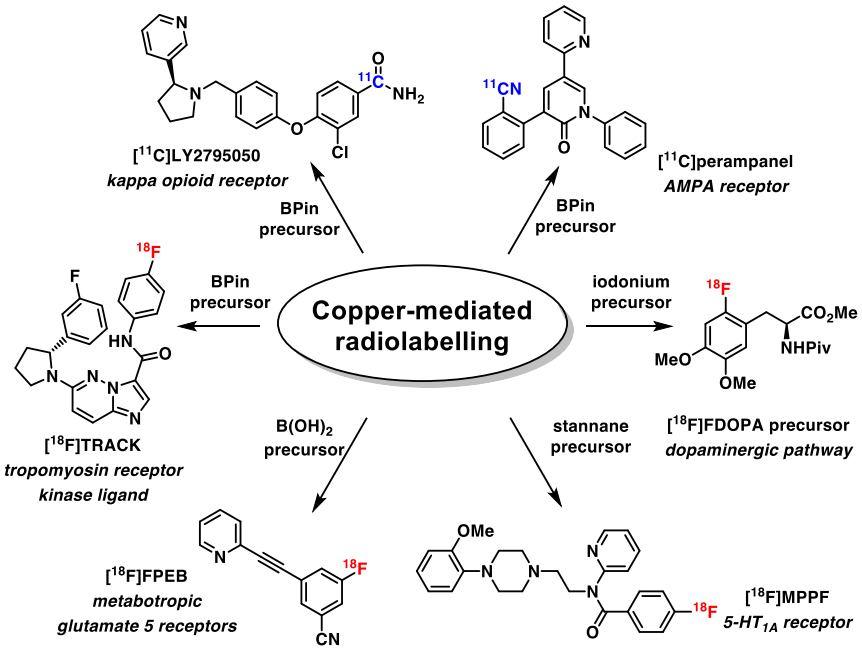

Materials and Methods:

$[^{11}C]CO_2$ was converted to $[^{11}C]HCN$ using standard chemistry, before being trapped on platinum wire, and flushed from the wire with a solution of KOH to furnish aqueous $[^{11}C]KCN$, which was then reacted with the appropriate (hetero)aryl boronic acid, boronic ester, trifluoroborate, or trialkylstannane under copper-mediated conditions furnish the desired (hetero)aryl [^{11}C]cyanide. Similarly, [^{18}F]fluoride was eluted from a QMA cartridge with aqueous KOTf to furnish [^{18}F]KF. [^{18}F]KF was reacted with the appropriate (hetero)aryl iodonium salt (either neat, or generated in situ from C-H precursors), boronic acids, boronic esters or trialkylstannanes under Cu-mediated conditions to furnish the desired (hetero)aryl [^{18}F]fluoride.

Results:

Using the newly developed methods, several radiotracers and radioligands for imaging neuroreceptors have been radiolabelled. [^{11}C]Perampanel was synthesised from the corresponding BPin derivative in 10.4% RCY with a A_M of 68 GBq/μmol (1.8 Ci/μmol).[3] [^{11}C]LY2795050 was synthesised in 5.6% isolated RCY with a A_M of 62 GBq/μmol (1.7 Ci/μmol).[3] [^{18}F]FPEB was synthesised from the corresponding boronic acid derivative in 8% TLC-RCY, with a A_M of 30 GBq/μmol (0.75 Ci/μmol).[4] [^{18}F]TRACK was synthesised from the corresponding BPin derivative in 8% isolated RCY, with a A_M of 100 GBq/μmol (3 Ci/μmol).[5] A protected version of [^{18}F]FDOPA was synthesised from the corresponding iodonium precursor in 17% TLC-RCY and a A_M of 150 GBq/μmol (4 Ci/μmol).[6] [^{18}F]MPPF was synthesised from the corresponding stannane precursor in 13% isolated RCY.[7]

Discussion and Conclusion:

The radioligands described above are agents for imaging specific neuroreceptors and are useful for probing both normal and pathophysiology. Specifically, perampanel is an AMPA receptor agonist and drug for treating epilepsy; LY2795050 is a potent kappa opioid antagonist; FPEB is an agent for interrogating metabotropic glutamate 5 receptors; TRACK

is a high affinity ligand for tropomyosin receptor kinases which have been implicated in a variety of neurodegenerative diseases; FDOPA is an agent for interrogation of the nigrostriatal dopaminergic pathway and MPPF is a $5HT_{1A}$ receptor ligand. These compounds had been challenging to access using traditional radiochemical methods, and the development of Cu-mediated radiolabelling methods with both ^{18}F and ^{11}C with the appropriate precursor, has greatly facilitated the transfer of selected agents to preclinical and clinical PET imaging for probing the function of the brain.

Acknowledgements:

We acknowledge the NIH, DOE and Merck for funding.

References:

1. Miller, P.W et al. [2008] Ang. Chem. Intl. Ed. 47:8998
2. Brooks, A.F et al. [2014] Chem. Sci. 5:4545
3. Manuscript Submitted
4. Mossine, A.V et al. [2015] Org. Lett. 17:5780.
5. Bernard-Gauthier, V et al. [2017] J. Med. Chem. DOI:10.1021/acs.jmedchem.7b01607
6. Ichiishi, N., et al. [2014] Org. Lett. 16:3224
7. Makaravage, K.J., et al. [2016] Org. Lett. 18:5440.

P88
MAGIA: Robust automated modelling and image processing pipeline for PET neuroinformatics

Tomi Karjalainen[1*], **Severi Santavirta**[1], Tatu Kantonen[1], Jouni Tuisku[1], Lauri Tuominen[1,2], Jussi Hirvonen[1,3], Jarmo Hietala[1], Juha O. Rinne[1], and Lauri Nummenmaa[1,4]

[1]Turku PET Centre, University of Turku, Finland

[2]Department of Psychiatry, Massachusetts General Hospital and Harvard Medical School, Boston, MA, USA

[3]Department of Radiology, University of Turku, Finland

[4]Department of Psychology, University of Turku, Finland

Introduction:

Processing PET data typically requires substantial manual labour including retrieving data from PACS, processing input functions, drawing reference regions, preprocessing the images and finally modelling the tracer kinetics. Such approach is not well suited for large-scale standardized reanalysis as processing one single image may take many hours. To resolve this problem, we have introduced the MAGIA analysis pipeline for brain-PET and MRI data that enables automatic processing of brain-PET data with minimal user intervention. Obtaining reliable input function is critical for accurate modelling. We investigated the accuracy of MAGIA's automatic reference region generation and subsequent modelling with four tracers binding to different binding sites: [^{11}C]raclopride, [^{11}C]carfentanil, [^{11}C]MADAM, and [^{11}C]PiB by comparing the automatically derived input functions and outcome measures against those derived with conventional manual techniques using pMod.

Materials and methods:

For each tracer, we selected 30 previously acquired images and generated the reference regions using traditional manual methods and the new automatic method. In the manual method, five persons familiar with human neuroanatomy delineated the reference regions (cerebellum and occipital cortex) for each image according to written instructions with visual landmarks shown on MR images. The automatic method was based on optimized FreeSurfer (https://surfer.nmr.mgh.harvard.edu) parcellations of the corresponding areas. The outcome measures derived by these two techniques were assessed as follows: First, we investigated the *anatomical* similarity by computing the overlap between automatic and manual reference regions (overlap percentage). Second, we determined the Pearson correlation coefficient of the manually and automatically obtained reference tissue time-activity curves (TAC). Third, we investigated how the differences in reference tissue TACs propagate into outcome measures in regions of interest (ROI) for each tracer. For [^{11}C]raclopride, [^{11}C]carfentanil and [^{11}C]MADAM binding potential (BP_{ND}) and for [^{11}C]PiB

ROI-to-cerebellum ratio between 60 and 90 minutes were used as outcome measures. Simplified reference tissue model [1] was used to estimate BP_{ND}.

Results:

Anatomically, MAGIA-generated reference regions differed from manual reference regions. The mean overlap percentage per tracer ranged from 20.3 % (SEM 1.70 %) for [^{11}C]raclopride to 7.3 % (SEM 0.28 %) for [^{11}C]MADAM. Mean overlap percentages for [^{11}C]carfentanil and [^{11}C]PiB were 8.1 % (SEM 0.92 %) and 8.0 % (SEM 0.25 %), respectively. The manually and automatically generated reference region TACs correlated nearly perfectly ($r > 0.99$ for every tracer) with negligible bias (Figure 1). Outcome measures for all tracers were also practically unbiased (Figure 2).

Conclusion:

Our results confirm that although the automated reference regions overlap poorly with the manually generated reference regions (mainly because the former are larger), the TACs themselves are nearly identical. Also the differences between the outcome measures are within acceptable limits. Based on these results and taking into account the intersubject variation in manual reference region delineation, the high level of standardization and strong scalability of MAGIA suggest that it can be used efficiently for producing reliable reference regions and inputs for these four tracers.

Acknowledgements:

This work was supported by the Academy of Finland grants #265915 and #294897 to LN and Sigrid Juselius Foundation grant to LN.

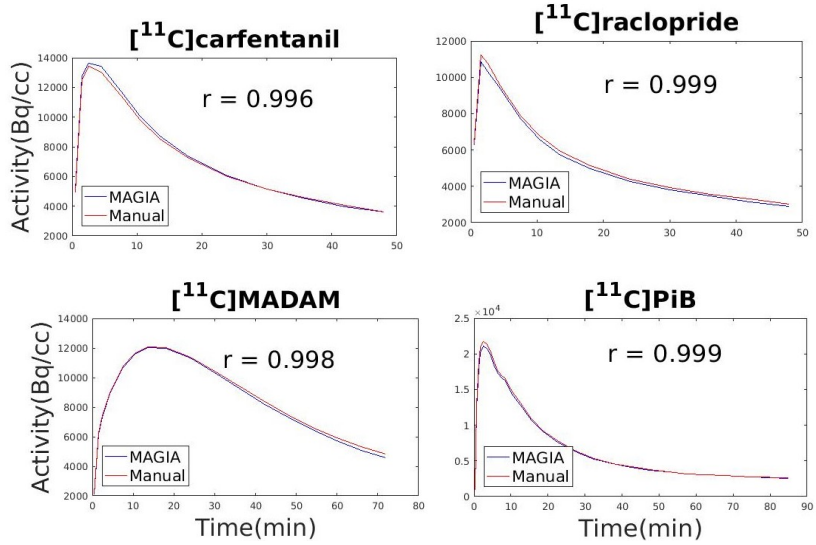

Fig 1. MAGIA and manual -derived reference region TACs and the Pearson correlation coefficient for each tracer.

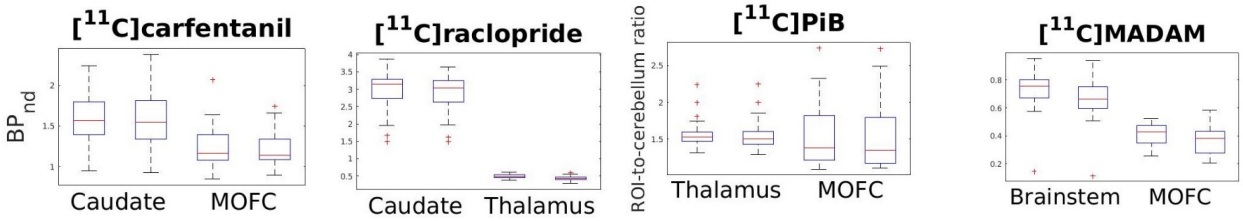

Fig 2. Boxplots of MAGIA and manual -derived outcome measures for two ROIs per tracer (MAGIA-derived on the left). For [^{11}C]carfentanil the difference of BP_{ND} was 1.5 % in caudate, and 2.0 % in medial orbitofrontal cortex (MOFC), for [^{11}C]raclopride 4.7 % in caudate and 10.6 % in thalamus, for [^{11}C]MADAM 10.3 % in brainstem and 12.4 % in MOFC. For [^{11}C]PiB the difference of ROI-to-cerebellum ratio was 0.4 % in caudate and 0.2 % in thalamus.

References:

Gunn R et. al. [1997] Neuroimage 6: 279-287

P89
Comparison of regional SV2A density in the rodent, monkey and human brain using ^{3}H-UCB-J

Kyle C. Wilcox, Timothy J. Montavon, Marc B. Skaddan, Aimee D. Reed, Manolo X. Mugnaini, and Sjoerd J. Finnema

AbbVie, 1 N. Waukegan Rd., North Chicago, IL, USA

Introduction:

Synaptic density imaging with PET has potential to further our understanding of brain function, aging, disease-associated neurodegeneration, and brain disorders. Synaptic vesicle glycoprotein 2A (SV2A) provides a useful biomarker of synaptic density as it appears to be present in a uniform copy number per synaptic vesicle [1-2].^{11}C-UCB-J has recently been reported as a promising PET radioligand for SV2A imaging and is being applied in PET studies in patients with epilepsy [3] and Alzheimer's disease [4]. Thorough in vitro characterization of UCB-J binding will enable interpretation of these in vivo PET studies. Here, we report in vitro radiopharmacological studies evaluating regional ^{3}H-UCB-J binding in rodent, monkey and human brain tissue.

Materials & Methods:

^{3}H-UCB-J was prepared with high radiochemical purity (98.9%) and specific activity (34.9 Ci/mmol). Freshly frozen brain tissue was dissected from C57BL mice, Wistar rats, Cynomolgus macaques and African green monkeys. Human temporal cortex and hippocampus tissue was obtained from Banner Sun Health Research Institute. Homogenates of freshly frozen brain samples in PBS were evaluated with ^{3}H-UCB-J in filter binding assays performed in a 96-well format to assess association and dissociation kinetics, B_{max}, and K_d. Nonspecific binding was determined in the presence of 1 mM levetiracetam. Phosphor-autoradiography was performed on thaw-mounted cryosections of nonhuman primate brain and spinal cord, as well as human hippocampus and inferior temporal gyrus.

Results:

Kinetic ^{3}H-UCB-J binding assays revealed an association constant of 2.6 x 10^{8} $M^{-1}min^{-1}$ and a dissociation rate of 0.15 min^{-1} (half-life = 4.6 minutes) following levetiracetam displacement at room temperature (Fig. 1A). Equilibrium saturation filter binding assays compared ^{3}H-UCB-J binding in mice, rats, nonhuman primates, and human brain tissue. Across species, a consistent K_d of approximately 3 nM was observed. In NHP, SV2A densities ranged from 16 to 23 pmol/mg protein with the highest density in hippocampus (B_{max} = 23±1.7 pmol/mg) and slightly lower in other regions (B_{max} ~16-18 pmol/mg in neocortical areas, cerebellum and basal ganglia; Fig. 1B). Rodent species exhibited a different pattern of regional SV2A density with highest signal in cortex (rat: 28±1.2 pmol/mg; mouse: 33±0.9 pmol/mg) and lower in the hippocampus (rat: 16±1 pmol/mg; mouse: 15±2 pmol/mg) and cerebellum (rat:

16±0.6 pmol/mg; mouse: 14 ±0.7 pmol/mg). Basal ganglia SV2A density was higher in rat than mouse (25±0.5 and 15±0.3 pmol/mg, respectively). Preliminary results indicate that SV2A density in human temporal cortex samples is similar as in NHPs (human: 13±1.2 pmol/mg; NHP: 16±0.7).

Finally, autoradiography studies comparing ^{3}H-UCB-J binding in either DPBS or Tris buffer containing NaCl and KCl found a reduced binding intensity and image resolution when using DPBS relative to Tris (Fig. 1C). NHP brain and spinal cord tissues showed strong ^{3}H-UCB-J binding in areas of grey matter and negligible uptake in the white matter (Fig. 1D).

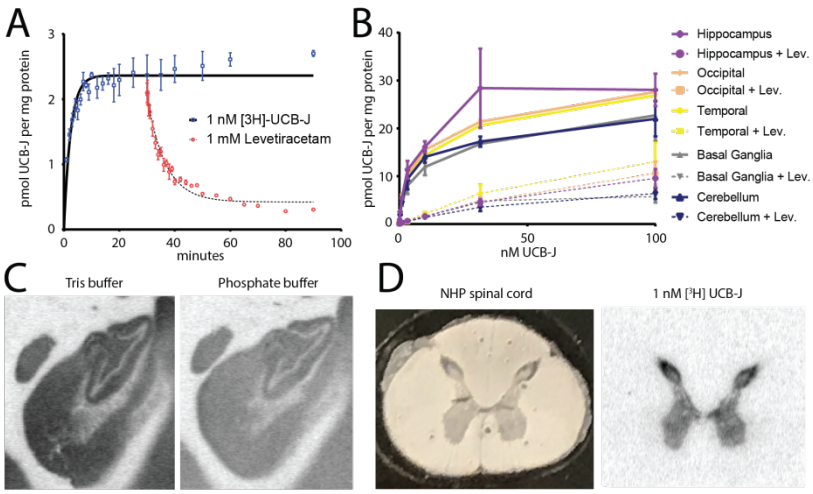

Figure 1. *In vitro binding of ^{3}H-UCB-J to NHP brain and spinal cord* A) Kinetics of association and dissociation in NHP cortex; B) Regional comparison of ^{3}H-UCB-J binding to homogenates of cynomolgus monkey grey matter; C) comparison of buffer conditions for ^{3}H-UCB-J autoradiography; and D) demonstration of ^{3}H-UCB-J binding in NHP spinal cord.

Discussion/Conclusion:

This preliminary evaluation supports that SV2A densities are comparable in brain tissues across the examined species. Radiolabeled UCB-J may also be suitable for imaging SV2A in the spinal cord in primates. Further work examining SV2A binding in brain tissue from patients is ongoing and will provide validation of SV2A PET imaging as a synaptic density imaging approach.

References:

1. Takamori S, Holt M, Stenius K, et al. [2006] Cell 127:831

2. Mutch SA, Kensel-Hammes P, Gadd JC, et al. [2011] J. Neurosci. 31:1461.

3. Finnema SJ, Nabulsi NB, Eid T, et al. [2016] Science Translational Medicine 348:348

4. Chen MK, Mecca AP, Naganawa M, et al. [2017] Clinical Trials on Alzheimer's Disease Abstract #LB10

Disclosures: All authors are employees of AbbVie. The design, study conduct, and financial support for this research were provided by AbbVie. AbbVie participated in the interpretation of data, review, and approval of the publication.

P90
Characterization of [^{11}C]PXT012253 as a PET radioligand for mGlu4 allosteric modulators in non-human primates

Akihiro Takano[1], Ryosuke Arakawa[1], Sangram Nag[1], Zhisheng Jia[1], Mahabuba Jahan[1], Anton Forsberg[1], Per Grybäck[2], Guillaume Duvey[3], Christer Halldin[1], Delphine Charvin[3]

1 Department of Clinical Neuroscience, Center for Psychiatry Research, Karolinska Institutet and Stockholm County Council, Stockholm, Sweden

2 Department of Medical Radiation Physics and Nuclear Medicine, Karolinska University Hospital; Department of Molecular Medicine and Surgery, Karolinska Institute, Stockholm, Sweden

3 Prexton Therapeutics, 14 Chemin des Aulx, 1228 Plan-les-Ouates, Geneva, Switzerland

Introduction:

Modulation of presynaptic metabotropic glutamate receptor 4 (mGlu4) has been proposed as a promising therapeutic target in several neurological disorders such as Parkinson's disease. C11-labelled PET radioligand, [^{11}C]PXT012253, (formerly [^{11}C]KALB012) has been recently developed and evaluated in rodents (Kil et al., 2016). In this study, in order to characterize [^{11}C]PXT012253 for further application in clinical studies, we investigated the kinetics of [^{11}C]PXT012253 in nonhuman primate (NHP) brains quantitatively, and whole body dosimetry PET measurements of NHP were performed to calculate the effective dose.

Materials & Methods:

A total of four 93-minute brain PET measurements (three baseline conditions and one blocking condition) were performed in three male cynomolgus monkeys (body weight 6.4 – 8.3kg) using a High Resolution Research Tomograph (HRRT) (Siemens Molecular Imaging). As the blocking study, a mGlu4 positive allosteric modulator (PAM), PXT002331 (2 mg/kg), currently in clinical trial for Parkinson's disease, was administered intravenously with bolus infusion in one NHP. As the outcome measure, the total distribution volume (V_T) was calculated with metabolite corrected plasma radioactivity as the input function. Four models were used for calculation of V_T; K_1/k_2 by one tissue compartment (1TC) model, $(K_1/k_2)\times(k_3/k_4+1)$ by two tissue compartment (2TC) model, Logan graphical analysis and MA1. The fitness of model curves in 1TC and 2TC were evaluated by the model selection criterion (MSC). The identifiability of V_T in Logan plot and MA1 was evaluated by the percentage of the coefficient of variation (%COV). These analyses were performed using the PMOD 3.4 software package (PMOD Group, Zurich, Switzerland).

125-minute whole body PET measurements were performed using a GE Discovery PET/CT 710 (GE healthcare) in two female cynomolgus monkeys (5.6 and 6.3kg) in order to estimate the effective dose of [^{11}C]PXT012253. Regions of interest were drawn on the heart, liver, kidney, spleen, lung, parotid gland, submandibular gland, thyroid, brain, bone marrow

(lumbar vertebra), gall bladder, small intestine, and urinary bladder with the help of the CT images for anatomic landmarks. Estimates of the absorbed radiation dose in humans were calculated with OLINDA/EXM 1.1 (Organ Level INternal Dose Assessment Code) software, using the adult male (70 kg) reference model. The fractional uptake in NHP organs was assumed to be equal to the uptake in human organs.

Results:

Brain regional time activity curves of [^{11}C]PXT012253 were well described in 2TC with lower MSC than 1TC although 2TC showed unstable values in some cases. In the linear graphical analysis, both Logan plot and MA1 were well fitted and V_Ts were well correlated with those by 2TC (R=0.9 and 0.9, respectively). MA1 showed slightly better identifiability than Logan plot with lower %COV. Under the blocking condition with PXT002331, VTs decreased significantly, which indicated high specific binding in the total distribution volume (Figure 1). Whole body PET showed high accumulation of [^{11}C]PXT012253 in the liver, kidney, heart, and brain in the initial phase. The radioligand was excreted through both the gastrointestinal and the urinary tracts. Effective dose of [^{11}C]PXT012253 was estimated to be 0.0042 mSv/MBq.

Discussion/Conclusion

[^{11}C]PXT012253 is a promising PET radioligand for mGlu4 allosteric modulators in the brain. MA1 would be the choice of quantitative method for [^{11}C]PXT012253. Based on the dosimetry results, multiple PET measurements in the same subjects can be performed, which is useful for the target occupancy or longitudinal studies. Further development of [^{11}C]PXT012253 is warranted in the human subjects.

Fig.1 V_T parametric images under the conditions at the baseline and after pretreatment with a mGlu4 PAM.

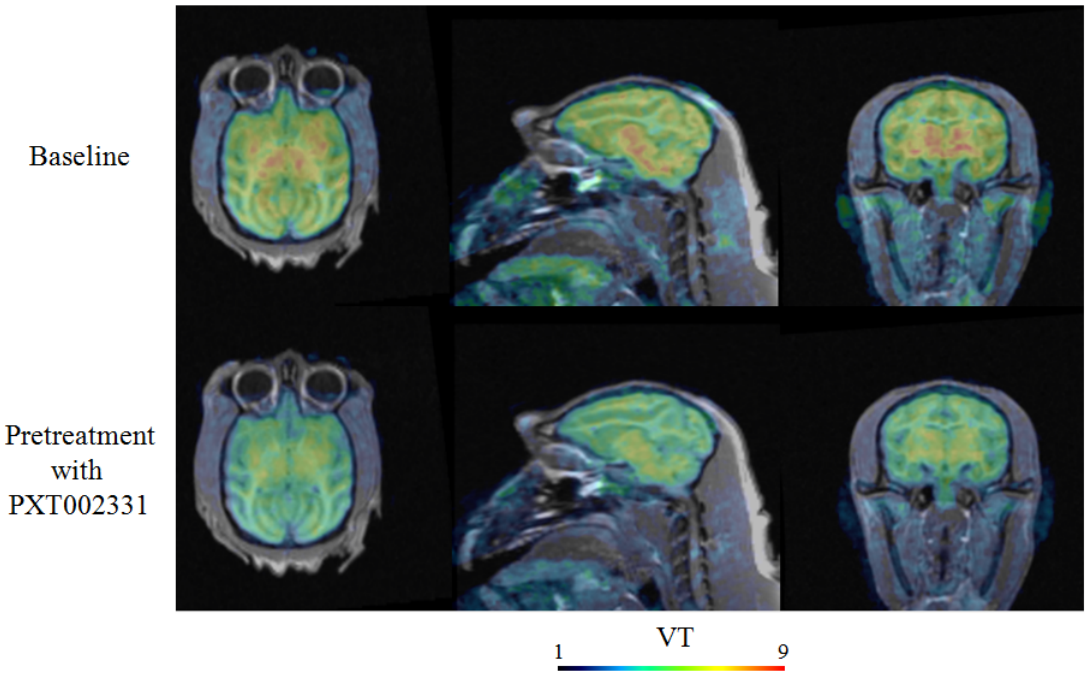

Acknowledgements

The study was sponsored by Prexton Therapeutics.

References

Kil KE, Poutiainen P, Zhang Z, et al.[2016], Bioorg Med Chem Lett, 26(1):133-139.

P91

Abstract Withdrawn

P92
Evaluation of a novel radiotracer for PET imaging of sigma-1 receptors in the brain of nonhuman primates

Hongmei Jia[1], Zhengxin Cai[2], Daniel Holden[2], Yingfang He[1], Shu-fei Lin[2], Songye Li[2], Evan Baum[2], Anupama Shirali[2], Michael Kapinos[2], Hong Gao[2], Jim Ropchan[2], Yiyun Huang[2]

[1]College of Chemistry, Beijing Normal University, Beijing, China; [2]PET Center, Department of Radiology and Biomedical Imaging, Yale University, New Haven, CT, USA

Introduction:

As a unique "ligand-operated receptor chaperone" located on the mitochondria-associated endoplasmic reticulum membrane (MAM), the sigma-1 receptor (Sig1R) interacts with a structurally diverse group of functional proteins and is regarded as a "pluripotent modulator" in living systems. Multiple lines of evidence have implicated Sig1R in the pathophysiology of a variety of diseases, including neurologic disorders, neuropathic pain, myocardial hypertension, and cancers. In particular, as a protein on the MAM, Sig1R is essential to neuronal survival and its alterations have been shown in the brain of patients with Alzheimer's disease (AD) and AD mouse models. Further, Sig1R agonists have been shown to be efficacious in the treatment of cognitive deficits in AD. As a result, Sig1R may represent yet another important biomarker in the pathophysiology of AD, and PET imaging studies with Sig1R-specific radiotracer will help shed new light on AD pathogenesis and progression.

We recently discovered a simple Sig1R-binding chemical scaffold for the synthesis of novel, selective Sig1R ligands. One radiotracer developed from this novel series of compounds, 1-(4-[^{18}F]fluorobenzyl)-4-[(tetrahydrofuran-2-yl)methyl]piperazine (^{18}F-FBFP), was found to localize in the rodent brain in high concentration and bind to Sig1R with high specificity [1]. Hence, we evaluated the pharmacokinetic and imaging properties of this novel radiotracer in nonhuman primates to assess its potential for translation to humans for PET imaging of Sig1R.

Materials & Methods:

The radiotracer ^{18}F-FBFP was prepared in an improved, one step radiosynthesis from an iodonium ylide precursor. PET scans with ^{18}F-FBFP were acquired for 120 or 180 min on the FOCUS 220 PET scanner in two cynomolgus monkeys. A blocking experiment was performed with the Sig1R-selective ligand SA4503 (0.5 mg/kg) given at 10 min before ^{18}F-FBFP injection. Arterial input function was measured during each PET scan for use in kinetic analysis. Plasma free fraction (f_P) was measured by the ultrafiltration method. Regions of interest were drawn on an anatomical monkey brain MR image registered to a template image for generation of regional time-activity curves (TACs). TACs were fitted with 1- and 2-tissue compartment (1TC & 2TC) models, and the multilinear analysis-1 (MA1) method to calculate regional volumes of distribution (V_T). Non-displaceable volume of distribution (V_{ND})

and receptor occupancy were determined from the occupancy plot. Regional binding potential (BP_{ND}) values were calculated from baseline 1TC V_T values and V_{ND} taken from the occupancy plot.

Results:

Radiosynthesis of ^{18}F-FBFP was facile and efficient (**Figure 1A**), with radiochemical yield of >20% (decay-uncorrected, n = 3). Radiochemical purity was >99%. In the plasma parent tracer fraction was 25% and 56% at 60 min post-injection for the two baseline scans, and 31% for the blocking scan, indicating a moderate rate of metabolism for this radiotracer. Plasma f_P value was 68 ± 4% (n = 3), consistent with the low lipophilicity of the tracer (log *D* = 1.3). Uptake of ^{18}F-FBFP in the monkey brain was high, and tissue kinetics was fast (**Figure 1B & C**). All three kinetic models provided good fitting of regional TACs and similar values in regional V_T estimation. Regional V_T values were higher in the amygdala, hippocampus and cortex, and lower in the striatum and cerebellum, in line with the distribution of Sig1R in primates. Specific binding of the tracer was nearly completely blocked by 0.5 mg/kg of SA4503, which produced receptor occupancy of 96% with V_{ND} value of 6.21 mL/cm^3. 1TC BP_{ND} values were 5.16, 4.24, 3.93, 3.58, 3.48, 3.16, 3.06, 2.95 and 2.95, respectively, for the amygdala, hippocampus, frontal cortex, cingulate cortex, temporal cortex, thalamus, putamen, caudate and cerebellum. When compared with the other Sig1R tracer (*S*)-^{18}F-fluspidine, ^{18}F-FBFP BP_{ND} values are 2.8 times higher on average across brain regions.

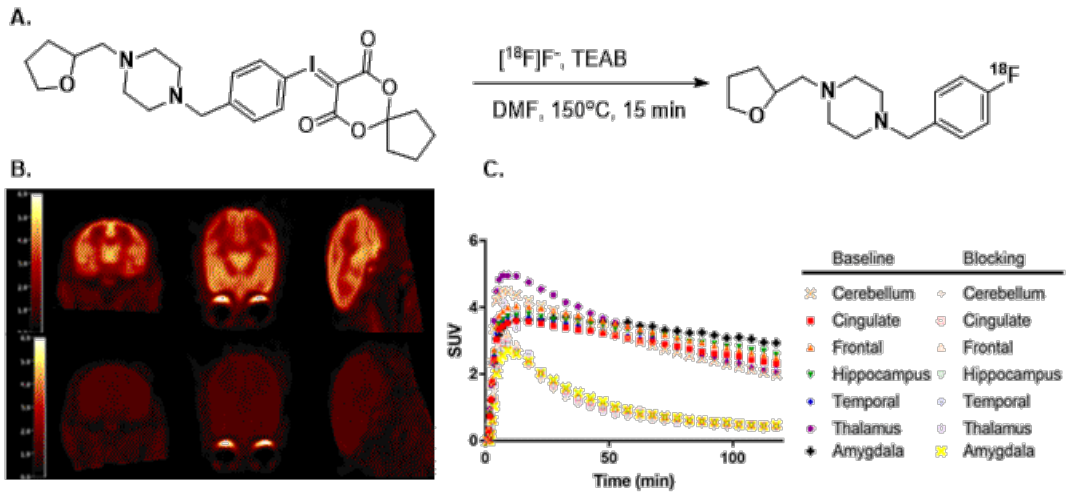

Figure 1. **A**. One step radiosynthesis of ^{18}F-FBFP; **B**. Summed SUV images of ^{18}F-FBFP from 30-45 min post-injection from a baseline scan (top) and a blocking scan with 0.5 mg/kg of SA4503 (bottom); **C**. Time-activity curves in selected brain regions from the baseline and blocking scans in the same monkey.

Discussion/Conclusions:

The novel Sig1R radiotracer ^{18}F-FBFP demonstrated high brain uptake and fast tissue kinetics suitable for quantitative analysis and reliable estimation of kinetic and binding

parameters. Among the known S1R tracers ^{18}F-FBFP displayed the highest plasma free fraction due to its simple structure and low lipophilicity. *In vivo* binding was highly specific, and specific binding signals of ^{18}F-FBFP also appeared to be the highest among the known S1R tracers. Taken together, ^{18}F-FBFP represents the most promising Sig1R PET radiotracer for PET imaging of Sig1R in the brain. Further evaluation in humans is thus warranted.

Acknowledgements:

This work was supported by the National Natural Science Foundation of China (No. 21471019).

References:

1. He Y, Xie F, Ye J, Deuther-Conrad W, Cui B, Wang L, Lu J, Steinbach J, Brust P, Huang Y, Lu J, and Jia H. [2017], *J. Med. Chem.*, 60:4161-4172.

P93
Synthesis, Radiolabeling and *in vivo* Evaluation of [^{18}F]ENL30, a Potential Positron Emission Tomography (PET) Radioligand for the 5-HT$_7$ Receptor

Elina T. L'Estrade[a),b),c)], Fraser G. Edgar[b)], Mengfei Xiong[a),b)], Vladimir Shalgunov[b)], Maria Erlandsson[c)], Tomas Ohlsson[c)], Gitte M. Knudsen[a)] and Matthias M. Herth [a),b),d)]

a) Neurobiology Research Unit, Copenhagen University Hospital, Rigshospitalet, Copenhagen, Denmark

b) Department of Drug Design and Pharmacology, Faculty of Health and Medicine, University of Copenhagen, Copenhagen, Denmark

c) Radiation Physics, Nuclear Medicine Physics Unit, Skånes University Hospital, Lund, Sweden.

d) Department of Clinical Physiology, Nuclear Medicine & PET, Copenhagen University Hospital, Copenhagen, Denmark

Introduction:

PET is a non-invasive, molecular imaging tool used to study, for example, central nervous system (CNS) receptor systems in the living brain. The 5-HT$_7$ receptor is the most recently discovered subfamily of serotonin receptors. These serotonin receptors have been shown to be involved in several CNS disorders, such as depression and schizophrenia[1]. SB-269970 is a known 5-HT$_7$ receptor antagonist, which can penetrate the blood brain barrier (BBB) and it has been used to elucidate new and important information about the receptor *in vitro*. Several analogues of SB-269970 have been labeled with fluorine-18 and subsequently, applied to *in vivo* PET studies[2-3]. Recently, a head-to-head comparison was performed between those derivatives with two promising ^{11}C-labeled tracers[4,5,6]. Both ^{11}C-labeled tracers showed better imaging characteristics than the published ^{18}F-labeled SB-269970 derivatives (manuscript in preparation). In light of that, our goal of this study was to develop one of our ^{11}C-labeled tracers into an ^{18}F-labeled analogue and evaluate its *in vivo* behavior.

Materials and methods:

The precursor (3-[[(2R)-2-[2-(4-methyl-1-piperidinyl)ethyl]-1-pyrrolidinyl]sulfonyl]-phenol, monohydrochloride) is commercially available, and the reference was successfully synthesized in house. ^{18}F-labeling succeeded using 2-[^{18}F]fluoroethyl tosylate which was produced in a fully automated system, similar to previously published[7]. The radioligand [^{18}F]ENL30 was evaluated *in vivo* using PET imaging in female Long-Evans rats and selectivity was tested with a competition study. SB-269970 was used as a competition agent, as previously published[5,6]. In some experiments, we gave Elacridar, a known P-glycoprotein (Pgp) efflux inhibitor, prior to radiotracer injection in order to assess if the compounds were Pgp substrates.

Results:

300 MBq of the final product could be isolated with sufficient molar activity and > 98 % radiochemical purity. Preliminary PET results from the Long-Evans rats showed that the tracer is a Pgp substrate. After inhibition of the Pgp transporter using Elacridar, PET studies of [^{18}F]ENL30 revealed high brain uptake and specific binding (see figure 1). Furthermore, the tracer showed reversible kinetics.

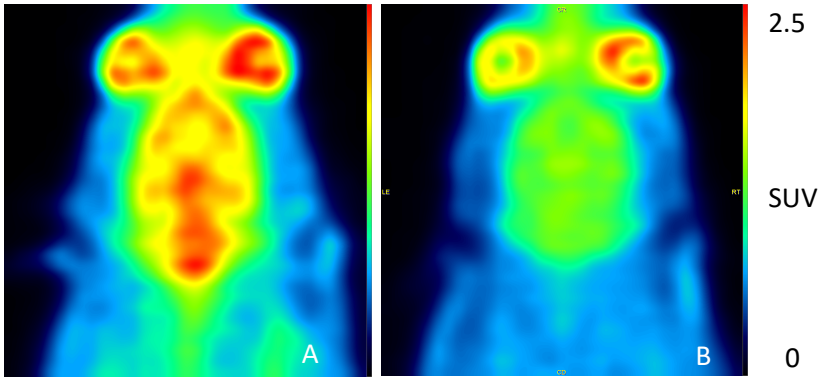

Figure 1: Averaged [^{18}F]ENL30 PET images (5.5-117.5 min) of female Long-Evans rats brain. A) Pretreatment with Elacridar (5mg/kg) i.v. 30 min prior tracer injection B) Pretreatment with Elacridar (5mg/kg) i.v. 30 min prior injection and SB-269970 (3mg/kg) i.v. 15min prior injection.

Conclusion:

The novel tracer, [^{18}F]ENL30 show promise and is a potential candidate to be further evaluated in higher species, such as the Danish Landrace pig.

References:

[1] Matthys A, Haegeman G, Van Craenenbroeck K *et al*. [2011] Mol. Neurobiol, 43:228–253

[2] Andriès J, Lemoine L, Mouchel-Blaisot A *et al.* [2010] Bioorg. Med. Chem. Lett, 20:3730–3733

[3] Lemoine L, Andriès J, Le Bars D e*t al*. [2011] J. Nucl. Med, 52:1811–1818

[4] Herth M M, Volk B, Pallagi K, *et al.* [2012] ACS Chem. Neurosci, 3:1002–1007

[5] Hansen H D, Herth M M, Ettrup A *et al*. [2014] J. Nucl. Med, 55:640–646

[6] Herth M M, Andersen V, Hansen H D, *et al*. [2015] J. Med. Chem, 58:3631−3636

[7] Block D, Coenen H H, Stöcklin G [1987] J Label Compd Radiopharm, 24:1026-1042.

P94
A Predictive Model of Chronic Low Back Pain Using Brain [^{11}C]-PBR28 Radiomic Features

Torrado-Carvajal A[1], Albrecht DS[1], Chang K[1], Beers AL[1], Akeju O[2], Kim M[1], Bergan C[1], Edwards RR[3], Zhang Y[2], Hooker JM[1], Napadow V[1], Kalpathy-Cramer J[1], Loggia ML[1]

[1]A.A. Martinos Center for Biomedical Imaging, Massachusetts General Hospital, Harvard Medical School (MGH/HMS), Boston MA

[2]Department of Anesthesia, Critical Care and Pain Medicine, MGH/HMS, Boston MA

[3]Department of Anesthesiology, Perioperative and Pain Medicine, Brigham and Women's Hospital, HMS, Boston, MA

Introduction:

Chronic pain affects more than 100 million individuals in the United States alone[1]. Despite the enormity of the phenomenon, both our understanding of its pathophysiological mechanisms and the efficacy of treatment options currently available are limited. Among the factors hindering the development of novel treatment approaches is the lack of reliable biomarkers. In chronic low back pain (cLBP), for instance, the presence or absence of anatomical alterations (e.g. in the lumbar spine) is a very unreliable predictor of pain. Recent developments in artificial intelligence, and their application to brain imaging, demonstrate great promise in aiding the search for biomarkers of pain and other conditions.

Using [^{11}C]-PBR28, we recently showed that cLBP patients demonstrate elevated brain levels of the 18kDa translocator protein (TSPO), a marker of glial activation, particularly in the thalamus[2]. In this work, we assess the performance of a model based on brain [^{11}C]-PBR28 radiomic features for the prediction of cLBP. Radiomics, so far mostly used in oncology, uses data-characterization algorithms to extract large amounts of quantitative features, potentially uncovering characteristics that may be invisible to the naked eye[3].

Materials & Methods:

25 cLBP patients and 27 healthy controls underwent [^{11}C]-PBR28 brain scanning using an integrated positron emission tomography/magnetic resonance imaging (PET/MRI) scanner. Standardize uptake values from [^{11}C]-PBR28 data collected 60-90 min post-injection ($SUV_{60\text{-}90min}$) were normalized by whole brain ($SUVR_{WB}$) and by occipital cortex ($SUVR_{occip}$). SUVR images were corrected for the Ala147Thr TSPO polymorphism (which predicts binding affinity to [^{11}C]-PBR28[4]), injected dose, and age. A T1-weighted multi-echo MPRAGE (TR/TE1/TE2/TE3/TE4= 2530/1.64/3.5/5.36/7.22ms, flip angle=7°, voxel size=1x1x1mm, acquisition matrix=256x256x176) was collected simultaneously to the PET data. Subcortical segmentation of the T1 was performed using FSL. Resulting labels were used to extract PET data from two regions of interest (ROIs): left and right thalamus.

We calculated 140 shape, intensity, and gray-level contrast matrices (GLCM) features[5] using the feature extraction package QTIM_Tools. From the GLCM matrices, we calculated contrast, dissimilarity, homogeneity, angular second moment (ASM), energy, and correlation at five different distances (1, 2, 3, 4, 5 voxels), and four different directions (0, 45, 90, and 135 degrees). These features were calculated for each axial slice of a given ROI and averaged. Shape features included surface area, volume, compactness, sphericity, and spherical disproportion. Intensity features included typical distribution statistics, e.g. standard deviation, energy, entropy, kurtosis, and skewness.

The machine learning algorithm was generated using the scikit-learn python module[6]. A random forest (RF) classifier with 256 trees (estimators), using 5-fold cross-validation, was used to perform the classification task. Performance was assessed by calculating the area under the curve (AUC) from receiver operating characteristic (ROC) curve analysis. A paired t-test was used to compare the results of the univariate analyses to determine whether $SUVR_{WB}$ or $SUVR_{occip}$ radiomic features showed a better predictive value. The top features (AUC≥0.8) were input into the RF classifier.

Results:

Univariate analyses demonstrated that $SUVR_{occip}$ radiomic features overall show a better predictive value than $SUVR_{WB}$ ($p<0.01$) (Fig. 1), hence the top 6 $SUVR_{occip}$ features (AUC≥0.8) were used to train the RF classifier.

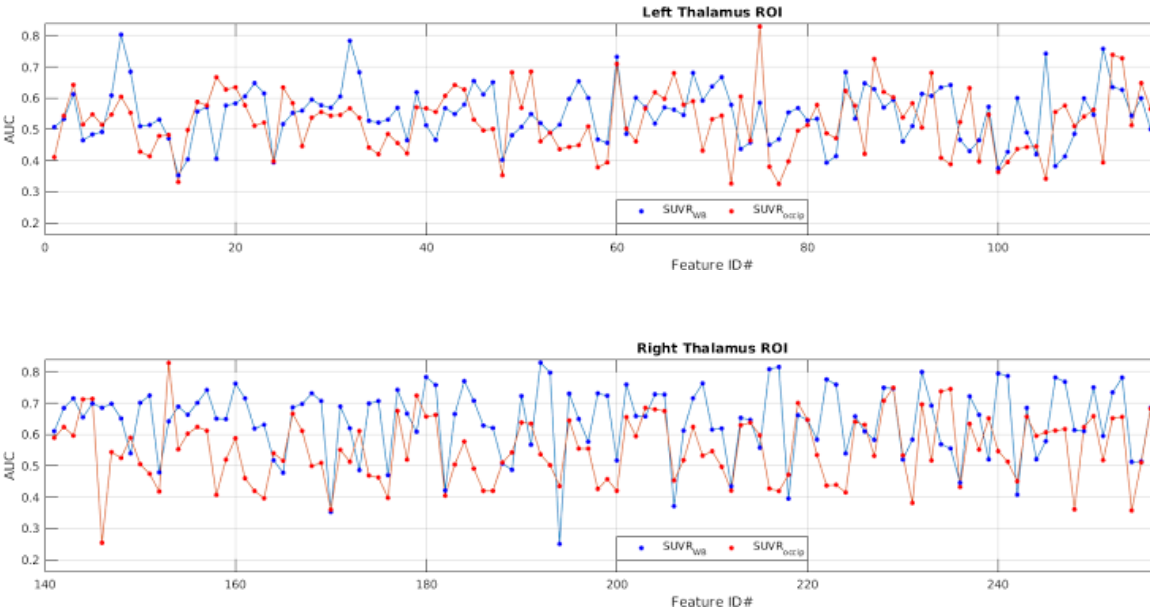

Fig 1. Performance of the prediction models for each radiomic feature in the univariate analysis.

The RF was thus grown to 256 trees with the number of features per decision tree set to 6. The mean AUC/sensitivity/specificity statistics for this classifier were 0.83±0.09/0.76±0.08/0.71±0.17, respectively.

Conclusion:

We have demonstrated the predictive ability of radiomic features derived from [^{11}C]-PBR28 images, further showing how $SUVR_{occip}$ features have a better predictive value than $SUVR_{WB}$ features when discriminating between patients and healthy subjects. PET radiomics is still in development, but its use may lead to a personalized pain management approach in the future. Further research in refining the predictive value of these models is needed. Likewise, with the advent of combined PET/MRI multi-modal imaging, the addition of anatomical as well as advanced MR modalities (e.g. perfusion, diffusion, or connectivity) may improve the performance of the classifier.

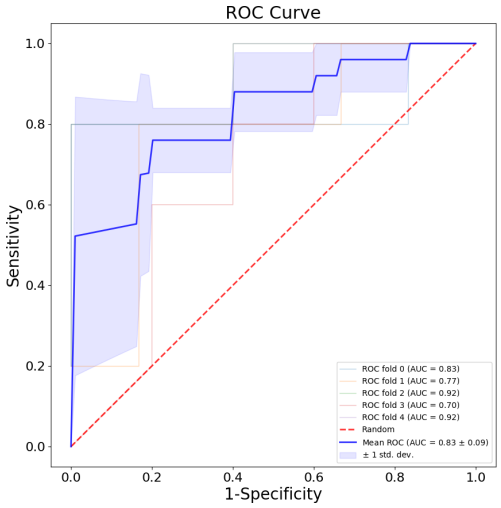

Fig 2. ROC curve for the RF classifier using the top (AUC≥0.8) $SUVR_{occip}$ radiomic features.

Acknowledgements

Support: 1R21NS087472-01A1/1R01NS095937-01A1(MLL).

References

[1]Harstall C. [2003] Pain: Clinical Updates, X:1–4.

[2]Loggia ML et al. [2015], Brain, 138(3):604-615.

[3]Gillies RJ et al. [2015], Radiology, 278(2):563-577.

[4]Owen DR et al. [2012], J Cerebr Blood F Met 32:1-5.

[5]Haralick RM et al. [1973], IEEE T Syst Man Cyb, SMC-3(6):610-621.

[6]Pedregosa F et al. [2011], J Mach Learn Res, 12:2825-2830.

P95
Synthesis and biological evaluation of a novel F-18 labelled radioligand [^{18}F]GEH200449 for detection of MAO-B activity

S. Nag[1], A. Jackson[2], A. Takano[1], J. Zhisheng[1], R. Arakawa[1], M. Jahan[1], R. Ahmad[2], S-K. Luthra[2], R- S. Maior[1] and C. Halldin[1,3]

[1]Karolinska Institutet, Department of Clinical Neuroscience, Stockholm, Sweden;

[2]GE Healthcare; [3]Lee Kong Chian School of Medicine, Nanyang Technological University, Singapore

Objective:

Monoamine oxidases (MAO) are important enzymes regulating the levels of monoaminergic neurotransmitters and of bioactive monoamines by catalyzing their deamination. MAO-B inhibitors are widely used in the treatment of e.g. Parkinson's disease (PD). L-deprenyl, a MAO-B inhibitor has been labelled with ^{11}C and used in PET studies to image the distribution of available MAO-B in the human brain. Carbon-11 labelled L-deprenyl is less suitable for its relatively short half life, irreversible binding kinetics and the formation of methamphetamine a metabolite deprenyl that can enter the brain. In this project our aim was to develop a fast and efficient synthetic method for labeling GEH200449 with ^{18}F and its biological evaluation for detection of MAO-B.

Method:

The precursor and the cold reference standard were provided by GE healthcare. Radiolabeling was achieved by classical one-step fluorine-18 nucleophilic substitution reaction (figure 1). The reaction was carried out in DMSO at 125 °C for 10 min. The stability and radiochemical yield was analyzed with HPLC. [^{18}F]GEH200449 was tested in human whole hemisphere autoradiography experiments. [^{18}F]GEH200449 was also examined in cynomolgus monkeys by PET. Two baseline and one pretreatment measurement with L-deprenyl (1,0 mg/kg) 30 min prior to the administration of the radioligand were performed and radiometabolites were measured in monkey plasma using gradient HPLC.

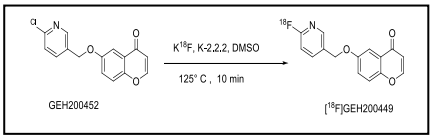

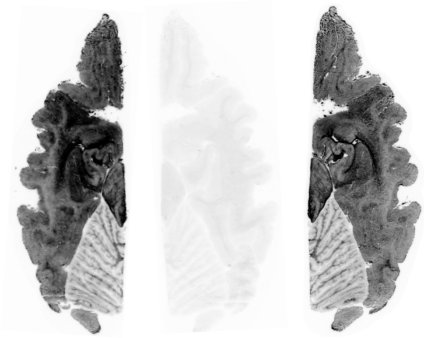

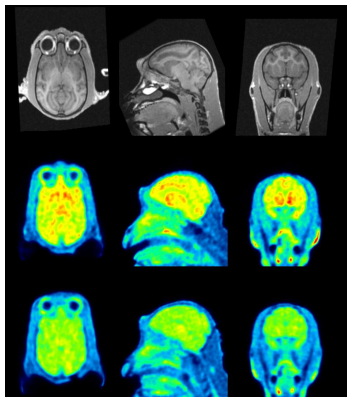

Figure 1: Synthesis scheme. Figure 2: ARG image Figure 2: PET image.

Results:

[^{18}F]GEH200449 was successfully synthesized. The incorporation yield of the fluorination reactions was >25%. The radiochemical purity was higher than 99% at EOS. Molar activity was >110 GBq/μmol at the time of administration. Radioligand was found to be stable, with a radiochemical purity of >99% at 2h after formulation in a sterile phosphate buffered solution (pH = 7,4). Autoradiography on human brain tissue section demonstrated specific binding to MAO-B (Figure 2). Additionally in the cynomolgus monkey brain a high brain uptake (5.5% ID at 4 min) and a pronounced blocking effect of pretreatment by L-deprenyl was found (figure 2). Metabolite studies demonstrated with 15% unchanged radioligand remaining 120 min post injection.

Conclusion:

Radiolabeling of new fluorine-18 MAO-B inhibitor [^{18}F]GEH200449 was successfully accomplished. Compound [^{18}F]GEH200449 binds specifically to MAO B and can be potential candidate for human PET studies.

Acknowledgements: This study was supported by GE Healthcare.

P96

Blood glucose levels interact with dopamine $D_{2/3}$ receptor availability at baseline and in presence of d-amphetamine inversely in patients with schizophrenia and in healthy volunteers. A (^{11}C)-(+)-PHNO PET study.

Sauerzopf U[1], Weidenauer A[1], Bauer M[1,2], Bartova L[1], Meyer B[1], Nics L[3], Philippe C[3], Pfaff S[3], Mitterhauser M[3,4], Lanzenberger R[1], Kasper S[1], Pezawas L[1], Wadsak W[3,5], Praschak-Rieder N[1], Willeit M[1]

(1) Medical University of Vienna, Department of Psychiatry and Psychotherapy, Division of General Psychiatry
(2) Medical University of Vienna, Department of Clinical Pharmacology
(3) Medical University of Vienna, Department of Biomedical Imaging und Image-guided Therapy, Division of Nuclear Medicine

(4) Ludwig-Boltzmann-Institute Applied Diagnostics, Vienna

(5) Center for Biomarker Research in Medicine CBmed, Graz

Introduction:

Patients with schizophrenia show increased insulin resistance in both, treated and medication-naïve states (Takayanagi et al. 2012; Chen et al. 2013). It has been suggested that deficiency of insulin receptors on dopaminergic midbrain neurons may play a role in the development of psychosis in schizophrenia (Caravaggio et al. 2015a), and that antipsychotic compounds prone to increase peripheral insulin resistance (Allison et al. 1999) confer part of their antipsychotic action via modulating of insulin signalling.

We have explored the relationship between blood glucose levels and dopaminergic neurotransmission with (^{11}C)-(+)-PHNO and positron emission tomography (PET) in healthy volunteers and patients with schizophrenia.

Materials and Methods:

Eighteen (13m, 5f) young medication-naïve first episode patients with schizophrenia and 27 (14m, 13f) young healthy volunteers without prior exposure to psychostimulant drugs underwent an (^{11}C)-(+)-PHNO PET scan at baseline and a second scan approximately 1.5 hours after ingestion of 0.4 mg/kg bodyweight d-amphetamine sulfate. Non-displaceable (^{11}C)-(+)-PHNO binding potential (BP_{ND}) values were derived employing the simplified reference tissue model (SRTM2) using the cerebellar cortex as a reference region. Parametric maps (SPM) have been calculated employing PMOD 2.6. Utilizing a linear mixed effects model, we have analysed the dependency of radioligand BP_{ND} values on blood glucose measured at start of the PET Scan, disease status, and amphetamine ingestion.

Results:

Blood glucose levels were significantly higher in medication-naïve patients with schizophrenia than in healthy volunteers, at baseline as well as after d-amphetamine administration ($p < 0.0005$) indicating some degree of metabolic dysfunction in the patient collective. Administration of amphetamine had no significant effects on blood glucose levels in either group.

SPMs revealed two significant clusters in the left head of the caudate nucleus, comprising some of the ventral striatum, and the right substantia nigra / ventral tegmental area (SNVTA) (FDR corrected p-values < 0.01) indicating dependency of (^{11}C)-(+)-PHNO BP_{ND} values on the independent variables. At baseline, healthy volunteers displayed a positive relationship between blood glucose levels and (^{11}C)-(+)-PHNO BP_{ND} values ($p < 0.01$) which shifted to a negative relationship during the amphetamine-challenged condition ($p < 0.01$). In patients, however, at baseline, higher blood glucose levels were related to lower (^{11}C)-(+)-PHNO BP_{ND} values ($p < 0.01$). In the amphetamine condition, higher blood glucose levels were associated with higher (^{11}C)-(+)-PHNO BP_{ND} values.

In an uncorrected correlation, healthy volunteers displayed a moderate positive relationship between blood glucose levels and (^{11}C)-(+)-PHNO BP_{ND} values in the left head of the caudate (r: 0.48 $p < 0.05$) and the right SNVTA (r: 0.66, $p < 0.001$). No significant correlations were observed in the patient cohort or amphetamine challenged condition. However, changes in the direction of the correlations (as shown in the full mixed effects model) were observed.

Discussion:

(^{11}C)-(+)-PHNO BP_{ND} has been shown to be highly sensitive to changes in endogenous dopamine levels (Willeit et al. 2008), with some evidence that variance in unstimulated (^{11}C)-(+)-PHNO BP_{ND} values is in part reflecting endogenous dopamine levels (Caravaggio et al. 2014). In a previous study in healthy volunteers, insulin resistance was associated with higher (^{11}C)-(+)-PHNO BP_{ND} values, indicating lower levels of the endogenous ligand, dopamine (Caravaggio et al. 2015b). The negative correlation of blood glucose levels with (^{11}C)-(+)-PHNO BP_{ND} values in our patients (instead of positive correlations in healthy subjects) corroborates the hypothesis an alteration in the functional link between dopamine signalling and insulin functions in the SNVTA in psychosis.

References:

Allison, D; Mentore, JL; Heo, M; Chandler, LP; Cappelleri, JC; Infante MC and Weiden PJ (1999). *Antipsychotic-Induced Weight Gain: A Comprehensive Research Synthesis*, American Journal of Psychiatry 156 : 1686-1696.

Chen, S.; Broqueres-You, D.; Yang, G.; Wang, Z.; Li, Y.; Wang, N.; Zhang, X.; Yang, F. and Tan, Y. (2013). *Relationship between insulin resistance, dyslipidaemia and positive symptom in Chinese antipsychotic-naive first-episode patients with schizophrenia*, Psychiatry Research 210 : 825 - 829.

Caravaggio, F.; Hahn, M.; Nakajima, S.; Gerretsen, P.; Remington, G. and Graff-Guerrero, A. (2015a). *Reduced insulin-receptor mediated modulation of striatal dopamine release by basal insulin as a possible contributing factor to hyperdopaminergia in schizophrenia*, Medical hypotheses 85 : 391-396.

Caravaggio, F.; Borlido, C.; Hahn, M.; Feng, Z.; Fervaha, G.; Gerretsen, P.; Nakajima, S.; Plitman, E.; Chung, J. K.; Iwata, Y.; Wilson, A.; Remington, G. and Graff-Guerrero, A. (2015b). *Reduced Insulin Sensitivity Is Related to Less Endogenous Dopamine at D(2/3) Receptors in the Ventral Striatum of Healthy Nonobese Humans*, International Journal of Neuropsychopharmacology 18 : pyv014-.

Caravaggio, F.; Nakajima, S.; Borlido, C.; Remington, G.; Gerretsen, P.; Wilson, A.; Houle, S.; Menon, M.; Mamo, D. and Graff-Guerrero, A. (2014). *Estimating Endogenous Dopamine Levels at D(2) and D(3) Receptors in Humans using the Agonist Radiotracer ((11)C)-(+)-PHNO*, Neuropsychopharmacology 39 : 2769-2776.

Willeit, M.; Ginovart, N.; Graff, A.; Rusjan, P.; Vitcu, I.; Houle, S.; Seeman, P.; Wilson, A. A. and Kapur, S. (2008). *First Human Evidence of d-Amphetamine Induced Displacement of a D2/3 Agonist Radioligand: A [11C]-(+)-PHNO Positron Emission Tomography Study*, Neuropsychopharmacology 33 : 279-289.

P97
Evidence for neuroinflammation in semantic dementia

B Pascual[1], P Zanotti-Fregonara[1], N Pal[1], E Rockers[1], Q Funk[1], M Yu[2], GC Román[1], PE Schulz[3], JC Masdeu[1]

[1]Houston Methodist Neurological Institute, and [2]Cyclotron and Radiopharmaceutical Core, Houston Methodist Research Institute, Weill Cornell Medicine, 6560 Fannin Street, Houston, Texas 77030, EEUU; [3]Department of Neurology, UT Physicians, 6431 Fannin Street, Houston, Texas 77030, EEUU

Introduction:

Semantic dementia (SD) is a progressive naming disorder with atrophy in the anterior portion of the left temporal lobe. It is associated with a propensity for autoimmune disease and increased inflammation in peripheral blood; however, brain inflammation has not been assessed *in vivo.* Our main objective was to measure brain inflammation in SD using the PET translocator protein (TSPO) radioligand ^{11}C-PBR28.

Materials and Methods

We performed ^{11}C-PBR28 PET in five SD patients and six healthy controls. Patients (3/5 women, mean age 71.2±4.6 years) were amyloid-negative, and did not differ significantly in age from the controls (2/6 women, mean age 67±5.8 years). The PET scan lasted 90 minutes, and started immediately after automatic injection of about 740 MBq of ^{11}C-PBR28. The metabolite-corrected arterial input function consisted of 24 samples per subject, drawn from a catheter in the radial artery. The samples were centrifuged and analyzed by liquid chromatography to separate the parent from its radiometabolites. The parent fraction for the whole duration was obtained by fitting the individual parent measurements with an extended Hill function [1]. The regions of interest were obtained by segmenting the MR images and coregistering them to the PET images using the Pneuro pipeline of Pmod 3.8. The brain regions were defined with the Hammers atlas. The total volume of distribution (VT) was calculated with a Logan plot, with and without correction for partial volume effect using the Geometric Transfer Matrix algorithm.

Results

Compared to controls, patients with SD had increased V_T mainly in the anterior portion of left temporal cortex, but also in the tip of the right temporal pole ($p < 0.05$). After partial volume correction, patients showed increased V_T in left temporal cortex from the tip to the posterior portion of the temporal lobe, and in the right temporal pole ($p < 0.01$). An increased V_T was also found in regions of the orbitofrontal cortex adjoining anterior temporal cortex ($p < 0.05$).

Discussion

This study provides the first direct *in vivo* evidence for neuroinflammation in SD. It was greatest in regions known to be associated with loss of volume, namely the temporal poles and, to a lesser extent, orbitofrontal cortex. TSPO imaging can be used to follow disease progression and determine the association between inflammation and other features of the neurodegenerative process, such as the accumulation of misfolded proteins or neuronal loss.

Acknowledgements:

This study was partially funded by the Chao, Graham, Harrison and Nantz Houston Methodist Foundation Funds.

References:

Tonietto M, et al. [2017] J. Cereb. Blood Flow Metab. 36(2): 326-39.

P98
PET imaging of the neuroimmune response to alcohol with [^{18}F]DPA-714 in an adolescent binge-drinking model

G Pottier, B Jego, J Negroni, M Goislard, S Demphel, F Caille, C Coulon, E Jaumain**, W Saba**

IMIV, CEA-SHFJ, 4, place du Général Leclerc 91400 Orsay, France.

Introduction:
Binge drinking during adolescence induced important and long lasting brain damages. Neuroinflammation is highly implicated in this process. This work aimed to evaluate, *in vivo*, the neuroimmune compound of alcohol related toxicity in a binge-like ethanol administration to adolescent rats using PET and [^{18}F]DPA-714, a selective TSPO radioligand.

Materials and Methods:
Adolescent (PND 33) rats received an i.p. injection of ethanol [3 g/kg in 25% (v/v); n=5] or saline (n=5) in an intermittent ethanol administration pattern (two consecutive days at 48-h intervals over a 14-day period) (1). MicroPET imaging with [^{18}F]DPA-714 (38.6± MBq, i.v.) was performed 24h after last alcohol injection. PET time activity curves were generated in different brain areas using PMOD and results were expressed as % of ID/cc. Blood alcohol concentration was measured on arterial blood plasma in an independent group using *gas chromatography* (2).

Results:
Ethanol administration to adolescent rats induced an alcohol blood concentration of 2.40 ± 0.5 g/L at 5 min after injection. In control animals, brain uptake of [^{18}F]DPA-714 is relatively low: 0.097±0.012 ; 0.210±0.036 and 0.11±0.018 %ID/cc at 30 min after tracer injection in the thalamus, cerebellum and hippocampus respectively. Ethanol administration increases the brain uptake of [^{18}F]DPA-714, this increase was observed globally across all studied brain regions including cerebellum (73%), thalamus (55%), cortex (32%) and in the hippocampus (58%).

Discussion:
These results indicate an overexpression of TSPO in the brain after alcohol exposure in adolescent rats and confirm that excessive alcohol consumption induces significant neuroinflammation in this animal model. PET imaging using [^{18}F]DPA-714 is an excellent tool to follow up the neuroinflammatory compound of alcohol in vivo.

Funding : Fondation pour la recherche en alcoologie

References:
(1) Pascual M, Montesinos J, Marcos M et al. [2017]. Addict Biol. 22:1829-1841.
(2) Kristoffersen L, Stormyhr L-E & Smith-Kielland A [2006]. Forensic Sci Int *161:151–157.*

P99

Evaluation of binding and chemical development of [^{18}F]GE387 - a candidate radiotracer for Imaging TSPO with low binding sensitivity to human polymorphism rs6971.

Luxi Qiao‡,[1] Emily M. Fisher‡,[1] Lindsay McMurray,[1] Eryn Werry[2], **Matthew Hird**,[1] Selena Milicevic Sephton[1], Ella Hirani, Michael Kassiou[2], Saijinder Luthra[3], Will Trigg[3] and Franklin I. Aigbirhio*,[1]

[1] *Molecular Imaging Chemistry Laboratory, Wolfson Brain Imaging Centre, University of Cambridge, Cambridge Biomedical Campus, CB2 022, UK.*

[2] *School of Chemistry, University of Sydney.*

[3] *GE Healthcare, Amersham, UK*

‡ Authors made equivalent contributions

Introduction:

[^{11}C]PK11195 is the most widely clinically employed PET radiotracer for imaging neuroinflammation by the biomarker translocator protein 18 kDa (TSPO). However it is limited by the short half-life of the carbon-11 radionuclide, low brain signal and an unreliable radiosynthesis.[1,2] In efforts to overcome these limitations, second generation radiotracers have been developed. However, these radiotracers unlike [^{11}C]PK11195 can be hindered in use by inter-individual variability in their binding affinities caused by a genetic polymorphism (rs6971) in exon 4 of the TSPO gene.[3] Thus there is a need to develop a TSPO PET imaging probe radiolabeled with fluorine-18, that has low sensitivity to this genetic polymorphism. We have identified a new compound, GE387 (**1**, Scheme 1) which may have these properties. Herein, we report on its binding properties to TSPO, methods for synthesis of precursor and reference material, separation and identification of its enantiomers and radiolabeling with fluorine-18.

Materials and Methods:

Binding affinity was determined using competition radioligand binding on membranes (20 □g/well) from HEK-293 cells stably transfected with either human wild type TSPO cDNA or human rs6971 TSPO cDNA. [^{3}H]PK11195 was used as the competing ligand. Standard synthetic procedures were employed in the syntheses of reference materials as well as radiolabelling precursors including as the key step tertiary amine formation/Zn-mediated cyclisation (Scheme 1). The separation of the racemic mixture into enantiomers was attempted using chiral moiety (using menthyl to form diastereomeric ester intermediates), a SFC (Lux C1 column, 21.2x250 mm, 5 μm, at 40 °C, eluting with 50:50 MeOH:CO_2 with 0.2% v/v NH_3 at 50 mL/min) as well as HPLC (Whelk-O1 (S,S) Kromasil 5um, 2.1x150mm, eluting with 80:20 MeOH:H_2O). The absolute configuration was determined using Circular Dichroism spectroscopy by comparison to a known GE180 enantiomer. The radiosynthesis employing nucleophilic substitution was performed both manually (with racemic material) and in

automated synthesizer (FX_{FN} TracerLab, using each enantiomer) using cyclotron produced fluorine-18. The reaction was performed in acetonitrile and heated to 100 °C over 20 min (Scheme 1). The material was purified *via* semi-preparative HPLC (eluting with 48% aq. MeCN) and formulated as a saline solution. The time of synthesis was 60 min from EOB.

Results:

The binding affinity of *R,S*-GE387 for WT TSPO was 36.3 ± 6.9 nM, and was 47.3 ± 7.0 nM for the polymorphic TSPO. The reference material was synthesized in 7 steps with 9% overall yield. The radiolabelling precursors mesylate and tosylate were prepared *via* the similar 7-step route in 10% and 11% overall yields, respectively. Separation of racemic mixture was accomplished either using SFC: 92% recovery of the material for fluorinated reference compound and 98% recovery for the tosylate precursor each in >98% ee and >97% chemical purity. Manual radiochemical experiments identified tosylate as a favorable radiolabelling precursor. Using FX_{FN} automated synthesis was developed yielding 15.1±5.6% decay corrected *S*-enantiomer and 11.5±7.3% *R*-enantiomer, both with >98% radiochemical purity and 76.5±42.4 GBq/μmol and 158.4±113.1 GBq/μmol molar activities, respectively.

Discussion/Conclusion:

The ratio of the affinity of *R,S*-GE387 at the polymorphic TSPO compared to wild type TSPO was similar to that of PK11195 (1.3 to 1), thus presenting a promising new lead for the development of a PET radiotracer for TSPO imaging.

The syntheses of both reference material and radiolabelling precursor proceeded smoothly with good yields. Initial efforts to employ intermediate acid for chiral separation of GE387 enantiomers failed due to the presence of the highly acidic proton thus directing the course of the study to application of either SFC or HPLC methods for enantiomer separation. The tosylate precursor proved superior with respect to radiochemical yields and also ease of handling a solid. The established automated radiochemical synthesis was reproducible and enabled *in vitro*/*in vivo* evaluation of PET radiotracer candidate [^{18}F]GE387.

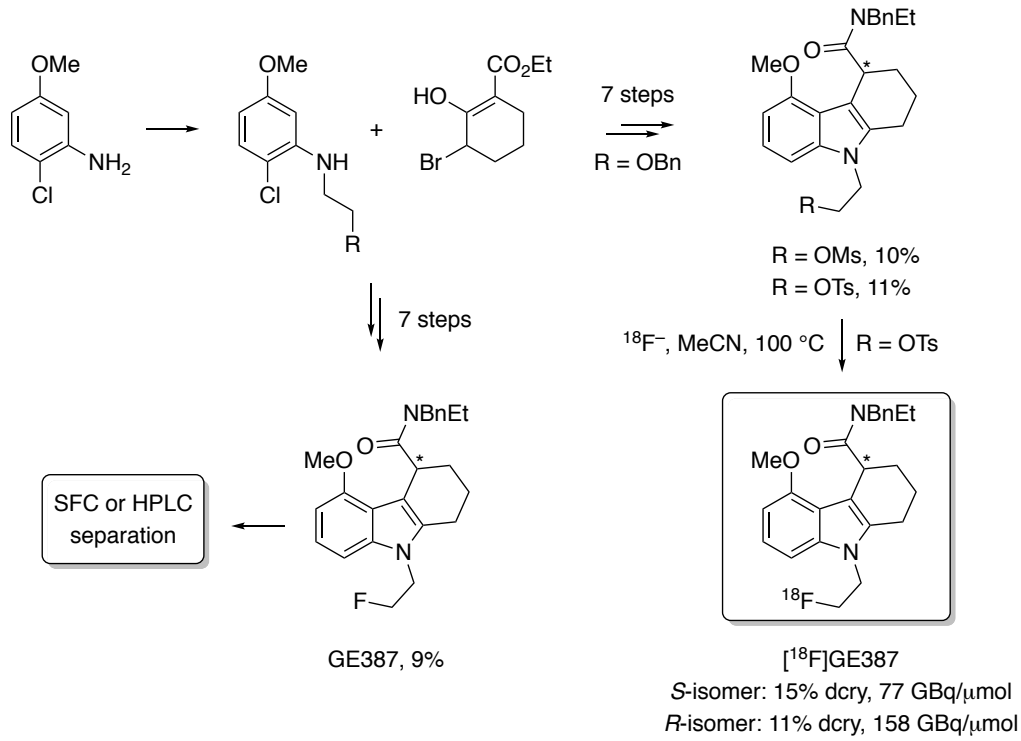

Scheme 1. Synthesis, chiral separation and radiolabelling of novel PET radiotracer candidate [^{18}F]GE387

References

[1] F. E. Turkheimer, G. Rizzo, P. S. Bloomfield *et al*. [2015], *Biochem. Soc. Trans*. The Methodology of TSPO Imaging with Positron Emission Tomography, 43:586.

[2] L. Vivash, T. J. O'Brien, [2016], *J. Nucl. Med*. Imaging Microglial Activation with TSPO PET: Lighting Up Neurologic Diseases?, 57:165.

[3] D. R. J. Owen, A. J. Yeo, R. N. Gunn *et al*. [2011], *J. Nucl. Med*. Mixed-Affinity Binding in Humans with 18-kDa Translocator Protein Lingands, 52:24.

P100
Effects of early environmental variables on striatal D2/3 receptors, impulsivity, novelty-seeking and cocaine-seeking behavior in rats.

Lidia Bellés[1], Andrea Dimiziani[1], Stergios Tsartsalis[2], Phillipe Millet[1,2], François Herrmann[3,4], Nathalie Ginovart[1,2]

[1]Department of Psychiatry, University of Geneva, Switzerland; [2]Laboratory for Translational Imaging in Psychiatric Neuroscience, Department of Mental Health and Psychiatry, University Hospitals of Geneva, Switzerland; [3]Department of Internal Medicine, Rehabilitation and Geriatrics, University Hospitals of Geneva, Switzerland; [4]Division of Geriatrics, Geneva University Hospitals, Switzerland.

Introduction:

Vulnerability to addiction is considered to result from the complex interaction of highly entangled factors, including genetic make up, personality, life experience and social environment. Among personality traits, high impulsivity and high novelty seeking (NS) have both been linked with an increased vulnerability to drug abuse through possibly a common underlying neurochemical substrate, namely a deficit in striatal D2/3R (Dalley et al.; 2007; Belin et al.; 2008). On the other hand, previous studies suggested that early environmental variables might influence individual's impulsivity, NS and their related predisposition to drug abuse (Gipson et al.; 2011; Perry et al.; 2008). The current study investigated the effects of environmental enrichment (EE) and environmental impoverishment (EI) rearing conditions on dopamine D2/3 receptors (D2/3R) availabilities in the striatum and its relationship with traits of impulsivity and NS as well as vulnerability to cocaine addiction in high impulsive Roman high avoidance (RHA) rats.

Materials & Methods:

RHA outbred rats were raised in an enriched condition (EE, n=8), or impoverished condition (EI, n=8) beginning at post-natal day 21. Beginning *at three months of age*, rats were tested in novelty-induced place preference (NIPP) paradigm and straightaway trained in the five-choice serial reaction time task (5-CSRTT) for impulsivity testing. Striatal D2/3R density was then measured using SPECT imaging and [123I]IBZM. Binding potential (BP_{ND}) values were quantified as indexes of D2/3R density in striatum, using the simplified reference region model (SRTM). Rats were then implanted with an intravenous catheter and trained to self-administer cocaine (0.4 mg/kg/infusion) for 14 days (2 hours/day).

Results:

Compared to EI rats, EE rats were significantly ($p \leq 0.001$) more impulsive as revealed by a greater number of premature responses (77±30 vs. 39±12) and less novelty-seekers as shown by the time spent in a novel compartment (44% of total time for EE rats vs. 64% of total time for EI rats; $p \leq 0.01$). In addition, EE rats showed significantly ($p \leq 0.01$) higher BP_{ND} (3.01±0.52) than EI rats (2.04±0.46). When rats were trained to self-administer cocaine, EE rats showed a faster rate of acquisition of cocaine self-administration (7 sessions) compared with EI rats (12 sessions), indicating a higher vulnerability of EE rats to initiate drug abuse.

Discussion:

This study confirms that early environmental variables have an effect on D2/3R availability in striatum and influences personality traits thought to predispose to drug abuse. When compared with EI, EE was associated with lower levels of novelty seeking but higher levels of impulsivity, higher striatal D2/3R densities and higher vulnerability to drug abuse. This study contrasts to the view that positive early-life circumstances or experiences decrease the risk of drug abuse later in life. It also challenges the finding that striatal D2/3R deficits are associated with higher levels of impulsivity and predispose to drug abuse. Taken together, these data suggest that environmental enrichment could increase the reinforcing effects of psychostimulants and may facilitate the development of drug addiction.

Acknowledgements:

This work was supported by the Swiss National Science Foundation

References:

Dalley JW, et al (2007) Science 315:1267-70

Belin D, et al (2008) Science 320:1352-5

Gipson CD, et al (2011) Psychopharmacology 214:557-66

Perry JL, et al (2008) Behav Brain Res 193:48-54

P101
[^{11}C]clozapine PET in hemiparkinsonian rhesus with iPSC-derived dopaminergic neuronal grafts expressing DREADDs

Matthew Zammit, Tobey Betthauser, Miles Olsen, Maxim Slesarev, Carissa Boettcher, Scott C. Vermilyea, Jeanette Metzger, Yunlong Tao, Su-Chun Zhang, Marina E. Emborg, and Bradley Christian

University of Wisconsin-Madison, Madison, WI, USA

Introduction:
Parkinson's disease (PD) is a neurodegenerative disorder characterized by the loss of dopaminergic nigral neurons. Cell replacement with induced pluripotent stem cell-derived midbrain dopaminergic neurons (iPSC-mDA) is proposed as a candidate therapeutic strategy for PD. Genomic edited iPSC-mDA expressing DREADD (designer receptors exclusively activated by designer drugs) are envisioned as a way to modulate graft activity. The goal of this study was to assess in hemiparkinsonian rhesus whether [^{11}C]clozapine PET would be able to detect grafts of rhesus iPSC-mDA neurons expressing DREADDs.

Materials & Methods:
The present study was performed in strict accordance with the recommendations in the NIH Guide for the Care and Use of Laboratory Animals in an AAALAC accredited facility (Wisconsin National Primate Research Center, University of Wisconsin-Madison). Experimental procedures were approved by the Institutional Animal Care and Use Committee of the University of Wisconsin-Madison. Four adult male rhesus monkeys received a unilateral (right) intracarotid artery injection of the neurotoxin MPTP under sterile surgical conditions and isoflurane anesthesia. Six to eight months later the monkeys received iPSC-mDA expressing DREADD into the right substantia nigra. Cell delivery was performed using real-time intraoperative magnetic resonance imaging (RT-IMRI) in a 3-T GE SIGNA MRI scanner. Two months after brain surgery, 2 monkeys received low daily doses of clozapine (0.04 mg/kg p.o.) and the other 2 monkeys received placebo dosings. Twelve months after brain surgery, the animals were evaluated with [^{11}C]clozapine PET in a microPET Focus 220. Clozapine dosing was withheld for 24 hours prior to the scan. PET data were acquired for 90 minutes post-injection of the radioligand (5 mCi). Hand-drawn regions of interest (ROI) were created in the left and right caudate and putamen nucleus, and time-activity curves (TAC) were generated from the dynamic PET data for each ROI. Activity concentrations for each ROI were normalized to that of the grey matter cerebellum, and normalized TACs were generated for each monkey.

Results:

Qualitatively (Figure 1) [^{11}C]clozapine uptake was easily identified in the caudate and putamen nuclei of the placebo-treated brain hemisphere of the 4 monkeys. Substantia nigra uptake could not be visualized with this radiotracer. In the grafted hemisphere, [^{11}C]clozapine uptake differed between the animals that received daily dosing of clozapine or placebo. The clozapine-treated animals had low-level uptake of [^{11}C]clozapine in the right caudate and putamen compared to contralateral side, while uptake in the placebo animals was similar to the contralateral side. This was confirmed through quantification of the PET images. From the normalized TACs (Figure 2), [^{11}C]clozapine uptake was similar in all ROIs (ipsilateral and contralateral caudate and putamen) for the 2 placebo monkeys, while the clozapine treated animals had less uptake of [^{11}C]clozapine in the right caudate and putamen.

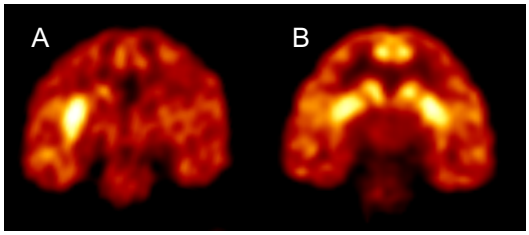

Figure 1. Uptake of [^{11}C]clozapine in (A) clozapine- and (B) placebo- treated monkeys.

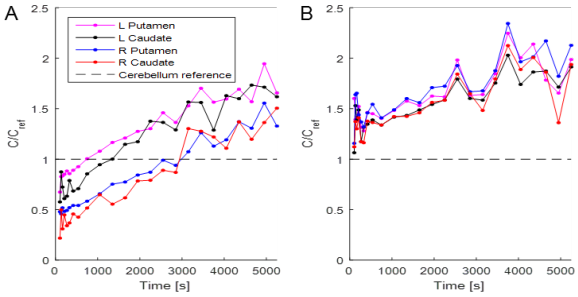

Figure 2. Normalized TACs for (A) clozapine- and (B) placebo- treated monkeys. The dashed line represents the threshold at which uptake of [^{11}C]clozapine elevates above cerebellar uptake.

Discussion/Conclusion:

Our results underscore the complexity of PET for visualization of DREADDs. The diverse binding profile and moderate D2 affinity of [^{11}C]clozapine does not permit the assessment of nigral DREADD receptors. However, it is suitable for striatal assay with high dopaminergic receptor expression. A surprising finding was the lack of [^{11}C]clozapine uptake in the MPTP+ graft brain hemisphere of clozapine-treated animals. Several explanations are possible: 1) Individual variability (unlikely due to the clear difference between treatment groups); 2) clozapine from the last dosing could still be occupying receptors (unlikely as the effects are not bilateral); 3) DA produced by the grafts could be competing with the radioligand; 4) If the grafts are chronically producing DA, it may have induced downregulation of striatal DA receptors, thus reducing binding sites. Next steps will include postmortem morphological assessment of the rhesus brains to assess iPSC-mDA neuron survival, phenotype and projections that will clarify the current PET imaging results.

Acknowledgements:

This research was supported by grants from the NIH (P51OD011106) and the UW-Madison Office of the Vice Chancellor for Research and Graduate Education.

P102
Serotonin 1A Autoreceptor Binding Correlates With Neural Responses to Emotion Reactivity and Regulation

Jeffrey M. Miller[1,2], Bruce Doré[3], Francesca Zanderigo[1,2], Barbara Stanley[1,2], Harry Rubin-Falcone[1,2], Noam Schneck[1,2], Elizabeth Sublette[1,2], Chelsea Boccagno[4], Odile Rodrick[5], Maria A. Oquendo[6], J. John Mann[1,2], Kevin Ochsner[5]

1. Columbia University, Department of Psychiatry; 2. New York State Psychiatric Institute; 3. Annenberg School, University of Pennsylvania; 4. Harvard University, Department of Psychology; 5. Columbia University, Department of Psychology; 6. Now at University of Pennsylvania, Department of Psychiatry

Introduction:

The serotonin neurotransmitter system modulates activity in emotion-processing-relevant brain regions, with prominent amygdala innervation. In raphe nuclei (RN), the serotonin 1A (5-HT_{1A}) receptor serves as an inhibitory autoreceptor on serotonergic neurons, and is thus a key regulator of serotonergic output. Consistent with this model, prior multimodal PET/fMRI studies have identified relationships between 5-HT_{1A} binding in RN and the neural responses to aversive stimuli in amygdala assessed by fMRI (1-3). We sought to expand this work by relating RN 5-HT_{1A} receptor binding to both emotion processing and regulation (specifically, reappraisal) assessed by fMRI, a relationship that has not been investigated previously to our knowledge.

Materials and Methods:

Fig 1. Responses to emotionally negative images in bilateral amgydala correlate positively with raphe nuclei 5-HT_{1A} receptor binding (SVC $p<.05$).

Twenty-one participants with current, unmedicated major depressive disorder (MDD) and 16 healthy volunteers participated in this study. **PET images** were acquired on a Siemens Biograph mCT in 3D mode over 120 minutes following transmission scan and bolus infusion of [^{11}C]CUMI-101. A high-resolution T1-weighted **structural MRI** was acquired for coregistration, segmentation, and identification of regions of interest (ROIs) using automated methods. The **fMRI task** used emotionally neutral and negative images selected from the International Affective Pictures Set (IAPS; (4)). Participants viewed IAPS pictures associated with three trial types: *Look Neutral* (look and respond naturally to emotionally neutral images), *Look Negative* (look and respond naturally to emotionally negative images), and *Reappraise Negative* (focus on positive aspects or outcomes of emotionally negative images). Each trial consisted of a 2s cue, 8s of image presentation, a 2-4s jittered interstimulus interval, and an 8s affective rating period. Participants were trained in the Look and Reappraise strategies prior to scanning. fMRI data were collected with a 3T GE MR750 magnet and 32-channel RF head coil. First-level general linear model analyses were implemented in NeuroElf v1.1. Analyses focused on activity during the stimulus (image presenation) period. Second-level (group) random-effects analyses were implemented in NeuroElf v1.1. A ROI for bilateral amygdala was identified using the Harvard-Oxford

probabilistic atlas. Within this ROI, small-volume correction was applied to achieve a corrected p value of <0.05. For whole-brain analyses, cluster-extent thresholding was applied to achieve a whole-brain FWE rate corrected p value of <0.05, with a primary threshold of p = 0.005 ($z \approx 2.6$) and smoothness parameters estimated from the residuals of the statistical map (12.2), yielding a k (minimum cluster size) of 148. We conducted individual differences analyses to determine whether contrasts of interest (reactivity: Look Negative > Look Neutral; reappraisal: Reappraise Negative > Look Negative and its inverse) correlated with variability in RN [^{11}C]CUMI BP_{ND}. Following pre-processing, [^{11}C]CUMI-101 binding potential (BP_{ND}) was estimated using the simplified reference tissue model (5), with cerebellar gray matter as reference region. We computed a voxel map reflecting the correlation between neural activity within these contrasts and RN [^{11}C]CUMI BP_{ND}.

Results:

Emotion Reactivity Contrast: RN [^{11}C]CUMI BP_{ND} was positively correlated with emotion reactivity contrast (Look negative > Look neutral) in clusters in bilateral amygdala within the *a priori* amygdala ROI mask (**Figure 1**; SVC p<0.05). In whole-brain analysis, RN [^{11}C]CUMI BP_{ND} was positively correlated with emotion reactivity in a cluster spanning posterior cingulate and precuneus (**Figure 2**; FWE p<0.05). These relationships persisted after controlling for age, sex, and diagnosis. There were no significant differences in the magnitude of these correlations as a function of diagnosis (MDD vs. healthy volunteer). We did not observe significant correlations between RN [^{11}C]CUMI BP_{ND} and the emotion reactivity contrast within either the MDD or healthy volunteer group when examined separately, likely due to sample size.

Emotion Regulation Contrast:

RN [^{11}C]CUMI BP_{ND} correlated with less BOLD response during the Reappraise Negative condition as compared to the Look Negative condition in a cluster in left amygdala within the *a priori* amygdala ROI mask (**Figure 3**; SVC p<0.05). No clusters were identified in whole-brain voxelwise analysis of reappraisal contrast that correlated with RN [^{11}C]CUMI BP_{ND}.

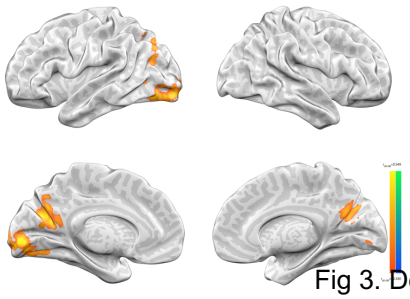

Fig 2. Responses to emotionally negative images in posterior cingulate/precuneus correlate positively with raphe nuclei 5-HT_{1A} receptor binding (FWE p<.05).

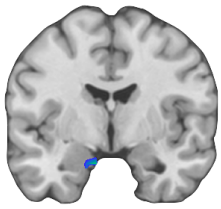

Fig 3. Decreased BOLD signal during reappraisal in left amygdala is positively correlated with raphe nuclei 5-HT_{1A} receptor binding (SVC p< .05).

Discussion:

In this study, we observed that RN 5-HT_{1A} autoreceptor binding was associated with both A) higher amygdala BOLD responses while spontaneously responding to affectively negative stimuli and B) lower amygdala BOLD responses while reappraising negative stimuli, consistent with effective emotion regulation. The emotion reactivity findings are partially convergent with a recent study (3), though divergent from earlier work (1, 2), all of which used a different radiotracer and different fMRI paradigms. In future work, we will examine these relationships in an expanded sample, incorporate subject-reported trial-by-trial ratings of emotional valence into fMRI analyses, and consider measures of task-based functional connectivity. Consistent with our previous findings of elevated 5-HT_{1A} binding in depression, these findings suggest that excessive spontaneous responding to emotionally negative stimuli may be partly mediated by lower serotonin release due to 5-HT_{1A} autoreceptor upregulaton. Paradoxically, this neurochemical profile may facilitate the neural correlates of effective emotion regulation. Treatment implications in depression will be discussed.

References:

1. Fisher PM, Meltzer CC, Ziolko SK et. al. [2006] Nat Neurosci 9: 1362-1363.
2. Selvaraj S, Mouchlianitis E, Faulkner P, et. al. [2015] Biological Psychiatry 78: 563-571.
3. Kranz GS, Hahn A, Kraus C, et. al. [2017] Neuroimage 171: 1-5.
4. Lang PJ, Greenwald MK, Bradley MM et. al. [1993] Psychophysiology 30: 261-273.
5. Lammertsma AA, Hume SP [1996] Neuroimage 4: 153-158.

P103
Endogenous opioid system is associated with inhibitory control: a combined fMRI-PET study

Tatu Kantonen[1], Tomi Karjalainen[1], Lihua Sun[1], Laura Pekkarinen[1], Pirjo Nuutila[1] and Lauri Nummenmaa[1,2]

[1]*Turku PET Centre, University of Turku, Finland*

[2]*Department of Psychology, University of Turku, Finland*

Introduction:

Obesity is linked with reduced inhibitory control leading to increased palatable food intake (Appelhans et al., 2011). Brain basis of inhibitory control is typically studied using go/no-go tasks, revealing activity in prefrontal and parietal cortical areas during response inhibition (Rubia et al., 2001). At molecular level, the endogenous opioid system is intimately linked with pathophysiology of obesity, likely due to its contribution to rewarding aspects of feeding (Gosnell and Levine, 2009). Positron emission tomography (PET) studies have shown that brain's μ-opioid receptor (MOR) availability is reduced in morbidly obese subjects (Karlsson et al., 2015) and also associated with the sensitivity of the reward system (Karjalainen et al., 2016). Here we tested whether individual differences in MOR availability are associated with inhibitory control responses in the brain.

Materials and Methods:

We scanned 11 healthy non-obese males with PET and MOR receptor specific ligand [11C]-carfentanil. Data were normalized to MNI space and the MOR availability was expressed in terms of BP_{ND} calculated for each voxel using the simplified reference tissue model with reference-tissue (occipital cortex) time activity curves as input data (Gunn et al., 1997). Subjectwise BP_{ND} values were extracted from regions of interest including striatum, thalamus, amygdala, cingulate, insular and orbitofrontal cortices.

Subsequently the subjects underwent a go/no-go fMRI experiment, where they saw three types of simple round-shaped color stimuli in random order (60 "no-go" cases, 60 "rare-go" cases, 300 "go" cases, duration = 0.4 s each, interstimulus-interval = 0.8 s). Subjects were instructed to press a button with their left thumb after each stimulus except the "no-go" stimuli. We then computed subjectwise BOLD contrast maps for "no-go" minus "go" contrast. These maps were subjected to a random effects analysis, and modelled with the regional MOR BP_{ND} values. The resulting maps thus show voxels whose go/no-go responses depend on MOR availability.

Results:

The go/no-go task activated frontal and parietal areas, anterior cingulate cortex (ACC) and bilateral insula (Fig 1 upper row) in accordance with prior studies (Levy and Wagner, 2011). In PET-fMRI fusion analysis (Fig 1 lower row), MOR availabilities particularly in insula, thalamus and putamen predicted inhibitory responses in fMRI especially in ACC, insula, thalamus and frontal areas. Negative associations were not observed in any brain region.

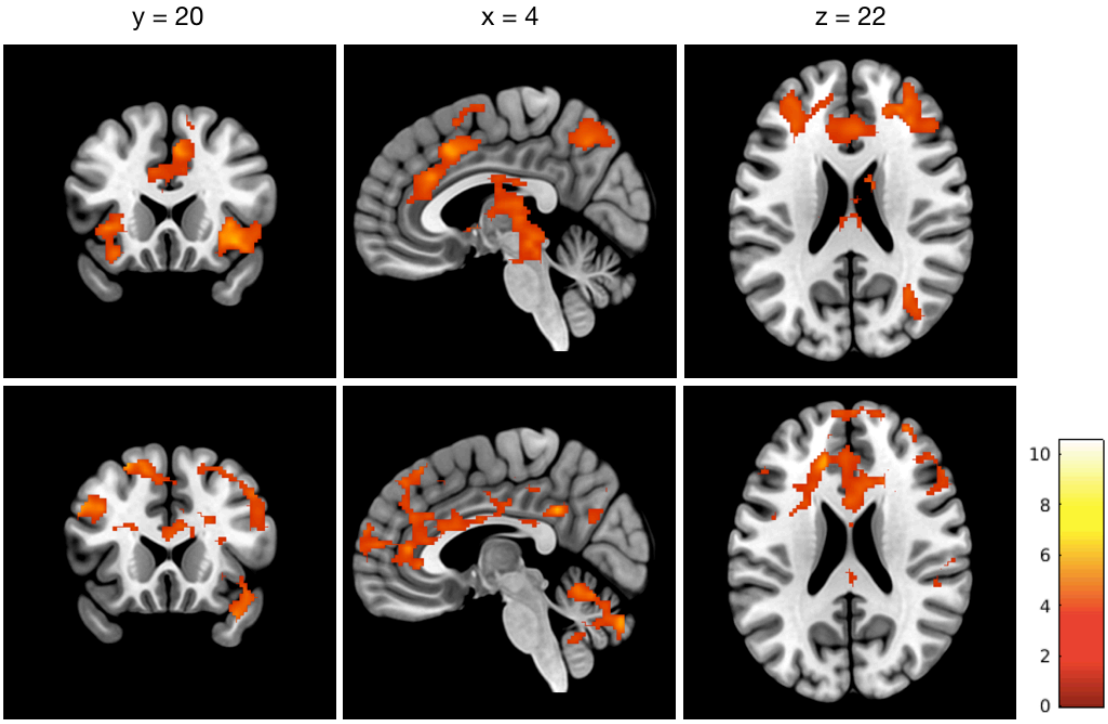

Fig 1. Upper row: The BOLD contrast of no-go activity with the subtraction of go activity showing the inhibitory network activation. Lower row: The positive correlation between insular MOR availability (BP_{ND}) and no-go activity. The data are thresholded at $p < 0.05$ (FDR corrected) and clusters of voxels > 1000.

Conclusion:

We showed that MOR availability in insula, thalamus and striatum predicts inhibition-related BOLD responses. The more opioid receptors the subjects had, the stronger their inhibitory responses were. These results link together the data on opioidergic basis of obesity and its cognitive phenotype associated with dampened inhibitory control in the brain, and suggest that individual differences in MOR expression may explain why some people are better in resisting their urges to eat.

Acknowledgements:

The study was financed by the Academy of Finland (decision number 304385).

References:

Appelhans BM, Woolf K, Pagoto SL et al. [2011] Obesity 19: 2175–2182

Rubia K, Russell T, Overmeyer S et al. [2011] NeuroImage 13: 250–261

Gosnell BA and Levine AS [2009] International Journal of Obesity 33: S54–S58

Karlsson HK, Tuominen L, Tuulari JJ et al. [2015] J. Neurosci. 35(9): 3959–3965

Karjalainen T, Tuominen L, Manninen S et al. [2016] Social Cognitive and Affective Neuroscience 11: 1310–1316

Gunn RN, Lammertsma AA, Hume SP and Cunningham VJ [1997] NeuroImage 6: 279–287

Levy BJ and Wagner AD [2011] Ann. N.Y. Acad. Sci. 1224: 40–62

P104
Frontostriatal functional connectivity and its relationship with striatal dopamine capacity in schizophrenia

Seoyoung Kim, M.D.[1] , Euitae Kim, M.D., Ph.D.[1,2]

[1] *Department of Neuropsychiatry, Seoul National University Bundang Hospital, Gyeonggi-do, Republic of Korea*

[2] *Department of Psychiatry, Seoul National University College of Medicine, Seoul, Republic of Korea*

Introduction:

Schizophrenia is thought to be a heterogeneous disorder and evidences reflect categorically distinct subtypes according to the antipsychotic treatment response. Altered frontostriatal functional connectivity (FC) in schizophrenia and its correlation with antipsychotic treatment response also suggests divergence of underlying pathophysiologic mechanism. Meanwhile, the observations that prefrontal activity correlates with striatal dopaminergic function, has led to the hypothesis that disrupted frontostriatal FC would be related with altered dopaminergic pathway in schizophrenia. The aim of this study was to investigate the relationship between frontostriatal FC and striatal dopaminergic activity in patients with schizophrenia according to responsiveness to first-line antipsychotic drug.

Materials & Methods:

24 symptomatically stable patients with schizophrenia were recruited from Seoul National University Hospital, 12 of which responded to first-line antipsychotic drugs (first-line AP group) and 12 stable under clozapine (clozapine group), along with 12 matched health controls. All participants underwent resting-state functional MRI and [^{18}F]DOPA positron emission tomography.

Results:

There was no significant difference in the total PANSS score between the first-line AP group and the clozapine group (mean difference=0.67, s.e.=3.21, df=33, p=1.000). Voxel-based analysis found significant negative correlation between frontal FC to the left associative striatum and the k_i^{cer} in the corresponding region in first-line AP group but not in clozapine group or healthy control. Additional region of interest analysis confirmed the result (control group: R^2=0.032, p=0.572; first-line AP group: R^2=0.551, p=0.005; clozapine group: R^2=0.108, p=0.297) and the correlation coefficients were significantly different between first-line AP group and clozapine group (z=-2.75, p=0.006).

Discussion:

Different patterns of relationship between striatal dopamine capacity and frontostriatal FC observed in this study indicate different pathophysiology underlying schizophrenia according to antipsychotics treatment-responsiveness.

Acknowledgements:

This work was supported by the Ministry of Health & Welfare, Republic of Korea (Grant no. HI15C3104) and grant no. NRF-2015R1C1A1A01054583 from the National Research Foundation of Korea (NRF). The authors have nothing to disclose.

References:

Kim E, Howes OD, Veronese M, *et. Al.* [2017]. *Neuropsychopharmacology.* Presynaptic Dopamine Capacity in Patients with Treatment-Resistant Schizophrenia Taking Clozapine: An [18F]DOPA PET Study. **42**: 941-950.

Howes OD, Kapur S. [2014], *Br J Psychiatry.* A neurobiological hypothesis for the classification of schizophrenia: type A (hyperdopaminergic) and type B (normodopaminergic). **205**: 1-3.

P105
Quantifying muscle amyloid content in inclusion body myositis using [18f]florbetapir positron emission tomography

J B Lilleker[1,2], R Hodgson[3,4], M E Roberts[2], K Herholz[5], J Howard[2], R Hinz*[5], H Chinoy*[4,6] * joint last author

1. *Centre for Musculoskeletal Research, School of Biological Sciences, Faculty of Biology, Medicine and Health, Manchester Academic Health Science Centre, The University of Manchester, Manchester, M13 9PT, UK*
2. *Greater Manchester Neurosciences Centre, Salford Royal NHS Foundation Trust, Stott Lane, Salford, UK*
3. *Radiology department, Salford Royal NHS Foundation Trust, Manchester Academic Health Sciences Centre, Stott Lane, Salford, M6 8HD*
4. *The National Institute for Health Research Manchester Biomedical Research Centre, Central Manchester University NHS Foundation Trust, The University of Manchester, Manchester, UK*
5. *Wolfson Molecular Imaging Centre, University of Manchester, Manchester, UK*
6. *Rheumatology Department, Salford Royal NHS Foundation Trust, Salford, UK*

Introduction:

Inclusion body myositis (IBM) shares some histopathological features with polymyositis (PM) but does not respond to conventional immunosuppressive treatments. Current investigations have low sensitivity for identification of amyloid deposits that are characteristic of IBM, contributing to frequent misdiagnosis.

We performed a prospective case control study comparing muscle amyloid content, quantified using a novel positron emission tomography (PET) technique, in IBM and PM.

Materials & Methods:

Ten cases with IBM and six controls with PM underwent clinical review, [18F]florbetapir PET/computed tomography, and magnetic resonance imaging (MRI) of whole-body skeletal musculature.

[18F]florbetapir standardised uptake value ratios (SUVRs, reference = lumbar fat pad) in skeletal muscle were compared between cases and controls. The relationship in IBM of [18F]florbetapir SUVRs to clinical and MRI-derived measures of disease severity were also investigated.

Results:

[18F]florbetapir SUVRs were significantly higher in those with IBM for all muscle regions assessed (total SUVR 1.45 [IQR 1.28-2.05] *versus* 1.01 [IQR 0.80-1.22], p=0.005) (Figures 1 & 2).

Strong negative correlation between MRI-derived muscle inflammation levels and [18F]florbetapir SUVRs were observed only in calf muscles bilaterally (right -0.73, p=0.02; left -0.68, p=0.03). No significant relationship between [18F]florbetapir SUVRs and clinical measures of disease severity were identified.

Conclusion:

Muscle amyloid imaging using [18F]florbetapir PET may be useful in the diagnostic workup of IBM, particularly when differentiating from PM. The observed correlation between inflammation and muscle amyloid content may provide clues to pathways of amyloidogenesis in IBM.

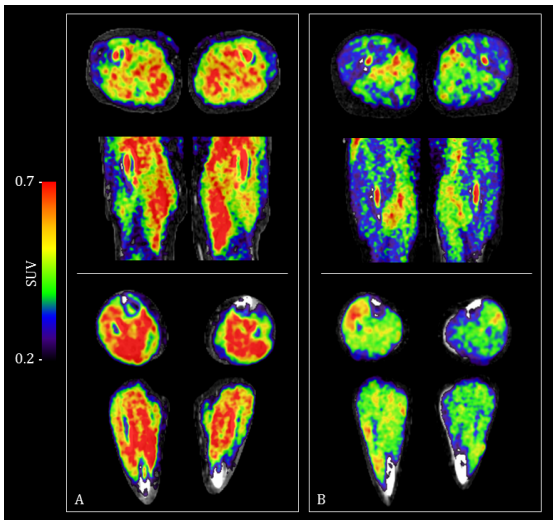

Figure 1: Differences in [18F]florbetapir positron emission tomography (PET) derived standardised uptake values (before reference tissue normalisation) between a case with inclusion body myositis (A) and a control with polymyositis (B)

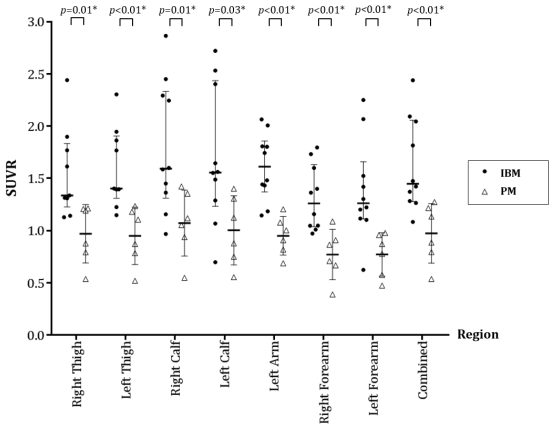

Figure 2: Comparison of standardised uptake value ratios (SUVRs) of [18F]florbetapir between cases (inclusion body myositis, filled circles) and controls (polymyositis, open triangles) across seven different muscle regions and a combined region (total SUVR)

P106
Dopamine-D_2-receptors in hemiparkinsonian rats - impact of intrastriatal Botulinum Neurotoxin-A Injection

Mann T[1], Kurth J[2], Hawlitschka A[1], Stenzel J[3], Lindner T[3], Polei S[3], Hohn A[2], Krause BJ[2], Wree A[1]

[1] Institute of Anatomy, Rostock University Medical Center, Gertrudenstrasse 9, 18057 Rostock, Germany
[2] Department of Nuclear Medicine, Rostock University Medical Centre, 18057 Rostock, Germany
[3] Core Facility Multimodal Small Animal Imaging, Rostock University Medical Center, Rostock, Germany

Introduction:

Intracerebral injection of botulinum neurotoxin A (BoNT-A) results in improved motor behavior of hemiparkinsonian (hemi-PD) rats, a widespread animal model for Parkinson's disease (PD) (Wree et al., 2011). To disclose receptor-mediated explanations of the therapeutic BoNT-A effect, we analyzed the Dopamine-D_2-receptor in the striatum (CPu) of 6-hydroxydopamine (6-OHDA)-induced hemi-PD rats by [^{18}F]fallypride-PET/CT and quantified D_2/D_3 receptor availability in controls and sham- or BoNT-A treated hemi-PD rats.

Materials & Methods:

Twenty-six male Wistar rats were assigned to 3 different groups: controls, sham-treated hemi-PD rats and BoNT-A-treated hemi-PD rats. Dopaminergic deafferentation was caused by stereotaxic injection of 6-OHDA into the median forebrain bundle. The therapeutic substance BoNT-A was subsequently injected at two sites into the striatum. Disease-specific motor impairment was verified by rotational testing with apomorphine (dosage: 0.25 mg/kg) and amphetamine (dosage: 2.5 mg/kg). Each animal was scanned by dynamic [^{18}F]fallypride-PET/CT scans over 90 min one, three and six months post BoNT-A or sham treatment. A MRI scan was performed for anatomical reference. Quantification of the non-displaceable Binding Potential (BP_{nd}) was assessed separately for the left and right striatum using PMOD software. The reference region was the cerebellum, expressing no D_2/D_3 receptors and being validated as a suitable reference for [^{18}F]fallypride uptake before (Constantinescu et al., 2011).

Results:

Kinetic analysis revealed no relative interhemispheric right-left differences in control animals. In hemi-PD rats we found a 23% increase of D_2/D_3 receptor ipsilateral to the 6-OHDA injection which remained constant up to 6 months. Notably, this pathological imbalance was almost normalized by the intrastriatal application of BoNT-A (Fig. 1A). A highly significant correlation of the degree of interhemispheric differences in D_2/D_3 receptor availability and apomorphine-induced rotations between the analyzed groups was found one month post sham-BoNT-A or BoNT-A injection (Fig. 1B).

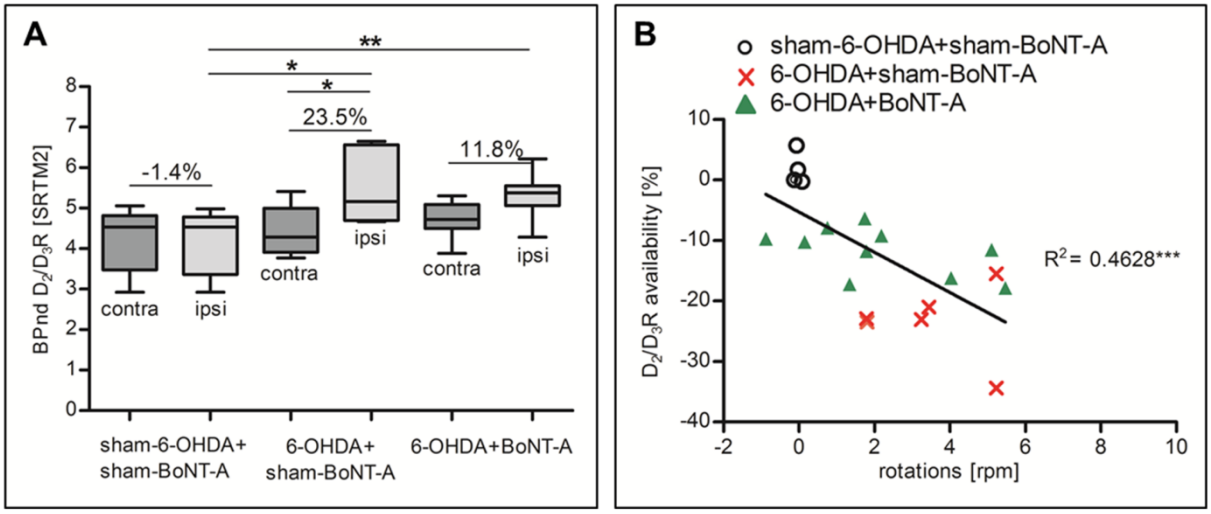

Fig. 1: A) Box plots for BP_{nd} values of D_2/D_3 receptors depicting median ± SD for the contralateral (dark grey) and ipsilateral (light grey) CPu for controls (sham-6-OHDA+sham-BoNT-A), sham-injected hemi-PD rats (6-OHDA+sham-BoNT-A) and BoNT-A-injected hemi-PD rats (6-OHDA+BoNT-A) one month post BoNT-A or sham-BoNT-A injection (*$p < 0.05$, **$p < 0.01$). B) Linear correlation of the right-left differences of D_2/D_3 receptor availability in [%] and apomorphine-induced rotations one month after BoNT-A or sham-BoNT-A (***$p < 0.001$).

Discussion/Conclusion:

We here provide a longitudinal study on changes of D_2/D_3 receptor availability in the 6-OHDA-induced hemi-PD rat model. We found a constant increase in D_2/D_3 receptor availability which was significantly reduced after striatal injection of BoNT-A. Interestingly, this decrease of pathological D_2/D_3 receptor imbalance by intrastriatal BoNT-A injection significantly correlated with behavior in apomorphine rotation testing. Altogether, our results emphasize the therapeutical capability of BoNT-A in hemi-PD rats and provide insights in the underlying mechanisms.

Acknowledgements:

The Core Facility Multimodal Small Animal Rostock and this project was funded and supported by EFRE funding (UHROM 16) and by the Deutsche Forschungsgemeinschaft (INST 2268/6-1 FUGG).

References:

Constantinescu CC, Coleman RA, Pan M-L, Mukherjee J (2011) Striatal and extrastriatal microPET imaging of D2/D3 dopamine receptors in rat brain with [^{18}F]fallypride and [^{18}F]desmethoxyfallypride. Synapse 65:778–787

Wree A, Mix E, Hawlitschka A, Antipova V, Witt M, Schmitt O, Benecke R (2011) Intrastriatal botulinum toxin abolishes pathologic rotational behaviour and induces axonal varicosities in the 6-OHDA rat model of Parkinson's disease. Neurobiol Dis 41:291–298

P107
Microglial activation in recent ischemic stroke: comparison of two TSPO tracers

E. Visi[1], R Hinz[1], W Trigg[2], K. McDonald[1], M. Punter[3], A. Majid[4], A. Gerhard[1], K. Herholz[1]

(1)Wolfson Molecular Imaging Centre, The University of Manchester, UK (2) GEHC Life Sciences, Little Chalfont, UK (3) Salford Royal NHS Foundation Trust, Manchester, UK (4) SITRAN, University of Sheffield, UK

Introduction:

Activated microglia play a complex role in neuro-inflammation associated to acute ischemic stroke and can be imaged by positron emission tomography (PET) using TSPO radiotracers. As a potential target for anti-inflammatory therapy it is crucial to understand the correlation between its intensity/extent and the clinical outcome of the stroke. While the "gold-standard" is the ^{11}C-labelled PK11195, ^{18}F-labelled compounds could be potentially applied as diagnostic tools in routine clinical settings. We therefore are studying microglia activation in human brain using [^{18}F]GE180 with PET in patients after mild to moderate stroke. In a first stage we have been comparing [^{18}F]GE180 with [^{11}C](R)-PK11195 to characterize the new tracer.

Patients and Methods:

10 participants (age 67$\pm$ 23, 8m/2f) with history of recent (36.5$\pm$18.5 days) ischemic stroke of mild-to-moderate severity (modified Rankin scale 2-3) in middle cerebral artery territory were scanned 18 to 63 days (median 34.5) after the stroke by MRI (Philips 1.5T), [^{18}F]GE180 (200MBq, 30 min dynamic scan) and [^{11}C](R)-PK11195 (740MBq, 60 min dynamic scan) PET (Siemens HRRT). The two PET scans were performed on two separate days (median 3.4 days apart). 5 patients were randomized to receive the [^{18}F]GE180 scan at the first session and 5 patients to receive it at the second session. All PET and MR data sets were co-registered with T1-weighted MR scans. Volume of interest (VOIs) of ischemic lesions and contralateral mirror regions were drawn manually. Distribution volume ratio (DVR) for the target (infarct) and reference (contralateral mirror) region were calculated from the [^{11}C](R)-PK11195 binding potential (SRTM, bilateral cerebellar grey matter input function [1,2]). Tissue activity concentrations of [^{18}F]GE180 were read out from summed images 15-30 min post injection. As shown in previous studies[3,4] intravascular activity of [^{18}F]GE180 remains high during the scanning time. We estimated intravascular activity from 0-5 min post injection summed images and calculated corrected tissue tracer uptake by subtracting intravascular activity from 15-30 minutes post injection scans. Target-to-reference ratios (TRRs) were then calculated for both tracers, based on the DVRs for [^{11}C](R)-PK11195 and tracer uptake 15-30 min post injection with and without correction for [^{18}F]GE180.

Results:

All patients showed recent ischemic lesions (n=15) associated with the recent ischemic stroke. Two patients also showed evidence of old clinically silent ischemic lesions (n=4). Across all lesions the contrast between the lesion and the reference region was very similar with [C](R)-PK11195 and [^{18}F]GE180 without intravascular activity correction **(Fig.1).** With correction for [^{18}F]GE180 intravascular activity, the contrast increased while the correlation coefficient between the tracers decreased **(Fig.2).** The pattern is similar across the recent lesions. As expected, recent infarcts showed higher tracer uptake with both tracers than old infarcts. Recent lesions with contrast enhancement (CE) showed higher uptake with both tracers **(Fig.3)**

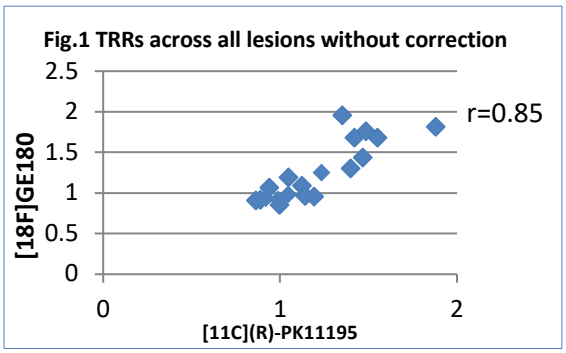

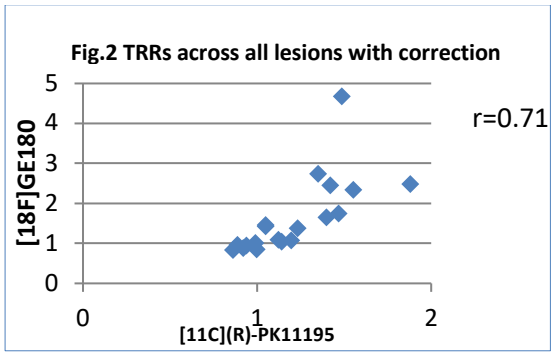

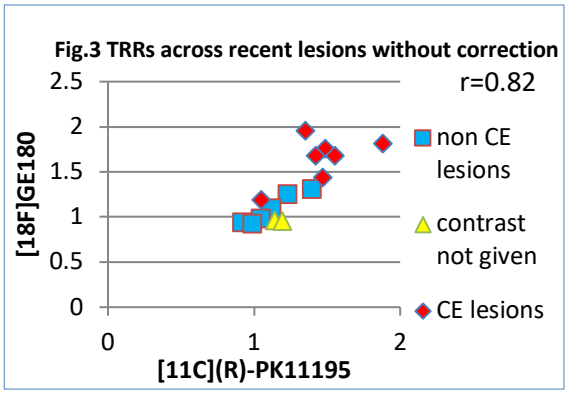

Conclusion:

The study demonstrates that microglial activation in ischemic stroke can be imaged by [^{18}F]GE180 and [^{11}C](R)-PK11195 PET. Target-to-reference ratios are similar with both tracers. Correction for intravascular activity increases target-to-reference ratios of [^{18}F]GE180. Further studies using dynamic data analysis and longer or delayed data acquisition are needed to determine the optimum time window for data acquisition with [^{18}F]GE180. We have not yet analysed whether the [^{18}F]GE180 signal is influenced by a TSPO gene polymorphism, but the close correlation with [^{11}C](R)-PK11195 suggests that any such effect on the target-to-reference ratios would likely be minor.

Acknowledgement:

The study is funded by a grant from NIHR EME programme and supported by GEHC and INMIND (European Commission Framework Programme 7)

References:

[1]Turkheimer, F. E., P. Edison, N. Pavese, et al. (2007).J Nucl Med 48(1): 158-167.

[2] Su, Z., K. Herholz, A. Gerhard, et al. (2013). Eur J Nucl Med Mol Imaging 40(9): 1406-1419. [3] Fan, Z., V. Calsolaro, R. A. Atkinson, et al. (2016) J Nucl Med 57(11): 1753-1759 [4] Feeney, C., G. Scott, J. Raffel, et al. (2016). Eur J Nucl Med Mol Imaging 43(12): 2201-2210.

P108
Impact of electroconvulsive therapy on the adenosine A_1 receptor in the human brain: A PET study in depressive patients

Tina Kroll[1], Maria Klingebiel[1], Michael Grözinger[2], Andreas Matusch[1], Ana Novakovic[2], David Elmenhorst[1,3], Andreas Bauer[1,4]

[1]*Molecular Neuroimaging, Institute of Neurosciences and Medicine, Jülich Research Center, Jülich, Germany*
[2]*Department of Psychiatry and Psychotherapy, Medical Faculty, RWTH Aachen University, Aachen, Germany*
[3]*Psychiatry and Psychotherapy, Medical Psychology, Rheinische Friedrich-Wilhelms-University Bonn, Bonn, Germany*
[4]*Neurological Department, Medical Faculty, Heinrich-Heine-University Düsseldorf, Düsseldorf, Germany*

Introduction:

Major depressive disorder (MDD) severely influences life quality and is one of the major causes of suicides. Currently, over 320 million people are affected by MDD world-wide [1]. Besides pharmaco- and psychotherapy, sleep deprivation (SD) and electroconvulsive therapy (ECT) are effective treatments. Both are associated with an enhancement of adenosine concentrations [2,3]. Moreover, SD causes an upregulation in A_1AR expression [4] and an increase of A_1AR-signalling inhibited depressive-like behavior in a transgenic mouse model [5]. The aim of the current study was to investigate if changes of A_1AR density could account for anti-depressive efficacy of ECT treatment in patients with MDD.

Material & Methods:

14 depressive patients (mean age: 49.5 ± 11.8 years, mean duration of illness: 17 ± 11.5 years) were investigated twice by means of [^{18}F]CPFPX A_1AR-PET. The first scan served as baseline whereas the second was performed after ECT treatment (10.4 ± 1.2 sessions, last ECT 5.7 ± 2.7 days before the second scan). The ninety-minutes dynamic [^{18}F]CPFPX PET scans were performed using a bolus plus continuous infusion protocol. Frequent blood samples were used to generate a metabolite corrected arterialized input function. As outcome parameter the tissue-to-plasma ratio under equilibrium conditions (min 50-90 after start of injection) was chosen which is directly proportional to A_1AR receptor availability. Regions of interest were delineated on individual anatomical MRI planes.

Additionally, all patients repeatedly underwent neuropsychological testing including Becks Depression Inventory-2 (BDI-2), Global Assessment of Functioning (GAF), Montgomery-Åsberg Depression Rating Scale (MADRS) and Mini Mental State Test (MMST).

Alterations in A_1AR expression due to ECT were analyzed by a mixed model analysis of variance with regions and scan session treated as within-subject factors and responder/non-responder as between-subject factor if applicable. Clinical outcome parameters of

neuropsychological testing were correlated (Pearson correlation coefficient) with molecular changes in A_1AR densities.

Results:

Outcome parameters of neuropsychological testing classified 7 patients as ECT-responders (decrease in HAM-D score of >50%) and 7 patients as non-responders.

Group comparison of cerebral A_1AR expression before and after ECT did not reveal significant differences in any of the investigated regions ($F_{(1,13)} = 0.026$; $p = 0.88$). Furthermore, responders and non-responders did not show any differences in A_1AR alterations due to ECT treatment (factor “responder/non-responder”: $p = 0.31$, interaction “region × scan session × responder/non-responder”: $p = 0.16$). Mean relative changes in A_1AR densities before and after ECT ranged from 1 ± 22% (anterior temporal lobe) to 11 ± 28% (nucleus accumbens, explorative paired t-test: $p = 0.4$). Noteworthy, individual patients showed striking increases or decreases in A_1AR expression after ECT treatment. However, there was no correlation between changes in clinical outcome parameters and regional A_1AR densities (e.g. HAM-D, gyrus parietalis superior: $R^2 = 0.04$; $p = 0.49$).

Discussion/Conclusion:

In the investigated sample of severely depressed patients, ECT did neither lead to consistent changes in A_1AR expression, nor did clinical outcome after ECT correlate with alterations in A_1AR availabilities. In conclusion, the results of the present study imply that clinical effects of ECT cannot be explained by long-lasting changes of the cerebral A_1AR. This does, however, not rule out that other routes of purinergic signaling are involved in ECT efficacy.

References:

[1] World Health Organization [2017], Global Health Estimates

[2] Porkka-Heiskanen T, Strecker RE, Thakkar M et. al. [1997] Science 276: 1265-1268

[3] Sadek AR, Knight GE, Burnstock G [2011] Purinergic Signal 7: 447-452

[4] Elmenhorst D, Meyer PT, Matusch A et. al. [2007] J Neurosci 27: 2410-2415

[5] Serchov T, Clement HW, Schwarz MK et. al. [2015] Neuron 87: 549-562

P109
Borderline Personality Disorder and the Endocannabinoid System: A [^{11}C]-CURB Positron Emission Tomography Study

Nathan J. Kolla[1], Pablo Rusjan[1], Shelley McMain[1], R. Michael Bagby[1], Sylvain Houle[1], Romina Mizrahi[1], Isabelle Boileau[1]

1 = Centre for Addiction and Mental Health Research Imaging Centre, Toronto, Ontario, Canada

Introduction:

Borderline personality disorder (BPD) is a serious psychiatric condition that presents with emotional dysregulation, poor impulse control, and unstable relationships. Self-harming behavior (SHB), such as cutting or hitting oneself, is common in the disorder and may function to maladaptively reduce stress. Despite the burden of SHB on health care systems, there has been little research investigating the neurochemical correlates of this pervasive symptom, although functional imaging studies suggest that the frontal cortex and amygdala may be involved in the pathogenesis. The endocannabinoid system (ECS) represents a novel opportunity to better understand SHB in BPD, as the ECS controls the release of several neurotransmitters and is a potent modulator of myriad neural circuits influencing human behavior, including violence. Fatty acid amide hydrolase (FAAH) is a brain enzyme that regulates the ECS by metabolizing anandamide (AEA), an endocannabinoid that binds to CB1 receptors to stimulate neurotransmission. Higher serum levels of AEA were reported in one BPD sample [1] as well as reduced AEA in the cerebrospinal fluid [2]. Overall, the relationship between plasma endocannabinoids and brain function is difficult to interpret. Hence, there is a real need for *in vivo* neuroimaging techniques that can probe the living human brain. [^{11}C]-CURB is an effective positron emission tomography (PET) radioligand that binds selectively, specifically, and irreversibly to FAAH. Biodistribution studies indicate that the regional brain uptake of [^{11}C]-CURB is consistent with the known distribution of FAAH in rat brain; [^{11}C]-CURB brain uptake is dose-dependently inhibited by increasing doses of unlabeled FAAH inhibitors; and chromatographic analyses confirm that the radiotracer is irreversible in brain and that metabolites do not cross the blood-brain-barrier [3]. We hypothesized that [^{11}C]-CURB binding would be higher in the prefrontal cortex and amygdala of BPD with persistent self-harm compared with healthy controls, consistent with the notion that CB1 receptor signaling is reduced in BPD.

Materials & Methods:

20 individuals with BPD and 28 healthy control comparison subjects each underwent one [^{11}C]-CURB PET scan. Inclusion criteria for the BPD group included at least 12 self-harming episodes in the past year and a SCID-II diagnosis of BPD. Exclusion criteria included lifetime history of psychotic or bipolar disorder; current mood or substance use disorder ascertained with the SCID-I; any psychotropic medication use in the past 6 weeks; cigarette smoking, which was corroborated by carbon monoxide testing; and illicit substance use, confirmed by urine toxicology. Healthy control subjects were free of any psychiatric illness, determined by the SCID-I and SCID-II; did not smoke; took no medications; and provided negative urine drug

screens. The regions of interest (ROI), including prefrontal cortex and amygdala, were automatically delineated using ROMI [4], an in-house program. An irreversible two-tissue compartment model with arterial input function was used to fit the time activity curves and provide an identifiable net influx constant [Ki = $K_1 \times k3/(k_2 + k_3)$], where K_1 (mL × cm^{-3} × min^{-1}) is the plasma-to-tissue transfer constant, k_2 (min^{-1}) is the tissue-to-plasma transfer constant, and $k3$ is the rate constant of irreversible trapping of the tracer in tissue due to the reaction of the radioligand with the enzyme and is proportional to the concentration of catalytically active FAAH. The composite parameter λk_3 is a reliable index of FAAH activity [5]. Subjects also underwent a standard T1-weighted MRI scan to aid in ROI delineation of the PET images. We also collected blood samples to test for a functional polymorphism of the FAAH gene (rs324420, C385A) that is rare (homozygotes represent 2-6% of the population).

Results:

Among the BPD subjects, there were 2 males and 18 females, which differed significantly from the proportion of males and females in the healthy control group (12 males and 16 females, $\chi^2 = 6.1$, $p = 0.023$). The mean age of the two groups did not differ significantly (BPD = 28.0 years; healthy control = 25.9 years; $p = 0.40$). PET data are currently being analyzed and will be presented in full at the conference.

Discussion/Conclusion:

To the best of our knowledge, the ECS has never been studied in BPD with SHB using PET. There is a strong rationale to believe that FAAH binding may be higher in BPD, given the existing biochemical evidence. A fulsome set of PET results is forthcoming.

References:

[1] C. Schaefer, F. Enning, J.K. Mueller, J.M. Bumb, C. Rohleder, T.M. Odorfer, J. Klosterkotter, M. Hellmich, D. Koethe, C. Schmahl, M. Bohus, and F.M. Leweke, Fatty acid ethanolamide levels are altered in borderline personality and complex posttraumatic stress disorders. Eur Arch Psychiatry Clin Neurosci 264 (2014) 459-63.

[2] D. Koethe, Schwarz E, Schaefer C, Enning F, Mueller JK, Bumbe JM, Herpertz S, Schmahl C, Bohus M, Leweke FM, Endocannabinoids and neuropeptides in CSF and serum from borderline personality disorder, Society of Biological Psychiatry, New York, 2014, pp. 148S.

[3] A.A. Wilson, A. Garcia, J. Parkes, S. Houle, J. Tong, and N. Vasdev, [11C]CURB: Evaluation of a novel radiotracer for imaging fatty acid amide hydrolase by positron emission tomography. Nuclear medicine and biology 38 (2011) 247-53.

[4] P. Rusjan, D. Mamo, N. Ginovart, D. Hussey, I. Vitcu, F. Yasuno, S. Tetsuya, S. Houle, and S. Kapur, An automated method for the extraction of regional data from PET images. Psychiatry Res 147 (2006) 79-89.

[5] P.M. Rusjan, A.A. Wilson, R. Mizrahi, I. Boileau, S.E. Chavez, N.J. Lobaugh, S.J. Kish, S. Houle, and J. Tong, Mapping human brain fatty acid amide hydrolase activity with PET. Journal of Cerebral Blood Flow and Metabolism: Official Journal of the International Society of Cerebral Blood Flow and Metabolism 33 (2013) 407-14.

P110
Evaluation of microglial activation and test-retest studies with [^{18}F]PBR06 in patients with amyotrophic lateral sclerosis and healthy volunteers

Christine Sandiego[1], Olivier Barret[1], Vincent Carroll[1], Alexandra Gouasmat[1], Caroline Papin[1], David Russell[1], Jennifer Madonia[1], Kenneth Marek[1], Sofia Mosesova[2], Carole Ho[2], Jonas Hannestad[2]

[1]Invicro, New Haven, CT, USA

[2]Denali Therapeutics Inc., South San Francisco, CA, USA

Introduction:

Amyotrophic lateral sclerosis (ALS) leads to the deterioration of motor function and is associated with over-activated microglia, the brain's immune cells. Previous PET studies with [^{11}C]PBR28 have shown higher translocator protein (TSPO) levels, a biomarker for activated microglia, in ALS patients compared with healthy volunteer (HV) subjects, after normalizing activity (SUVr) to whole brain or occipital cortex [1,2]. The aim of this study was to examine differences in TSPO levels with [^{18}F]PBR06 in ALS and HV subjects and to evaluate test-retest (T-RT) reliability using invasive and non-invasive measures.

Materials & Methods:

Seventeen (13M/4F) subjects completed T-RT imaging (7±5 days apart) with [^{18}F]PBR06, acquired on a Siemens HR+ camera. High (HA) and mixed (MA) affinity binders for TSPO were included with eight HV (3 MA, 5 HA; 52.5±7.8 y) and nine ALS (3 MA and 6 HA; 61.6±11.2 y). In ALS subjects, upper motor neuron burden score was 13±9, and ALS functional rating scale score was 37±5. Arterial input function data were obtained in 13 subjects (7 HV, 6 ALS), venous samples were collected between 60-90 min in 3 subjects (1 HV, 2 ALS), and blood was unattainable in 1 ALS subject.

[^{18}F]PBR06 images were normalized to Montreal Neurological Institute atlas space and time-activity curves were extracted to evaluate the following regions: frontal (inferior, mid, superior, precentral gyrus and orbital), parietal and temporal (inferior and superior lateral and mesial) cortices, anterior and posterior cingulate, cerebellum, brainstem and thalamus. Invasive measures included V_T, estimated over 90 min using the 2-tissue compartment model (2T), and tissue to plasma ratio (C_T/C_P) evaluated between 60-90 min. Non-invasive measures included SUV (60-90min) and SUVr (60-90 min). For SUVr, whole brain (WB), occipital cortex (OC) and corpus callosum (CC) pseudo-reference regions were evaluated based on having the smallest difference in SUV between groups. Between ALS and HV groups across measures, percent difference was computed and averaged across regions and differences were tested using a 2-tailed unpaired t-test (p=0.05). T-RT reliability across measures was described with mean difference (i.e., bias) and typical error (i.e., variability) assessed globally (averaged across regions) and in the precentral gyrus (motor cortex).

Results:

Global T-RT bias and variability, respectively, were smaller for non-invasive (SUVr CC: 0% and 3%, SUVr WB 1% and 2% and SUV: -4% and 7%) as compared with invasive (C_T/C_P: 12% and 10% and V_T: -8% and 7%) measures, and was similar in the motor cortex. SUV differences in pseudo-reference regions between ALS and HV subjects were 1% in CC, 8% in WB and 10% in OC (not used for further analysis). Averaged across regions, uptake was higher in ALS than in HV for: V_T (65% MA, 5% HA), C_T/C_P (68% MA, 4% HA), SUV (18% MA, 4% HA), SUVr CC (11% MA, 9% HA), but not for SUVr WB (0% MA, 2% HA), shown in Fig. 1. Group differences were significant in several regions and were outside of test-retest typical error ranges, using a 95% confidence limit (CI), for MA binders with V_T, C_T/C_P, SUV, and SUVr CC and HA binders with SUVr CC only.

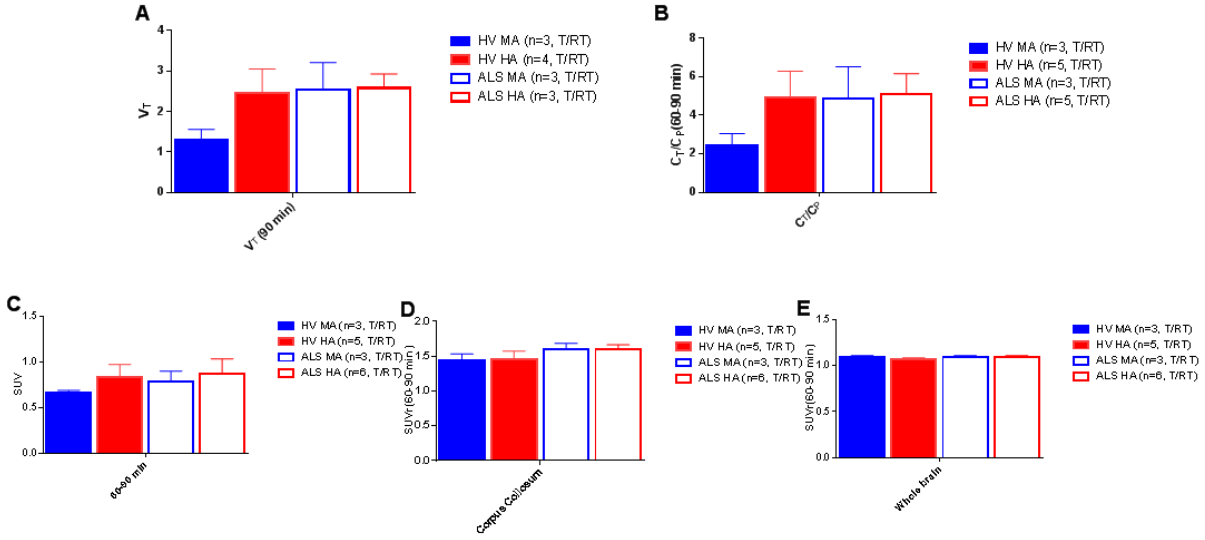

Fig 1 [^{18}F]PBR06 summary for HV and ALS mixed (MA) and high (HA) affinity binders with A) V_T over 90 min and between 60-90 min for B) tissue to plasma ratio (C_T/C_P), C) SUV, and SUVr to D) corpus callosum and E) whole brain averaged across test and retest (T/RT) in the regions examined. Error bars are SD.

Discussion:

The current findings with [^{18}F]PBR06 suggest higher TSPO levels in ALS vs HV subjects across measures; however, differences were small in high binders. Interestingly, binding status was more apparent in HV than ALS subjects with invasive measures. T-RT reliability was good, with higher variability using invasive quantification, mainly attributed to noise in blood measurements. Observed differences in [^{18}F]PBR06 blood measures with binding status (i.e., higher parent fraction, plasma to blood ratio and parent in plasma in MA binders) are important to consider when interpreting invasive modeling outcomes between cohorts. SUV can be used, but does not correct for genotype as with SUVr. SUVr WB showed no group differences, whereas SUVr CC was most sensitive to detecting differences that were outside of T-RT error limits (95% CI).

Acknowledgements

Dr. Kevin J. Felice, D.O. from the Hospital for Special Care (New Britain, CT) for ALS subject recruitment.

References:

[1] Zurcher N, Loggia M, Lawson R et. al. [2015], *Neuroimage Clinical*, 7:409-414

[2] Albrecht D, Normandin M, Shcherbinin S et al. [2018], *Journal of Nuclear Medicine*, 59(1):107-114.

P111
Preliminary Imaging of Neuroepigenetics in Huntington's Disease

HD Rosas[1], AB Sidwell[2], I Gonzalez[2], C Lois[2], JM Hooker[2], C Wang[2], JC Price[2].

Department of Neurology[1] and Radiology[2] Massachusetts General Hospital, Athinoula A. Martinos Center for Biomedical Imaging, Harvard Medical School, Charlestown, MA, USA

Introduction:

Histone deacetylases (HDACs) are a family of epigenetic enzymes that regulate gene expression in the human brain by chemically modifying chromatin (removing acetyl groups from histone tails), a fundamental network of proteins and DNA in chromosomal structure. HDAC expression in the brain has been evaluated by groups investigating the molecular mechanisms underlying neuropsychiatric disorders and neurodegeneration, including Huntington's Disease (HD). The goal of this work is to perform a first evaluation of the magnitude and distribution of regional HDAC expression *in vivo*, in HD, using positron emission tomography (PET) and [^{11}C]Martinostat, an imaging probe selective for class I HDACs (isoforms 1-3).

Materials & Methods:

[^{11}C]Martinostat PET and MR imaging were simultaneously acquired using a Siemens BrainPET PET/MR. Imaging began 60 minutes after radiotracer injection (Patients: 4.97±0.13 mCi; Controls: 5.39±0.31 mCi) and data were acquired for 30 minutes. Seven control subjects (57±4.9 years) and seven HD patients (60.9±6.2 years) were studied. T1-weighted MRI data were used for PET/MR co-registration and regional parcellation was performed using Freesurfer software. HDAC binding was evaluated for several volumes-of-interest: brainstem, caudate, putamen, pallidum, occipital, thalamus, pre-central gyrus, cuneus, and cortical white matter. The [^{11}C]Martinostat image data were averaged over 60-90 min post-injection and SUVR tissue ratios were computed by normalizing the regional SUV value by the whole brain SUV value.

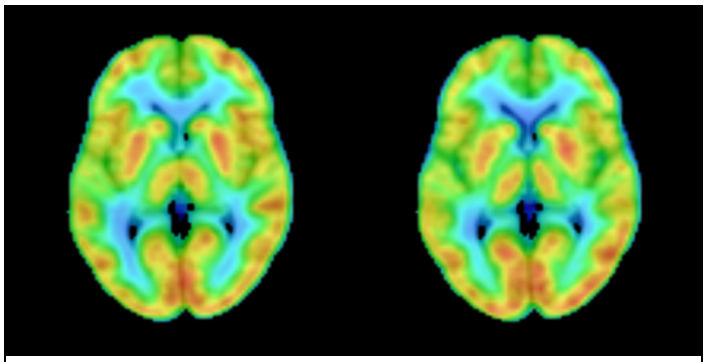

Figure 1. Average [^{11}C]Martinostat SUVR images for 7 Control (Left) and 7 Huntington Disease subjects (Right). Images are overlaid on MRI and image display ranges from 0-2 SUVR units.

Results:

No group differences were noted for age or injected dose. The regional rank order of [^{11}C]Martinostat binding was consistent with that previously observed in healthy control subjects [1], with putamen > occipital and cuneus > pallidum and thalamus and pre-central gyrus > caudate. The lowest [^{11}C]Martinostat binding was observed in cortical white matter and brain stem. The regional

SUVR values (normalized to whole brain uptake) ranged from about 0.7 - 1.5. Lower regional SUVR values were observed in the caudate region of HD patients (relative to controls). Correlation between caudate SUVR and age (n=14) did not reach statistical significance.

Discussion/Conclusion:

The results of this preliminary study support the use of [^{11}C]Martinostat to study epigenetic mechanisms in Huntington's Disease patients relative to control subjects. The caudate SUVR values observed in patients are inconclusive given the small sample size, but consistent with previous literature regarding HD pathology and atrophy. Greater sample sizes will enable interpretation of group differences, along with careful future consideration of age- and disease-related atrophy.

Acknowledgements: This work was supported by NIH grants R21NS098407, R21AA025192, and R21AG051931.

References:

[1] Wey H-Y et al. 2016. Sci. Transl. Med. 8(351): 351ra106.

P112

Mapping alteration of dopaminergic neurons in a rat model of Parkinson Disease through the comparison of the presynaptic PET tracers, [^{18}F]-LBT999 and 6-[^{18}F]fluoro-L-m-tyrosine

Pauline Roost, Francesco Gubinelli, Mylène Gaudin, Martine Guillermier, Noémie Cresto, Leopold Eymin, Charlène Josephine, Marie-Claude Gaillard, Alexis Bemelmans, Yann Bramoullé, Emmanuel Brouillet, Philippe Hantraye, Nadja Van Camp

Commissariat à l'Energie Atomique et aux Energies Alternatives (CEA), Direction des Recherches Fondamentales (DRF), Institut de Biologie François Jacob,

MIRCen, F-92260 Fontenay-aux-Roses, France and Centre National de la Recherche Scientifique (CNRS), Université Paris-Sud, UMR 9199, Neurodegenerative Diseases Laboratory, F-92260 Fontenay-aux-Roses, France

Introduction:
The pathological features of Parkinson's Disease (PD) are mainly driven by the loss of the dopaminergic projection neurons in the substantia nigra (SN) resulting in a dopamine (DA) deficiency in the striatum [1]. We developed a pathologically relevant rodent PD model; overexpressing the mutant (A53T) human alpha-synuclein protein in the SN [2]. Our aims are triple: 1- map neuronal loss and DA deficiency over time using two different presynaptic PET tracers, 2- evaluate the respective sensitivity of each radioligand, and 3- correlate individual PET data to behavioural and histological results.

Materials & Methods:
A total of ten rats were unilaterally injected in the SN with a viral vector (AAV2/6) overexpressing mutated (A53T) human alpha-synuclein, and were studied either at 6 weeks post-injection (6wpi, n=6, 543±36g) or 12wpi (n=4, 573±40g). PET imaging was performed using a ligand substrate for AADC, 6-[18F]fluoro-L-m-tyrosine ("FMT", 60min acquisition, 31.3-60.8MBq; pre-treatment by IP injection of 10mg/kg benserazide 30' before imaging [3]), or a ligand for DA transporter (DAT), [18F]-LBT999 [4] ("LBT", 90min acquisition, 40.3-63.0MBq). For behaviour, rats were subjected for 5 minutes to the cylinder test, in which contralateral and ipsilateral paw use was compared. After the *in vivo* studies rats were sacrificed for histological studies using tyrosine hydroxylase immunohistochemistry. From LBT and FMT PET scans, quantitative uptake images (BPnd and Ki, respectively) were calculated using Logan and Patlak graphical methods, with the cerebellum as a reference. Unilateral AAV injections allowed the contralateral striatum to serve as internal control. Paired student t-test were used to compare the contra- and ipsilateral sides in imaging studies, while an ANOVA was used to compare contralateral paw use to a control group.

Results:
Injection of benserazide was not effective in 42% of the animals, thus Ki values could not reasonably be estimated for FMT. Additionally, Ki images showed more non-specific binding than LBT BPnd images. At 6wpi we did not observe any asymmetry in the Ki of quantifiable scans (n=5, p=0.084, Fig 1A, D), however LBT data show decreased BPnd in the ipsilateral caudate putamen (n=6, p=0.027; Fig 1B, D). At 12wpi we observed a similar pattern (Ki, n=2, p=0.336; BPnd, n=4, p=0.003; Fig 1A, B, D). These results are in concordance with the behavioural observations, showing roughly only 30% use of the contralateral forepaw at 8wpi (n=7, p=0.044) and 12wpi (n=8, p=0.045; Fig 1C). No significant correlations between PET data and behaviour were observed. Histological comparisons are still ongoing.

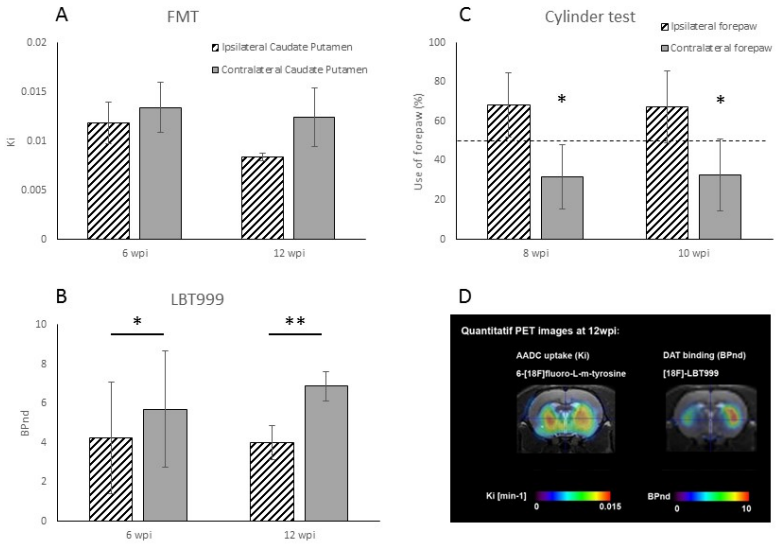

Fig 1: Positron emission tomography and behavioural studies. PET scans were obtained from α-syn-A53T rats at 6wpi and 10/12wpi, using a tracer substrate of AADC (18F-FMTyr) (A), or a dopamine transporter ligand (DAT, 18F-LBT999) (B). (A) Neither at 6wpi (n=5) nor at 12wpi (n=2) a difference was observed in AADC metabolism (FMT). (B) In contrast the DAT tracer (LBT999) showed a significant difference at 6wpi (n=6) and 12wpi (n=4). (C) Cylinder tests at 8wpi (n=7) and 10wpi (n=8) detected motor deficits in α-syn-A53T overexpressing rats. (D) Representative PET images of both tracers.

Discussion/Conclusion:

We created an AAV rat model of PD that shows progressive DA deficiency and neuronal loss detectable by FMT and LBT PET imaging. Our parametric data suggest that the DAT tracer is more sensitive to detect a mild PD phenotype as compared to the AADC tracer. This phenomenon has previously been described, and is possibly due to a combination of reduced nerve terminal DAT binding sites and downregulation of DAT in surviving neurons, in an attempt to increase DA availability [5]. More FMT scans will have to be done to increase numbers and compensate for ineffective benserazide blocking. Further analysis of PET data will allow correlating PET data to behavioural and histological measurements.

Acknowledgements:

This project has been funded by the European Union Horizon 2020 Programme (H2020-MSCA-ITN-2015) under the Marie Skłodowska-Curie Innovative Training Network and Grant Agreement No. 676408.

References:

1. Dauer W. and Przedborski S. [2003], Neuron, 39(6): p. 889-909.
2. Cresto N. et al. [2017], Neurodegener Dis 2017;17(suppl 1):8-590 – Page 448, 2017.
3. Becker G. et al. [2017] J Neurochem, 141(4):626-635.
4. Serriere S. et al. [2014] Nucl Med Biol, 41(1): p. 106-13.
5. Arena J. and Stoessl A. [2016] Relat Disord, 22 Suppl 1: p. S47-51.

P113
Preclinical evaluation of [^{18}F]GE387, a novel 18 kDa translocator protein (TSPO) PET radioligand with low binding sensitivity to human polymorphism rs6971

Nisha K. Ramakrishnan[1], Emily Fisher[1], Luxi Qiao [1], David J. Williamson[1], Matthew Hird[1], E. Hirani[2], S. Luthra[2], W. Trigg[2], Franklin I. Aigbirhio[1]

[1] Molecular Imaging Chemistry Laboratory, Wolfson Brain Imaging Centre, University of Cambridge, [2] GE Healthcare, Amersham,

Introduction:

18 kDa translocator protein receptors (TSPO), are upregulated in activated microglia, hence are biomarkers for neuroinflammation. However, the established TSPO radioligand, [^{11}C](R)-PK11195, suffers from high non-specific binding and difficult radiosynthesis, while second-generation radiotracers have variability in binding affinity due to a genetic polymorphism of the TSPO gene (rs6971), which makes their use challenging for quantitative imaging[1]. A novel compound (GE387) has been shown to have low binding sensitivity to this polymorphism and hence has the potential to be applied to TSPO PET imaging. Therefore, in our study, we aimed to perform preclinical PET imaging evaluation of this compound.

Materials & Methods:

Time dependent uptake of racemic [^{18}F]GE387, [^{18}F]*(S)*-GE387 and [^{18}F]*(R)*-GE387 in the brain of naive male Wistar rats (n=3 each) were measured over 60min using a preclinical PET scanner. Specific binding of [^{18}F](S)-GE387 was investigated in rats (n=3) pretreated with (R)-PK11195 (1mg/kg, i.p). Arterial blood sampling was performed to measure the time course of the radiotracer in the plasma. Radioactive metabolites in plasma were analysed using radio-TLC and radio-HPLC. A biodistribution study of brain and peripheral organs was performed at the end of the scan. Logan graphical analysis was used to estimate total volume of distribution (V_T) in the whole brain.

Results:

Initial metabolite analysis of the racemic mixture indicated the presence of a polar metabolite in plasma that does not cross the blood brain barrier and is excreted in urine. However, analysis of the individual enantiomers indicated the possible presence of a metabolite that entered the brain in the case of [^{18}F]*(R)*-GE387. Biodistribution data shows higher uptake of [^{18}F]*(S)*-GE387 in the olfactory bulb compared to the striatum as expected in healthy naive animals. The uptake of [^{18}F]*(S)*-GE387 in TSPO rich peripheral organs was blocked by (R)-PK11195 pretreatment. Whole brain V_T was also significantly reduced by the (R)-PK11195 pretreatment.

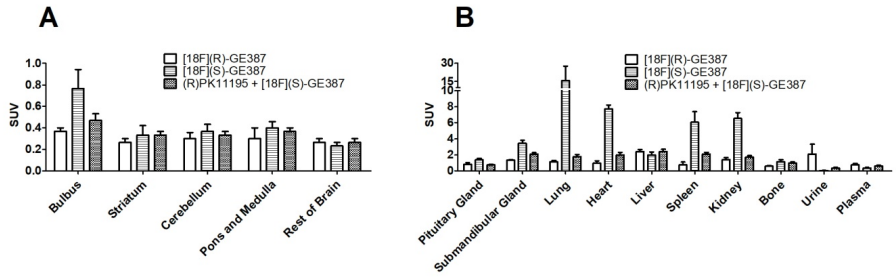

Figure 1: Biodistribution of [^{18}F]*(S)*-GE387 with and without pretreatment with (R)-PK11195, and [^{18}F]*(R)*-GE387 in brain (A) and peripheral organs (B)

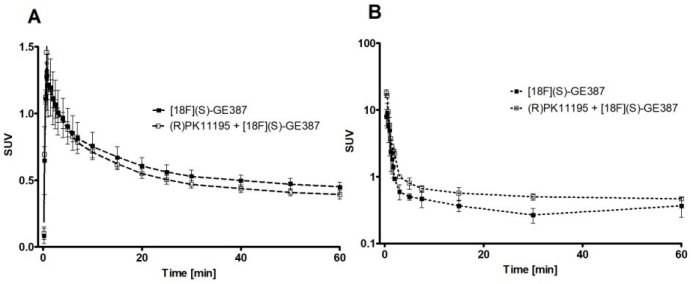

Figure 2: Brain and plasma time-activity curves of [^{18}F]*(S)*-GE387 with and without (R)-PK11195 pretreatment

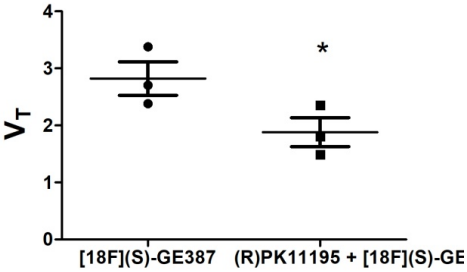

Figure 3: Total volume of distribution of [^{18}F]*(S)*-GE387 with and without (R)-PK11195 pretreatment, estimated using Logan graphical analysis

Discussion/Conclusion:

Preliminary results from this ongoing study indicates that [^{18}F]GE387 enters the brain and the uptake of [^{18}F]*(S)*-GE387 in the whole brain can be blocked by pretreatment with (R)-PK11195. Based on the metabolite profile and distribution, [^{18}F]*(S)*-GE387 appears to be a better candidate than [^{18}F]*(R)*-GE387. Studies are ongoing to further understand the differing metabolite profiles of these enantiomers.

References:

1. Owen *et al*., [2011], *J. Nucl. Med*. 52:24.

P114

Two for the price of one: voxelwise “bandpass" spectral analysis of [^{11}C]Ro15-4513 PET reveals bidirectional GABA$_A$ receptor subunit expression changes in temporal lobe epilepsy

Colm J. McGinnity[a, b, c, †], Daniela A. Riaño Barros[a, b, †], Rainer Hinz[d], James F. Myers[a], Siti N. Yaakub[c], Rolf A. Heckemann[e], John S. Duncan[f], Josemir W. Sander[f, g], Anne Lingford-Hughes[a], Matthias J. Koepp[f], Alexander Hammers[a, b, c, f, h].

[a] Imperial College London, London, UK; [b] MRC Clinical Sciences Centre, London, UK; [c] King’s College London, London, UK; [d] University of Manchester, Manchester, UK; [e] MedTech West, Gothenburg University, Sweden and Institute of Clinical Sciences, Gothenburg University, Sweden; [f] UCL Institute of Neurology, London, UK and Chalfont Centre for Epilepsy, Chalfont St Peter, UK; [g] Stichting Epilepsie Instellingen Nederland (SEIN), Heemstede, Netherlands; [h] Neurodis Foundation, Lyon, France; [†] These authors contributed equally.

Introduction:

Gamma-aminobutyric acid (GABA) A receptors that contain the α5 subunit mediate tonic inhibition, and are widely expressed in the limbic lobes. In animal models, expression of the α5 subunit is reduced in epilepsy (Schwarzer et al., 1997), whereas other α subunits are inconsistently altered. However, as epilepsy patients often have memory problems, and α5 antagonism is promnestic (Sternfeld et al., 2004), α5 binding might be increased. [^{11}C]Ro15-4513 binds with high affinity to α5-subunit-containing receptors and with lower affinity to those containing other α subunits. We compared GABA$_A$ α5 subunit binding in participants with temporal lobe epilepsy (TLE) with that of healthy controls, using ‘bandpass’ exponential spectral analysis.

Materials and Methods:

Eleven participants with MRI-normal TLE (seven males; median age 40 years, range 32–64 years) and 23 healthy male controls (median age 49 years, range 36–61 years), had a 90-minute PET scan after bolus injection of a median dose ± interquartile range of 450±45 MBq of [^{11}C]Ro15 4513, as previously described (McGinnity et al., 2017). Participants with TLE were seizure-free for a median of six (range 1 – 304) days. Data were acquired on a Siemens/CTI ECAT EXACT HR+ 962 camera, with arterial blood sampling, and reconstructed using filtered backprojection.

Voxelwise “bandpass” exponential spectral analyses (SA; (Lingford-Hughes et al., 2016)) were used to calculate fast-component ($0.00137s^{-1}$–$0.1s^{-1}$; “α1/α2/α3”), and slow-component ($0.00063s^{-1}$–$0.00137s^{-1}$; “α5”) volumes-of-distribution (V_Ts). These boundaries were selected based on inspection of spectra derived from the α5-rich hippocampus and the occipital lobe, which has considerable non-α5 binding (Myers et al., 2017). Groupwise comparison of V_Ts was made at the global, regional (limbic lobes, via MAPER (Heckemann et al., 2010)) and voxel levels (SPM12) after resolution recovery via iterative SFS-RR (McGinnity et al., 2013). For ROI and voxel analyses, participants with TLE were x-flipped so the epileptogenic side appeared on the right for all; eight randomly selected controls were also x-flipped. A5 V_Ts were also compared for each individual patient (versus 23 controls), at the voxel level.

Results:

Patients had non-significantly higher global “α5” V_T (3.48±0.87, controls 3.10±0.78, p=0.10). After linear regression to control for a correlation with specific activity (ρ=0.43, p=0.01), there was no significant difference in residual global “α1/α2/α3” V_T between groups (TLE 0.08±0.43, controls 0.03±0.26, p=0.41).

At the regional level, the TLE group had visibly but non-significantly higher “α5” (p>0.37) and slightly lower “α1/α2/α3” V_Ts (p>0.05) than controls in the limbic lobes (Figure 1). Significant negative correlations were observed between the log-transferred interictal interval and the “α5” V_Ts in the limbic lobes (left/contralateral ρ=-0.67/p=0.02; right/ipsilateral ρ=-0.66/p=0.03). There were no significant correlations with the limbic lobe “α1/α2/α3” V_Ts (p>0.38).

On voxelwise analyses, the TLE group had significantly higher “α5” V_T in the anterior cingulate gyri and medial temporal lobes (maximal in the contralateral hippocampus; 3560 mm^3 cluster, p_{FWE}=0.02). After linear regression to control for a correlation with specific activity the TLE group had extra-temporal clusters of both significantly higher and lower fast component V_Ts. On individual comparisons, 8/11 participants with TLE had clusters of significantly increased “α5” V_T, which were largely bilateral.

Discussion/Conclusion:
Bandpass SA revealed bidirectional alterations of $GABA_A$ receptor alpha subunit binding in MRI-normal TLE, with bilaterally increased limbic lobe “α5” V_T in particular revealed by voxelwise analyses. Our results are consistent with dynamic alterations in α5 subunits, increasing after spontaneous epileptic seizures. Where tissue kinetics permit, bandpass SA can be used to distinguish binding to different targets. This may allow re-investigation of other tracers with selectivity for more than one target.

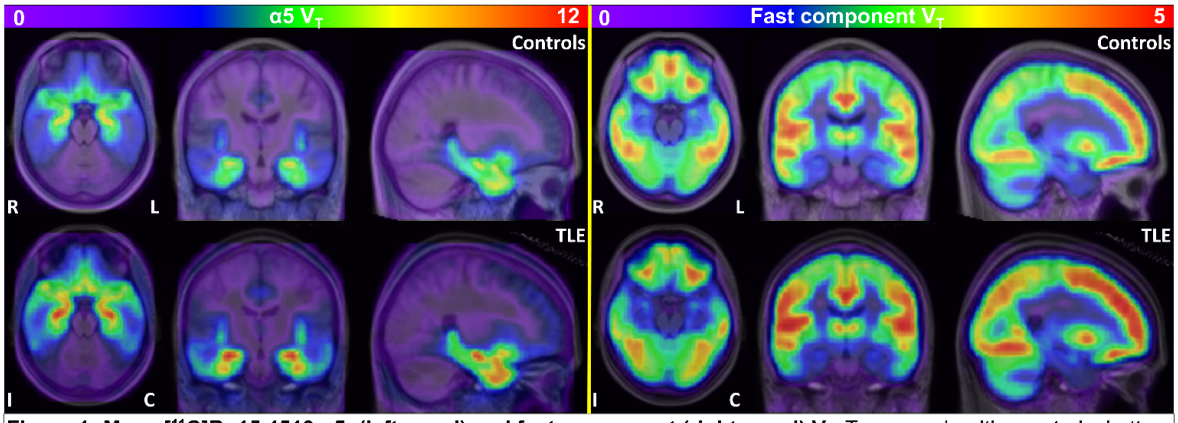

Figure 1: Mean [^{11}C]Ro15 4513 α5- (left panel) and fast component (right panel) V_T. Top row – healthy controls; bottom row – TLE group.

References:

Heckemann, R.A., Keihaninejad, S., Aljabar, P. et al. [2010], *Neuroimage*, 51:221-7.
Lingford-Hughes, A., Myers, J., Watson, B. et al. [2016], *NeuroImage*, 132:1-7.
McGinnity, C.J., Riano Barros, D.A., Rosso, L. et al. [2017], *NeuroImage*, 152:270-282.
McGinnity, C.J., Shidahara, M., Feldmann, M. et al. [2013], *Neuroimage*, 79:72-80.
Myers, J.F., Comley, R.A., Gunn, R.N. [2017], *J Cereb Blood Flow Metab*, 37:2137-48.
Schwarzer, C., Tsunashima, K., Wanzenbock, C. et al. [1997], *Neuroscience*, 80:1001-17.
Sternfeld, F., Carling, R.W., Jelley, R.A. et al. [2004], *J Med Chem*, 47:2176-9.

P115
[^{11}C]raclopride – long term reliability and extrastriatal validity

Jonas Svensson[1], Martin Schain[1,2], Pontus Plavén-Sigray[1], Mikael Tiger[1], Christer Halldin[1], Johan Lundberg[1]

[1] Department of Clinical Neuroscience, Center for Psychiatry Research, Karolinska Institutet and Stockholm County Council, SE-171 76 Stockholm, Sweden;
[2]Neurobiology Research Unit, Copenhagen University Hospital, Copenhagen, Denmark

Introduction:

[^{11}C]raclopride is an established radioligand for quantification of dopamine D_2 receptor (D_2R) binding in striatum. In extrastriatal regions, where the receptor density has been estimated to 1/100 of that of striatum, the signal to noise ratio for [^{11}C]raclopride binding have been considered unreliable [1]. However, a recent [^{11}C]raclopride test-retest study showed high reliability in extrastriatal regions, including thalamus and cortex [2].
In order to employ a radioligand in clinical studies, it is important to confirm both reliability and validity. Long term (>2weeks) test-retest studies can be used to evaluate the reliability as well as the variability of outcome measures, such as binding potential (BP_{ND}), in a setting relevant for clinical applicability. A common method for assessing the validity of the PET signal in vivo is to use a blocking agent to examine displaceability and thus specificity for the target protein. The objectives of this study were to 1) replicate the previous published long-term test-retest findings, and 2) evaluate displacement of the extrastriatal [^{11}C]raclopride binding using the D_2R antagonist quetiapine.

Material and Methods:

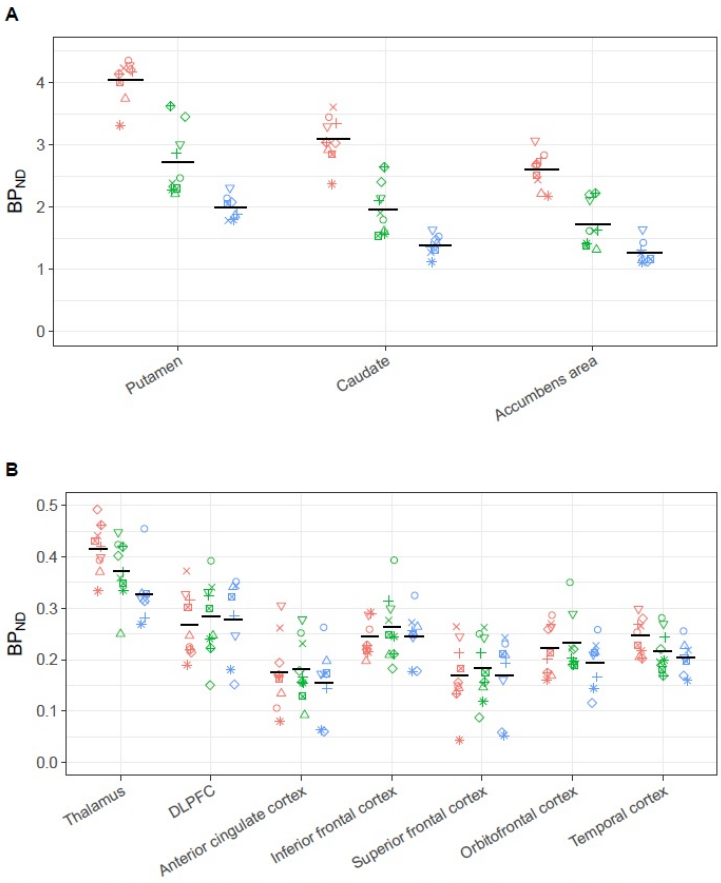

Figure 1. Raw data. Striatum in A). For each ROI three examinations, in order from left to right: Baseline (red); Quetiapine XR (green); Quetiapine IR (blue). Horizontal bars representing mean BP_{ND}. B) Extrastriatal ROIs, same order of examinations. DLPFC = dorsolateral prefrontal cortex.

Two groups of healthy controls were examined with PET and [^{11}C]raclopride. To test long-term reliability, nine subjects were examined twice with a mean interval of 22 days between PET experiments. Reliability was quantified using the mean absolute percentage difference between first and second examination (APD). To confirm extrastriatal displaceable binding of [^{11}C]raclopride, eleven subjects were examined three times: at baseline and after administration of two different formulations of quetiapine: extended release (XR) and immediate release (IR), both 300mg. Displacement was defined as significant difference in baseline experiment BP_{ND} compared to the respective quetiapine pretreatment experiments using paired t-test ($p<0.05$). Occupancy was calculated as mean percentage change of [^{11}C]raclopride BP_{ND} from baseline. Difference in occupancy between different regions of interest (ROIs) was tested with paired t-test.
FreeSurfer 6.0 was used on T1-weighted MR-images to delineate regions of interest (ROIs), see Figure 1

for a list of ROIs. BP_{ND} was estimated using the simplified reference tissue model (SRTM) with cerebellar cortex as reference region.

Results: In putamen, APD was 3.71%; in thalamus 16.6%; and in cortical regions 12.9-58.9%. Significant displacement of [^{11}C]raclopride binding was seen in all striatal ROIs as well as in temporal cortex (TC) and thalamus, but not in any other examined ROIs (Figure 1). In putamen the highest occupancy of quetiapine was 50.6±4.1% (mean±S.D.); thalamus 19.5±16.6%; TC 17.8±16.8%. The occupancy in TC and thalamus was significantly lower compared to putamen, both after IR and XR pretreatment.

Discussion:
Long term test-retest reliability for BP_{ND} in striatum was in line with previous studies [2,3]. In extrastriatal regions, the reliability was generally poor. Our results do not support previous reports stating that raclopride can be reliably quantified in extrastriatal regions.

Furthermore, in most cortical ROIs our data show a BP_{ND} around 0.2 that could not be displaced, suggesting little to no specific signal. BP_{ND} in thalamus and TC were significantly decreased after pretreatment with quetiapine, but the level of occupancy was significantly lower compared to striatum.
We see two possible explanations for these results: 1) different occupancy of quetiapine in different regions, or 2) spatially varying non-specific binding (V_{ND}). Several studies using high affinity radioligands have shown that quetiapine has similar or higher D_2R occupancy in cortex compared to striatum [4]. We therefore suggest that [^{11}C]raclopride have a systematically lower V_{ND} in cerebellar cortex compared to cerebral regions. This would violate an assumption of the reference tissue model resulting in an inflated BP_{ND}, more pronounced in regions with lower density of D_2R [5].
Our findings indicates that use of [^{11}C]raclopride to quantify D_2R outside of striatum is highly problematic. Strong caution is in general warranted for applying reference tissue models on data where the difference in binding between reference and target is small.

References

1. Farde L, Pauli S, Hall H, et al. [1988] *Psychopharmacology (Berl)*; 94: 471–478.
2. Alakurtti K, Johansson JJ, Joutsa J, et al. [2015] *J Cereb Blood Flow Metab*; 35: 1199–1205.
3. Hietala J, Någren K, Lehikoinen P, et al. [1999] *J Cereb Blood Flow Metab*; 19: 210–7.
4. Kessler RM, Ansari MS, Riccardi P, et al. [2006] *Neuropsychopharmacology*; 31: 1991–2001.
5. Salinas CA, Searle GE, Gunn RN. [2014] J *Cereb Blood Flow Metab*; 35: 304–311

P116
Evaluation of the new CB_2R radioligand: a PET study with ^{18}F-FC024 in rhesus monkeys

Sylvain Auvity[1, 2, 3], Fabien Caillé[4], Maud Goislard[4], Jérôme Cayla[4], Françoise Hinnen[4], Stéphane Demphel[4], Bertrand Kuhnast[4] and Marie-Anne Peyronneau[4]

[1] Inserm, U1144, Paris, F-75006, France
[2]Université Paris Descartes, UMR-S 1144, Paris, F-75006, France
[3]Université Paris Diderot, UMR-S 1144, Paris, F-75013, France
[4]UMR 1023 IMIV, Service Hospitalier Frédéric Joliot, CEA, Inserm, Université Paris Sud, CNRS, Université Paris-Saclay, Orsay, France

Introduction:

Neuroinflammation is a key process occurring during several diseases such as multiple sclerosis, Alzheimer's or Parkinson's diseases. Upregulation of the cannabinoid type 2 receptors (CB_2R) in activated microglia during neuroinflammation is a relevant biomarker which can be sensitively and quantitatively monitored by positon emission tomography (PET) imaging [1].

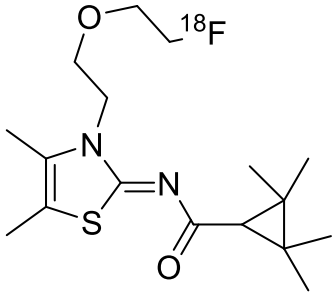

We have recently synthetized and characterized ^{18}F-FC024 ((Z)-N-(3-(2-(2-fluoroethoxy)ethyl)-4,5-dimethylthiazol-2(3H)-ylidene)-2,2,3,3-tetramethylcyclopropane-1-carboxamide) (Fig.1) as a promising CB_2R radiotracer for PET imaging neuroinflammation in rats [2]. In the course of translating this tracer to clinical trials, we report herein a preliminary evaluation of this radiotracer in healthy rhesus monkeys.

Figure 1: Chemical structure of ^{18}F-FC0324

Material and Methods:

Four male rhesus monkeys (9.5 ± 2.8 kg) were included in this study. Two PET scans were performed in each animal with a minimum rest period of two weeks. Dynamic cerebral PET scans were acquired during 120 minutes under propofol anaesthesia after radiotracer injection in a sural vein (218.1 ± 29.5 MBq), including the measurement of arterial input function corrected for radiometabolites and binding to plasma proteins. A 3D T1-weighted (T1-w) image was also acquired prior to PET study with a 1.5T MRI scanner for each subject allowing for segmentation of several brain regions. Whole brain and regional total volume of distribution (V_T) were estimated using logan plot analysis and PMOD software (version 3.8; PMOD Technologies Ltd.). The test-retest variability (within subject variability) was calculated for whole brain V_T.

Results:

In plasma, unchanged ^{18}F-FC0324 rapidly decreased with time and accounted for 7.2 ± 2.3 % of radioactivity 120 min after radiotracer injection (Fig. 2). ^{18}F-FC0324 was converted into four main polar radiometabolites. Binding to plasma protein was important with a free fraction for ^{18}F-FC024 of 2.8 ± 0.8 %.

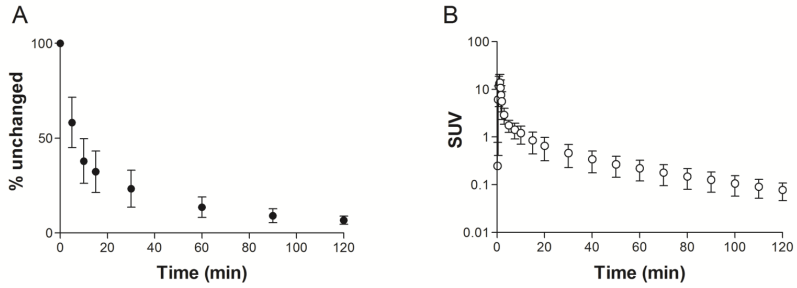

Figure 2: (A) Percentage of parent fraction evolution over time in plasma, (B) Arterial input function corrected for radiometabolites. Data are expressed as mean ± SD.

Within the brain, time-activity curves (TACs) of ^{18}F-FC024 rapidly increased, with a pic at 2-3 min, followed by a fast wash-out from the brain. Radioactivity was homogenous throughout the cerebral parenchyma, with no significant difference in regional V_T ($p>0.05$) (Fig. 3). Whole brain distribution of ^{18}F-FC024 estimated by Logan plot graphical analysis was 1.6 ± 0.4 mL.cm^{-3}. The within-subject variability of whole brain V_T was 26.4 %.

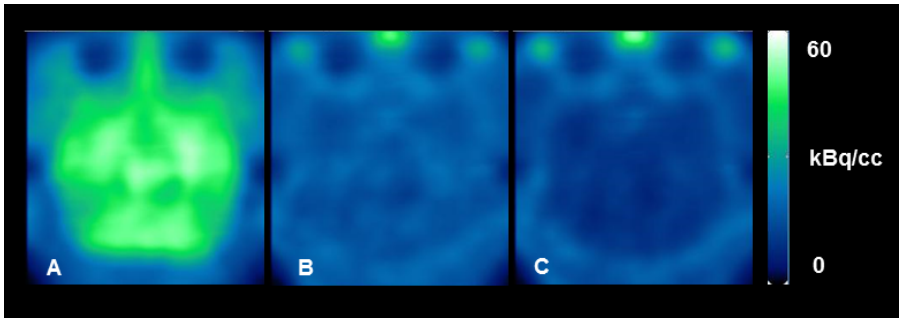

Figure 3: Representative PET images for one subject, summed from (A) 0 to 40 min, (B) 40 to 80 min and (C) 80 to 120 min.

Discussion/Conclusion:

We have previously demonstrated that ^{18}F-FC024 was a promising tracer to perform in vivo CB_2R PET imaging. This preliminary evaluation in non-human primate demonstrated that ^{18}F-FC024 is able to cross the blood-brain barrier with a low retention in the brain in accordance with the cerebral level of expression of the CB_2R in healthy animals. Blocking and displacement experiments using unlabeled FC024 and specific ligands for each subtype of cannabinoid receptors are currently ongoing. Whole body scans with dosimetry evaluation is also currently being performed.

Acknowledgments: The authors thank the InMiND research consortium (HEALTH-F2-2011-278850) for financial support.

References

[1] Evens N, Bormans G M [2010] Curr. Topics Med. Chem. 10: 1527-1543
[2] Caillé F, Cacheux F, Peyronneau M-A et. al. [2017] Mol. Pharm. 14: 4064-4078

P117
The Influence of Amphetamine Sensitization on the Binding Potential of [^{11}C]-(+)-PHNO to Dopamine $D_{2/3}$ receptors: A Study in Healthy Humans

Ana Weidenauer (1), Ulrich Sauerzopf (1), Martin Bauer (1,2), Lucie Bartova (1), Lukas Nics (3), Verena Pichler (3), Cecile Philippe (3), Sarah Pfaff (3), Markus Mitterhauser (3,4), Wolfgang Wadsak (3,5), Siegfried Kasper (1), Rupert Lanzenberger (1), Nicole Praschak-Rieder (1), Matthäus Willeit (1)

(1) Medical University of Vienna, Department of Psychiatry and Psychotherapy, Division of General Psychiatry
(2) Medical University of Vienna, Department of Clinical Pharmacology
(3) Medical University of Vienna, Department of Biomedical Imaging und Image-guided Therapy, Division of Nuclear Medicine
(4) Ludwig-Boltzmann-Institute Applied Diagnostics, Vienna
(5) Center for Biomarker Research in Medicine CBmed, Graz

Introduction:
Repeated administration of a constant dose of amphetamine leads to increased behavioral effects such as euphoria, alertness and openness and to enhanced amphetamine-induced dopamine release. This phenomenon is termed sensitization and can be observed in patients with schizophrenia without previous exposure to stimulants. Sensitization of the dopamine system is regarded as part of the underlying neurobiology of the disorder comprising increased dopamine synthesis capacity and disturbances of functional and structural brain networks (1). The amphetamine sensitization model of schizophrenia and the utilization of positron emission tomography with the dopamine $D_{2/3}$ agonist radioligand [^{11}C]-(+)-PHNO, the current gold standard for measuring changes of extracellular dopamine, might therefore serve as a tool to extend the knowledge on dopaminergic alterations in schizophrenia.

Materials and Methods:

To investigate the effect of amphetamine sensitization on non-displaceable [^{11}C]-(+)-PHNO binding potentials (BP_{ND}) twenty healthy stimulant-naive subjects (12 female, 12 male) underwent two positron emission tomographies: a baseline scan followed by two amphetamine sensitization visits, and, two weeks after, another scan 90-120 min. after an oral amphetamine challenge (0.03mg/KG bodyweight). [^{11}C]-(+)-PHNO BP_{ND} were extracted with ROMI from putamen, caudate, ventral striatum, globus pallidus and substantia nigra/ventral tegmental area using the simplified reference tissue model SRTM-2 with the cerebellum as reference region. Behavioral effects of amphetamine were recorded using the Drug Effects Questionnaire (DEQ) and the Subjective States Questionnaire (SSQ) in regular intervals. Dopamine release was calculated as ($BP_{ND}^{baseline} - BP_{ND}^{amphetamine}$) / $BP_{ND}^{baseline}$ *100. Baseline BP_{ND} values and amphetamine induced changes in BP_{ND} were compared with two-sided t-tests, significance level was set at $p < 0.05$.

Results:

As expected amphetamine led to significant reduction of [^{11}C]-(+)-PHNO BP_{ND}. After compared to before sensitization there was a higher amphetamine-induced reduction of BP_{ND} in all

regions with significant results in the putamen (14% vs. 19.8% displacement, $p<0.05$) and in the ventral striatum (12.8% vs. 20.6% displacement, $p<0.05$). Higher baseline BP_{ND} was observed in the ventral striatum after compared to before sensitization. Sensitization on a neurochemical level was paralleled by an increased behavioral response after sensitization on the SSQ items “focused”, “outgoing” and “lively” ($p<0.05$).

Discussion:

Comparable to previous data we observed significant amphetamine-induced displacement of [^{11}C]-(+)-PHNO (2) and a significant sensitization on a neurochemical and behavioral level after repeated amphetamine administration in healthy subjects (3). We furthermore observed increased $D_{2/3}$ receptor binding in the ventral striatum after sensitization, which might be an indicator of compensatory self-regulation of dopamine receptors. When compared to data of patients with schizophrenia, the amphetamine sensitization protocol might help elucidate important pathophysiological mechanisms in schizophrenia.

Acknowledgements:

This study was funded by the Austrian Science Fund FWF [Proj. No. P23585-B09], the Anniversary Fund of the Austrian National Bank [Proj. No.16723], the Medical Scientific Fund of the Mayor of Vienna (Medizinisch-Wissenschaftlichen Fonds des Bürgermeisters der Bundeshauptstadt Wien) [Proj. No. 15189], and the Vienna Science and Technology Fund (WWTF) [CS15-033] granted to M.W.

References:

(1) Weidenauer A, Bauer M, Sauerzopf U et.al. [2017] The International Journal of Neuropsychopharmacology;20(1):1-10.

(2) Willeit M, Ginovart N, Graff A, et al. [2008] Neuropsychopharmacology ;33(2):279-89

(3) Boileau I, Dagher A, Leyton M, et al. [2006] Archives of General Psychiatry 2006;63(12):1386-95. doi: 10.1001/archpsyc.63.12.1386

P118
Quantification of striatal serotonin transporter occupancy using reduced PET/MR scan time and [^{11}C]DASB bolus plus constant infusion

Silberbauer L[1], Gryglewski G[1], Berroterán-Infante N[2], Rischka L[1], Vanicek T[1], Philippe C[2], Hienert M[1], Kautzky A[1], Pichler V[2], Godbersen GM[1], Komorowski A[1], James GM[1], Hartenbach M[2], Wadsak W[2, 3], Mitterhauser M[2,4], Hacker M[2], Kasper S[1], Hahn A[1], Lanzenberger R[1]

[1]*Department of Psychiatry and Psychotherapy, Medical University of Vienna*

[2]*Department of Biomedical Imaging and Image-guided Therapy, Division of Nuclear Medicine, Medical University of Vienna*

[3]*Center for Biomarker Research in Medicine (CBmed), Graz, Austria*

[4]*Ludwig Boltzmann Institute Applied Diagnostics, Vienna Austria*

Introduction:

In-vivo quantification of the serotonin transporter (SERT) is among the most promising biomarker candidates in the field of neuropsychiatric disorders. Using the highly specific radioligand [^{11}C]DASB and dynamic PET data is considered state-of-the-art in the quantification of cerebral SERT [1]. While this method yields reliable measures of *in-vivo* SERT expression, applicability is hampered by the elaborate and sophisticated procedure of kinetic modeling and the economic pressure to reduce scan time. Here, we refined a recently introduced approach using [^{11}C]DASB bolus plus constant infusion aiming to reduce scan time and thereby increasing efficiency of SERT imaging [2].

Materials & Methods:

7 healthy volunteers underwent both two PET/MR (SIEMENS mMR) and two PET (GE advance) scans after double blind application of 7.5 mg citalopram or saline solution. During PET/MR scans [^{11}C]DASB was applied as bolus plus constant infusion (mean dosage = 10.7 ± 0.86 MBq/kg). PET scans started simultaneously with a bolus injection of [^{11}C]DASB (mean dosage = 4.9 ± 0.22 MBq/kg) resulting in a total acquisition time of 90 minutes. For PET scans the non-displaceable binding potential (BP_{ND}) was calculated using the multi-linear reference tissue model (MRTM2) [3]. For PET/MR BP_{ND} was calculated using data acquired between 110 and 115 minutes after start of tracer application as follows: $BP_{ND} = (V_T - V_{ND})/V_{ND}$ using average activity at tracer equilibrium [4]. Occupancies were calculated as the relative decrease in BP_{ND} between saline and citalopram scans. Bias was calculated as the difference in occupancy between scans divided by the value of the bolus measurement.

Results:

Occupancies calculated from striatal BP_{ND} were highly correlated between PET and PET/MR scans (r = 0.94, ICC = 0.74) (Figure). Compared to SERT occupancy derived from PET scans, occupancy obtained from PET/MR scans was underestimated by an average of 8%.

Conclusion:

Striatal occupancy of SERT can reliably be obtained with a dramatically reduced scan time of 5 minutes performed 110 minutes after start of [^{11}C]DASB bolus plus constant infusion and simple quantification models. Occupancy measures are consistent with data obtained from standard protocols comprising 90 minutes of scan time. This approach might help to overcome limitations that are imposed by long time spans of scanning and aid the transition of SERT imaging to clinical practice.

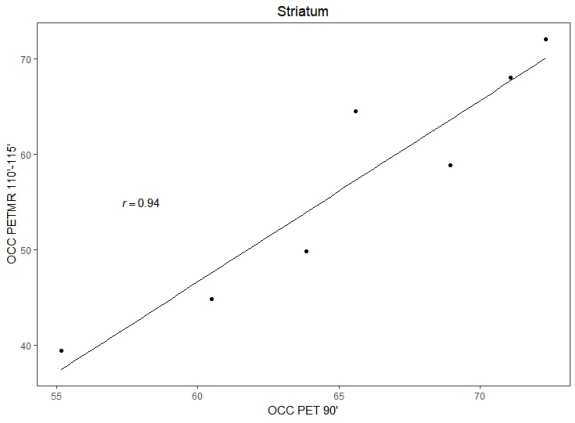

Figure: Scatter plot of occupancies obtained from PET/MR [11C]DASB bolus plus infusion scans and PET bolus scans.

References

1. Ginovart N, et al. [2001], J Cereb Blood Flow Metab, 21(11): 1342-53
2. Gryglewski G, et al. [2017], Neuroimage, 149: 23-32
3. Ichise M, et al. [2003], J Cereb Blood Flow Metab, 23(9): 1096-112
4. Innis R.B, et al. [2007], J Cereb Blood Flow Metab 27(9): 1533-9

Acknowledgements: Gryglewski G. and Rischka L. are recipients of DOC Fellowships of the Austrian Academy of Sciences at the Department of Psychiatry and Psychotherapy, Medical University of Vienna. This study was performed with the support of the Medical Imaging Cluster of the Medical University of Vienna, a grant from the Else Kröner-Fresenius-Stiftung (2014_A192) and funding by SIEMENS (CA-ID: C00214938/06).

P119
Amyloid-β load is related to worries in individuals with subjective cognitive decline

Sander C.J. Verfaillie[1,2], Tessa Timmers[1,2], Rosalinde E.R. Slot[2], Chris W.J. van der Weijden[1], Linda Wesselman[2], Niels D. Prins[2], Sietske A.M. Sikkes[2], Adriaan A. Lammertsma[1], Philip Scheltens[2], Rik Ossenkoppele[2], Bart N.M. van Berckel[1], Wiesje M. van der Flier[1,3]

Departments of [1]Radiology & Nuclear Medicine, [2]Neurology & Alzheimer Center, and [3]Epidemiology & Biostatistics, VU University Medical Center, Amsterdam, Netherlands. All authors are affiliated with Amsterdam Neuroscience

Background:
Self-perceived cognitive decline is associated with an increased risk of AD.[1] The majority of individuals with subjective cognitive decline (SCD), however, do not harbor preclinical AD. The aim of this study was to investigate whether amyloid-β load is associated with a specific pattern of cognitive complaints.

Methods:
We included 106 SCD memory-clinic patients (mean±SD age: 64±8, 45%F) with [^{18}F]florbetapir PET scans from the ongoing SCIENCe study. Mean cortical amyloid-β binding potential (BPnd) was derived from 90-minutes dynamic PET scans using optimized receptor parametric mapping (RPM). We used following questionnaires to assess SCD: cognitive change index (CCI, self-reported& informant; 2x20 items), subjective cognitive functioning (SCF), and the two closed questions “Do you have memory complaints?” (response: memory, attention, organization, language complaints “yes/no”), and “Does this worry you?”. We used the Rivermead Behavioral Memory Test (RBMT)-Stories (delayed recall) and the Rey Auditory verbal learning test (Dutch version; delayed recall) to assess delayed memory performance. Additionally, we calculated a self-awareness index (Z-transformed delayed memory performance minus self-reported CCI [i.e. complaint severity>memory performance]), and a self-proxy index (z-transformed self- minus informant-reported CCI). We used linear regression analyses, adjusted for age, sex and education, to investigate associations between amyloid BPnd (independent variable) and measures of SCD (dependent variables). Standardized betas were reported if $p<0.05$.

Results:
Increased mean cortical amyloid-β load was associated with worries (Figure 1; Beta=0.53, p=0.03), but not with the CCI (informant and self-reported, total scores or individual items) or SCF. Additionally, we found that higher amyloid-β load was associated with a higher self-awareness index (figure 2) based on the RBMT (Beta=0.25, p=0.01), but not with the self-awareness index based on the RAVLT (Beta=0.20, p=0.05) or self-proxy index (Beta=0.15, p=0.14).

Conclusions:
Our results suggest that amyloid-β load is associated with worries and higher degree of insight, but not with severity or specific pattern of cognitive complaints. These findings suggest that worries about self-perceived cognitive decline is the strongest indicator of preclinical AD, while other items seem less sensitive.

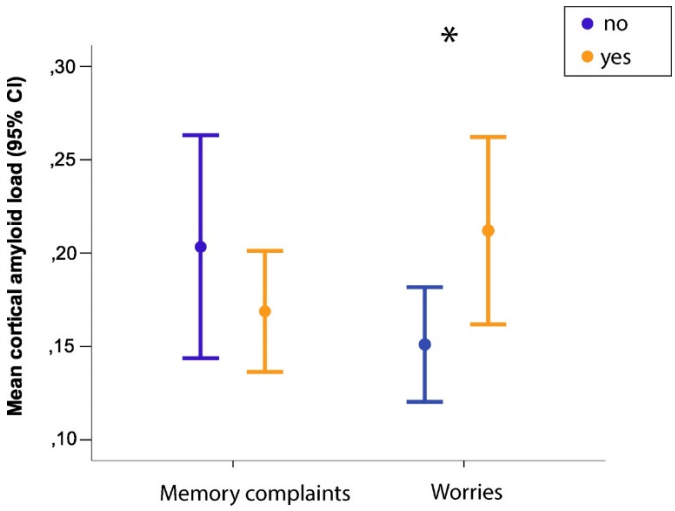

Figure 1. Mean cortical amyloid-beta load stratified for memory complaints (yes/no) and worries (yes/no). *p<0.05$_{FDR}$

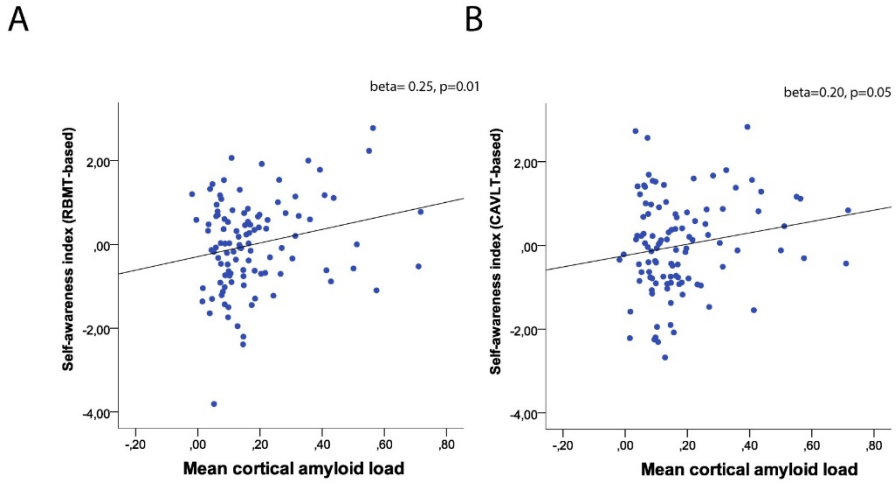

Figure 2. Associations between mean cortical amyloid load and self-awareness indexes based on the RBMT (A) and RAVLT (B) delayed recall. Self-awareness index; a positive beta estimate reflects a positive association between amyloid and higher self-awareness (subjective impairment more severe than objective impairment).

P120
[^{18}F]-AV-1451 binding quantification in AD using SUVr: choosing the optimal time window

Catriona Wimberley[1], Julien Lagarde[1,2], Pauline Olivieri[1,2], Bertand Kuhnast[1], Fabien Caillé[1], Philippe Gervais[1], Irène Buvat [1], Marie Sarazin[1,2], **Michel Bottlaender**[1,3]

[1] *UMR 1023 IMIV, Service Hospitalier Frédéric Joliot, CEA, Inserm, Université Paris Sud, CNRS, Université Paris-Saclay, Orsay, France.*

[2] *Unit of Neurology of Memory and Language, Université Paris Descartes, Sorbonne Paris Cité, INSERM UMR S894, Centre Hospitalier Sainte Anne, Paris, France.*

[3] *UNIACT, Neurospin, CEA, Gif-sur-Yvette, F-91191, France*.

Introduction :

AV-1451 binds selectively to neurofibrillary tangles in Alzheimer's disease (AD). The radiotracer [^{18}F]-AV-1451 has been shown to have increased binding in PET scans of AD patients. Several quantification methods have been proposed (Barret et al. 2017, Golla et al. 2017, Baker et al. 2016) and a correlation has been found between the SUVr and gold standard binding parameter estimates from compartmental modelling. However, it has been shown that the SUVr from the acquisition windows used (80-100 or 110-130 min) are not in a pseudo-equilibrium for subjects with AD, meaning that they could be unreliable depending on the level of binding. The later time points are more likely to be in equilibrium but are often disregarded due to the higher level of noise. The aim of this work was to apply denoising techniques to allow the use of the later time window and to compare the SUVr with the earlier acquisition window.

Materials & methods:

Six amyloid-positive (PIB-index >1.45) Alzheimer patients and 5 amyloid-negative age-matched healthy volunteers were included. [^{18}F]-AV-1451 was synthesized on site with precursor supplied by Avid Radiopharmaceuticals (Philadelphia, USA). PET scans were performed on a HRRT camera (Siemens) for two acquisition windows (70-120 and 180-220 min after 370 MBq tracer injection) and five minute frames images were reconstructed using OSEM with PSF correction. The images were then denoised using a principal components analysis with the first 2 components used and the rest were discarded as noise (PIXIES, http://www.apteryx.fr/).

For all images (original and denoised), voxel-vise SUVr kinetics images were generated with the cerebellum gray matter as the normalisation region. PET images were co-registered with 3D T1 MRI images (3 Tesla, PRISMA, Siemens) and VOIs were defined using AAL atlas segmentation warped to the T1 MRI and corrected for atrophy by intersecting AAL regions with gray matter. The regional SUVr from the early (80-100 min) and late acquisition (190-220 min) windows were compared and the percentage difference between them calculated.

Results:

The coefficient of variation of the SUVr was calculated for all VOIs for the patients before and after denoising. The average coefficient of variation was reduced by 38 % for the late frames using the denoising.

In healthy controls, the SUVr appears stable between the 2 windows (mean regional variation: 6.2±5.7%; fig 1 dotted line). In AD patients, SUVr increases during the early acquisition window, and were higher at the later acquisition window (180-220 min; Fig 1), but are more stable (at pseudo-equilibrium) within the window. The % difference of SUVr between the two acquisition windows depended on the late SUVr: the higher the late SUVr, the larger the % difference. The underestimation was up to 60- 70 % in the structures with the highest [^{18}F]-AV-1451 uptake (Fig 2).

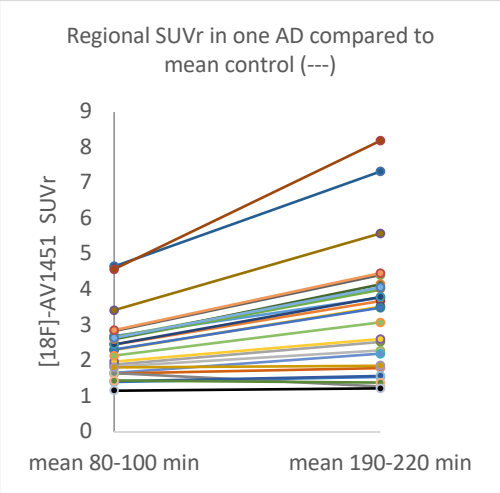

Fig 1.

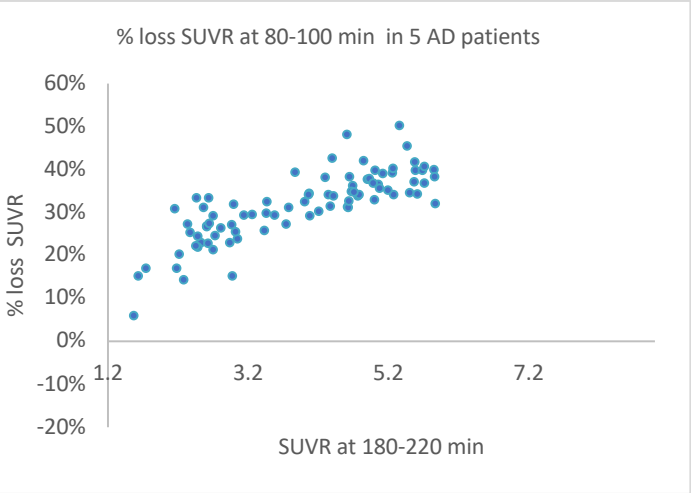

Fig 2.

Conclusion:

The SUVr from early time windows are underestimated when compared to the more stable SUVr at the late windows. This underestimation is not linear: the higher the late SUVr, the higher the loss of values at early times. The use of denoising greatly improves the stability of the SUVr calculated for the late time window, therefore allowing the use of the later time frame. This result should be taken into account, as the underestimation of the SUVr, especially in the structures presenting high tau burden, may alter the interpretation of the analyses in correlation studies.

References:

Golla S, Timmers T, Ossenkoppele et al. [2017],Mol.Imaging.biol 19 : 963-971

Barret O, Alagille D, Sanabria et al. [2016], Human amyloid Imaging

Baker S, Lockhart S, Price J et al. [2017], J. Nucl.Med. 58:332-338

P121
α4β2-nicotinic receptor availability in Parkinson's disease MCI and healthy controls: a pilot imaging study using [^{18}F]-XTRA PET

Kelly A. Mills, M.D., M.H.S,[a] Yong Du, Ph.D.,[b] Jennifer M. Coughlin, M.D.,[b,c] Andrew Horti, Ph.D.,[b] Martin Pomper, M.D, Ph.D.,[b] Gwenn Smith, Ph.D.,[c]

[a] *Department of Neurology, The Johns Hopkins University School of Medicine, Baltimore, Maryland, USA.*
[b] *Department of Radiology and Radiological Science, The Johns Hopkins University School of Medicine, Baltimore, Maryland, USA.*
[c] *Department of Psychiatry and Behavioral Sciences, Johns Hopkins Bloomberg School of Public Health, Baltimore, Maryland, USA.*

Introduction:

Cognitive dysfunction is observed in up to 24% of newly diagnosed Parkinson's disease (PD) patients[1] and is an independent contributor to poor quality of life.[2] Discovery of biomarkers specific to cognitive symptoms is an essential step in the development and assessment of therapeutic strategies targeting PD-related cognitive impairment. The neurobiology of cognitive impairment in PD is multifactorial, but there is substantial evidence for a role of disordered cholinergic signaling at nicotinic receptors.[3, 4] Elucidating the role of nicotinic cholinergic signaling in PD has been challenging due to the relatively low affinity of the available radiotracers for imaging of cortical regions involved in cognition.[4, 5] We hypothesized that a radiotracer with higher affinity to cortical and hippocampal α4β2-nicotinic cholinergic receptors[6, 7] would be reduced in regions associated with PD-related cognitive deficits, including the anterior and posterior cingulate, pre-frontal cortex, mesial temporal cortex/hippocampus, and precuneus in PD patients compared with age- and gender-matched controls

Materials and Methods:

Seven subjects with Parkinson's disease of moderate severity (Hoehn & Yahr 2.5-3), mean age 6.85 years, mild cognitive impairment (PD-MCI level I criteria) or normal cognition, and no use of anticholinergic medications underwent brief cognitive assessment with the Montreal Cognitive Assessment (MoCA) and then underwent a 120 minute PET scan on the High Resolution Research Tomograph after injection of 3.70e+8 Bq (10 mCi) of [^{18}F]XTRA, after withholding dopaminergic medications for at least 12 hours. PMOD v3.7 was used for motion correction and PET-MRI co-registration. Cortical and hippocampal (extrathalamic) regions of interest were selected based on previously described associations between these regions and typical cognitive deficits in PD. Tracer kinetic modeling used the Logan graphical method with metabolite-corrected arterial input function to calculate regional total distribution volumes (V_T). These data were compared to those from three age-matched healthy controls without MCI or Parkinson's disease.

Results:

[^{18}F]XTRA V_T in the extrathalamic ROI's did not differ between healthy controls and PD patients regardless of MCI status. V_T tended to be lower in PD-MCI patients compared to healthy controls or when compared with PD-normal cognition (PD-NC). When comparing healthy controls and PD-MCI patients, [^{18}F]XTRA V_T was 19.4% lower in the hippocampus, 28.5% lower in the anterior cingulate, and 17.4% lower in the posterior cingulate (Figure 1), but none of these differences were statistically significant. In comparing cortical and hippocampal α4β2-nicotinic receptor availability in PD-MCI patients and PD-NC patients, the anterior cingulate V_T was significantly lower (23.2%, p=0.048) in the PD-MCI patients, while the hippocampus, anterior and posterior cingulate, parietal cortex, and precuneus tended to be lower in the PD-MCI group as well (12.5%, 23.2%, 16.1%, 13.3%, and 13.7%, respectively (Figure 2)). Among patients with PD, total MoCA score correlated with VT in the anterior cingulate (r=0.7739, p=0.041, Figure 3), which appeared to be the strongest ROI-MoCA correlation

Figure 1. [18F]XTRA V_T in age-matched healthy controls and patients with PD-MCI.

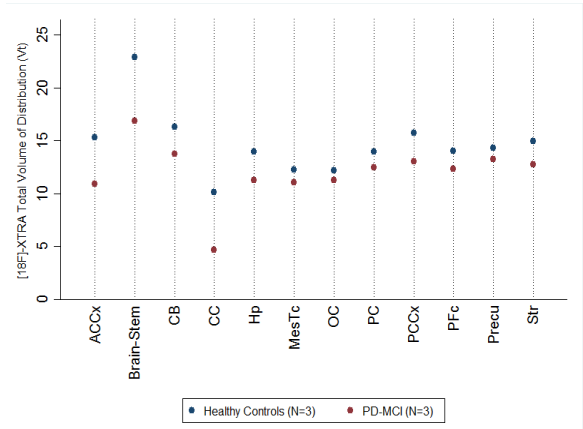

Figure 2. [18F]XTRA V_T in PD patients with- and without PD-MCI.

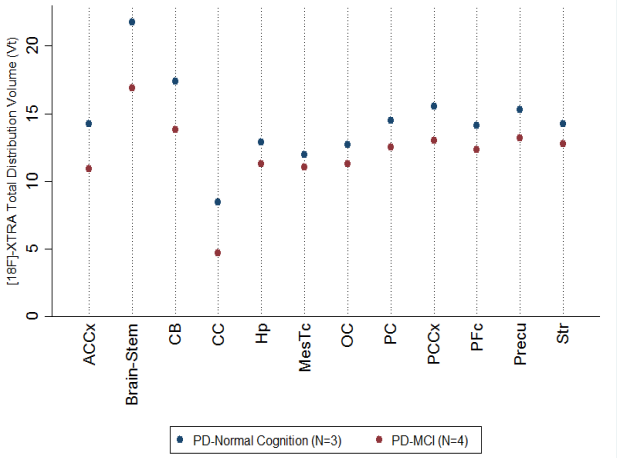

Figure 3. Correlation between anterior cingulate V_T and MoCA score in 7 subjects with PD.

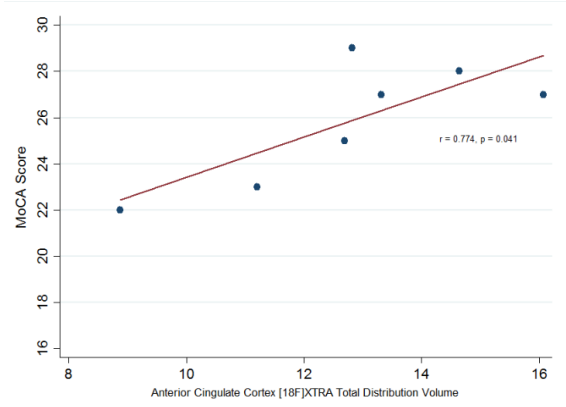

Discussion: As a measure of cortical and hippocampal (extrathalamic) α4β2-nicotinic receptor availability, these preliminary data support further studies of [18F]XTRA as a possible marker of cognitive impairment in PD. Future studies will focus on scanning more patients and evaluating the relationship between regional [18F]XTRA and specific cognitive tests.

Acknowledgements: This work was supported by the National Center for the Advancement of Clinical and Translational Research [KL2 scholar fund (KL2TR001077), as part of parent grant to Johns Hopkins (UL1TR001079)] and and is now funded by the NINDS/NIH (1K23NS101096-01A1). The authors thank all the participants for their donated time.

1. Muslimovic D, Post B, Speelman JD, Schmand B. Cognitive profile of patients with newly diagnosed Parkinson disease. Neurology 2005;65:1239-1245.

2. Lawson RA, Yarnall AJ, Duncan GW, et al. Severity of mild cognitive impairment in early Parkinson's disease contributes to poorer quality of life. Parkinsonism Relat Disord 2014;20:1071-1075. 4194347

3. Rinne JO, Myllykyla T, Lonnberg P, Marjamaki P. A postmortem study of brain nicotinic receptors in Parkinson's and Alzheimer's disease. Brain Res 1991;547:167-170.

4. Meyer PM, Strecker K, Kendziorra K, et al. Reduced alpha4beta2*-nicotinic acetylcholine receptor binding and its relationship to mild cognitive and depressive symptoms in Parkinson disease. Arch Gen Psychiatry 2009;66:866-877.

5. Isaias IU, Spiegel J, Brumberg J, et al. Nicotinic acetylcholine receptor density in cognitively intact subjects at an early stage of Parkinson's disease. Front Aging Neurosci 2014;6:213. 4132266

6. Kuwabara H, Gao Y, Stabin M, et al. Imaging alpha4beta2 Nicotinic Acetylcholine Receptors (nAChRs) in Baboons with [18F]XTRA, a Radioligand with Improved Specific Binding in Extra-Thalamic Regions. Molecular imaging and biology : MIB : the official publication of the Academy of Molecular Imaging 2017;19:280-288.

7. Coughlin JW, Kuwabara H, Wang Y, et al. [18F]XTRA: first-in-human PET imaging of α4β2 nicotinic acetylcholine receptors. J Nucl Med 2015;56.

P122
SPECT Imaging and brain retention of recombinant bispecific and unmodified antibodies in an amyloid beta mouse model

Tobias Gustavsson[1], Stina Syvänen[1], Dag Sehlin[1]

[1]*Department of Public Health and Caring Sciences, Uppsala University, Uppsala, Sweden*

Introduction:

Antibodies are an attractive alternative in molecular imaging due to their high target specificity compared to small molecules. For an antibody to be successful as a radioligand for neuroimaging it must be able to pass the blood-brain barrier (BBB) to reach its brain parenchymal target. Antibodies can be engineered to actively bind to receptors at the BBB, e.g. the transferrin receptor (TfR), to enable receptor mediated transcytosis across the BBB. In this project, we have evaluated long-term brain retention and distribution of a bispecific antibody targeting Aβ protofibrils and the TfR, RmAb158-scFv8D3, in comparison with unmodified RmAb158.

Materials and methods:

RmAb158-scFv8D3 and RmAb158 were labeled with iodine-125 (^{125}I) and administered i.v. to tg-ArcSwe and WT mice, aged 18-24 months. Blood pharmacokinetics were evaluated over a period of 27 days and SPECT scans were performed at 6, 14 and 27 days. Brain was isolated following SPECT scanning and radioactivity was measured *ex vivo.* Autoradiography was performed on 20 µm brain sections to investigate antibody intrabrain distribution while Aβ pathology was examined with Aβ immunohistochemistry.

Results:

[^{125}I]RmAb158-ScFv8D3 showed a faster blood clearance compared to [^{125}I]RmAb158. SPECT showed a considerably higher uptake and more uniform distribution of [^{125}I]RmAb158-scFv8D3 in the brain compared with [^{125}I]RmAb158. Antibody brain retention, expressed as percent of injected dose (%ID), was 0.8±0.25% and 0.3% at 3 days; 0.3±0.13% and 0.15% at 14 days; and 0.12±0.03% and 0.05±0.008% at 27 days for [^{125}I]RmAb158-scFv8D3 and [^{125}I]RmAb158, respectively. *Ex vivo* autoradiography of [^{125}I]RmAb158-scFv8D3 and [^{125}I]RmAb158 injected mice revealed that while RmAb158-scFv8D3 was uniformly distributed throughout the brain, coinciding with Aβ pathology, [^{125}I]RmAb158 was confined to central brain areas and a few high intensity hotspots in the brain parenchyma.

Conclusion:

The bispecific antibody RmAb158-scFv8D3 showed higher brain concentrations than unmodified RmAb158 at all studied time points after administration demonstrating the feasibility of TfR mediated transcytosis. In addition, the global distribution pattern in the brain parenchyma was fundamentally different between the two types of antibodies; RmAb158-scFv8D3 was detected throughout the brain in line with the abundant brain Aβ pathology while RmAb158 appeared in a more scattered pattern.

P123
In vitro characterisation of TDP-43 and Tau protein distribution in frontotemporal lobe dementia (FTLD) using [^{18}F] AV-1451 autoradiography, T-557 fluorescence microscopy and immunohistochemistry

David J. Williamson[1], Nisha Kuzhuppilly Ramakrishnan[1], James Rowe[2], John O'Brien[3] and Franklin I. Aigbirhio[1]

[1]Molecular Imaging Chemistry Laboratory, Wolfson Brain Imaging Centre and [2]Department of Clinical Neurosciences and [3]Department of Psychiatry, Cambridge Biomedical Campus, Cambridge, CB2 0QQ, UK.

Introduction:

FTLD is the second most common form of dementia in the under 65 age group and is characterised by focal atrophy in frontal and temporal lobes of the brain. Unlike Alzheimer's disease (AD), where deposits of abnormal brain beta-amyloid and tau proteins are characteristics hallmarks, there are different subtypes of FTLD. Most cases, the two most common are associated with either tau or TAR-DNA binding protein 43 (TDP-43). The radioligand [^{18}F]AV-1451 was developed as a positron emission tomography (PET) tracer with selectivity for tau neurofibrillary tangles in AD. The utility of [^{18}F] AV-1451 remains controversial, due to potential binding to non-Tau targets (e.g. neuromelanin and monoamine oxidase) and discrepancies between *in vivo* clinical data and *in vitro* studies on post mortem tissues. It has also been shown using PET that [^{18}F]AV-1451 binds in cases with the semantic dementia (Bevan Jones et. al., 2017) associated with TDP-43+ but not tau pathology at post-mortem. Here we investigated these clinicopatholgoical correlations using [^{18}F]AV-1451 autoradiography, fluorescence microscopy with the AV-1451 analogue T-557 and tau and TDP-43 immunohistochemistry on post-mortem FTLD brains *in vitro*.

Material and Methods:

All studies performed in this study used frozen 20 □m brain slices of frontal cortex from FTLD TDP43+/tau-, TDP43-/tau+, AD patients and healthy control tissue kindly provided by Cambridge University Hospital and King's College Brain Banks. Briefly, for autoradiography studies, samples were defrosted, washed in PBS/triton X100 buffer and incubated with [^{18}F]AV-1451 (0.2 MBq/slide) for 1 hour. Following a further wash and water dip samples were dried, opposed to a phosphor screen and left overnight. Subsequent images were produced using a phosphor imaging system and analysed using Aida software. For immunohistochemistry studies sections were incubated with acetone for 10 min, washed and the specific antibody to TDP-43 or tau (AT8) added and left overnight. The secondary antibody (Alexa Flour 555) was added for 1 hour, sections washed and prepared for fluorescence microscopy. Similarly for T-557 studies, sections were fixed, washed, incubated with T-557 (10□M) and analysed using fluorescence microscopy.

Results:

Immunohistochemistry with the tau antibody (AT8) revealed higher fluorescence in TDP43-/Tau+ over TDP43+/Tau- FTLD tissues confirming a) the correct pathological diagnosis of FTLD and b) retention of tau signal in FTLD TDP43-/tau+ post-mortem tissue (data not shown).

AD TDP-43+/Tau- TDP-43-/Tau+

Figure 1. [^{18}F]AV-1451 Autoradiography**.** In AD brain there was a clear and characteristic increase in [^{18}F]AV-1451 binding in frontal cortex. In FTLD brains there was reduced binding on both tissues and no obvious differences between FTLD tau+ and tau- sections.

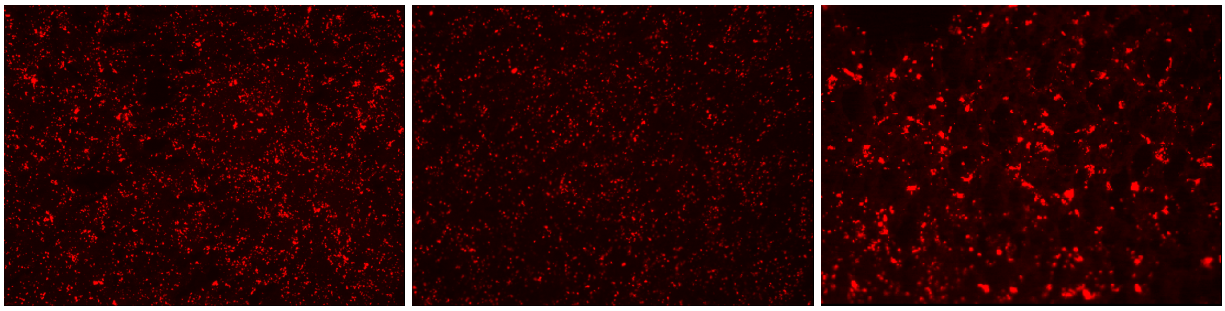

Control **TDP-43-/Tau+** **TDP-43+/Tau-**

Figure 2 Immunohistochemistry with TDP-43 antibody showed, as expected, an increase signal in TDP-43+/Tau- brain sections versus control and TDP-43-/Tau+ FTLD brain sections

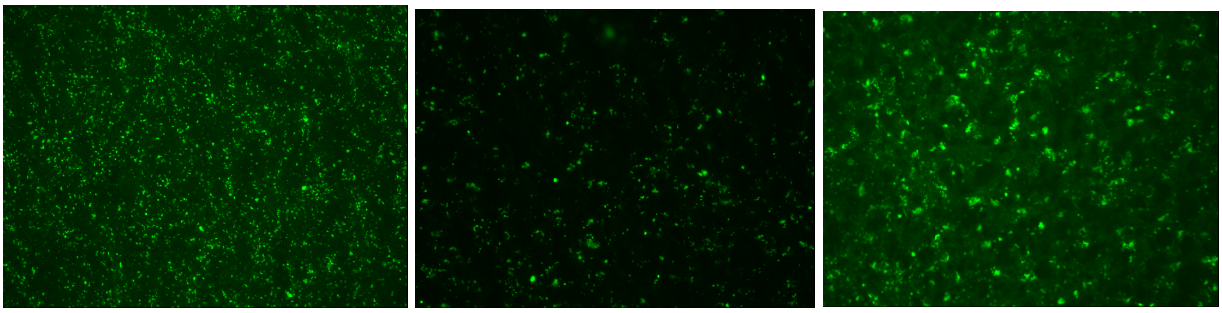

Control **TDP-43+/Tau -** **TDP-43-/Tau+**

Figure 3: Fluorescence microscopy with the AV-1451 analogue T-557 revealed an increased signal in TDP-43-/Tau+ versus control and TDP-43+/Tau- FTLD brain sections

Conclusions:

There was prominent [^{18}F]AV-1451 binding in AD, but less in FTLD tissue, with similar binding in TDP43+ and Tau+ tissue. There was reduced binding of T-557 in TDP-43+/Tau- negative versus TDP-43-/Tau+ tissues suggesting no binding to TDP-43 protein. The increased retention of [^{18}F]AV-1451 in clinical FTLD PET scans of patients with presumed TDP-43 but not tau pathology remains unexplained. It may represent binding of [^{18}F]AV-1451 to another pathological substrate closely associated with TDP-43, and further indicates the disparity between *in vivo* and in *vitro studies* on post mortem tissues as has previously been reported.

Acknowledgments:

The authors thank King's College and CUH brain banks for providing the brain sections used in this study

Reference:

Bevan-Jones WR, Cope TE, Jones PS, et al., [2017]. J. Neurol. Neurosurg. Psychiatry (in press).

P124
[^{18}F]Flutemetamol PET imaging reveals interaction between relative cerebral blood flow, fibrillar amyloid pathology and memory in non-demented elderly

Stephen F. Carter[1], **Rainer Hinz[1]**, C. Hardcastle[2], C. Amadi[2], Laura Parkes[2], Neil Pendleton[2], Karl Herholz[1]

[1] *Wolfson Molecular Imaging Centre, University of Manchester,UK*

[2] *Division of Neuroscience and Experimental Psychology, University of Manchester, UK*

Introduction:

There is extensive evidence that many elderly individuals >70 years old can harbour pathological quantities of fibrillar amyloid-beta (Aβ) pathology, a hallmark of Alzheimer's disease (AD), in their brains and remain cognitively normal. The present neuroimaging study investigated whether fibrillar amyloid pathology moderates the relationship between cerebral blood flow (CBF) and memory performance in a group of cognitively normal advanced elderly.

Subjects and Methods:

72 cognitively normal elderly, age= 84.7 ± 4.2 years, Mini-Mental State Examination (MMSE)= 28.8 ± 1.2, were included. All participants completed detailed cognitive testing including the Rey Auditory Verbal Learning Test. Dynamic [^{18}F]flutemetamol PET data (injected dose 185.7 ± 9.1 MBq) were acquired on a High Resolution Research Tomograph (Siemens) using the 'tea-break' protocol (30 min early emission scan, 60 min break, 20 min late emission scan). The Simplified Reference Tissue Model (SRTM) was used to generate parametric maps of relative delivery RI with cerebellum grey matter as reference tissue input [1]. From the target-to-reference region activity ratios of the late images, the study population was divided by the presence / absence of fibrillar Aβ pathology (Aβ+ ≥1.5 in a composite neocortical region). The Aβ+ (*n*= 36) and Aβ- (*n*= 36) groups were matched for age, sex and MMSE scores though the Aβ- group had more years of full time education (14.9 ± 3.1 years versus 13.4 ± 2.6 years, t= 2.3, $p < 0.05$). In addition, structural T1-weighted and pseudo-continuous arterial spin labelling (pcASL) MR images were acquired on a 3 Tesla Achieva (Philips).

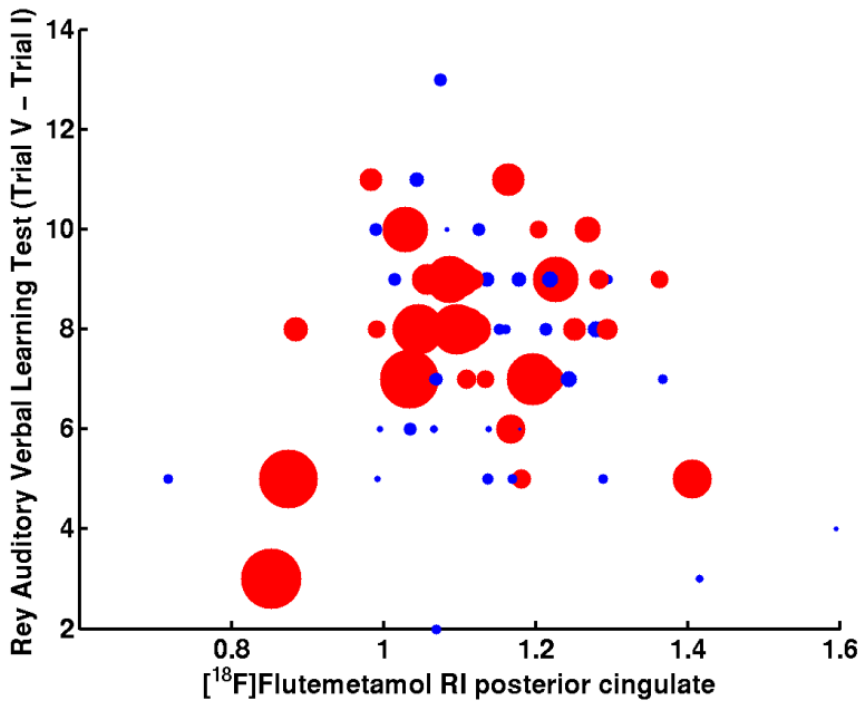

Results:

In the Figure, the size of the circles is proportional to the [^{18}F]flutemetamol target-to-reference region ratio with red circles indicating Aβ+ status and blue circles indicating Aβ- status. Across the whole population (*n*= 72) it was found that fibrillar Aβ moderated the effect between relative CBF and memory, as a significant interaction was found between SRTM RI in the posterior cingulate and the target-to-reference region activity ratio in the neocortical composite region.

Within the Aβ+ group alone (red circles, *n*=36) there was a significant interaction between SRTM RI in the hippocampus and parietal lobe and Aβ in the neocortical composite region. There were no significant interactions found in the Aβ- group. The results indicate that Aβ+ individuals with low Aβ have a negative association with relative CBF and memory such that, counter intuitively, Aβ+ individuals with lower relative CBF had better memory performance. When comparing CBF measures from each modality (SRTM RI [^{18}F]flutemetamol PET and pcASL MRI), only a moderate correlation (r= 0.51) was found.

Discussion:

A longstanding viewpoint is that preserved/higher relative CBF is associated with better cognitive performance. The present results challenge that idea, since it was found that Aβ moderated the relationship between CBF and memory performance. In Aβ+ individuals, higher [^{18}F]flutemetamol binding to Aβ and higher [^{18}F]flutemetamol delivery (SRTM RI) reflecting relative CBF were both associated with worse Rey Auditory Verbal Learning Test performance. The evidence suggests that there is an as yet poorly understood physiological process ongoing in non-demented individuals with transitional amounts of Aβ.

Further work is required to understand the moderate correlation between CBF measures acquired from the different imaging modalities (pcASL MRI versus amyloid PET SRTM RI) since the published MRI recommendations may not apply to the oldest old (> 80 years) [2].

Acknowledgements:

This work was primarily funded by the EU/EFPIA Innovative Medicines Initiative Joint Undertaking EMIF grant agreement n°115372. Funding was also received from GE Health Care in the form of FASTlab cassettes for the production of [18F]Flutemetamol.

References:

[1] Heurling K, Buckley C, Van Laere K, Vandenberghe R, Lubberink M (2015), Neuroimage 121: 184-192.

[2] Alsop DC, Detre JA, Golay X, Günther M, Hendriske K, *et al*. (2015), Magnetic Resonance in Medicine 73: 102-116.

P125
Comparison of *in vivo* [^{11}C]DED imaging and immunohistochemical *ex vivo* markers of astrogliosis in a mouse model of Alzheimer's Disease

Malin Olsen[1], Ximena Aguilar[1], Dag Sehlin[1], Xiaotian T Fang[1], Gunnar Antoni[2,3], Anna Erlandsson[1], **Stina Syvänen[1]**

[1]Department of Public Health and Caring Sciences/Geriatrics, Uppsala University, Rudbeck Laboratory, Dag Hammarskjölds väg 20, SE-751 85 Uppsala, Sweden
[2]Department of Medicinal Chemistry, Preclinical PET Platform, Uppsala University, Dag Hammarskjölds väg 20, SE-751 83 Uppsala, Sweden
[3]PET Centre, Uppsala University Hospital, Entrance 70, Sjukhusvägen 10, 75185 Uppsala, Sweden.

Introduction:

Astrocytes, the most abundant glial cell type in the nervous system, convert to a reactive inflammatory state as a response to neurodegenerative disorders in a process called "astrogliosis". Astrogliosis can be imaged using positron emission tomography (PET) radioligand deuterium-L-[^{11}C]deprenyl ([^{11}C]DED). [^{11}C]DED binds to enzyme monoamine oxidase-B (MAO-B) which is overexpressed in reactive astrocytes. The aim of this study was to investigate how *in vivo* quantification of astrogliosis using [^{11}C]DED corresponds to expression of glial fibrillary acidic protein (GFAP) and vimentin, i.e. two well-established markers of astrogliosis, during Aβ pathology progression in a mouse model of Alzheimer's disease (AD).

Materials and Methods:

Radioligand [^{11}C]DED was administered to 8 month old tg-ArcSwe, 8 month old WT, 16 month old tg-ArcSwe and 16 month old WT mice (n = 4-6 per group). Binding potential (BP_{ND}) using time-activity curves from the whole scan time of 30 min was obtained in hippocampus, striatum, thalamus and cerebral cortex using the simplified reference tissue model with cerebellum as a reference region. Immunohistochemistry was performed to evaluate amyloid-beta (Aβ) pathology and the expression of GFAP, vimentin, macrophage-associated lectin (Mac-2) and MAO-B in mice of 8 month, 12 month and 16 month (n = 4 tg-ArcSwe, n = 2 WT for each age group). To further analyze the protein concentration of GFAP and Aβ in tg-ArcSwe mice in relation to disease progression, sandwich ELISAs were performed in brain homogenates obtained from mice aged 2-16 months (n=4-5 per age group).

Results:

The intra-brain levels of aggregated Aβ and markers of astrogliosis were found to be elevated in tg-ArcSwe mice compared with WT mice. Immunohistochemistry showed that GFAP and vimentin expression increased with increasing Aβ pathology in tg-ArcSwe mice. [^{11}C]DED showed elevated binding of the same magnitude in tg-ArcSwe mice compared with WT mice at both 8 and 16 months. Thus, although presence of Aβ lead to increased BP_{ND} values already at an early disease stage, pathology progression did not lead to further

elevated BP_{ND} values. Immunohistochemistry also indicated that there was only limited co-expression of MAO-B and GFAP.

Conclusion:

MAO-B levels are increased early in Aβ pathology progression, while GFAP and vimentin appear to increase later, most likely as a consequence of abundant Aβ plaque formation. Thus, [^{11}C]DED can be used for the detection of changes in MAO-B, but does not measure the total extent of astrogliosis at advanced stages of Aβ pathology.

P126
Synthesis and characterization of heterocyclic sulfoxides: New reversibly binding radiotracers for positron emission tomography imaging of tau neurofibrillary tangles.

Waqas Rafique[1+], **Vasko Kramer**[2+], Tania Pardo[3], René Smits[4], Mona M. Spilhaug[1], Alexander Hoepping[4], Eduardo Savio[3], Henry Engler[3], Horacio Amaral[2], Patrick J. Riss[1,5,6]

[1]Realomics SFI, Kjemisk Institutt, Universitetet i Oslo, Sem Sælands vei 26, Kjemibygningen, 0371 Oslo, Norway. [2]Positronpharma SA, Santiago de Chile, Rancagua 878, Providencia, Chile. [3]Uruguayan Centre of Molecular Imaging (CUDIM), Av. Dr. Américo Ricaldoni 2010, 11600 Montevideo, Departamento de Montevideo, Uruguay. [4]Advanced biochemical compounds GmbH, Heinrich-Glaeser-Strasse 10-14, D-01454 Radeberg, Germany. [5]Klinik for Kirurgi og Nevrofag, Oslo Universitets Sykehus HF–Rikshospitalet, Postboks 4950 Nydalen, 0424 Oslo. [6]Norsk Medisinsk Syklotronsenter AS, Gaustad, Postboks 4950 Nydalen, 0424 Oslo

Introduction:

Neurodegeneration is a complex mechanism of diseases, which leads to dysfunction and death of the neurons. Neurodegeneration associated with dementia, specifically Alzheimers disease (AD) affects more than 7 million people in Europe only.[1]

Although noticeable neurological symptoms can be observed during progression of the disease, diagnosis is challenging. Significant research is ongoing to develop non-invasive and accurate means of early detection, and differentiation of pathologic hallmarks, albeit with mild to moderate success. Despite the promising results in clinical trials, the available generation of radiotracers confound with non-specific or off-target binding, blood-brain barrier (BBB) penetration and/or false positive evaluations due to interfering radio-metabolites.

The objective of current study was to prove the aptness of 2 benzimidazole analogues, named [^{18}F]Lansoprazole (^{18}F-LSP) and [^{18}F]*N*-methyl Lansoprazole (^{18}F-NML), which are previously known to target the neurofibrillary tangles (NFTs) *ex vivo,*[2] through first-in-man evaluation using PET. In addition, a library of compounds was designed with aim to identify new ligands, with possibility to label the formation of neurofibrillary tangles (NFTs) in high specificity, and could potentially be labeled with the PET nuclides ^{18}F and/or ^{11}C for in vivo evaluation.

Material and methods:

First-in-man PET studies with both ^{18}F-LSP and ^{18}F-NML were performed. 4 healthy elderly controls (mean age 60,2±6,0 years, MMSE≥29) underwent T1-weighted volumetric MRI and dynamic PET scans after injection of 305±36 MBq ^{18}F-LSP (n=2) or 297±56 MBq ^{18}F-NML (n=2), respectively. PET images, time-activity-curves, SUV-ratios in different brain regions, and % injected dose in brain were analysed using PMod quantification software.

A total of 22 compounds based on known pharmaceuticals named astemizole and LSP, were synthesized to validate the molecular scaffold, benzimidazol-2-yl-heteroarylmethyl-

sulfoxide.[3] *In vitro* binding affinities of synthesized compounds were measured via radioligand binding assay using [^{3}H]Astemizole and heparin induced Tau filaments (HITF) derived from synthetic htau-441. Binding to ß-amyloid and α-synuclein fibrils was also determined to access the cross affinity of new compounds.

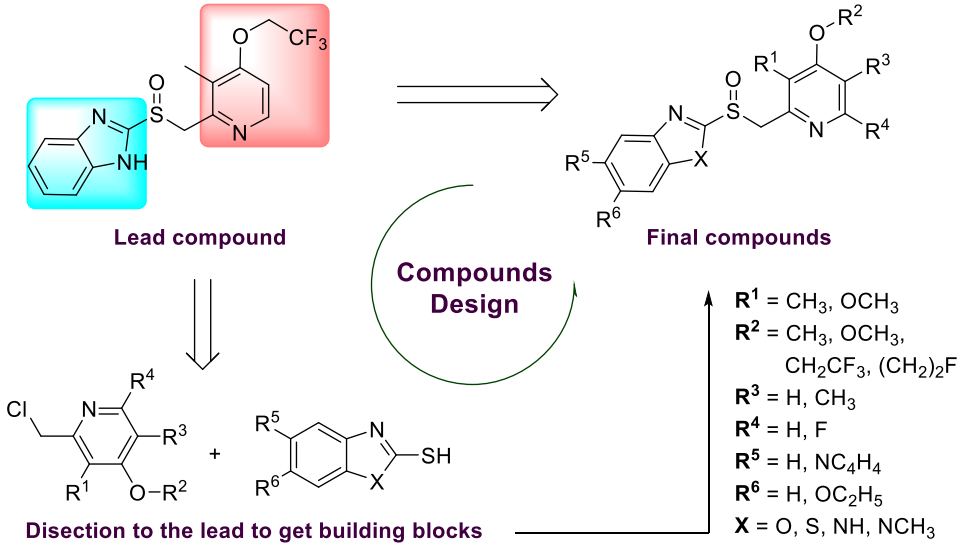

Figure – 1: Synthesis of new analogues from the lead compound with variable building blocks in blue and red.

Results and discussion:

Ex vivo binding studies of both ^{18}F-LSP and ^{18}F-NML show specific binding to NFTs on human tissue samples. *In vivo* PET studies showed insufficient penetration of BBB for ^{18}F-LSP,whereas ^{18}F-NML showed good BBB penetration, fast washout and low non-specific binding throughout the brain.

In-vitro binding affinities (IC_{50}) of new compounds range from 0.2 to 100 nM towards NTFs and show good selectivity compared to ß-amyloid and α-synuclein.^{18}F-NML and an additional compound ,(identified from the library) are currently being evaluated for performance of NFT imaging agents in human studies and animal models.

Acknowledgement:

This study was funded by the faculty of Mathematics and Natural Sciences (SFI-leader PJR), the Department of Chemistry, University of Oslo (startup grant to PJR) and PositronPharma SA, Santiago, Chile.

References:

[1] http://www.neurodegenerationresearch.eu/about/. [2] Fawaz MV, Brooks AF, Rodnick ME, Carpenter GM, Shao X, Desmond TJ, Sherman P, Quesada CA, Hockley BG, Kilbourn MR, Albin RL. [2014], ACS Chem. Neurosci, 5(8):718-730. [3]. Rojo LE, Alzate-Morales J, Saavedra IN, Davies P, Maccioni RB. [2010], J Alzheimers Dis.19(2):573–589.

P127
Dopamine synthesis capacity correlates with mu-opioid receptor availability in the human basal ganglia: a triple-tracer PET study

Joonas Majuri[a,b,c], Juho Joutsa[b,c,d,e], Eveliina Arponen[c], Sarita Forsback[c], Valtteri Kaasinen[a,b,c]

a. *Division of Clinical Neurosciences, Turku University Hospital, Turku, Finland*
b. *Department of Neurology, University of Turku, Turku, Finland*
c. *Turku PET Centre, University of Turku, Turku, Finland*
d. *Athinoula A. Martinos Center for Biomedical Imaging, Massachusetts General Hospital and Harvard Medical School, Charlestown, MA*
e. *Berenson-Allen Center for Noninvasive Brain Stimulation, Beth Israel Deaconess Medical Center and Harvard Medical School, Boston, MA*

Introduction:

Animal studies have suggested that dopamine and opioid neurotransmitter systems interact in brain regions that are relevant for reward functions, but data in humans is very limited. Brain μ-opioid receptor (MOR) activation has been linked to increased dopamine release in ventral tegmental area (Jalabert 2011). Here, we investigated if subcortical MOR availability and presynaptic dopamine synthesis capacity are correlated in the healthy human brain, and in pathological gamblers (PG). The specificity of the findings was further investigated by including a serotonin transporter (SERT) ligand as a negative control.

Materials and Methods:

13 PG patients and 15 age-, sex- and weight-matched controls underwent the positron emission tomography (PET) with tracers 6-[^{18}F]fluoro-L-dopa, [^{11}C]carfentanil and [^{11}C]MADAM. The PET scans were performed using a High Resolution Research Tomograph PET scanner (HRRT, Siemens Medical Solutions, Knoxville, TN, USA). Patlak plot was used to calculate [^{18}F]fluorodopa influx constant rates (K_i), and simplified reference tissue model were used to calculate the ratios spesifically relative to the non-displaceable binding (BP_{ND}) with [^{11}C]carfentanil and [^{11}C]MADAM (Patlak 1985, Gunn 1997). Parallel voxel-by-voxel analysis was performed with VoxelStats MATLAB package (Mathotaarachchi 2016). The data was statistically approached using general linear model.

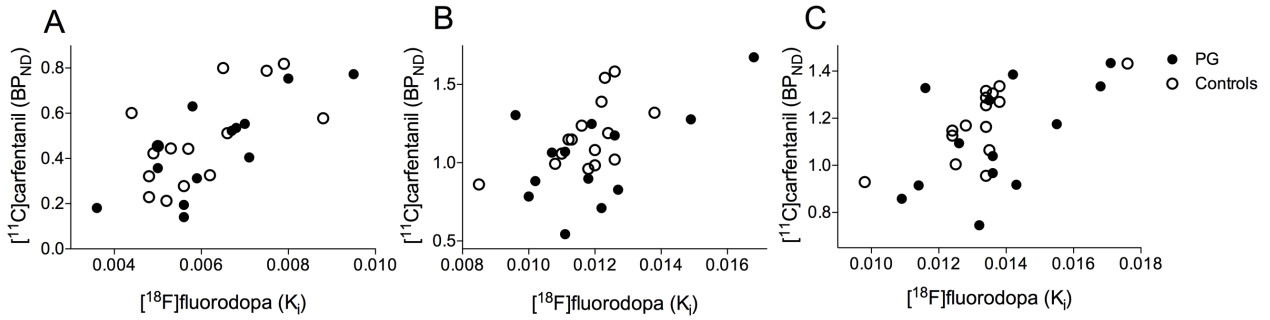

Figure 1. Scatter plots for correlations between [^{18}F]fluorodopa uptake and [^{11}C]carfentanil binding in (A) the globus pallidus, (B) the caudate nucleus and (C) the putamen. Solid circles = PG patients, open circles = healthy controls.

Results:

There were positive associations between 6-[^{18}F]fluoro-L-dopa and [^{11}C]carfentanil uptakes in the putamen (p=0.001), caudate nucleus (p=0.002) and globus pallidus (p<0.001) in both groups (Figure 1). No similar connections were seen between 6-[^{18}F]fluoro-L-dopa and [^{11}C]MADAM binding. The correlations did not differ between healthy volunteers and PG patients. Voxel-by-voxel analysis confirmed the findings by showing bilateral clusters in the caudate nuclei and in the left putamen (Figure 2).

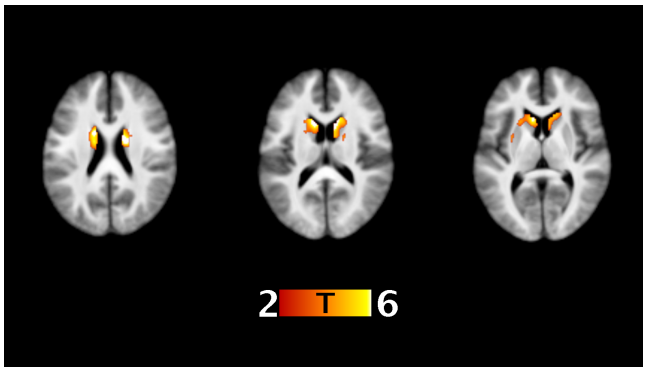

Figure 2. Significant clusters from the voxel-by-voxel analysis for correlations between [^{18}F]fluorodopa and [^{11}C]carfentanil.

Conclusions:

Here we demonstrated that 6-[^{18}F]fluoro-L-dopa and [^{11}C]carfentanil binding are correlated in the human striatum and the globus pallidus. Correlations were similar between the groups, suggesting that the dopamine-opioid link is general and unaffected by the behavioral addiction. The lack of connection between dopamine synthesis capacity and SERT density supports a specific interplay between presynaptic dopamine neurotransmission and opioid receptor function in the basal ganglia. The results of this corroborate animal data, providing additional evidence about the connection of endogenous opioid and dopamine signaling in the living human brain.

Acknowledgements:

We thank the staff of the Turku PET Centre for their expertise and assistance in PET and MR imaging.

References:

Gunn RN, Lammertsma AA, Hume SP, Cunningham VJ. [1997] Parametric imaging of ligand-receptor binding in PET using a simplified reference region model. Neuroimage 6(4): 279-287.

Jalabert M, Bourdy R, Courtin J, Veinante P, Manzoni OJ, Barrot M, et al. [2011] Neuronal circuits underlying acute morphine action on dopamine neurons. Proc Natl Acad Sci U S A 108(39): 16446-16450.

Mathotaarachchi S, Wang S, Shin M, Pascoal TA, Benedet AL, Kang MS, et al. [2016] VoxelStats: A MATLAB Package for Multi-Modal Voxel-Wise Brain Image Analysis. Front Neuroinform 10: 20.

Patlak CS, Blasberg RG. [1985] Graphical evaluation of blood-to-brain transfer constants from multiple-time uptake data. Generalizations. J Cereb Blood Flow Metab 5(4): 584-590.

P128
Childhood family size is associated with striatal type 2 dopamine receptor density and protects against its age-related decline

Vesa Putkinen[1], Janne Isojärvi[1], Tomi Karjalainen[1], Jouni Tuisku[1], Robin I.M. Dunbar[2], Mikko Sams[3,4], Riitta Hari[5], Juha O Rinne[1], Jani Erola[6] & Lauri Nummenmaa[1,7].

[1]Turku PET Centre, University of Turku, Turku, Finland.

[2]Department of Experimental Psychology, Oxford University, United Kingdom

[3]Department of Neuroscience and Biomedical Engineering, Aalto University, Finland

[4]Department of Computer Science, Aalto University, Finland

[5]Department of Art, School of Arts, Design and Architecture, Aalto University, Finland

[6]Derpartment of Sociology, University of Turku, Finland

[7]Department of Psychology, University of Turku, Finland

Introduction:

A large social network is one of the most important protective factors against age-related decline in somatic wellbeing and cognitive functions (Charles & Carstensen, 2010; Holt-Lunstad, Smith, Baker, Harris, & Stephenson, 2015). Thus, the extent of one's family network could be inversely associated with neurobiological markers of cognitive aging. We tested this hypothesis by examining the relationship between the number of siblings—a proxy for the number of close social contacts—and age-related reduction in striatal type 2 dopamine receptor (D2R) density that contributes to corresponding cognitive decline particularly in executive functions (Bäckman et al., 2000; Grady, 2012).

Materials & Methods:

We retrieved positron emission tomography (PET) data from the AIVO database at Turku PET Centre, obtained in 308 scans conducted with the D2R agonist radioligand [^{11}C]raclopride in 19–58-year-old subjects. Data were normalized to MNI space and the D2R density was expressed in terms of BP_{ND} calculated for each voxel using a simplified reference-tissue model with reference-tissue (cerebellum) time activity curves as input data (Gunn, Lammertsma, Hume, & Cunningham, 1997). The effects of age and the number of siblings on D2 binding potential in putamen and caudate were examined using linear mixed modeling.

Results:

Caudate and putamen D2R densities were positively associated with the number of siblings (main effect of number of siblings, $p > .05$) and negatively associated with age (main effect of age, $p > .001$) (Figure 1 A). Importantly, however, the age-related decline in D2R density was significantly attenuated in subjects with more than 1 siblings in both structures (age × number of siblings interaction, $p > .05$) (Figure 1 B).

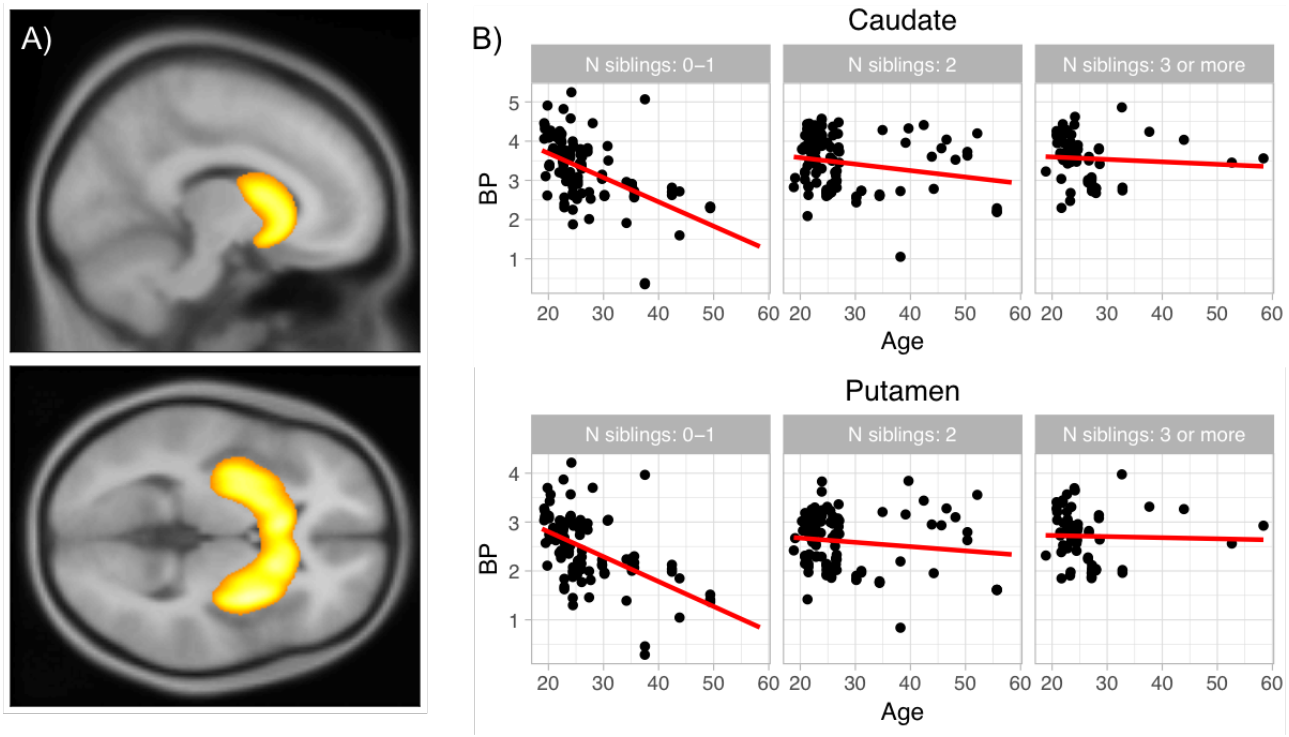

Figure 1 A) Regions showing significant (p > .001 uncorrected) age-related reduction in D2R density. B) age-related D2R-density reduction in caudate and putamen in subjects with different number of siblings.

Conclusions:

The number of siblings was associated with higher D2R density in caudate and putamen, and with slower age-related reduction in striatal D2R density. We conclude that the cognitive and social/emotional stimulation provided by close family ties may stave off age-related cognitive decline by promoting the integrity of the underlying neural networks.

Acknowledgements:

This project was supported by Sigrid Jusélius Foundation

References:

Bäckman L, Ginovart N, Dixon RA et. al. [2000]. Am.J.Psychiatry 157: 635–637

Charles ST & Carstensen LL [2010 Annu.Rev.Psychol 61: 383–409

Grady C. [2012] Nat.Rev.Neurosci 13:491-505

Gunn RN, Lammertsma AA, Hume SP et. al. [1997] NeuroImage 6: 279–287

Holt-Lunstad J, Smith TB, Baker M et. al. [2015] Perspect.Psychol.Sci 10: 227–237

P129
The relation between cerebrovascular stress, dopamine system integrity and cognitive performance

Nina Karalija[1,3], Anders Wåhlin[1,3], Goran Papenberg[4], Alireza Salami[4], Anna Rieckmann[1,3], Jarkko Johansson[1,3], Micael Andersson[2,3], Jan Axelsson[1,3], Katrine Riklund[1,3], Martin Lövdén[4], Ulman Lindenberger[5,6], Lars Bäckman[4] & Lars Nyberg[1,2,3]

1. *Department of Radiation Sciences, Umeå University, S-90187 Umeå, Sweden*
2. *Department of Integrative Medical Biology, Umeå University, S-90187 Umeå Sweden*
3. *Umeå Center for Functional Brain Imaging (UFBI), Umeå University, S-90187 Umeå, Sweden*
4. *Aging Research Center, Karolinska Institutet & Stockholm University, Gävlegatan 16, 11330, Stockholm, Sweden*
5. *Center for Lifespan Psychology, Max Planck Institute for Human Development, Lentzeallee 94, D-14195 Berlin, Germany*
6. *Max Planck UCL Centre for Computational Psychiatry and Ageing Research, Berlin, Germany, and London, UK*

Introduction:

The aging brain undergoes several changes, including reduced cerebrovascular integrity and dopamine system degeneration (Brickman et al., 2011; Bäckman et al., 2006; Raz et al., 2017). Both changes have been associated with age-related cognitive decline. However, there is lack of multimodal imaging studies addressing their interplay. The present work studied interrelations of cerebrovascular parameters (blood flow, perfusion, and white-matter lesions), dopamine system integrity (D2-receptors), and cognitive performance in a sample of healthy, older adults.

Materials and Methods:

The study was carried out using data from the Cognition, Brain, and Aging (COBRA) sample, which consists of healthy, older adults (n=181, 100 men, age:64-68 years (Nevalainen et al., 2015)). The participants have undergone magnetic resonance imaging (MRI) to measure arterial blood flow (ml/s), perfusion (ml·100 g^{-1}·min^{-1}), and white-matter lesions (cm^3), and also positron emission tomography (PET) with ^{11}C-raclopride to determine dopamine D2-receptor availability (BP_{ND}), and cognitive testing. Furthermore, the impact of lifestyle-related risk factors such as consumption of medication for hypertension, systolic blood pressure>140 mmHg, medication for hyperlipidemia, overweight (BMI>25), and nicotine consumption were evaluated and integrated into an aggregated risk score (min:0, max:5).

Results:

Dopamine D2-receptor availability (^{11}C-raclopride BP_{ND}) in regions important for cognitive functions, such as caudate nucleus, hippocampus, prefrontal cortex, anterior cingulate cortex was negatively correlated with total white-matter lesion burden (cm^3; r= -.17 to -.36, p's<0.05). For the size of single lesions, rather than total lesion burden, individuals with lesions exceeding 20mm in diameter had reduced ^{11}C-raclopride BP_{ND} in caudate, putamen and prefrontal cortex (p<0.01) and performed worse on tasks of episodic memory (p<0.05)

compared to individuals with smaller lesions (<9mm). No associations were found between D2-receptor availability and cerebral blood flow or perfusion. However, perfusion and WMH burden were correlated (r=-0.18 to -0.19, p<0.05 for caudate, hippocampus, and cortex).

The risk score was positively related with number of white matter lesions (r=.17, p<0.05), and negatively related to perfusion in caudate (r=-0.23), putamen (r=-0.25), and hippocampus (r=-0.22, p<0.01). Furthermore, the risk score was negatively related with cerebral blood flow in the internal carotid artery (r=-0.19, p<0.05) and to performance on a timed processing-speed subtest from the Wechsler Adult Intelligence Scale (r=-0.16, p<0.05).

Discussion/Conclusion:

Even though we cannot infer the temporal order of events, as that would require longitudinal measurements, these cross-sectional data suggests a relationship between reduced cerebrovascular integrity and dopamine decline that may underlie reduced cognitive performance in aging. The putative link to lifestyle factors for brain integrity holds promise for preventive strategies.

Acknowledgements:

This work was funded by the Swedish Research Council, Umeå University, Umeå University–Karolinska Institute Strategic Neuroscience Program, the Knut and Alice Wallenberg Foundation, the Torsten and Ragnar Söderberg Foundation, an Alexander von Humboldt Research award, a donation from the Jochnick Foundation, Swedish Brain Power, Swedish Brain Foundation, Västerbotten County Council, Innovation Fund of the Max Planck Society, and Gottfried Wilhelm Leibniz Research Award 2010 of the German Research Foundation (DFG).

References:

Brickman, A.M., Siedlecki, K.L., Muraskin, J., Manly, J.J., Luchsinger, J.A., Yeung, L.K., Brown, T.R., DeCarli, C., Stern, Y., 2011. White matter hyperintensities and cognition: testing the reserve hypothesis. Neurobiol. Aging 32, 1588-1598.

Bäckman, L., Nyberg, L., Lindenberger, U., Li, S.C., Farde, L., 2006. The correlative triad among aging, dopamine, and cognition: current status and future prospects. Neurosci. Biobehav. Rev. 30, 791-807.

Nevalainen, N., Riklund, K., Andersson, M., Axelsson, J., Ogren, M., Lovden, M., Lindenberger, U., Backman, L., Nyberg, L., 2015. COBRA: A prospective multimodal imaging study of dopamine, brain structure and function, and cognition. Brain Res. 1612, 83-103.

Raz, N., Daugherty, A.M., Sethi, S.K., Arshad, M., Haacke, E.M., 2017. Age differences in arterial and venous extra-cerebral blood flow in healthy adults: contributions of vascular risk factors and genetic variants. Brain Struct Funct.

P130

Human fMRI response in striatum is accompanied by changes in dopamine D2-receptor occupancy: Results from an in-vivo hybrid PET-fMRI study in healthy humans during task performance.

Anna Rieckmann[1,2], Jarkko Johansson[1,2], Patrik Brynolfsson[1], Jan Axelsson[1], Filip Grill[1], Katrine Riklund[1], Lars Nyberg[1,2]

Umeå Center for Functional Brain Imaging and Departments of (1) Radiation Sciences and (2) Integrative Medical Biology, Umeå University, Umeå, Sweden

Introduction:

Human fMRI studies are valuable for studying the large-scale functional architecture of the human brain. However, in the quest for fMRI as a marker of disease and a potential biomarker for pharmaceutical targets, a shortcoming of fMRI is that the blood-oxygen-level-dependent (BOLD) response lacks neurochemical information. The current study tests whether it is possible to supplement fMRI BOLD responses with complementary neurochemical information from dynamic PET during human task performance. A pharmacological PET-fMRI study in anesthetized monkeys by Sander et al. (2013) has demonstrated feasibility of this approach. We investigate overlap of the task-dependent BOLD response with a PET-derived measure of dynamic changes in dopamine D2 receptor occupancy using data from a single scan acquired on a hybrid PET-MRI scanner.

Materials & Methods:

11 healthy, young participants took part in a single 60-minute PET-MR scan (GE Signa 3T). Dynamic PET data were acquired in list-mode for 60 minutes following a bolus+infusion of 250 MBq 11C-Raclopride, and reconstructed to 50 frames of varying duration. For the last 40 minutes, fMRI (echo planar imaging TR = 4 s, TE = 30 ms, 3.6 mm slice thickness) was acquired continuously during PET. Participants were instructed to stay awake during the fMRI acquisition and follow instructions to periodically tap all fingers on their right hand. Task timing varied between participants. Here, preliminary data is presented for 4 subjects who performed the tapping task for 13 minutes and rested for the remainder of the scan time. Analyses for the other participants with shorter tapping periods are ongoing.

The fMRI data were pre-processed using conventional procedures and a general linear model of task on- and offsets was fitted voxelwise to BOLD time series. PET data were motion-corrected and smoothed. A linear parametric neurotransmitter PET (lp-ntPET) model was fitted voxelwise to time-activity curves (TACs) in order to identify where TACs follow functions that deviate from the simplified reference tissue model (SRTM) for 11C-Raclopride, which are interpreted as “activations” (Wang et al. 2017). The set of activation functions included in the lp-ntPET was informed by simulation work.

Results:

All 4 subjects showed reliable fMRI activations in bilateral putamen ($p < 0.0001$) during finger tapping. Peak PET activations were also located in putamen, in spatial proximity, and partially overlapping, with fMRI activations (Figure 1). Three subjects showed predominant fMRI and PET signal changes in left putamen, while one subject had peak fMRI and PET signal changes in right putamen. Further inspection of active clusters in PET data showed that they were driven by a transient decrease in the TAC, which we interpret to reflect competition with endogenous dopamine release during task. Notably, however, we found individual differences in the shape and lag of PET activations as well as significant PET activations that are not overlapping with fMRI activation, which require further investigation to fully understand.

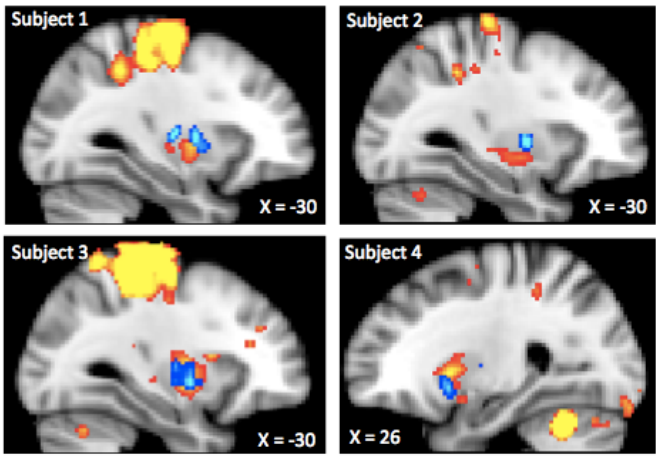

Figure 1. Individual PET-fMRI maps for 4 subjects from a finger-tapping task. Red-yellow activations are fMRI activations of the motor circuit including motor cortex, putamen and cerebellum. Blue activations are derived from 11C-Raclopride PET data and show voxels where TACs deviate from an SRTM fit. It can be seen that fMRI and PET activations partially overlap in lateral putamen. For illustration, fMRI and PET maps were thresholded differently in different subjects but fMRI activations all exceeded a significance threshold of $p < 0.0001$ and PET maps had an F value of 5 and cluster extent of 19 voxels (cf. Wang et al. 2017).

Discussion:

Extending pharmacological PET-fMRI work in monkeys, we show that PET-based signal fluctuations are detected in areas that partially overlap with task-related changes in fMRI. Assuming that dynamic changes in the TAC reflect task-induced dopamine release, our data show that non-specific information gained from fMRI can be supplemented with neurochemical information acquired with PET in a single scan, and that the modalities provide converging information on the neurobiological basis of a specific cognitive function. Nevertheless, further analyses are required to fully understand the limits of the technique (e.g. in terms of task timing), the relationship between the two modalities in overlapping signals and how PET-fMRI can inform our understanding of brain functions where they do not overlap.

Acknowledgements:

This work was supported by the Swedish Research Foundation (VR) to AR, Umeå University and Västerbotten County Council.

References:

- Sander CY, Hooker JM, Catana C et al. [2013] PNAS 110: 11169-74
- Wang S, Kim S, Cosgrove KP et al. [2017] Neuroimage 146: 701-714

P131
Regional Vesicular Acetylcholine Transporter Distribution in Human Brain: A [^{18}F]FEOBV Study

Roger L. Albin[1,2,3,4], Martijn L.T. Muller[3,5], Nicolaas I. Bohnen[1,2,3,5], William T. Dauer[1,2,3], Martin Sarter[3,6], Kirk A. Frey[2,5], Robert A. Koeppe, PhD[3,5]

[1]Neurology Service & GRECC, VAAAHS, Ann Arbor, MI, 48105; [2]Dept. of Neurology, University of Michigan, [3]University of Michigan Morris K. Udall Center of Excellent for Research in Parkinson's Disease, [4]Michigan Alzheimer Disease Center, [5]Dept. of Radiology, University of Michigan, [6]Dept. of Psychology, University of Michigan, Ann Arbor, MI, 48109

Introduction:

Cholinergic projection systems are key mediators of several important brain processes. Abnormalities of brain cholinergic projection systems are implicated in several neurodegenerative and psychiatric diseases. We used positron emission tomography (PET) with the vesicular acetylcholine transporter (VAChT) ligand [^{18}F]Fluoroethoxybenzovesamicol ([^{18}F]FEOBV) to define the distribution of cholinergic projection system terminals in normal human brain.

Materials and Methods:

We studied 29 (18:11 Male:Female; mean age 47 [range 20-81] years) neurologically normal individuals. [^{18}F]FEOBV PET was performed as described previously (Albin et al., eNeuro, 2017; Petrou et al., J Nuc Med, 2014). Volumes of interest were determined from co-registered T1-weighted MRI scans. Averaged late static images were normalized using white matter VOIs derived from co-registered T1-weighted MRI scans (Albin et al., eNeuro, 2017).

Results:

[^{18}F]FEOBV binding was inhomogeneously distributed throughout the brain (**Fig. 1**). [^{18}F]FEOBV binding was conspicuous in the striatal complex, thalamus, cortical mantle, mesopontine junction, and portions of the cerebellar cortex. Cortical [^{18}F]FEOBV binding was relatively high in the amygdala, hippocampal formation, insula, BA24, BA27, BA28, and BA34. Thalamic [^{18}F]FEOBV binding was inhomogeneous with higher binding in lateral geniculate nuclei and more medial thalamus with lower binding in anterior thalamus and pulvinar complex. [^{18}F]FEOBV binding was conspicuous at the mesopontine junction, likely including the pedunculopontine - laterodorsal tegmental complex and the parabigeminal nuclei. There was moderate binding throughout the brainstem reticular formation and the facial nerve nuclei were identifiable. [^{18}F]FEOBV binding was notable in the cerebellar vermis and flocculus with lower binding in the cerebellar hemispheres.

Discussion:

CNS [^{18}F]FEOBV binding is largely consistent with the distribution of cholinergic projections established in non-human animals and some prior post-mortem studies of human brain. A significant exception is the distribution of cerebellar cortical vermal [^{18}F]FEOBV binding, which is more extensive than described in other mammals. [^{18}F]FEOBV PET identifies cholinergic terminals associated with major cholinergic systems, including the basal forebrain corticopetal projection, striatal cholinergic interneurons, the pedunculopontine - laterodorsal tegmental complex, and medial vestibular nuclei. The latter may have more extensive projections to cerebellar vermis than found in other mammals. [^{18}F]FEOBV PET will be a useful method for quantifying changes in these projection systems in normal aging and neurodegenerative disorders.

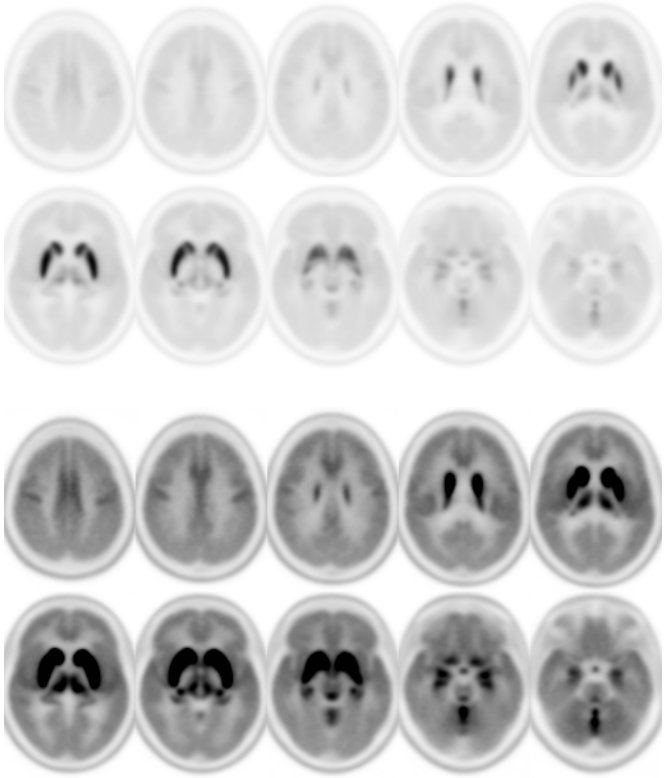

Figure 1: Group averaged Images (n=29) scaled to white matter; Upper image set peak display is 9.5; lower image set peak is 3.0.

Acknowledgments:

Supported by P50 NS091856, R21 NS088302, and the Michael J. Fox Foundation.

References:

Albin RL, Minderovic C, Koeppe RA. [2017] eNeuro 4: ENEURO.0178-17.2017; Petrou M, Frey KA, Kilbourn MR, et al. [2014] J. Nuc. Med. 55: 396-404

P132

Abstract Withdrawn

P133
Adaptive optimal design based PK/PD modeling determines enzyme occupancy of O-GlcNAcase (OGA) inhibitor by PET imaging

Talakad G. Lohith[1], Cristian Salinas[1], Wenping Li[1], Chandni Valiathan[1], Junghoon Lee[1], Kerry Riffel[1], Claire Li[1], David R. Hagen[1], Brittany Walker[1], Daniel Dreyer[1], Punam Sandhu[1], Daniel Jonathan[1], Ruben Declercq[2], Tom Reynders[2], Kim Serdons[3], Guy Bormans[3], Jan de Hoon[3], Corinne Vandermeulen[3], Koen Van Laere[3], Ernest McEachem[4], David Vocadlo[4], Sean Smith[1], Arie Struyk[1], Jeffrey L Evelhoch[1], and Eric D. Hostetler[1]

[1]MRL, Merck & Co., Inc., West Point, PA, USA

[2]MRL, Merck Sharp & Dohme Inc., Brussels, Belgium

[3]UZ Leuven and KU Leuven, Leuven, Belgium

[4]Alectos Therapeutics Inc., Burnaby, BC Canada

Introduction:

Positron emission tomography (PET) is a powerful translational pharmacokinetic/pharmacodynamic (PK/PD) tool that facilitates dose selection for novel therapeutic candidates when used early on in Phase 1 clinical trials by characterizing relationship between time course of plasma concentration (a measure of PK) and target occupancy (a measure of PD). This study describes the use of [^{18}F]MK-8553 *(1)*, a novel PET tracer targeting O-GlcNAcase (OGA) to characterize brain enzyme occupancy (EO) to enable dose selection for MK-8719, an OGA inhibitor targeted for reducing tau aggregation in patients with progressive supranuclear palsy.

Materials and Methods:

An adaptive, optimal-design, open-label, single-dose trial of three panels in up to 3 subjects each were performed in healthy women of non-childbearing potential. Each subject underwent a baseline [^{18}F]MK-8553 PET scan, followed by a single dose of MK-8719, and then two serial post-dose PET scans over a period of 4 days to characterize the relationship between plasma PK and peak/time-on-target kinetics of brain EO. Doses and scan times were selected using an optimal design that leveraged a population PK (PopPK) model linked to a brain EO model. The PK parameters were obtained by fitting a PopPK model to data from a MK-8719 first-in-human single ascending dose (FIH SAD) study. A starting dose of 5 mg was predicted to achieve ~50% peak brain EO based on preclinical data as well as human PK data from the FIH SAD study.

Results:

The first panel of 5 mg MK-8719 dosing resulted in about 70% peak EO between 2 – 6 h (scan 1) and about 40% EO at ~30 h (scan 2) post-dosing. For subsequent panels, dose and scan times were selected based on informed decisions and D-optimality criteria that maximized the confidence around the model parameters. The doses selected using the optimal design were 2 mg and 300 mg which captured a low-to-high range of PET EO values. A simple diffusion limited brain occupancy model fitted the PET EO data from all panels (Figure 1). The PK/PD model characterized the single dose-EO relation by a sigmoidal relationship with an Occ_{50} of 10.6 nM and a brain $t_{1/2}$ of 10.7 h.

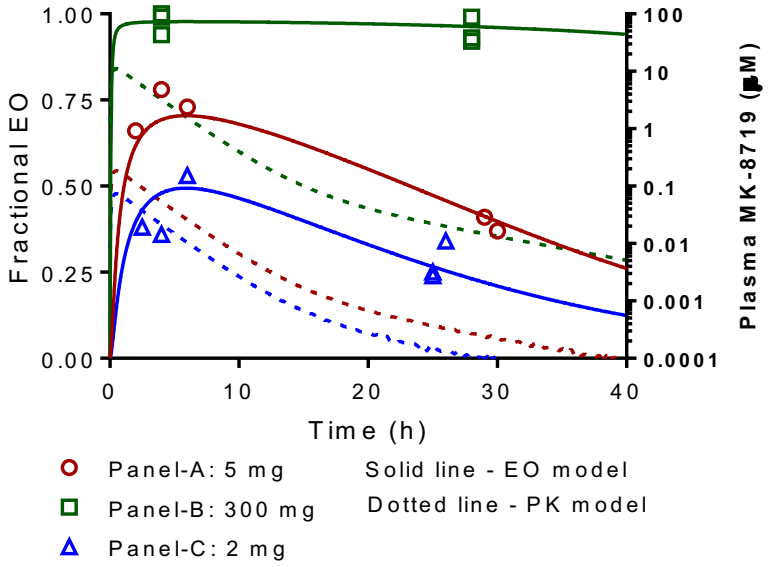

Figure 1: Time occupancy plot with PK/PD model that fits well to measured occupancies from all three panels.

Conclusion:

The PK/PD relationship established using an adaptive optimal design approach successfully characterized the time-on-target kinetics of MK-8719 in an early clinical Phase 1 trial. The PK/PD model is useful to define an appropriate dosage and administration regime required to achieve a level of enzyme occupancy capable of eliciting a desired pharmacological effect, thereby ensuring proper testing of the OGA mechanism as well as increasing the probability of a successful clinical trial.

References:

Li W, Salinas CA, Riffel K, Miller P, Zeng Z, Lohith TG, et al. “The Discovery and Characterization of [^{18}F]MK-8553, A Novel PET Tracer for Imaging O-GlcNAcase (OGA).” Neuroreceptor Mapping 2016, Boston, USA (July 2016). Abstract No. O-001.

P134
In vivo demonstration of COX-2 upregulation after neuroinflammation in monkey brain using the novel PET radioligand [11C]MC1

Stal Shrestha[1]

[1]*NIH*

Introduction:

Neuroinflammation is implicated in several brain diseases such as multiple sclerosis and a specific biomarker to diagnose and stage neuroinflammation is warranted. The cyclooxygenase (COX) isozymes, COX-1 and COX-2, mediate inflammatory responses, and are potential biomarkers of neuroinflammation. Nonsteroidal anti-inflammatory drugs (NSAIDs) inhibit the function of the COX isozymes. Previously, we showed that ^{11}C-PS13 (COX-1 selective) showed specific uptake in normal monkey brain, but ^{11}C-MC1 (COX-2 selective) did not. However, it remains unknown whether ^{11}C-MC1 exhibits specific binding under conditions that elicit significant COX-2 expression. This study sought to examine whether ^{11}C-MC1 could image COX-2 during inflammation triggered via an intracerebral injection of lipopolysaccharide (LPS). As a comparator, COX-1 was measured before and after LPS using ^{11}C-PS13.

Methods:

LPS was injected into the right putamen of rhesus macaque monkeys (n=4; 10µg at a concentration of 1µg/µL; infusion rate=0.5 µL/min). Dynamic brain PET scans were acquired for two hours both pre- and post-LPS injection. Approximately 315 MBq of radioligand was injected intravenously into the monkey before each scan. Blocking studies were also conducted with non-radioactive MC1 or PS13 (0.3-1 mg/kg) to assess the specific uptake of the radioligands in the brain. Distribution volume (V_T) was measured using arterial sampling before and after LPS injection. As a positive control, ^{11}C-PBR28 PET and T1- and T2-weighted MRI scans were done. Cellular localization of COX-1/2 proteins was measured using *in vitro* immunofluorescence, and their mRNA was measured using fluorescent multiplex *in situ* hybridization.

Results:

After the first injection of LPS, a widespread, 60% increase of ^{11}C-MC1 uptake was observed in the brain, which was displaced by non-radioactive MC1. An even more dramatic, and localized increase (>200%) in ^{11}C-MC1 uptake was observed after the second LPS injection. No increase in COX-1 was seen after LPS injection. ^{11}C-PBR28, a radioligand for translocator protein (TSPO), showed increased uptake, as expected, at the site of injection. Both T1- and T2-weighted MRI scans showed robust changes after LPS injection. COX-2

mRNA and protein were upregulated in the inflamed brain and were located primarily in neurons and infiltrating neutrophils.

Conclusion:

^{11}C-MC1 successfully imaged and quantified COX-2 upregulation in monkey brain from basal levels to 160% after a single injection and >300% after a second injection. The findings demonstrate that COX-2, but not COX-1, is upregulated in monkey brain after inflammation, consistent with the general notion that COX-2 expression is inducible and COX-1 is constitutive. We plan to go ahead with first-in-human studies to measure COX-2 in rheumatoid arthritis and myositis using ^{11}C-MC1.

Figure 1. The effect of inflammogen, LPS, on ^{11}C-MC1 uptake in a monkey brain shown as volume of distribution (V_T). In normal brain (pre-LPS), there was no detectable uptake. After the second injection of LPS into right putamen, ^{11}C-MC1 uptake increased by >200% in the area of lesion, and blocked by non-radioactive MC1 (1 mg/kg i.v.).

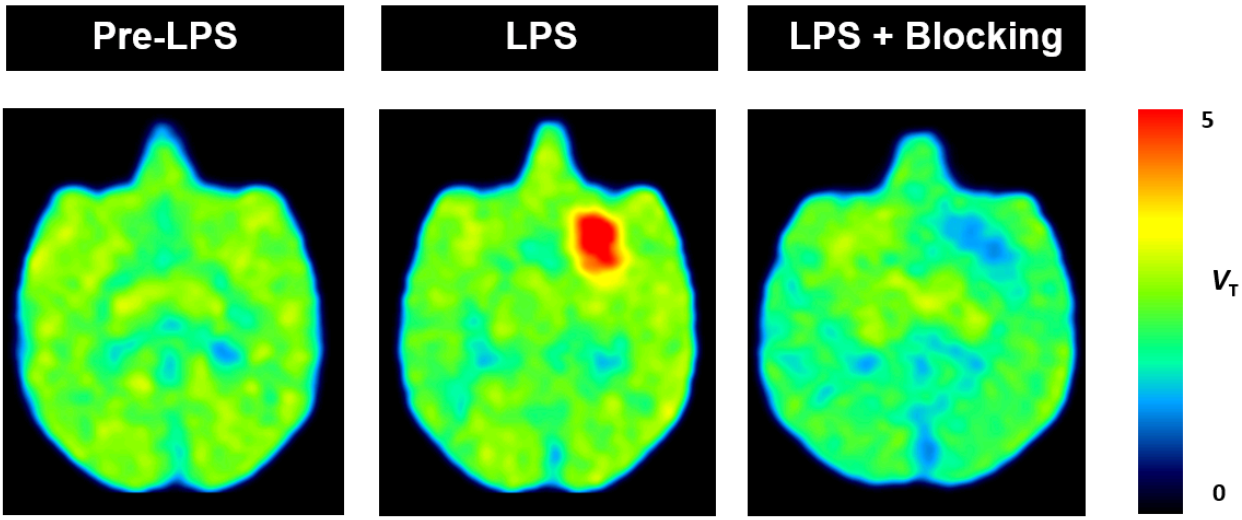

P135
Evaluation of [^{11}C]TMI as a COX-2 selective PET tracer in baboon

J S Dileep Kumar[a], Francesca Zanderigo[a,b], Jaya Prabhakaran[a,b], Harry Rubin-Falcone[b], Ramin V Parsey[c], **J John Mann**[a,b]

[a]Molecular Imaging and Neuropathology Division, New York State Psychiatric Institute, New York, USA; [b]Department of Psychiatry, Columbia University Medical Center, New York, USA; [d]Department of Psychiatry, Stony Brook University, Stony Brook, NY, USA

Introduction:

Cyclooxygenase-2 (COX-2) is an inducible enzyme involved under normal physiological conditions. Enhanced expression of COX-2 in brain is associated with neurological and neuropsychiatric disorders, stroke, head injuries and infections. Outside the brain COX-2 over-expression occurs in organ rejection, arthritis, infarcts and other conditions associated with inflammation. Positron-emitting labeling of COX-2 selective inhibitors may permit in vivo imaging of COX-2 binding in diseases, as well as relating nonsteroidal anti-inflammatory drug (NSAID) occupancy of COX-2 to therapeutic effect. At present there is no target-specific or validated PET tracer available for in vivo monitoring of COX-2. We disclosed the synthesis of [^{11}C]3-(4-methylsulfonylphenyl)-4-phenyl-5-trifluoromethylisoxazole ([^{11}C]TMI).[1] TMI is a highly selective COX-2 inhibitor with COX-2 enzyme IC_{50} <1 nM and >500,000 times higher selectivity for COX-2 over COX-1 (IC_{50} = >500 μM).[2] Herein we describe the in vivo evaluation of [^{11}C]TMI in baboon brain.

Materials and Methods:

Synthesis of reference standard TMI, and corresponding thiobuturic ester precursor were achieved as previously described.[1] Cross selectivity of TMI to an extensive panel of other brain targets was assessed through NIMH-PDSP. [^{11}C]TMI radiosynthesis was accomplished by reacting the corresponding butyrate ester with [^{11}C]CH_3I, followed by oxidation with oxone in a one pot procedure.[1] Two PET scans were acquired in a male baboon (*papio anubis*) with an ECAT ACCEL (Siemens Medical Solutions, Inc. Knoxville) in two-dimensional mode for 120 minutes following an intravenous injection of 3 $\pm$ 0.5 mCi of [^{11}C]TMI. A blocking study was performed in different male baboon by administering 1 mg/kg meloxicam 30 minute prior to [^{11}C]TMI injection. [^{11}C]TMI total volume of distribution (V_T) was estimated using metabolite-corrected arterial input functions and both the one-tissue compartment model (1TC) and graphical methods, such as likelihood estimation in graphical analysis (LEGA) and Logan. A revised Lassen plot[3] was used to calculate occupancy and nondisplaceable binding (V_{ND}) using the baseline and blocking data from the blocking study.

Results:

Radiosynthesis of [^{11}C]TMI was achieved in 37 ± 3% radiochemical yield (EOS) with >99% radiochemical purity and a specific activity of 2.5 ± 0.5 Ci/□mol. TMI did not exhibit significant affinity to a variety of competitive brain receptors, transporters, biogenic amines and proteins (Ki >10 μM) in NIMH-PDSP binding assays. PET studies in baboon showed that [^{11}C]TMI penetrates the blood brain barrier (BBB) and accumulates in brain in a somewhat homogeneous pattern (Figure 1). Time activity curves (TACs) indicated a peak uptake of the radiotracer from 3-to-9 minutes post injection in various brain regions, followed by a gradual washout of activity. Metabolite analyses in baboon indicated that [^{11}C]TMI undergoes no significant metabolism with >90% of parent tracer retained in the baboon plasma after 90 minute injection. All the tested models show comparable V_T measurement in the range of 4.7-5.7 (mL/cm^3). Specific binding was about one third of total V_T values based on the blocking scan compared to baseline scan (Figure 1). Lassen plot estimates a modest occupancy of ~43%, and V_{ND} of ~2.

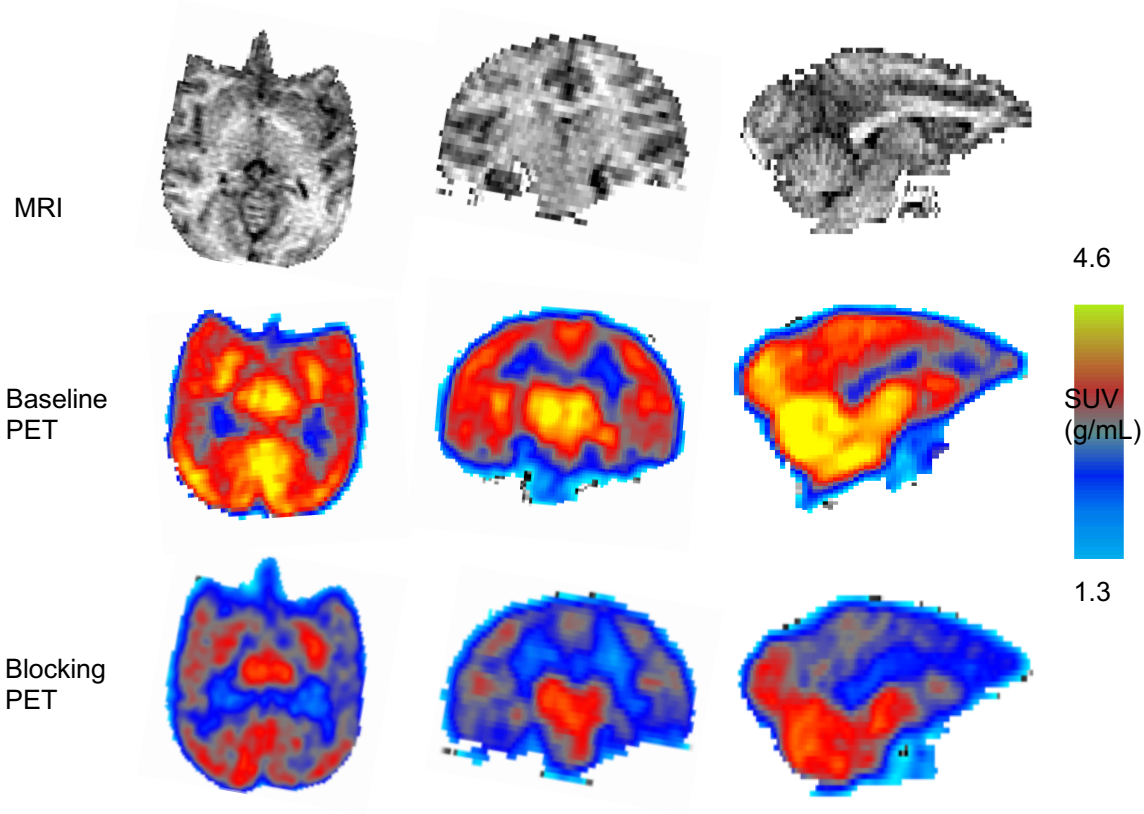

Figure 1. MRI and PET images (SUV: standard uptake value) of a representative [^{11}C]TMI brain study in baboon.

Conclusion:

PET study in anesthetized baboons show that [^{11}C]TMI penetrates the BBB and exhibits relatively homogeneous binding across brain regions and modest specific binding. The radiotracer exhibits good washout characteristics for binding parameter measurements. Determination of level of specific binding by PET imaging in animal models of inflammation with higher expression of COX-2, can better establish the utility of this tracer.

Acknowledgement:

Diane Goldberg Foundation (NYSPI/CUMC) and Pfizer Inc.

References:

1. Majo, V. J., Prabhakaran, J., Simpson, N. R., Van Heertum, R. L., Mann, J. J., Kumar J. S. D. (2005) A General Method for the Synthesis of Aryl[11C]Methylsulfones: Potential PET probes for Imaging Cyclooxygenase-2 Expression. Bioorg. Med. Chem. Lett 15: 4268-4271.Majo VJ et al., Bioorg Med Chem Let., 15: 4268.
2. Habeeb, A. G., Rao, P. N. P., Knaus, E. E. (2000) Design and Syntheses of Diarylisoxazoles: Novel Inhibitors of Cyclooxygenase-2 (COX-2) With Analgesic-Antiinflammatory Activity. Drug Deveop. Res. 51:273–286.
3. Cunningham V.J., Rabiner E.A., Slifstein M., Laruelle M., Gunn R.N. (2010) Measuring drug occupancy in the absence of a reference region: the Lassen plot re-visited. J Cereb Blood Flow Metab. 30(1): 46-50.

P136
Development of PET Imaging of Colony Stimulating Factor 1 Receptor expressed on microglia

Aya Ogata[1], Yasuyuki Kimura[1,2], Takashi Yamada[1], Bin Ji[2], Chie Seki[2], Masanori Ichise[1,2], Junichiro Abe[1], Hiroshi Ikenuma[1], Hiroko Koyama[1], Masaaki Suzuki[1], Takashi Kato[1], and Kengo Ito[1].

[1] National Center for Geriatrics and Gerontology, 7-430, Morioka, Obu, Aichi, 474-8511, Japan, [2] National Institutes for Quantum and Radiological Science and Technology, 4-9-1, Anagawa, Inage, Chiba, 263-8555, Japan

Introduction:

Neuroinflammation is involved in the pathophysiology of neurodegenerative diseases including Alzheimer's diseases. Neuroinflammation has recently been recognized as a promising target for the treatment of neurodegenerative diseases. Thus, positron emission tomography (PET) imaging for a specific molecule related to neuroinflammation could provide useful information for the drug development targeting neuroinflammation.

In this study, we developed a novel PET ligand for the colony stimulating factor 1 receptor (CSF1R). CSF1R is expressed only on microglia in the central nervous system, and its activation by two endogenous ligands, CSF-1 and IL-34, is essential for the proliferation and the differentiation of microglia. Therefore, PET imaging of CSF1R could provide unique information on neuroinflammation and the regional distribution of microglia in the brain.

Materials and Methods:

As a CSF1R PET ligand, we synthesized a novel ^{11}C-labeled compound, named [^{11}C]NCGG401, derived from BLZ945, which is a selective inhibitor of CSF1R with a high potency (IC_{50} = 1.0 nM) and a capability of brain penetration (Pyonteck *et al.*, Figure 1). We conducted 120-min dynamic [^{11}C]NCGG401 PET scans to evaluate its kinetics in the brain after intravenous administration in normal rats (Cal:CD (SD), male. 8-week old). To verify if there is any specific binding of the ligand to CSF1R, a blocking PET study was conducted using unlabeled BLZ945 (10 mg/kg body weight). An autoradiography using brain samples of a normal rat was also conducted.

Results:

We were able to synthesize [^{11}C]NCGG401, with a high radiochemical purity (>99%) and a good yield by methylation of BLZ945 (0.25 mg) with [^{11}C]methyl iodide. After the intravenous administration of [^{11}C]NCGG401, brain radioactivity showed a fast initial peak (SUV 1.0) and good washout thereafter (Figure 2). Administration of a blocking agent, unlabeled BLZ945, increased the rate of washout significantly suggesting that there is specific binding of the

ligand in the rat brain (Figure 2). Specific binding was also suggested by the autoradiography blocking experiment.

Discussion:

We have successfully synthesized a novel PET ligand, [^{11}C]NCGG401, based on a selective inhibitor of CSF1R. Although [^{11}C]NCGG401 showed a favorable kinetics and presence of specific binding in rat brain, the property of the ligand should be confirmed with *in vitro* assays and *in vivo* imaging in model animals with neuroinflammation.

Acknowledgements:

This work was supported by the Research Funding for Longevity Sciences (29-29) from National Center for Geriatrics and Gerontology (NCGG), Japan.

References:

Pyonteck S. M., Akkari L., Joyce J. A., *et al.*, [2013] *Nature Medicine*, 19, 1264-1272.

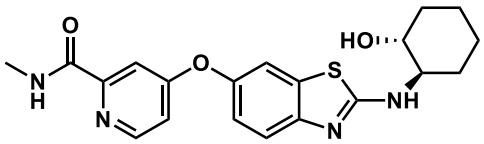

Figure 1. The structure of BLZ945

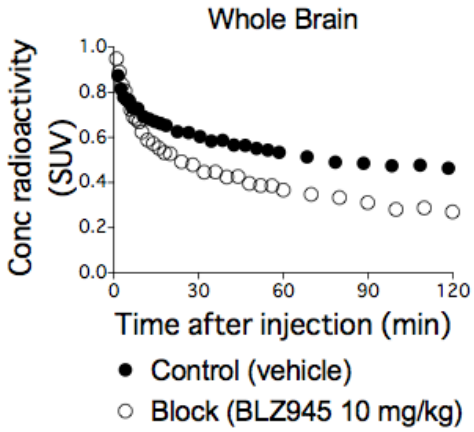

Figure 2. Time-activity curves in the whole brain after injection of [^{11}C]NCGG401 with and without blocking in normal rats

P137
Decrease in dopamine release in the striatum after a single session of continuous Theta Burst Stimulation (cTBS).

Lucero Aceves-Serrano[1], Jason L Neva[2], Katelyn E Brown [3], Lara A Boyd[1,2,3] , Doris Doudet[1,4].

[1]Faculty of Medicine, Graduate program in Neuroscience, University of British Columbia, Vancouver, Canada

[2]Department of Physical Therapy, Faculty of Medicine, University of British Columbia, Vancouver, Canada

[3] Faculty of Medicine, Graduate program of Rehabilitation Sciences, University of British Columbia, Vancouver, Canada

[4]Department of Neurology, University of British Columbia, Vancouver, British Columbia, Canada

Introduction:

Repetitive Transcranial Magnetic Stimulation (rTMS) has been studied as a tool for the treatment of movement and mood disorders. rTMS modifies cortical excitability locally, and likely affects activity in widespread brain regions. Theta Burst Stimulation (TBS), a patterned high-frequency form of rTMS, can produce robust and long-lasting changes in excitability. Stimulation of cortico-striatal projections, using rTMS, modulates activity in the striatum, affecting dopamine release presumably through direct glutamatergic stimulation of the dopamine terminals. A session of excitatory rTMS has been shown to decrease raclopride binding by positron emission tomography (PET), presumably through increase striatal dopamine release [1].

Here, we tested the effect of a single session of continuous TBS (cTBS, which has a net inhibitory effect) on dopamine release by assessing the changes of ^{11}C-Raclopride, a D_2 antagonist, before and immediately after administration of cTBS in non-human primates (NHP).

Materials & Methods:

Two ^{11}C-Raclopride scans were acquired, one at baseline and the second immediately after cTBS stimulation. NHP received either cTBS or sham stimulation over left motor cortex (M1) using a figure-8 shaped coil. Both scans were obtained on the same day. The resting motor threshold (RMT) was determined prior to the stimulation using surface electromyography (EMG) over the contralateral deltoid. Location of M1 was determined using stereotaxic neuronavigation. For cTBS, a continuous train of 600 pulses was applied for 40 seconds over left M1, at 90% RMT. Sham stimulation was administrated with the same parameters

but with the coil held perpendicular, with the magnetic field facing away from the head of the subject.

Logan's reference tissue model was used to obtain the non-displaceable binding potential (BP_{ND}), using the cerebellum as the reference tissue.

Results:

NHP that received the cTBS showed an increase in ^{11}C-Raclopride binding in caudate and putamen. Surprisingly, the increase in ^{11}C-Raclopride binding was observed in both left and right striatum.

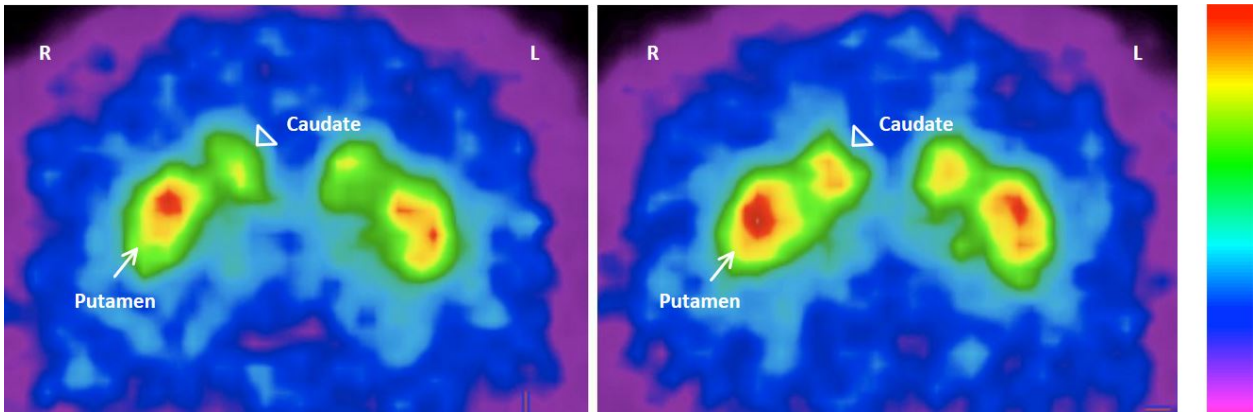

Coronal view of PET scan. Baseline ^{11}C-Raclopride scan is shown at the left side. Acute post-stimulation scan is shown at the right side. The amount of tracer binding is represented in heat color scale.

Discussion/Conclusion:

We show that cTBS-induced modulation of M1 may indirectly affect dopamine release in the ipsilateral and contralateral striatum, at least in NHP. Increased ^{11}C-Raclopride binding suggests that there is a drop of dopamine release in the striatum. This may be mediated through inhibition of local circuitry within M1, which in turn may modulate activity in downstream areas through cortico-striatal projections. The change in dopamine observed in both sides is most likely due to modulation via interhemispheric connections between the striatum.

References:

[1] A. P. Strafella, J. H. Ko, J. Grant, M. Fraraccio, and O. Monchi, "Corticostriatal functional interactions in Parkinson's disease: A rTMS/[11C]raclopride PET study," *Eur. J. Neurosci.*, vol. 22, no. 11, pp. 2946–2952, 2005.

P138
TSPO radioligand ^{18}F-DPA-714 binding quantification in genotyped Parkinson patients and healthy volunteers

Sonia Lavisse[1,2], Catriona Wimberley[3] , Mickaël Labit[4,5] , Claire Thiriez[6] , Luce Dauphinot[7,8], Michel Bottlaender[3,5], Philippe Hantraye[1,2] and Philippe Remy[1,2,6,9]

[1]CEA-DRF-JACOB, MIRCen, Fontenay-aux-Roses, France, [2]CNRS-UMR9199, Universités Paris-Sud and Paris-Saclay, Fontenay-aux-Roses, France, [3]CEA-DRF-JOLIOT, SHFJ and IMIV, UMR1023 Inserm/CEA/Paris-Sud University, Orsay, FranceM [4] CATI Multicenter Neuroimaging Platform, France, [5]CEA-DSV-I2BM, Neurospin, Gif-sur-Yvette, France, [6]Centre Expert Parkinson, Neurology Department, CHU Henri Mondor, AP-HP, Créteil, France, [7]Institut du Cerveau et de la Moelle épinière, Inserm-U1127 and Sorbonne University, UPMC-UMRS-1127, Paris, France ; [8]CNRS-UMR7225, Paris, France, [9]Paris-Est University, Créteil, France

Introduction:

The up-regulation of the translocator protein (TSPO) under inflammatory condition can be directly associated with the degree of damage in neurodegenerative diseases and makes this protein a sensitive marker and an attractive target for imaging the neuroinflammation state in Parkinson disease (1). Reported studies on neuroinflammation with PET imaging in this pathology used either the ^{11}C-PK11195 or the ^{18}F-FEPPA ligand. With the ^{11}C-PK11195, Ouchi et al. (2) found increased binding in the midbrain while Gerhard et al. (3) found increased level in the pons and basal ganglia compared to healthy volunteers (HV). In the more recent ^{18}F-FEPPA study (4), no evidence of increased binding could be found in the brain of patients.

The ^{18}F-DPA714 tracer has shown high specificity in non-human primates (5) and was quantified in genotyped HV using either the 2-TCM compartmental analysis with arterial input function (6) or the supervised cluster analysis (SVCA) approach (7). Here we examined genotyped Parkinson patients and HV with this tracer. We aimed to explore the best discriminative quantification method using two types of reference regions: the anatomically defined cerebellum grey matter and the region defined by supervised clustering. In addition, the loss of dopaminergic innervation in the brain was measured with ^{11}C-PE2I to explore correlation between neuroinflammation and a sensitive marker of disease severity.

Material and Methods:

Parkinson's patients (n=24, 64.0 ±9.8y; motor UPDRS [6-34]) and age-matched HV (n=29; 54.4±15.5y) were enrolled. The genotyping of the rs6791 polymorphism in the TSPO gene revealed 13/13 mixed affinity binders (MABs), 7/15 high affinity binders (HABs) and 4/1 low affinity binders (LABs) in patients and volunteers, respectively. PET data were acquired on a HRRT scanner for 90 minutes after injection of 207.2±41.6 MBq ^{18}F-DPA714 and for 60min after injection of the ^{11}C- PE2I. A T1-weighted MRI was performed within the same day.

^{18}F-DPA714 SUV images were calculated and a regions-of-interest-based approach was performed using the AAL atlas including 90 lateralized ROIs on individual MRI. Substantia nigra (SN) was manually segmented on individual MRI and included in the analysis. Most and less affected sides of SN were defined based on the lateralized UPDRS scores confirmed by reduction of ^{11}C-PE2I in the putamen.

Grey matter of the cerebellum was used as reference region to calculate $SUVr_{Cerv}$ values. The SVCA was conducted to extract an individual reference region (Ref_{SCA}). $SUVr_{SCA}$ values were then compared to $SUVr_{Cerv}$.

Finally, a SRTM analysis was computed to extract BP_{ND} estimates using either grey matter cerebellum (BP_{cerv}) or Ref_{SCA} (BP_{SCA}) as reference region.

Results:

For each subject, time-activity curves of Ref_{SCA} displayed a faster and higher wash-out than in the cerebellar region. In each group, difference in the mean radioactivity between HABs and MABs was smaller in the Ref_{SCA} region than in the cerebellum.

Using the $SUVr_{Cerv}$, the highest difference in HABs compared to MABs was found in the thalamus. In this region, the difference in HV was significant (+13.05%, *P*=0.0039) whereas this was not the case in patients (+22.15% but more variability). In HABs, $SUVr_{Cerv}$ was slightly higher in patients compared to HV in all regions (putamen, frontal, temporal, parietal cortices, thalamus, globus pallidus, hippocampus) and the maximal difference was seen in the most affected SN (*+28.9%*). No difference was observed between MAB patients and MAB volunteers for any region.

$SUVr_{SCA}$ in HABs compared to MABs was higher in most regions and was significantly higher in the thalamus in patients (+21.9%, *P*=0.002) and in HV (+12.0, *P*=0.0002). In HABs, comparison between patients and HV followed the same trend as with $SUVr_{Cerv}$ in all regions. Maximal and significant difference between patients and HV was found in the most affected SN (+39.0%, *P*=0.0453). No difference was observed between MAB patients and MAB volunteers.

BP_{ND} estimates from the SRTM were poorly identified using cerebellum (25%) whereas Ref_{SCA} systematically provided accurate BP_{ND}. In HABs, BP_{SCA} in patients were higher than in volunteers in all regions with a maximal difference in both SN: BP_{ND} ranged from 0.487±0.18 (HV) to 0.70±0.63 (patients, +44.3%) in the most affected side and from 0.418±0.19 to 0.73±0.63 (+ 74.4%) in the less affected side. In each genotyped group however, no significant difference was observed.

Finally, BP_{SCA} and $SUVr_{SCA}$ in the SN did not correlate with disease severity (motor UPDRS scores) but both parameters correlated to each other in bilateral SN (most affected: r=0.70, *P*=0.0017 and less affected: r=0.50, *P*=0.038, *Pearson*).

Discussion/Conclusion:

The SVCA appeared to be a more accurate method to provide a reference region than using the cerebellum to analyze ^{18}F-DPA714 PET data in the absence of arterial blood sampling.

$SUVr_{SCA}$ images showed that ^{18}F-DPA714 binding was increased in Parkinson HAB patients compared to HAB healthy volunteers, especially in the SN. SRTM analysis confirmed the increased PET binding in this region in HAB patients. Analysis on ^{11}C- PE2I images are still ongoing and other correlations will be performed.

Acknowledgements:

This work was supported by Association France Parkinson and Neuratris.

References

1. Hirsch EC, Hunot S. [2009], The Lancet Neurology,8(4):382-97
2. Ouchi Y, Yoshikawa E and Futatsubashi M. [2002], Journal of cerebral blood flow and metabolism, 22(6):746-52
3. Gerhard A, Pavese N and Hotton G. [2006], Neurobiology of disease, 21(2):404-12
4. Ghadery C, Koshimori Y and Coakeley S. [2017], J Neuroinflammation, 14(1):8.
5. Lavisse S, Inoue K and Jan C. [2015] European journal of nuclear medicine and molecular imaging.;42(3):478-94
6. Lavisse S, Garcia-Lorenzo D and Peyronneau MA. [2015], J Nucl Med.;56(7):1048-54
7. Garcia-Lorenzo D, Lavisse S and Leroy C. [2017], Journal of cerebral blood flow and metabolism, 271678X17692599.

P139
Neuropharmacological fMRI of MDMA – A Novel, Multimodal Analytical Approach Informed by PET

Ottavia Dipasquale[1], Pierluigi Selvaggi[1], Anthony Gabay[1], Mattia Veronese[1], Steve Williams[1], Federico Turkheimer[1], Mitul Mehta[1]

1 Department of Neuroimaging, Institute of Psychiatry, Psychology & Neuroscience, King's College London, London, UK

Introduction:

In the last decade, resting state fMRI (rfMRI) has been increasingly used in pharmacological applications to investigate drugs effects on brain function [1]. Pharmacological MRI studies strongly rely on the assumption that haemodynamic measures can be considered a proxy of altered neurotransmission function. However, the haemodynamic MRI signal has no intrinsic selectivity to any particular receptor sites. Indeed, the degree to which the functional MRI response indexes the action at drug target sites, and thus could be useful in parsing mechanistic underpinnings, is still an open question. The aim of this work is to address this question with a compound with a known mixed profile of serotonergic action. Specifically, we test whether haemodynamic response to 3,4-Methylenedioxymethamphetamine (MDMA) measured with rfMRI mirrors receptor 5-HT density profiles measured with PET.

Methods:

Twenty healthy subjects participated in this placebo-controlled crossover study. Images were acquired under two different conditions, i.e. placebo and 3,4-Methylenedioxymethamphetamine (MDMA), with a 3T scanner. rfMRI was acquired with a multi-echo EPI sequence (TR=2500ms, TEs=12, 28, 44ms, resolution = 3.75×3.75×4.2 mm^3, slice thickness=3 mm, 27 axial slices; 192 volumes). High-resolution T1-weighted images were also acquired. rfMRI images were preprocessed with AFNI [2] and de-noised with the AFNI tool *meica.py* [3-5]. Then, data were spatially smoothed with a with an 8-mm FWHM Gaussian kernel, WM and CSF signals were regressed out and a high-pass temporal filter, with a cut-off frequency of 0.005 Hz, was applied. Finally, images were normalized to MNI space using the Advanced Normalization Tools (ANTs) [6]. MDMA has its highest affinity for serotonin 1A, 2A receptors and the transporter [7]. We used a high-resolution in vivo atlas [8] of four serotonin receptors ($5\text{-}HT_{1A}$, $5\text{-}HT_{1B}$, $5\text{-}HT_{2A}$, and $5\text{-}HT_{4}$) and its transporter (5-HTT) as a template in a two-step multivariate regression analysis [9] to estimate the subject-specific spatial maps and time series of the BOLD response to placebo and MDMA. For each 5-HT target, the spatial maps of the two conditions were then compared using permutation tests with Randomise [10].

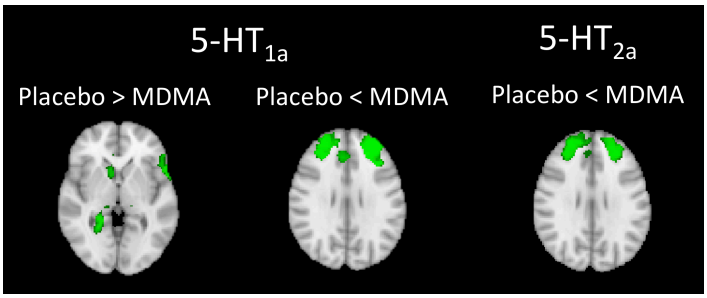

Figure: Results of PET-based dual regression. Significantly different BOLD response to MDMA was detected only in the 5-HT_{1A} and 5-HT_{2A} maps, due to the strong affinity of MDMA for these two receptors.

Results:

By comparing the two conditions for every 5-HT target, significant differences were found only for the maps derived by two of the drug targets, namely the 5-HT_{1A} and 5-HT_{2A} receptors ($p_{FWE} < 0.05$, figure). Specifically, subjects under MDMA showed a lower BOLD response (5-HT_{1A}-related maps) in the precentral and postcentral gyri, supplementary motor cortex, insular cortex, anterior cingulate cortex, inferior frontal gyrus and subcortical structures (right thalamus, right caudate, right and left putamen, right accumbens and right hippocampus). A higher BOLD response to MDMA was also found in the frontal pole, middle frontal gyrus, paracingulate gyrus and anterior cingulate cortex (5-HT_{1A} and 5-HT_{2A} maps).

Discussion:

The areas showing a significant different haemodynamic response to placebo/MDMA are those reported in published ASL and fMRI studies [11, 12]. Moreover, significant differences between placebo and drug were found only in the maps determined by 5-HT_{1A} and 5-HT_{2A} density profiles. This result is in keeping with the strong affinity of MDMA for these two receptors [7]. This study provides new evidence that rfMRI changes following MDMA administration reflect the known binding profile of the drug. This approach may provide an interesting new fingerprint in the characterisation of novel compounds and potentially greater insight to the commonly observed eclectic response to treatment.

Figure 2. Results of PET-based dual regression. Significantly different BOLD response to MDMA was detected only in the 5-HT_{1A} and 5-HT_{2A} maps, due to the strong affinity of MDMA for these two receptors.

References:

1. Khalili-Mahani N et al (2017) Hum Brain Mapp; 38(4):2276-325. doi: 10.1002/hbm.23516. PubMed PMID: 28145075.

2. Cox RW (1996) Comput Biomed Res; 29(3):162-73. PubMed PMID: 8812068.

3. Kundu P et al (2014) NeuroImage; 102:861-74.

4. Kundu P et al (2013) PNAS; 110(40):16187-92. doi: 10.1073/pnas.1301725110 [doi].

5. Dipasquale O et al (2017) Plos One; 12(3):e0173289. doi:10.1371/journal.pone.0173289.

6. Avants BB et al (2011) Neuroimage; 54(3):2033-44. doi: 10.1016/j.neuroimage.2010.09.025. PubMed PMID: 20851191; PubMed Central PMCID: PMCPMC3065962.

7. Lyon RA et al (1986) Psychopharmacology (Berl); 88(4):525-6. PubMed PMID: 2871581.

8. Beliveau V et al (2016) J Neurosci; doi: 10.1523/JNEUROSCI.2830-16.2016. PubMed PMID: 27856786.

9. Filippini N et al (2009) Proc Natl Acad Sci U S A; 106(17):7209-14. doi: 10.1073/pnas.0811879106.

10. Winkler AM et al (2014) Neuroimage; 92:381-97. doi:10.1016/j.neuroimage.2014.01.060.

11. Carhart-Harris RL et al (2014) Int J Neuropsychopharmacol; 17(4):527-40. doi: 10.1017/S1461145713001405.

12. Walpola IC et al (2017) Neuropsychopharmacology; 42(11):2152-62. doi: 10.1038/npp.2017.35.

P140
Association between tau neuropathology in TBI patients and late-onset psychiatric symptoms: A PET study

Keisuke Takahata[1,2], Yasuyuki Kimura[1,3], Hitoshi Shimada[1], Masanori Ichise[1], Naruhiko Sahara[1], Sho Moriguchi[1,4], Soichiro Kitamura[1], Manabu Kubota[1], Jin Mizushima[2], Hajime Tabuchi[2], Kazunori Kawamura[1], Ming-Rong Zhang[1], Masaru Mimura[2], Tetsuya Suhara[1], Makoto Higuchi[1]

(1) National Institute of Radiological Sciences, National Institute of Radiological Sciences, 4-9-1 Anagawa, Inage, Chiba, Chiba, Japan
(2) Department of Neuropsychiatry, Keio University School of Medicine, 35 Shinanomachi, Shinjuku, Tokyo, Japan
(3) National Center for Geriatrics and Gerontology, 7-430 Morioka, Obu, Aichi, Japan
(4) Research Imaging Centre, Centre for Addiction and Mental Health, Toronto, Canada, 250 College Street, Toronto, Ontario, Canada

Introduction:

Compelling clinical evidence indicates that late-onset psychiatric symptoms can be initiated by diverse types of traumatic brain injury (TBI)[1]. Neuropathological studies have revealed that late-life neurodegenerations due to TBI are characterized by abnormal accumulations of tau fibrils[2]. However, distribution of tau depositions in the living brains of TBI patients and its association with late-onset psychiatric symptoms remain unknown. The current study was aimed to compare tau depositions measured by positron emission tomography (PET) among age-matched controls and TBI patients with and without late-onset symptoms, and to evaluate associations between TBI-induced tau depositions and clinical symptoms.

Materials and Methods:

30 subjects at a chronic stage of mild-repetitive or single-severe TBI and 17 normal control subjects were recruited in the neighboring hospitals of psychiatry and neurology. Depositions of tau and amyloid β were investigated by conducting dynamic PET scans after injecting 543.5 ± 50.2 MBq of [^{11}C]pyridinyl-butadienyl-benzothiazole 3 ([^{11}C]PBB3) and 543.5 ± 50.2 MBq of [^{11}C]Pittsburgh compound B ([^{11}C]PIB), respectively. As two TBI patients who did not receive MRI, 1 TBI patient and 1NC subjects who did not receive tau PET scan were excluded, 27 TBI patients with (n=13) or without (n=17) late-onset psychiatric symptoms and 16 age-matched normal controls were included in the present analysis. Binding potential (BP^*_{ND}) of [^{11}C]PBB3 was calculated using an optimized reference region method[3]. Since patchy distributions of tau lesions and consequent partial volume effects on tau PET signals in the TBI brains hamper accurate quantification of these pathologies, we calculated [^{11}C]PBB3 binding capacity [cm^3] as a total volume of voxels whose binding potential values (BP^*_{ND}) above a threshold in a target region. Amyloid β depositions were evaluated by estimating standardized uptake value ratio (SUVR) for [^{11}C]PiB between the entire cerebral cortex and cerebellar cortex. A cortical [^{11}C]PiB SUVR above 1.21 was considered to be high uptake[4]. All PET scans were performed with a Bigograph mCT flow system (Siemens Healthcare, Erlangen, Germany). Psychiatric symptoms were evaluated by clinical scales and neuropsychological tests.

Results:

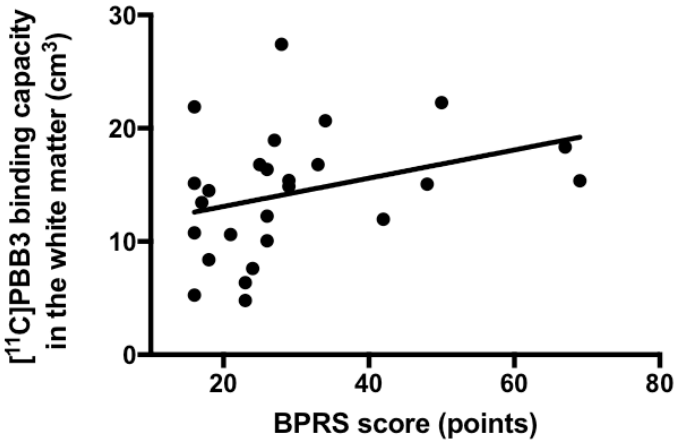

TBI patients showed higher [^{11}C]PBB3 binding capacities in the neocortical gray and white matter but not in the subcortical gray or subcortical white matter compared to controls. TBI patients with late-onset psychiatric symptoms had higher [^{11}C]PBB3 binding capacities in the white matter compared to those without late-onset psychiatric symptoms. Among TBI patients, [^{11}C]PBB3 binding capacity in the cortical and subcortical white matter showed positive correlation with severity of psychosis as assessed by Brief Psychiatric Rating Scale (BPRS). Among TBI patients and normal control subjects, only one single-severe TBI patients was [^{11}C]PiB positive (cortical [^{11}C]PiB PET SUVR: 1.32).

Discussion/Conclusion:

Our results provide the *in vivo* evidence of distinctive distribution of tau neuropathology in TBI brains. Late-onset symptoms following TBI are associated with higher tau depositions in the cortical white matter, implicating physical injury-provoked axonal tau accumulations in the deteriorations of the brain functions.

Acknowledgment: This study was supported by JSPS KAKENHI 16K19789.

References:

1.Smith DH, Johnson VE, Stewart W. [2013] *Nate Rev Neurol*. 9:211-221

2.McKee AC, Stein TD, Nowinski CJ et al. [2013] *Brain*. 2013;136:43-64.

3.Kimura Y, Endo H, Ichise M et al. [2016] *EJNMMI Research* 6:1-6

4.Villeneuve S, Rabinovici GD, Cohn-Sheehy BI et al. [2015] Existing *Brain* 138 2020-2033

P141
Multimodal ASL/PET/mRNA-expression analysis reveals CBF changes after single dose of antipsychotics depends on dopamine D2 receptor density profiles.

Pierluigi Selvaggi[1], Peter C.T. Hawkins[1], Ottavia Dipasquale[1], Gaia Rizzo[2,3], Alessandro Bertolino[4], Juergen Dukart[5], Fabio Sambataro[6], Steven C.R. Williams[1], Federico Turkheimer[1], Mattia Veronese[1] and Mitul Mehta[1].

[1]Department of Neuroimaging, Institute of Psychiatry, Psychology and Neuroscience, King's College London, London, United Kingdom
[2]Imanova Ltd., Centre for Imaging Sciences, Hammersmith Hospital, London, UK
[3]Division of Brain Sciences, Department of Medicine, Imperial College London, London, UK
[4]Department of Basic Medical Science, Neuroscience and Sense Organs, University of Bari Aldo Moro, Bari BA, Italy
[5]Translational Medicine Neuroscience and Biomarkers, F. Hoffmann-La Roche Ltd, Basel, Switzerland
[6]Department of Experimental and Clinical Medical Sciences, University of Udine, Udine, Italy

Introduction:

Antipsychotic drugs produce marked functional effects as measured with MRI haemodynamic markers like Cerebral Blood Flow (CBF) [1-3]. These effects are thought to depend on dopamine D2 receptor (D2R) blockade[4], although their relationship with antipsychotic pharmacodynamics has not been fully established yet. In fact, the haemodynamic nature of CBF measures makes difficult to interpret drug effects in terms of altered neurotransmission function. In the present work, we tested whether CBF changes induced by different antipsychotics mirror receptor distribution profiles of one of the main target of these compounds, namely the D2R. We evaluated the correlation of CBF variation with receptor density as measured with PET and brain mRNA expression extracted from the Allen Human Brain Atlas[5].

Methods:

Forty-two healthy male subjects were enrolled in a double blind, randomized, placebo-controlled, crossover study[3]. Regional CBF was assessed with arterial spin labelling, acquired on a 3T scanner using a pseudo-continuous ASL (pCASL) sequence. For each antipsychotic, a paired T-test was performed in SPM12. A template image of dopamine D2 receptor density was derived from PET scans using the high affinity D2/D3 antagonist ligand [18F]-Fallypride[6]. Brain mRNA expression values for *DRD2* gene (coding for D2R) were extracted from the Human Allen Brain Atlas dataset[5] by using the MENGA toolbox[7]. CBF contrast images and the [18F]Fallypride BP_{ND} template were segmented into 83 ROIs by using the Desikan-Killiany Atlas[8]. The regional changes in CBF against placebo (ΔCBF) were compared with BP_{ND} and gene expression maps using multivariate correlations.

Results:

PET profiles

Drug	R^2 (linear)	sign	p value
HAL	0.61	+	<0.001
lowRIS	0.54	+	<0.001
highRIS	0.52	+	<0.001
OLA	0.24	+	<0.001

mRNA expression

Drug	R^2	sign	Chance likelihood
HAL	0.15	+	0 %
lowRIS	0.19	+	0 %
highRIS	0.20	+	0 %
OLA	0.04	+	2 %

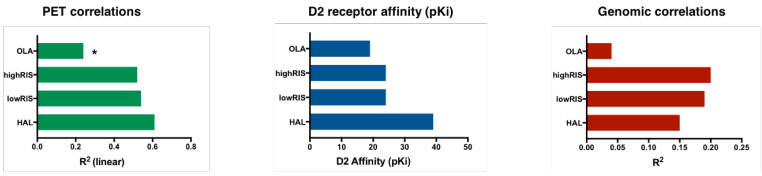

Figure 1. Summary of the multivariate correlation analyses. For all antipsychotics ΔCBF values were positively correlated with [18F]Fallypride BP and *DRD2* mRNA levels. pKi values are from the National Institutes of Mental Health (NIMH) Psychoactive Drug Screening Program (PDSP) K_i database[9]. * p<0.01 vs HAL, lowRIS and highRIS. All the other comparisons were not significant (p>0.05)

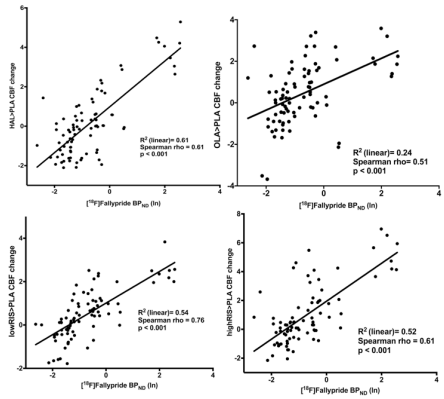

Figure 2. Top row: Scatterplot of the correlation between HAL ΔCBF profiles and [18F]Fallypride BP (left) and of the correlation between OLA ΔCBF profiles and [18F]Fallypride BP (right). Bottom row: Scatterplot of the correlation between lowRIS ΔCBF profiles and [18F]Fallypride BP (left) and of the correlation between highRIS ΔCBF profiles and [18F]Fallypride BP (right)

Discussion:

CBF increase after antipsychotics were directly proportional to D_2R concentration in the brain, as indexed by PET BP_{ND} maps and mRNA expression levels. Microarray mRNA expression data explained less variance in ΔCBF than PET derived map. Interestingly, the association strength between ΔCBF and brain receptor distribution profiles mirrored differential D2R affinity between the tested drugs[9]. Overall, these results indicate that CBF increases after administration of a single dose of antipsychotics actually reflect known pharmacodynamics profile of these compounds. Further work will determine whether this

approach is able to separate the specific contribution of different receptor systems (i.e. dopamine and serotonin receptors) for drugs with multiple targets like antipsychotics. While individualised receptor profile maps may bring more precision to the method, CBF is ultimately a functional marker and this work is important in bridging the considerable gap between the pharmacokinetic and pharmacodynamic effects of compounds.

Acknowledgements:

This work represents independent research part funded by the National Institute for Health Research (NIHR) Biomedical Research Centre at South London and Maudsley NHS Foundation Trust and King's College London. The views expressed are those of the author(s) and not necessarily those of the NHS, the NIHR or the Department of Health.

References:

1. Handley, R. *et al.* Acute effects of single-dose aripiprazole and haloperidol on resting cerebral blood flow (rCBF) in the human brain. *Hum. Brain Mapp.* **34,** 272–282 (2013).

2. Fernández-Seara, M. A. *et al.* Effects on resting cerebral blood flow and functional connectivity induced by metoclopramide: a perfusion MRI study in healthy volunteers. *Br. J. Pharmacol.* **163,** 1639–1652 (2011).

3. Hawkins, P. C. T. *et al.* An investigation of regional cerebral blood flow and tissue structure changes after acute administration of antipsychotics in healthy male volunteers. *Hum. Brain Mapp.* **39,** 319–331 (2018).

4. Goozee, R., Handley, R., Kempton, M. J. & Dazzan, P. A systematic review and meta-analysis of the effects of antipsychotic medications on regional cerebral blood flow (rCBF) in schizophrenia: Association with response to treatment. *Neuroscience & Biobehavioral Reviews* **43,** 118–136 (2014).

5. Hawrylycz, M. J. *et al.* An anatomically comprehensive atlas of the adult human brain transcriptome. *Nature* **489,** 391–399 (2012).

6. Mukherjee, J., Yang, Z.-Y., Das, M. K. & Brown, T. Fluorinated benzamide neuroleptics—III. Development of (S)-N-[(1-allyl-2-pyrrolidinyl)methyl]-5-(3-[18F]fluoropropyl)-2,3-dimethoxybenzamide as an improved dopamine D-2 receptor tracer. *Nuclear Medicine and Biology* **22,** 283–296 (1995).

7. Rizzo, G., Veronese, M., Expert, P., Turkheimer, F. E. & Bertoldo, A. MENGA: A New Comprehensive Tool for the Integration of Neuroimaging Data and the Allen Human Brain Transcriptome Atlas. *PLoS ONE* **11,** e0148744–20 (2016).

8. Desikan, R. S. *et al.* An automated labeling system for subdividing the human cerebral cortex on MRI scans into gyral based regions of interest. *NeuroImage* **31,** 968–980 (2006).

9. McCormick, P. N. *et al.* The antipsychotics olanzapine, risperidone, clozapine, and haloperidol are D2-selective ex vivo but not in vitro. *Neuropsychopharmacology* **35,** 1826–1835 (2010).

P142
Dysregulation of mGluR5 in borderline personality disorder: A Pilot PET Study with [^{18}F]FPEB.

Margaret T. Davis, Sophie E. Holmes, Ansel T. Hillmer, Nicole DellaGioia, Sarah O'Grady, Nabeel Nabulsi, David Matuskey, Richard E. Carson, Irina Esterlis

Yale University School of Medicine, New Haven, CT

Introduction:

Borderline Personality Disorder (BPD) is a debilitating psychiatric condition, characterized by affective instability, impulsivity, disruption of interpersonal relationships and self-image, and chronic self-harm. Despite relatively low prevalence (1-3% in the United States[1]), BPD is associated with 75% rate of lifetime suicide attempt, and 10% suicide mortality[2]. However, relatively little is known about the pathophysiology of BPD on a molecular level, and available pharmacological agents largely fall short of significantly reducing overall symptom severity and suicide risk[3]. Promisingly, the metabotropic glutamate receptor type 5 (mGluR5) has recently been implicated in the pathophysiology of both BPD and suicidal behavior. MGluR5 is of particular interest given its role in emotional regulation, social and cognitive functioning, and pain processing, all of which are central to both BPD and suicidal behavior[4]. Further, recent postmortem studies have supported a relationship between glutamate dysregulation[5,6], including altered mGluR5[7], and death by suicide. This novel pilot study examined the role of mGluR5 in BPD symptomatology *in vivo*.

Materials & Methods:

Twenty individuals in a current depressive episode and twenty healthy controls (HC) participated in a single [^{18}F]FPEB PET scan to quantify mGluR5 availability *in vivo* [11 with major depressive disorder (MDD) alone (age=36±4 years; MADRS=23±6); 9 with both MDD and comorbid BPD (age=40±10 years; MADRS=24±6); 20 age-, sex-, and smoking-matched comparison controls (HC; age=37±9 years)]. All participants completed a comprehensive battery of psychiatric rating scales and cognitive testing on scan day. Volume of distribution (V_T: ratio of parent radioligand concentration in tissue relative to that in blood) in grey matter regions was computed using a venous input function Radiotracer was injected as bolus plus constant infusion and subjects were scanned during steady state (90-120mins post-injection).

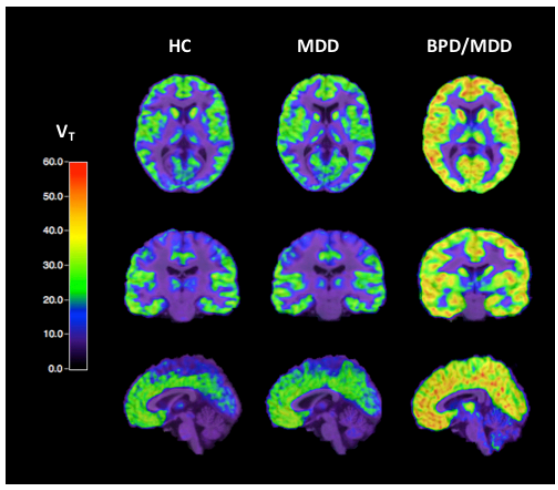

Figure 1. Parametric VT images of representative subjects from each patient group imaged with [18F]FPEB.

Results:

We observed significantly greater mGluR5 V_T in individuals with comorbid BPD and MDD compared to both MDD only [(amygdala; 31% higher, p<.001), dorsolateral PFC (dlPFC; 24% higher, p=.015); and orbitofrontal cortex (OFC; 29% higher, p=.002)], and HC [(amygdala; 32% higher, p<.001), dorsolateral PFC (dlPFC; 31% higher, p<.001); and orbitofrontal cortex (OFC; 30% higher, p=.002)] across brain regions implicated in the neurobiology of BPD (See Figure 1). Among individuals with comorbid BPD and MDD, higher mGluR5 V_T was associated with history of suicide attempt (28-33% higher, p's=.002-.046) and positively correlated with impulsivity (r's=.85-.77, p's<.005) across regions of interest. No relationship between mGluR5 V_T suicide attempt history or impulsivity was observed among individuals with MDD only.

Discussion/Conclusion:

This is the first *in vivo* investigation implicating mGluR5 dysregulation in BPD. Previous studies in MDD report lower or no difference in mGluR5 availability in the MDD group as compared to control. Here, however, comorbidity with BPD appears to be associated with higher mGluR5 availability, which is likely a unique contribution of BPD. Importantly, higher mGluR5 availability was associated with history of suicide attempt and impulsivity in individuals with BPD. Accordingly, these findings suggest that mGluR5 may represent a novel biomarker for suicidal behavior and a potential therapeutic target in BPD. Of note, these results are preliminary and warrant replication in a larger sample of subjects to validate current implications. Further, the nature of mGluR5 abnormalities in this population warrant exploration to determine whether they are part of a causative mechanism underlying the development of BPD symptoms, including suicidal behavior. While preliminary, these findings implicate mGluR5 as a potentially critical treatment for the core symptoms in this disorder.

Acknowledgments:

This study was funded in part by the VA National Center for PTSD, and NIH grant R01MH104459 (PI: Esterlis). Dr. Davis is funded by NIH grant T32 DA022975-9.

References:

1. Grant BF, Chou SP, Goldstein RB et al. [2008] J Clin Psychiat. Prevalence, correlates, disability, and comorbidity of DSM-IV borderline personality disorder: results from the Wave 2 National Epidemiologic Survey on Alcohol and Related Conditions.69:533.
2. Oldham, JM [2006]. Am. J. Psychiat. Borderline personality disorder and suicidality.163: 20-26.
3. Hancock-Johnson E, Griffiths C, Picchioni M. [2017]. CNS Drugs. A Focused Systematic Review of Pharmacological Treatment for Borderline Personality Disorder. 5:345-356.
4. New AS, Triebwasser J, Charney DS. [2008]. Biol Psychiat. The case for shifting borderline personality disorder to Axis I. Biol Psychiat.64:653-659.
5. Lutz P, Mechawar N, Turecki G. [2017]. Mol. Psychiat. Neuropathology of suicide: recent

findings and future directions.
6. Zhao J, Verwer R, van Wamelen D et al. [2016]. J. Psychiat. Res. Prefrontal changes in the glutamate-glutamine cycle and neuronal/glial glutamate transporters in depression with and without suicide. 82:8-15.
7. Chandley MJ, Szebeni A, Szebeni K et al. [2014]. Int. J. Neuropsychop. Elevated gene expression of glutamate receptors in noradrenergic neurons from the locus coeruleus in major depression.17:1569-1578.

P143

Synthesis and microPET evaluation of [^{11}C]7-iodo-2-[4-methoxy-3-(2-(4-methylpiperidin-1-yl)ethoxy)phenyl]isoindolin-1-one as a candidate 5-HT$_{2C}$ receptor imaging agent

Fanxing Zeng, Jonathon A. Nye, Ronald J. Voll, and **Mark M. Goodman**

Department of Radiology and Imaging Sciences, Center for Systems Imaging, Emory University, Atlanta, Georgia 30322

Introduction:

The serotonin 5-HT$_{2C}$ receptor (5-HT$_{2C}$R) is abundantly expressed throughout the central nervous system, and is involved in a variety of neuroendocrine and neurobehavioral processes. With the availability of selective agonists and antagonists, 5-HT$_{2C}$R has been indicated as a novel pharmacotherapeutic target for the treatment of depression, schizophrenia, anxiety, drug abuse, obesity, and Parkinson's disease. However, a direct relationship between 5-HT$_{2C}$R physiology and brain diseases has proven difficult to establish due to an inability to accurately quantify 5-HT$_{2C}$R density and functional status in vivo. The radioligands developed so far are not ideal for in vivo brain imaging. As part of an ongoing research project in our laboratories to develop 5-HT$_{2C}$R imaging agents using PET, we synthesized [^{11}C] 7-iodo-2-[4-methoxy-3-(2-(4-methylpiperidin-1-yl)ethoxy)phenyl]isoindolin-1-one (**1**). We report here the radiosynthesis and microPET evaluation of (**1**) in rodents.

Materials and Methods:

(**1**) and its corresponding normethyl precursor (**2**) were synthesized *via* multi-step synthetic approaches. In vitro competition binding assays of (**1**) were conducted by NIMH Psychoactive Drug Screening Program (PDSP). [^{11}C]**1** was prepared *via O*-methylation of (**2**) with [^{11}C]CH_3I in the presence of 0.1 M Bu_4NOH in DMF followed by HPLC purification. Log P of **1** was measured between 1-octanol and phosphate buffer at PH 7.4. MicroPET brain images of [^{11}C]**1** were acquired in Sprague-Dawley rats using a Siemens Inveon microPET/CT imaging system. Baseline studies were initially performed to determine the extent of brain uptake *in vivo* (n=3). Pretreating the rats with a dose of 0.3 mg/kg of 5-HT$_{2C}$R antagonist, SB-242084, 30 min prior to injection of [^{11}C]**1** was also conducted to assess the in vivo specific binding to 5-HT$_{2C}$R (n=3).

Results:

(**1**) displayed a high affinity for 5-HT$_{2C}$R (Ki = 1.1 nM) and a high selectivity over 5-HT$_{2A}$R (Ki > 1000 nM) and 5-HT$_{2B}$R (Ki = 126 nM). [^{11}C]**1** was obtained in an average 36% ± 10% decay-corrected radiochemical yield (n = 8) with a radiochemical purity of >97% and a specific activity of 0.5-1.2 Ci/μmol. (**1**) displays moderate lipophilicity with a log P7.4 of 2.89.

After injection of [^{11}C]**1**, high binding was observed in the choroid plexus, the region with the highest density of 5-HT$_{2C}$R, whereas the bindings in all other brain regions were low. Overall, [^{11}C]**1** did not enter the brain in high amounts during the time course of PET studies, but the contrast of binding to the choroid plexus was excellent at greater than 10:1 compared to the cerebellum. Administration of a dose of SB-242084 resulted in a marked reduction of radioactivity at the choroid plexus, suggesting that the uptake of [^{11}C]**1** in choroid plexus reflected specific bindig.

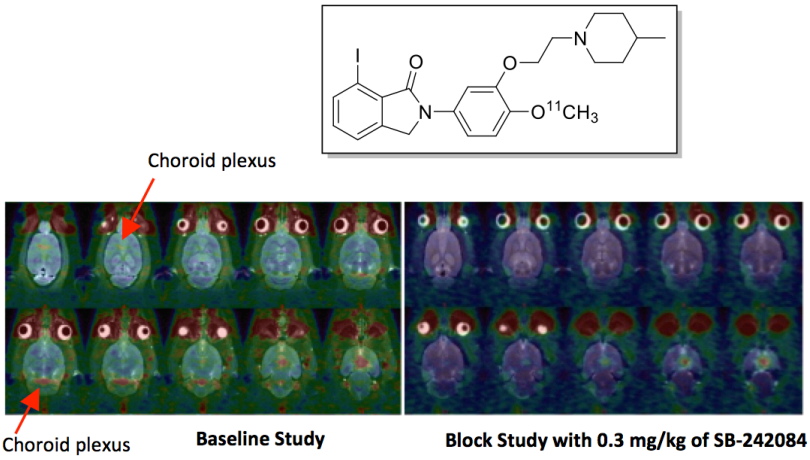

Discussion/Conclusion:

A new 5-HT$_{2C}$R imaging ligand [^{11}C]**1** was successfully prepared. The poor brain availability of [^{11}C]**1** does not appear to be explained by its logP7.4 value, suggesting a factor other than lipophilicity prevents [^{11}C]**1** from entering brain such as high level of protein binding in the plasma or active action of efflux pumps (e.g. P-gp) at the blood-brain barrier, but further studies would need to be conducted for validation. MicroPET brain image studies demonstrated that [^{11}C]**1** was suitable for detecting 5-HT$_{2C}$R in the choroid plexus of the rodent brain. Structural modification of **1** will be conducted in order to increase binding affinity and brain penetration.

Acknowledgements:

This work was funded by a grant from the National Institute of Health (1R21MH108928). We thank Dr. Bryan Roth and his team for providing the binding affinity data. We thank Dr. Jaekeun Park for his help in the microPET studies.

References:

Monck N J, and Kennett G A [2008] Progress in Medicinal Chemistry 46: 281-390.
Jensen N H, Cremers T I, and Sotty F. [2010] Scientific World Journal 10:1870-1885.
Hamprecht D, Micheli F et al. [2007] Bioorg. Med. Chem. Lett. 17: 428-433.

P144
α7-nAChR: [^{18}F]ASEM binding potentials and receptor density in human brain in vivo

Albert Gjedde, MD, DSc[1,2] , Jenny A. Phan, MBBS[2-4], Andrew G. Horti, PhD[2], Elise Weerts, PhD[5], Heather Valentine, BS[2], William Kem[6] , Robert Freedman MD[7], Dean F. Wong, MD, PhD[2,5]

1 Department of Nuclear Medicine, Odense University Hospital, University of Southern Denmark, Odense, Denmark
2 Russell H Morgan Dept of Radiology and Radiological Sciences, Johns Hopkins University School of Medicine, Baltimore, MD
3 Department of Biomedicine, Aarhus University, Aarhus, Denmark
4 Department of Nuclear Medicine and PET Centre, Aarhus University Hospital, Aarhus University. Aarhus, Denmark
5 Department of Psychiatry and Behavioral Sciences, Neurosciences and Neurology, Johns Hopkins Medical Institutions, Baltimore, MD
6 Department of Psychiatry, University of Colorado, Aurora, CO
7 Department of Pharmacology, University of Florida , Gainesville, FL

Introduction: [^{18}F]ASEM is a radioligand of human α7-nAChR (Wong et al 2014). The lack of a reference region of nonspecific binding has limited the quantification of specific binding. We used the novel Extended Inhibition Plot method to identify the volume of distribution of the tracer in a virtual reference volumes before and after receptor blockade (Phan et al. 2017) to obtain occupancy and affinity estimates of a partial agonist, and binding potentials of the tracer and measures of receptor density in five healthy non-smoking volunteers.

Methods: We completed PET with [^{18}F]ASEM at baseline and after 150 mg DMXB-A(GTS21) (see companion abstract by Wong et al., NMR 2018). Regional volumes of distribution (V_T) of [^{18}F]ASEM yielded reference volumes of non-displaceably bound radioligand (V_{ND}), competitor saturation of receptors (s), tracer binding potentials (BP_{ND}), and estimates of receptor density estimates (B_{max}) and competitor affinity (IC_{50}, K_I) in the five subjects.

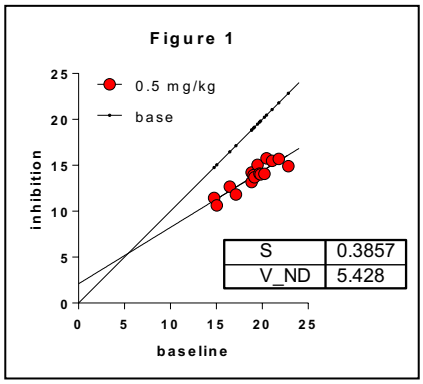

Baboon: We estimated the radioligand's baseline V_{ND} in baboon brain in vivo (Horti *et al,* 2014), using the conventional Inhibition Plot (Gjedde and Wong 2000). Applied to regional values of V_T, the plot yielded values of V_{ND} and saturation (s),

$$V_{T(i)} = (1 - s)\, V_{T(b)} + s\, V_{ND} \quad (1)$$

where $V_{T(b)}$ refers to baseline, $V_{T(i)}$ to competition with the high affinity inhibitor SSR180711. When plotted as function of the baseline condition in baboon brain (Figure 1), the V_T values yielded the V_{ND} and the occupancy of the competitor, s.

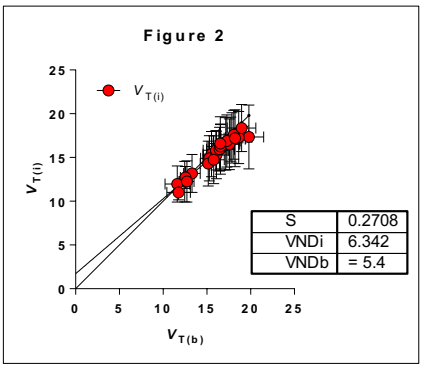

Humans: We obtained near identical V_T estimates before and after a single dose of 150 mg DXMB-A (Figure 2), assumed to be due to changing V_{ND}. To resolve the change, we applied the Extended Inhibition Plot (EIP; Phan *et al.* 2017) that related the distribution volumes at inhibition and baseline,

$$V_{T(i)} = (1 - s)\left[\frac{V_{ND(i)}}{V_{ND(b)}}\right] V_{T(b)} + s\, V_{ND(i)} \quad (2)$$

where $V_{ND(b)}$ and $V_{ND(i)}$ represent V_{ND} at baseline and inhibition. The EIP yielded the inhibition $V_{ND(i)}$, when the baseline $V_{ND(b)}$ was adopted from baboon. The volume estimates yielded binding potentials (BP_{ND}) for the two conditions,

$$BP_{ND(b)} = \frac{V_{T(b)}}{V_{ND(b)}} - 1 \text{ and } BP_{ND(i)} = \frac{V_{T(i)}}{V_{ND(i)}} - 1 \quad (3)$$

where $BP_{ND(b}$ and $BP_{ND(i)}$ are the binding potentials at baseline and inhibition. The BP_{ND} together with inhibitor concentrations (Ci) yielded B_{max} and K_I (IC_{50}) estimates for receptor and inhibitor,

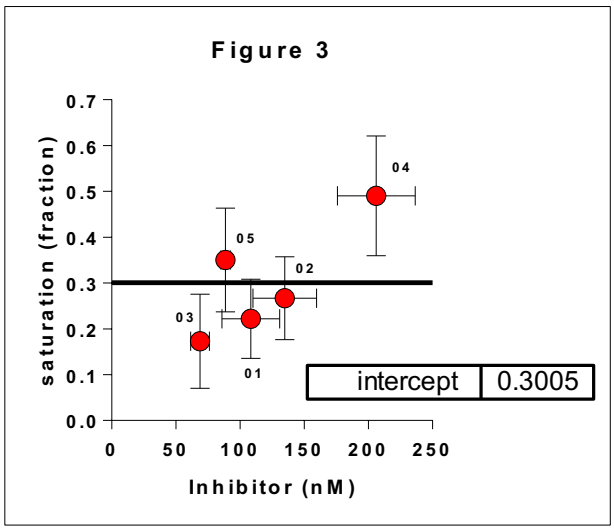

$$BP_{ND} = \frac{B_{max}}{K_d\left(1 + \frac{[DMXB\text{-}A]}{K_I}\right)} \quad (4)$$

where the receptor density is determined relative to the affinity of the radioligand, K_d, with known values of the [DMXB-A] concentration and the inhibitor affinity, K_I, and the value of ASEM K_d of 0.35 nM from the estimate of K_I of 0.4 nM for [^{123}I]bungarotoxin.

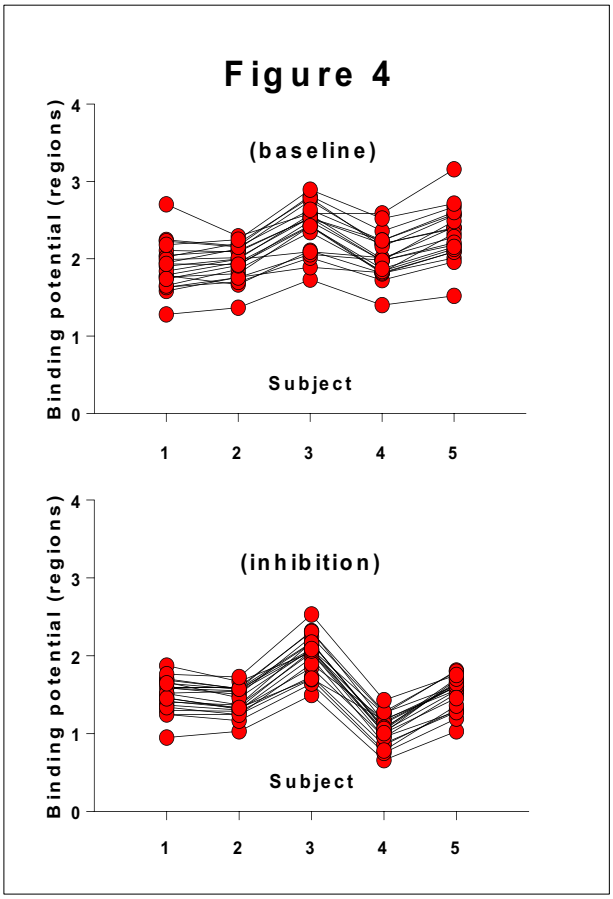

Results and Discussion: In baboon, the reference volume V_{ND} assessed by the Inhibition Plot shown in **Figure 1** yielded the estimate of $V_{ND(b)}$ of 5.4 ml/cm^3 at the lowest dose of the SR180711. The application of this baseline value of V_{ND} to the five subjects yielded the degree of inhibition shown in **Figure 2**, obtained with the Extended Inhibition Plot (Phan et al. 2017). From the reduction of binding (occupancy), the Extended Inhibition Plot yielded individual values of the occupancy of α7-nAChR by DMXB-A at 17-49% for plasma concentrations at 60-200 nM DMXB-A, as shown in **Figure 3**. From equations 3, the estimates of regional binding potentials (BP_{ND}) declined significantly in all examined regions after blocking with DMXB-A, as shown in **Figure 4.** The average values of receptor density (B_{max}) and average values of the receptor's affinity (K_I) to DMXB-A ranged from 0.67-0.82 nM for B_{max} and from 170 to 385 nM for K_I, as presented in **Figure 5**, in agreement with evidence from post-mortem human brain with the radioligand ([^{125}I]-α-BTX) (Horti et al. 2014).

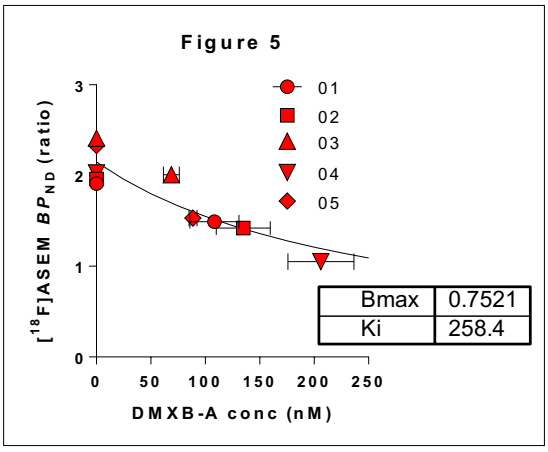

References

Gjedde A and Wong DF (2000). Receptor occupancy in absence of reference region. *Neuroimage* **11:** S48.

Horti AG, Gao Y, Kuwabara H, Wang Y, Abazyan S, Yasuda RP *et al* (2014). [18F]ASEM (18F]JHU82132), a radiolabeled antagonist for imaging the a7-nicotinic acetylcholine receptor (α7-nAChR) with positron emission tomography (PET). *J Nucl Med* **55:** 672-677.

Phan J, Landau AM, Jakobsen S, Gjedde A (2017). Radioligand binding analysis of α 2 adrenoceptors with 11C]yohimbine in brain in vivo: Extended Inhibition Plot correction for plasma protein binding. *Scientific Reports* **7:** 15979.

Wong DF, Kuwabara H, Pomper M, Holt DP, Brasic JR, George N *et al* (2014). Human Brain Imaging of Alpha-7 nAChR with [18F]ASEM: a New PET Radiotracer for Neuropsychiatry and Determination of Drug Occupancy. *Molecular Imaging and Biology* **16:** 730-738.

LONDON NRM2018 *is sponsored by:*

abbvie

UNITED IMAGING

Eisai

pmod

ACS Chemical Neuroscience

wellcome EPSRC centre medical engineering

iel.

KING'S College LONDON